

Lecture Notes in Civil Engineering

Andrei Petriaev
Anastasia Konon *Editors*

Transportation Soil Engineering in Cold Regions, Volume 2

Proceedings of TRANSOILCOLD 2019

 Springer

Lecture Notes in Civil Engineering

Volume 50

Series Editors

Marco di Prisco, Politecnico di Milano, Milano, Italy

Sheng-Hong Chen, School of Water Resources and Hydropower Engineering,
Wuhan University, Wuhan, China

Ioannis Vayas, Institute of Steel Structures, National Technical University of
Athens, Athens, Greece

Sanjay Kumar Shukla, School of Engineering, Edith Cowan University, Joondalup,
WA, Australia

Anuj Sharma, Iowa State University, Ames, IA, USA

Nagesh Kumar, Department of Civil Engineering, Indian Institute of Science
Bangalore, Bangalore, Karnataka, India

Chien Ming Wang, School of Civil Engineering, The University of Queensland,
Brisbane, QLD, Australia

Lecture Notes in Civil Engineering (LNCE) publishes the latest developments in Civil Engineering - quickly, informally and in top quality. Though original research reported in proceedings and post-proceedings represents the core of LNCE, edited volumes of exceptionally high quality and interest may also be considered for publication. Volumes published in LNCE embrace all aspects and subfields of, as well as new challenges in, Civil Engineering. Topics in the series include:

- Construction and Structural Mechanics
- Building Materials
- Concrete, Steel and Timber Structures
- Geotechnical Engineering
- Earthquake Engineering
- Coastal Engineering
- Ocean and Offshore Engineering; Ships and Floating Structures
- Hydraulics, Hydrology and Water Resources Engineering
- Environmental Engineering and Sustainability
- Structural Health and Monitoring
- Surveying and Geographical Information Systems
- Indoor Environments
- Transportation and Traffic
- Risk Analysis
- Safety and Security

To submit a proposal or request further information, please contact the appropriate Springer Editor:

- Mr. Pierpaolo Riva at pierpaolo.riva@springer.com (Europe and Americas);
- Ms. Swati Meherishi at swati.meherishi@springer.com (Asia - except China - and Australia/NZ);
- Ms. Li Shen at li.shen@springer.com (China).

Indexed by Scopus

More information about this series at <http://www.springer.com/series/15087>

Andrei Petriaev · Anastasia Konon
Editors

Transportation Soil Engineering in Cold Regions, Volume 2

Proceedings of TRANSOILCOLD 2019

 Springer

Editors

Andrei Petriaev
Emperor Alexander I St. Petersburg State
Transport University
St. Petersburg, Russia

Anastasia Konon
Emperor Alexander I St. Petersburg State
Transport University
St. Petersburg, Russia

ISSN 2366-2557 ISSN 2366-2565 (electronic)
Lecture Notes in Civil Engineering
ISBN 978-981-15-0453-2 ISBN 978-981-15-0454-9 (eBook)
<https://doi.org/10.1007/978-981-15-0454-9>

© Springer Nature Singapore Pte Ltd. 2020

This work is subject to copyright. All rights are reserved by the Publisher, whether the whole or part of the material is concerned, specifically the rights of translation, reprinting, reuse of illustrations, recitation, broadcasting, reproduction on microfilms or in any other physical way, and transmission or information storage and retrieval, electronic adaptation, computer software, or by similar or dissimilar methodology now known or hereafter developed.

The use of general descriptive names, registered names, trademarks, service marks, etc. in this publication does not imply, even in the absence of a specific statement, that such names are exempt from the relevant protective laws and regulations and therefore free for general use.

The publisher, the authors and the editors are safe to assume that the advice and information in this book are believed to be true and accurate at the date of publication. Neither the publisher nor the authors or the editors give a warranty, expressed or implied, with respect to the material contained herein or for any errors or omissions that may have been made. The publisher remains neutral with regard to jurisdictional claims in published maps and institutional affiliations.

This Springer imprint is published by the registered company Springer Nature Singapore Pte Ltd. The registered company address is: 152 Beach Road, #21-01/04 Gateway East, Singapore 189721, Singapore

Organizing Committee

Honorary Chair

Dr. Alexander Y. Panychev, Rector of Emperor Alexander I St. Petersburg State Transport University, Russia

Conference Chair

Dr. Andrei Petriaev, “Construction of roads” Department, Emperor Alexander I St. Petersburg State Transport University, Russia

Vice-chairs

Prof. Jiankun Liu, School of Civil Engineering, Sun Yat-sen University, China
Prof. Erol Tutumluer, Chair of TC202, ISSMGE, University of Illinois, Urbana-Champaign, USA

Conference Secretary

Dr. Anastasia Konon, “Construction of roads” Department, Emperor Alexander I St. Petersburg State Transport University, Russia

Conference Committee Members

Local Committee

Vice-chairs

Prof. Tamila S. Titova, Vice-rector, Emperor Alexander I St. Petersburg State Transport University, Russia

Prof. Nikolai S. Bushuev, Dean of Transport Construction Faculty, Emperor Alexander I St. Petersburg State Transport University, Russia

Prof. Vladimir V. Egorov, Dean of Civil Construction Faculty, Emperor Alexander I St. Petersburg State Transport University, Russia

Dr. Alexey F. Kolos, Head of “Construction of roads” Department, Emperor Alexander I St. Petersburg State Transport University, Russia

Prof. Larisa B. Svatovskaya, Head of “Engineering Chemistry” Department, Emperor Alexander I St. Petersburg State Transport University, Russia

Prof. Alexander P. Lediaev, Head of “Tunnels and Underground Railways” Department, Emperor Alexander I St. Petersburg State Transport University, Russia

Viktor V. Gachits, “Construction of roads” Department, Emperor Alexander I St. Petersburg State Transport University, Russia

Dr. Antonina S. Sakharova, “Engineering Chemistry” Department, Emperor Alexander I St. Petersburg State Transport University, Russia

Svetlana A. Petrenko, “Construction of roads” Department, Emperor Alexander I St. Petersburg State Transport University, Russia

International Committee

Prof. Charles Ng, President of the International Society for Soil Mechanics and Geotechnical Engineering (ISSMGE), The Hong Kong University of Science and Technology, Kowloon

Prof. Chungsik Yoo, President of International Geosynthetics Society (IGS), College of Engineering, Sungkyunkwan University, Seoul

Prof. Martin Ziegler, Geotechnical Engineering and Institute of Foundation Engineering, Soil Mechanics, Rock Mechanics and Waterways Construction, RWTH Aachen University, Aachen

Prof. Antonio Gomes Correia, Immediate past Chair of the TC202, ISSMGE, University of Minho, Braga

Prof. Abdelmalek (Malek) Bouazza, Chair of TC215 Environmental Geotechnics, ISSMGE, Monash University, Australia

Prof. Takashi Ono, Chair of TC216 Frost Geotechnics, ISSMGE

Prof. Jorge G. Zornberg, University of Texas at Austin

Dr. Jacek Kawalec, Silesian University of Technology, Poland
Prof. Askar Zhussupbekov, Eurasian National University, Astana
Prof. Eun Chul Shin, College of Urban Science, Incheon National University, Incheon
Prof. Devendra Narain Singh, Indian Institute of Technology Bombay, Mumbai
Prof. Satoshi Akagawa, Cryosphere Engineering Laboratory, Hachioji, Tokyo
Prof. Jong-Sub Lee, School of Civil, Environmental and Architectural Engineering, Korea University, Seoul
Prof. Valentin V. Vinogradov, Russian University of Transport, Moscow
Prof. Taisiya V. Shepitko, Russian University of Transport, Moscow
Prof. Alexander L. Isakov, Siberian Transport University, Novosibirsk
Prof. Evgeniy S. Ashpiz, Russian University of Transport, Moscow
Dr. Daniele Cazzuffi, President of the Italian Chapter of IGS—CESI SpA, Milano
Prof. Gökhan Baykal, Department of Civil Engineering, Faculty of Engineering, Bogazici University, Istanbul
Prof. Armen Z. Ter-Martirosyan, Moscow State University of Civil Engineering (National Research University), Moscow
Prof. Svyatoslav Ya. Lutskiy, Russian University of Transport, Moscow
Simon Dumais, President of Permafrost Young Researchers Network (PYRN), University Laval, Quebec
Prof. Tatsuya Ishikawa, Hokkaido University, Sapporo
Prof. Ivan Vanicek, ISSMGE Vice-president for Europe 2009–2013, Czech Technical University, Prague
Prof. Andreas Loizos, Laboratory of Pavement Engineering, National Technical University of Athens
Prof. Jean Cote, University Laval, Quebec
Prof. Pauli Kolisoja, Tampere University of Technology
Prof. Sergey A. Kudryavtsev, Nominated Member of TC216 Frost Geotechnics, ISSMGE, Far Eastern State Transport University, Khabarovsk
Prof. Vladimir N. Paramonov, Emperor Alexander I St. Petersburg State Transport University, Russia
Prof. José Neves, University of Lisbon
Prof. Zhaohui Yang, University of Alaska Anchorage
Prof. Katarzyna Zabielska-Adamska, Bialystok University of Technology
Prof. Inge Hoff, Department of Civil and Environmental Engineering, Norwegian University of Science and Technology (NTNU), Trondheim
Prof. Luljeta Bozo, Polis University, Tirana
Dr. Andrey A. Zaitsev, Moscow State University of Railway Engineering, Moscow
Dr. Elena Scibilia, Department of Civil and Environmental Engineering, Norwegian University of Science and Technology (NTNU), Trondheim
Dr. Nikolai K. Vasiliev, Department of Soil Mechanics and Geotechnics, JSC “Vedeneev VNIIG”, St. Petersburg
Prof. Xinglong Wang, Heilongjiang Institute of Highways and Transport Research
Prof. Xiong Zhang, Missouri University of Science and Technology

Prof. Dongqing Li, State Key Laboratory of Frozen Soil Engineering Cold and Arid Regions Environmental and Engineering Research Institute, Chinese Academy of Sciences, Lanzhou, Gansu

Prof. Igor Sakharov, Saint-Petersburg State University of Architecture and Engineering

Prof. Gennadiy M. Stoyanovich, Far Eastern State Transport University, Khabarovsk

Dr. Kazunori Munehiro, Senior Researcher, Civil Engineering Research Institute for Cold Regions, Sapporo

Alexey A. Maslakov, Department of Cryolithology and Glaciology, Faculty of Geography, Lomonosov Moscow State University

Dmitry Yu. Nekrasov, Coordinator, PYRN Russia 2018–2020

Dr. Pavel I. Kotov, Department of Geocryology, Faculty of Geography, Lomonosov Moscow State University

Prof. Viktor V. Pupatenko, Far Eastern State Transport University, Khabarovsk

Prof. Fujun Niu, Chinese Academy of Sciences, Beijing

Dr. Stephan Saboundjian, Chair of AFP50, Committee on Seasonal Climatic Effects on Transportation Infrastructure, TRB

Prof. Ma Wei, State Key Lab of Frozen Soil Engineering, Gansu

Prof. Yuanming Lai, Academician, Chinese Academy of Sciences, Beijing

Prof. Qing-Bai Wu, State Key Lab of Frozen Soil Engineering, Gansu

Prof. Zhou Guoqing, Vice-president, China University of Mining and Technology, Xuzhou

Prof. Adelino Jorge Lopes Ferreira, University of Coimbra

Pietro Rimoldi, Professional Civil Engineer, Council member of IGS

Prof. Dimitrios Zekkos, University of Michigan, Ann Arbor

Prof. Hemanta Hazarika, Kyushu University, Fukuoka

Prof. Zhuangzhuang Liu, School of Highway, Chang'an University, Xi'an

Prof. Erol Guler, Bogazici University, Istanbul

Prof. Heinz Brandl, President of the Austrian Chapter of IGS, Vienna University of Technology

Editorial Committee

Dr. Dali Naidu Arnepalli, India

Prof. Talal Awwad, Syria

Prof. Gokhan Baykal, Turkey

Prof. Daniele Cazzuffi, Italy

Prof. Krzysztof Czech, Poland

Prof. Hamed Farshbaf Aghajani, Iran

Prof. Erol Guler, Turkey

Ing. Viktor Ganchits, Russia

Prof. Wojciech Gosk, Poland

Prof. Tatsuya Ishikawa, Japan
Prof. Jacek Kawalec, Poland
Prof. Jong-Sub Lee, South Korea
Prof. Dongqing Li, China
Prof. Xu Li, China
Prof. Zhuangzhuang Liu, China
Prof. Dongdong Ma, China
Prof. Kazunori Munehiro, Japan
Prof. José Neves, Portugal
Prof. P. L. Ng, Hong Kong
Dr. Yu Qian, USA
Prof. Pietro Rimoldi, Italy
Dr. Antonina Sakharova, Russia
Prof. Yupeng Shen, China
Ing. Arina Sivolobova, Russia
Prof. Šarūnas Skuodis, Lithuania
Prof. Bagdat Teltayev, Kazakhstan
Prof. Ivan Vaníček, Czech Republic
Prof. Nicolai Vasiliev, Russia
Prof. Yuanjie Xiao, China
Prof. Zhaohui Yang, USA
Prof. Katarzyna Zabielska-Adamska, Poland
Prof. Andrey Zaytsev, Russia
Prof. Dimitrios Zekkos, USA
Prof. Feng Zhang, China
Prof. Askar Zhussupbekov, Kazakhstan

Preface

The International Scientific Conference “Transportation Soil Engineering in Cold Regions” (TRANSOILCOLD2019) provides an international forum on the latest technologies and research in the field of transportation geotechnics in cold regions.

The conference was organized by the Emperor Alexander I St. Petersburg State Transport University, Permafrost Young Researchers Network, Russian University of Transport, Siberian Transport University, Far Eastern State Transport University, Transportation Research Board, Russian Chapter of International Geosynthetics Society (RCIGS) with the support of IGS Technical Committee on Stabilization, Russian Society for Soil Mechanics, Geotechnics and Foundation (RSSMGFE) with the support of ISSMGE Technical Committee TC202 on Transportation Geotechnics, ISSMGE Technical Committee TC215 on Environmental Geotechnics and ISSMGE Technical Committee TC216 on Frost Geotechnics.

The “Cold Regions” of the world cover large areas in the northern hemisphere, including Canada, Alaska, Finland, Norway, Sweden, a vast portion of China and Russia and all the northern tier of the USA. The cold regions cover 50% of the world’s total land area.

TRANSOILCOLD2019 aims to provide a broader look at the overall problems faced by designers, contractors and infrastructure owners during the planning and building of transport infrastructure in cold regions.

TRANSOILCOLD2019 was organized as the follow-up to TRANSOILCOLD symposiums, held in 2013 (Xining, China), 2015 (Novosibirsk, Russia) and 2017 (Gui-de, China).

The conference programme included Young Geotechnical Engineers Symposium. The different themes covered in this conference include:

- permafrost dynamics in changing climate and under technogenic impact,
- green technology in construction and reconstruction of transport facilities for Arctic and cold regions,
- design, construction and exploitation of high-speed railway subgrade,
- geotechnical problems in permafrost regions,
- geotechnical modelling of transport facilities base,

- use of geosynthetics in construction and reconstruction of transport facilities,
- geotechnical problems of underground construction in complex geotechnical conditions,
- frost heaving and thaw weakening of subgrade, ballasted subgrade and base of slab track.

The Organizing Committee of the TRANSOILCOLD2019 received more than 200 abstracts from 16 countries. Each submitted paper went through an exacting peer review with at least two independent reviewers. Following a thorough review, 109 full papers were selected for submission to Springer series Lecture Notes in Civil Engineering. More than 200 researchers, practitioners and students from all over the world registered to attend the conference.

We would like to thank the Organizing Committee members for their support. We would also like to thank all the authors who submitted their papers at this conference and the reviewers.

St. Petersburg, Russia

Dr. Andrei Petriaev
Dr. Anastasia Konon

Contents

Use of Geosynthetics in Transport Construction. Stabilization in Transportation	
Bearing Capacity Mechanism of Geocell Reinforced Soil Foundations	3
Shintaro Miyamoto and Yoshihisa Miyata	
The Influence of Sand Composition on Railway Track Pumping and Deformation in Winter Period	13
V. I. Shtykov and A. B. Ponomarev	
Experimental Investigation of Railway Maintenance with Stoneblowing Techniques	19
A. A. Abrashitov and A. V. Semak	
Modeling of a Railway Roadbed Reinforcement	27
Andrei Petriaev	
Mechanistic-Experimental Approach for Determination of Basic Properties of Mechanically Stabilized Layers	37
Zikmund Rakowski, Jacek Kawalec, Leoš Horníček and Sławomir Kwiecień	
Stamp Test of Railway Ballast, Stabilized by Geogrids	45
Andrei Petriaev, Victor Ganchits, Maria Chetina, Ivan Kozlov and Svetlana Petrenko	
Relevant Properties of PET-Geosynthetics in Cold Regions	55
Viktor Poberezhnyi	
The Technology of Mechanically Stabilized Layers for Road Structures in Cold Regions	63
Zikmund Rakowski and Jacek Kawalec	

Modelling, Design, Construction and Exploitation of Railway and Highway Subgrade

Numerical Simulation of the Work of a Low-Settlement Embankment on a Pile Foundation in the Process of Permafrost Soil Thawing	73
Sergey Kudryavtsev, Tatiana Valtseva, Semen Bugunov, Zhanna Kotenko, Vladimir Paramonov, Igor Saharov and Natalya Sokolova	
Experimental Evaluation of the Deformational Calculation Method of Foundations for Overpasses of High-Speed Railways	83
Vladimir Ulitskiy, Sergey Alekseev and Stanislav Kondrat'ev	
Numerical Modeling of Railway Embankment Deformations in Permafrost Regions, Central Yakutia	93
Petr P. Permyakov, Aleksandr F. Zhirkov, Stepan P. Varlamov, Pavel N. Skryabin and Georgy G. Popov	
Calibration of PLAXIS Frozen/Unfrozen Soil Model According to Results of Laboratory Tests and In-situ Monitoring	105
Alexey A. Korshunov, Sergey V. Churkin and Alexander L. Nevzorov	
The Frozen Depth and Its Prediction Affected by Shallow Phreatic Groundwater by Modified Berggren Equation	121
Xiaoqiang Liu, Jiankun Liu, Yahu Tian and Yupeng Shen	
Calculation of Soil–Transport Structure Interaction	135
A. G. Shashkin, K. G. Shashkin and V. M. Ulitsky	
Considering the Strength Soils Variability in the Consolidation by Numerical Modeling	147
Evgeniy Fedorenko	
Engineering Survey and Field Testing	
Identification of the Emergency Condition Reasons at Railway Lines that Are in Difficult Geocryological Conditions	155
D. N. Gorobtsov, I. K. Fomenko, V. V. Pendin and M. E. Nikulina	
Experimental Researches in Defining Deformations by Free Station Method and Results Processing by Search Method	163
G. G. Shevchenko, M. J. Bryn, D. A. Afonin and D. A. Gura	
The Use of Terrestrial Laser Scanning for the Development and Control the Design Documentation of Reconstruction Projects	177
A. A. Kuznetsova	

Three-Dimensional Laser Scanning for Safety of Transport Infrastructure with Application of Neural Network Algorithms and Methods of Artificial Intelligence 185
 D. A. Gura, Y. V. Dubenko, G. G. Shevchenko, E. E. Dyshkant and N. I. Khusht

Use of Geoinformatics for Landslide Susceptibility Mapping: A Case Study of Murree, Northern Area, Pakistan 191
 Menal Zaheer, Anoosh Zaheer and Ali Hamza

Bridge Leveling Network Monitoring in Construction on Highly Heaving Soils 201
 Dmitry Afonin, Nikolay Kanashin and Andrey Nikitchin

Determining the Refraction Coefficient Based on the Differences of the Measured and Known Zenith Distances in Short-Distance Trigonometric Leveling 209
 Yulia Lobanowa, Mikhail Bryn and Evgeniy Svintsov

Features of Engineering Surveys in Areas of Permafrost Prevalence by the Example of the Project “Northern Latitudinal Way” 215
 Natalia Bogomolova, Yuriy Milyushkan, Sergey Shkurnikov, Nikolay Bushuev, Evgeniy Svintsov and Vladimir Anisimov

The Study of Railway Embankment Deformations in Cold Regions 223
 Natalia Bogomolova, Mikhail Bryn, Andrey Nikitchin, Alexey Kolos and Andrey Romanov

Laboratory Soil Testing

Compression Curves’ Extrapolation to High Pressures for Soft Clay Soils 233
 Peter Klemyatsionok, Svetlana Kolmogorova and Sergey Kolmogorov

Experimental Study on Pore Water Pressure and Microstructures of Silty Clay Under Freeze-Thaw Cycles 239
 Dan Wang, Chengsong Yang, Guodong Cheng, Wei Ma and Lianhai Zhang

Technical Improvements in Testing Small-Strain Deformation Behaviour of Frozen Soil 255
 Jinyuan Wang, Satoshi Nishimura, Bhakta Raj Joshi and Shota Okajima

Experimental Study on Induced Anisotropies of Remolded Loess in Cold Region 265
 Yongzhen Feng, Lingxiao Liu, Wuyu Zhang and Yanxia Ma

Investigation of Frost Heave Considering the Boundary Conditions of Artificial Ground Freezing	273
Katharina Niggemann	
Frost-Heaving Pressure and Stiffness of Compacted Roadbed Material by Laboratory Model Test	285
Eun Chul Shin, Byung Hyun Ryu and Hee-Mun Lee	
The Effect of Different Additives on the Swelling Process of Heavy Clays	295
Alexey Kolos, Vera Alpysova, Grigoriy Osipov and Irina Levit	
Geocoprotective Materials, Structures and Technologies for Transportation	
The Method of Estimation of the Technical Conditions of Transport Facilities Used in Cold Regions After the Accidents Caused by Temperature Anomalies	309
Nikolay Gusev, Larisa Svatovskaya and Alexandr Kucherenko	
Geocoprotective Building Structures for Transport Construction Using Mineral Technogenic Silicates and Their Properties	319
Maria Shershneva, Ivan Kozlov, Galina Pankrateva and Ivan Drobyshev	
Geocoprotective Technologies from Heavy Metal Ions Pollution for Transport Construction in Permafrost Regions	329
Maria Shershneva, Yuliya Puzanova and Antonina Sakharova	
High-Strength Concrete with Improved Deformation Characteristics for Road Surfaces	339
Valentina Solovieva, Irina Stepanova and Dmitriy Soloviev	
Geocoprotective Screens for Road Construction and Operation in Cold Regions	347
Maria Shershneva, Antonina Sakharova and Ivan Kozlov	
Efficiency Evaluation of the Use of Mineral Technogenic Substances in Geocoprotective Technologies of Transport Construction	357
Maria Shershneva, Antonina Sakharova, Denis Anpilov and Egor Ereemeev	
A High-Performance Repair Mixture to Restore and Protect Damaged Concrete Structures	369
Valentina Solovieva, Irina Stepanova, Dmitriy Soloviev and Anna Kasatkina	
Multifunctional Nanomodified Concrete of New Generation	377
Valentina Solovieva, Irina Stepanova, Dmitriy Soloviev and Tatyana Kravchenko	

Increasing the Level of Properties of Composite Materials for Civil Engineering Geoconstruction with the Use of New Generation Additives	387
Valentina Solovieva, Irina Stepanova, Dmitriy Soloviev and Nikolay Yorshikov	
Geoechemical Basis of Geocoprotective Technologies	395
Larisa Svatovskaya, Kseniia Mikhailova, Tatyana Supeliuk and Ivan Drobyshev	
Information Assessment of Natural Geosystem Preservation in Geoconstruction by Improving the Quality of Concrete	405
Larisa Svatovskaya, Oleg Urov, Kseniia Mikhailova and Tatyana Supeliuk	
Safing Technologies for Lithosphere Geocoprotection	413
Larisa Svatovskaya, Kseniia Mikhailova, Ivan Drobyshev and Elena Bodenکو	
Specificities of Soling Processes in Technologies of Geoconstruction	421
Larisa Svatovskaya, Kseniia Mikhailova, Alexander Kabanov and Nikolay Khamenok	
Criteria of Green Geocoprotective Technologies in Transport Construction	431
Larisa Svatovskaya, Ivan Drobyshev, Kseniia Mikhailova and Nikolay Khamenok	
Modification of Mineral Substance Surfaces for Geosphere Protection	441
Larisa Svatovskaya, Maxim Sychov, Kseniia Mikhailova, Alexander Kabanov and Elena Bodenکو	
A Structure of Atoms of the Main Phase of Industrial Wastes Predict Properties of Building Materials in Transport Construction in Cold Regions	451
Natalia Babak	
Silica Sol in Transport Construction	459
Ivan Kozlov	
The Method of Producing Non-autoclaved Foam Concrete Based on Polymers for the Construction of Various Road Structures in Cold Regions	469
Anastasiya Sychova, Yuriy Kamenev, Larisa Svatovskaya and Alexandr Avseenکو	

Conservation of Mineral Resources in Transport and Civil Construction 479
Marina Baydarashvili, Antonina Sakharova and Natalia Shrednik

The Acceleration of Hardening of Non-autoclaved Foam Concrete with the Mechano-Activated Binder When Constructing in the Arctic and Cold Regions 487
Andrey Solomahin, Larisa Svatovskaya and Yuriy Kamenev

Effective Building Ceramics for Transport Infrastructure 495
Ludmila Maslennikova, Natalia Babak, Anna Slavina and Igor Naginskii

About the Editors



Dr. Andrei Petriaev is a senior researcher in the Emperor Alexander I St. Petersburg State Transport University, Russia and the President of Russian Chapter of IGS. Dr Petriaev's research expertise is in geoecology and the geotechnics of railways and road design, with specific focus on the challenges faced in cold and arid regions. He has served as the conference chair for the Transportation Geotechnics and Geoecology conference in 2017, and on the scientific committee for various other conferences.



Dr. Anastasia Konon is an associate professor in Emperor Alexander I St. Petersburg State Transport University, Russia, where she joined in 2005. Dr Konon's research interests are primarily in road and railway engineering, with specific emphasis on the geotechnical challenges faced in cold and arid environmental conditions. She has worked as a technician, researcher and engineer in railway design and geotechnics projects for JSC Russian Railways, and has served as the conference secretary for Transportation Geotechnics and Geoecology conference in 2017, and on the scientific committee for various other conferences.

Use of Geosynthetics in Transport Construction. Stabilization in Transportation

Bearing Capacity Mechanism of Geocell Reinforced Soil Foundations



Shintaro Miyamoto  and Yoshihisa Miyata 

Abstract The technology for restoring a damaged road system is critical for reaching victims and reconstructing damaged areas in large-scale natural disasters caused by earthquake and tsunami. Soil reinforcement technology with geocell materials can be useful in the above situation. This technology has been applied to road construction on soft soil ground, and its usefulness has been recognized. However, its reinforcement mechanism has not been investigated adequately. The current design method for geocell mattress under vertical load is based on classical pavement engineering and not on the actual mechanism of geocell reinforcement. Further technical investigation is required to achieve the rational design and construction of geocell mattress. The authors have developed a visualization technique for geocell mattress by using particle image velocimetry (PIV) analysis. The results obtained in the current stage are as follows: (1) mixing of colored sand with laboratory fill material is useful in visualizing the bearing capacity model test with PIV analysis. This paper proposes a method to determine the mixing ratio of two types of sand by conducting basic calibration tests. (2) This method can be used to visualize the behavior of soil confined by the geocell through a laboratory model test. This paper reports the results of the visualization.

Keywords Reinforced soil · Geocell mattress · Bearing capacity · Visualization

1 Introduction

There has been a rise in large-scale natural disasters in recent years. The technology for restoring damaged road systems is important for reaching victims and reconstructing areas damaged by earthquake and tsunami. The authors have focused on the soil reinforcement technology with geocell materials and have investigated its usefulness in the restoration of damaged roads [1–3]. Previous studies have explained the reinforcement effects of a geocell mattress under a vertical load by the lateral

S. Miyamoto (✉) · Y. Miyata
National Defense Academy of Japan, 1-10-20, Yokosuka, Japan
e-mail: miyamoto@nda.ac.jp

© Springer Nature Singapore Pte Ltd. 2020
A. Petriaev and A. Konon (eds.), *Transportation Soil Engineering in Cold Regions*,
Volume 2, Lecture Notes in Civil Engineering 50,
https://doi.org/10.1007/978-981-15-0454-9_1

resistance effect, vertical stress dispersion effect, and tensioned membrane effect. Limit equilibrium equations based on Terzaghi's equation have been proposed to estimate the bearing capacity of the reinforced ground by considering the above effects [4–7]. To estimate it with higher accuracy, it is necessary to revise the current equations proposed by previous researchers or to establish it newly by using a different approach for observing the reinforcement mechanism in the model tests.

In this study, laboratory model tests were conducted to observe the behavior of a geocell mattress under a vertical load. The precision improvement technique of Particle image velocimetry (PIV) was examined for visualizing the results of the model test. The new findings from the experiment on precision improvement of PIV were applied to the model test, and the reinforcement mechanism of the geocell mattress under the vertical load was analyzed. This paper reports the results of the precision improvement test of the PIV analysis and visualization of the model test.

2 Precision Improvement of PIV Analysis

PIV analysis is a well-known visualization technique for model tests in the geotechnical research field since the 2000s [8–11]. Commercial software has become popular, and it has become relatively easy to use visualization techniques.

The technique of PIV analysis can be divided into the method for direct tracking of target markers arranged in the model ground (particle tracking method) and the method for tracking of the image correlation from the intensity of the digital signal (image correlation method). With regard to the use of the image correlation method, there are cases where a model ground is constructed with only natural materials or it is constructed with mixed materials comprising natural and colored sand. The image correlation method is considered capable of visualizing a wide range of behaviors with high precision, even after omitting the preparation time such as the time spent on arranging the target markers. However, the details of the visualization technique such as deciding the mixing ratio of the colored material and the shooting interval are not sufficiently established. In order to improve the accuracy of visualization, further technical investigations relating to the experimental method, photography method, and analysis method are required.

This study focused on a visualization technique using the image correlation method against the planar deformation field of a model test conducted with mixed materials. Prior to the model test, the precision of visualization using mixed sand comprising silica sand and colored sand was investigated for various mixing ratios. The test apparatus for determining the precise mixing ratio of silica sand and colored sand is shown in Fig. 1 [12]. The silica sand having an average diameter of 0.4 mm is used as the natural material. The black colored sand having the same particle size distribution as silica sand was used as the colored material. The appearances of both sands are shown in Fig. 2. The mixing ratios of colored sand investigated in this test are listed in Table 1. In the series of tests, a specimen of the thin mixed sand was measured by a micrometer, which showed a horizontal displacement of 0.1 mm

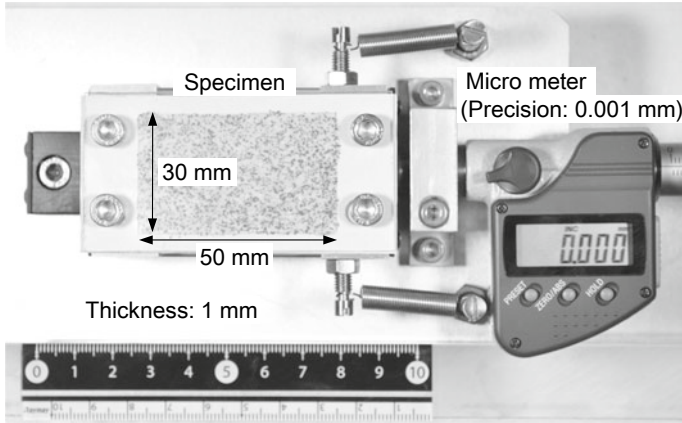
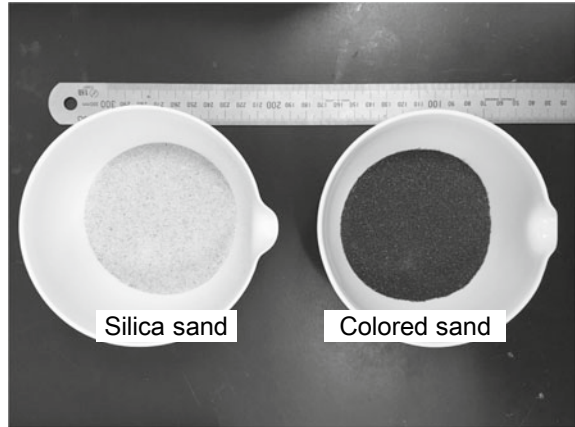


Fig. 1 Test apparatus for precision improvement of PIV

Fig. 2 Used sand samples

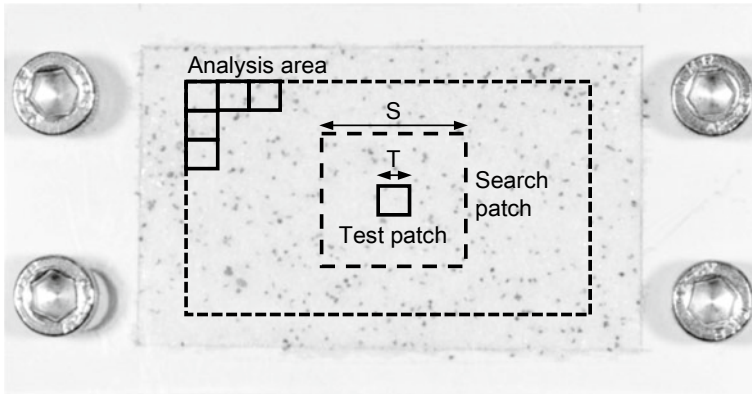


(≈ 1 pixel). The images of the specimen were captured using a single-lens reflex camera with an image resolution of 1760×1168 pixels.

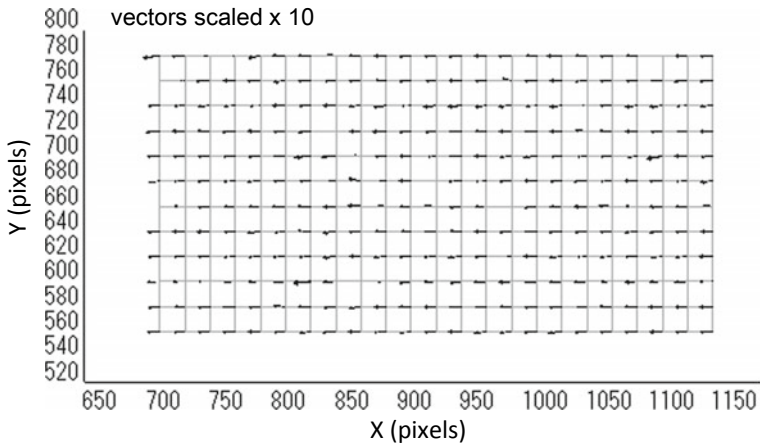
The schematic diagram for explaining the visualization condition in this study is shown in Fig. 3. The test patch is a square visualization unit area. The search patch is a region for searching for high correlation of the test patch. The sizes of both patches were specified in units of pixel in the analysis. In this test, the effect of the test patch size was investigated for 1–30 pixels. The search patch size was set to 51 pixels in all cases. The search patch size was set as a condition where the influence on the analysis result could be ignored. The calculated displacements within the range of 0.5–2.0 times the actually applied displacement were used as the effective data. The calculated displacements outside this range, which were significantly different from the actual applied displacement, were judged as the error points.

Table 1 Case of precision improvement tests

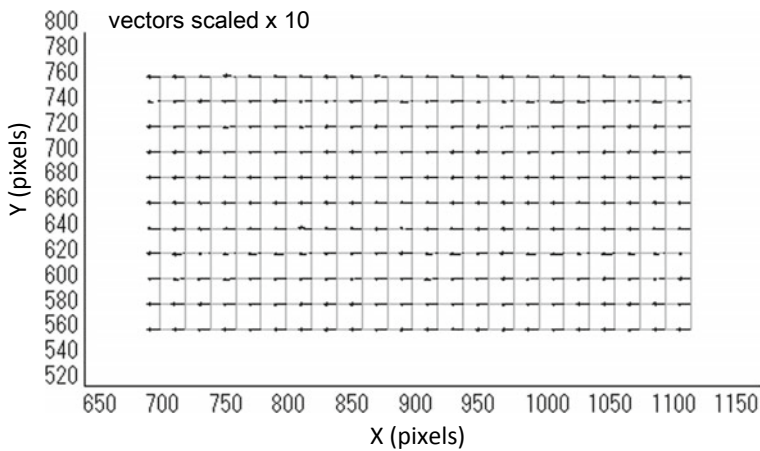
Case	Silica sand g	Colored sand μ g	Mixing ratio %
B05	100	5	4.8
B09	100	10	9.1
B13	100	15	13.0
B17	100	20	16.7
B23	100	30	23.1
B29	100	40	28.6
B33	100	50	33.3
B41	100	70	41.2
B50	100	100	50.0
B60	100	150	60.0
B70	100	230	69.7
B80	100	400	80.0
B90	100	900	90.0
B95	100	1900	95.0

**Fig. 3** Image manipulation of PIV analysis

The results of analyzing test cases B05 (mixing ratio of colored sand: 5%) and B50 (mixing ratio: 50%) with test patch size of 20 pixels in the PIV analysis are shown in Fig. 4. The results of B50 are ideal. The horizontal components of the calculated displacement vectors in all grid points are almost the same as the actual applied displacement. The results of B05 are compared with these ideal results. There are some points which displacement has not been calculated. Several of the calculated displacement vectors are not at the same level and do not correspond to the actual applied displacement.



(a) Case B05 (mixing ratio of colored sand: 5%)



(b) Case B50 (mixing ratio of colored sand: 50%)

Fig. 4 Examples of vector distribution of precision improvement test

The ratio of the number of error points to the total number of grid points was evaluated based on the error rate, and the relationship between the error rate and test patch size is shown in Fig. 5. The precision of measurement was evaluated by the standard deviation in pixels, and the relationship between the standard deviation and test patch size is shown in Fig. 6. When the mixing ratio was more than 30%, the error rate became almost 0%, regardless of the test patch size. In these cases, the standard deviation became less than 0.04 pixels, that is, the variation was 4% or less.

Fig. 5 Relationship between error rate and test patch size

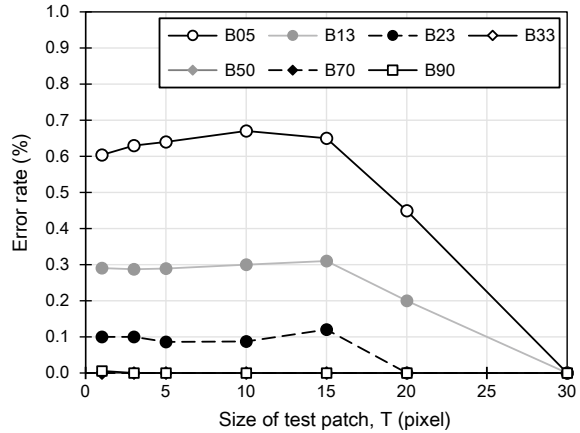
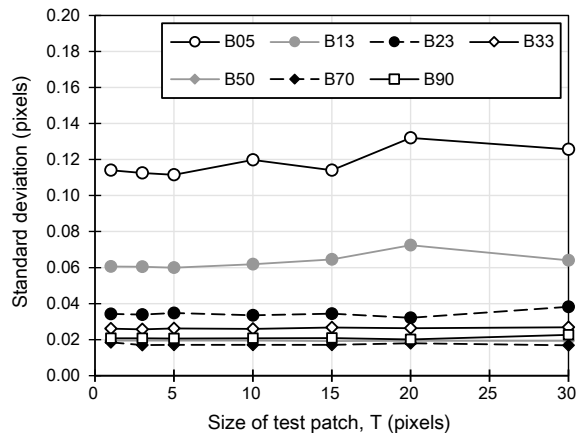


Fig. 6 Relationship between standard deviation and test patch size



3 Visualization of Model Test

The visualization of the model test was realized based on the findings obtained in Sect. 2. The schematic diagram of the model test apparatus is shown in Fig. 7. The dimensions of the model ground are 1200 mm length, 305 mm depth, and 400 mm height.

The front wall in Fig. 7 is made of acrylic, and the two-dimensional displacement field of the model ground can be captured from this observation front wall. Loading is realized by applying a rigid flat plate of dimensions 100 mm width, 300 mm depth, and 50 mm height, with displacement control in the vertical direction. Sandpaper of 0.5 mm roughness is affixed on the bottom surface of the loading plate for attaining the rough surface condition of the bearing test. The loading speed was 1 mm/min in all cases.

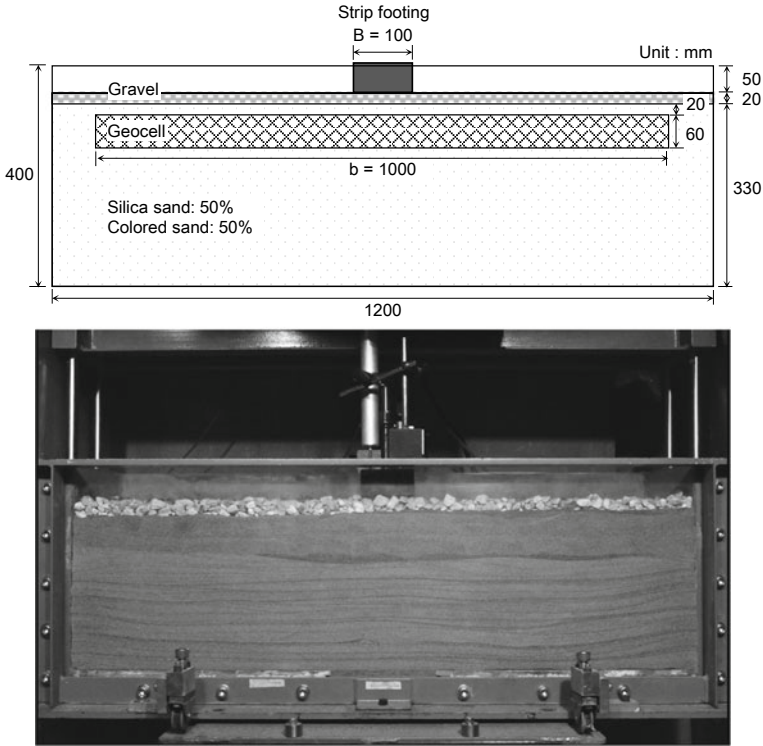


Fig. 7 Apparatus of bearing capacity model test

The model test was conducted for the two cases of unreinforced foundation and geocell reinforced foundation. The mixed sand comprising silica sand and colored sand, mentioned in Sect. 2, was used in the series of tests at a mixing ratio of 50%. In both cases, the relative density of the mixed sand was set to $D_r = 90\%$, and a gravel layer having an average particle diameter of 10 mm was laid with a thickness of 20 mm on the model ground surface. The geocell mattress using in this study was made of polyethylene strip having a thickness of 0.1 mm. The physical properties of the polyethylene strip are shown in Fig. 7. The geocell mattress, which was composed of a unit cell having a side length of 60 mm and height of 60 mm, was prepared using this polyethylene strip, as shown in Fig. 8. The geocell mattress was placed 20 mm below the model ground surface, as shown in the figure. The images of the two-dimensional displacement fields of the model test were captured using a CCD camera with an image resolution of 1392×1040 pixels.

The relationship between vertical stress and settlement normalized by width of the loading plate is shown in Fig. 9. This figure shows the results for both unreinforced foundation and the geocell reinforced foundation. The reinforcement with geocell mattress showed a significant increase in the modulus and bearing capacity under vertical loading. The visualization results of the two-dimensional displacement fields

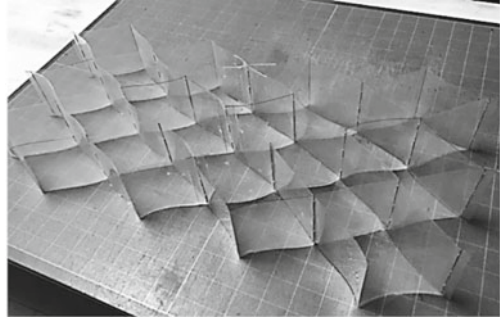
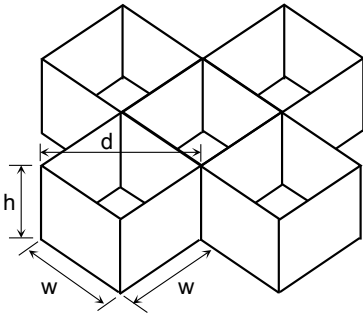
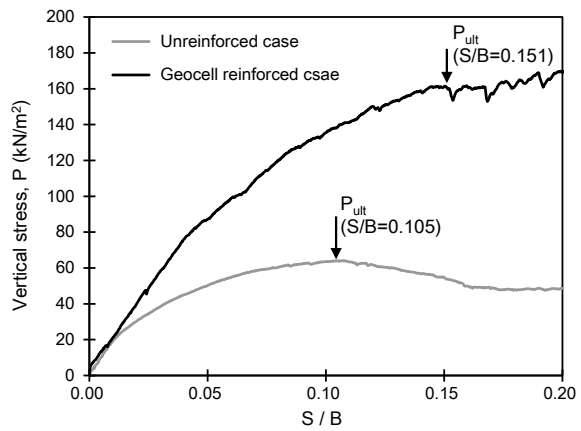


Fig. 8 Configuration of geocell mattress

Fig. 9 Relationship between vertical stress and normalized settlement



of both the unreinforced foundation and geocell reinforced foundation are shown in Fig. 10. Here, the behaviors of both cases were compared with the normalized settlement at the peak bearing capacity of the unreinforced case. This figure shows the PIV results analyzed with test patch size of 10 pixels. As in the results of the precision improvement test mentioned in Sect. 2, error points did not occur under this analysis condition. The general shear failure mode was observed in the unreinforced case. A comparison of the results of the geocell reinforcement with those of the unreinforced case shows that the displacement in the horizontal direction is greatly reduced despite the nearly equal degree of displacement in the vertical direction. The horizontal displacement of the sand around the geocell mattress is confined, and the development of failure surface is suppressed.

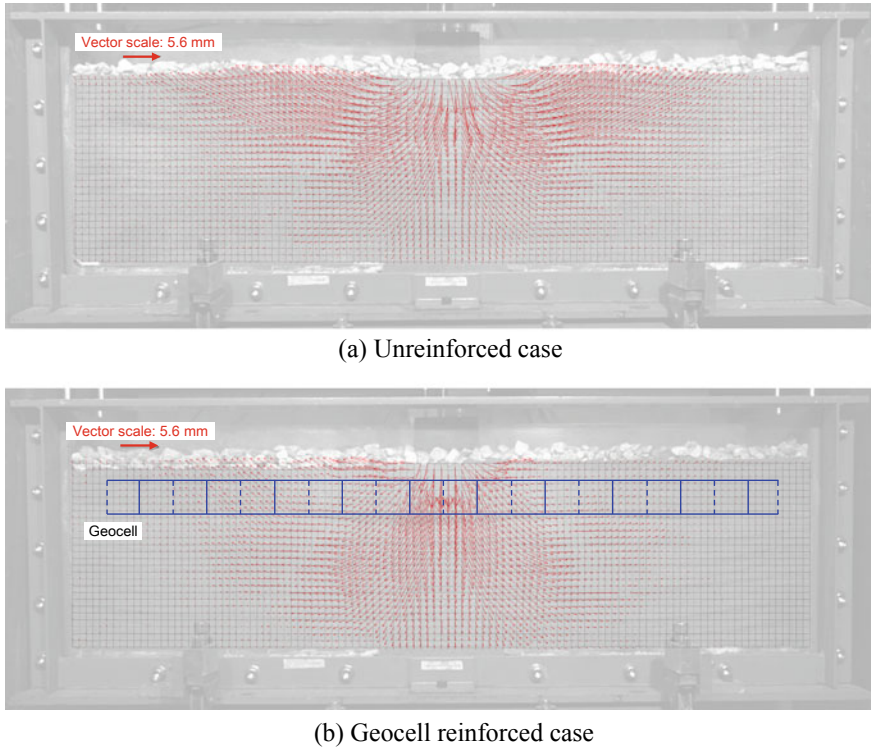


Fig. 10 Two-dimensional displacement fields of unreinforced and geocell reinforced cases

4 Conclusion

An experimental method based on PIV analysis using colored sand was proposed and applied to the model test to clarify the reinforcement mechanism of geocell mattress under a vertical load. The results obtained in this study are as follows:

1. To advance the accuracy of the PIV analysis of the model test, a precision improvement test was conducted, which employed mixed sand comprising natural sand and colored sand. The error rate and standard deviation of the displacement tended to decrease with increasing ratio of colored sand. When the ratio of colored sand was more than 30%, it was possible to reduce the error rate to 0% and the standard deviation to 0.04 pixels regardless of the test patch size in the PIV analysis.
2. The model test was performed using mixed sand containing 50% colored sand to clarify the two-dimensional displacement fields of both unreinforced foundation and geocell reinforced foundation. It was proven that error points do not occur when the proposed experimental method for PIV analysis was used, regardless of the test patch size.

3. It was revealed that the displacement in the horizontal direction was greatly reduced by the reinforcement effect of the geocell mattress. The horizontal displacement of the sand around the geocell mattress was also confined, and the development of failure surface was suppressed.

Acknowledgements This study was conducted as part of “Grant-in-Aid for Scientific Research (number: 18K13832).” The PIV analysis of this study was performed using the software “Flow-PIV” provided by Library Co., Ltd. I’d like to express my appreciation.

References

1. Webster SL (1979) Investigation of beach sand. Trafficability enhancement using sand-grid confinement and membrane reinforcement concept. Report GL-79-20, U.S. Army Engineer Waterways Experiment Station, Vicksburg Miss
2. Bathurst RJ, Jarrett PM (1988) Large-scale model tests of geocomposite mattresses over peat subgrades. *Transp Res Rec* 1188:28–36
3. Hegde A (2017) Geocell reinforced foundation beds-past findings, present trends and future prospects: A state-of-the-art review. *Constr Build Mater* 154:658–674
4. Koerner RM (2005) *Designing with geosynthetics*, 5th edn. Prentice Hall, New Jersey
5. Zhang L, Zhao M, Shi C, Zhao H (2010) Bearing capacity of geocell reinforcement in embankment engineering. *Geotext Geomembr* 28:475–482
6. Avesani Neto JO, Bueno BS, Futai MM (2013) A bearing capacity calculation method for soil reinforced with a geocell. *Geosynthetics Int* 20(3):129–142
7. Sitharam TG, Hegde A (2013) Design and construction of geocell foundation to support embankment on soft settled red mud. *Geotext Geomembr* 41:55–63
8. Taylor RN, Grant RJ, Robson S, Kuwano J (1998) An image analysis system for determining plane and 3-D displacements in soil models. *Proceedings on centrifuge '98*, Balkema, Rotterdam, pp 73–78
9. Paikowsky SG, Xi F (2000) Particle motion tracking utilizing a high-resolution digital CCD camera. *ASTM Geotech Test J* 23(1):123–134
10. Iskander M (2010) *Modeling with transparent soils, visualizing soil structure interaction and multiphase flow, non intrusively*. Springer, New York
11. Stanier SA, Blaber J, Take WA, White DJ (2016) Improved image-based deformation measurement for geotechnical applications. *Can Geotech J* 53:727–739
12. White DJ, Take WA, Bolton MD (2003) Soil deformation measurement using particle image velocimetry (PIV) and photogrammetry. *Geotechnique* 53(7):619–631

The Influence of Sand Composition on Railway Track Pumping and Deformation in Winter Period



V. I. Shtykov and A. B. Ponomarev 

Abstract The current standards for the effective pore diameter in geotextile materials both in Russia and in other countries have been determined by the techniques using natural sands of certain composition. However, particles that fall into geotextiles from railway ballast differ in form from natural sands. Thus, the existing requirements for the diameter of geotextile filtration passages need to be corrected. The calculation methodology for determining the possibility of colmated layers in sands is described. The requirements for the size of geotextile filtration passages preventing them from colmatage and ensuring the preservation of their filtration properties within the required limits throughout the standard service life are presented. In case of non-compliance with the requirements for sands, colmated layers will occur in them, which will lead in pumping.

Keywords Pumping · Sand · Geotextile · Colmatage

1 Introduction

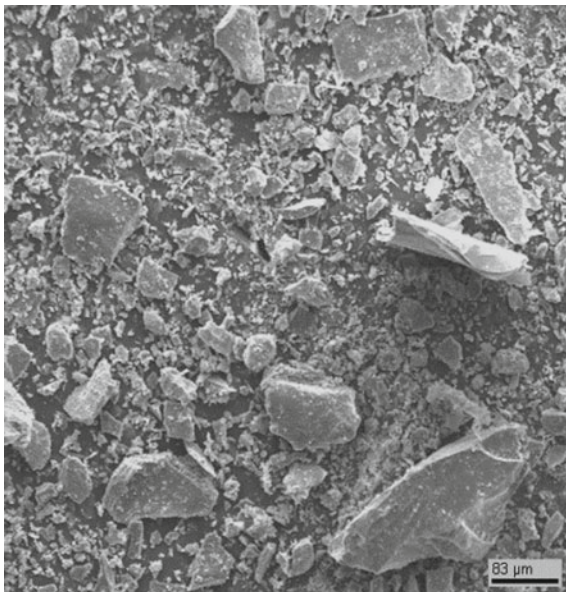
At the present time, both in Russia and in other countries the standards for existing pore diameter in geotextile materials have been determined by the techniques using natural sands of certain composition [1, 2]. However, as it follows from Fig. 1, the particles taken from colmated geotextile materials differ significantly in form from natural sands. Being of the same mean and maximum mean size in diameter, plate-shaped particles, unlike quartz sand particles whose shape is close to spherical one, have essentially different particle distribution curves. Plate-shaped particles are formed by shearing when ballast stones are colliding under vibrodynamic loads of train movement.

After decades of laboratory and field studies, hydraulic engineers have formulated the following requirements for reverse filters of hydraulic installations, including

V. I. Shtykov · A. B. Ponomarev (✉)
Emperer Alexander I Petersburg State Transport University, 9, Moscovsky Prospect, Saint Petersburg 190005, Russia
e-mail: pollnom@yandex.ru

© Springer Nature Singapore Pte Ltd. 2020
A. Petriaev and A. Konon (eds.), *Transportation Soil Engineering in Cold Regions*, Volume 2, Lecture Notes in Civil Engineering 50,
https://doi.org/10.1007/978-981-15-0454-9_2

Fig. 1 Particles taken from colmatated geotextile



sands [3]. Filters must freely pass all the particles of size <0.05 mm, which are classified as colmatage particles. Let us apply these requirements to geotextile materials as the water flows through filtration passageways in them. The theoretical, laboratory and field studies have been carried out on textile materials in Alexander I St. Petersburg State Transport University for a considerable number of years [4, 5].

To prevent geotextile materials from colmatage, the following correlation must be established [3]:

$$d_u \geq (3.3 \dots 4.4)d_{ci}^{\max}, \quad (1)$$

where d_u is estimated value of the diameter of the filtration passageway, calculated by formula (2) [4];

d_{ci}^{\max} is maximum diameter of suffusion particles accepted in the study to be 0.05 mm.

$$d_u \geq 2 \cdot d_p \left(\frac{1}{\sqrt{1-n}} - \frac{1}{\sqrt{\pi}} \right), \quad (2)$$

where

d_p is diameter of geotextile fiber, mm;

n is geotextile porosity, fractions.

The predisposition of a number of geotextiles toward colmatage was established by verifying the compliance with criterion (1). The paper [5] presents the data on the colmatage level of various brands of geotextiles, laid in the railway track in

different years. The terms of full colmatage of the pores of these geotextiles were calculated. By the time of full colmatage, their coefficient of permeability becomes around 0, n m/day, which is significantly less than required. At the end of this term, colmatage particles will be partly deposited on the surface of the geotextile and partly transported away by the flow through the pores of the ballast section. The coefficient of permeability of the geotextile material will not practically change, remaining close to the value indicated above. The regulations stipulate that the geotextile's filtration properties must remain within the required limits corresponding to the geotextile service life declared by the manufacturer. As follows from the above-mentioned paper [5], such brands of geotextiles exist. The results of field and laboratory studies have confirmed that for the geotextile material used as a separating layer in a railway track, the calculated diameter of the filtration passageway, determined by formula (2), should meet the following requirement [5]:

$$0.165 \text{ mm} \leq d_u \leq 0.220 \text{ mm}. \quad (3)$$

The requirements for reverse filters of hydraulic installations may also be applied with underground drainage fills of sand and sand-gravel mixtures.

We will analyze these requirements to determine the cause of pumping in the site with the sand roadbed, and the groundwater is at a depth of 2.4 m below the surface.

The sand composition is:

$$d_{10} = 0.02 \text{ mm}; d_{17} = 0.23 \text{ mm}; d_{60} = 0.80 \text{ mm}; \eta = \frac{d_{60}}{d_{10}} = 4; \psi = 1.2,$$

where d_{10} , d_{17} and d_{60} are diameters of sand particles, the sand containing, respectively, 10, 17 and 60% of particles by mass; η is a sand non-homogeneity ratio; and ψ is a particle shape factor.

The coefficient of permeability determined at the site was averaging 24 m/day.

The non-colmatage of sands is provided by easy passage of particles <0.05 mm which tend to aggregate, which ensures the compliance with condition (1). Wherein:

$$d_{ci}^{\max} = \frac{d_u^{\max}}{(3.3 \dots 4.4)} \quad (4)$$

where d_u and d_u^{\max} are diameters of estimated and maximal values of the filtration passage which are calculated by formulas (5) and (6) [6].

$$d_u^{\max} = d_u(1 + 0.05\eta) \quad (5)$$

$$d_u = 0.57\sqrt[3]{\eta} \cdot \frac{n}{1-n} \cdot \frac{d_{17}}{\psi}. \quad (6)$$

The calculations give $d_u^{\max} = 0.092 \text{ mm}$, and $d_{ci} = \frac{d_u^{\max}}{4} = 0.023 \text{ mm}$.

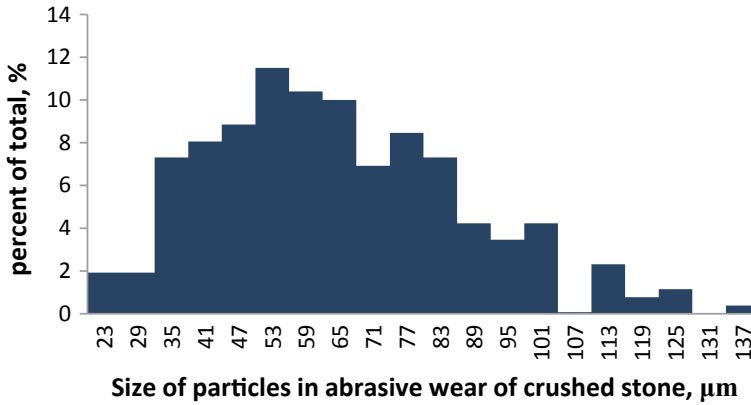


Fig. 2 Size of particles formed in abrasive wear of crushed stone

The studies on abrasion products (Fig. 2) have shown that they contain a quite high percentage of particles sized $0.023 \text{ mm} \leq d_{ci} \leq 0.05 \text{ mm}$, which will not seep through the sand, and therefore, the sand will be colmated.

The sand is medium-grained and is able to filter even in the frozen condition. The coefficient of permeability of the sand in frozen state is calculated by formula (7) [7]:

$$K_f = K_t \frac{\left(1 - \frac{i+0.04}{n}\right)^3}{\left[1 + \frac{2.8(i+0.04)}{(1-n)(1-0.6\sqrt{i+0.04})}\right]^2} \quad (7)$$

where K_f and K_t are coefficient of permeability of the sand in frozen and thawed states, respectively; n is porosity in a thawed state; and i is volumetric ice content.

$$i = \frac{(n - \mu)\rho_w}{\rho_i} \quad (8)$$

where μ is specific yield; ρ_w and ρ_i are the density of water and ice, respectively. The specific yield for medium-grained sands is (0.12–0.2) [8]. If we assume its value equal to 0.16, then:

$$i = \frac{0.36 - 0.16}{0.917} = 0.218, \quad (9)$$

and $K_t = 0.089 \text{ m/day}$.

In this case, precipitation more than 4 mm/h, which in North-West of Russia conditions corresponds to 98% of precipitation norm, with partial thawing of the sandy layer in spring, will cause pumping while trains are running.

2 Results and Discussion

Calculations show that the formation of colmated sand layers will also lead to heaving (characteristics of colmatage particles are presented in Fig. 2).

The colmatage particles formed due to vibrodynamic loads are deposited in the sand pores with a density of at least 1.1 g/cm^3 . In this case, the porosity of the colmatage particles will be averaging 0.59, and the effective porosity (n_e) of the colmated sand layer will be equal to 0.21, whereas its coefficient of permeability will be 0.45 m/day in thawed state. The specific yield adduced to the effective porosity will be 0.03. Consequently, the ice content will be:

$$i = \frac{(n_e - \mu)\rho_w}{\rho_i} = \frac{(0.21 - 0.03) \cdot 1}{0.917} = 0.20.$$

From formula (7), it follows that frozen sands will not filter the water when $i + 0.04 = 0.24$, which exceeds the effective porosity value of 0.21. The average content of trapped air in the sand layer is 0.04. Since the trapped air will not move freely, the colmated layer will heave. The degree of heaving depends on the thickness of the colmated layer. When running on this section, a track meter car detected local deviations of the rail location by level up to $\pm 6 \text{ mm}$, which could have been caused by soil heaving in the areas of pumping. Over the time, the thickness of the colmated layers and, consequently, the heaving rates will only increase. Heaving will continue in the intervals between thawing periods. In the spring period, before the complete thawing of the colmated layer, pumping will occur during precipitation.

In view of the above, it is of interest to find out whether the protective sub-ballast layers recommended for use [9] are exposed to colmatage. To verify the calculation, the grading of the sand was taken from the Guidelines [9]. The following initial data were used in the calculation: $d_{10} = 0.14 \text{ mm}$; $d_{17} = 0.42 \text{ mm}$; $d_{60} = 6.4 \text{ mm}$; $\eta = \frac{d_{60}}{d_{10}} = 46$; $\psi = 1.2$; $\nu = 0.01 \text{ cm}^2/\text{c}$; $n = 0.36$.

The calculations were carried out by formulas (4), (5) and (6) gave the following results: $d_u = 0.021 \text{ cm}$; $d_u^{\max} = 0.069 \text{ cm}$; $d_{ci} \leq \frac{d_u^{\max}}{4} = 0.017 \text{ cm}$.

Since $d_{ci} = 0.017 \text{ mm} > 0.05 \text{ mm}$, the sand will definitely let all the colmatage particles pass through. However, the sand should not be suffusional. The coefficient of permeability of this sand in frozen state is (10–12) m/day, which is much higher than any possible precipitation intensity in the spring period when the sub-ballast layers have not thawed completely.

3 Conclusions

1. In the sand, subgrade pumping and heaving can occur over time unless the sand is able to let all the colmatage particles $< 0.05 \text{ mm}$ pass through. The particles are the product of crushed stone abrasion when exposed to vibrodynamic loads of train movement.

2. The calculation methodology for determining the possibility of formation of colmated layers in sands is described. The requirements for the size of geotextile filtration passages ensuring the preservation of their filtration properties within the required limits throughout the standard service life are presented.
3. The sands recommended for use by the Guidelines [9] as sub-ballast layers are not colmated by the particles present in the products of crushed stone abrasion caused by vibrodynamic loads of moving trains. However, the sands themselves should not be suffusional.

References

1. Polymer materials application guides (foams, geotextiles, geogrids, and polymer drainpipes) for strengthening a railway roadbed, MPS of Russia, Moscow Akademkniga 2002, 111 p
2. BS EN 13250:2016, Geotextiles and geotextile-related products. The characteristics required for railway construction, 46 p
3. Guidelines for designing reverse filters in hydraulic engineering installations. Leningrad VNIIG, 1981, 87 p
4. Shtykov VI, Ponomarev AB (2012) Specific requirements for protective-filtrating materials of underground drains used in permafrost zones. *Civ Eng J* N4(30):39–45
5. Blazhko LS, Shtykov VI, Kanziber YUA, Ponomarev AB, Chernayev YEV (2014) The colmatage protection of geotextile materials applied as a separating layer in the ballast section. *Proc PGUPS* N4:22–26
6. Shtykov VI (1998) The study on filtration properties of granular materials based on the model of curved filtration passages, *Bulletin of the Ukraine State Academy of Water Management*. In: *The materials of the international conference “Relevant Issues of the Filtration Theory”*, Rovno, 1–3 June 1998, pp 170–173
7. Shtykov VI (1980) Characteristics of design and function of underground drains in frozen soils. *Hydraul Eng Land Reclam* N11:53–56
8. Maslov BS (2004) Specific yield coefficient, *land reclamation encyclopedia*, vol 2. RosInformAgroTech University, Moscow, p 39
9. “Guidelines for placing sub-ballast protective layers in the course of reconstruction (upgrading) of a railway track”, JSC “Russian Railways”, 12.12.2012, N2544 p

Experimental Investigation of Railway Maintenance with Stoneblowing Techniques



A. A. Abrashitov  and A. V. Semak

Abstract This work presents the results of experiments carried out to investigate the potential application of the technology of railway track alignment: “stoneblowing”. In this technology, ballast stones are injected into gaps of the ballast bed beneath sleepers. Despite potential benefits, this technology has a limited application. In order to understand the performance of the ballast aligned by stoneblowing and to develop maintenance procedures, we conducted series of experiments at the Experimental Railway Ring in Shcherbinka, Russia. It was found out that the railway track, aligned by stoneblowing and flat reinforcement geogrid, showed better track stability in vertical plane in comparison to the track aligned only by stoneblowing. Finally, railway tracks aligned by stoneblowing techniques proved to show good results under high loads.

Keywords Stoneblowing ballasted railway track · Track maintenance · Flat reinforcement geogrid

1 Introduction

The stoneblowing technology has previously attracted the attention of researchers, and in some countries, it has even been included in the railroad maintenance system [1–3]. However, the positive effects of the use of this technology are often accompanied by the examples of increased pollution, where stoneblowing was used with crushed stone of small fractions. The objective of this study was to find technological methods for eliminating these defects.

A. A. Abrashitov (✉) · A. V. Semak
Russian University of Transport (MIIT), St. Obraztsova, 9, p. 9, 127994 Moscow, Russia
e-mail: abr54@yandex.ru

© Springer Nature Singapore Pte Ltd. 2020
A. Petriaev and A. Konon (eds.), *Transportation Soil Engineering in Cold Regions*,
Volume 2, Lecture Notes in Civil Engineering 50,
https://doi.org/10.1007/978-981-15-0454-9_3

2 The Design of Test Sections

The procedure of stoneblowing includes of the insertion of stones between the sleeper and the surface of the ballast layer, filling the gap between both components and, therefore, recovering the original position of the railway track. Moved by pneumatic air flow, the stones effectively penetrate under the lifted sleeper. For this purpose, a pipe is inserted into the sleeper bottom. In current experiments, crushed stone with size fraction 5–10 mm was used for stoneblowing. To create crushed stones—air flow a blower device STIL BR 200 was used.

The VNIIZHT experimental ring consists of three circle tracks. Circle track 1 is for testing of locomotives, electric and diesel trains, passenger and freight cars, brake systems, catenary and overhead system, current-collecting, etc. Circle tracks 2 and 3 are for durability testing of freight cars and the structures of the permanent way. All the experiments were conducted on circle track 2.

Specifications of circle track 2:

- length 5700 m;
- curves 390–1200 m;
- grade 12‰.

Every day, a train weighing up to 10,000 tons with the axial load of cars up to 30 tons runs on Track 2. The operation time of the passed tonnage equals from 200 to 300 million tons per year (1–1.5 million tons of the operation time per day).

Speeds of the circulating trains on the tracks:

passenger trains—up to 140 km/h
freight trains—up to 90 km/h [4].

The joints between the rails № 291 and № 292 and ones between the rails № 293 and № 294 on the circle track 2 were chosen for the experiments (Fig. 1). The distance between joints was 12.5 m. The design of the joints is presented in Table 1.

The tonnage hauled on the section at the time of testing equaled 2 billion 200 million gross tons. This value exceeded the standard overhaul tonnage limit in 1.5 times and the standard limit between ballast cleaning periods in 3 times. These studies are a continuation of studies carried out by RUT (MIIT) and JSC VNIIZhT in 2017 [5].

2.1 Joints' Alignment with Stoneblowing

The measurement of the range of the hidden settlement was done with a flexometer (voltmeter) in the sleepers supposed to be aligned. Flexometers were installed on the rail base on each sleeper box of the joint zone (four sleeper boxes from the joint on both sides) (Fig. 2). The metal bar (a nail) was lowered to the pre-installed hard stone surface of the plywood or metal plate. The flexometer readings were registered with the help of Vernier caliper before and after the passage of a set of rolling stock.



Fig. 1 Scheme of the VNIIZHT experimental ring (the testing site is marked with an asterisk)

Table 1 Permanent way design of the testing sections

Joint	Kilometer stone	Rail type	Track structure	Fastening, sleeper type	Ballast	Position in the plan
291–292	6 KS 3	R-65	Jointed	KB, RFC	Hard stone	Straight
293–294	6 KS 3	R-65	Jointed	KB, RFC	Hard stone	Straight

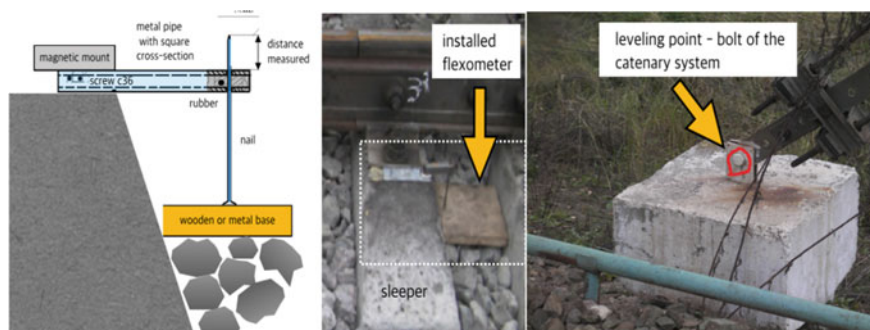


Fig. 2 Scheme of the installation and photographs of the installed flexometers

After measuring the value of the hidden settlement under and between the sleepers, which had been selected for the alignment, the boxed of the next but one sleepers were dug at the depth of 50 cm, at the distance of 25 cm from the rail.

The height of lifting of the rail head in the joints 291–292 and 293–294 was determined with the extensive settlement of the assembled rails and sleepers under their own weight after the alignment and the jack removal (10–15 mm) and the settlement of fine gravel during the first 6 days after the alignment (20 mm). The

distance from the “bed” of the sleeper to the bearing surface was not less than 35 mm [6]. The track was hung up on the hydraulic jacks installed opposite each other on the both sides of the track rails. The rail-gauge template was used to determine the height at which the assembled rails and sleepers were to be raised, and on laying the test sections, the height was exactly 35 mm. After having been hung upon the jacks, a plastic grid with the mesh of 5 mm in the clear (the so-called “masonry” grid) was placed under the two sleepers, the nearest ones to the joints; meanwhile, the alignment in the joint 293–294 was made with the mixture of hard stone and rubber crumbs of 5–8 mm in a ratio of 4–1 respectively.

After having hung up both track rails with the help of the blower device STIL BR 200, equipped with the special nozzle, the stoneblowing alignment was made with the use of specially colored crushed stone with the fraction of 5–10 mm and the mixture of crushed stone and rubber crumbs (Fig. 3).

When leveling, the bolt of the stayed pole № 103 of the catenary system was used as a stake (Fig. 2).

3 Results

3.1 *Unloaded Profile Measurements*

The leveling of the test joint 291–292 and joint 293–294 led to the following results (Fig. 4).

3.2 *Loaded Profile Measurements*

According to the results of the grade measurement alongside with the data of leveling and the amount of rail deflection, we got the force rail head profiles under the rolling stock. The most distinctive force profile was obtained on the left rail of the joint 291–292 (Fig. 5).

3.3 *Results*

Due to the visual examination and the examination after the ballast removal out of the sleeper boxes, aligned with stoneblowing, it was found that:

1. There are signs of the intensive action of stoneblowing crushed stone in the joint under the aligned sleepers (Fig. 6a).

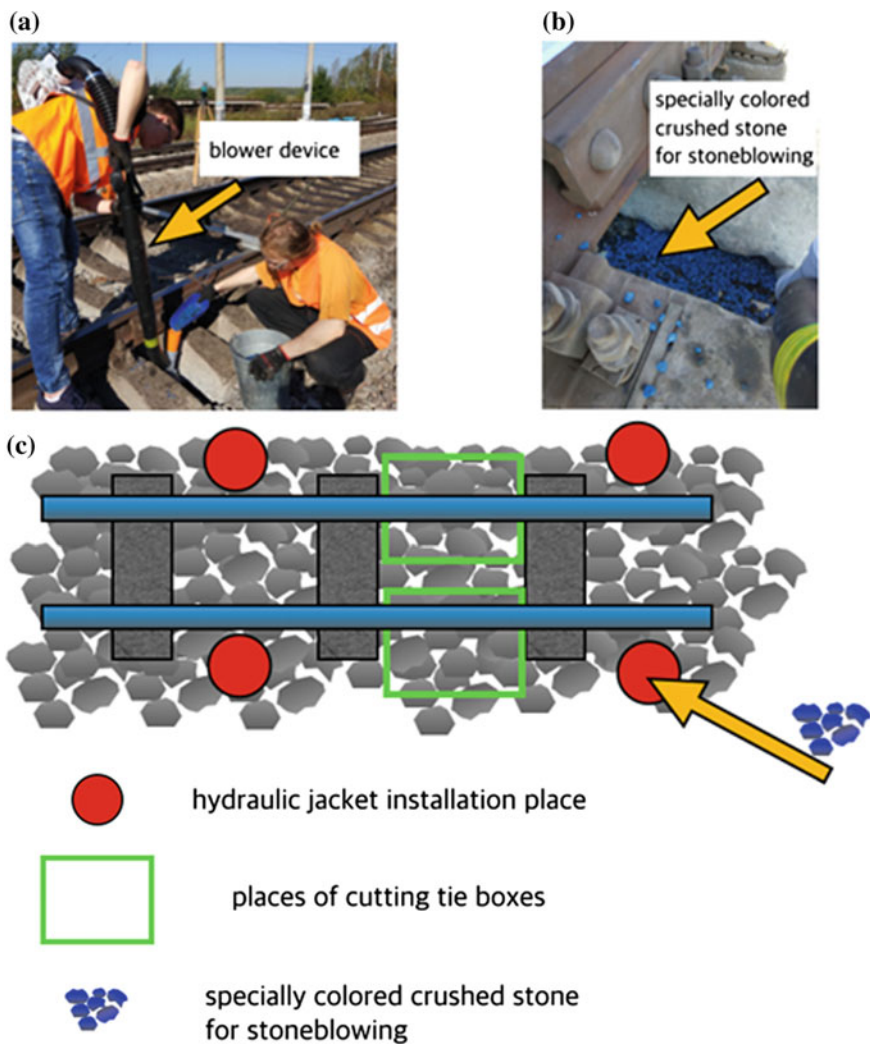


Fig. 3 **a** Elimination of a two-side settlement in the joint with the use of stoneblowing, **b** sleeper position after alignment, and **c** places of excavation of ballast and installation of jacks during alignment

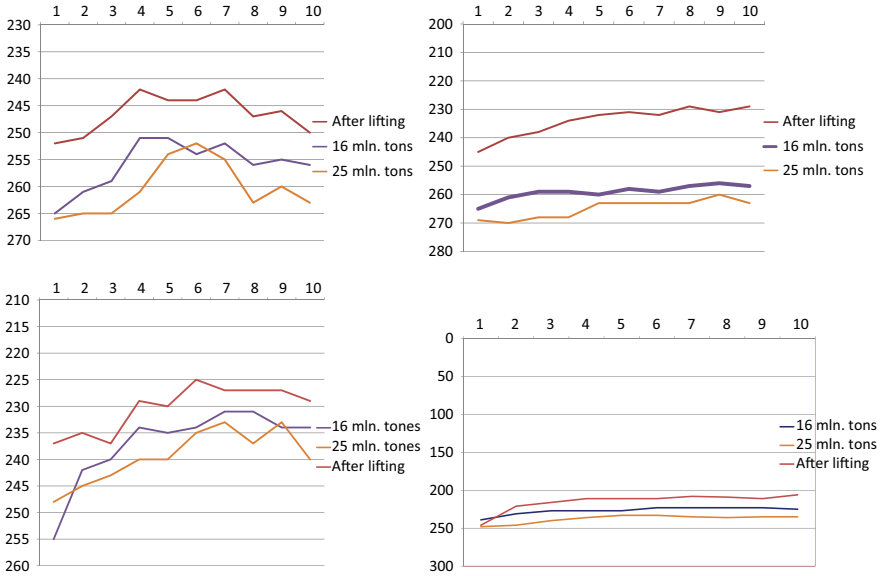


Fig. 4 Leveling of the joint 291–292, aligned with stoneblowing: **a** the left rail and **b** the right rail. Leveling of the joint 293–294, aligned with stoneblowing: **a** the left rail and **b** the right rail

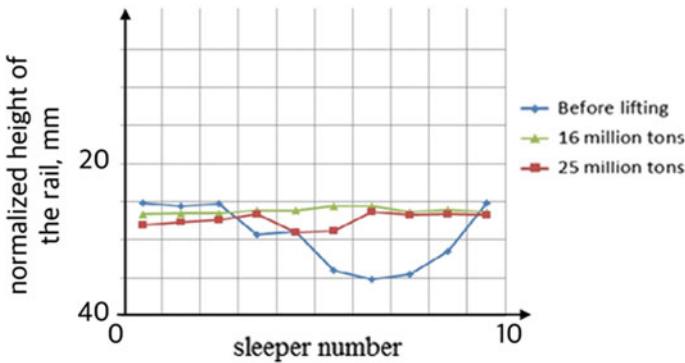


Fig. 5 Force profile of the left rail of the joint 291–292

2. Only in the areas where a plastic grid were laid under the ballast, the stoneblown crushed stone has not penetrated into the lower layers of the ballast even after the passage of 25 million tons of traffic (Fig. 6b).
3. In the areas where a plastic grid was not laid under the crushed stone for measured shovel packing, the crushed stone has penetrated into the track crushed stone just after the passage of 6 million tons of traffic that corresponds to laboratory researches carried out in RUT (MIIT) [7] (Fig. 6c).

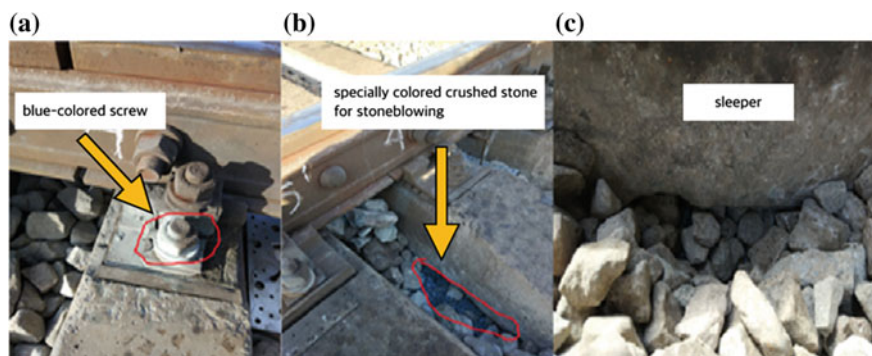


Fig. 6 a Signs of the intensive action of stoneblowing crushed stone under the aligned sleepers, b stoneblown crushed stone under the sleeper after the passage of 25 million tons of traffic, and c the penetration of the crushed stone after the passage of 6 million tons of traffic when there is no plastic grid under the crushed stone

4 Conclusion

Testing of a new equipment for stoneblowing should be recognized to be a success (the applied blower device STIL BR 200 extremely reduced the complexity of the stoneblowing operation and provided a high mobility of the alignment).

Stoneblowing can be successfully applied for the alignment of the joint settlements on the railway track with the high operating tonnage and even for the sections with expired overall repair.

The research, which was carried out on an extremely loaded element of the track structure, presupposes a successful stoneblowing alignment of such areas as bridge pits, frogs, and switch sleepers.

Summarizing all written above, we can formulate an intermediate result.

Stoneblowing technology will certainly be more effective on the track with high operating time of the passed tonnage that may exceed significantly the normative value. The possibility of alignment in some ballast section locations without repacking the bulk of the ballast granules will lead to an extension of the service life of the track ballast section. This is especially important for the countries with a cold climate, where the number of temperature transitions below zero can reach 50 or more. Moreover, when applying stoneblowing, the consumption of the alignment material is 20–60 times less than with the typical mechanized alignment of the track [8].

According to the test results, it can also be concluded that the use of a flat geogrid (mesh size 5 mm) used in construction to reduce the consumption of concrete mortar in the construction of masonry prevents the penetration of stoneblowing small particles into the pores of railway track stones.

References

1. Zarembski AM, Newman GR (2008) Comparative technical and economic analysis of Stoneblowing vs. tamping. In: AREMA 2008 annual conference and exposition, Salt Lake City, UT, September 2008
2. McMichael P, McNaughton A (2003) The Stoneblower—delivering the promise, TRB 2003 annual-meeting
3. Cope DL, Ellis JB (2001) British railway track, vol 4. Plain Line Maintenance Permanent Way Institution
4. Stepov VV, Savin AV (2017) Experimental ring of JSC “VNIIZHT”, history, advantages, prospects. Bulletin of the JSC RZD, Moscow
5. Pevzner VO, Kaplin VN, Abdrashitov AA, Semak AV (2018) Alignment of the track on the crushed stone ballast with the installation under sleeper pads and stoneblowing. Bull Res Inst Railway Transp (Vestnik VNIIZHT) 77(2):104–109
6. Abrashitov AA (2014) Pneumatic stoneblowing for the alignment of the track on the crushed stone ballast. Track Track Facil 5:11–14
7. Abrashitov A, Semak A (2017) Experimental study of stoneblowing track surfacing technique procedures of transportation geotechnics and geotechnology, TGG 2017
8. Selig ET, Waters JM (1994) Track geotechnology and substructure management. Thomas Telford Services Ltd., London

Modeling of a Railway Roadbed Reinforcement



Andrei Petriaev 

Abstract The purpose of the conducted model tests was to study the possibility of using a number of design solutions with geosynthetic materials to increase the bearing capacity and reduce the deformability of the sub-base, as well as to evaluate the effectiveness of their use. Small-scale modeling tests were conducted to investigate the stress–strains behavior of embankment reinforced in the upper part with geosynthetics. A series of model experiments have shown that an increase in the number of geosynthetic layers does not significantly effect on the roadbed bearing capacity. Reinforcement in a single layer is sufficient if the geosynthetic has required strength.

Keywords Roadbed · Geosynthetics · Model

1 Introduction

Modern geosynthetics are used on the railways of all European countries in the construction and reconstruction of the track structures for different purposes. A common feature of the reconstruction and construction of new Railways is needed to have a high-quality track base. In this case, the geosynthetics can play an important role, for example, to improve the quality of the soil layer and the bearing capacity of the roadbed, and to increase the service life of the track structure as a whole.

Small-scale modeling is one of the methods for the evaluation of different design solutions for the strengthening of the subgrade. Even approximate satisfaction of the similarity theory requirements in the soil model allows us to obtain very valuable data covering the qualitative side of the studied phenomena and revealing the studied processes mechanism. The data obtained on the models can be used for the quantitative evaluation of issues related to the roadbed stress–strain state.

A. Petriaev (✉)

Emperer Alexander I St.Petersburg State Transport University, 9, Moscovsky Prospect, Saint Petersburg 190031, Russia
e-mail: pgups60@mail.ru

© Springer Nature Singapore Pte Ltd. 2020

A. Petriaev and A. Konon (eds.), *Transportation Soil Engineering in Cold Regions*, Volume 2, Lecture Notes in Civil Engineering 50,
https://doi.org/10.1007/978-981-15-0454-9_4

In previous studies [1], authors have received a significant increase in bearing capacity and a decrease in the adjacent foundations incline when reinforcing sand with geogrid during the model tests.

During of sandy base model stamp tests [2], it was shown that the bearing capacity can be significantly increased by strengthening the zone directly under the foundation by short panels of geosynthetic material with a width equal to the width of the foundation. In this case, the reinforced zone behaved as a part of a deep foundation.

Having conducted stamp tests on soil-analog from the ceramic material [3], the authors note that the use of geogrid increases the stiffness of the soil layer and its bearing capacity.

The results of experimental studies showed that the bearing capacity of the soil was improved by reinforcement and the effect of improvement significantly depended on the depth at which the reinforcing elements were located.

In engineering practice, it is recommended that the distance from the sole of the foundation to the top layer of geosynthetic material and the distance between its layers were from 0.2 to 0.4 width of the foundation (B). The total depth of geosynthetic materials under foundation should be from 1.4 B to 1.6 B , and the length of the reinforced elements would be from 4 B to 6 B [4].

According to the results of the tests presented in [3], the bearing capacity of the base increases when the geogrid was laid at a depth of 0.065–0.5 of the stamp width.

The stamp tests to determine the bearing capacity of the sand base [5] allowed to conclude that the maximum increase in the bearing capacity was obtained at a ratio of the laying geogrid depth to the width of the stamp less than one. Reinforcement below the foundation at a depth of more than 2.25 times the width of the foundation did not contribute to an increase in bearing capacity for the case of a strip foundation.

The carried out tests of the sandy base, reinforced with a woven geotextile, allowed to obtain the dependence of the base elasticity modulus and its bearing capacity on the number of reinforcement layers located at depths of 0.25, 1, and 2 of the diameter of the stamp [6]. From these studies, it can be concluded that the laying of additional layers of the geogrid at a depth of more than the diameter of the stamp does not lead to a significant increase in the base elasticity modulus and its bearing capacity. In addition, it is seen that as the distance between the layers of reinforcement increases, its efficiency decreases.

Using a mixture of aluminum rods in stamp tests as a similarity of the sand base [7], the authors concluded that the reinforcement effect is more affected by the width of the geosynthetics and the number of layers than its rigidity. For practical use, the installation of geosynthetics in two layers is quite suitable, because a larger load-bearing capacity is achieved with less deformation. It is also noted that the sliding surfaces of reinforced foundations spread more in the horizontal direction than in the vertical direction with the increase in the width of the geosynthetic material. This increase in the sliding surface cannot be caused by the stiffness of the valve.

From the experimental studies described in the literature, there are two main mechanisms that contribute to an increase in the bearing capacity of the reinforced base. The first is blocking effect that is caused by the interaction of soil and geogrid.

In this case, the lateral deformation or potential deformation of stretching is limited and as a result, the vertical deformation of the soil is reduced, its strength and, consequently, the bearing capacity is increased.

The membrane mechanism is because both the soil and geosynthetic material are deformed and stretched under the foundation loading. In this case, the geosynthetic material takes part of the load. The geosynthetic material must be of sufficient length and strength not to be torn or pulled out from the ground.

2 Railway Subgrade Modeling

To achieve the similarity of the model and the railway roadbed, it is necessary to take into account numerous parameters (the design of the rolling stock, the upper structure of the track, the roadbed, elastic and plastic properties of materials, soil characteristics of the roadbed, etc.). It is not possible to preserve the numerical values of all similarity criteria when moving to models. However, the correct idea of the roadbed behavior can be obtained, as well in cases where only part of the similarity criteria is satisfied.

It is currently extremely difficult to accurately model such process, and it is not advisable for the goals of engineering practice. It is enough to create a model that will take into account the basic conditions of the soil in the roadbed. In our experiments, the main attention was paid to the strain-state modeling under the action of static loads.

One of the earliest methods of the subgrade modeling is small-scale modeling. Using this method, you can make significant additions to the calculations. In many cases, this method allows you to solve such complex and unexplored issues that are not yet amenable to study either analytically or by field observations.

The choice of the model scale is primarily due to the technological features of the model elements manufacturing. Modeling is associated with high costs when the scale of the models is close to the natural value; there may be large differences between the mechanical values of the model and the original at very small scales, and it is difficult to install the measuring equipment on this model, which can lead to large errors.

3 Model Test Facility and the Scale Model Choice

Model tests were carried out in a large test tray of the laboratory of soil mechanics. The tray is a reinforced concrete tank with dimensions of 300×400 cm and a depth of 203 cm.

The fine sand was used as a ground for carrying out model tests, the granulometric composition and properties of which are given in Table 1.

Table 1 Soil granulometric composition

Particle size, mm	>10	10–5	5–2	2–1	1–0.5	0.5–0.25	0.25–0.1	<0.1
% Finer	0.009	0.73	3.13	9.41	15.02	40.67	16.84	14.11

Table 2 Properties of subgrade soil

Property	Unit	Average values by depth H, cm		
		0–50	75	100–125
Unit weight ρ	kN/m ³	1,667	1,652	1,982
Dry unit weight	kN/m ³	1,624	1,535	1,748
Soil moisture	%	3.26	7.6	13.39
Voids ratio		0.65	0.76	0.63
Cohesion	kPa	3		
Friction angle	°	36		
Young modulus	MPa	38		

The use of fine-grained sand made it possible to reduce the impact of soil particle size on the test results of the small size model and to assess the impact of soil strength characteristics on the bearing capacity of the embankment model (Table 2).

The tray filling with sand was carried out to the level of 1.0 m. The model of the embankment was formed above the base by a special template with a mechanical compaction. The tray was equipped with a system of metal beams that allow you to transfer the load to the model up to 500 kN.

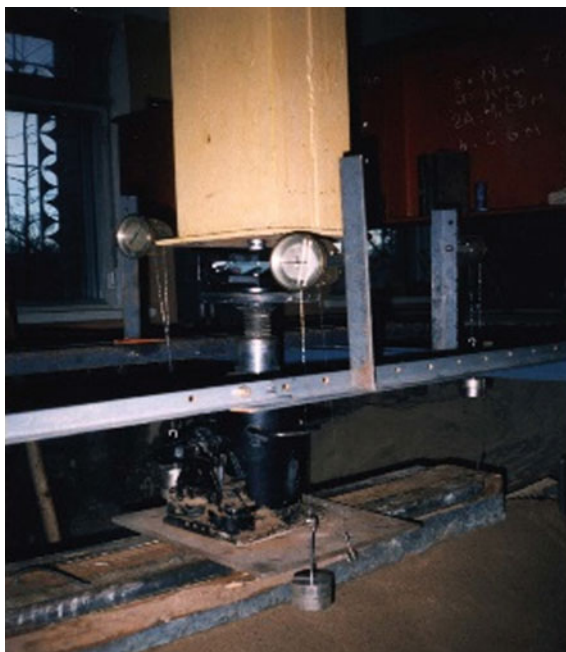
The model was loaded with the hydraulic Jack DG-100-2 capacity 1000 kN. The load value, which was transferred to the embankment model, was fixed by means of dynamometer DS-5, designed for a maximum force of 50 kN. The dynamometer was duplicated by manometer on the jack to increase the reliability of the test load measurement.

The metal plate in the size of 450 × 350 × 25 mm was placed under the jack for ensuring stability of the jack on a bar and for the transfer loading centrality on the embankment. The bar horizontal position was checked with the help of the level. A device for stamp deformation measuring consists of four indicators with divisions of 0.1 mm.

A metal ball with a diameter of 8 mm was used in the center of the model to ensure a strictly vertical load transfer. A plumb controlled the vertical position of the jack during the installation and experiment.

A general view of the installation for model tests is shown in Fig. 1.

The embankment models were made in the scale of 1:19 with the purpose of the model experimental studies. The bar with dimensions 150 × 16 × 10 cm (contact area 0.24 m²) was adopted as an upper structure model, which bottom and top were reinforced by four metal corners (45 × 45 mm) to protect from the splitting. The embankment model is with a width of 18 cm on the top and with a slope of 1:1.25. The height of the embankment model remained constant—60 cm.

Fig. 1 Test device

4 Geosynthetics Properties and Their Laying

Geosynthetics were laid at different depths (10–40 cm), in one or two layers, with or without layer-by-layer compaction. The compaction was made by manual electric tamping (method from slopes to the middle).

Some characteristics of the used geosynthetics are given in Table 3.

The schemes of the subgrade reinforcement, investigated in our experiments, are shown in Figs. 2 and 3.

Table 3 Tested geosynthetics

Material characteristics	Type 1	Type 2	Type 3
Structure	Geocells	Bi-oriented geogrid	Bi-oriented geogrid
Polymer type	Polyethylene	Polypropylene	Polyester
Aperture size MD/TD, mm	200/200	39/39	50/50
Strength at 5% strain MD/TD, kN/m		21/21	28/28
Peak tensile strength MD/TD, kN/m	29/29	30/30	80/80
Yield point elongation MD/TD, %	25/25	12	13/13

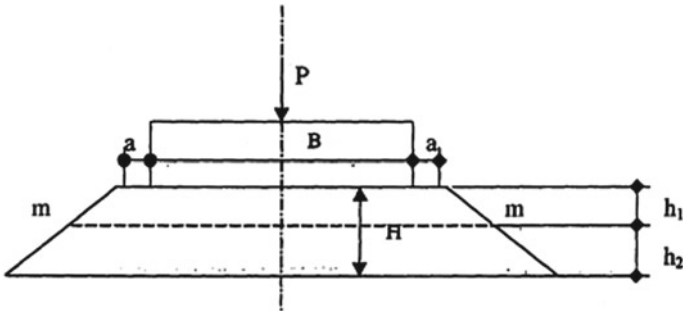


Fig. 2 Roadbed specimen reinforced with one geogrid layer, $m = 1:1.25$; $B = 16$ cm; $a = 1$ cm; $H = 60$ cm; $h_1 = 25$ cm; $h_2 = 35$ cm

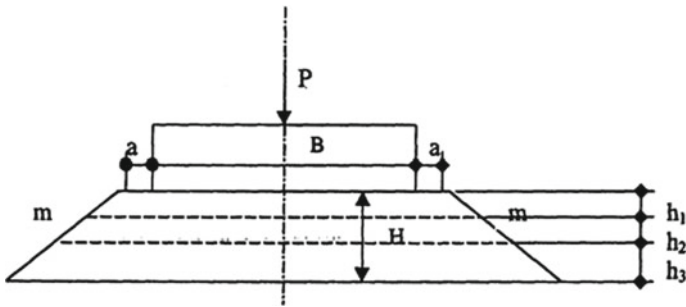


Fig. 3 Roadbed specimen reinforced with two geogrid layers, $m = 1:1.25$; $B = 16$ cm; $a = 1$ cm; $H = 60$ cm; $h_1 = 25$ cm; $h_2 = 35$ cm; $h_3 = 20$ cm

5 Test Procedure

Several experimental series were conducted in the course of small-scale model studies. The deformation properties of the embankment model without reinforcement were determined in the first series. In the following series deformation properties of embankment models, which were reinforced with geosynthetics in the upper part, were determined.

The weight of the track upper structure model was taken into account in the pressure and sediment at the first stage of loading. The loading of embankment model was carried out before its destruction. The embankment was considered to be destroyed when the deformation was occurred with a soil heave failure from all sides of the model or by a shift of the soil mass toward the least resistance (toward to the one of the slopes).

6 Discussion

Tests have shown that the embankment model deformations (in cases of reinforcement and without it) increase in linear dependence until complete destruction (Fig. 4). The settlements in the first phase of deformation occurred due to compaction of the soil under the model of the track upper structure. The limit of proportionality occurred when the load on the embankment model was 70–80% of the limit. Its deformation in this case was 40–45% from the deformation at the maximum load.

A further increase in the load caused a faster increase in settlement, and the dependence of settlement on the load took a nonlinear character. The settlement occurred in both due to further compaction of the soil and due to the formation of shear zones. At the beginning of the second phase cracks on the ground surface began to diverge, they were lengthened and were expanded from the corners of the embankment model as the load increased.

Cracks on the ground surface appeared at a vertical load of 75–80% of the maximum load. Cracks on the main site were developed mainly in the direction of one of the slopes. The angle of crack direction with the sides of the model was about 120°. On the slope, the cracks developed as a continuation of the cracks of the top of embankment then sharply went down about 2/3 of the height of the embankment model.

With a further increase in the applied load, the third phase of settlement occurred, when the model of the track upper structure failed at a fixed load value, while the surrounding soil shifted to the sides and upward. The shifted soil was limited by cracks

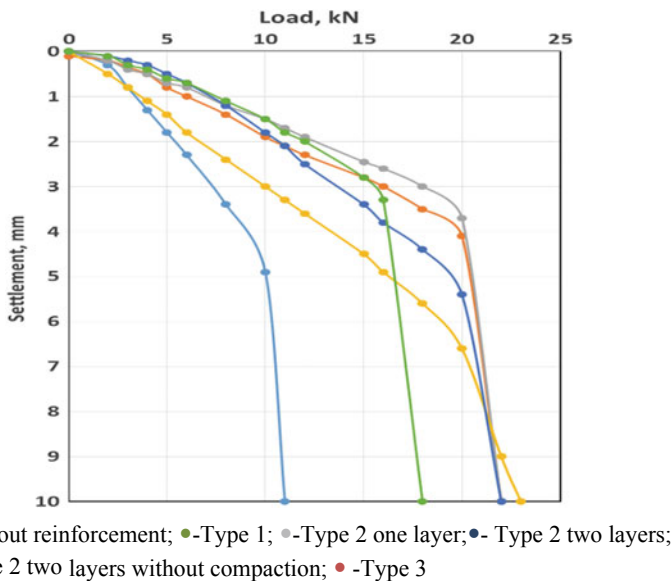


Fig. 4 Stress–strains response of reinforced roadbed model

Table 4 Model tests results

Reinforcing type	Settlement at load 10 kN, mm	Load at rupture, kN	K _p	K _s	KE
Without reinforcement	4.9	11.0	1.0	1.0	1.0
Type 1	1.5	18.0	1.6	3.3	2.6
Type 2 1 layer	1.7	22.0	2.0	2.9	3.3
Type 2 2 layers	1.8	23.0	2.1	2.7	1.7
Type 2 1 layer without compaction	3.1	22.0	2.0	1.6	1.8
Type 3	1.9	22	2.0	2.6	2.6

formed at the beginning of the second phase of deformation during the destruction of the embankment model. In the final phase, the destruction was usually two-sided and occurred in the plane of geosynthetic material laying.

For a visual and objective assessment of the effect of reinforcement of the upper part of the embankment model on its precipitation, destructive forces and the general deformation modulus, the coefficients of the relative decrease (increase) of the above values were used—K_S, K_R, K_E, respectively. K_S is the ratio of the embankment model deformation non-reinforced and reinforced with geomaterials at a load of 10 kN; K_P is the ratio of the embankment model bearing capacity reinforced and non-reinforced with geomaterials; K_E is the ratio of the embankment model total strain modulus reinforced and non-reinforced with geomaterials. The values of these coefficients for a series of model tests are given in Table 4.

Analysis of this results showed that the presence of geomaterials in the embankment model design leads to a decrease in its sediment under load in the range of from 1.6 to 3.3 times, increases the total strain modulus of the embankment model by 1.7–3.3 times and increases the embankment model bearing capacity by 1.6–2.1 times. The tests have shown that the geogrid type does not significantly affect on the bearing capacity of the embankment model.

Laying the second layer of geogrid does not lead to a significant increase in the bearing capacity of the subgrade. The effect of its application in comparison with a single-layer structure is about 5%. Bearing capacity of the embankment model reinforced by geogrid is 20% higher than when using geogrids.

7 Conclusions

The presence of geosynthetic material in the soil, absorbing tensile deformation, prevents the formation of continuous sliding surfaces and thus increases its shear strength. At the initial stage of loading in the phase of soil compaction, geosynthetic layer has no effect on the process of embankment deformations. Further horizontal deformation of the soil in the shear phase causes stretching of the geosynthetic

material caused by friction, which limits the lateral displacement. Destruction occurs when there is insufficient strength or stiffness of geosynthetics or if its adhesion to the soil is overcome. The shear occurs over the surface of a geosynthetic material if the adhesion of the geosynthetic material to the soil is less than the shear resistance of the soil itself.

The reinforcing geosynthetic material must be placed in the zone of tensile stresses in the direction coinciding with the main soil-strain rate of stretching.

A series of model experiments have shown that an increase in the number of geosynthetic layers does not significantly effect on the roadbed bearing capacity. Reinforcement in a single layer is sufficient if the geosynthetic has required strength.

References

1. Lavasan AA, Ghazavi M (2012) Behavior of closely spaced square and circular footings on reinforced sand. *Soil Found* 52(1):160–167
2. Huang C, Tatsuoka F (1990) Bearing capacity of reinforced horizontal sandy ground. *Geotext Geomembr* 9:51–82
3. Raymond G, Ismail I (2003) The effect of geogrid reinforcement on unbound aggregates. *Geotext Geomembr* 21:355–380
4. Chen Q, Abu-Farsakh M (2015) Ultimate bearing capacity analysis of strip footings on reinforced soil foundation. *Soils Found* 55(1):74–85
5. Khing KH, Das BM, Puri VK, Cook EE, Yen SC (1993) The bearing-capacity of a strip foundation on geogrid reinforced sand. *Geotext Geomembr* 12:351–361
6. Basudhar PK, Saha S, Deb K (2007) Circular footings resting on geotextile-reinforced sand bed. *Geotext Geomembr* 25:377–384
7. Yamamoto K, Kusuda K (2001) Failure mechanisms and bearing capacities of reinforced foundations. *Geotext Geomembr* 19:127–162

Mechanistic-Experimental Approach for Determination of Basic Properties of Mechanically Stabilized Layers



Zikmund Rakowski, Jacek Kawalec , Leoš Horníček
and Sławomir Kwiecień 

Abstract Mechanically stabilized layers have rather good potential for the application in construction of transport structures in cold regions. But determination of mechanical properties, which could be used in practice, remains still quite problem both theoretically and practically. The paper describes a new approach how to solve that problem. Presented method, it is a combination of laboratory experiment and inversion FEM modelling. The approach is called mechanistic-experimental. The experiment should be in scale 1:1 and should provide data of at least two independent parameters so that FEM model could be calibrated by iterative inverse modelling accordingly. Then mechanical properties like deformation modulus, Poisson ratio and minimum initial shear resistance of mechanically stabilized layer (composite like) could be determined. The real laboratory and FEM model are described and discussed. The paper is a continuation of earlier published papers (Rakowski in *Procedia Eng* 189:166–173, [1]; Horníček and Rakowski in *Mechanically stabilized granular layers an effective solution for tunnel project*. Springer Nature America Inc., New York, [2]; Rakowski et al. in *The applicability of recent mechanically stabilized granular layer concept in ME pavement design*. Springer Nature America Inc., New York, [3]).

Keywords Geogrids · Stabilization function · Granular material · Interlocking · FEM · Mechanical properties

Z. Rakowski (✉)
Český Těšín, Czech Republic
e-mail: zyraki44@gmail.com

J. Kawalec
Tensar International, Český Těšín, Czech Republic

L. Horníček
Faculty of Civil Engineering, Czech Technical University, Prague, Czech Republic

J. Kawalec · S. Kwiecień
Department of Geotechnics and Roads, Silesian University of Technology, Gliwice, Poland

© Springer Nature Singapore Pte Ltd. 2020
A. Petriaev and A. Konon (eds.), *Transportation Soil Engineering in Cold Regions*,
Volume 2, Lecture Notes in Civil Engineering 50,
https://doi.org/10.1007/978-981-15-0454-9_5

1 The Structure of Mechanically Stabilized Layer

The key mechanism involved in the field of stabilization is the interlocking of aggregates provided by a stiff geogrid structure [4, 5]. It was confirmed. Three different zones were distinguished: the immobilized/stiffened zone h_i , the transition zone h_T , the untouched zone h_o [1–3]. Transition zone means transition from fully confinement zone to not confined stone at all. It is assumed [2, 3] that changing of properties in vertical direction through that zone has nonlinear character (Fig. 1). At the moment we are not able to define the parameters of that curve properly. For practical reasons and certain simplification, the transition zone can be divided on the set of thin layers each with different parameters according to the position in the zone (Fig. 1). Following this concept, mechanically stabilized layer has a vertically layered structure. The performance of the whole mechanically stabilized layer is the function of the intensity of confinement in the zone GGC and thicknesses of the other zones [6, 7].

The approach according to Fig. 1 enables to construct a model representing numerically transition zone as shown in Fig. 2. This approach is then applied in inverse FEM described in Chap. 3.

Another important consequence of the confinement is shown in Fig. 3. The element is loaded vertically by σ_v and due to abutting to geogrid ribs confinement stress component σ_{co} is generated. By this resulting horizontal stress σ_h is reasonably smaller than in not confined granular material. The knowledge of this mechanism can be used in further procedure in the laboratory and the following FEM [8, 9].

Fig. 1 Layered model of mechanically stabilized layer

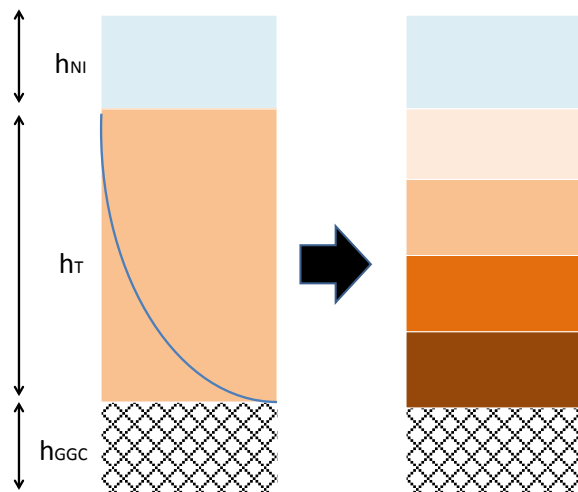


Fig. 2 Approximate model of the distribution of properties in transition zone

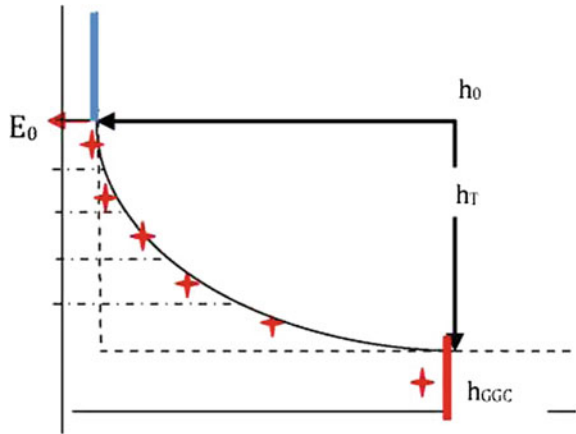
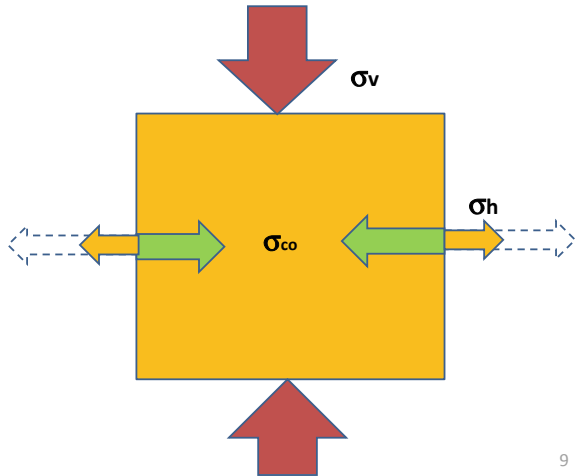


Fig. 3 Reduction of horizontal stress in the GGC due to effective confinement



9

2 Laboratory Experiments

Laboratory configuration (Figs. 4, 5, 6) was exactly the same as described in the earlier work [3], crushed aggregates graded 0–31.5 layers and a triaxial geogrid (rib pitch 40 mm). Model was formed by three granular layers (250, 250, 150 mm), between which the geogrid was located. On both lateral walls vibrating wire pressure cells were installed to measure horizontal pressure.

The load was applied through prefabricated circular reinforced concrete plate, 790 mm in diameter and 140 mm thick. Circular steel plate, 40 mm in height and 390 mm in diameter, was placed on the concrete plate. Static load of 100 kN (0.20 MPa under concrete plate) was applied in 4 steps by 25 kN. The measurement of plate

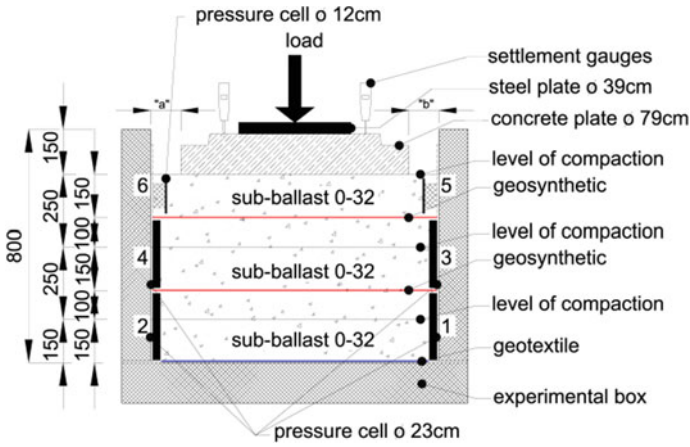


Fig. 4 Laboratory model—cross section—perpendicular

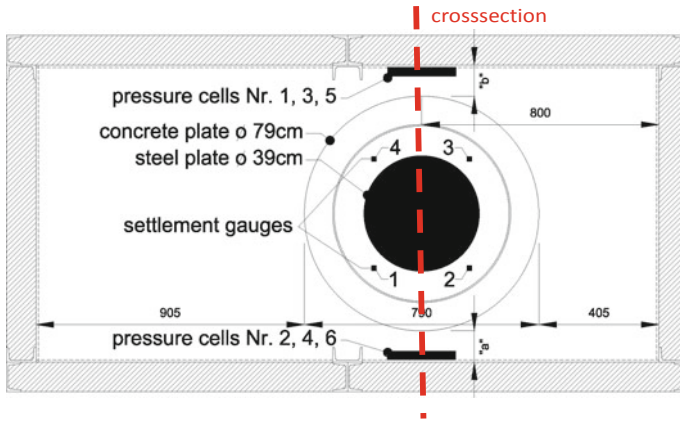


Fig. 5 Laboratory model—top view

settlement and the pressure on sidewalls formed basic data. After t static loading, the model n was exposed to cyclic loading with a force ranging between 3 and 100 kN with a sinusoidal mode and a frequency of 3 Hz. The readings were done at 1000, 10,000, 100,000, 200,000, 500,000, 1,000,000, 1,500,000 and 2,000,000 loading cycles.



Fig. 6 Experimental box assembled with the actuator

3 Inverse FEM Modelling

FEM models are used to analyse pavement structures [10]. In our case, FEM model was assembled exactly according to the geometry of physical laboratory model (Fig. 7) [11, 12].

Modelling was executed in several iterative steps to find parameters of the MSL, with which the model performs similarly to physical laboratory model. Vertical settlement and soil pressures on box sides during vertical loading through concrete-steel plate were measured as the performance parameter. The last model results fitted to the measured ones almost perfectly. Loading plate was always modelled with $E = 26 \text{ GPa}$ and $\nu = 0.2$.

Figure 8 shows a very good agreement between measured and last FEM model vertical settlement (Fig. 9).

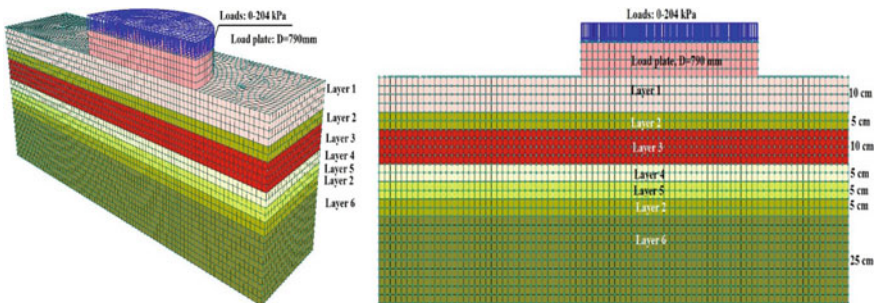


Fig. 7 3D FEM model mesh assembly—linear elastic

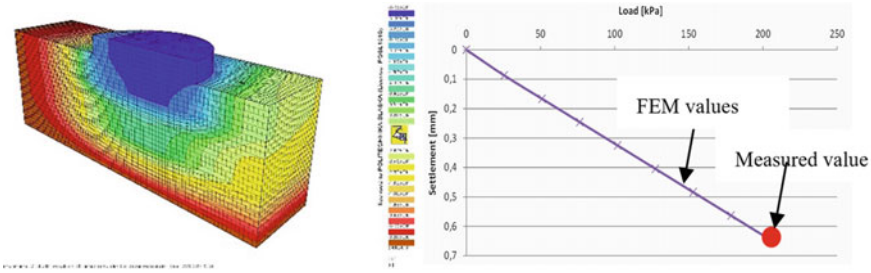


Fig. 8 Total final vertical settlement in FEM model comparing with measured value

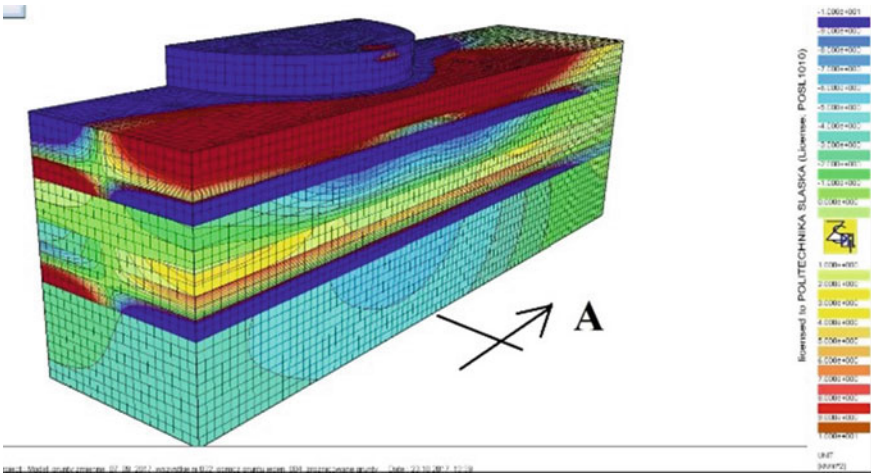


Fig. 9 Horizontal stress field in FEM model

Table 1 shows the results of the calibration of the FEM model with the data measured in the laboratory. In the level of MSL, the figures are exactly the same in the non-stabilized layer and the similarity is satisfactory.

The results of FEM as described above were achieved by modelling with parameters shown in Table 2.

We can observe reasonably increased modulus for fully confined zone and adequately higher values for transition zones. The last are different and difference is in

Table 1 Comparison of measured and modelled pressures on sidewalls

Position in model	Physical model/MPa/average	FEM/MPa
Lowest part of the model	5.3	5.17
In MSL level	2.21	2.21

Table 2 Parameters of FEM by layers as used in the best-calibrated model, FC—fully confined zone, T—transition zones

Layer	E/MPa	$\nu/-$
1 T	500	0.2
2 FC	2000	0.02
3 T	500	0.02
4 T	250	0.1
5 T	750	0.02
6	50	0.4

the position of the layer against fully confined layer. Poisson number for fully confined zone is very low and it explains well the reason for strongly reduced horizontal pressure on the box sidewalls in the level of that zone [13–15].

4 Conclusions

Direct measurement of MSL mechanical parameters is recently impossible. The mechanistic-experimental approach based on full-scale physical model and its inverse modelling by FEM using measured data was proven as satisfactory way for determination of basic parameters of the MSL. Parameters obtained as the results of the process showed high elastic modulus and very low Poisson number. It confirms the principle of mechanical stabilization as strong reduction of deformability of fully confined layer. Such a low deformability agrees with some time used name for fully confined zone as “quasi rock”. It is obvious that as that was one experiment with certain type of used materials the results can not be generalized yet. For more general conclusions more experiments as described should be done.

Acknowledgements Authors thanks Tensar International, Ltd., UK for sponsoring the research and access to the technical library.

References

1. Rakowski Z (2017) An attempt of the synthesis of recent knowledge about mechanisms involved in stabilization function of geogrids in infrastructure constructions. *Procedia Eng* 189:166–173
2. Horníček L, Rakowski Z (2019) Mechanically stabilized granular layers an effective solution for tunnel project, chap 12. Springer Nature America Inc., New York
3. Rakowski Z, Kawalec J, Kwiecień S (2019) The applicability of recent mechanically stabilized granular layer concept in ME pavement design, chap 14. Springer Nature America Inc., New York
4. Byun YH, Tutumluer E, Feng B, Kim JH, Wayne MH (2019) Horizontal stiffness evaluation of geogrid-stabilized aggregate using shear wave transducers. *Geotext Geomembr* 47(2):177–186

5. Tutumluer E, Huang H, Bian X (2012) Geogrid-aggregate interlock mechanism investigated through aggregate imaging-based discrete element modeling approach. *Int J Geomech* 12(4):391–398
6. Chen X, Zhang J, Li Z (2014) Shear behavior of a geogrid-reinforced coarse-grained soil based on large-scale triaxial tests. *Geotext Geomembr* 42(4):312–328
7. Correia NS, Zornberg JG (2016) Mechanical response of flexible pavements enhanced with geogrid-reinforced asphalt overlays. *Geosynthetics Int* 23(3):183–193
8. Fischer S, Szatmari T (2016) Investigation of the geogrid-granular soil combination layer with laboratory multi-level shear box test. In: *Proceedings of EuroGeo6 conference, Special Session on “geosynthetics in road construction”*, Ljubljana, Slovenia
9. Konietzky H, te Kamp L, Groeger T, Jenner C (2004) Use of DEM to model the interlocking effect of geogrids under static and cyclic loading. Numerical modeling in micromechanics via particle methods. In: *Proceedings of the 2nd international PFC symposium, Kyoto*, pp 3–12
10. Akbulut H, Aslantas K (2005) Finite element analysis of stress distribution on bituminous pavement and failure mechanism. *Mater Des* 26(4):383–387
11. Grygierek M (2017) Change in stiffness of pavement layers in the linear discontinuous deformation area. In: *IOP conference series: materials science and engineering*, vol 245, no 4. IOP Publishing, UK
12. Jenner CG, Watts GRA, Blackman DI (2002) Trafficking of reinforced, unpaved subbases over a controlled subgrade. In: *Geosynthetics: state of the art-recent developments. Proceedings of the seventh international conference on geosynthetics, 7-ICG, vol 3. Nice, France*
13. Matys M, Baslik R (2004) Study of interlocking effect by the push test. In: *Proceedings of Asian regional conference on geosynthetics geoAsia 2004, Seoul*, pp 341–347
14. Sun X, Han J, Kwon J, Parsons RL, Wayne MH (2015) Radial stresses and resilient deformations of geogrid-stabilized unpaved roads under cyclic plate loading tests. *Geotext Geomembr* 43(5):440–449
15. Wu H, Huang B, Shu X, Zhao S (2015) Evaluation of geogrid reinforcement effects on unbound granular pavement base courses using loaded wheel tester. *Geotext Geomembr* 43(5):462–469

Stamp Test of Railway Ballast, Stabilized by Geogrids



Andrei Petriaev , Victor Ganchits , Maria Chetina , Ivan Kozlov 
and Svetlana Petrenko

Abstract In accordance with the objectives of the study, the program of works provided for stamp tests of ballast reinforced with geomaterials. The need for stamp tests is primarily due to the lack of reliable data to assess the impact of geomaterials on the stabilized railway ballast deformability. Thus, the main purpose of the stamp tests was to study and evaluate the impact of different geomaterials types on the crushed stone deformation properties in different reinforcement variants in a wide range of operating loads.

Keywords Geogrids · Ballast · Stamp

1 Introduction

The soil moisture in the frozen layers is greatly increased in the process of subgrade freezing. The load from the rolling stock during the thawing is perceived not by the soil skeleton, but by the free water formed at the thawing boundary. This leads to a significant reduction in the bearing capacity of the roadbed soils. The low bearing capacity of the roadbed during thawing often causes a geometry violation of the upper structure due to the deformation of subgrade top in the under rail zones. Laying the geogrid in the ballast reduces these deformations due to the redistribution of pressure.

Previous laboratory researches and numerical simulation results have highlighted the benefits of geosynthetics reinforcement [1–3]. As a result of stamp tests, it was noted that with a thickness of the protective layer 10 cm above the geogrid, the increase in the deformation module is relatively small, which was explained by the fact that the specified layer thickness is not enough to activate the geogrid [4]. By increasing the thickness of the protective layer up to 20 cm, the geogrid effect on increasing the deformation module can already be clearly traced. In this case, it increases by 31–70%.

A. Petriaev (✉) · V. Ganchits · M. Chetina · I. Kozlov · S. Petrenko
Emperer Alexander I St. Petersburg State Transport University, 9, Moscovsky Prospect, Saint Petersburg 190031, Russia
e-mail: pgups60@mail.ru

© Springer Nature Singapore Pte Ltd. 2020
A. Petriaev and A. Konon (eds.), *Transportation Soil Engineering in Cold Regions*,
Volume 2, Lecture Notes in Civil Engineering 50,
https://doi.org/10.1007/978-981-15-0454-9_6

In a series of laboratory studies [5], it was determined that the effect of the geogrid in the ballast layer is more obvious for soft ground than hard. The size of the geogrid cell relative to the nominal size of the ballast particles is a very important parameter for effective stabilization. For maximum ballast particles size up to 50 mm, the optimal geogrid cell size is 60–80 mm. The more rigid geogrid gives a more significant effect in the ballast.

The geogrid that placed on the boundary ballast base stabilizes part of its layer, thereby reducing the degree of ballast lateral displacement [6]. The geogrid influence zone in the ballast limited to the value of 16 cm. A stronger locking of the ballast particles is observed during the laying of the geogrid in the ballast layer compared to laying on the border of the ballast-subballast. This is because in the first case, crushed stone particles can protrude through the holes of the geogrid due to the presence of the same material both above and below the grid, thereby significantly increasing the geogrid influence zone.

The present study focuses on the different parameters, such as the depth under stamp foot of first and second geogrid layers, number of reinforcement layers, on settlement and bearing capacity of the rectangular stamp resting on the ballast.

2 Experimental Setup

Model tests were carried out in a large test tray of the laboratory of soil mechanics. The tray is a reinforced concrete tank with dimensions of 300×400 cm and a depth of 203 cm. The tray eliminates the deformation of the base and, accordingly, their additional impact on the value of deformation of stabilized and non-stabilized crushed stone layer.

The pure crushed stone of 40–70 mm fractions was used for carrying out stamp tests, which corresponds to the fractional composition of crushed stone used as ballast on railways. Geosynthetics were laid at different depths (10–40 cm), in one or two layers with layer-by-layer compaction. The compaction was made by manual electric tamping. The tray was equipped with a system of metal beams that allow you to transfer the load to the model up to 500 kN.

The stamp was loaded with the hydraulic jack with capacity 1000 kN. The load value, which was transferred to the stamp, was fixed by means of dynamometer, designed for a maximum force of 250 kN. The dynamometer was duplicated by manometer on the jack to increase the reliability of the test load measurement.

A rectangular metal plate of dimensions $1200 \text{ mm} \times 700 \text{ mm} \times 25 \text{ mm}$ was used as the stamp with the area of the stamp-working surface 8400 cm^2 . A metal ball with a diameter of 8 mm was used in the center of the model to ensure a strictly vertical load transfer. A plumb controlled the vertical position of the jack during the installation and experiment.

It is allowed to use any devices, the measuring system which allows the measurement of the stamp settlement with error not exceeding 0.1 mm. In our tests, the device for stamp settlement measuring consisted of four-deflectometer system Maksimova with a scale measuring sensitivity of 0.01 mm, mounted on a reference system. The stamp was connected to the deflectometer by means of a steel wire in diameter of 0.3 mm. Immediately before the filling process, a steel wire with a diameter of 0.3 mm was attached to each of the edges of the laid geomaterial with the help of special carbiners to control a horizontal displacement of the geomaterial. The other end of the wire was connected to the deflectometer through the system of blocks and carabiners. The wire was passed in a steel tube with a diameter of 20 mm to prevent it jamming with ballast. The reference system consisted of four beams and placed before each experiment on the tray walls. This ensured the immobility of the reference system during the test.

3 Material Properties and Their Laying

Magmatic and sedimentary rocks are used as a source of ballast materials in various countries because they tend to have high hardness and compressive strength and resistance to weathering.

The tested ballast in this study is a sharp angular coarse particles of volcanic granites crushing. The grain size distribution of fresh ballast is shown in Fig. 1. The

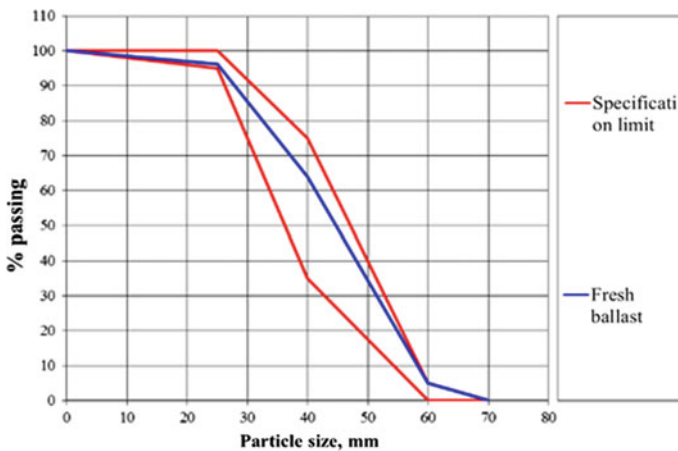


Fig. 1 Particle size distribution of tested ballast

selected particle size distribution, which is used in laboratory tests, is typical for railways of JSC “Russian Railways”.

Some characteristics of the used geosynthetics are given in Table 1.

The schemes of the subgrade reinforcement and layers dimension, investigated in our experiments, are shown in Fig. 2 and Table 2.

Table 1 Tested geosynthetics

Characteristics of the material	Type 1	Type 2	Type 3	Type 4
Structure	Bi-oriented geogrid	Bi-oriented geogrid	Bi-oriented geogrid	Geocells
Polymer type	Polypropylene	Polypropylene	Polyester	Polyethylene
Aperture size MD/TD, mm	39/39	35/45	50/50	200/200
Strength at 5% strain MD/TD, kN/m	21/21	28/30	28/28	
Peak tensile strength MD/TD, kN/m	30/30	40/40	80/80	29/29
Yield point elongation MD/TD, %	12	10/10	13/13	25/25

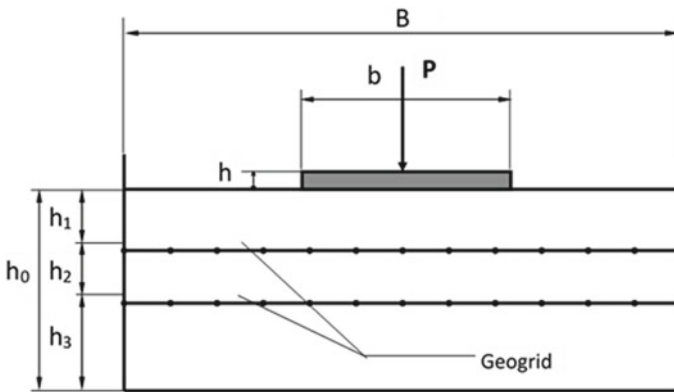


Fig. 2 Schemes of the subgrade reinforcement

Table 2 Dimensions of test construction

Test number	Geosynthetics type	Geometric parameters in accordance with Fig. 2 $B = 300$ cm, $b = 70$ cm, $h = 2.5$ cm			
		h_0 , cm	h_1 , cm	h_2 , cm	h_3 , cm
1	Crushed stone	120	–	–	–
2	Type 1	120	50	–	70
3	Type 2	120	50	–	70
4	Type 3	120	50	–	70
5	Type 4	120	50	–	70
6	Type 1	120	40	10	70
7	Type 1	120	30	20	70
8	Type 1	120	20	30	70

4 Test Procedure

The next main parameters were varied during the tests: the total ballast thickness, geosynthetics type, the geomaterial depth under stamp, the number of geosynthetics layers, and the distance between them.

The loading of stamp was carried out in steps of 0.048 and 0.06 MPa. The maximum load was 0.228 MPa. The value of the maximum pressure was established based on the considerations that the actual pressure under the sleeper with rails P65 and axial loads up to 230 kN is about 0.2 MPa. The weight of the stamp and jack was included in the first pressure step.

Each next stage of pressure was withstood to the conditional stabilization of ballast deformation, and the speed of stamp settlement, not exceeding 0.1 mm for 30 min, was taken as a criterion of deformation stabilization. The value of the total deformation was determined as the arithmetic mean of the readings. When the maximum load value of 0.228 MPa was reached, the investigated sub-base was fully unloaded.

In the final stage of each test cycle, the measuring system and used ballast were removed, and geomaterial samples were inspected.

Design solutions variants implemented in the stamp tests are given in Table 2.

5 Results and Discussion

It should be noted that the dependences of the deformation on the load is nonlinear (Fig. 3). This is especially noticeable in structures where there is a geosynthetic reinforcing layer. On the first stage, there are a compression and compaction of the ballast top layer, grinding in the stamp surface, which leads to a slightly larger value of the total strain in comparison with the second step of the load in all variants of constructive solutions. The absolute value of settlement is almost the same for all

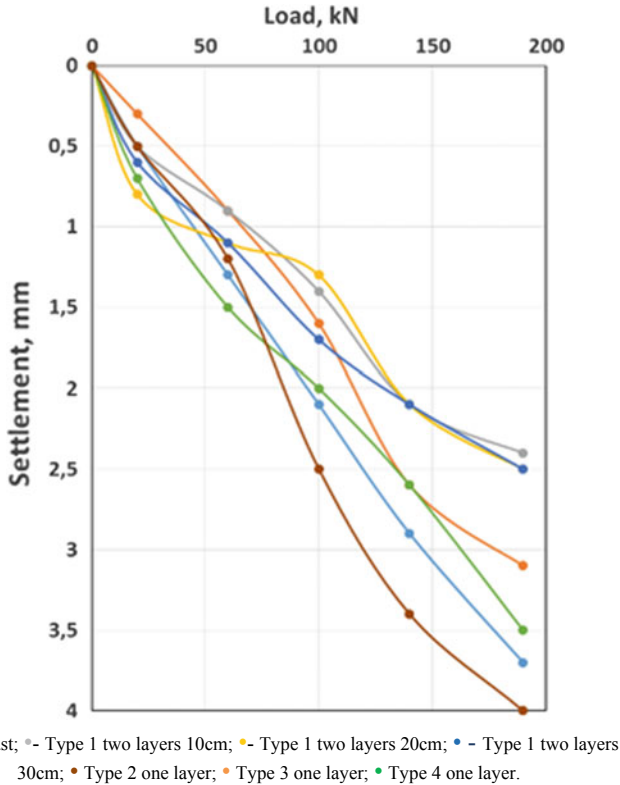


Fig. 3 Dependence of settlement on stamp load

variants of structures after the first stage, except for the structure with three layers, and is about 0.5 mm. Starting from the second stage of the load, the dependence of deformation on the load for non-stabilized ballast becomes almost linear.

The calculated value of the deformation modulus in this case is 72 MPa. In the further, the deformation process of reinforced and not reinforced ballast is different. Structures with reinforcing layers have a slightly increased deformability in comparison with the non-reinforced structure in the load range of 0.07–0.12 MPa. It is due to the ballast compaction at the depth of geosynthetic laying, reorientation, and final jamming of individual ballast grains in the geogrid cells. With a further increase in the load, the geogrids are included in the work, which leads to a sharp change in the deformation module at these stages. It should be noted that the inclusion of geogrids in the work with one-layer structure occurs when the load on the stamp is 0.17 MPa. For two layers reinforcement, this is also at the load 0.17 MPa, but there is a slight decrease in the base deformability in the range of 0.12–0.17 MPa. The inclusion in the work of geogrid in the three-layer structure occurs earlier, exactly when the load on the stamp is 0.12 MPa. This is connected with the fact that the top layer in

the three-layer structure was situated on the depth only 10 cm, and this led to the inclusion of the top layer in the work at an earlier stage of loading.

The design with geosynthetic Type 4 in the load range of 0.12–0.23 MPa showed a linear dependence of the total strain on the applied load, and the value of the deformation modulus of such a structure does not differ from the value of the deformation modulus of crushed stone. This means that in these conditions, there was no full inclusion of geocells in the work of the reinforcement structure. This fact is related to the impossibility of ballast normal compaction in the cells due to the relative size of the material cells and the predominant fractions of crushed stone. It is most likely that in fine crushed stone or sand, the inclusion of geocells in the work will occur at a lower load.

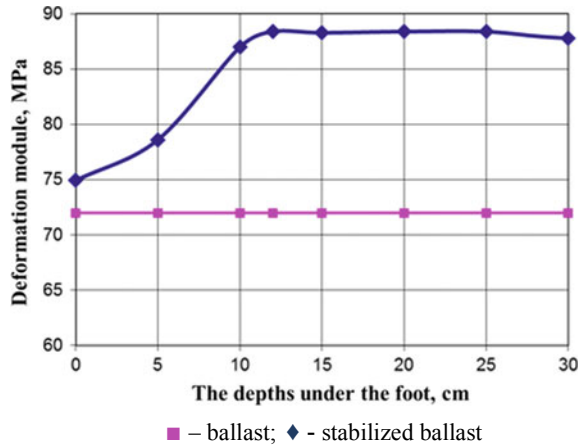
When the load on the stamp is more than 0.23 MPa, the value of the stamp settlement for reinforced structures becomes less than for crushed stone. This fact allows us to predict that at the loads exceeding the specified value, the geomaterials will contribute to the ballast deformation reduction.

A significant geosynthetic horizontal movement was not recorded from the action of vertical load in all tests. This indicates that in this range of loads, the geometric dimensions of the studied materials are sufficient to become anchored, and they perceive the tensile forces without pulling out from the ballast. On the other hand, this indicates that the geogrid does not work as a membrane in the ballast, which is located on a sufficiently strong base, and the effect of blocking of gravel particles in the geogrid is observed. The specified property of a composite material consisting of crushed stone and a geogrid allows its use in the construction of the ballast prism of railway tracks to decrease its deformability.

Inspection of geogrids after the experiments did not reveal any changes in the geometry of the cells, such as breaks, geometric distortions, etc., which indicates the normal operation of geosynthetics in the ballast under tested load up to 0.23 MPa. The results showed that the stabilized ballast deformation properties are directly dependent on the stamp load and the geosynthetics depth laying. Both of these factors depend on stresses that are realized at the geosynthetics level. Thus, an important task is to determine the stresses at the geosynthetics level, at which it is included in the work. This stress may be determined in accordance with the known solutions for the stresses attenuation under the rigid rectangular stamp [7]. For the stamp that we used in tests, this value is 0.1 MPa.

The obtained results show a positive effect of geomaterials on the ballast deformability, but do not provide an opportunity for an objective assessment of geogrids impact on the ballast deformed state in other design solutions. We have so far used the value of the total deformation modulus, which, obviously, will largely depend on the total thickness of structure. The greatest interest for us is only a layer of soil, the deformation characteristics of which have changed during reinforcement with geogrid. The fact that total deformation module increases in reinforced ballast indicate the possibility to consider this construction as a sandwich structure, where there is an additional conditionally homogeneous layer in crushed stone. This layer equivalently replaces the geogrid impact on the ballast layer stress-strain condition.

Fig. 4 The dependence of the total deformation module on the geogrid laying depth



The series of experiments was carried out to determine the thickness and deformation module of this layer. The geogrid Type 1 was consistently placed at different depths from the surface of the stamp. The results are shown at Fig. 4.

The deformation module is 75 MPa when the geogrid was placed at the ballast surface, under the stamp foot. This module slightly (4%) differs from the total deformation module of unreinforced construction. This is because there is no geogrid anchorage, and it works due to the friction forces in the contact zone of the crushed stone and geogrid. Geogrid gradually activates with increasing laying depth from 0 to 12 cm under the stamp, and the total deformation module increases from 75 to 88 MPa. A further increase in the geogrid depth from the stamp foot does not change the total deformation module. This fact indicates that geogrid is fully involved in the work with the layer thickness above it 11 cm. Therefore, it can be assumed that the influence zone of geogrid Type 1 on the overlying layer of ballast is about 11 cm. The geogrid Type 1 influence zone in this ballast type is 22 cm as the geogrid reinforces both the overlying and the underlying layers.

The deformation modulus 480 MPa of this equivalent layer with thickness 22 cm was determined analytically in accordance with [7, 8].

6 Conclusions

The stamp tests results analysis of ballast that was stabilized by geogrids allows us to note the following. Inclusion geogrid in the work occurs at some external load values, which are due to the achievement of certain values of stresses acting at the geogrid laying level. The external load and the geogrid laying depth are factors that affect the deformability designs.

These experimental studies have obtained the ballast stress value 0.1 MPa, at which geogrid is included in the work. Geosynthetics horizontal movement was not

occurring in ballast under the load up to 0.23 MPa. When the ballast is reinforced with a single-layer geogrid, the deformation modulus increases by 1.22 times in the load range on a stamp of 0.12–0.23 MPa; when reinforced in two layers, the deformation modulus increases 1.79–2.08 times.

The deformation properties of the crushed stone layer during the joint work with geocells in the same load range slightly deteriorated by 22.4%. It is caused by impossibility of fractions 40–70 crushed stone normal compaction in the cells. The depth of geocells laying from the stamp surface in the range from 10 to 50 cm does not affect the deformation of the ballast. The total deformation module increases in reinforced ballast that point on the possibility to consider this construction as a sandwich structure. In this design, the reinforcing properties of the geogrids may be modeled by the introduction of an equivalent layer with certain geometric and deformation properties. The thickness and deformation modulus of this equivalent layer that are determined by the ballast stamp tests results are 22 cm and 480 MPa.

References

1. Biabani MM, Indraratna B (2015) An evaluation of the interface behaviour of rail subballast stabilized with geogrids and geomembranes. *Geotext Geomembr* 43(4):240–249
2. Qian Y, Mishra D, Tutumluer E, Kazmee H (2015) Characterization of geogrid reinforced ballast behavior at different levels of degradation through triaxial shear strength test and discrete element modeling. *Geotext Geomembr* 43(4):412–422
3. Petriaev A (2017) Stress response analyses of ballasted rail tracks, reinforced by geosynthetics. In: Petriaev A, Konon A (eds) *Transportation geotechnics and geoecology (TGG-2017)*, vol 189. Elsevier, Amsterdam, pp 660–665
4. Gobel G, Weisemann UC (1994) Effectiveness of a reinforcing geogrid in a railway subbase under dynamic loads. *Geotext Geomembr* 13:91–99
5. Brown SF, Kwan J, Thom NH (2007) Identifying the key parameters that influence geogrid reinforcement of railway ballast. *Geotext Geomembr* 25:326–335
6. Indraratna B, Hussaini SKK, Vinod JS (2013) The lateral displacement response of geogrid-reinforced ballast under cyclic loading. *Geotext Geomembr* 39:20–29
7. Gorbunov-Posadov MI, Malikova TA, Solomin VI (1984) *Calculation of structures on elastic base*. 3rd edn. Stroiizdat, Moscow
8. Berezantsev VG (1961) *Soil mechanics, bases and foundations*. Transgeldorizdat, Moscow

Relevant Properties of PET-Geosynthetics in Cold Regions



Viktor Poberezhnyi

Abstract Nowadays, the use of the geosynthetics in infrastructural projects is a well-known practice, which has shown its advantages worldwide. Market demands as well as technical challenges have led to the development of a wide range of geosynthetics made of different raw materials, in particular, polymer-based materials. This paper focuses on the properties of geosynthetics, made of polyester-terephthalate (PET), which are relevant to their performance in cold regions. In different researches and publications, it has been concluded that some of the main mechanical properties of polymeric geosynthetics, such as stress-strain behavior, including tendency to creep, change if the same material is exposed to different temperatures. The awareness of the properties alterations at different temperatures is indispensable for designing geosynthetic reinforced structures safely and efficiently. With regard to design procedures which are generally calibrated for areas with moderate climate, it allows to come up with more cost-effective solutions by taking into account the temperature regimes of the geosynthetic reinforced structures. The paper shows the dependency of the properties of PET-geosynthetics to different temperatures and indicates its potential utility.

Keywords Temperature-dependent properties · PET-geosynthetics · Soil temperature regimes

1 Introduction

The development of infrastructure, including rehabilitation or construction of new roads, retaining walls, bridges, landfills, and other structures, is an intrinsic demand of the economic growth also in the cold regions of the world. The utilization of the modern construction materials, such as geosynthetics, in combination with the

V. Poberezhnyi (✉)
Huesker Synthetic GmbH, Fabrikstraße 13, 48712 Gescher, Germany
e-mail: poberezhnyi@huesker.de

understanding of the working conditions of geosynthetic reinforced structures allows to implement highly cost-effective solutions even in harsh conditions of the northern regions.

Taking into account the alteration of the properties of polymeric geosynthetics in different service conditions, it is possible not only to design safer structures, but also to make them more cost-effective.

Polymeric geosynthetics are typically produced from polyester-terephthalate (PET), polypropylene (PP), polyvinyl alcohol (PVA), aramid (AR), or high-density polyethylene (HDPE). Each of them performs differently at different temperatures. For instance, investigations on HUESKER products show that strength and tensile moduli of the PET-geotextiles can increase with the temperature getting lower than the standard reference temperature of 20 °C. At the same time, the creep and the chemical sensitivity decrease. The existing data on HUESKER PET-geosynthetics behavior reveal that the structures, which are designed with the properties of the geosynthetics determined at 20 °C, but operated at the temperatures less than 20 °C, can perform with a greater margin of safety and less deformations than designed.

2 PET Behavior at Different Temperatures

The mechanical properties of polymeric materials, including creep, depend not only on type and morphology of raw materials, but also on the external physical and chemical impacts.

As a rule, such physical processes as creep do not lead to the transformation of the chemical properties of the material, i.e. the polymers can only move with respect to each other until they fully disconnect, which is considered as rupture.

Chemical reactions, such as degradation due to hydrolysis or oxidation, in its turn cause rupture or linking of the polymers. As a result, the average molecular weight alters, which eventually leads to the degeneration of the mechanical performance.

The degree of impact of physical or chemical processes is determined by the intensity of the mechanical stress as well as by the temperature at which they take place.

A number of tests made with HUESKER PET-geosynthetics, such as woven geotextiles Stablenka and geogrids Fortrac T, show an enhancement of the mechanical performance at temperatures lower than the normative reference temperature of 20 °C. Tests performed in 2004, 2007, and 2018 in TRI/Environmental, Inc. (TRI) allow to estimate the influence of the temperature on the character of creep and hydrolytic degradation. Furthermore, in order to estimate the influence of strain rate on tensile strength of woven geotextile in the selected range of temperatures, a set of tests was performed in Warsaw University of Life Science.

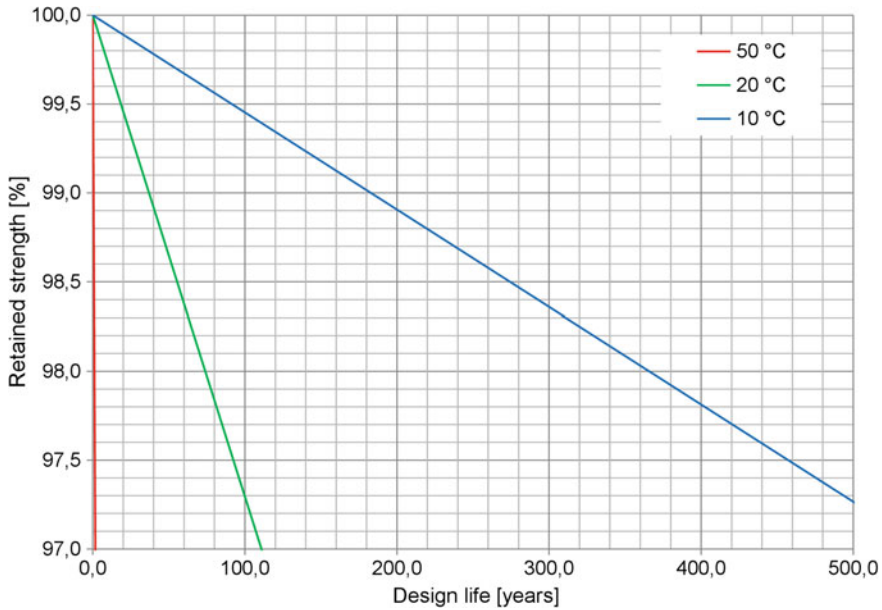


Fig. 1 Hydrolytic degradation curves for HUESKER PET-products at different temperatures

2.1 Hydrolytic Degradation

Figure 1 presents the rates of hydrolytic degradation of HUESKER PET-products at different temperatures.

The results of the tests show that the design life of the material decreases to 1.5 years if it is tested at 50 °C considering a target value of the retained strength of 97.1%. This target value corresponds to the impact of chemical degradation on the retained strength of HUESKER PET-products after 114 years of being exposed to the neutral environment. The same tests indicate that the designed life increases to more than 500 years if the material is tested at 10 °C with the same target value of the retained strength.

2.2 Creep-Rupture

Figure 2 shows the creep-rupture curves of Stablenka woven geotextile at different temperatures.

It can be concluded from the graph that the design life drops to 0.23 years if the material is tested at 50 °C at the target load level equal to 66% of the ultimate tensile strength. The design life is expected to reach 114 years if the material is tested at

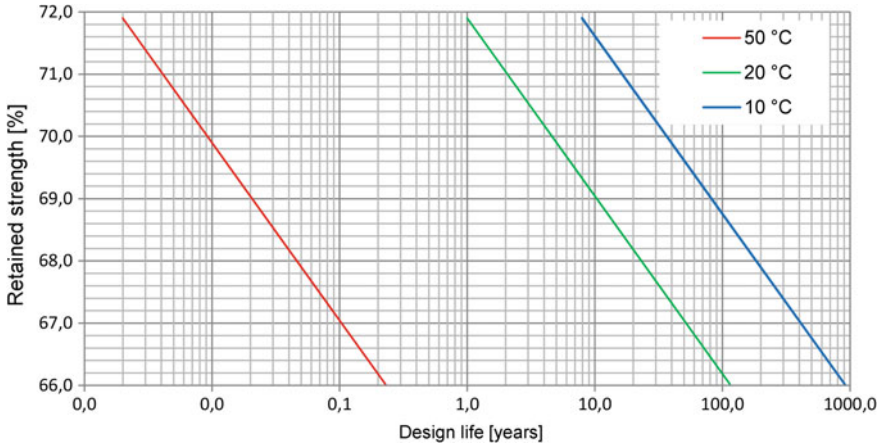


Fig. 2 Creep-rupture curves of Stablenka at different temperatures

20 °C at the load level equal to 66%. The data also confirm that the design life attains about 900 years if the same material is tested at 10 °C with the same loading ratio.

2.3 Stress-Strain Behavior

The next set of laboratory data on Stablenka and Fortrac T reinforcement products shows the stress-strain behavior alterations at different temperatures [1]. Both products perform identically in terms of stress-strain behavior.

Figure 3 presents the ratio of the ultimate tensile strength determined at various temperatures in relation to the ultimate tensile strength at reference temperature of 20 °C, which is set as 100.0%.

Figure 4 presents the ratio of the strain at rupture determined at various temperatures in relation to the strain at the ultimate tensile strength at 20 °C, which is set as 100.0%.

It can be seen that the tensile strength of PET-geosynthetics increases with the temperature getting less than 20 °C, whereas the strain at rupture decreases. At the same time, this results in a higher tensile stiffness at temperatures lower than 20 °C.

3 Soil Temperature Regimes

Long-term observations of the soil temperatures in different regions give some prospects for further investigation into the behavior of geosynthetics in geosynthetic reinforced structures.

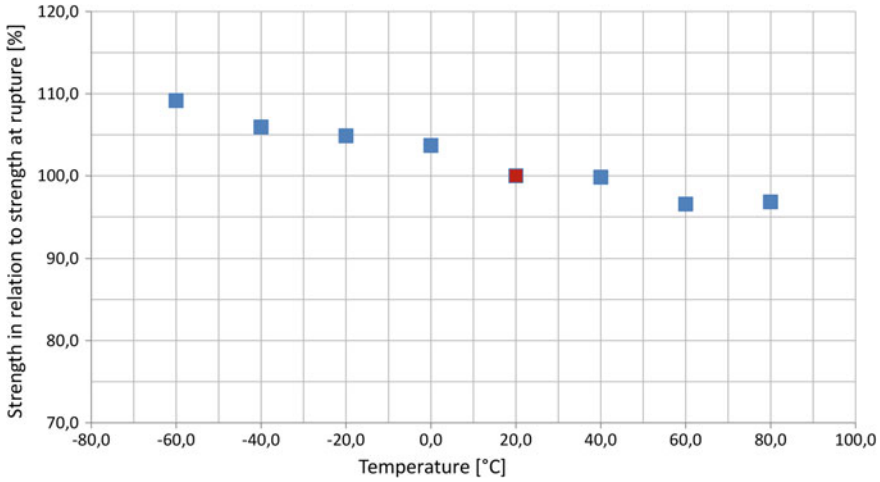


Fig. 3 Ultimate tensile strength of Stabilenka and Fortrac T determined at different temperatures in relation to the ultimate tensile strength at reference temperature of 20 °C

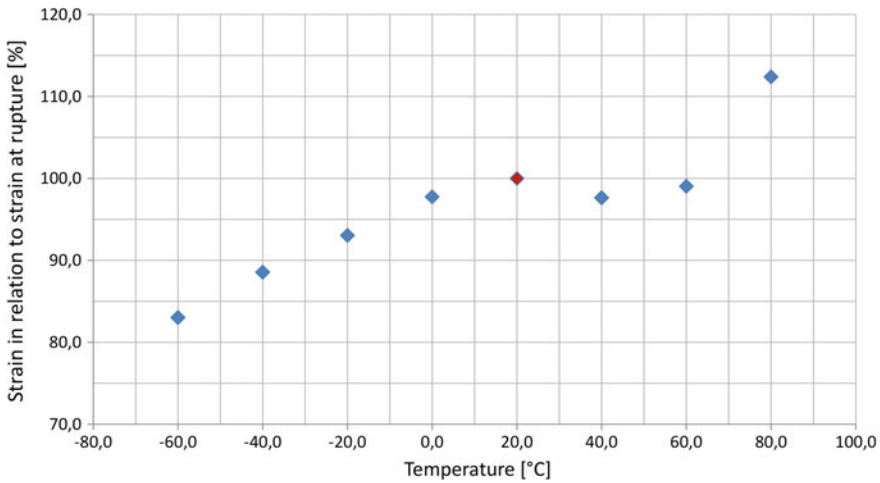


Fig. 4 Strain at rupture of Stabilenka and Fortrac T determined at various temperatures in relation to the strain at the ultimate tensile strength at reference temperature of 20 °C

In accordance with the data provided by the United States Department of Agriculture, soil temperature regimes such as mesic, frigid, cryic, and gelisol prevail in many regions [2]. Mean soil temperatures at a depth of 50 cm from the soil surface or at a densic, lithic, or paralithic contact, whichever is shallower in those soil temperature regimes do not exceed 15 °C [3]. Such soil temperature regimes imply the need

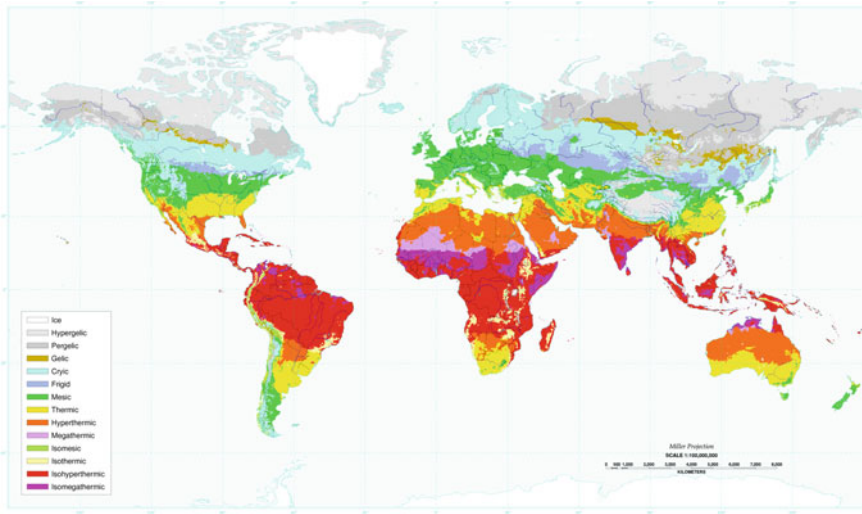


Fig. 5 The global soil temperature regimes map

for further investigation into the temperature regimes of the geosynthetic reinforced structures. Figure 5 shows the global soil temperature regimes map.

Further investigations are required due to the apparent difference in the temperature conditions of geosynthetic reinforced structures and soils, which are used for agricultural purposes. Certain impacts of different temperature conductivities, water content, presence or absence of snow cover, solar insolation, and other factors are to be considered. In addition, a significant role of climate change and global warming must be taken into account.

4 Conclusion

The paper describes the positive changes in the performance of PET-geosynthetics at temperatures less than 20 °C. The results of the tests performed on HUESKER PET-products at different temperatures show the decrease in the creep rate, higher ultimate strength, and lower strain at rupture in relation to the values measured at the reference temperature of 20 °C. The tested materials also showed less sensitivity to the hydrolytic degradation at temperatures less than 20 °C. The results are valid for the tested PET-products.

The enhanced performance of PET-geosynthetics can be developed in the geosynthetic reinforced structures in which they are operated at temperatures less than 20 °C. This can lead to better performance including a higher factor of safety, less deformations, or significantly increased allowable lifetime of already existing geosynthetic

reinforced structures. It is also possible to design more efficient structures from technical and commercial points of view having sufficient amount of data on the behavior of the geosynthetics in different temperature regimes of geosynthetic reinforced structures.

Some regions of the world are of a particular interest due to the present soil temperature regimes at which the improved properties of PET-geosynthetics can be utilized.

Further investigations are required on this topic.

References

1. Stępień S, Szymański A (2015) Influence of strain rate on tensile strength of woven geotextile in the selected range of temperature. *Studia Geotechnica et Mechanica* 37(2):57–60
2. Soil climate map, USDA-NRCS. Soil Science Division, World Soil Resources, Washington, DC
3. Soil Survey Staff (2014) Keys to soil taxonomy, 12th edn. Books Express Publishing, Washington, DC

The Technology of Mechanically Stabilized Layers for Road Structures in Cold Regions



Zikmund Rakowski and Jacek Kawalec 

Abstract The paper describes the technology of mechanically stabilized layers in road structures. Special attention is paid to weak soils extreme cold regions Theoretical approach to the application of MSL technology in such conditions supported by practical experience is presented. Special attention is paid to the distribution of load through the mechanically stabilized layer. There are described examples of structures where the influence of parameters and structure of mechanically stabilized layers are demonstrated. By proper selection of the structure, the performance of the road can be essentially influenced. Recommendations for future development and widen application are formulated.

Keywords Geogrids · Mechanically stabilized layer · Interlocking · Road structure · Weak soil · Cold regions

1 Introduction

Roads over weak soils in cold regions meet several technical problems. Building of the road in such conditions in the warm season is technically almost impossible due to problems with machinery access on site. Layers of granular materials are typical construction elements of paved and/or unpaved roads, railways and hard-standing structures. The granular layers experience only the relatively insignificant permanent load from the weight of the layers on top. When construction or in-service traffic passes (vehicles, trains, etc.), these layers are under transient increased pressure resulting in associated strain. Passing of the trafficking load induces both vertical and horizontal stress components in granular layers, where the associated horizontal

Z. Rakowski (✉)
Český Těšín, Czech Republic
e-mail: zyraki44@gmail.com

J. Kawalec
Tensar International, Český Těšín, Czech Republic

strains have a radial distribution. The stabilization is defined as the beneficial consequence on the serviceability of an unbound granular layer via the inhibition of the movement of the particles of that layer under applied load [1–3]. Load distribution through different structures with and without mechanically stabilized layer (MSL) is analysed and evaluated from the point of view of roads over weak soils in cold regions. This paper describes continuation of earlier published results of the research [4–6].

2 Actual Concept of Mechanically Stabilized Layer (MSL)

The interlock of aggregate is the key mechanism involved in the stabilization [5–7]. During the placement and compaction of a granular layer over a geogrid, the aggregate partially penetrates into the geogrid apertures. Abutting of grains against ribs leads to their immobilization (Fig. 1) The inhibition of the movement of the grains under load is the essential effect and the principle of mechanical stabilization.

When wheels are passing over granular layer, the rotation of loading forces is observed in both interlocked and untouched grains. But in case of the presence of the geogrid, their ribs are also involved in force distribution due to abutting of grains (Fig. 2).

The difference in mechanism of loading in not interlocked and interlocked grains is shown in Fig. 3. Shear displacements between grains are almost completely restricted. The system is much stiffer and performs as quasi rock. The scheme on Fig. 2 shows that the stone grain is properly locked in the aperture and when loaded abutting forces are becoming active. It is not any more discrete system of granular material and geogrid but a kind of composite performing like stiff continuum. By that the system—composite—represents completely new quality which is not a simple sum of properties of components. It is called grain-geogrid-composite (GGC).

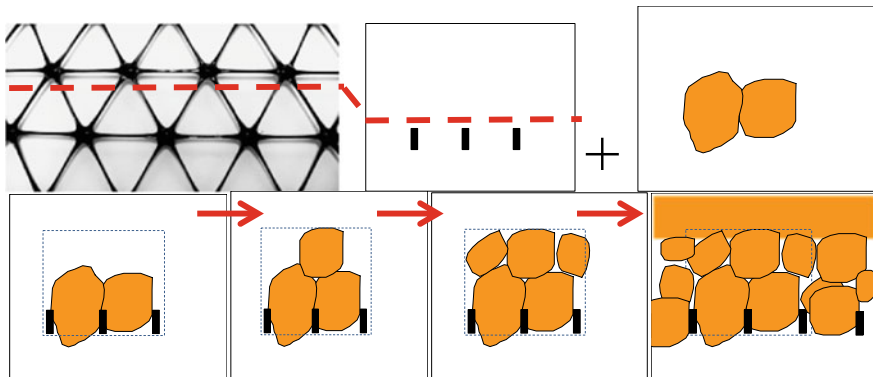


Fig. 1 Process of stone grains immobilization in geogrid aperture

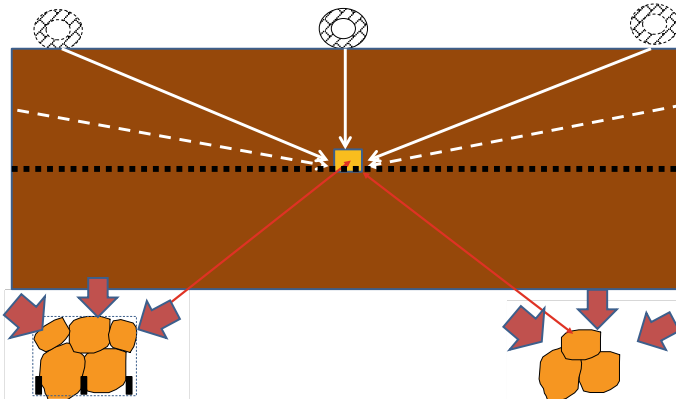


Fig. 2 Rotation of loads during wheel passing in interlocked (left) and not touched grains (right)

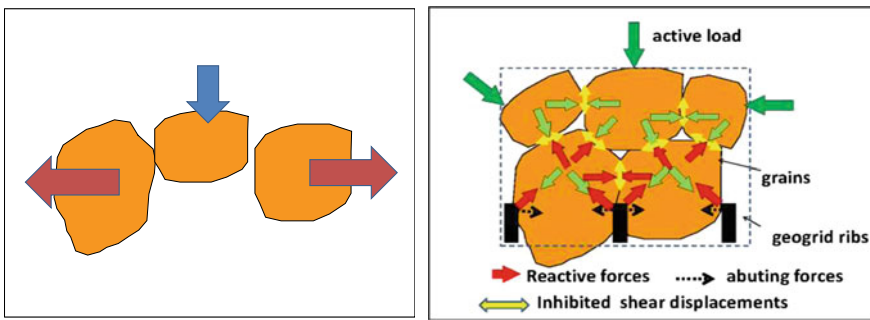


Fig. 3 Difference in mechanism of loading in not interlocked (left) and interlocked (right) grains [5, 6]

Mechanically stabilized layer should be characterized, namely by its thickness, deformation modulus and shear strength, namely in the vertical direction. It was confirmed, e.g. [3, 8, 9], that fully immobilized zone can achieve the thickness $h_i = 7-10$ cm. In case of hexagonal geogrid, it can be even up to 15 cm; it means few times D_{max} . According to [5, 6], the effect of interlocking is decreasing with the distance from the geogrid.

The layer mechanically stabilized by stiff geogrid is vertically not homogenous with different intensity of mechanical immobilization of grains. Three different zones are distinguished [5, 6]: immobilized/stiffened zone GGC, transition zone and not influenced zone (Fig. 4).

Increasing the thickness of granular layer is a typical measure for traditional way of improving the layer stability. In case of mechanically stabilized layer, simple increasing of the thickness should be applied carefully as by this just not influenced zone could be increased (Fig. 5) what may lead to worse mechanical properties of the whole layer in fact.

Fig. 4 Zonality of the MSL

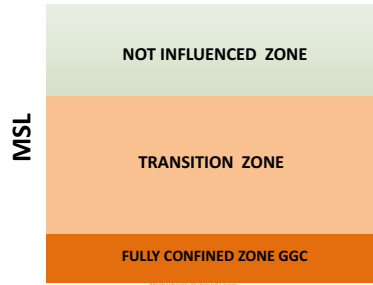
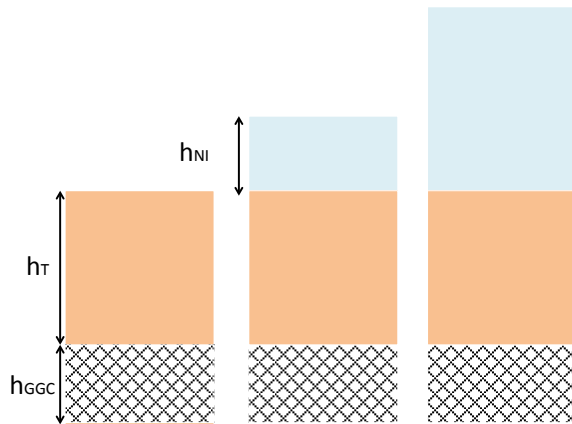


Fig. 5 Zonality of mechanically stabilized layer depending on the total thickness of the layer



3 MSL Potential for Roads on Weak Soils in Cold Regions

Roads over weak soils in cold regions meet several technical problems. Building of the road in such conditions in the warm season is technically almost impossible due to problems with machinery access on site. Of course, then the final stability of structure is next important one. Often the first problem is approached by shifting construction period to winter season when frozen ground enables construction works. But when the thawing period comes, the overall stability can be problematic. One of the promising solutions could be the application of mechanically stabilized layer (MSL) in road structure. The interlocking and resulting immobilization of grains in stiff geogrid limit their vertical and horizontal displacements and so stabilize the layer. Also, mixing of granular material with soft subsoil is prevented effectively [4, 10–13]. Other fundamental contribution of the MSL is effective load distribution.

Load distribution through standard (unconfined) crushed stone may be typically considered by angle of 35° . Loaded zone on the base of the layer is $d_1 = 0.7 * h_1$ (Fig. 6) [4, 14].

Let us have mechanically stabilized layer of thickness $h_2 = h_1/2$. Load distribution through MSL is more complex due to nonlinearity in transition zone. Generalized

Fig. 6 Load distribution through standard layer

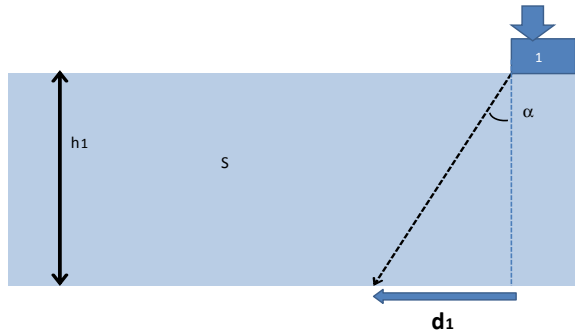
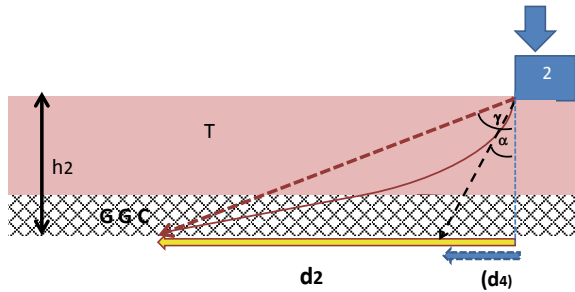


Fig. 7 Load distribution through MSL, $h_2 = h_1/2$



angle of total distribution is considered as 70° [5]. Loaded zone on the base of the layer is $d_2 = 2.75 * h_1/2$ (Fig. 7).

The next example shows combined structure when bottom half of the layer is formed by MSL and upper one by unconfined standard granular material (Fig. 8). In such a case, the width of load distribution zone is $d_3 = d_2 + d_4$ (Fig. 8).

The last example shows the structure formed by double MSL (Fig. 9). The load zone $d_5 = 2.75 * h_1$.

Fig. 8 Load distribution through MSL+ unconfined layer

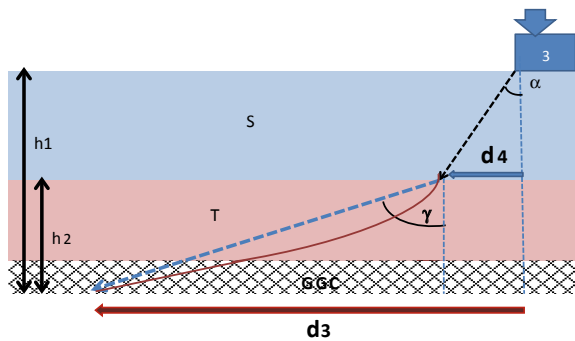
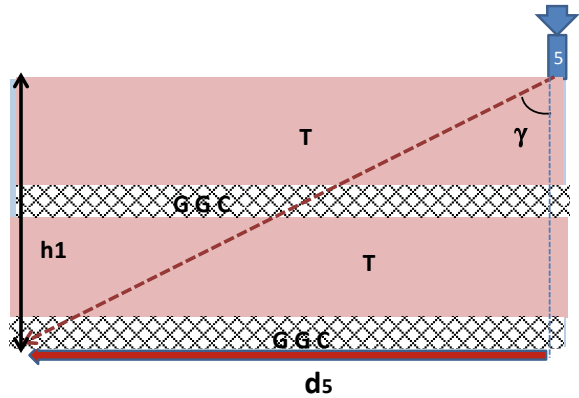


Fig. 9 Load distribution through double MSL



4 Discussion

Based on the results shown above, we can evaluate and compare the efficiency of different presented types of structures.

- A comparison of the first two structures shows that the ratio is $d_2/d_1 = 1.96$. It means that even just half thickness of the MSL is almost two times more efficient than full thickness standard layer.
- The next ratio is $d_3/d_2 = 1.25$. It means that adding above MSL the same thickness of unconfined granular material is relatively less efficient.
- Although comparing d_3/d_1 gives the ratio 2.4, so that structure, it is still very good improvement.
- Comparing d_5/d_1 gives the ratio 3.92. It is the most efficient structure from all presented ones.

In principle, there are two types of benefits from using MSL as follows:

1. Reasonable savings of granular material due to smaller thickness of MSL comparing with standard layer.
2. Reasonable increase of bearing capacity when applying the same thickness in both cases can be important, e.g. when transporting of heavy equipment is considered.

Practical experience with the installation of stiff geogrids in the extreme cold weather confirmed the possibility to use this technology already (Fig. 10).

Fig. 10 Installation of geogrids in temperature – 53°. Yakutia, Russia (courtesy of Tensar International)



5 Conclusion

Mechanically stabilized layer confirms its high potential also for roads in cold regions. All benefits provided by geogrid to aggregate known from other applications are achievable in low temperatures.

References








1. Cook J, Dobie M, Blackman D (2016) The development of APT methodology in the application and derivation of geosynthetic benefits in roadway design. In: The roles of accelerated pavement testing in pavement sustainability. Springer, Cham, pp 257–275
2. EOTA non-reinforcing hexagonal geogrid for the stabilization of unbound granular layers by way of interlock with the aggregate. EOTA report TR41 (2012)
3. Fischer S, Szatmari T (2016) Investigation of the geogrid-granular soil combination layer with laboratory multi-level shear box test. In: Proceedings of EUROGEO 6 conference special sessions on “Geosynthetics in road construction”, Ljubljana, Slovenia
4. Jenner CG, Watts GRA, Blackman DI (2002) Trafficking of reinforced, unpaved subbases over a controlled subgrade. In: Geosynthetics: state of the art-recent developments. Proceedings of the seventh international conference on geosynthetics, vol 3. 7-ICG, Nice, France
5. Rakowski Z (2017) An attempt of the synthesis of recent knowledge about mechanisms involved in stabilization function of geogrids in infrastructure constructions. *Procedia Eng* 189:166–173
6. Rakowski Z, Kawalec J, Kwiecień S (2019) The applicability of recent mechanically stabilized granular layer concept in ME pavement design, chap 14. Springer Nature America, Inc, New York
7. Byun YH, Tutumluer E (2018) Local stiffness quantification of geogrid stabilized aggregates in relation to deformation behavior. In: Geo Shanghai international conference. Springer, Singapore, pp 109–114
8. Grygierek M, Kawalec J (2017) Selected laboratory research on geogrid impact on stabilization of unbound aggregate layer. *Procedia Eng* 189:484–491
9. Konietzky H (2002) Numerical modeling in micromechanics via particle methods. In: International PFC symposium, Gelsenkirchen, Germany, CRC Press, Boca Raton

10. Horníček L, Rakowski Z (2018) The mechanically stabilized granular layers—an effective solution for tunnel projects. In: International congress GEOMEAST 2018, Cairo, Egypt
11. Konietzky H, te Kamp L, Groeger T, Jenner C (2004) Use of DEM to model the interlocking effect of geogrids under static and cyclic loading. In: Numerical modelling in micromechanics via particle methods, Balkema, Leiden, Netherlands, pp 3–12
12. Kwon J, Tutumluer E, Al-Qadi I, Dessouky S (2008) Effectiveness of geogrid base-reinforcement in low-volume flexible pavements, pp 1057–1064. In: GeoCongress 2008: geosustainability and geohazard mitigation
13. Kwon J, Tutumluer E (2009) Geogrid base reinforcement with aggregate interlock and modeling of associated stiffness enhancement in mechanistic pavement analysis. *Transp Res Rec J Transp Res Board* 2116:85–95
14. Robinson WJ, Tingle JS, Norwood GJ, Wayne MH, Kwon J (2018) Performance of multi-axial geogrid stabilised flexible pavements. In: Proceedings of the institution of civil engineers—ground improvement, pp 1–32
15. Giroud JP (2009) An assessment of the use of geogrids in unpaved roads and unpaved areas. In: Proceedings of the jubilee symposium polymer geogrid reinforcement. Institution of Civil Engineers, London, UK, pp 23–36
16. Giroud J, Han J (2016) Mechanisms governing the performance of unpaved roads incorporating geosynthetics. *Geosynthetics* 34(1):22–36
17. Matys M, Baslik R (2004) Study of interlocking effect by the push test. In: Proceedings of the 3rd Asian regional conference on geosynthetics GEOASIA2004, Seoul, pp 341–348
18. Qian Y, Tutumluer E, Mishra D, Kazmee H (2018) Triaxial testing and discrete-element modelling of geogrid-stabilised rail ballast. In: Proceedings of the institution of civil engineers—ground improvement, pp 1–22
19. Stahl M, Konietzky H, Te Kamp L, Jas H (2014) Discrete element simulation of geogrid-stabilised soil. *Acta Geotech* 9(6):1073–1084
20. Tutumluer E, Huang H, Bian X (2012) Geogrid-aggregate interlock mechanism investigated through aggregate imaging-based discrete element modeling approach. *Int J Geomech* 12(4):391–398
21. Tutumluer E (2016) Geogrid-aggregate interlock mechanism investigated. Special session on “Geosynthetics in road construction” EUROGEO 6, Ljubljana, Slovenia
22. Zornberg J (2016) Stabilization of roadways using geosynthetics. Special session on “Geosynthetics in road construction” EUROGEO 6, Ljubljana, Slovenia
23. Zornberg JG (2017) Functions and applications of geosynthetics in roadways. *Procedia Eng* 189:298–306

**Modelling, Design, Construction and
Exploitation of Railway and Highway
Subgrade**

Numerical Simulation of the Work of a Low-Settlement Embankment on a Pile Foundation in the Process of Permafrost Soil Thawing



Sergey Kudryavtsev , Tatiana Valtseva , Semen Bugunov , Zhanna Kotenko , Vladimir Paramonov , Igor Saharov  and Natalya Sokolova 

Abstract The article presents numerical modeling techniques, calculations, and recommendations for rational roadbed structures in the zone of permafrost and soft soils in the independent railway line construction areas that are in the zone of influence of the constructed reservoir in the Far East Federal District of Russia, taking into account constructional measures that reduce the intensity and uneven deformation of the defrost base. The usage of a geomaterials in the structure allows to lessen considerably the volume of expensive hard mineral volcanic filling of high quality. Numeric modeling of the structure behavior was done using a programming geotechnical complex, an “FEM model.” This allowed to give a quantitative and qualitative assessment of freezing and thawing processes in conditions of annual cycle construction.

Keywords Permafrost soils · Deformations · Integral grid

1 Engineering-Geological Structure of a Considered Site

The roadbed on permafrost high-temperature soils of the reorganization of a section of the railway line that falls into the zone of influence of the reservoir of the Bureyskaya HPP is designed according to the second principle—with the assumption of thawing of the base from the weight of the embankment [1–3].

S. Kudryavtsev · T. Valtseva (✉) · S. Bugunov · Z. Kotenko
Far Eastern State Transport University, Khabarovsk, Russia
e-mail: vtu25@mail.ru

V. Paramonov
Saint-Petersburg State Transport University, Saint-Petersburg, Russia

I. Saharov
Saint-Petersburg State University of Architecture and Civil Engineering, Saint-Petersburg, Russia

N. Sokolova
Financial University Under the Government of the Russian Federation, Moscow, Russia

The roadbed is designed for winter dumping conditions, with the soil of the active layer completely frozen; therefore, the widening of the embankment for the possibility of filling after full thawing is 1.5 total precipitation in each direction [4–6].

The width of the roadbed on the straight sections of the road is taken as 5.8 m for embankments filled with rocky pebbles and rocky silt wood and low-strength sandstone draining. The width of 6.5 m is taken in the level of the profile edge, and 5.8 m is the level of the design edge, which is 0.35 m (0.15 m drain prism + 0.20 m difference in ballast thickness) higher than the profile, and in the curves, the subgrade is broadened from the outside according to SNiP 32-01-95.

Gentle flat watershed areas are mainly represented by peatlands.

Ground cover is formed by moisture-loving mosses. The surface of the peatlands is cut up by subtle sikes, frost knobs, thermokarst-collapsed funnels and lakes. Approaches to the sikes are very swamped, overgrown with sedge and a thick bump.

The climate of the region is harsh, extreme continental, formed under the influence of the Asian continent and the Pacific Ocean, thus preserving the monsoon character. The influence of the continent manifests itself mainly in the winter, when dry and heavily cooled continental air penetrates the study area.

Soil temperature, as well as air temperature, is determined by climate-forming factors of a large scale: atmospheric circulation and radiation regime. In addition, the thermal conditions of the soil, even more than the air temperature, are influenced by local conditions: microrelief, slope steepness, the mechanical and chemical composition of the soil itself, vegetation, groundwater level, and human activity.

The actual depth of seasonal freezing of soils on the basis of a full-scale inspection of soil samples during drilling varies widely from 0.6 to 3.5 m, depending on the penetrated soils. The greatest depth of seasonal freezing is recorded in coarse-grained soils and reaches 3.0–3.5 m.

The area of research is located in the zone of discontinuous distribution of permafrost. There are taliks in the area, both of hydrogeological and hydrological origin, as well as taliks of radiation genesis. The first are developed in the valley of the river Bureya and in the floodplain parts of its tributaries Adnikan and Dublikan with the river Soloni. The latter are confined to the slopes of the southern exposition and to areas composed of rocks that well infiltrate rainwater. Taliks are developed not only in the valleys, but also in the watersheds. The thickness of the permafrost soil varies from 25 to 60 m. The temperature of the permafrost varies from -0.7 to -1.8 °C.

In the valleys of the rivers Adnikan, South Elga, Dublikan, and Soloni, marshes of the lowland type are widely developed.

The length of the swamps along the bypass road reaches 30%, and the peat thickness is 2–3 m, averaging 1 m. In terms of subsidence, permafrost peat belongs to the W and IV subsidence categories.

2 Deformations of an Embankment

As a result of the influence of the reservoir of the Bureyskaya HPP and the fact that permafrost rocks with taliks are widespread in the study area, permafrost is in unstable equilibrium and is subject to the formation of thermokarst and degradation. The presence of high bogs developed on the aboriginal slopes and watersheds, as well as the heterogeneity of the soil surface, and therefore its temperature can vary greatly over a distance of even several meters, causing deformation of the railway embankment [7–9]. Figures 1 and 2 show the sections of the railway embankment on thawing permafrost with measures to stabilize deformations.

In this regard, it is necessary to develop structures of the railway embankment and the roadbed to ensure the safety and uninterrupted movement of trains [6, 10].

3 Methodology of Geotechnical Modeling of the Subgrade Thawing on Weak Grounds

This method of numerical modeling was used to determine the thermophysical process of the ground. The FEM models can to model condition of structures in its stress and strain state, the processes of freezing and thawing and any other necessary parameters of structures. This complex was developed by the geotechnical



Fig. 1 Deformations of the railway embankment on thawing permafrost soil



Fig. 2 Construction of anti-deformation measures of the railway embankment on thawing permafrost

engineers. Module «Termoground» is one of the main parts of all complex of «FEM models» software, which can define the thermophysical parameters of foundations and structures.

The thermophysical processes described in the work are described in the work of such authors as Ulitckiy et al. [11].

The main parameters are the air temperature and the heat exchange conditions. It depends on the solar radiation, wind conditions, and many other factors. Main parameters are taken in accordance with the SR 25.13330.2012—Permafrost Foundation Engineering Standards [12, 13].

4 Heat-Engineering Calculation of Bulk on a Permafrost Base

The transverse profile of the simulated embankment height $H = 2.7$ m is located on a slope with a cross-slope of 64%.

At the base of the embankment, a moss-vegetative layer with a thickness of up to 0.3 m lies down; below, sandy loam occurs with a thickness of up to 1.2 m; below lies soft plastic loam thickness up to 1.4 m; the loam of permafrost is layered below with layered cryo-textures up to 1.2 m below; under it lies a sandstone of low-strength permafrost massive cryo-texture. The design scheme of the embankment is shown in Fig. 3 (3D model).

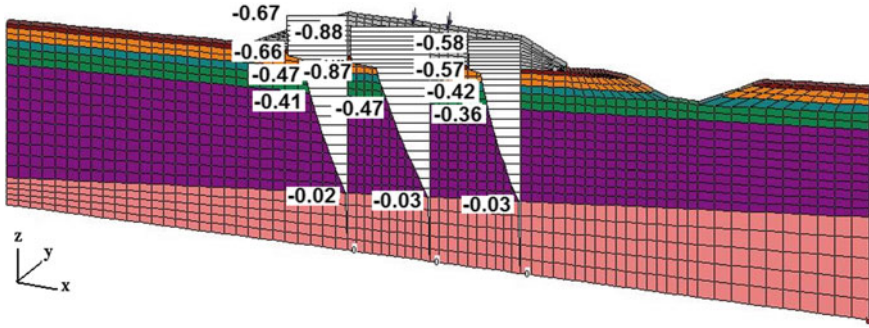


Fig. 5 Diagrams of vertical deformations of the body of the mound and grounds for the initial period of operation

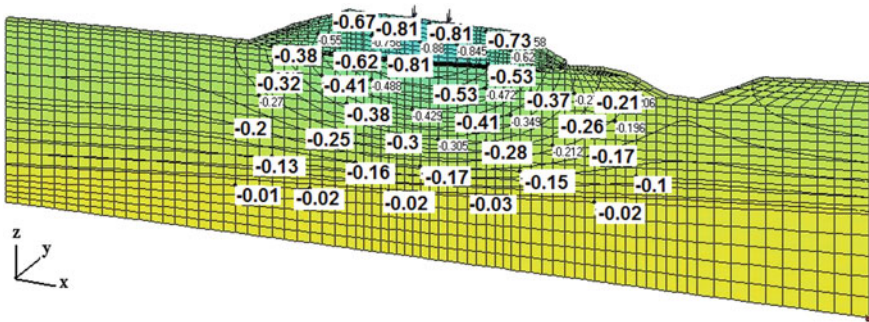


Fig. 6 Isolines of vertical deformations of the body of the mound and the grounds for the initial period of operation

of the sediment values fall on the compression of the moss-vegetative layer, sandy loam, and soft plastic loam [14–16].

Due to the fact that the embankment is located on a slope, the basis of the slope, especially in the moss-vegetation layer and sandy loam in the lower part, develops horizontal deformations of more than 21 cm (Fig. 7, 3D model).

To reduce the vertical and horizontal deformations of this embankment, a construction of a low-cage embankment (Fig. 8, 3D model) is proposed, which includes:

1. Construction of a pile field of reinforced concrete piles 11.0 m long, 20 × 20 cm in cross section, 2 m in length, and 1.6–2.5 m in diameter across the embankment for transferring train load and from embankment weight to a low-compressible layer of low-density cryogenic sandstone;
2. To evenly distribute the train load and the weight of the embankment on the piles, it is advisable to install two layers of a Tensor geogrid over the heads of the piles over the entire width of 21.0 m and a height of up to 0.7 m. The length of the transition section to the bridge should be at least 100 m finally determined by local conditions.

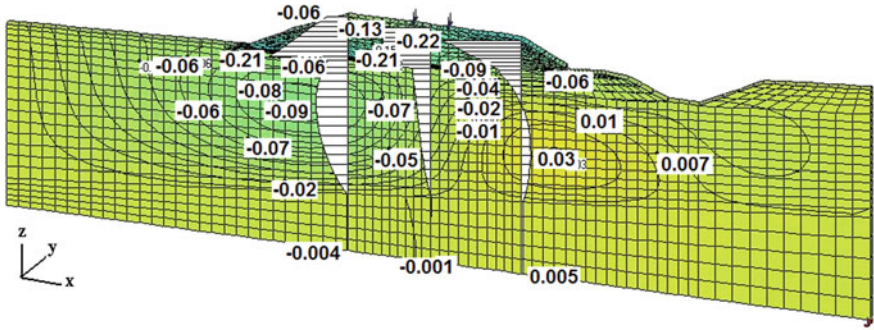


Fig. 7 Isolines and diagrams of horizontal deformations of the body of the embankment and the bases for the initial period of operation

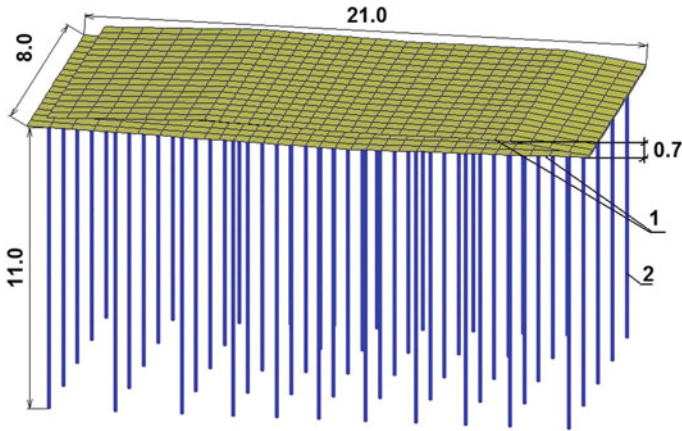


Fig. 8 Construction of a low-settlement embankment on the approaches to the bridges: 1—two layers of Tensor geogrid; 2—reinforced concrete piles 11.0 m long and a section of 20 × 20 cm

The vertical deformations of the embankment with this design of the low-settlement embankment device will be from 21 to 71 mm in the initial period of operation, that is, the sediment reduction will be at least 92% (Fig. 9, 3D model).

With the given construction structure of a low-mound embankment, horizontal deformations will reach up to 15 mm, i.e., the reduction will be up to 93% (Figs. 10, 11, 3D models).

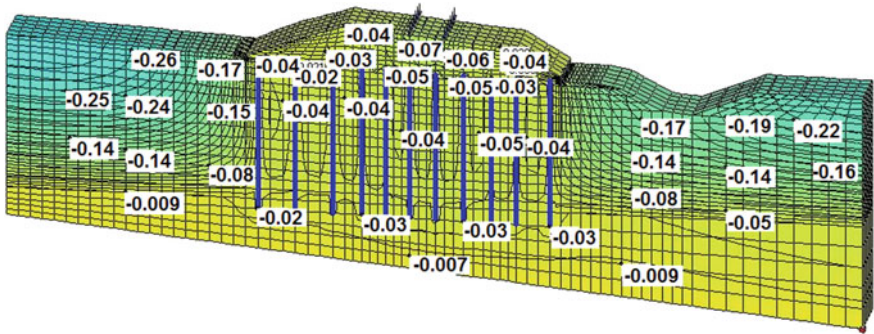


Fig. 9 Isolines of the vertical deformations of the body of the low-settlement embankment and foundations for the initial period of operation

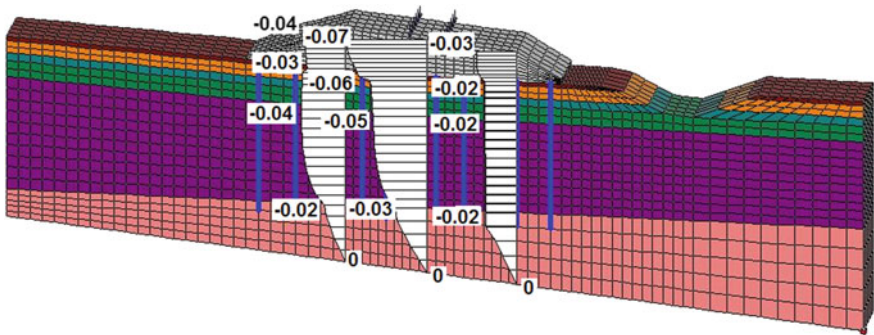


Fig. 10 Diagrams of vertical deformations of the body of the low-settlement embankment and bases for the initial period of operation

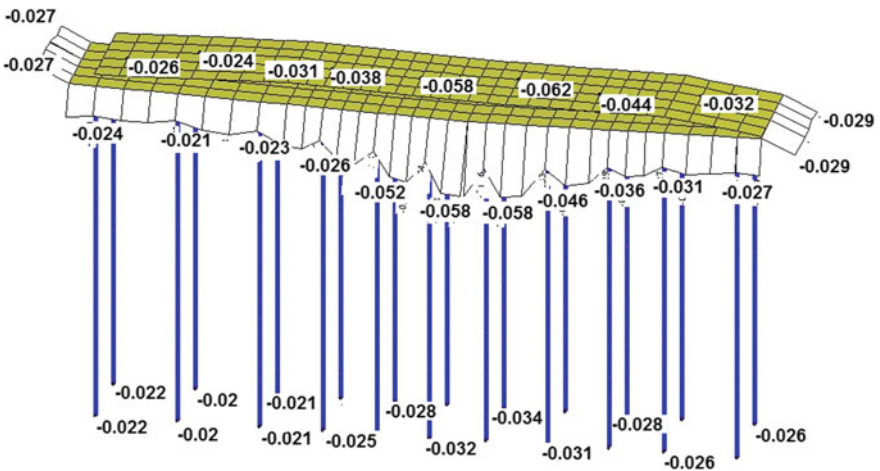


Fig. 11 Diagrams of vertical deformations of the structure low-mass embankment for the initial period of operation

6 Conclusions

1. The actual depth of seasonal soil freezing on the basis of a full-scale inspection of soil samples during drilling varies widely from 0.6 to 3.5 m, depending on the penetrated soils. The greatest depth of seasonal freezing is recorded in coarse-grained soils and reaches 3.0–3.5 m.
2. It is advisable to design the subgrade and foundations of artificial and transport structures according to the principle—with the degradation of permafrost.
3. The software package “Termoground” allows to solve three-dimensional thermophysical and stress–strain.
4. The heat-engineering calculation is performed in the annual cycle of freezing and thawing. In subsequent years, the depth of thawing will increase due to changes in the heat-engineering parameters of the base soils prone to compressive train load and embankment weight.
5. Deflected mode calculation of the embankment in the process of thawing from train load and embankment weight was made in the initial period of operation and does not take into account the subsequent cyclicity of the trains. Therefore, the final draft will be 20–30% more than calculated.
6. To exclude horizontal and vertical deformations of embankments on thawing permafrost soils, it is advisable to build pile foundations on a grillage from a biaxial integral grid on approaches to bridge crossings. The developed design reduces the vertical and horizontal deformations of the embankment by more than 90%.

References

1. Kudryavtsev S, Berestianyi I, Goncharova E (2013) Engineering and construction of geotechnical structures with geotechnical materials in coastal arctic zone of Russia. In: Proceedings of the international offshore and polar engineering conference, pp 562–566
2. Paramonov VN, Sakharov II, Kudryavtsev SA (2016) Forecast the processes of thawing of permafrost soils under the building with the large heat emission. In: MATEC web of conferences 2016, “15th international conference “topical problems of architecture, civil engineering, energy efficiency and ecology—2016”, TPACEE 2016”
3. Kazharsky AV, Valtseva TY, Goncharova ED, Kudryavtsev SA, Kotenko ZI (2016) Thermo-physical feasibility of railway embankment design on permafrost when projecting side tracks. In: 15th international scientific conference “underground urbanisation as a prerequisite for sustainable development”, vol 165, pp 1080–1086
4. Maleev DYu, Tsvigunov DG, Goncharova ED, Kudryavtsev SA (2016) Disalignment of railroad poles as dynamic effect of rolling stock. In: 15th international scientific conference “underground urbanisation as a prerequisite for sustainable development”, vol 165, pp 1858–1865
5. Goncharova ED, Mikhailin RG, Kudryavtsev SA, Kotenko ZI, Grigoriev DO (2017) Disalignment of railroad poles as dynamic effect of rolling stock. In: MATEC web conference international science conference SPbWOSCE-2016 “SMART City”, vol 106

6. Sakharov II, Paramonov VN, Kudryavtcev SA (2016) Strengthening thawed permafrost base railway embankments cutting berms. In: MATEC web of conferences 15. Cep. "15th international conference "topical problems of architecture, civil engineering, energy efficiency and ecology—2016", TPACEE 2016"
7. Kazharsky AV, Goncharova ED, Kudryavtcev SA, Kotenko ZI, Grigoriev (2017) Embankment on permafrost Eastern polygon of Baikal-Amur Mainline. Embankment on permafrost Eastern polygon of Baikal-Amur Mainline. PROENG394962 Journal Procedia Engineering, pp 774–782
8. Valtseva TY, Goncharova ED, Kudryavtcev SA, Kazharsky AV (2017) Strengthening design for weak base using geomaterials on "Amur" automobile road section. In: International scientific conference energy management of municipal transportation facilities transport EMMFT 2017, advances in intelligent systems and computing. Springer International Publishing AG, ISSN: 0038-0741, pp 145–153
9. Kovshun VS, Mut AD, Kudryavtcev SA (2017) The investigation of freezing and thawing processes of metal foundations ground of pipelines. In: International scientific conference energy management of municipal transportation facilities transport EMMFT. Advances in Intelligent Systems and Computing. Springer International Publishing AG, ISSN: 0038-0741, pp 953–961
10. Zhussupbekov A, Shakhmov Z, Lukpanov R, Tieulena G, Kudryavtcev SA (2017) Frost dept monitoring and evaluation of frost susceptibility at soil ground of Kazakhstan. In: 19th ICSMGE—19th international conference on soil mechanics and geotechnical engineering. COEX, vol 2. Seoul, Korea. Proceedings 2017, pp 1455–1458
11. Ulitckiy VM, Sakharov II, Paramonov VN, Kudryavtcev SA (2015) Calculation of the "base—construction" system during freezing and thawing of soils using the "Thermoground": basis, foundations and soil mechanics № 5, pp 3–7
12. Bugunov SA, Pogulyaeva EV, Kudryavtcev SA, Kotenko ZI, Grigoriev DO (2018) Construction of high-rise buildings in the Far East of Russia. In: E3 web of conferences 33
13. Berestianyi YB, Kudryavtsev SA, Kazharskyi AV, Goncharova ED (2014) Study of moisture migration in clay soils considering rate of freezing. In: The 10th international symposium on permafrost engineering in cold regions. Sciences in Cold and Arid regions 2014. № 6, p 474
14. Berestyanyy YB, Kudryavtcev SA, Goncharova ED, Valtseva TY, Mikhailin RG (2014) Motorway structures reinforced with geosynthetic materials in Polar Regions of Russia. In: The 24rd international off-shore (ocean) and Polar engineering conference 2014, pp 502–506
15. Zhussupbekov AZ, Kudryavtsev SA, Arshinskaya LA, Valtseva TU, Berestyanyy UB (2008) Developing design variants while strengthening roadbed with geomaterials and scrap tires on weak soils. In: Proceedings of the international workshop on scrap tire derived geomaterials—opportunities and challenges, IW-TDGM 2007, pp 171–178
16. Bugunov SA, Pogulyaeva EV, Kudryavtcev SA, Kotenko ZI (2018) Investigation of light embankment on weak soils. In: MATEC web of conferences 2018, vol 193

Experimental Evaluation of the Deformational Calculation Method of Foundations for Overpasses of High-Speed Railways



Vladimir Ulitskiy , Sergey Alekseev  and Stanislav Kondrat'ev 

Abstract One of the most important issues of the foundation design for overpasses of high-speed railways is consideration of soil strata heterogeneity (along the track line) influence on differential foundation soil settlements. The possibility of their limiting is directly related to the degree of conformity of predictable (calculated) and actual (obtained) values of foundation soil settlement. The purpose of the article is to optimality substantiation of using the predetermined soil settlement criterion (deformational calculation method) for the design of foundations for overpasses of high-speed railways, because this method allows decreasing the values of differential soil settlements to minimum. The following research tasks were solved: experimental studies on deformation of soil under the model of a shallow foundation (the model tests); comparison of experimentally measured and calculated soil settlements using the deformational calculation method and the numerical simulation; comparison of experimentally measured and calculated soil settlements using the proposed method and the most common approximate (“engineering”) methods; economic efficiency substantiation of the deformational calculation method. Based on the obtained results, the proposed method can be considered as promising for solving problems associated with the design of foundations for overpasses of high-speed railways.

Keywords Soil settlement · Overpass foundation · High-speed railways

1 Introduction

The solution of tasks, related to transportation process, cannot be achieved without railway infrastructure construction. In the construction of the high-speed railways (HSR) on overpasses [1], the issue of foundation soil deformation becomes particularly important. Contemporary regulations (e.g., [2]), concerning the HSR design, limit the values of soil settlement in the range of 2–3 cm. These strict limitations cause

V. Ulitskiy · S. Alekseev · S. Kondrat'ev (✉)
Emperor Alexander I St. Petersburg State Transport University, Saint Petersburg, Russia
e-mail: kondratev.s@yandex.ru

© Springer Nature Singapore Pte Ltd. 2020
A. Petriaev and A. Konon (eds.), *Transportation Soil Engineering in Cold Regions*,
Volume 2, Lecture Notes in Civil Engineering 50,
https://doi.org/10.1007/978-981-15-0454-9_10

the development of foundation calculation method, which is based on the criterion of soil deformation [3].

The proposed solution is connected with using the predetermined soil settlement criterion, with reference to which an appropriate method for soil deformation calculation (relating to “engineering” (approximate) group of methods) is developed. Deformational calculation method prescribes the required values of soil settlement at the initial design stage for a number of foundations and allows taking into account the influence of soil strata heterogeneity along the course of track on differential foundation settlements of overpasses (angles of break-in profile) and to minimize it [4]. In order to set the value of soil settlement for a number of foundations, it is necessary to consider the nonlinear soil deformation behavior. This circumstance allows transferring greater pressure to the foundation soil or reducing foundation sizes and, therefore, allows designer to make more cost-effective decisions.

An important aspect of the proposed method application is an assessment of disagreement between predicted (theoretical) and obtained (actual) values of soil settlement. Thus, the purpose of the article is to optimality substantiation of using the deformational calculation method for foundations design with respect to high-speed railways’ overpasses.

2 Experimental Studies on Deformation of Soil Under the Model of a Shallow Foundation (The Model Tests)

In order to assess the reliability of the proposed method, it is necessary to compare a variety of soil settlement values, which are obtained by different methods in specific conditions. The theoretical (calculated) values of soil settlement are not informative in themselves; therefore for estimation of their deviations, it is necessary to consider the experimental data as a “standard of reference.”

Due to technical difficulties [5] (and often the impossibility) of in situ testing with the desired degree of reproducibility, concerning foundation soil deformation in the condition of reaching its limit state, it was carried out the test series in laboratory trays (the models’ tests). A necessary condition for the tests is compliance with the modeling conditions, which are presented in publications [6–9]. It is allowed the identity of tray soil characteristics to their natural values; therefore, the scale factors γ and φ are taken to be one. Consequently, in order to similarity of distribution of stresses and shapes of the limit state zones in soil below the foundation model, and in kind, it is necessary to provide the proportionality of the most characteristic foundation dimension and an actual loading.

The tests were carried out in a cylindrical tray. The foundation soil in the tray was represented by slightly wet fine sand ($\varphi = 35^\circ$), which was compacted layer by layer before each test on average to $\gamma = 13.6 \text{ kN/m}^3$. In the framework of the research, round rigid foundation models with the diameter of 7.5 and 10 cm were used. The size of the tray exceeded the diameters of the models by six–seven times. Details of

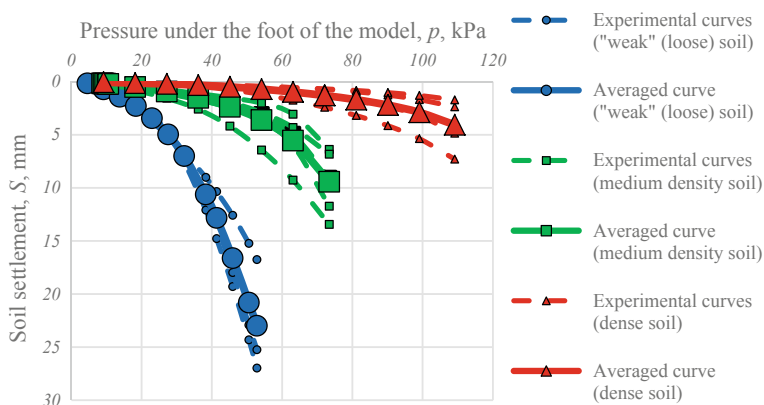


Fig. 1 Actually accepted and averaged experimental dependencies $S = f(p)$

the tests are presented in the work [3]. After elimination of gross errors by Grubbs outlier test [10], the experimental dependencies “soil settlement—pressure under the foot of the model” ($S = f(p)$) were obtained for three test series with different soil density. Actually accepted and averaged dependencies $S = f(p)$ are presented in Fig. 1.

3 Comparison of Experimentally Measured and Calculated Soil Settlements Using the Deformational Calculation Method and the Numerical Simulation

The conditions of the experiments were recreated for the numerical simulation of the laboratory test series. The simulation was carried out in tridimensional statement using the Mohr–Coulomb model [11–13]. The cylindrical shape of the tray was taken into account using the equivalent square of the design area. The finite element mesh qualitatively is described as fine. The foundation model was considered as a plate element. The force transfer to it was carried out by means of step-by-step loading to the limit load (the bearing capability of soil), which was established by the results of the experiments. The dependencies of $S = f(p)$ for different series of the soil tests, obtained experimentally, as a result of numerical simulation and by the proposed method, are presented in Figs. 2, 3, and 4.

Thus, as a result of comparison, the following is established: the deviation of the proposed method from all experimental series averaged 6.3% (minimum—4.3% maximum—7.6%), the numerical simulation—15.5% (minimum—8.2%, maximum—29.3%) in considering the pressure under the foot of the model p in the interval from $1.1 \cdot p_{in.cr.}$ ($p_{in.cr.}$ —the initial critical soil pressure [6]) to $0.7 p_{ult}$ [9, 14]. Such deviations can be estimated as satisfactory, allowing to draw the conclusion

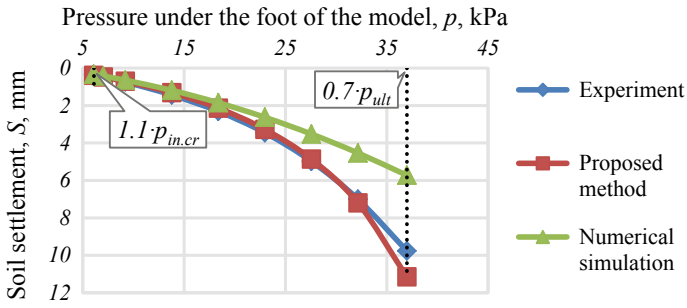


Fig. 2 Comparison of $S = f(p)$ dependencies for series with “weak” (loose) soil

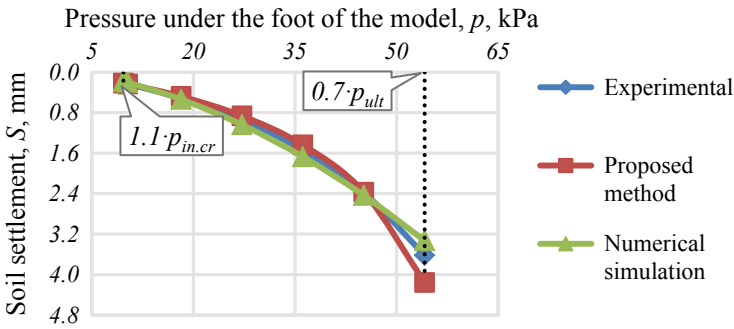


Fig. 3 Comparison of $S = f(p)$ dependencies for series with medium density soil

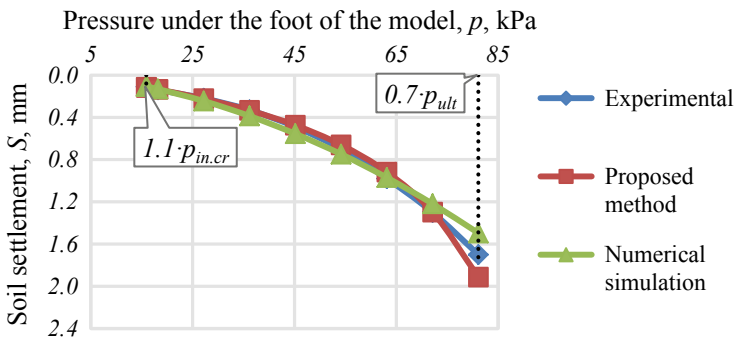


Fig. 4 Comparison of $S = f(p)$ dependencies for series with dense soil

about the reliability of the proposed “engineering” method of foundation calculation with respect to high-speed railways’ overpasses.

4 Comparison of Soil Settlements Using the Proposed Method and the Most Common Approximate (“Engineering”) Methods

Approximate (“engineering”) methods, concerning the soil settlement calculation out of the applicability limits of the linear theory of elasticity, are based on use, as a rule, of the phenomenological dependencies. The dependencies reflect the change of soil stress and strain state for the considered types of foundations in certain soil conditions [15, 16]. Consider the comparison of experimentally measured and calculated soil settlements using the proposed method and well-known approximate methods of Vyalov and Mindich [17], Malyshev and Nikitina [18], and Kirillov [19].

The dependencies of $S = f(p)$ for different series of the soil tests, obtained experimentally, as a result of calculation using the approximate methods of other authors and by the proposed method, are presented in Figs. 5, 6, and 7.

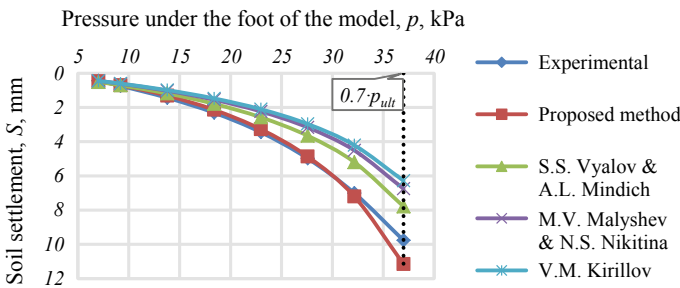


Fig. 5 Comparison of $S = f(p)$ dependencies for series with “weak” (loose) soil

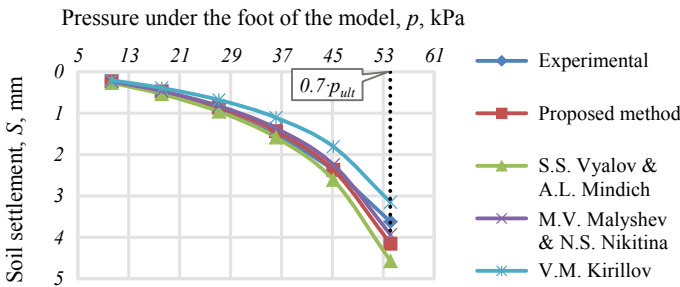


Fig. 6 Comparison of $S = f(p)$ dependencies for series with medium density soil

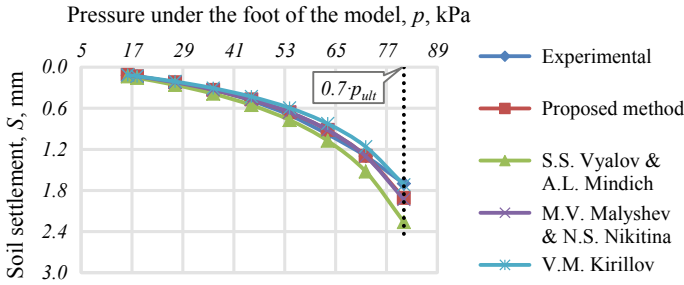


Fig. 7 Comparison of $S = f(p)$ dependencies for series with dense soil

Thus, as a result of comparison, the following is established: The proposed method had the least divergence from the experiment (average 6.3% for all series), and in doing so, the approximate methods of other authors also showed quite satisfactory results. The deviation of soil settlement was from 7.1 to 28.6% in the series with medium density soil and from 4.3 to 16% in the series with dense soil in the pressure interval from $1.1 \cdot p_{in.cr.}$ to $0.7 \cdot p_{ult.}$ The deviation of soil settlement in the series with “weak” (loose) soil using the proposed method was an average of 7.6%, according to the methods of other authors—from 25 to 47.4%—in this case, it is acceptable to talk about their ability to qualitatively describe the process of soil deformation.

Thus, the comparison of soil settlement values showed that the resulting deviations were generally acceptable for “engineering” methods and, mainly, comparable with each other. It should be noted that the deviations of theoretical values of soil settlement (calculated by the proposed method) from the experimental were the smallest among other considered methods, which led to the conclusion about deformational calculation method reliability.

5 Economic Efficiency Substantiation of the Deformational Calculation Method

To assess the economic efficiency of the proposed method, it is necessary to compare it with the alternative type—the traditional approach presented in the Russian special technical regulations [2]. The main criterion is the consumption of construction materials, which are necessary to build the foundation during calculating it by the corresponding method. Consider an example of calculation of the overpass foundation for high-speed railway [20]. It is necessary to solve the following tasks: Determine the dimensions of the foundations ($F-1$ and $F-2$) using the traditional (regulatory) approach and the proposed method; determine the economic efficiency of the proposed method relative to the traditional (regulatory) approach.

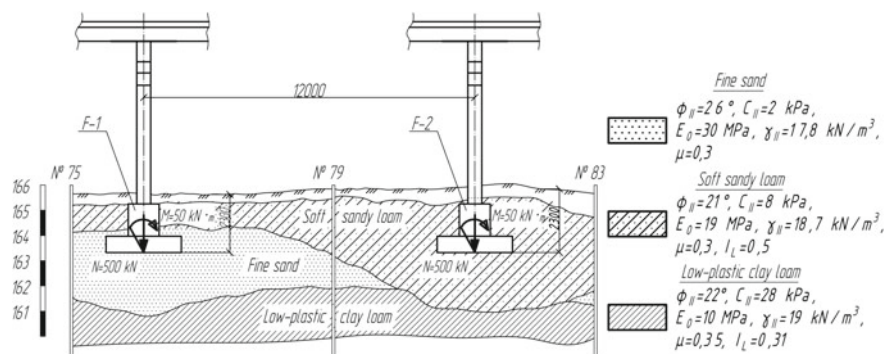


Fig. 8 Initial data for calculation example

The initial data for the calculation example, including the actual loads, the schematic representation of overpass structures and the soil characteristics, are shown in Fig. 8.

The aspect ratio of the foundations is equal to one (width $b = \text{length } l$). According to the requirements [2], the predetermined soil settlement of the overpasses foundations is equal to 2 cm, the maximum allowable angle of break-in profile (dS/l)—1‰. The calculation results are presented in Table 1.

Thus, the proposed method made it possible to obtain satisfactory and more cost-effective solutions of the foundations with respect to the requirements [2]: The foundation base width of $F-1$ was 1.1 m versus 1.4 m, for the $F-2$ —1.4 m versus 1.7 m. It should be noted that the obtained value of the soil settlement of $F-1$ ($1.8 \text{ cm} \neq 2 \text{ cm}$) by the proposed method was connected with the usage of type design of the foundation. The assessment of the moment influence was carried out on the basis of limiting the foundation tilt by its maximum allowable value according to the decisions outlined in the work [21]. Analysis of the calculation results showed that the actual foundation tilt was admissible ($F-1: 0.0045 < 0.0083; F-2: 0.00182 < 0.00606$).

Taking into account the nonlinear soil deformation behavior allowed to make less material-intensive decisions of the foundations. Design of foundations by the proposed method allowed in this case to reduce more than 2 times the actual angle of break-in profile (0.16‰ vs. 0.36‰). It should be noted that all calculation decisions were satisfactory with respect to the soil bearing capacity ($p \ll p_{ult}$) and had sufficient

Table 1 Results of the calculation example

Calculation method	N ^o	$1.1 \cdot p_{in.cr.}, \text{ kPa}$	$p, \text{ kPa}$	$p_{ult}, \text{ kPa}$	$S, \text{ cm}$	$dS/l, \text{ ‰}$	$b, \text{ m}$	γ_n
Traditional approach [2]	F-1	217.5	301	1081	1.13	0.36	1.4	3.2
	F-2	204.8	219	667	1.57		1.7	2.7
Proposed method [3]	F-1	217.5	459	1064	1.8	0.16	1.1	2.1
	F-2	204.8	302	658	2		1.4	1.96

reliability, which significantly exceeded the requirements ($[\gamma_n] = 1.2$) for buildings of III geotechnical category [14, 22].

The calculation of economic efficiency was based on an assessment of reduction of concrete and reinforcing steel consumption, reduced to 1 m³ and 1 kg of consumption, respectively. This calculation is presented in [20].

Thus, on the basis of considered example it is necessary to note: Use of the deformational calculation method allows ensuring the compliance with sufficiently stringent regulatory requirements related to the absolute values of foundation soil settlements and their irregularity. In addition, the use of the proposed method allows reducing the cost of foundations. On the basis of the example, the consumption reduction of concrete on average amounted to 35.2% and reinforcing steel—15.8%. The presented values had generalized character because they were determined by the conditions of the example. Mainly, the economic effect of the application of deformational calculation method depends on the degree of risk of specific foundation design. The greatest economic effect is possible with the smallest regulatory permissible safety margin of soil bearing capacity $[\gamma_n] = 1.2$ [14] or with the predetermined soil settlement equal to 0.7–0.8 of its maximum permissible value.

6 Conclusion

As a result of comparisons of experimentally determined soil settlements, the numerical simulation, the calculations by “engineering” methods of other authors and by the proposed method it was established: The resulting deviations were generally acceptable and, mainly, comparable with each other. The deviations of theoretical values of soil settlement calculated by the proposed method from the experimental were the smallest among other considered methods, which led to the conclusion about deformational calculation method reliability.

The advantages of the proposed method are the following: minimization of differential foundation soil settlements, use of “standard” soil test results, low computational complexity, considering the nonlinear soil deformation behavior—the ability to make the most cost-effective decisions of overpasses foundations. Thus, the proposed method can be considered as promising for solving problems associated with the design of foundations for overpasses of high-speed railways.






References

1. Ulitskiy VM, Shashkin AG (2016) Successful construction of high-speed motorways: the geotechnical constituent (in Russian). *J Trans Russia* 63–64:36–39
2. Smirnov VN, Kavkazskii VN, D'yachenko LK et al (2016) Artificial structures on Moscow–Kazan–Ekaterinburg high-speed railway mainline. In: Design and construction norms and requirements. Technical specifications (in Russian). PGUPS Publication St. Petersburg (2016)

3. Alekseev SI, Kondrat'ev SO (2018) Spread foundation calculation according to predetermined settlement (in Russian). *J Constr Arch* 20:194–206. <https://doi.org/10.31675/1607-1859-2018-20-2-194-206>
4. Kudryavtsev S, Ulitskiy V, Alekseev S, Kondrat'ev S (2019) Consideration of soil strata heterogeneity influence on differential foundation settlements of overpasses for high-speed railways. *MATEC Web Conf* 265:02003. <https://doi.org/10.1051/mateconf/201926502003>
5. Dvornavich SV (1973) Dependence of settlement of test plates on size of plate. *J Soil. Mech Found Eng* 10(3):196–199. <https://doi.org/10.1007/BF01706685>
6. Florin VA (1959) Soil mechanics. In: General dependencies and the stress-state state of foundation soils (in Russian), vol 1. Gosstroizdat Publishing, Leningrad–Moscow
7. White DJ, Take WA, Bolton MD (2001) Measuring soil deformation in geotechnical models using digital images and PIV analysis. In: 10th international conference on computer methods and advances in geomechanics, Balkema, Rotterdam, pp 997–1002
8. Chrisopoulos S, Vogelsang J, Triantafyllidis T (2017) FE Simulation of model tests on vibratory pile driving in saturated sand. In: Holistic simulation of geotechnical installation processes. *LNACM*, vol 82, pp 124–149. Springer, Cham. https://doi.org/10.1007/978-3-319-52590-7_5
9. Terzaghi K (1951) Theoretical soil mechanics. John Wiley and Sons Inc., New York
10. Grubbs FE (1969) Procedures for detecting outlying observations in samples. *Technometrics* 11(1):1–21. <https://doi.org/10.2307/1266761>
11. Das BM (2010) Principles of geotechnical engineering. Cengage Learning, Stamford
12. Ishibashi I, Hazarika H (2015) Soil mechanics fundamentals and applications. CRC Press, Boca Raton
13. Murthy VNS (2002) Geotechnical engineering: principles and practices of soil mechanics and foundation engineering. CRC Press, New York
14. Petrukhin VP, Sorochan EA, Kolybin IV et al (2016) Building code SP 22.13330.2016. The bases of the buildings (in Russian). Minstroy RF Publishing, Moscow
15. Duncan JM, Chang CY (1970) Nonlinear analysis of stress and strain in soils. *J Soil Mech Found Div ASCE* 96(5):1629–1653
16. Lade PV, Duncan JM (1975) Elastoplastic stress-strain theory for cohesionless soil. *J Geotech Eng Div ASCE* 101(10):1037–1053
17. Vyalov SS, Mindich AL (1974) Settlement and limiting equilibrium of a layer of weak soil underlain by a rigid foundation bed. *J Soil Mech Found Eng* 11(6):381–386. <https://doi.org/10.1007/BF01703809>
18. Malyshev MV, Nikitina NS (1982) Computing foundation settlements for a nonlinear relationship between stresses and strains in the soils. *J Soil Mech Found Eng* 19(2):70–79. <https://doi.org/10.1007/BF02304606>
19. Kirillov VM (1992) Approximate accounting of zones of plastic deformation in the bed of a rigid plate. *J Soil Mech Found Eng* 29(4):95–100. <https://doi.org/10.1007/BF02104231>
20. Alekseev SI, Kondratev SO (2018) Analysis of economic efficiency of shallow foundations design using the predetermined soil settlement (in Russian). In: Titova TS (eds) Proceedings of professional education, science and innovation in XXI century conference, vol 12, pp 17–18. PGUPS Publication, St. Petersburg (2018)
21. Alekseev SI, Kondrat'ev SO (2017) Specification of limiting value of foundation heel as a result of its interaction with over-foundation construction (in Russian). *J Proc Univ Investments Constr Real Estate* 7(1):53–58
22. Orr TLL, Farrell ER (1999) Basis of geotechnical design. In: Geotechnical design to Eurocode 7, pp 7–39. Springer, London. https://doi.org/10.1007/978-1-4471-0803-0_2

Numerical Modeling of Railway Embankment Deformations in Permafrost Regions, Central Yakutia



Petr P. Permyakov , Aleksandr F. Zhirkov , Stepan P. Varlamov , Pavel N. Skryabin  and Georgy G. Popov 

Abstract In this article, we consider the problem of thermal response of the near-surface ice-rich permafrost to the effects of linear infrastructure and current climate change. First, we emphasize the scientific and practical significance of the study and briefly describe permafrost conditions and related hazards in the study area. Then we present a mathematical model which accounts for the actual process of soil thawing and freezing and consists of two nonlinear equations: heat conduction and moisture transfer. Numerical calculations were made to predict temperature and moisture conditions in the railroad embankment, taking into account solar radiation, snow cover, rainfall infiltration, and evaporation from the surface. The numerical results indicate that moisture migration and infiltration play the primary role in the development of frost heaving and thaw settlement. During winter, the frost-heave extent is monotonously increased due to pore moisture migration to the freezing front. Strong volume expansion (dilatation) is observed near the surface of the active layer with the onset of the warm season and meltwater infiltration. Settlement of the upper layers of the soil occurs in the summer months (June–August) when there is intense evaporation due to drying. Autumn rains stop the process of thaw settlement by increasing the soil moisture. The above processes are repeated cyclically every year. A “frozen core” shifts to the shaded side of the embankment under the influence of variations in the solar radiation. Over time, the total moisture content of the frozen core is increased which increases differential heaving and negatively affects the stress–strain state in the embankment. The quantitative and qualitative characteristics of the processes of frost heaving and thaw settlement are obtained in the annual and long-term cycles.

Keywords Climate change · Frozen soils · Heat and moisture transfer · Infiltration · Frost heaving · Thaw settlement · Railway embankment

P. P. Permyakov · G. G. Popov

Larionov Institute of Physical and Technical Problems of the North, SB RAS, 677890 Yakutsk, Russia

P. P. Permyakov · A. F. Zhirkov (✉) · S. P. Varlamov · P. N. Skryabin

Melnikov Permafrost Institute, SB RAS, 677010 Yakutsk, Russia

e-mail: zhirkov_af@mail.ru

© Springer Nature Singapore Pte Ltd. 2020

A. Petriaev and A. Konon (eds.), *Transportation Soil Engineering in Cold Regions*,

Volume 2, Lecture Notes in Civil Engineering 50,

https://doi.org/10.1007/978-981-15-0454-9_11

1 Introduction

Routes of linear infrastructure (pipelines, railways, and highways) traverse areas with different geocryological conditions. Ensuring the sustainability of engineering structures under current climate change requires predictive modeling studies. Assessing the thermal condition of permafrost foundations during climate warming is a high-priority research problem in geocryology [1–3].

This paper deals with the problem of adverse geocryological processes that may develop during the operation of linear structures with account for climate change. Thawing and freezing of ice-saturated soils are accompanied by the development of thaw settlement or frost heaving.

Depending on the moisture regime, two types of frost heave, either migration or injection, occur in the “open” (with moisture supply) or “closed” (without moisture supply) systems. Thermokarst processes lead to various degrees of thaw settlement depending on the ice content of embankment and foundation soils.

The Tommot–Nizhny Bestyakh Railway route traverses the areas with very ice-rich permafrost (IV thaw susceptibility class), especially within the Pre-Lena Plateau and the high terrace of the Lena River [4]. Based on the data from geotechnical investigations along the route, various designs were used for the railroad embankment to prevent deformation. Deformations of the road embankments on permafrost are associated with degradation of underlying permafrost. The main factors causing degradation include solar radiation, infiltration of summer precipitation into the embankment, snow cover on the embankment sideslopes, and toes.

The purpose of this study is numerical modeling of the heat and moisture regimes in the railroad embankment for various conditions of temporary railway operation.

2 Embankment Description

The Tommot–Nizhny Bestyakh Railway crosses ice-rich permafrost terrain between KP 692 and 734, where the total volumetric ice contents within the layer of annual temperature fluctuations are as high as 0.7–0.8 (fractional) [4, 5]. Ice wedges occur in the depth range of 1.5 and 12.0 m.

In 2007–2010, a monitoring site was established at KP 694 in sloping ice-rich permafrost terrain to observe the thermal regime in the embankment, as well as in the underlying and adjacent ground (Fig. 1). Right of way clearing was carried out in winter of 2006 and a 7-m high rockfill embankment was placed continuously during the period from April 2009 to September 2010. Boreholes for temperature monitoring beneath the future embankment were drilled and instrumented in the fall of 2007 after ROW clearing. Sites in the adjacent areas (ROW, larch forest, and bog) were established during embankment construction.

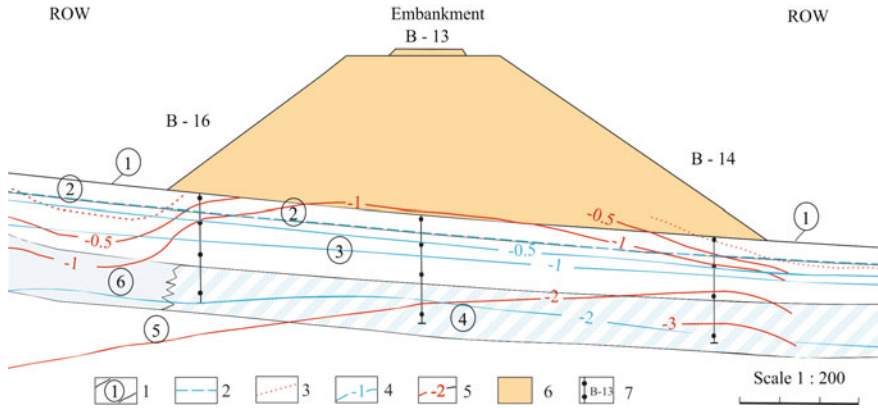


Fig. 1 Changes in temperature isotherms and permafrost table beneath the embankment at KP 693.4 [6]: 1—number of soil layer: 1—moss-mountain cranberry cover, $\delta=0.10$; 2—clayey silt, soft-plastic, $\delta=0.10$; 3—clayey silt, liquid, $\delta=0.27/3$; 4—clayey silt, liquid (icy), $\delta=0.62/4$; 5—clayey silt, soft-plastic, $\delta=0.13/3$; permafrost table: 2—in 2007, 3—in 2017; temperature contours: 4—23.09.2007, 5—30.08.2017; 6—rock with $\leq 10\%$ fines; 7—temperature borehole. The layer of massive ice is colored in blue and the icy soil layer is shown in blue hatching

The study site is located in the lower part of the east-facing gentle slope. The 0.1–0.15 m thick moss-cowberry cover of larch forest is characterized by high moisture contents (42–62%), and the active layer consisting of clayey silts has moisture contents of 24–29%. Permafrost soils consist of soft-plastic and liquid clayey silts with moisture contents varying over a wide range, from 27 to 132%. Ground ice bodies and icy soils of 2.3–3.5 m in thickness occur at a depth of 1.2–2.1 m. The mean annual ground temperature at a depth of 10 m ranges from -2.4 to -2.8 °C, and the thickness of the active layer in the forest is 0.8–0.9 m [6].

3 Problem Definition

The heat and moisture regime of the soil is described by the following system of differential equations in the Cartesian coordinate system [7]:

$$c \frac{\partial T}{\partial \tau} = \frac{\partial}{\partial x} \left(\lambda \frac{\partial T}{\partial x} \right) + \frac{\partial}{\partial y} \left(\lambda \frac{\partial T}{\partial y} \right) - c_w V_x \frac{\partial T}{\partial x} - c_w V_y \frac{\partial T}{\partial y} + L\rho \frac{\partial W_i}{\partial \tau}, \quad (1)$$

$$\left(\frac{\partial W_w}{\partial \tau} = \frac{\partial}{\partial x} \left(k \frac{\partial W_w}{\partial x} \right) + \frac{\partial}{\partial y} \left(k \frac{\partial W_w}{\partial y} \right) - \frac{\partial k_h}{\partial y} - \frac{\partial W_i}{\partial \tau} \right), \quad (2)$$

$$\frac{\partial \theta_w}{\partial \tau} = \frac{\partial}{\partial x} \left(k_h \frac{\partial H}{\partial x} \right) + \frac{\partial}{\partial y} \left(k_h \frac{\partial H}{\partial y} \right) - \frac{\partial \theta_i}{\partial \tau}, \quad (2^*)$$

$$(x, y) \in \Omega, \quad \tau > 0.$$

The system of Eqs. (1)–(2) is closed by the equilibrium function of the amount of unfrozen water:

$$W_w = W_{uw}(T, W) \quad (3)$$

Equation (1) describes the soil freeze–thaw process with account for heat transfer by moisture. Water movement and ice formation are taken into account by expressions (2) and (3). To predict the moisture regime, we can use any of these equations. The Richards Eq. (2*) is commonly used for saturated and unsaturated soils, while Eq. (2) for unsaturated soils.

On the surface bounded above by atmospheric air:

$$\begin{aligned} -\lambda \frac{\partial T}{\partial n} &= \alpha_{ef} \left(T_w + \frac{Q_c(1-A)}{\alpha_{ef}} - T \right), \\ -k \frac{\partial W_B}{\partial n} &= q_w(\tau) \end{aligned} \quad (4)$$

In the remaining sections, the heat flux is zero:

$$\begin{aligned} \lambda \frac{\partial T}{\partial n} &= 0 \\ k \frac{\partial W_w}{\partial n} &= 0 \end{aligned} \quad (5)$$

$$(x, y) \in (E, F) \cup (H, Q) \cup (A, H)$$

Initial temperature distribution:

$$\begin{aligned} T(x, y, 0) &= T_0(x, y) \\ W(x, y, 0) &= W_0(x, y) \end{aligned} \quad (6)$$

$$(x, y) \in \Omega$$

The mathematical model of heaving is based on the assumption that the volume expansion of the soil occurs vertically (toward the ground surface) due to the increase in the pore material caused by the freezing of water, i.e. laterally confined condition—an assumption applied to the problem of soil compression.

The frost-heave extent can be described, using the total volumetric moisture content θ , as follows [3]:

$$S_1 = \int_0^i (\theta - n) dz, \quad M \quad (7)$$

Similarly, a mathematical model of thaw settlement (compression) of frozen soil is derived, taking into account the depth of thawing, compressibility and load on the frozen soil:

$$S_2 = k_0 \xi + \alpha (P_s + 0.5 \rho_d (1 + W) \xi) \xi, \quad M \quad (8)$$

The parameters θ , ξ in Eqs. (7)–(8) are determined by solving the system of coupled heat and moisture transfer Eqs. (1)–(6). Other input parameters, P , n , α , are set based on the physical and mechanical properties of the soil. The total volumetric moisture content θ is expressed in terms of gravimetric moisture as follows [8]:

$$\theta = \frac{\rho_d W}{\rho_i \rho_w} (\rho_i + (\rho_w - \rho_i) \cdot i(T)).$$

Here T —temperature, K; c , c_w volumetric heat capacity of the soil and water, J/(m³ K); τ —time, s; ρ , ρ_w , ρ_i —bulk density of dry soil, water and ice, respectively, kg/m³; $W = W_i + W_w$ —total gravimetric moisture contents in the form of ice and water; λ —soil thermal conductivity, W/(m K); x , y —spatial coordinates, m; L —volumetric latent heat of fusion, J/m³; $V = (V_x, V_y)$ —flow rate, m/s; k —diffusion coefficient, m²/s; $H = P - z$ —pressure, m; P —suction pressure, m; k_h —hydraulic conductivity, m/s; $\theta = \theta_i + \theta_w$ —total volumetric moisture content, bulk ice and water content; $\frac{\partial T}{\partial n}$ —derivative along the normal line; $i(T)$ —function of ice content ($i(T) = W_i(T)/W$); n —porosity of the soil; ξ —thaw bulb, m; k_0 —thaw–strain parameter (relative settlement under no pressure); α_{ef} —effective heat transfer coefficient on the soil surface, W/(m² K); α —compressibility coefficient, MPa^{−1}; P_s —pressure on thawed soil, MPa; Q_s —net solar radiation, W/m²; and A —surface albedo.

The two-dimensional mathematical model presented here takes into account variations in atmospheric air temperature and effects of net solar radiation and surface albedo, as well as variations in the air-to-ground heat transfer coefficient depending on wind speed, vegetation, snow depth, and snow thermal properties. The mathematical model, which takes into account the actual process of soil thawing and freezing, consists of two nonlinear equations: heat conduction and moisture transfer. The heat conduction equation contains convective terms that can be represented in non-divergent (non-conservative) and divergent (conservative) forms. In numerical solution, the focus is on the approximation of convective components. In practice, convective terms are widely used in the schemes with directed differences, taking into account the sign of the filtration rate. The numerical implementation of this system of nonlinear equations is carried out by an implicit finite-difference scheme using iteration [7].

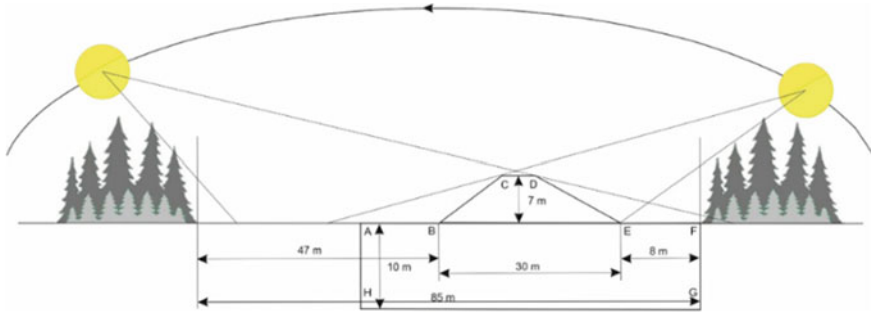


Fig. 2 Cross-section of the modeled railway embankment

4 Numerical Experiment

4.1 Input Data

The cross section of the railway embankment on ice-rich permafrost used for modeling is illustrated in Fig. 2. The rockfill embankment has the following dimensions: height—7 m, crest width (CD)—8 m, and base width (BE)—30 m. The underlying permafrost consists of ice-rich clayey silts (see Fig. 1).

The input values for air temperature, precipitation, albedo, and wind speed were taken from weather records from the Pokrovsk, Yakutsk, and Amga stations.

Snow depths measured annually during the period of maximum snow accumulation are presented in Table 1. The thermal properties of the soils are given in Table 2. The initial distributions of temperature and total moisture content are specified on the basis of field measurements [6].

4.2 Results and Discussion

Figure 3(I) presents the temperature and moisture distribution in the embankment in 10 years calculated with no account for solar exposure. A frozen core is formed in the center of the high embankment, due to the annual accumulation of moisture. Snow depth on the sideslopes is significantly less than at the toe of the embankment. Snow cover on the right and left toes of the embankment has a warming effect on the ground during the winter.

Figure 3(II) shows the distributions of temperature and total moisture content in the embankment in 10 years incorporating the effects of solar radiation. The left sideslope exposed to the sun has a warming effect on the embankment, causing the center of the frozen core to shift toward the shaded right side. As a result, soil drying occurs at the base of the sun-exposed slope, while the opposite, shaded base of the slope has favorable conditions for moisture accumulation. Uneven moisture distribution leads to differential heave and distress in the embankment.

Table 1 Variation in snow depth at KP 693.4, m

Location	Date											
	05.04 2010	04.04 2011	04.04 2012	04.04 2013	10.04 2014	01.04 2015	22.03 2016	03.04 2017	13.03 2018			
Forest left to ROW	0.41	0.58	0.50	0.45	0.64	0.56	0.60	0.68	0.58			
ROW	0.47	0.61	0.55	0.23	0.48	0.58	0.67	0.64	0.60			
Left embankment toe	0.41	0.71	0.84	0.69	0.71	0.59	1.10	0.78	0.89			
Left mid-slope	0.60	0.14	0.27	0.32	0.44/0.15	0.28	0.48	0.12	0.21			
Embankment centerline	0.02	0.24	0.04	0.08	0.10	0.06	0.17	0.10	0.08			
Right mid-slope	0.56	0.56	0.61	0.43	0.35/0.51	0.57	0.70	0.63	0.57			
Right embankment toe	0.47	0.62	0.59	0.59	0.73	0.70	0.88	0.50	0.69			
Forest right to ROW	0.50	0.60	0.57	0.50	0.44	0.53	0.62	0.63	0.56			

Table 2 Thermophysical characteristics of soils

Soil type	Depth interval, m	Dry density, kg/m ³	Moisture content, %	Thermal conductivity, W/(m K)		Specific heat capacity, J/(kg K)
				Thawed	Frozen	
Embankment fill	0.0–7.0	1300	5–10	2.73	2.90	690
Organic mat	0.0–0.1	970	15	0.46	0.64	950
Clayey silt, soft-plastic	0.1–0.5	1300	10	0.75	1.03	775
Clayey silt, liquid	0.5–3.0	1155	27	1.12	1.33	775
Clayey silt, liquid	3.0–7.0	1055	62	1.36	1.76	775
Clayey silt, liquid	7.0–...	940	13	0.62	0.84	775

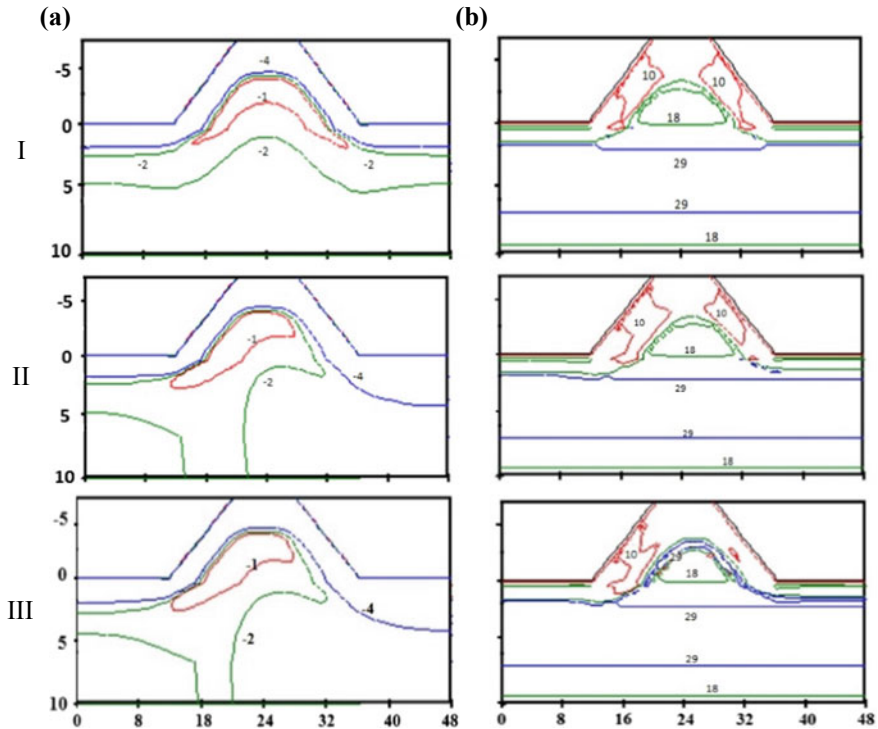


Fig. 3 Distributions of temperature (a) and total moisture content (b) in 10 years with no account for solar radiation (I) and incorporating solar radiation in 10 years (II) and in 50 years (III), indicating the size of the calculated region (in meters)

The model predicts warmer embankment temperatures under the unshaded sideslope after 50 years of operation of the railway (Fig. 3(I, II)). The thermal regime of the subgrade is stabilized till the year 50. The moisture regime of the embankment during the first 50 years is characterized by more intensive soil drying under the left, sunlit slope than below the right, shaded sideslope. Moisture migration to the freezing front contributes to increased ice contents at the base of the active layer (Fig. 3III).

The active layer freezes from above during the winter months (November to March), and this process is accompanied by the migration of pore water. Frost heave occurs due to the 9% volume expansion of pore water upon freezing and is enhanced at moisture values above saturation. This process is a major factor in the development of frost heaving. The frost-heave extent is monotonously increased during the winter due to the migration of pore moisture to the freezing front. In May, meltwater infiltration leads to a strong increase in the volume (dilatation) of the upper horizons of the active layer. Intense evaporation is observed during the summer months (June–August) which results in drying of the surface layers of the soil and subsequent subsidence of the active layer. In Central Yakutia, evaporation exceeds precipitation in the annual water balance. Autumn rains (August–September) stop the process of thermal settlement induced by drying. All the above processes are repeated cyclically every year.

Soil thawing is more intensive on the unshaded than on the shaded slope. The shaded sideslope experiences greater heave, shallower thaw, and less settlement compared to the unshaded slope. The long-term extent of migration-induced heaving is 5.2 cm on the sunny side and 4.6 cm on the shaded side (Fig. 4). The maximum values of soil deformation occur in mid-May while the minimum ones occur in late September. The results of numerical simulation are in good agreement with the field measurements. Over the long-term cycle, “seasonal deformations” in the embankment can contribute to the process of disintegration and lead to damage of the embankment.

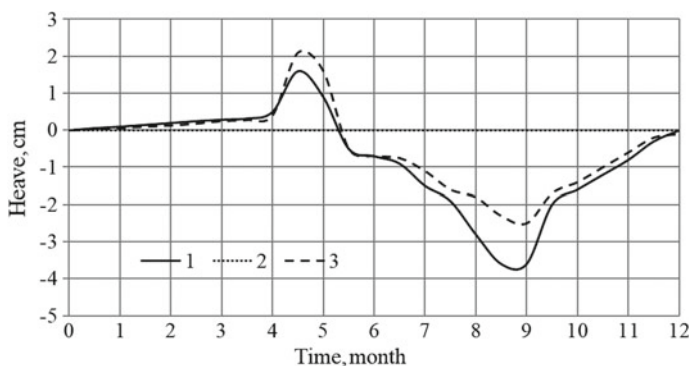


Fig. 4 Annual dynamics of surface heave: 1—unshaded ROW; 2—embankment; 3—shaded sideslope

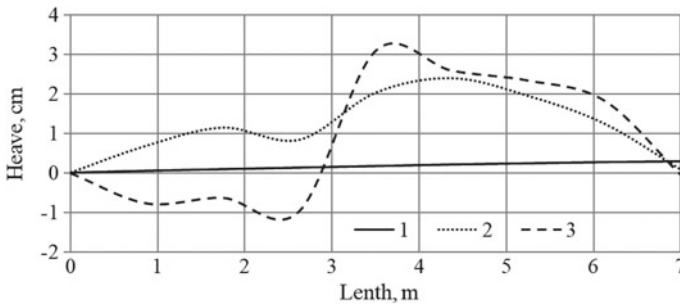


Fig. 5 Dynamics of embankment surface heave with time: 1—in 10 years; 2—in 25 years; 3—in 50 years

The moisture content in the embankment is considerably lower than saturation moisture contents, and the roadbed is not exposed to heaving during seasonal freezing–thawing in the annual cycle for the first 10 years. In the active layer, embankment heaving up to 1 cm is predicted to occur in 25 years and settlement of up to 1 cm in 50 years. Heave after 25 and 50 years is 2 and 3 cm, respectively, in the frozen core of the body of the embankment near the border of the active layer (Fig. 5). The calculated values approach the permissible heave value of 3.5 cm for speeds of 51–70 km/h after 50 years of operation of the subgrade [9].

5 Conclusion

We developed an algorithm for numerical prediction of frost heaving and thaw settlement of a railway embankment on permafrost in Central Yakutia. The algorithm was used to forecast changes in the temperature and moisture regime of the embankment with account for changes in air temperature, snow cover, solar radiation, and infiltration of summer precipitation. The “frozen core” is shown to shift to the shaded sideslope which experiences increased moisture contents and greater differential heaving. Moisture migration to the freezing front will be increased as well as ice contents at the bottom of the active layer.

Acknowledgements The study was performed as part of Russian Academy of Sciences Project IX.135.2.3, with additional support from the Russian Foundation for Basic Research (Grants 18-55-53041 and 18-41-140008).

References

1. Kondratyev VG (2001) Active ways to strengthen the foundation of the roadbed on the ever-frozen soils. Zabtrans, Chita

2. Hao Z, Kanie S, Niu F (2018) The thermal regime evaluation of high-speed railway foundation by mixed FEM. *Cold Reg Sci Technol* 155:333–342
3. Permyakov PP, Popov GG, Matveeva MV (2011) Forecast of the dynamics of the “seasonal loosening” of the pipeline. *Gazovaya Prom* 4:17–19
4. Varlamov SP (2006) Ground ice contents in the Northern Section of the Tommot-Kerem Railway Project (Olen Station to Kerem Station). In: *Proceedings of international conference, earth cryosphere assessment: theory, applications and prognosis of alterations*, vol 2, 29–31 May 2006. Tyumen, Russia, pp 212–214
5. Pozin VA, Korolev AA, Naumov MS (2009) The “ice complex” in Central Yakutia as a testing area for railway construction under extreme engineering-geocryological conditions. *Inzhener-naya Geologiya* 1:15–18
6. Varlamov SP (2018) Thermal monitoring of railway subgrade in a region of ice-rich permafrost, Yakutia, Russia. *Cold Regions Sci Technol* 155:184–192
7. Permyakov PP, Ammosov AP (2003) *Mathematical modeling of technogenic pollution in the cryolithozone*. Nauka, Novosibirsk
8. SNiP 2.02.04–88. *Foundations on permafrost soils/gostroy Russia*. GUP TsPP, Moscow
9. *Technical Instructions for Eliminating Deeps and Settlement of a Railway Track, Transport*, Moscow, 65 pp (1987)

Calibration of PLAXIS Frozen/Unfrozen Soil Model According to Results of Laboratory Tests and In-situ Monitoring



Alexey A. Korshunov , Sergey V. Churkin  and Alexander L. Nevzorov 

Abstract Frost heaving is a challenge for geotechnical engineers who deal with transportation infrastructure in a cold climate. To make a frost heave forecast and assess reliability of soil masses engineers apply different numerical soil models calibrated by results of in-situ and numerical simulation tests. The recently developed frozen/unfrozen soil model by PLAXIS bv and NTNU was used for reproduction of laboratory and field tests data. The model describes frost heaving as a function of frost front moving rate and water migration rate from unfrozen zone and has 25 parameters: 7 general ones, 12 parameters that are responsible for solid strains, 3 parameters responsible for suction strains and 3 ones that account for coupling effects between the variation of the solid phase stresses and the cryogenic suction. The results of oedometer tests of silt in the unfrozen and frozen states and frost heave tests, presented in the article, allow us to obtain such parameters as initial segregation threshold value, elastic and elasto-plastic compressibility coefficients, rate of change in Young's modulus with temperature. But we have to apply backward analysis in order to obtain a best-fit of simulated results with test results. Unfortunately, most parameters is to be obtained by only calibration method. Additionally, to validate the frozen and unfrozen soil model the results of geotechnical monitoring of the cold-storage building are used. The frost heave phenomenon was appeared for 29-years period of its operation. Results of in-situ monitoring and numerical simulation showed good correlation with depth of frost penetration but unsatisfied results of frost heave deformations.

Keywords Frost heaving · Frozen and unfrozen soil model · Numerical simulation · PLAXIS · Cryogenic suction

A. A. Korshunov (✉) · S. V. Churkin · A. L. Nevzorov
Northern (Arctic) Federal University named after M.V. Lomonosov, Severnaya Dvina Emb. 17,
163002 Arkhangelsk, Russia
e-mail: a.a.korshunov@yandex.ru

1 Introduction

Increasing activity in cold regions all over the world leads to technological challenges for geotechnical engineers. One of them is a frost heave phenomenon which has impact on decision how to design, build and maintain roads, bridges, railways, low-rise buildings to prevent negative effect or even a damage of structures. The prediction of the freezing soil behavior is possible by making numerical simulation. However, the prediction is to be made with applying only verified and calibrated numerical model. It will be achieved by reproduction of laboratory tests and in-situ experiments and comparison these results with outcomes of numerical simulation.

There are numerous soil models, which deal with thermo-hydraulic-mechanical analysis but distinguishing feature of such models is a numerous input parameters. Some of them are determined by standard laboratory tests, the others require advanced laboratory tests or using of iterative approach.

Recently developed frozen/unfrozen soil model [6] by PLAXIS bv and Norwegian University of Science and Technology (NTNU) is an example of the advanced models. It takes into account dependency of soil stiffness and shear strength from temperature and simulates frost heave deformations and thaw settlements. The model is available as a user-defined soil model in PLAXIS 2D. One of the crucial abilities of the model is prediction of frost heaving as a function of frost front moving rate and water migration rate from the unfrozen zone.

The main objective of this research is to determine the model parameters of silt which was found under object of transport logistic system. Model parameters are defined as the results of consolidation and frost heave tests. Additionally, the results of geotechnical monitoring of the object of transport logistic system are used to calibrate frozen and unfrozen soil model.

2 In-situ Verification Object

Cold-storage building for fishing preservation has been normally operated since 1985. The refrigeration equipment installed in the building was kept in the temperature from 249.15 to 251.15 K inside the building. Floor of building consists of two layers: one is heat-insulating, another is heated by electricity. Heated floor was operated normally until 1995. From 1995 heated floor wasn't work and by 2012 inner columns were uplifted up to 130–184 mm. Cracks in the floor and walls were appeared. After 2012 building wasn't operate. In 2014 to clarify geological conditions and to determine the frozen stratum thickness two boreholes were drilled. In the middle part of the building at the depth between 3.8 and 8.1 m, there were frozen soils—1.0 m of fine sand and 3.3 m of silt [4]. The temperature of the frozen soil was between 272.85 and 272.65 K. The cross-section of the building with soil strata is shown in Fig. 1. Physical and thermal parameters of silt (soil stratum № 3) are presented in Table 1.

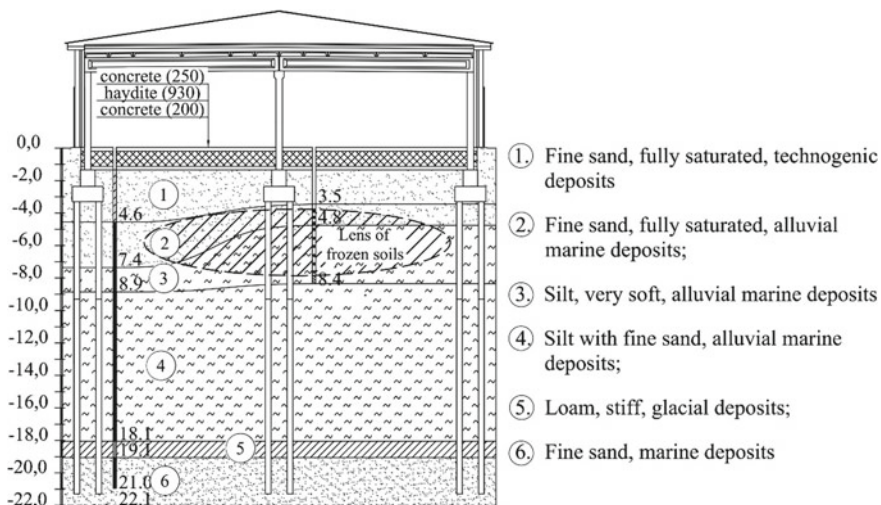


Fig. 1 Cross-section of the building

Table 1 Physical and thermal parameters of silt (ML)

Parameter	Unit	Unfrozen state	Frozen state
Density of solids	g/cm ³	2.47	–
Dry density	g/cm ³	1.49	1.40
Total water content	–	0.30	0.37
Void ratio		0.66	0.76
Ice content	–	–	0.05
Liquid limit	%	40.5	–
Plasticity index	%	14.4	–
Heat capacity	J/kg K	730	–
Thermal conductivity	W/m K	1.5	–

3 Model Parameter and Their Determination

3.1 General Description

The constitutive model for frozen and unfrozen (FU) soil is mainly based on Barcelona Basic Model developed for expansive unsaturated soils, but adopted for unfrozen/frozen states [3]. FU model is an elasto-plastic time-independent mechanical soil model formulated within the framework of two-stress state variables. The stress state variables are the cryogenic suction (S_c) and the solid phase stress or effective stress (σ'). The latter one is defined as [6]:

$$\sigma' = \sigma - S_{uw} p_w \quad (1)$$

where σ is the total stress, S_{uw} is the unfrozen water saturation and p_w is the pore water pressure. The effective stress is able to reflect the effect of unfrozen water on the mechanical behavior of soil.

Unfrozen water saturation S_{uw} is defined as relationship of volumetric unfrozen water content and porosity [3]:

$$S_{uw} = \frac{\theta_{uw}}{n} \quad (2)$$

$$\theta_{uw} = \frac{\rho_w}{\rho_b} \exp(0.2618 + 0.5519 \ln(\text{SSA}) - 1.4495(\text{SSA})^{-0.264} \ln|T|) \quad (3)$$

$$\text{SSA} = 3.89 \cdot d_g^{-0.905} \quad (4)$$

where ρ_b —dry density of unfrozen soil, T —temperature, SSA—specific surface area, d_g —geometric mean of the soil particle diameter.

The cryogenic suction, S_c , is used as the second state parameter. Cryogenic suction allows to take into account ice content and temperature variation. By considering the cryogenic suction, it is possible to take the effects of the ice content and temperature variation into account. S_c is defined as [5, 10]:

$$S_c = p_{ice} - p_w \approx -\rho_{ice} L \ln \frac{T}{T_f} \quad (5)$$

where p_w and p_{ice} indicate the pore water and ice pressure, respectively; ρ_{ice} the density of ice and L is the latent heat of fusion of water. T represents the current temperature and T_f is the melting/freezing temperature of ice/water for a given soil and value of pressure.

Strain increments are defined as:

$$d\varepsilon = d\varepsilon^{me} + d\varepsilon^{se} + d\varepsilon^{mp} + d\varepsilon^{sp} \quad (6)$$

where $d\varepsilon^{me}$ and $d\varepsilon^{mp}$ are the elastic and plastic parts of strain due to the solid phase stress variation ($d\sigma'$) respectively; $d\varepsilon^{se}$ and $d\varepsilon^{sp}$ are the elastic and plastic parts of strain due to cryogenic suction variation (dS_c), respectively.

3.2 Model Parameters

The FU soil model has 25 parameters: 7 general parameters, 12 parameters that are responsible for solid strains, 3 ones responsible for suction strains and 3 parameters that account for coupling effects between the variation of solid phase stresses and the cryogenic suction (Table 2).

Table 2 Parameters of FU model

Parameter	Description	Unit
<i>General parameters</i>		
T_{ref}	Reference temperature ($T = 273.15$)	K
p_c^*	Reference stress	N/m ²
P_{at}	Atmospheric pressure ($P_{at} = -10^5$)	N/m ²
K_w	Water bulk modulus ($K_w = 10^9$)	N/m ²
λ_r	Parameter for fitting unfrozen water saturation curve	–
p_r	Parameter for fitting unfrozen water saturation curve	N/m ²
α	Parameter for the pressure dependency of ice thawing temperature	–
<i>Solid strains</i>		
$E_{f Ref}$	Frozen soil Young’s modulus at reference temperature	N/m ²
$E_{f Incr}$	Rate of change in Young’s modulus with temperature	N/m ² /K
ν_f	Frozen soil Poisson’s ratio	–
G_0	Soil shear modulus in unfrozen state	N/m ²
κ_0	Unfrozen Soil Elastic compressibility coefficient	–
λ_0	Elasto-plastic compressibility coefficient for unfrozen state	–
γ	Plastic potential parameter ($0 \leq \gamma \leq 1$)	–
M	Slope of critical state line	–
M	Yield parameter ($0 \leq m \leq 1$)	–
$(P_{y0}^*)_{in}$	Initial pre-consolidation stress for unfrozen condition	N/m ²
Y_{Ref}	Value of depth for pre-consolidation	M
ΔP_{Y0}^*	Rate of change in pre-consolidation stress $Y < Y_{ref}$	N/m ² /m
<i>Suction strains</i>		
$S_{c,seg}$	Initial segregation threshold	N/m ²
κ_s	Elastic compressibility coefficient for cryogenic suction variation	–
λ_s	Elasto-plastic compressibility coefficient for cryogenic suction variation	–
<i>Coupling effects between strains</i>		
β	Rate of change in soil stiffness with cryogenic suction	(N/m ²) ⁻¹
R	Coefficient related to the maximum soil stiffness	–
κ_t	Rate of change in apparent cohesion with cryogenic suction	–

Aukenthaler, Brinkgreve and Haxaire [2] proposed using results of oedometer tests to define pre-consolidation stress, $(P_{y0}^*)_{in}$, elasto-plastic compressibility coefficient for unfrozen state, λ_0 . Other parameters such as β , κ_0 , r and p_c^* can be determined by the calibration methods.

Simple shear test in unfrozen state are required to obtain the shear modulus G_0 and slope of critical state line M . To determine the Young’s modulus of frozen soil E_{ref} , rate of change in previous one with temperature $E_{f inc}$, Poisson’s ratio ν_f and

rate of change in apparent cohesion κ_t unconfined axial compression test is to be carried out.

Frost heave tests will allow determining initial segregation threshold value, by determining the temperature, at which the frost heave phenomena start, and two parameters—elastic (κ_s) and elasto-plastic (λ_s) compressibility coefficients.

Other parameters (κ_t , m , γ , λ_r , p_r , α) for FU model are determined by empirical correlations and iterative calibration methods [3].

4 Determination of Input Parameters

4.1 Correlations and Default Values

To minimize efforts and to reduce time-consuming laboratory tests known correlations equations were used for determination input parameters. Poisson's ratio for frozen soil is approximately equal Poisson's ratio of ice ($\nu_f \approx \nu_{ice} = 0.31$).

Slope of critical state line (M) is defined as function from residual friction angle (φ'). For low plasticity silt $\varphi' = 25^\circ$. So for triaxial compression $M = 0.98$ and for triaxial extension $M = 0.74$.

Rempel [9] defines the temperature (T_{ice}) when ice formation lens are to start, for three types of soil: sand, Chena silt and Inuvik Clay. Temperatures are equal 0.57, 1.27 and 3.48 °C respectively. Aukenthaler et al. [2] propose transforming the given temperatures to obtain values of initial segregation threshold when no frost heaving has been performed. It is proposed to define as function of $|T_{ref} - T_{ice}|$ and for silt it is equal 1.25 MPa for the first estimation. The value of initial segregation threshold is recommended to calibrate in results of frost heave tests.

Other parameters should be defined as result of laboratory tests and their numerical simulation to order to obtain best-fit combination of input parameters.

4.2 Oedometer Tests

Oedometer tests were carried out on a cylindrical specimens of silt in frozen and unfrozen states. Dimensions of soil samples were 73 mm diameter and 20.85 mm thick.

Consolidation test results for unfrozen silt are presented in Fig. 2. Elasto-plastic compressibility coefficient, λ_0 , is defined as compression index C_c divided into $\ln 10$ and is equal 0.0249 ± 0.0173 . Compression index C_c was determined as slope of “ e - $\lg P$ ” straight line in the range from preconsolidation pressure to 300 kPa. The elastic compressibility coefficient is generally of minor importance for unfrozen soils and it can be taken in 5 times less than λ_0 . At reference stress, $p_c^* = 100$ kPa, Young's modulus is equal 5.88 MPa and G_0 is estimated 2.18 MPa.

Fig. 2 “e-lg P” line for unfrozen silt

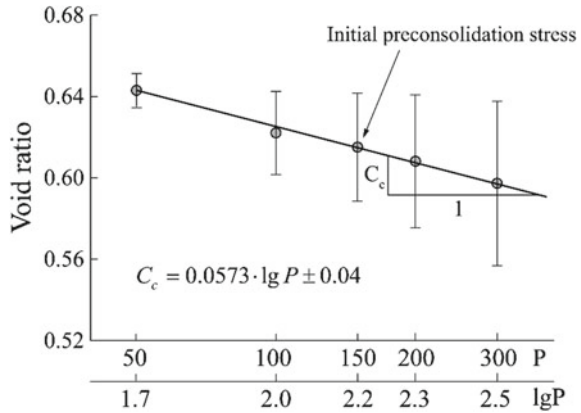
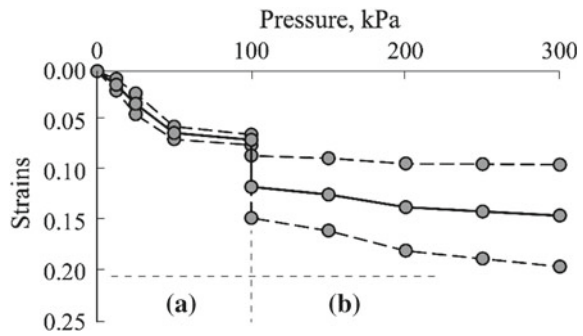


Fig. 3 “Strain-stress” curve of silt for frozen (a) and unfrozen (b) state



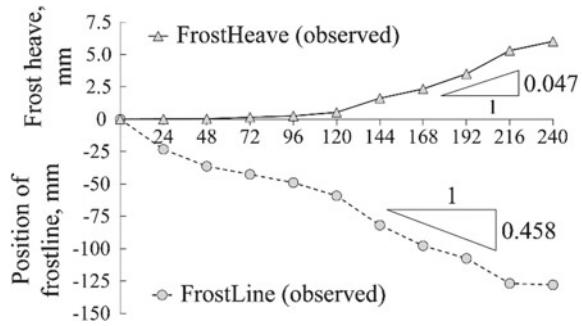
At the beginning of the test for frozen silt, temperature was 271.15 K. The pressure was applied in several steps: 12.5, 50 and 100 kPa. When pressure was equal 100 kPa, the temperature was uplifted to 275.15 K, dramatically thaw settlements were observed. After finishing full consolidation of soil a pressure was continued to apply up to 300 kPa. Results of tests are presented in Fig. 3. Initial pre-consolidation stress for unfrozen soil is estimated as 150–190 kPa for given geotechnical situation.

According to Fig. 3 Young’s modulus for frozen silt at $T = 271.15$ K is estimated in 8.4 MPa. So rate of change in Young’s modulus with temperature is equal 1.2 MPa/K.

4.3 Frost Heave

Frost heave tests allow to determine the initial segregation threshold value and two parameters: elastic (κ_s) and elasto-plastic compressibility coefficient (λ_s). Frost heave test was carried out under applied pressure 50 kPa and in subject to keep up the rate of frost front penetration equal to 10–12 mm/day. Results are presented in Fig. 4. The

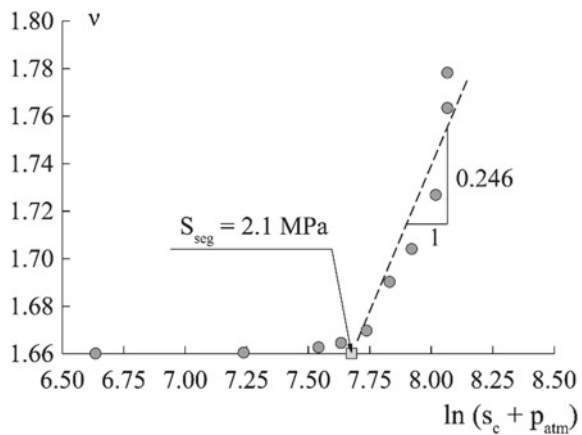
Fig. 4 “Frost heave versus time” curve



frost heave rate was 1.12–1.15 mm/day that corresponds to medium frost-susceptible soils [3].

We reconstructed the “frost heave vs. time” curve in “ $v - \ln(S_c + p_{atm})$ ”, where v —specific volume, to obtain input parameters $S_{c,seg}$, κ_s and λ_s . It should be noted that s_c is defined according to Eq. [5], where T represents the current temperature under bottom of loading cap. Elasto-plastic compressibility coefficient is estimated as 0.246, initial segregation threshold—2.1 MPa (see Fig. 5). Unfortunately, we obtained negligible value of elastic compressibility coefficient and accepted in 150 times less than λ_s , $\kappa_s = 1.64 \times 10^{-3}$. Other parameters are recommended to define by different optimization methods to get best-fit of simulated results with laboratory test results.

Fig. 5 “ $v - \ln(s_c + p_{atm})$ ” curve



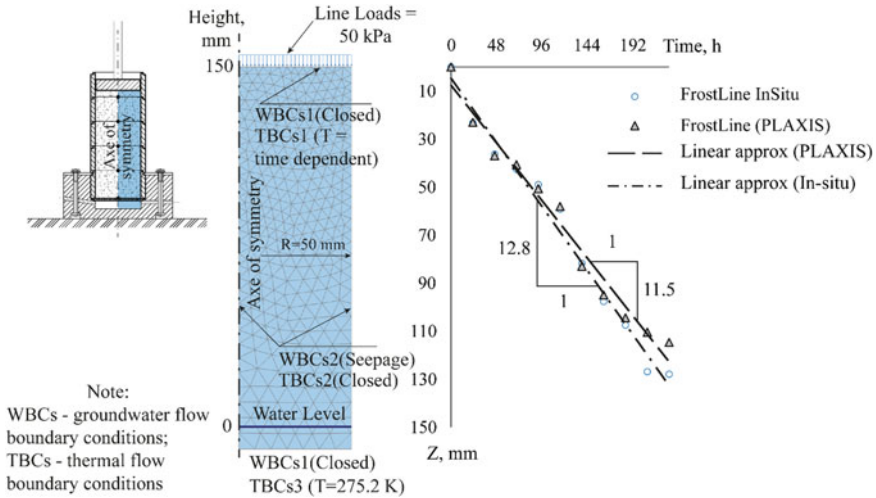


Fig. 6 Model geometry and boundary conditions

5 Numerical Simulation and Calibration Procedure

5.1 General Settings

The frost heave and compression tests were simulated in axisymmetry model with radius 50 mm and height 150 mm. Ground water flow and thermal flow boundary conditions are presented in Fig. 6. Ten stages were simulated for frost heave tests and additional five stages—to simulate compression tests. Duration of each stage was 1 day and total—10 days.

Average temperature of sample was 275.15 K as a result of initial stage. Temperature on the top of sample was a time-dependent function provided almost equal rate of frost front in PLAXIS (11.5 mm/day) and in-situ (12.8 mm/day). On each stage fully coupled flow-deformation analysis were carried out. On 2–10 stages excluding initial stage line loads (50 kPa) were applied.

After finishing the frost heave test compression under load 50, 100 kPa started. At 100 kPa load the sample was fully thawed. Average temperature was 275.15 K. Then following loads 150, 200 and 300 kPa at each stage were applied to continue compression test.

5.2 Influence of Selected Parameters

More than 100 numerical simulations of frost heave and compression tests were carried out to calibrate the input parameters of model. For assessment of influence

rate of input parameters on output results for silt (Table 1) and given boundary conditions, we varied only one parameter, other characteristics were without changes. We selected five parameters for calibration procedure: elasto-plastic compressibility coefficient for cryogenic suction variation (λ_s), elasto-plastic compressibility coefficient for unfrozen state (λ_0), segregation threshold (S_{seg}), initial pre-consolidation stress for unfrozen condition ($(P_{y0}^*)_{in}$) and rate of change in Young's modulus with temperature ($E_{f,inc}$). The initial values of the above parameters were applied: $\lambda_0 = 0.0249$ $\kappa_0 = 0.00498$ $\lambda_s = 0.246$ $\kappa_s = 1.64 \times 10^{-3}$; $s_{seg} = 2.1$ MPa, $P_{y0}^* = 190$ kPa, $E_{f,inc} = 1.2$ MPa/K.

Effects of selected parameters on frost heave and compression tests are shown in Fig. 7.

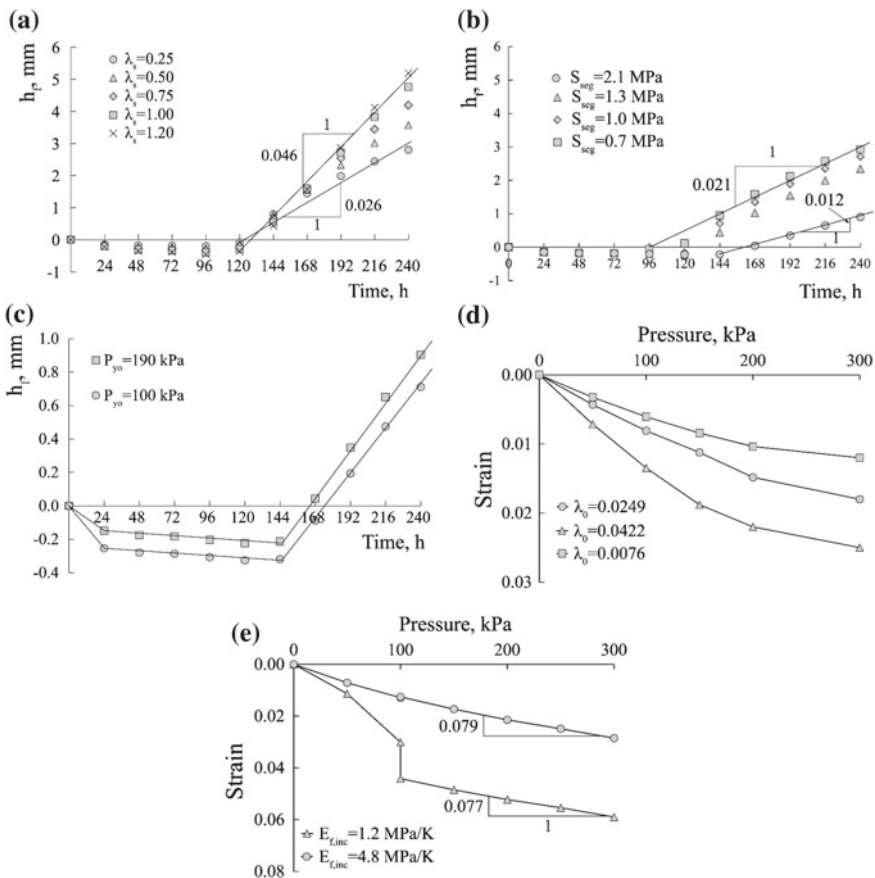


Fig. 7 Effects of most sensitive parameters on simulated frost heave and compression tests

5.3 Results

Results of the numerical simulation showed that elasto-plastic compressibility coefficient for cryogenic suction variation (λ_s) has major effect on result of simulated frost heave tests. So increasing value from 0.25 to 1.2 leads to increasing frost heave rate from 0.62 to 1.1 mm/day. Decreasing of segregation threshold (S_{seg}) from 2.1 to 0.7 MPa increases the frost heave rate from 0.29 to 0.5 mm/day.

Initial pre-consolidation stress for unfrozen condition ($(P_{y0^*})_{in}$) has a minor effect on output parameters for the given soil properties, boundary conditions and applied loads. So the increasing of pre-consolidation pressure from 100 to 190 kPa slightly decreases consolidation displacement (from 0.3 to 0.2 mm) before frost heaving is occurred.

Deviation of elasto-plastic compressibility coefficient for unfrozen state (λ_0) from mean on ± 0.0173 gives us deviation of compression strains (from 0.012 to 0.025). Unusual phenomenon was occurred when the rate of change in Young's modulus was increased in 4 times and was become 4.8 MPa/K. Thawing displacements weren't observed on the compression curve (see Fig. 7e).

It should be noted that results of numerical simulation and laboratory experiments have a good correlation. So slope of straight line of simulated consolidation curve (Fig. 7e) is equal $0.077\text{--}0.079 \text{ MPa}^{-1}$. The experimental results show that slope of straight line of "e-Ig P" (Fig. 2) is similar and is equal to $\Delta e/(1+e_0)/\Delta P = 0.77 \text{ MPa}^{-1}$. In addition, the slope of straight line of curve for unfrozen state (Fig. 3B) is equal to $0.046\text{--}0.110 \text{ MPa}^{-1}$.

Thus λ_s and S_{seg} have major effect on results of simulated frost heave test. The study of influence rate of input parameters on results allowed to calibrate parameters of the model. The frost heave and compression tests were simulated with these parameters (see Fig. 8). Initial and calibrated parameters are presented in Table 3.

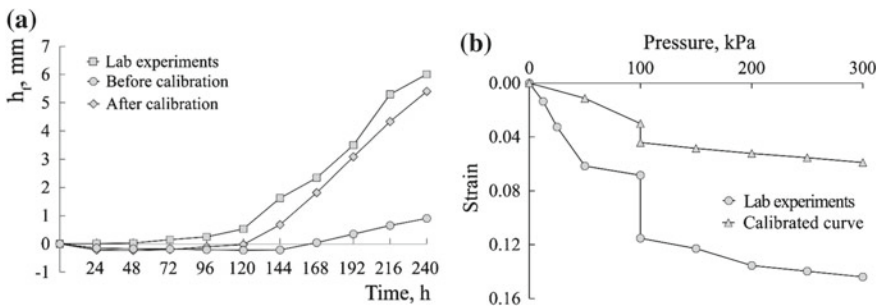


Fig. 8 Results of numerical simulation of frost heave (a) and compression (b) tests

Table 3 Model parameters for silt before and after calibration

Parameter	Before	After	Unit	Parameter	Before	After	Unit
$E_{f\text{Ref}}$	6×10^6	6×10^6	N/m ²	M	0.74	1.2	–
$E_{f\text{Incr}}$	1.2×10^6	1.2×10^6	N/m ² /K	$S_{c,\text{seg}}$	2.1×10^6	0.5×10^6	N/m ²
κ_0	0.00498	0.00152	–	κ_s	1.64×10^{-3}	8×10^{-3}	–
λ_0	0.0249	0.0076	–	λ_s	0.246	1.2	–

6 Reproduction of Field Test Data

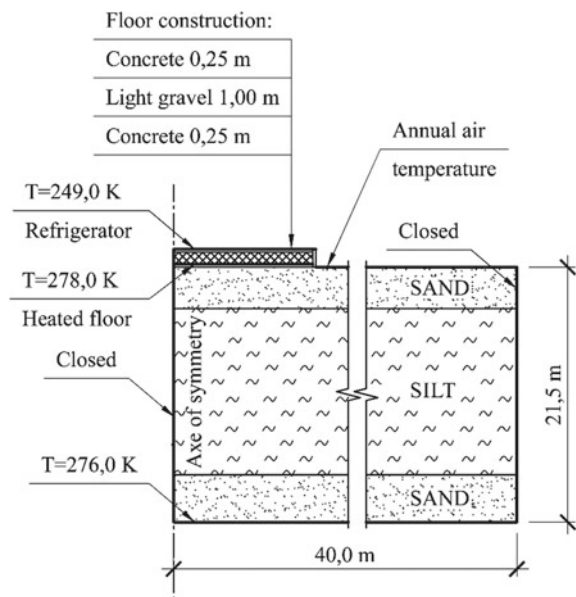
6.1 Geometry and Boundary Conditions

The next step of research was numerical modeling of process of freezing and thawing soils under cold-storage building during its life cycle from 1985 to 2014 year.

The main input parameters were the following: geometry of building, soil strata, thermal and physical properties of the soils, structure materials and annual air temperature distributed on each month. Properties of silt calibrated as result of laboratory soil tests were applied. The cross-section of geometry model is shown in Fig. 9.

Two types of temperature conditions were applied: constant and time-dependent temperature. The constant temperature was specified at the bottom of soil strata ($T = 276.0$ K) and inside building ($T = 249.0$ K).

Fig. 9 Cross-section of geometry model



The time—dependent temperature was specified for simulating the climate conditions which were presented by annual air temperature. Ground surface boundary conditions were correlated with the air temperature using an empirically determined coefficient called the “ n -factor”. The n -factor (n_f) was defined as the ratio of the surface freezing index (I_{sf}) to the air freezing index (I_{af}).

For given geotechnical situation n -factor was equal 0.3 [1]. Soil and material properties are shown in Table 4 and Sect. 5.

6.2 Simulation and Results

For simulation of temperature distribution the initial phase was applied with two thermal boundary conditions. The temperature at the surface was equal to the average annual temperature ($T = 274.15$ K). The temperature at a depth 21.5 m was set 276.15 K.

There were three stages for numerical modelling. The first stage simulated normal operation of refrigerator for the period of 10 years (April, 1985–April, 1995). Temperature inside building was 249.0 K. The heated layer under the insulation in the floor had been functioning normally for the 10 years. Temperature under floor was set 278 K.

The results are presented in Fig. 10(left). Simulated height of frost front penetration out of refrigerator ($H_f^{\text{sim}} = 1.75\text{--}1.90$ m) is approximately equal to the same height in-situ ($H_f^{\text{obs}} = 1.60\text{--}1.80$ m). There were no ice lens in soil strata under the building.

The next stage heated layer failure was simulated. For 16.5 years the heated floor hadn't been operating normally. The temperature inside the building was 249.0 K. The temperature of the heated layer in the floor was ignored in the model. Frozen soils were observed under building, simulated height of frost penetration was reached up to 10.9 m. At the end of this period frost heave phenomenon appeared.

At the last stage (September, 2012–September, 2014), heated floor and refrigerator failures were simulated. The temperature inside building was correlated to climate conditions. During geotechnical survey ice lens were observed at depth from 4 to 8 m.

The results of numerical simulation are presented in Fig. 10(right). Ice lens were located at depth from 5.2 to 10.1 m, obviously, it's rather good correlation with in-situ results. But model gives us unsatisfied values of frost heaving and as a consequence thawing displacements. Thus, in-situ uplift displacements is equal 130–180 mm and simulated displacements is only 50–60 mm.

Table 4 Soil and material properties

Parameters	Name	Soil		Material		Unit
		Silt	Sand	Concrete	Light gravel	
<i>General</i>						
Material model	Model	FU model	Mohr-Columb	Linear elastic	Linear elastic	–
Type of material behaviour	Type	Drained	Drained	Non-porous	Non-porous	–
Soil unit weight above phreatic level	γ_{unsat}	19.4×10^3	16.5×10^3	20×10^3	8×10^3	N/m ³
Soil unit weight below phreatic level	γ_{sat}	19.6×10^3	19.9×10^3	20×10^3	8×10^3	N/m ³
Initial void ratio	e_{init}	0.66	0.65	0	0	–
Young's modulus	E'	–	28×10^6	20×10^9	20×10^6	N/m ²
Poisson ratio	ν'	0.31	0.30	0.15	0.15	–
Cohesion	c'_{ref}	–	2000	–	–	N/m ²
Frictional angle	φ'	–	30	–	–	°
<i>Groundwater</i>						
Data set	–	USDA	USDA	–	–	–
Model	–	Van Genuchten	Van Genuchten	–	–	–
Soil type	–	Silt	Sand	–	–	–
<i>Thermal</i>						
Thermal conductivity	λ_s	1.50	2.70	1.40	0.16	W/m/K
Specific heat capacity	c_s	730	700	504	938	J/kg/K
Soil density	ρ_s	2710	2650	2000	900	kg/m ³
Unfrozen water content	–	Grain size distribution	Grain size distribution	None	None	–
Specific surface area	SSA	100	5.58	–	–	m ² /g

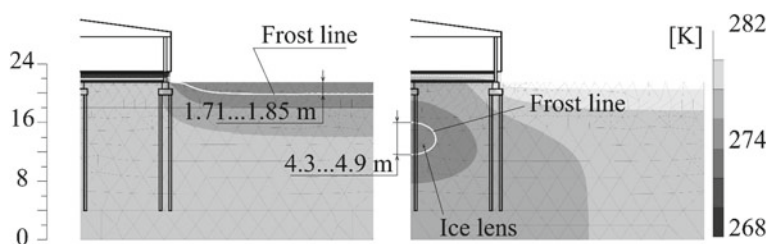


Fig. 10 (Left) Seasonal frost depth in April from 1985 to 1995. (Right) Temperature distribution after two years operation pause (September 2014)

7 Discussions

Results of numerical simulation and experiments showed that the laboratory frost heave and compression tests allow us to define such parameters of FU model as elasto-plastic compressibility coefficient for cryogenic suction variation (λ_s), elasto-plastic compressibility coefficient for unfrozen state (λ_0), segregation threshold (S_{seg}), initial pre-consolidation stress for unfrozen condition ($(P_{y0^*})_{in}$). But it's required to apply calibration coefficients to get best-fit results. For instance, to obtain calibrated λ_s the latter is to be multiply on coefficient equal 4–5. For segregation threshold, the calibrated coefficient should be equal 1/4–1/3.5. For elasto-plastic compressibility coefficient for unfrozen state the initial input value is to be multiplied on 0.3–0.5. Elastic compressibility coefficient for cryogenic suction variation (κ_s) is too difficult to define because the “ $v \cdot \ln(s_c + p_{atm})$ ” approximation is close to horizontal line. To define precise value of κ_s another test should be used, for instance, unconfined compression test.

Numerical simulation of in-situ investigations showed that frozen and unfrozen soil model is rather good in frost front rate within freezing and thawing process. Deviation of depth of frost penetration from observed one doesn't exceed 0.10–0.15 m below undeveloped area and 0.5–0.85 m under building. But model gives us unsatisfied values of frost heaving and as a consequence thawing displacements. Thus, in-situ uplift displacements is equal 130–180 mm and simulated displacements is only 50–60 mm.

Values of three parameters (λ_s , κ_s , S_{seg}) which is responsible for suction strains, have a huge gap between observed and calibrated input parameters. The gap can be explained by peculiarity of determination of crysuction. In FU model crysuction is varied from 100 kPa to 6 MPa. Actually, the crysuction at the frost front in frozen fringe doesn't exceed 80 kPa according investigation performed by Konrad and Morgenstern [8]. Knutsson S. et al. showed that for highly frost susceptible soils suction values also doesn't exceed 9 kPa. Hohmann [7] obtained low value of cryogenic suction, which vary from 10 to 400 kPa. So to get predicted input parameters FU model should be modified according to result of laboratory experiments and in-situ investigations.

8 Conclusions

The paper presents the results of calibration procedure of frozen and unfrozen soil model (FU model) developed by PLAXIS bv and NTNU according to outcomes of laboratory test and in-situ investigations. The model describes frost heaving as a function of frost front penetration rate and water migration rate from unfrozen zone.

Initial input parameters of the model obtained as result of lab tests and in-situ are required to be calibrated. For silts with or without fine sand elasto-plastic compressibility coefficient for cryogenic suction variation (λ_s) is to be multiplied on 4–5, elasto-plastic compressibility coefficient for unfrozen state (λ_0)—0.3–0.5, segregation threshold (S_{seg})—0.25–0.29.

To get predicted results of numerical simulation according to laboratory and in-situ tests FU model should take into account the peculiarity of determination of cryogenic suction and its in-situ observed values.

The FU model has proven itself in the simulation of separate processes, for example, frost heaving or thawing and consolidation processes. However, when all processes are simulated consistently with using unified geometry and boundary conditions, in some cases FU model works unstable. There is a good possibility to improve and enhance the model.

References

1. Andersland O, Ladanyi B (2004) Frozen ground engineering. 2nd edn. Am Soc Civ Eng. XII + 363 p. Chichester: John Wiley & Sons. ISBN: 978-0-471-61549-1
2. Aukenthaler M, Brinkgreve R, Haxaire A (2016) Evaluation and application of a constitutive model for frozen and unfrozen soil. In: Proceedings of the GeoVancouver 2016: the 69th Canadian geotechnical conference. Vancouver, Canada, pp 1–8
3. Aukenthaler M (2016) The frozen & unfrozen barcelona basic model. A verification and validation of a new constitutive model. Thesis report. TU Delft and Plaxis bv, Delft
4. Churkin S, Nikitin A, Nevzorov A et al (2015) Deformation of building on pile foundation due to frost heave. In: 15th Asian regional conference on soil mechanics and geotechnical engineering, ARC 2015. Kyushu, Japan, pp 1420–1423
5. Ghoreishian Amiri S, Grimstad G, Kadivar M et al (2016) Constitutive model for rate-independent behavior of saturated frozen soils. *Can Geotech J* 53(10):1646–1657
6. Ghoreishian Amiri S, Grimstad G, Aukenthaler M et al (2016) Frozen and unfrozen soil model. Plaxis Company, Delft
7. Hohmann M (1997) Soil freezing—the concept of soil water potential. State of the art. *Cold Reg Sci Technol* 25:101–110 (1997)
8. Konrad J, Morgenstern N (1981) The segregation potential of a freezing soil. *Can Geotech J* 18:482–491
9. Rempel A (2007) Formation of ice lenses and frost heave. *J Geophys Res* 112:F02S21
10. Thomas HR et al (2009) Modelling of cryogenic processes in permafrost and seasonally frozen soils. *Geotechnique* 59(3):173–184

The Frozen Depth and Its Prediction Affected by Shallow Phreatic Groundwater by Modified Berggren Equation



Xiaoqiang Liu, Jiankun Liu, Yahu Tian and Yupeng Shen

Abstract In order to study the influence of shallow phreatic groundwater on the maximum frozen depth of the subgrade in the seasonally frozen region, this paper verified the applicability of the modified Berggren equation predicting the maximum frost depth based on the monitoring geotemperature and air temperature in stratum whether the shallow phreatic groundwater does exist. The shallow phreatic groundwater lowers the mean geotemperature, delays it to the extreme value, and reduces the maximum frozen depth in the cold season. The shallow phreatic groundwater lowers the surface freezing index, which makes the average surface n -factor smaller. The influence of shallow phreatic groundwater on the thermal diffusivity of the stratum is small but has a significant influence on the thermal conductivity. The slope of the modified Berggren equation is almost unaffected by shallow phreatic groundwater, and the applicability of the equation predicting the maximum frozen depth is verified based on the thermal conductivity calculation, no matter the shallow phreatic groundwater does exist.

Keywords Shallow phreatic groundwater · Temperature monitoring · Thermal parameters · Modified Berggren equation

1 Introduction

The geotemperature is mainly determined by the thermal properties of soil, the heat flow inside the earth, and the temperature of the air (surface). The thermal properties of soil are affected by many factors such as soil mineral composition, dry density, and water content [1, 2]. The existence of shallow phreatic groundwater can significantly influence the geotemperature, especially the line engineering crosses the seasonally frozen region where the shallow phreatic groundwater is shallow, and the correlation

X. Liu · J. Liu (✉) · Y. Tian · Y. Shen
School of Civil Engineering, Beijing Jiaotong University, Beijing 100044, China
e-mail: liujiank@mail.sysu.edu.cn

J. Liu
School of Civil Engineering, Sun Yat-Sen University, Zhuhai 519082, Guangdong, China

© Springer Nature Singapore Pte Ltd. 2020
A. Petriaev and A. Konon (eds.), *Transportation Soil Engineering in Cold Regions*,
Volume 2, Lecture Notes in Civil Engineering 50,
https://doi.org/10.1007/978-981-15-0454-9_13

between the frost penetration in the cold season and the shallow phreatic groundwater is strong [3, 4].

Many simple methods were tried to obtain the frozen depth in the seasonally frozen region, and the air or geotemperature was essential. Based on the meteorological data along the Moscow-Kazan high-speed railway, Liu et al. adopted numerical simulation to analyze the temporal and spatial variation characteristics of the 0 °C isotherm inside the embankment [5]. Liu et al. explored the influence of structural type on the 0 °C isotherm in subgrade by analyzing the geothermal monitoring data in different structure types along the Harbin-Dalian high-speed railway in China [6]. Li et al. compared the freezing depth with the frost heaving of Harbin-Dalian high-speed railway in two freeze-thaw cycles and analyzed the interrelation between the air temperature and frost depth [7]. The design frozen depth in typical embankments of Moscow-Kazan high-speed railway was estimated by both the maximum freezing index over the years and average aggregate particle size based on the railway subgrade design code in Russia [8]. Zhang estimated the more accurate frozen depth modified by the polynomial regression analysis based on the geothermal data and proposed the frozen depth prediction equation according to the linear regression between the frozen depth and air freezing index [9].

Numerical methods may be adapted to model complex geometrical boundaries and time-dependent thermal properties. The two methods most often referred to include the Stefan equation and the modified Berggren equation which assume that the latent heat of soil moisture is the only heat that must be removed when freezing soil [10]. Due to the insufficient in calculating the multi-layer soil freeze-thaw interface based on the Stefan equation JL and NM algorithm, the XG algorithm can determine the freeze-thaw interface more rigorously [11]. Gao et al. analyzed the correlation between the maximum frozen depth of many meteorological stations and the calculated values based on the Stefan equation in the Tibetan seasonally frozen regions and then calculated the maximum freezing depth in other parts of Tibet [12]. The air freezing index and the semi-empirical method of modified Berggren equation were directly used to compare the frozen depth prediction value with the field measured value of the high-speed railway subgrade in the seasonally frozen regions and proposed the calculation formula of the frozen depth for the high-speed railway subgrade design [13]. Wang et al. discussed the modified Berggren method which can calculate the freezing depth of the multi-layer soil structure by using the air freezing index, and the feasibility of the method to predict the frozen depth was confirmed by comparing the calculated value with the monitored value [14]. Based on the surface freezing index transformed from the air freezing index in eastern Turkey, Stefan equation and modified Berggren equation were used to predict the frozen depth of highway multi-layer structure and verify the superiority of the modified Berggren equation by comparing with the measured values [15]. Ai calculated the maximum frozen depth through the surface freezing index of five cities along the Harbin-Dalian high-speed railway by using the modified Berggren equation, and the applicability of the equation was verified [16].

The mean daily air temperature and the mean daily geotemperature of two typical zero-section subgrades of the Shenchu section of the Shenshuo heavy-haul railway in

the seasonally frozen region are monitored in the past two years. Firstly, the freezing indices, the surface n -factor, and the thermal diffusion coefficient of the unfrozen soil are obtained from the monitoring data. The thermal conductivity of the frozen soil in the stratum is calculated based on the slope of the modified Berggren equation. Both the thermal properties of unfrozen or frozen soil are compared to discuss influence of the shallow phreatic groundwater. Then, the feasibility of the modified Berggren equation in predicting the frozen depth is verified by comparing the estimated and calculated thermal conductivity, no matter the shallow phreatic groundwater does exist.

2 Geothermal Data Analysis

2.1 Monitoring Points

The geothermal monitoring points are located in Shenchu County, Shanxi Province of China which has an altitude of over 1400 m. Monitoring point A is located 25 m outside the left shoulder where the terrain is flat, and the vegetation cover around point A is mainly grass. There was no apparent surface water in the vicinity, and no shallow phreatic groundwater was found in the borehole. Monitoring point B is located 10 m outside the right side of the subgrade. Although vegetation cover near the borehole is grass, there are tall trees and the waste bank blocking the sunlight from the east or the south orientations. There is no surface water at this location. However, it was found in the borehole that there is shallow phreatic groundwater at a depth of 0.6 m in July 2017, which can be regarded as a research point for the influence of shallow phreatic groundwater on geotemperature. Point C is the meteorological station of Shenchu County in Shanxi Province, and the ground surface temperature sensor is buried at a depth of 5 cm. The soils in the strata are the same at the three monitoring points, and the detailed information and earth-surface appearance are shown in Table 1 and Fig. 1, respectively.

Table 1 Information of monitoring points

Monitoring point	Location	Elevation (m)	Shallow phreatic groundwater table (m)	Monitoring depth (m)
A	N39°04'05" E112°04'51"	1433	N/A	10
B	N39°05'11.96" E112°12'41.61"	1530	0.6	10
C	N39°06'27" E112°12'42"	1525.4	N/A	5

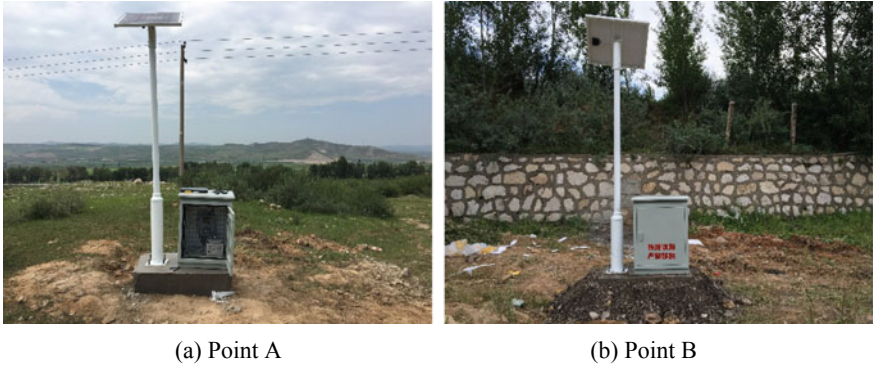


Fig. 1 Earth surface appearance of the monitoring points

2.2 Geotemperature

During the two years from August 1, 2016, to July 31, 2018, geotemperature data were collected every six hours from 0 o' clock everyday, and the mean value was taken as the average daily geotemperature. Figures 2 and 3 show the change of geotemperature within two years in point A and B, respectively.

The curve form of the geotemperature over time can utilize sine wave. Except for the curve fluctuation of the ground temperature measured by the shallowly buried sensors, the geotemperature curves at other buried depths are the smooth sine wave. The sinusoidal function is used to fit the ground temperature variation law at different depths as shown in Eq. (1).

$$T = T_{0H} + A_H \times \sin(2\pi(t - t_{cH})/p) \tag{1}$$

Fig. 2 Geotemperature of point A

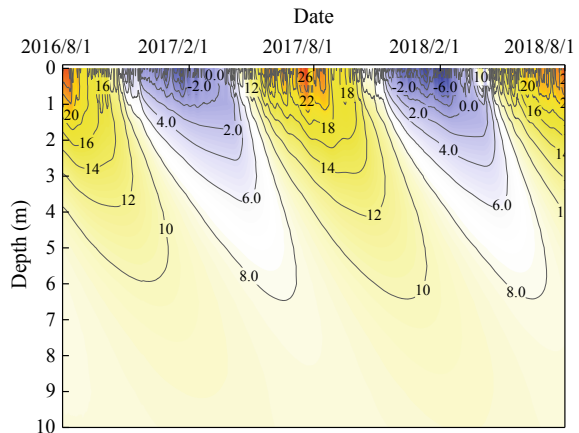
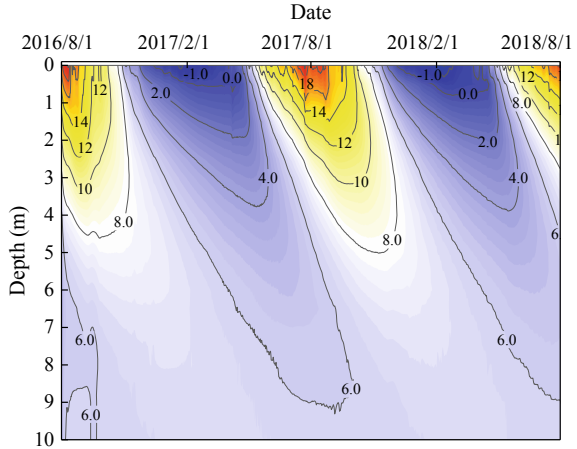


Fig. 3 Geotemperature of point B



where T_{0H} is the mean annual geotemperature in buried depth H , A_H is the geotemperature amplitude in buried depth H , p is the period equals to 365.25 days, and t_{cH} is the phase difference in buried depth H and represents the delay of the extremum. The parameters in Eq. (1) are fitted and listed in Tables 2 and 3.

The relation between the mean annual geotemperature T_{0H} and the buried depth H in Table 2 can be fitted by a linear function, as shown in Eq. (2).

$$T_{0H} = a + bH \tag{2}$$

where a is the annual geotemperature at the ground surface and equals to 9.60 °C, and b is the gradient of -0.097 °C/m.

Table 2 Parameters of geotemperature in point A

Buried depth (m)	T_{0H} (°C)	t_{cH}	A_H (°C)	R^2
0	9.61	312.61	15.12	0.93
1.0	9.52	333.53	11.01	0.98
2.0	9.41	357.09	7.054	0.98
3.0	9.32	380.64	4.423	0.99
4.0	9.20	406.22	2.759	0.99
5.0	9.08	431.56	1.736	0.99
6.0	8.97	457.77	1.108	0.98
7.0	8.89	483.46	0.744	0.97
8.0	8.82	507.69	0.522	0.95
9.0	8.75	529.77	0.374	0.93
10.0	8.68	551.11	0.268	0.89

Table 3 Parameters of geotemperature in point B

Buried depth (m)	T_{0H} (°C)	t_{cH}	A_H (°C)	R^2
0	6.93	273.29	10.34	0.97
1.0	6.76	294.66	7.076	0.95
2.0	6.60	314.73	4.777	0.94
3.0	6.49	335.10	3.180	0.93
4.0	6.42	355.85	2.151	0.93
5.0	6.37	379.27	1.443	0.94
6.0	6.32	402.95	0.970	0.95
7.0	6.26	427.08	0.617	0.94
8.0	6.25	449.75	0.449	0.91
9.0	6.27	471.50	0.274	0.81
10	6.26	492.26	0.185	0.68

While the relation between the mean annual geotemperature T_{0H} and the buried depth H in Table 3 is not as simple as linearity and can be fitted by logistic function in Eq. (3).

$$T_{0H} = A_1 + (a - A_1) / (1 + (H/H_0)^p) \quad (3)$$

where a equals to 6.93 °C, A_1 is the mean annual geotemperature when the buried depth toward infinity and equals to 6.05 °C, H_0 is the turning point where the mean annual geotemperature increment approaches zero, the magnitude is about 3 m, and p is a dimensionless parameter indicating the curvature of the logistic function and equals to 1.315.

The amplitude of the annual geotemperature A_H changing with the buried depth H can employ Eq. (4) to fit the curves.

$$A_H = A_S \exp\left(-H\sqrt{\pi / (\alpha_u p)}\right) \quad (4)$$

where A_S is the amplitude at the ground surface and α_u is the unfrozen soil thermal diffusivity. The magnitudes of A_S and α_u in point A are 15.11 °C and 0.05392 m²/Day, respectively. And, the values of A_S and α_u in point B are 10.33 °C and 0.056 m²/Day, respectively.

The depth-dependent phase difference t_{cH} can adopt the linear equation in Eq. (2) to fit the relationships. The magnitudes of parameter b in both point A and point B are 24.60 and 22.18 m⁻¹, respectively.

The mean annual geotemperature T_{0H} , annual geotemperature amplitude A_H , and phase difference t_{cH} changing with the buried depth H and those fitting effect are plotted in Fig. 4, respectively. The mean annual geotemperature T_{0H} decreases with the buried depth H , which is a typically negative gradient geothermal curve. The

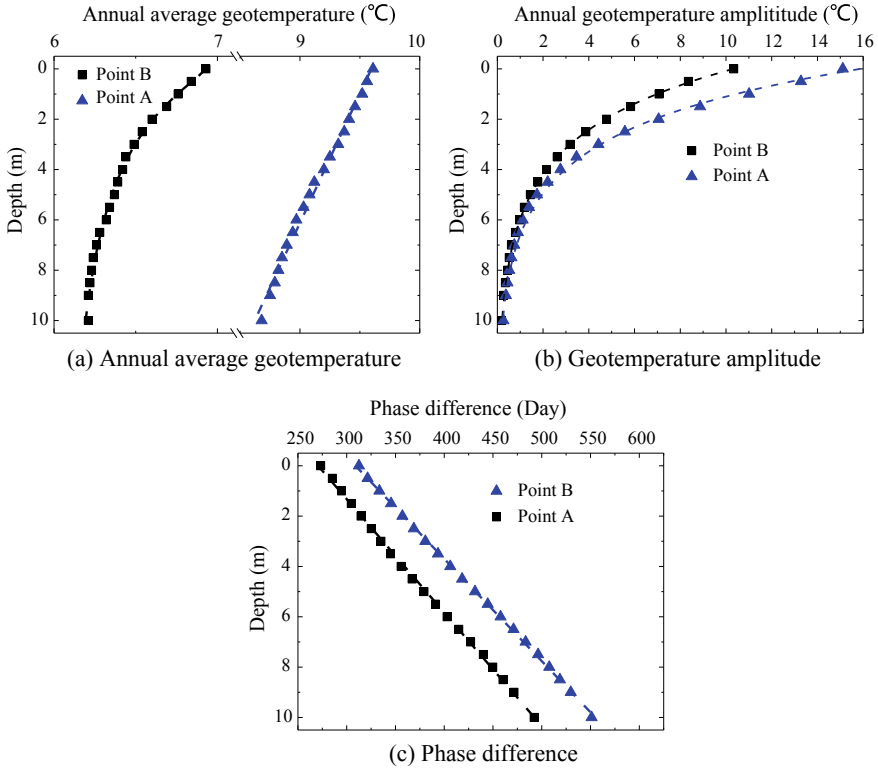


Fig. 4 Parameters in Eq. (1) changing with depth

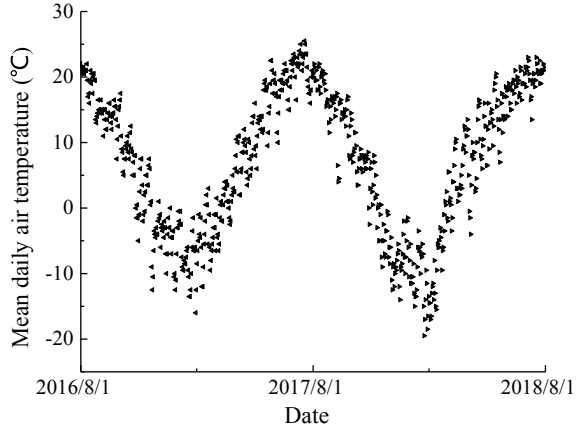
annual heat flow direction is from top to bottom, and the annual heat dissipation is less than the heat absorption. So, the stratum is an endothermic type whose temperature is increasing. The geotemperature amplitude range within 10 m is greater than 0.1 °C, which indicates that the depth of zero annual amplitude is deeper than 10 m. Phase difference t_{cH} increases with the buried depth, which indicates that the extremum of the geotemperature will delay with the increasing depth.

The average monthly ground surface temperatures of point C in cold seasons from 2011 to 2018 are given in Table 4. Any spring or autumn month that includes a

Table 4 Average monthly ground surface temperature of point C (Unit: °C)

Year	Month					
	10	11	12	1	2	3
2016–2017	7.2	0.2	−3.6	−6.6	−3.2	2.2
2017–2018	6.7	−0.8	−7.0	−8.3	−6.3	7.2

Fig. 5 Mean daily temperature from 2016 to 2018



seasonal maximum or minimum is called a changeover month. Namely, the November and March are the changeover month in autumn and spring, respectively. And, January is the coldest month.

2.3 The Calculation of Air Freezing Index

Figure 5 shows the mean daily air temperature in Shenchi meteorological station from 2016 to 2018. Based on the mean daily air temperature of the meteorological station from 2016 to 2018, the air freezing index is calculated as -596.5 °C Day and -883.0 °C Day, respectively.

3 Applicability of the Modified Berggren Equation

3.1 Ground Surface Freezing Index and Maximum Frost Depth

The Lagrangian interpolation method is used to determine the 0 °C isotherm over time in the stratum. The temporal and spatial variation of the 0 °C isotherm in the two cold seasons of the monitoring points is obtained in Fig. 6. The maximum frozen depth of monitoring point A in the first monitoring period is 1.08 m, while the maximum frozen depth of point B is only 0.63 m. The maximum frozen depth of point A in the second period is 1.36 m, while the maximum frozen depth of point B is 0.80 m. It is clear that the maximum frozen depth of the cold season is significantly affected by shallow phreatic groundwater. The phase change of abundant shallow

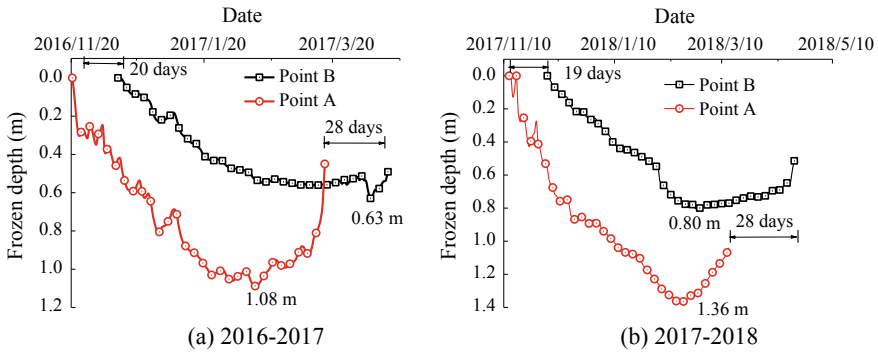


Fig. 6 Comparison of frozen depth

phreatic groundwater at point B releases a large amount of latent heat and inhibits the development of frozen depth during the frosting process in the cold seasons. Due to the high thermal conductivity of saturated soil, the much more heat in the deep stratum can transmit to the ground surface which leads to a positive impact on reducing the frozen depth.

Another significant feature in Fig. 6 is the difference of the freezing start dates and the melting end dates of the two monitoring points. The freezing start date of point B is about 20 days later than that of point A, and the melting end date of point B is also posterior to the date of point A. It indicates that a large quantity of shallow phreatic groundwater phase-change latent heat can delay the freezing of the stratum and cause ice layers appearing in the stratum which will eventually lead to longer time in melting process during the spring.

The ground surface freezing index (I_{sf}) is defined as the cumulative degree-days versus time when the temperature at the ground surface is subzero. The ground surface freezing indices of the point A and B are obtained directly from Figs. 2 and 3 by summation of the minus mean daily ground surface temperature, while the ground surface freezing index of point C can be calculated by the method based on Table 4 by Boyd’s method [17]. Surface n -factor is defined as the ratio of the ground surface freezing index to the air freezing index, and the results are shown in Table 5.

By comparing the air freezing index with the ground surface freezing index of different monitoring points, shallow phreatic groundwater can significantly reduce the ground surface freezing index, which makes the surface n -factor relatively smaller.

3.2 Parameters of the Modified Berggren Equation

The average value of the maximum frozen depth measured in a flat, bare, and open site outside the city for no less than ten years is called the maximum frozen depth of the area. In the deriving of the maximum frozen depth in modified Berggren

Table 5 Frost depth and surface frost index

Monitoring point	Monitoring period (year)	Ground surface freezing index (°C Day)	Mean surface <i>n</i> -factor	Maximum frost depth (m)
A	2016–2017	−384.627	0.645	1.08
	2017–2018	−659.847		1.36
B	2016–2017	−129.720	0.222	0.63
	2017–2018	−199.629		0.80
C	2016–2017	−465.32	0.794	0.82
	2017–2018	−714.26		1.13

equation, it was assumed that the latent heat is the only heat that must be removed when freezing the soil. Thermal energy stored in the form of volumetric heat, which is released as soil temperature drop to and below the freezing point, is neglected. And, the heat released by the soil moisture at the frost line, as it freezes a depth dX in time dt , equals the rate at which heat is conducted to the ground surface. So, the modified Berggren equation can be written as follows.

$$X = \lambda(2k_f I_{sf}/L)^{0.5} \tag{5}$$

where X is the depth, t the time, L the latent heat of the soil, k_f the frozen soil thermal conductivity, I_{sf} the ground surface freezing index, and λ the correction coefficient.

The frozen depth X has a linear relation with $I_{sf}^{0.5}$ as illustrated in Fig. 7, and whose gradient is $\lambda(2k_f/L)^{0.5}$. So, the gradients of point A and B are $0.0550 \text{ [m}^2\text{/(M Day } ^\circ\text{C)}]^{0.5}$ and $0.0561 \text{ [m}^2\text{/(M Day } ^\circ\text{C)}]^{0.5}$, respectively.

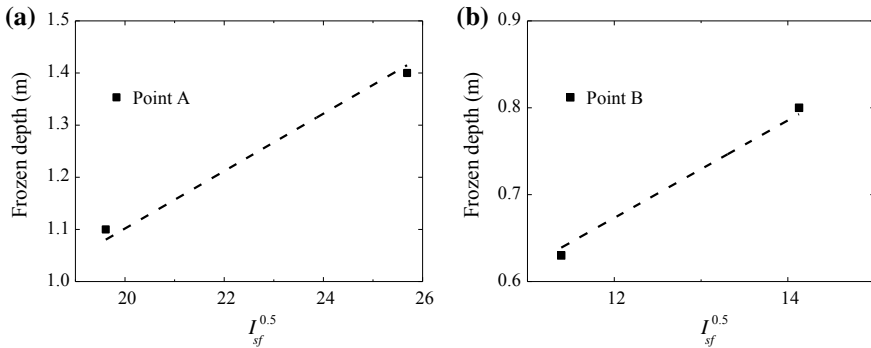


Fig. 7 Relation between $I_{sf}^{0.5}$ and maximum frozen depth

3.3 Applicability Check of the Modified Berggren Equation

The correction coefficient λ , which is dimensionless, is a function of two dimensionless parameters α and μ [10, 18].

$$\alpha = T_0 \times t / (I_{sf}) \text{ Thermal ratio} \tag{6}$$

$$\mu = c_v I_{sf} / (1000 Lt) \text{ Fusion parameter} \tag{7}$$

where T_0 is the mean annual ground surface temperature, t the dates which daily surface temperature below 0 °C, and c_v (kJ/m³ K) the soil volumetric heat capacity.

Using the specific heat of a material defined as the ratio of its heat capacity to that of water in degrees Celsius, volumetric heat capacity for unfrozen mineral soils can be calculated as

$$c_v = \rho_d / \rho_w (0.17 + 1.0 \times w / 100) c_{vw} \tag{8}$$

where $c_{vw} = 4.187 \text{ MJ}/(\text{m}^3 \text{ }^\circ\text{C})$, ρ_d and ρ_w are the unit mass of the dry soil and water, respectively. The specific heats 0.17 and 1.0 correspond to mineral soil and water, respectively.

For soils, the total energy involved in the phase change process will depend on the total water contained in a given soil volume and the fraction of this water that changes phase. For a given soil,

$$L = \rho_d L' (w - w_u) / 100 \tag{9}$$

where $L' = 33.7 \text{ kJ}/\text{kg}$ is the mass latent heat for water, w is the total water content, and w_u is the unfrozen water content in frozen soil. For practical problems, the assumption that w_u is zero will give acceptable L values.

Based on the stratum information of the monitoring points in Table 6, the unfrozen soil thermal conductivity can be calculated by the formula between the thermal diffusivity and conductivity. Also, the thermal ratio and fusion parameter can be obtained from the above monitoring and calculated values, and then, the correction coefficient is determined in Eq. (5) [10] (Aldrich and Paynter 1966). Therefore, the

Table 6 Geological survey of the monitoring points

Point	Depth (m)	Mean water content (%)	Dry density (g/cm ³)
A	0-4	12.1	1.732
	4-8	18.3	1.784
	8-10	12.2	1.883
B	0-6	21.5	1.760
	6-10	28.3	1.582

Table 7 Calculated values of thermal conductivity based on monitoring data (W/(m °C))

Point	Year	Thermal conductivity of unfrozen soil	Thermal conductivity of frozen soil
A	2016–2017	1.19	2.30
	2017–2018	1.21	2.13
B	2016–2017	1.74	3.83
	2017–2018	1.88	3.93

only parameter unknown in the gradient $\lambda(2k_f/L)^{0.5}$, which is the frozen soil thermal conductivity, can be calculated, as shown in Table 7.

The estimated thermal conductivity of unfrozen soil can be acquired by Eq. (10) based on the water content w and dry density ρ_d .

$$k_u = 0.1442(0.9 \log w - 0.2)10^{0.6243\rho_d} \quad (10)$$

As shown from Eqs. (11) to (14), the estimated thermal conductivity of unsaturated frozen soil is the combination of the saturated frozen soil thermal conductivity k_{sat} and dry frozen soil thermal conductivity k_{dry} , with Kersten number K_e related to saturation [19].

$$k_{\text{sat}} = k_s^{1-n} k_i^{n-w_u} k_w^{w_u} \quad (11)$$

$$k_{\text{dry}} = \frac{(0.137\rho_d + 64.7)}{(2700 - 0.947\rho_d)} \pm 20\% \quad (12)$$

$$K_e = S_r \quad (13)$$

$$k_f = (k_{\text{sat}} - k_{\text{dry}})K_e + k_{\text{dry}} \quad (14)$$

where, n is the soil porosity; ρ_d is the dry density (kg/m^3); k_s is the thermal conductivity of solid particles and $k_s = 5.2 \text{ W/m K}$ [20]; $k_i = 2.2 \text{ W/m K}$ and $k_w = 0.57 \text{ W/m K}$; and w_u is the unfrozen water content in frozen soil and assumed as zero.

The estimated thermal conductivity by empirical equations from Eqs. (10) to (14) and calculated thermal conductivity by monitoring data are demonstrated in Table 8. The errors between the thermal conductivity are less than 10%, so the applicability

Table 8 Comparison between the calculated and estimated thermal conductivity (W/(m °C))

Monitoring point	Unfrozen soil		Frozen soil	
	Calculated value	Estimated value	Calculated value	Estimated value
A	1.20	1.35	2.22	2.23
B	1.81	1.76	3.88	3.69

of the modified Berggren equation can predict the maximum frozen depth affected by shallow phreatic groundwater.

4 Conclusion

- (1) The shallow phreatic groundwater lowers the mean geotemperature, delays it to the extreme value, and reduces the maximum frozen depth in the cold season. The shallow phreatic groundwater also lowers the ground surface freezing index, namely reduces the average surface n -factor.
- (2) The influence of shallow phreatic groundwater on the thermal diffusivity of the stratum can be neglected, but it has an ignored influence on the thermal conductivity of the soil.
- (3) The slope of the modified Berggren equation is almost unaffected by shallow phreatic groundwater, and the equation predicting the maximum freezing depth affected by groundwater is effectively verified via comparison of the thermal conductivity.

Acknowledgements This research was supported by the project (No. 41731281 & 41801055) the National Natural Science Foundation of China, by the project (No. 2015-10) funded by Shenhua Shenshuo Railway Branch of China, and by the project (No. 2017G002-S) funded by China Railway Corporation.

References

1. Wei W, Zheng G, Luan Y (2010) Characteristics and influence factors of the shallow geothermal field in Beijing plain area. *Geol China* 34(6):1733–1739 (in Chinese)
2. Lanzhi L, Jin H, Wang S et al (2008) Dual influence of local environmental variables on ground temperature on the interior-eastern Qinghai-Tibet Plateau (II): Sand-layer and surface water bodies. *J Glaciol Geocryology* 20(4):546–555 (in Chinese)
3. Wang S (1982) Frost heave and its distribution in different layers influenced by shallow phreatic groundwater. *J Glaciol Cryopedology* 4(2):55–62 (in Chinese)
4. Wang X (1980) Experimental research of frost heave under different level of ground water in various soils. *J Glaciol Cryopedology* 2(3):40–45 (in Chinese)
5. Liu W, Zhang Y, Mi J et al (2018) Temperature distribution of Moscow-Kazan high-speed railway roadbed in Russia. *J Railway Sci Eng* 101(8):34–42 (in Chinese)
6. Liu H, Niu F, Nui Y et al (2015) Effect of structure style on subgrade frozen characteristics of high-speed railway in cold regions. *Rock Soil Mech* 26(11):3135–3142 (in Chinese)
7. Li X, Niu F, Liu H et al (2018) Characteristics and engineering significance of frost heaving in subgrade of Harbin-Dalian high-speed railway. *J Glaciol Geocryology* 40(1):55–61 (in Chinese)
8. Zhang D, Xue Y, Luo Q et al (2018) Research on the anti-frost subgrade bed structure of Moscow-Kazan high-speed railway in Russia. *J Railway Eng Soc* 235(4):29–33 (in Chinese)
9. Dongqing Zhang (2008) Research on the diseases of seasonally frozen roadbed and control measures. Jilin University, Jilin (in Chinese)

10. Aldrich HP Jr, Paynter HM (1996) Depth of frost penetration in non-uniform soil, vol 104. U.S. Army Cold Regions Research and Engineering Laboratory Special Report
11. Xie CW, Gough WA (2017) Comments on thaw-freeze algorithms for multilayered soil, using the Stefan equation. *Sci Cold Arid Reg* 9(6):0525–0533. <https://doi.org/10.3724/SP.J.1226.2017.00525>
12. Gao S, Zeng W, Wu Q et al (2018) Temporal and spatial variations of the maximum frozen depth of seasonally frozen soil in Tibet from 1990 to 2014. *J Glaciol Geocryology* 40(2):223–230 (2018) (in Chinese)
13. Du X, Ye Y, Zhang Q et al (2015) Frost depth of high-speed railway subgrade in the seasonally frozen ground region. *China Railway Sci* 141(2):13–19 (in Chinese)
14. Wang Z, Ye Y, Yan H et al (2013) Discussion on calculation method of frost depth in anti-freeze expansion design of railway subgrade in cold area. *Railway Eng* 2:57–59 (in Chinese)
15. Orakoglu M-E, Liu J, Tutumluer E (2016) Frost depth prediction for seasonal frost area in Eastern Turkey. *Cold Reg Sci Technol* 124:118–126
16. Ai Q (1975) Experimental research on high-speed railway subgrade frost-depth in cold areas. China Academy of Railway Science Corporation Limited, Beijing (in Chinese)
17. Boyd DW (1976) Normal freezing and thawing degree-days from normal monthly temperatures. *Can Geotech J* 13(2):176–180
18. Andersland OB, Ladanyi B (2004) *Frozen ground engineering*. ASCE, US, pp 57–67
19. Johansen O (1977) *Thermal conductivity of soils*. Norwegian Technical University, Trondheim
20. Qian J, Yin Z (1996) *Geotechnical principle and calculation*. China Water & Power Press, Beijing, pp 2–4 (in Chinese)

Calculation of Soil–Transport Structure Interaction



A. G. Shashkin, K. G. Shashkin and V. M. Ulitsky

Abstract The paper considers soil–transport structure interaction. Soil deformations, completely defining deformations of a road embankment, require an accurate prediction with a help of effective models of soil behavior, which take into account its non-linear and rheological behavior. There is given a visco-plastic model of behavior of soil of small and medium degree of lithification, which allows predicting development of deformations of transport structures in time. It is demonstrated that settlements of structures are defined not only by deformations of consolidation but also by deformation of form change. The authors implemented the soil model in the software complex FEM models, which is an import-substituting domestic production overtaking capacities of western analogs according to the speed of solution of non-linear and rheological problems. The paper shows the results of verification of the software for meeting the results of monitoring of a renown site of transport construction—the dam for protecting St. Petersburg against floods, which test grounds served for long-term investigations of the process of soil deformation under different draining conditions.

Keywords Visco-plastic soil model · Soil–structure interaction calculations · Verification · Soft clayey soil · Embankment deformations · Glacial and lacustrine-glacial deposits

1 Introduction

Transport construction in Russia is on the threshold of creating a new quality of aboveground facilities—emerging high-speed railways and highways. High-speed transit is associated with higher risks and, consequently, stricter requirements for road deformations. Requirements for deformations, which are set for railroads, are

A. G. Shashkin (✉) · V. M. Ulitsky
Emperor Alexander I St. Petersburg State Transport University, St. Petersburg, Russia
e-mail: mail@georec.spb.ru

K. G. Shashkin
PI “Georeconstruction”, St. Petersburg, Russia

© Springer Nature Singapore Pte Ltd. 2020
A. Petriaev and A. Konon (eds.), *Transportation Soil Engineering in Cold Regions*,
Volume 2, Lecture Notes in Civil Engineering 50,
https://doi.org/10.1007/978-981-15-0454-9_14

unprecedentedly tough: according to the draft of the new Russian set of regulations relative deformations should not exceed 0.00025 that is by order smaller than in civil construction. Absolute settlements of railroad bed are limited to the value of 15 mm. Evidently, it is impossible to meet these requirements using traditional approaches of road construction to engineering investigations, calculations, design, and construction.

One of the most important components of success is enhancing accuracy of calculations of strains of line structures. Also the necessary conditions of it include reliable initial data on engineering-geological and hydro-geological conditions of a road and physical–mechanical soil properties. It is noteworthy that contrary to civil and industrial buildings and structures, which have their own spatial rigidity allowing to redistribute forces and even align settlements, railway bed is an absolutely flexible structure, where strains are completely defined by soil deformations. Therefore, the accuracy of prediction of soil deformations is determined by an applicable physical model of soil behavior, which should reflect real behavior of subsoil. According to the Federal Law “The Technical Regulations of Safety of Buildings and Structures” calculation of soil–structure interaction should be made taking into account physical and geometrical non-linearity of soils and materials as well as their rheological properties. St. Petersburg-based geotechnical school is the Russian and world leader in the field of soilstructure interaction calculations.

For several decades, a special attention of St. Petersburg-based geotechnical engineers was drawn to saturated clayey soils of small and medium degrees of lithification, which are briefly called soft clayey soils. These soils were formed in the conditions of severe climate of the last glacial period and gradual retreat of the glacier accompanied by alternation of fresh water and salty lakes on the place of the modern Baltic Sea, on the bottom of which lacustrine-glacial and lacustrine-marine sediments accumulated [1, 2]. These deposits are spread in the area of Fennoscandia and the adjacent territories of the Russian plain and near-Arctic area [3]. For them it is intrinsic to respond to an external impact as a quasi-solid body at preservation of structural links and turn into liquefied milieu at violation of natural structure, i.e. explicit non-linear behavior.

2 A Model with Independent Strain Hardening

Nowadays many physical models of soil behavior have been developed in soil mechanics [4–7]. A part of these models was implemented in software complexes [8, 9]. We have conducted a critical analysis of these models [10], which showed that they do not adequately describe real behavior of saturated clayey soils of small and medium degree of lithification.

Stabilometrical tests demonstrate that at hydrostatic loading an area of strain hardening does not develop in a deviator direction. Therefore, in order to create a realistic model of soil behavior there is a need to make independent description of hardening at volumetric and shear loading. This approach was partly implemented in

hardening soil model of PLAXIS, developed by prof. Vermeer [11], gave it deserved prominence and success in the market of practical calculations for design. However, it is noteworthy, that separate description of volumetric and deviator deformations was not completely consistent there [10].

In the model, proposed by the authors, the idea of independent description of shear and volumetric hardening was brought to the logical end [12].

2.1 Making Dependencies of Volumetric Deformations on Ball Tensor and Shear Deformations on Stress Deviator

Dependencies of shear and volumetric deformations on a volumetric component and a stress deviator $\gamma_p(p, q)$ and $\varepsilon_{vp}(p, q)$ are made according to a number of tests. Dependencies $\gamma_p(p, q)$ and $\varepsilon_{vp}(p, q)$ can be drawn on the surface (p, q) in the form of contours (Fig. 1). The form of dependencies $\gamma_p(p, q)$ is well known. It is evident that approaching to the ultimate stress deformations increase, therefore, contours $\gamma_p(p, q)$ concentrate along the line according to Coulomb law.

The dependency $\varepsilon_{vp}(p, q)$ at $q = 0$ is defined based on the test on hydrostatic compression. Providing different values of stress deviator one can obtain the complete form of these dependencies. Deviation of contours $\varepsilon_{vp}(p, q)$ on the surface (p, q) from the vertical defines the phenomenon of dilatancy. As the points located above the ultimate line correspond to stress–strain behavior impossible for the soil stress state,

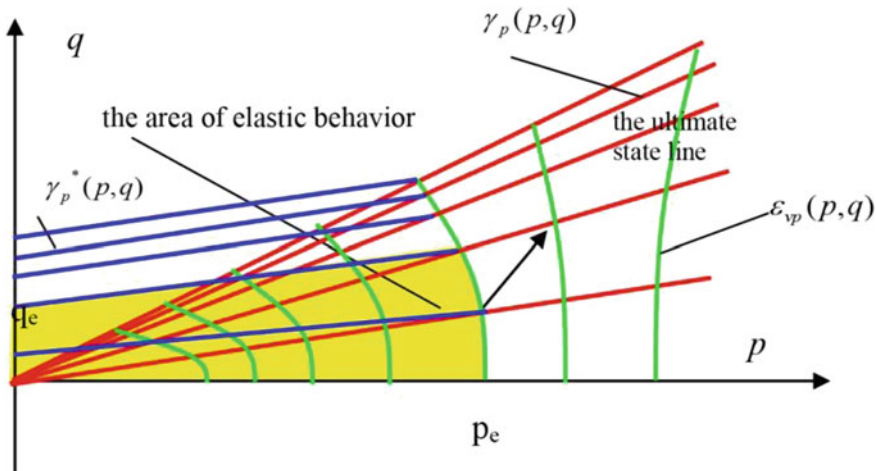


Fig. 1 Scheme of forming an elasto-plastic model with independent deformation hardening in FEM models software

there is a reason to draw the contours $\varepsilon_{vp}(p, q)$ below the ultimate line according to Coulomb law.

The set of dependencies $\gamma_p(p, q)$ and $\varepsilon_{vp}(p, q)$ completely defines the vector of plastic deformation at the given increment of stresses. Using this approach composing the model is free from any theoretical consideration on a shape of a “tent (marquee)” and the necessity of application of the associated law of plastic flow, which was already criticized with good substantiation by Iosilevich [13]. It allows to make maximum approximation of the model to the experimental results. In fact differences from the experiment are defined only by inaccuracy of approximation of the functions $\gamma_p(p, q)$ and $\varepsilon_{vp}(p, q)$.

For non-cohesive soils, the given contours are enough to describe deformation at any stress state as an increase of shear resistance in such a soil is explained by increased inter-particle friction. At unloading of volumetric stresses normal forces between particles decrease together with inter-particle friction forces and, consequently, an integral value of shear resistance also reduces.

2.2 A Dependency of Shear Deformations on Stress Deviator for Cohesive Soils

In cohesive soils, shear resistance at volumetric compression is explained by soil hardening accompanied by contingency of particles and an increase of amount of structural inter-particle connections. At unloading volumetric stress, there is no back softening, and the formed structural links define preservation of a value of shear resistance. Therefore, in case of cohesive soils it would be more correct in terms of physics to depict not the dependencies $\gamma_p(p, q)$, but the dependencies $\gamma_p(\varepsilon_{vp}, q)$, i.e. to define the dependency of soil behavior at shear based on an achieved degree of hardening rather than on volumetric pressure.

The most general solution of this problem is to introduce an additional set of dependencies $\gamma_p^*(p, q)(p, q)$ at the stage of unloading of volumetric stresses. Then, for ideal non-cohesive soils $\gamma_p^*(p, q) \approx \gamma(p, q)$, for ideal cohesive soils $\gamma_p^*(p, q) \approx \gamma(p_e, q)$, where p_e is an achieved level of hardening stresses. Introduction of an intermediate set of contours $\gamma_p^*(p, q)$ allows describing any degree of strength loss at unloading of volumetric stresses.

This approach allows describing most of phenomena recorded during experiments. Curving of contours of equal volumetric stresses allows reflecting the phenomenon of dilatancy without involvement of consideration on a shape of “tent” surface, etc. As regards clayey soils of small and medium degree of lithification dilatancy is understudied now, although there is some evidence of insufficiency of this effect. Therefore, in the future, in order to facilitate the model, we will approximate these contours by vertical straight lines (dilatancy is not taken into account).

2.3 Approximation of Dependencies

In order to approximate the dependency p – ε_{vp} , it is convenient to use the following formula:

$$\varepsilon_{vp}(p, q) = \varepsilon_{vp}(p) = \lambda \cdot \ln\left(\frac{p + p_0}{p_0}\right) \quad (1)$$

The parameters λ and p_0 , as it will be shown below, can be approximately obtained from compressive soil tests.

Approximation of the dependency q – γ at $q < \tau_{\text{lim}}$ can be made with a help of the degree function:

$$\gamma_p(p, q) = Aq^n, \quad (2)$$

where n —a degree index,

$$A = \frac{\gamma_c}{\tau_{\text{lim}}^n}, \quad \tau_{\text{lim}} = c + Mp, \quad M = \frac{3 \sin \phi}{3 - \sin \phi}.$$

Inserting these values in (2), we will get

$$\gamma_p(p, q) = \gamma_c \left(\frac{q}{c + Mp} \right)^n \quad (3)$$

In expression (3) the parameter γ_c defines a value of shear deformation achieved before a sample failure. In soft soils, where a sample failure occurs without forming a sliding surface, vertical deformation is usually limited by the value of 15%, that corresponds to the deformation of form change $\gamma_c = 0.225$ in unconsolidated undrained tests of a saturated sample. The parameter n defines a form of a curve.

The contours $\gamma_p^*(p, q)$ at unloading of volumetric stresses can be also approximated by straight lines, which are directed at an angle and a coefficient M^* . Then

$$\tau_{\text{lim}} = c + Mp_e - M^*(p_e - p),$$

$$\gamma_p^*(p, q) = \gamma_c \left(\frac{q}{c + Mp_e - M(p_e - p)} \right)^n \quad (4)$$

For convenience, the parameter M^* can be described analogous to the parameter M :

$$M^* = \frac{3 \sin \phi^*}{3 - \sin \phi^*}$$

where ϕ^* can be called an angle of internal friction at unloading.

Dependency (4) describes soil behavior at stresses, which are smaller than the ultimate ones. At stresses exceeding the strength limit and within the model of deformation of form change aspires to infinity a sample fails.

3 The Account of Development of Deformations in Time

Certainly, the model with independent deformation hardening, which provides more realistic description of soil behavior, is not sufficient to solve the problem of calculation of structure. Long-term in situ observations, which have been conducted during 150 years, show that there is no such a notion as “final settlement” for buildings and structures constructed in saturated soils of small and medium degree of lithification [14]. Therefore, in order to design line structures, it is very important to know a real speed of development of soil deformation in time.

3.1 Development of Deformations of Volume in Time

The theory of filtration consolidation is traditionally used for calculation of deformations in time. There is distinguished primary consolidation associated with dissipation of pore pressure and secondary consolidation caused by creeping of a structural frame of soil.

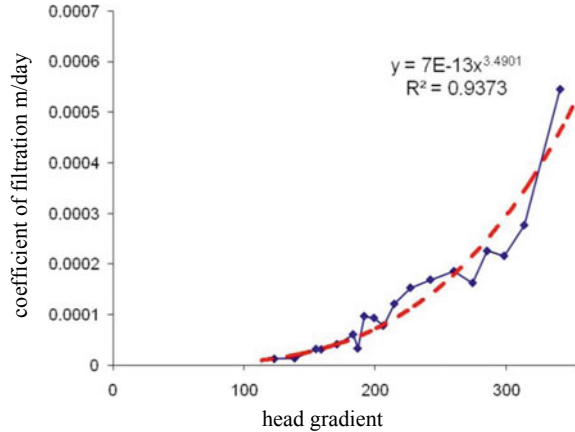
Creating the visco-plastic model, we implemented the effect of delay in volumetric deformations due to water removal in the traditional way. The non-linear dependency of a coefficient of filtration on a head gradient has been taken into account. The form of this non-linear dependency is well known due to research of many authors (Dashko [15], Gor'kov [16], etc.) of the national school. An example of the dependency of the coefficient of filtration on the head gradient is given in Fig. 2 [17]. According to the practice of calculations, the account of real coefficients of filtration makes us considerably revise the established opinion on a prevailing contribution of volumetric deformations into settlements of structures in soft clayey soils.

3.2 Development of Deformations of Form Change in Time

A shear component makes quite a considerable contribution into development of deformations. At the same time, today there are almost no models, which can adequately describe shear deformations in time. The majority of models imply immediate development of shear deformation that contradicts the whole experience of construction accumulated by the mankind.

The national school of soil mechanics devoted a large amount of attention to the phenomenon of shear creeping. The works of Maslov, Vyalov [18, 19] demonstrate

Fig. 2 Approximation of a coefficient of filtration on a head gradient for lacustrine-glacial deposits (lgIII)



theoretical and practical premises of calculation of deformations in time with account of shear creeping. However, until recently, there has not been created a generally accepted rheological model of behavior of soft clayey soil, which is convenient for implementation in calculation software.

We have made an attempt to summarize the existing data on soil deformation in time within a single visco-plastic model.

The proposed model utilized the simplest linear dependency: according to the linear law, viscosity reduces with an increase of shear stress and approaches to zero when reaching the strength limit:

$$\eta(\tau) = \eta_0 \frac{\tau_{lim} - \tau}{\tau_{lim}}, \tag{5}$$

where η_0 —initial viscosity, τ_{lim} —ultimate shear resistance.

Meanwhile, a speed of development of shear deformation is in non-linear dependence on the acting stresses that is quite consistent with the existing research [20] (Fig. 3).

As a result of using such a simple method, we have managed to unite different soil behavior within one model: slow development of deformations at small shear stresses and quick failure at stresses at the strength limit.

4 Comparison of Calculation Results and in Situ Investigations

In order to test the work of the visco-plastic model, let us consider the results of settlement calculation of test ground of the complex for St. Petersburg protection against floods [20]. The calculation scheme of the problem for calculating test ground #1 is shown in Fig. 4.

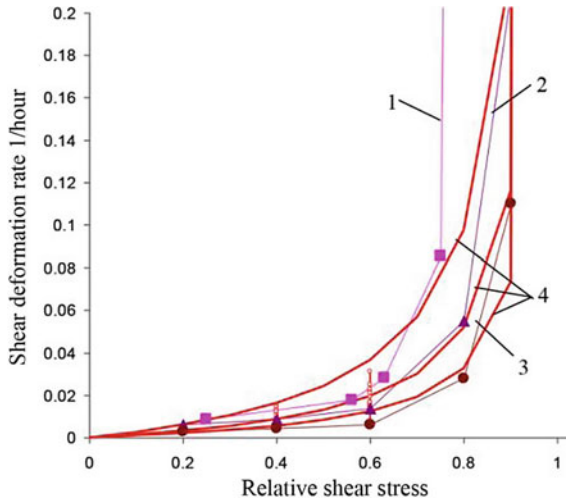


Fig. 3 Dependency of the rate deformation of form change on deviator stresses at various soil water content. 1—the water content of clayey soil $W = 30\%$; 2—the water content of clayey soil $W = 24\%$; 3—the water content of clayey soil $W = 21\%$; 4—approximation of test by dependency (5)

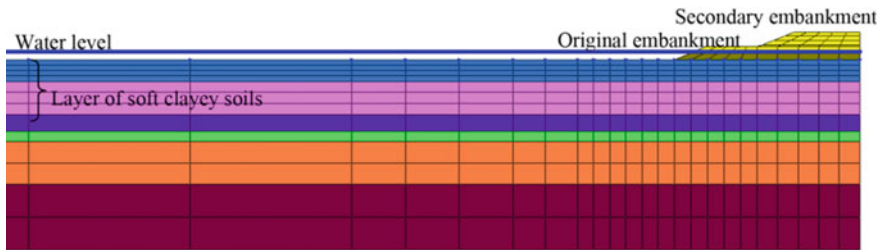


Fig. 4 Calculation scheme of the problem for calculating settlements of test ground #1

4.1 The Initial Data for Numerical Modeling

At the initial step of the problem distribution of natural stresses was modeled. Then loads exerted by the embankment were applied step by step. The elevation of the original embankment was +1.5 m from the water level of the Gulf of Finland. Then incremental filling of the secondary embankment to the elevations +2.15, +3.45, +4.75, and +5.8 m was modeled.

The following properties were accepted for the layer of soft soils: $E = 5000$ kPa; $c = 30$ kPa; $\phi = 10$; $\phi^* = 0$; $\eta_0 \approx 100cu = 2000$ kPa year, where cu is undrained strength of soil [20].

4.2 Simulation Results and Discussion

According to the calculations at small values of filtration coefficient of a bulk of soft soils ($10^{-8} \dots 10^{-9}$ cm/c), the values of settlements caused by filtration consolidation are very small. The main role is played by deformations of form change. Figure 5 shows the contours of displacement rates after applying the last step of load. The figure shows that soil is pressed out of the embankment, and the area of deformation development is similar to circular–cylindrical surfaces along which one can anticipate the loss of slope stability. In the given case, maximum shearing stresses do not reach the strength limit of soil; therefore, non-linear deformations are defined by development of shear deformations in the initial part of the graph $q-\gamma_p$, which is defined according to formula (2).

Therefore, expectedly, the main parameter for the problems of settlements calculation is characteristics of deformability at pre-limit stresses rather than strength limit of soil. Unfortunately, due attention is not always devoted to these characteristics, and many soil models [10] do not quite adequately describe this very initial step of deformation. The settlements of test ground #1, which have been defined using the proposed model, are in good agreement with observational result that is explained by proper account of deformations of form change of the model under consideration (Fig. 6).

The calculation scheme of the problem for calculating settlements of test ground #2 [20] is given in Fig. 7. The elevation of the original embankment was +1.2 m from the water level of the Gulf of Finland. Then incremental filling of the secondary embankment to the elevations +2.5, +3.65, +4.85, +5.69, and +6.12 m was modeled.

Contrary to test ground #1, in test ground #2, implementation of drains initiated settlement development without applying an additional load. The calculations

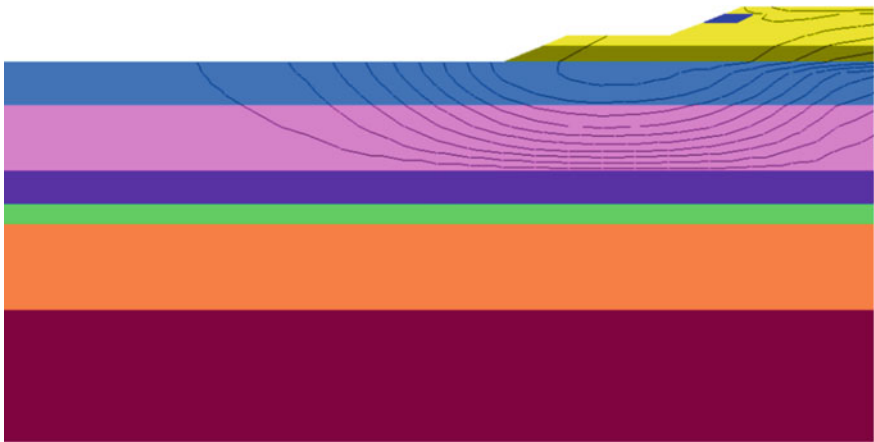


Fig. 5 Contours of rates of displacements after applying the last step of load

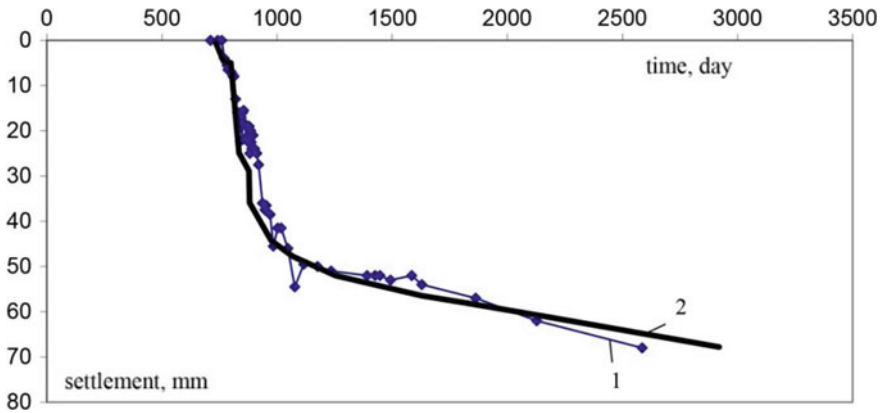


Fig. 6 Graph of development of settlements in time in test ground #1: 1—observation results; 2—the results of calculation according to the visco-plastic model

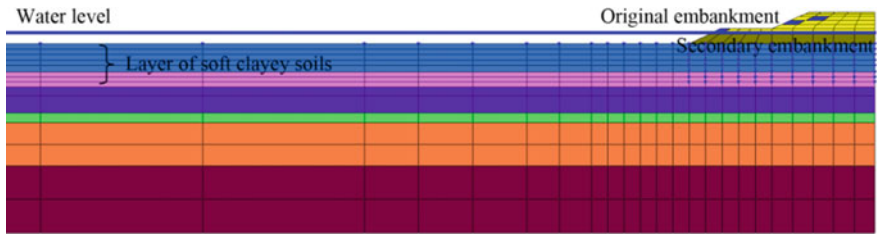


Fig. 7 Calculation scheme of the problem for calculating settlements of test ground #2

according to the model under consideration show the analogous effect, as at implementation of drains (change of boundary conditions for solving the problem of filtration consolidation) settlements start to be determined not only by deformations of form change but also by deformations of consolidation. The dependency of settlements for test ground #2 in time is also in good agreement with the results of field tests (Fig. 8).

Therefore, the comparison of calculation results and the results of long-term observations of settlements in the test grounds demonstrates that the proposed model provides adequate description of the process of development in time of both deformations associated with soil consolidation and deformations of form change, which prevail in test ground #1 without drainage.

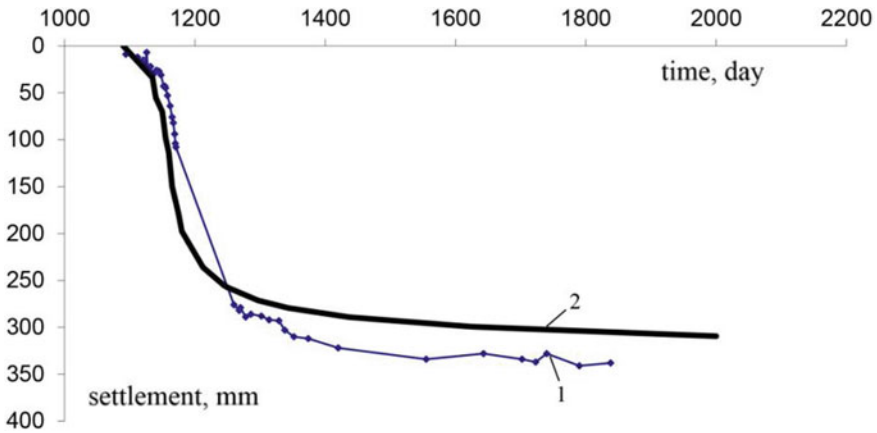


Fig. 8 Graph of development of settlements in time in test ground #2: 1—observation results; 2—the results of calculation according to the visco-plastic model

5 Conclusions

- 5.1. The visco-plastic model provides adequate description of the process of development in time of both deformations associated with soil consolidation and deformations of form change, which prevail in undrained soils; its use allows to increase significantly the accuracy of geotechnical calculations.
- 5.2. Deformation behavior of a line structure (transport roadbed, embankment) is completely defined by soil deformations. In saturated clayey soils of small and medium degree of lithification without special drainage deformations of form change prevail.

References

1. Stroeven A, Hättestrand C, Kleman J, Heyman J, Fabel D, Fredin O, Goodfellow B, Harbor J, Jansen J, Olsen L, Caffee M, Fink D, Lundqvist J, Rosqvist G, Strömberg B, Jansson NK (2016) Deglaciation of Fennoscandia. *Quat Sci Rev* 147:91–121
2. Wohlfarth B, Björck S, Funder SV, Houmark-Nielsen M, Ingolfsson O, Lunikka J-P, Mangerud J, Saarnisto M, Vorren T (2008) Quaternary of Norden. *Episodes* 31(1—Special Issue):73–81
3. Andrén T, Björck S, Andrén E, Conley D, Zillén L, Anjar J (2011) The development of the Baltic Sea basin during the last 130 ka. *The Baltic Sea Basin*, pp 75–97
4. Pietruszczak S (1980) Numerical analysis accounting for material hardening and softening. *Int J Rock Mech Min Sci Geomech Abstr* 17(4):199–207
5. Roscoe KH (1968) On the generalized stress–strain behaviour of “wet” clay. In: Roscoe KH, Burland JB (eds) *Heyman, Leskie*. Cambridge University Press, pp 535–609

6. Sanchez F, Gonzales NA (2005) Elastoplasticity within the framework of microplane models. Part II, applicable models for their use in geotechnical analyses. In: Sanchez F, Gonzales NA (eds) Prediction, analysis and design in geomechanical applications. The 11th conference of IACMAG, vol 1, pp 497–504. Torino
7. Wood DM (1990) Soil behaviour and critical state soil mechanics. Cambridge University Press, p 463
8. Vermeer PA (2005) On the numerical modeling of quasi-static cyclic problems. In: Benz T, Schwab R, Vermeer PA (eds) Prediction, analysis and design in geomechanical applications. The 11th conference of IACMAG, vol 1, pp 257–264. Torino
9. Vermeer PA (1998) PLAXIS: finite element code for soil and rock analyses, version 7 (ed: Brinkgreve RBJ, Vermeer PA). Balkema
10. Shashkin AG (2010) Critical analysis of the most wide-spread non-linear models of soil behavior. *Eng Geol* 3:29–37
11. Schanz T, Vermeer PA, Bonnier PG (1999) The hardening soil model: formulation and verification. In: Beyond 2000 in computational geotechnics—10 years of PLAXIS. Balkema, Rotterdam
12. Shashkin AG (2010) The description of deformation behavior of clayey soil with a help of visco-elasto-plastic model. *Eng Geol* 4:22–32
13. Iosilevich VA, Rasskazov LI, Sysoev YM (2005) The features of development of superficial loading at plastic soil hardening. In: Iosilevich VA (eds) Selected works. The Publishing House of Moscow University, Moscow
14. Vasenin VA (2013) Development of the geoinformation system for evaluation of long-term settlements of buildings of the historical center of St. Petersburg. *Eng Invest* 10–11:62–70
15. Dashko RE (2015) Engineering-geological analysis and evaluation of saturated clayey soils as the subgrade of structures. “PI “Georeconstruction”, St. Petersburg
16. Gor’kova IM (1975) Physical-mechanical studies of disperse sedimental deposits for construction purposes. Stroyizdat, Moscow (1975)
17. Shashkin KG, Mamonov AO, Kuvaldina OS (2010) Evaluation of the non-linear dependency of a filtration coefficient on a head gradient in laboratory tests of poorly filtered clayey soils and its use at calculation of filtration consolidation. In: Geotechnical problems of megacities/Proceedings of the international conference on geotechnical engineering, 7–10 June 2010. Moscow, pp 1407–1412
18. Vaylov SS (1978) Rheological basics of soil mechanics. Vyshaya shkola, Moscow
19. Maslov NN (1977) Soil mechanics in construction practice. Stroyizdat, Moscow
20. Shashkin AG (2011) Using data of engineering-geodetic studies when defining rheological soil properties in subsoil of buildings and structures. *Eng Invest* 2:18–30

Considering the Strength Soils Variability in the Consolidation by Numerical Modeling



Evgeniy Fedorenko

Abstract Representations in the field of mechanics of frozen and thawing soils require joint calculations: both thermophysical and stress–strain in a single calculation scheme. One of the criteria for assessing the reliability of the structure is to check the stability, the initial data for which are strength parameters. However, the process of transition from the frozen state to the thaw state entails a significant increase in moisture and, as a consequence, sharp decrease in strength, which gradually increases in the process of consolidation. Thus, in the calculations of transport facilities on thawing soils, it is necessary to take into account unstable strength parameters of soils in time and space. One of the methods of such accounting is the use of the type of behavior of undrained A soil models in PLAXIS software, working with the finite element method. The article describes an example of checking the design scheme when using this type of behavior based on the results of laboratory tests.

Keywords FEM · Plaxis · Soil strength · Undrained behavior · Undrained A type

1 Introduction

The design scheme in the form of an embankment with the corresponding geometry in numerical modeling allows to obtain a complex stress–strain state, the parameters of which are determined by the selected soil model. When using constitutive soil models, for example, soft soil or hardening soil, one of the modeling results is shear strains [2].

The models reflect that the shear leads to an increase in the excess pore pressure, and the analysis of the complete design scheme becomes very difficult. The calculation is based on the analysis of the effective characteristics, and in accordance with the principle of K. Terzaghi value of the excess pore pressure affects the effective stress and the resistance of soil against the shear. For visual analysis and simple

E. Fedorenko (✉)
MIAKOM SPb, Saint-Petersburg, Russia
e-mail: geotehnikfd@mail.ru

perception, further reasoning is conducted for a column of soil cut from the design scheme of the embankment on a weak base.

The height of the embankment is 5.2 m, below is IGE 40 (plastic sandy loam 2.4 m) and IGE 89 considered in the example (3 m), which is underlaid by crushed soil [4]. In the example, loam was selected for the analysis (IGE-89). The soil is in the stage of incomplete consolidation ($IL = 1.05$) and shows a slight hardening in depth in the form of increased strength, i.e., refers to the normally consolidated soils.

The embankment soil and other layers (except for the considered one) are given by a linear elastic model with $\gamma_{\text{unsat}} = 19 \text{ kN/m}^3$ and $\gamma_{\text{sat}} = 20 \text{ kN/m}^3$. The stiffness of the model is assumed to be conditional, and in this example this value does not matter.

The soil of IGE-89 with the type of undrained A behavior is given by soft soil model. The strength values of this model will be different depending on the selected behavior.

Parameters of soil strength are taken from the analysis of laboratory and field tests. In this example, we consider only triaxial tests: UU—unconsolidated-undrained and CD—consolidated-drained to facilitate the perception of information.

Evaluation of strength characteristics is made for two soil states:

- unstabilized (UU testing) of the corresponding point in time before consolidation (undrained state);
- stabilized (CD tests) corresponding to the moment of time after completion of consolidation (drained state).

1.1 Unstabilized State

In geotechnical practice, the profile of undrained strength C_u with depth is based on all available geotechnical engineering data: UU and CU triaxial testing, field methods (CPTu, dilatometer, vane tests), and so on [1]. In this example, profile with depth (Fig. 1) is obtained according to the protocols of unconsolidated-undrained (UU) tests.

The value of the undrained strength at the depth of the roof (-2.4 m) and sole (-7.4 m) of the IGE-89 layer is $C_u = 6.5 \text{ kPa}$ and $C_u = 10 \text{ kPa}$, respectively.

This line will be the lower limit of strength, i.e., it will characterize the strength in the unstabilized state, which the model should not exceed.

1.2 Stabilized Condition

The parameters of the stabilized state are obtained from the data of triaxial tests according to the consolidated-drained test consolidated-drained (CD). The results are processed in the p-q space. The drained friction angle in effective stresses φ'

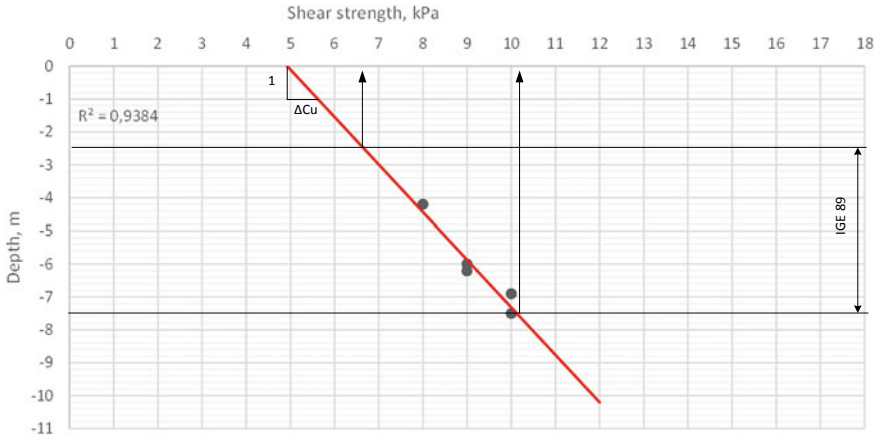


Fig. 1 Profile of undrained strength with depth

Table 1 Strength parameters for IGE-89 model

Unstabilized state	Stabilized state
$S_u = C_u = 5 \text{ kPa}$ Incremental on deeps $S_{u, inc} = C_{u, inc} = 0.65 \text{ kPa}$	$\phi' = 12^\circ; c' = 0 \text{ kPa}$

is determined by the slope of the limiting envelope in these axes. With this test processing, a drained friction angle $\phi' = 12^\circ$ was obtained.

The results of the analysis of the source data can be summarized in Table 1.

2 Numerical Modeling

The calculation is performed to estimate two states [3, 5]:

– unstabilized:

type of plastic calculation—activation of the embankment cluster, increase in excess pore pressure without taking into account the influence of the filtration coefficient and boundary conditions of the consolidation scheme (phase 1.1, Fig. 2);

– stabilized:

(1) type of consolidation calculation with a minimum pore pressure of 1 kPa (after phase with the unstabilized condition)—full dissipation of excess pore pressure with the definition of the consolidation time, which does not matter in this calculation (phase 1.2 after phase 1.1, Fig. 2).

(2) type of plastic calculation—activation of ignore undrained behavior option, which means the application of load (activation of embankment soil) without








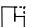
Undrained A	0 Initial phase	 K0 procedure  Staged construction
	1.1 1.2	Unstabilized state : Undrained condition Drain condition  Plastic  Staged construction  Consolidation  Minimum excess pore pressure
	1.3	Stabilized state (drain condition)  Plastic  Staged construction <input checked="" type="checkbox"/> Ignore undr. behaviour (A,B)

Fig. 2 Modeling stages

the formation of pore pressure (phase 1.3 after phase 0 initial, Fig. 2). This is a separate branch to map to phase 1.2.

Using the undrained behavior type allows to evaluate both the unstabilized and the stabilized state, i.e., it will show differences for the three selected calculation types and will change the strength in the consolidation process.

Unstabilized condition is specified by the type of plastic calculation and generates excess pore pressures, the value of which amounted to 98.08 kPa.

These values are related to laboratory tests as follows:

- at a depth of 2.4 m calculated $T_{max} = 4.5$ kPa, laboratory $C_u = 6.5$ kPa;
- at a depth of 7.4 m calculated $T_{max} = 12$ kPa, laboratory $C_u = 10$ kPa.

A geotechnician should decide on their own, how these values are acceptable. In addition, one should take into account the impact such of factors on these values as follows: parameter Skempton, type of calculation (plastic or consolidation), and drained effective strength (adjustment $\varphi' = 12^\circ$).

The values of the calculated parameters (effective and total) at one point in the lower part of the IGE 89 layer for the unstabilized state in the form of Mohr circles are shown in Fig. 3. This is the mechanism of undrained A type of behavior when generating the calculated strength of the soil shear at a given effective strength

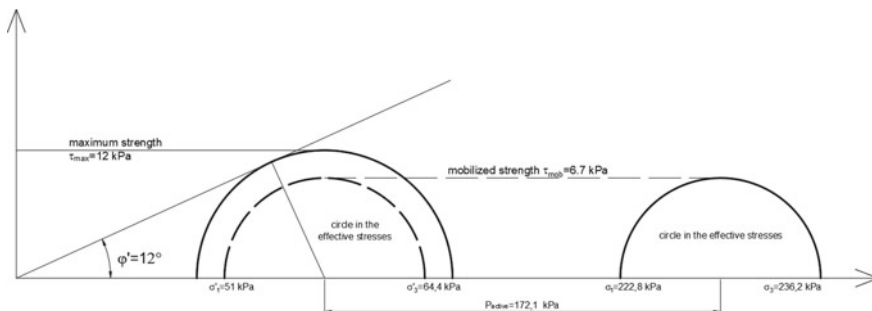


Fig. 3 Mechanism of undrained A behavior for non-stabilized state (phase 2.1)

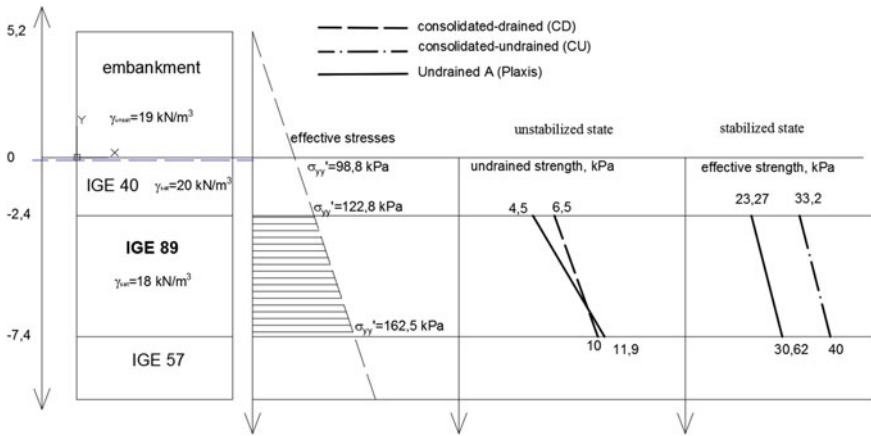


Fig. 4 Results of modeling with undrained A type

in the form of conditional untrained strength, determined by the parameter T_{max} . The displacement of the circles is made by the amount of active pressure: $P_{active} = 171.1 \text{ kPa}$.

Evaluation of the unstabilized state in the form of untrained strength when using undrained A type of behavior is made in an effective “coordinate system,” i.e., the safety margin is estimated in relation to the entered ultimate strength of the model in effective stresses— φ' .

Comparison of control (obtained in the laboratory) values and calculated values is shown in Fig. 4.

The selected strength parameters for undrained A type of behavior are as follows: $c' = 0 \text{ kPa}$; $\varphi' = 12^\circ$. The results obtained indicate satisfactory behavior of the model, the calculated strength values of which fall within the limits established by the laboratory (upper and lower). In this way, the modeling of this soil layer can be carried out with undrained A type of behavior. The main parameters of the calculation are shown in Fig. 5.

It should be noted that the considered version of the test is a conservative estimate, since it does not allow filtration consolidation in the process of filling five meters of soil (plastic mode). In fact, the filling will take place over a period of time and the process of filtration consolidation will take place, and, consequently, there will be a change in strength increasingly.

3 Conclusion

When designing embankments of transport facilities on weak soils, including thawing ones, a variable value of resistance against the shear plays an important role, both in time (consolidation) and in space (under the axis, the slope of the embankment

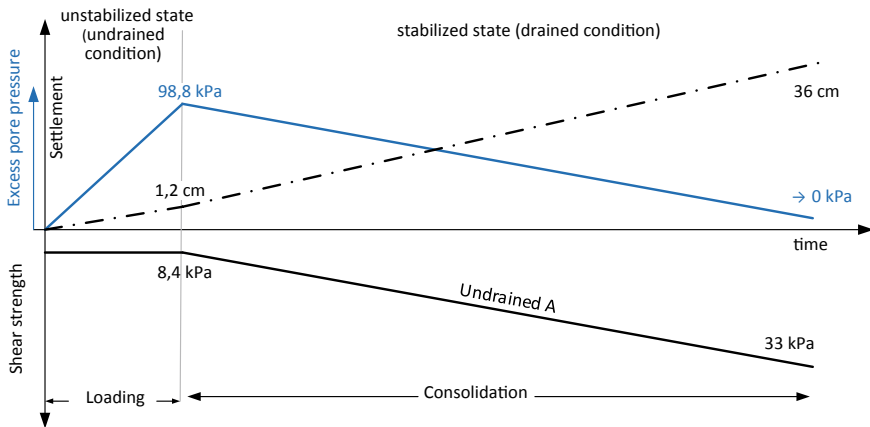


Fig. 5 Visualization of modeling results (strength values are taken for the middle of the layer)

and beyond it). Standards based on the use of calculations manually regulate the assessment of only two states: initial (unstabilized) and final (stabilized), while the ability to perform stage construction is very difficult. The use of geotechnical software makes it possible to perform both a conservative assessment in accordance with the requirements of regulatory documents (e.g., undrained B, C types of behavior) and a more complete analysis taking into account the changes in strength in the consolidation process and taking into account the influence of weak soil before the beginning of filtration consolidation (undrained A type of behavior).

Using the possibilities of numerical modeling provides a solution for such problems as considering the existing embankment (e.g., when widening or construction of the second track), the influence of hardening when using the system of vertical drainage (PVD), and stage-by-stage embankment construction costs calculated on the basis of excess reserves by conservative methods.

References

1. Abelev M (1973) Soft water-saturated clay soils as the basis of structures. Stroyizdat, Moscow
2. Brinkgreve RBJ, Broere W, Waterman D (2008) With other cooperators: Plaxis manual: Delft University of Technology & Plaxis b.v., The Netherland
3. Fedorenko E (2014) The method of calculation of sustainability by reducing the strength characteristics. Des Dev Reg Railroad Netw 2:124–130
4. Fedorenko E, Kovalsky A, Vavrinyuk T, Yerchenko D (2017) Numerical simulation of station tracks on soft soils. Procedia Eng 189:372–378
5. Fedorenko E, Vavrinyuk T (2015) Concerning the determination of the permissible load on a soft soil of the subgrade. Track Track Facil 10:10–12

Engineering Survey and Field Testing

Identification of the Emergency Condition Reasons at Railway Lines that Are in Difficult Geocryological Conditions



D. N. Gorobtsov , I. K. Fomenko , V. V. Pendin  and M. E. Nikulina 

Abstract The quantity slope stability assessment is an organization based on the engineering, geological, and geophysical investigations' analysis. The geomechanical slope's models creation realized along with stability assessment for slopes in natural conditions and in conditions of one estimated geological element soaking and thawing. Morgenstern–Price, Bishop's method, and Janbu's method were the main in stability assessment. The estimation analysis allows concluding that there are two main mechanisms of sliding processes on the slope. In the first case, landslide dislocations occur in the embankment's body. The second mechanism bases on the assumption of one estimated geological element soaking and thawing. In this case, sliding dislocations cover the whole embankment. The embankment's displacement comes along frozen moistening loams (main straining horizon (MSH)). This main straining horizon is the base for made ground. In addition, displacement may occur because of infiltration of the surface water along well-filtering macadam in warm period. The main sliding factors at the territory are significant relief energy, low strength properties of soils during it soaking and thawing, artificial cooperation. Fine probability sliding process activation predetermines the necessity of design and engineering protection measurements organization.

Keywords Quantity slope stability assessment · Geomechanical models · Mechanisms of sliding processes

1 Introduction

Temperature regime and factors that caused it during engineering surveys in permafrost areas were under much attention. In addition, the observation of the degree of frost heaving, assessment of the depth of seasonal thawing and determination of the types of cryogenic processes and areas of their distribution are also very important.

D. N. Gorobtsov · I. K. Fomenko · V. V. Pendin · M. E. Nikulina (✉)
Russian State Geological Prospecting University n. a. Sergo Ordzhonikidze (MSGU),
Miklouho-Maklay's Street 23, Moscow 117997, Russia
e-mail: nikulinamari93@mail.ru

© Springer Nature Singapore Pte Ltd. 2020
A. Petriaev and A. Konon (eds.), *Transportation Soil Engineering in Cold Regions*,
Volume 2, Lecture Notes in Civil Engineering 50,
https://doi.org/10.1007/978-981-15-0454-9_16

The aim of engineering and geological investigations is complex study of natural and technogenic conditions [1]. These conditions are necessary and sufficient for the development of the main measures for drainage system (as the main factor that influence on temperature regime) and strengthening sustaining capacity of railway tracks soils to the loading rack of petroleum products. The sustaining capacity complex assessment of permafrost soils is based on the engineering surveys. The main objectives of the investigations were:

1. Organizing the quantitative assessment of slope stability.
2. Developing the measures for strengthening and/or sustaining capacity preservation.
3. Composing the recommendations for further safe operation of investigated area.

2 Engineering and Geological Conditions of the Territory

The investigated area situates at the junction of the West Siberian lowland and the middle Siberian highland. The territory is extensive low hilly rolling plain with an average absolute strength altitude about 120–130 m and maximum altitudes about 215 m. In this area, various and complex relief and all-round permafrost forms are widespread. The oil base is located near the edge of Krasnoyarsk region.

Climate is arctic. It is characterized by abrupt temperature changes along the day and the year. There are also cold winters and short cool summers. The duration of stable frosts is 214 days. The average temperature of the coldest month is -28.0°C . All year-round, strong winds widespread there. The number of them is on average about a week in a month. Night frosts and snowfall are not rare in summer. Precipitation here falls a little (about 380 mm per year). The permafrost and slight evaporation of moisture from the surface cause strong quantity of bogs. The average duration of the frost-free period is 67 days.

Continuous spread of permafrost soils with merging type is typical for this region. The capacity is more than 100 m.

Modern technogenic, quaternary lake-alluvial, as well as quaternary marine and glacial deposits compose the investigated territory to a depth of 40.0 m. Quaternary sediments are represented by plastically frozen loam, with low ice content, icy. Such sediments also consist of medium size sand, frozen, icy.

At this territory, the most distributed geological forms are mounds of swelling, spot medallions, and frost-thaw subsidence.

According to thermometric observation in boreholes at the depth from 0 to 5 m, the soils temperature was positive (from 7.08 to 0.01°C). Above 10 m, temperature hesitates from -0.02 to -0.26°C . Temperature was from -0.37 to -0.93°C from 10 to 20 m.

The soils of the seasonal thawing layer represent bulk soils. The seasonal thawing and freezing layer depth was from 2.2 to 8 m along the investigations depth.

The processes of permafrost soils degradation may occur within the study area. Frozen soils' thawing occurs because of technogenic water leakage. Permafrost soil degradation appears as:

- formation and increase of technogenic unfrozen pockets;
- activation of dangerous cryogenic processes (especially thermokarst, thermal erosion, and rheological processes);
- increasing the seasonal soils' thawing depths;
- increasing the temperature in the frozen zone;
- decreasing the bearing capacity of soils;
- activation of cryogenic weathering.

In general, this territory is characterized by:

- high susceptibility of the natural environment to the technogenic impacts;
- widespread of permafrost;
- expand of cryogenic processes.

3 Slope Stability Assessment

There is a wide range of slope stability methods at present [2]. The choice of the method is determined by two factors. The first is the type of landslide process. The second is the mechanism of possible landslide masses displacement [3]. Each method is characterized by original force system [2]. The last one is obtained using one or another assumption. It is associated with the statistical uncertainty of the problem [4–8].

The preferred method of calculations was the class of limit equilibrium methods designed for inhomogeneous slopes [4–6]. This class includes:



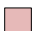
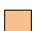
- Morgenstern–Price method;
- simplified Bishop's method;
- simplified Janbu's method.

The geotechnical model for stability calculations is based on the engineering and geological survey's results. The geomechanical models of slopes creation include construction of the geometric model for stability quantifying. Geometric model is schematic representation of the real object structure and its typical division into separate layers and structural elements. The elastic–plastic model of the Coulomb–Mohr soil behavior poses an adaptation in the calculations [3].

The slope stability calculations include the following variants:

1. Slope stability assessment in natural state. Strength properties (Table 1) of the calculated geological element (CGE) 3 based on soil section tests on the ground.

Table 1 Soils' properties and the legend for geomechanical scheme (variant 1)

Material name	Color	Unit weight (kN/m ³)	Cohesion (kPa)	Phi (°)
1		19	1	30
2		20	128	34
3		18	14.4	37
4		18	100	

2. Slope stability assessment in forecast state (assuming soaking of CGE). Strength properties (Table 2) of the calculated geological element (CGE) 3 based on soil section tests on the moist soil.
3. Slope stability assessment in forecast state (assuming frost retreat of CGE). Strength properties (Table 3) of the calculated geological element (CGE) 3 based on soil section tests on the thawed soil.

Table 2 Soils' properties and the legend for geomechanical scheme (variant 2)



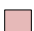
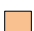


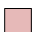
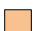
Material name	Color	Unit weight (kN/m ³)	Cohesion (kPa)	Phi (°)
1		19	1	30
2		20	128	34
3		18	31	2.4
4		18	100	

Table 3 Soils' properties and the legend for geomechanical scheme (variant 3)

Material name	Color	Unit weight (kN/m ³)	Cohesion (kPa)	Phi (°)
1		19	1	30
2		20	128	34
3		18	6	10
4		18	100	

4 Slope Stability Assessment Results

The considered landslide refers to landslides slip. The analysis of the performed calculations allows making a conclusion that there are two possible mechanisms for activating the landslide process on the slope.

The first mechanism corresponds to the calculation of variant 1 (Fig. 1). In this case, landslide displacements of soils occur in the embankment body. Calculations performed by the methods of limiting equilibrium in the natural state and with the external load application showed that the slope is in the state of limiting equilibrium ($1.00 < S_c < 1.25$).

Probability analysis allows assessing the danger of sliding activation [9, 10]. It was 0.2%. Sensitivity analysis of S_c is based on the soil heterogeneity in the mound and its strength characteristics [1]. This analysis includes definition of the soil’s internal friction angle composing the embankment (Fig. 2). The obtained relation showed that with internal friction angle about 24° , the slope becomes unstable ($S_c < 1.0$). The reduction internal friction angle may occur in the case of “clogging” the crushed clayey material. The last one acts, in the case of hydration, as a lubricant. In addition, sensitivity analysis allows assessing the impact of the external load on the calculated S_c . The results showed that the slope loses stability when the external load exceeds 175 kPa.

In this case, the landslide displacement captures the whole embankment. The offset of the mound occurs on the frozen moist loam (main straining horizon (MSH)). This is the underlying bulk soil (option 2). Thawing deformations (in the loams) occur due to penetration of the warm surface waters at the well-filtered gravel in the warm

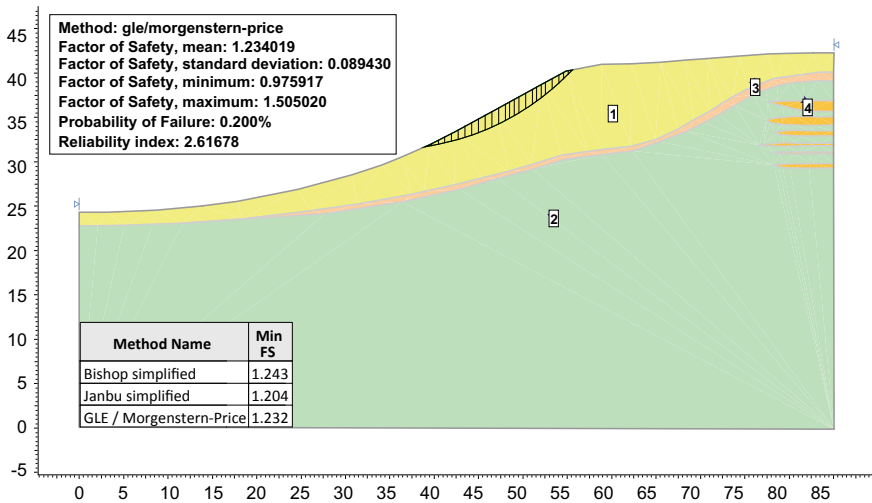


Fig. 1 Slope stability assessment with the results of probability analysis made by Morgenstern–Price method (variant 1)

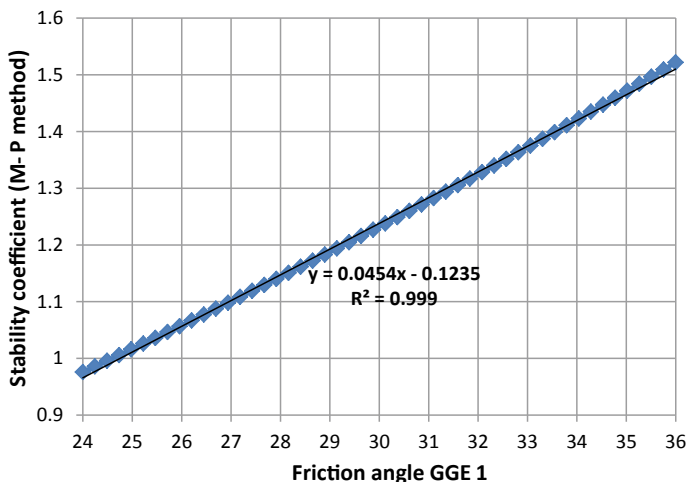


Fig. 2 Relationship between S_c and friction angle of CGE 1

season. The calculations performed on the second variant showed that the slope is in the state of ultimate equilibrium ($S_c < 1.25$). On the third, the slope is unstable ($S_c < 1.0$).

The second mechanism corresponds to variants 2 and 3 (Figs. 3 and 4).

The probability of activation of the sliding process for the second variant is 0.1%. Therefore, in spite of the drop in the S_c value, sliding hazard has decreased. The

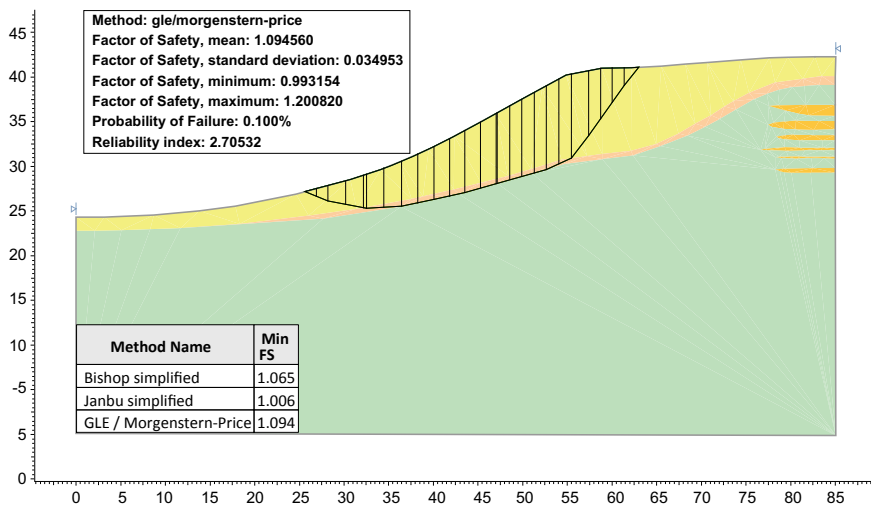


Fig. 3 Slope stability assessment with the results of probability analysis by the Morgenstern–Price method (variant 2)

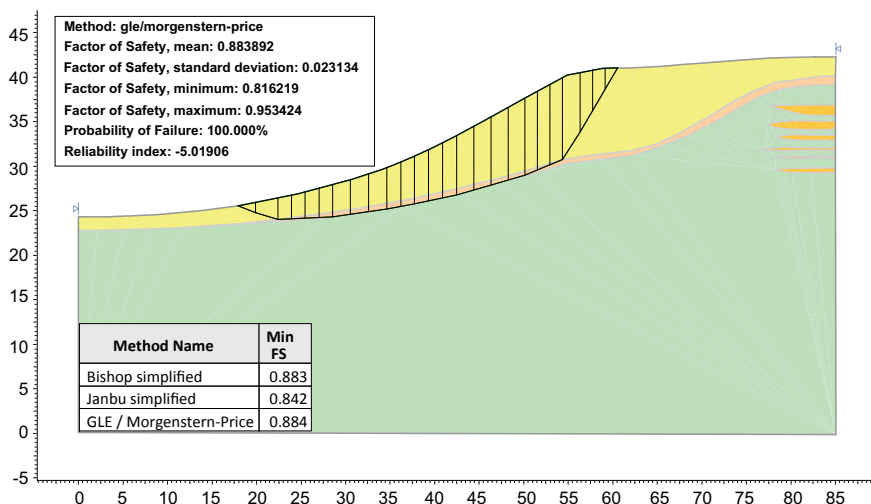


Fig. 4 Slope stability assessment by the Morgenstern–Price method (variant 3)

Table 4 Results of the calculation by various methods

Estimation methods	Computational methods		
	Morgenstern–Price (M-P)	Bishop	Janbu
Variant 1a	1.23	1.24	1.20
Variant 1b	1.135	1.17	1.11
Variant 2	1.09	1.065	1.01
Variant 3	0.88	0.88	0.84

probability of activation of the sliding process for the third variant is 100%. In the case of the third variant, slope loses the stability on the base of deterministic and probability analysis.

The estimation results are in Table 4.

5 Conclusion

The slope is generally stable (except for the results obtained by the third version of the calculation). This conclusion bases on quantitative assessment the stability by the methods of limit equilibrium.

The main factors of landslide processes’ activation are:

- significant energy of relief;
- low-strength properties of soils during their moistening and thawing;
- artificial interactions.

The high probability of landslide process activation determines the designing and implementation of appropriate measures for engineering protection. These measures should be directed to exclude the situation with the third estimation variant. It is necessary to:

1. Organize surface drainage, providing interception of surface runoff at the site and (or) waterproofing of the slope. It happens to prevent the groundwater horizon formation and thawing of MSH soils.
2. Develop the project of pile restraining structure that combines with heat stabilizer. This solution will prevent the thawing of MSH soils. It will significantly reduce the risks of sliding process activation on the slope.

The implementation of proposed measures will ensure regular operation without negative engineering and geological processes. It is necessary to create a system of operational monitoring to ensure quality control. The system should monitor for development of the negative engineering and geological processes. In order to clarify the calculations and choose the optimal solution it is necessary to conduct thermal logging of soils within the active zone and groundwater level measurements in the spring-summer period.

References

1. Ershov ED, Nikolaeva GV, Brushkov AV (1990) Temperature deformation of freezing and frozen soils under various thermal and mechanical influences. *Eng Geol* 5:38–46
2. Ginzburg LK (1986) Recommendations on the choice of methods for calculating the slope stability coefficient and landslide pressure. Central Bureau of Scientific and Technical Information, Moscow
3. Pendin VV, Fomenko IK (2015) Methodology of landslide hazard assessment and prediction in RF. Lenand, Moscow
4. Duncan JM (2000) Factors of safety and reliability in geotechnical engineering. *Geotech Geoenviron Eng* 4(April):307–316
5. Duncan JM, Wright SG, Brandon TL (2014) Soil strength and slope stability, 2nd edn. Wiley, Hoboken
6. Krahn J (2004) Stability modeling with SLOPE/W. An engineering methodology, 1st edn. GEO-SLOPE International Ltd., Calgary, Alberta
7. Javankhoshdel S, Luo N, Bathurst RJ (2017) Probabilistic analysis of simple slopes with cohesive soil strength using RLEM and RFEM. Georisk, Moscow
8. Low BK (2003) Practical probabilistic slope stability analysis. In: Proceedings soil and rock America, 12th Panamerican conference on soil mechanics and geotechnical engineering and 39th U.S. rock mechanics symposium. M.I.T., Cambridge, Massachusetts, Verlag Glückauf GmbH Essen, pp 2777–2784
9. Rocscience Inc. (2017) Slide beta version 8.0—2D limit equilibrium slope stability analysis. <http://www.rocsience.com/lncs>. Last accessed 28 Dec 2018
10. Zerkal OV, Fomenko IK (2016) The influence of various factors on the results of probability analysis the sliding processes activation. *Eng Geol* 1:16–21

Experimental Researches in Defining Deformations by Free Station Method and Results Processing by Search Method



G. G. Shevchenko , M. J. Bryn , D. A. Afonin  and D. A. Gura 

Abstract This article proposes a method of monitoring the buildings stability with free station positioning which includes a geodetic monitoring technique with a free station. Processing and adjustment of data are proposed to be conducted with the search method by a specially designed software program. The sequence of monitoring is as follows. The location of the stations is chosen in such a way that each of them shows as many deformation and support points as possible and at least three points should be determined from any other station. It is preferable to choose stations approximately in the alignment of one pair of support points so that the planes of the marks being defined are perpendicular to the line of sight. Measurements of all horizontal angles, zenith, and slant distances to all visible reference points, and deformation marks are made at each station with an electronic total station. As a result, redundant measurements appear in the measurement scheme, which in turn increase the accuracy of the final result. The coordinates determination of the defining marks is performed by deducing the minimal sum of the measured angles deviations squares and of distances squares calculated from the preliminary coordinates of the marks taking into account the weights of the measurements. It is proposed to search for the objective function minimum with a search method using a specially developed program in the form of a macro in the Microsoft Excel software product which provides special features to accelerate the problem-solving process. The buildings deformation monitoring technique mentioned above was successfully tested at several sites.

Keywords Geodetic monitoring · Three-dimensional coordinates · Setting and displacement · The search method of adjustment

G. G. Shevchenko (✉) · D. A. Gura
Kuban State Technological University, Krasnodar, Russia
e-mail: grettel@yandex.ru

M. J. Bryn · D. A. Afonin
Emperor Alexander I St. Petersburg State Transport University, Saint-Petersburg, Russia
e-mail: 3046921@mail.ru

© Springer Nature Singapore Pte Ltd. 2020
A. Petriaev and A. Konon (eds.), *Transportation Soil Engineering in Cold Regions*,
Volume 2, Lecture Notes in Civil Engineering 50,
https://doi.org/10.1007/978-981-15-0454-9_17

1 Introduction

When solving problems of determining the three-dimensional coordinates of deformation marks located along the perimeter of a building under construction as a rule, the measurements are performed from geodetic points fixed on the ground from cycle to cycle especially if such measurements are made by electronic total station [1–4]. However, there is often a problem to ensure the stability of such observation points due to the continuous work on the construction site. In addition, in a city, the high built-up density often complicates work arrangement [5]. This is especially evident when it is necessary to determine the planned-high-altitude position of deformation marks on the object.

The article describes issues related to the method of determining the displacement and settings of buildings. A newly developed technique is confirmed by experimental data.

The novelty of the proposed technique based on the fact that geodetic observations of the buildings deformation are suggested to be carried out by performing angular and linear measurements of the reference points and deformation marks by an electronic total station installed in any locations accessible for measurement without fixing observation stations. So, it is not needed to center the device above the point. In this case, the linking of stations with each other will be done at common points captured at all stations. So, this method of an object observation can be compared with shooting in scanning method. Thus, the linking of stations is carried out as well as during scanning by common points visible from several positions.

The vertical and horizontal displacements themselves are determined relatively to the stated reference points located in stable locations. The points used in the setting out of the axes of the structure are also offered as reference points. The reference points and initial geodetic points will be used to determine the location of the total station points. The presence of reference points is prerequisite in an amount of at least three pieces.

Thus, to monitor all three axes of the structure, it is proposed to measure the following types of points fixed in the work area:

- reference points;
- deformation marks (located along the perimeter of the object under study).

By observing each of these points, data are taken to determine the value data of horizontal angles, zenith, and slope distances.

Numerical methods and methods of comparative analysis were used in the processing of measurement results. Mathematical calculations were carried out in Microsoft Excel using a specially created macro written in the programming language Visual Basic. Processing and analysis of the measurement results are proposed to be made on the basis of the least squares search method.

2 The Sequence of Monitoring

Determination of three-dimensional coordinates of points, and displacements and settings based on them are supposed to be carried out in the following sequence.

Stage I. Reconnaissance of the territory. Preparation of the territory and the object under study for geodesic observations:

- (1) installation of deformation marks;
 - (a) marks are located at a certain height;
 - (b) marks are located along the perimeter of the building;
 - (c) in this case, reflective films fixed in the required place substitute the marks (Fig. 1). For the convenience of targeting deformation marks and to eliminate errors for the inclination of the collimating ray to the mark plane, a special rotating reflective film was proposed at the Cadastre and Geoengineering department of the Kuban State Technological University (Fig. 1c). It is mounted on the wall and allows to be targeted at almost any position due to the rotation of the mark without shifting the center. The usage of this kind of marks has increased greatly [6].
- (2) installation of reference points.

As reference points, the points on buildings nearby can be used, for example, buildings that have been built for a long time, fence posts, pylons of electric lines, etc.

Points received at setting out the axes of the structure can be used as reference points. The minimum number of reference points is three pieces. Theoretically, the reference point can be used to determine the location of standing points of the total station (stations) by linear–angular ticks.
- (3) Determination of the stations location.

Since this method of measurement is suggested to be carry out without fixing stations on the ground, the method to conduct observations of the location of the instrument is selected based on the following requirements:

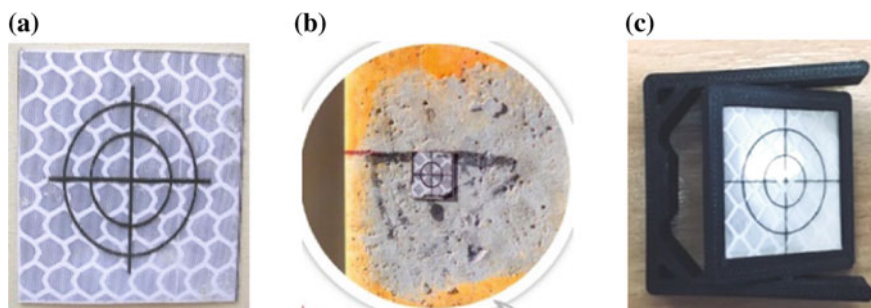


Fig. 1 Reflective film fixed on the object

- stations are selected in such a way that as many deformation marks, auxiliary marks, and reference points as possible can be observed from each of them;
- it is preferable to choose stations aligned to one pair of reference points so that the planes of the observed marks are perpendicular to the collimating line. The collimating ray and the plane of the reflective film should make an angle of at least 45° [7];
- every station is chosen to target at least three points detected by the previous station or some other one. This is necessary to ensure “rigid” connection between stations.

If the deformation marks and reference points are not enough to link the stations with each other, auxiliary points could be set.

Stage II. Conducting field work. Measurements are taken at all reference points and deformation marks visible from each station. To make these measurements, an electronic total station is used. At first, only reference points are measured thus creating a reference points network. Then, integrated measurements are performed on all deformation marks and reference points visible from the stated station. For each deformation mark, measurements should be taken by two or more stations, and however, the coordinates of the mark can be calculated by using only one station measurements. As a result, redundant measurements appear in the measurement scheme which in its turn increases the accuracy of the final result.

In order to determine the value of displacement or setting, it is necessary to carry out measurements in several stages (cycles), each of them contains three-dimensional coordinates computation of the observed marks. Positioning is carried out based on the measured values of the horizontal angles, zenith, and slope distances for each defined mark. That is, measurements for each determined point during field work are performed with a reciprocal observation. Sometimes the distance cannot be measured correctly due to the acute angle between the mark plane and the collimating ray. In this case, only two measured values will be processed—the horizontal angle and the zenith distance. Subsequently, the differences in the X -coordinate and Y -coordinate reveal the possible displacements of elements and the differences in the H marks show the setting of the structure.

Stage III. Processing and adjustment of measurement results. Processing and adjustment of data are proposed to be fulfilled by Microsoft Excel using specially designed software. At first, all the measured values of angles and distances (β_{taken} ; Z_{taken} ; D_{taken}) from the instrument are exported to this software. Then, the coordinates of the reference points are entered and the coordinates of the determined deformation marks are arbitrarily indicated.

The coordinates positioning of the detected marks is performed by finding the minimum of the squares sum of the measured angles and distances deviations v from the calculated values using the previously entered coordinates of the detected points taking into account weights p . The calculated values of β_{calc} , Z_{calc} , and D_{calc} are

deduced by a computer using the inverse geodesic problem formulas. The weight of the measurement p is taken into account by multiplying the difference between the measured and calculated values by \sqrt{p} [8]. As a result, the target cell contains the calculated sum $[pv^2]$.

To search for a minimum, a computer program is compiled as a macro in the Microsoft Excel software product [9]. To operate the target, cell is given a name. Then, the cells with previously entered coordinates of the detected marks are selected. To search for a minimum, it is needed to indicate the appropriate value of Δ to change arbitrarily entered values of X , Y , and H . The technique of finding the minimum is that the computer for each unknown calculates three values of y_0 , y_1 , and y_2 in the target cell which correspond to the three values of the selected unknown x_0 , x_1 , and x_2 . A parabola is constructed at three points, the parameters of which provide an allowance to go to the parabola vertex.

The program makes consequent calculations for all unknowns then proceeds to the second cycle of iterations over all unknowns and so on until the value in the target cell stops decreasing. Sometimes, it is useful to reduce the value of Δ at the end of the iterations.

3 Study Value

This software program is a useful addition to the well-known universal minimum search programs in Microsoft Excel and Math Cad software products. However, the studies show that the built-in functions of such search programs do not always give correct results, as calculations are made with gradient method. It is hard enough to deduce derivatives in the form of analytic functional relations as the problems have fairly great number of variable data [10–12]. As a result, the mentioned above minimum search program has been written.

When solving monitoring tasks, one of the two mentioned above programs is used first, and then the final adjustment to the minimum is made by the algorithm developed by the authors. Some special features are introduced into the program. So, in addition to automatically stopping the calculations when the minimum is reached, the calculations could be continued by setting the desired number of iteration cycles. The order of transition from one unknown to another in a cycle can be changed that sometimes speeds up the process of solving a problem.

4 Testing of the Technique

This technique was tested at several construction sites. So, four cycles of measurements of displacements and settings of three buildings under construction were performed. These buildings include a swimming pool, a hotel, and a house of athletes.

The measurements were made with the Nikon NPL-332 total station № 043256. The accuracy of the instrument is: 5'' when measuring angles of standard deviation and $3 \text{ mm} + 2 \text{ mm} \cdot D \cdot 10^{-6}$ when measuring distances.

For processing all measurements, a left system of spatial rectangular coordinates was used, where were given the coordinates of the marks for the setting out of the 3 buildings axis were given.

4.1 The Location Coordinate of Marks Along the Perimeter of the Objects

To monitor of buildings, measurements were made on reflective films placed along the perimeter of the objects.

So, 18 marks (B1–B18) are fixed at a height of 3–4 m from the ground along the perimeter of the basin. Along the perimeter of the hotel complex, there are 15 marks (G1–G15) at the floor level of the fourth floor at a height of about 17 m. Also, four marks (D1–D4) are fixed at a height of 3 m along the perimeter of the sports center.

Nine marks previously fixed and intended for superimposing down the axes of structures and nine aligning marks located along the perimeter of the sanatorium mainly on metal fences were used as reference and initial geodetic points. The view of both mark types is similar to the deformation marks (Fig. 1). Aligning marks are used to determine the standing points' coordinates of the total station (stations) with a linear–angular tick. The stations are selected approximately at the alignment of one pair of aligning marks in so that the plane of the marks to be perpendicular to the collimating line which gives the minimum error in the measured distance.

Measurements are made from 14 stations. Measurements were made on all the above-mentioned marks visible from this position from each station.

When targeting the marks, horizontal angles, zenith, and slope distances were measured and recorded in the memory of the total station. Measurements from one to two and up to five stations were made for each deformation mark.

The coordinates were calculated using the least squares method by means of a specially designed software program. The program changes one-by-one the coordinates of all points previously entered into the computer so that the sum of squared deviations of the measured values differ from the values calculated from the coordinates in minimum. The processing took into account the weights of measurements and errors of the initial data.

Table 1 shows the adjusted coordinates of all marks and deviations in the fourth cycle from the coordinates in the first and third cycles. Coordinates of stations, reference, and aligning marks are not given.

Comparing the deformation measurements between cycles shows the following.

1. The height difference for the five points of the sports center does not exceed 2 mm, which indicates the stability of the building in height over the observation period.

Table 1 Marks coordinates on the building

Points/marks	Coordinates in the fourth cycle			Differences: fourth cycle minus third cycle			Differences: fourth cycle minus first cycle		
	X (m)	Y (m)	H (m)	dX (mm)	dY (mm)	dH (mm)	dX (mm)	dY (mm)	dH (mm)
B1	224.865	116.992	6.911	-3	-1	0	0	-2	-1
B2	210.082	116.790	6.951	-3	-2	-1	2	-2	-3
B3	198.164	124.290	6.577	0	-2	-1	3	-5	-3
B4	168.916	124.296	6.599	5	-5	-3	17	-7	-3
B5	159.542	119.403	7.519	6	-6	-2	14	-7	-1
B6	143.071	117.695	7.060	4	-6	-1	13	-2	-2
B7	139.716	103.918	6.023	3	0	-2	10	0	-3
B8	139.711	73.336	6.165	1	-2	-1	11	3	-2
B9	139.714	43.934	6.205	3	3	-1	11	11	-2
B10	142.795	30.466	6.580	2	5	-1	10	9	-2
B11	157.819	30.299	6.791	3	6	-1	12	13	-3
B12	175.104	23.698	6.060	-6	2	-1	0	10	-4
B13	192.252	23.710	6.092	-8	1	0	-6	9	-2
B14	209.556	30.686	7.241	-2	0	-1	6	5	-4
B15	223.666	30.208	7.044	-3	1	-1	4	3	-2
B16	227.291	45.867	6.024	-2	-1	-1	0	6	-2
G1	81.703	197.145	20.070	7	2	-13	7	-1	-33
G2	74.428	197.310	20.142	7	2	-12	5	-4	-29
G3	66.177	192.298	20.097	7	-1	-12	0	-4	-36
G4	60.475	186.639	20.101	7	-1	-12	-2	-1	-36

(continued)

Table 1 (continued)

Points/marks	Coordinates in the fourth cycle			Differences: fourth cycle minus third cycle			Differences: fourth cycle minus first cycle		
	X (m)	Y (m)	H (m)	dX (mm)	dY (mm)	dH (mm)	dX (mm)	dY (mm)	dH (mm)
G5	37.493	160.869	20.178	3	5	-9	1	15	-26
G6	52.421	146.148	20.103	9	6	-7	17	18	-19
G7	70.490	159.188	20.001	8	5	-14	14	12	-32
G8	84.866	159.192	19.994	1	0	-13	10	9	-31
G9	97.757	151.414	20.355	-4	-2	-8	-	-	-
G10	103.742	146.062	20.129	-1	1	-6	4	10	-15
G12	118.088	160.390	20.122	-3	3	-7	-2	6	-17
G13	109.734	171.735	20.100	2	0	-8	0	3	-24
G14	98.429	183.185	19.950	2	2	-13	5	3	-34
G15	48.934	173.775	20.062	4	1	-11	0	3	-34
D1	105.107	72.151	6.382	0	-5	-2	6	-2	-1
D2	70.956	72.174	6.381	6	1	-1	14	5	-1
D3	70.942	55.143	6.388	5	0	0	13	7	2
D4	105.113	55.215	6.309	-1	-1	-2	4	6	-2

2. For a universal pool, there is a slight setting in average for all marks by 2–3 mm comparing to the 1st cycle.
3. The height difference for a hotel complex between four and three cycles (48 days) is from –6 to –14 mm, and between four and one cycles (126 days), it constitutes from –15 to –36 mm, which is apparently due to the increasing weight of the building during construction. For clarity, settings are shown in Figs. 2 and 3.

Analysis of the uneven setting of the hotel complex shows that the northwestern part of the building has a less setting. The unequal setting of the opposite parts of the building leads to a tilt of the hotel complex. The difference in settings over the observation period between the northwest and southeastern parts of the building is in average 18 mm, which at a distance of 60 m gives a tilt in relative units of about 1:3300.

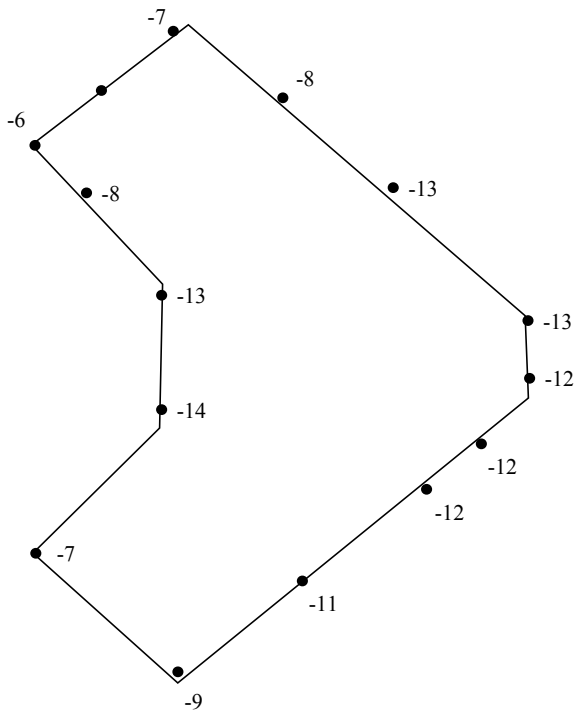


Fig. 2 Settings (mm) of the hotel complex in 48 days

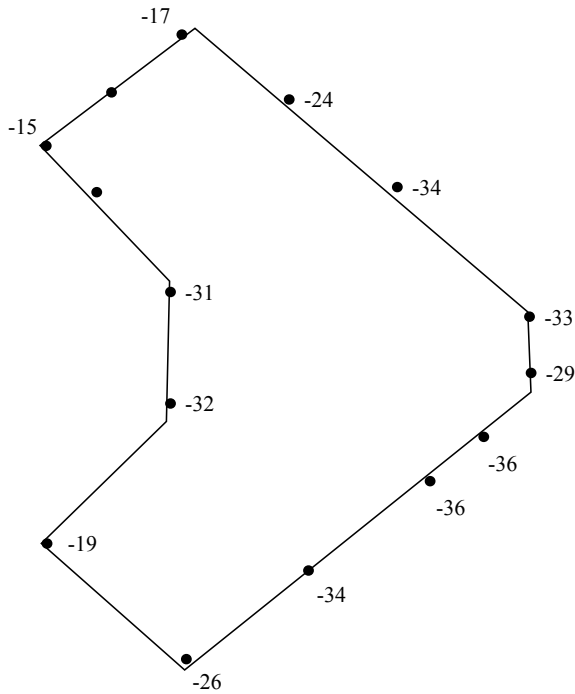


Fig. 3 Settings (mm) of the hotel complex in 126 days

4.2 Determining the Coordinates of the Pools Corners

Sixteen marks are fixed on the first story of the universal pool. Eight marks (B1b–B8b) are placed in the upper corners of both bowls of pools and eight marks (B1a–B8a)—on the floor of the first story at a distance of about 1 m from the first one so that both marks overlap the gap between the bowls of the pools and the ceiling of the ground floor. Marks are placed on a horizontal surface. In this case, the marks are not reflective films but have the shape of a cross with a dot in the middle for which all three coordinates are defined. The cross is patterned using red auto-enamel on a white circle with a diameter of 16 cm. The diameter of the center point is 6 mm.

The measurements were made with an electronic total station from one station, the coordinates and heights of which are determined by linear–angular tick of the reference points visible from the station. The coordinates of all points are calculated by the measured distances, horizontal and vertical angles (Table 2).

Discrepancies in the X -coordinate and Y -coordinate (columns 5, 6, 8, and 9 of Table 2) indicate deformations. Meanwhile, there is a slight setting of both the floor of the first story and the pool bowls of about 4–6 mm in the last 48 days.

Table 2 Points coordinates on the first story of the pool

Points/marks	The fourth cycle coordinates			Differences: the fourth cycle minus the third			Differences: the fourth cycle minus the third		
	X (m)	Y (m)	H (m)	dX (mm)	dY (mm)	dH (mm)	dX (mm)	dY (mm)	dH (mm)
<i>Floor points at the corner of the pool bowls</i>									
B1a	169.97	119.02	6.135	-6	-12	-3	1	0	-5
B2a	170.05	66.89	6.197	-2	-6	-3	5	7	-4
B3a	169.93	60.32	6.170	-4	-5	-3	3	9	-4
B4a	169.96	28.98	6.178	-13	-6	-6	-1	5	-11
B5a	197.03	28.96	6.138	-6	-3	-5	2	13	-9
B6a	197.01	61.02	6.162	-8	-3	-3	10	6	-4
B7a	197.09	67.76	6.164	-10	-4	-2	6	9	-4
B8a	197.08	119.08	6.148	-2	-3	-4	2	0	-6
<i>Top corners of pool bowls</i>									
B1b	170.83	118.18	6.288	-3	5	-6	1	2	-4
B2b	170.78	67.80	6.283	-10	-5	-3	5	10	-3
B3b	170.82	60.17	6.275	-5	-7	-3	11	0	-3
B4b	170.83	29.84	6.278	-8	-13	-4	8	6	-5
B5b	196.19	29.83	6.282	-12	-10	-5	5	10	-5
B6b	196.16	60.19	6.274	-4	0	-4	3	6	-4
B7b	196.22	67.79	6.281	1	-5	-4	5	12	-4
B8b	196.20	118.20	6.268	-10	-5	-6	-5	0	-5

5 Summary of the Results of the Deformations Determination

The results of measurements performed in the fourth cycle compared with the results of measurements in the first cycle showed the following:

1. Displacements and settings were not found in the building of the sports center.
2. There is setting of marks along the perimeter of the building on average 3–4 mm in a universal pool. Settings close to them of 4–6 mm were detected on 16 marks on the first story of the pool.
3. Marks around the perimeter of the hotel complex had uneven setting from 15 to 36 mm. The northwestern part of the building had less setting. As a result, there was a slight tilt of a building of about 1:3300.
4. Experimental studies have confirmed that the time spent on processing measurements is proportional to the cube of the number of unknowns. So, if the number of unknowns is about 10, the program calculates minimum in a split second, but if there are 200 unknowns like in this example, it takes several hours. In this case, the program performs calculations without operator intervention. Therefore, a large amount of computation time is not a significant drawback of the method.

References

1. Afeni TB, Cawood FT (2013) Slope monitoring using total station: what are the challenges and how should these be mitigated? *South Afr J Geomat* 2(1):41–53
2. Andrianova SD (2008) High-accuracy geodetic monitoring during construction and occupancy of modern buildings. *Soil Mech Found Eng* 45(2):66–70
3. Woźniak M, Odziemczyk W (2017) Investigation of stability of precise geodetic instruments used in deformation monitoring. *Rep Geodesy Geoinformatics* 104:79–90
4. Bird B (2009) Analysis of survey point displacement using total station measurements. A Technical report, Geomatics Engineering Department of British Columbia Institute of Technology, England
5. Mustafin MG, Valkov VA, Kazantsev AI (2017) Monitoring of deformation processes in buildings and structures in metropolises. *Procedia Eng* 189:729–736
6. Bryn MJ, Afonin DA, Bogomolova NN (2017) Geodetic monitoring of deformation of building surrounding an underground construction. *Procedia Eng* 189:386–392
7. Goryainov IV, Kodirov AA, Shevchuk AA, Averyanov SV, Delphonians EV (2017) Influence of the positions of the sighting target-the reflective mark on the accuracy of the measurements according to the linear-angle intersection scheme. *Izvestiya Vuzov. Geodesy and Aerophotography* 3:29–35 [in Russian]
8. Zheltko CHN, Shevchenko GG, Gura DA, Kuznetsov AA (2013) Algorithm for determining the coordinates of the monitoring facilities using the search method of equalization. *Sci Tech Technol (J Technol)* 3:60–64 [in Russian]
9. Shevchenko GG, Zheltko CHN, Gura DA, Pastuhov MA (2015) Universal program of determining three-dimensional coordinates of the points through the processing of measuring horizontal, vertical angles and distances search method. The Certificate on State Registration of the Computer Program, No. 2015617205

10. Muoi PQ, Hào DN, Maass P, Pidcock M (2016) Descent gradient methods for nonsmooth minimization problems in ill-posed problems. *J Comput Appl Math* 298:105–122
11. Wilke DN, Kok SI, Groenwold AA (2010) The application of gradient-only optimization methods for problems discretized using non-constant methods. *Struct Multidisc Optim* 40(1–6):433–451
12. Nesterov Yu (2013) Gradient methods for minimizing composite functions. *Math Program* 140(1):125–161

The Use of Terrestrial Laser Scanning for the Development and Control the Design Documentation of Reconstruction Projects



A. A. Kuznetsova 

Abstract Reconstruction of buildings is a complex engineering task, and the climatic conditions of cold regions further complicate and increase the cost of solving this task. Therefore, the delay in construction due to poor-quality design documentation leads to large financial losses. This article provides an analysis of results for four projects, where the main task was clash detection between the designed and existing engineering constructions. Each project used a combination of the technology of terrestrial laser scanning (TLS) and CAD. The article describes two ways to apply this methodology. At one of the projects, a point cloud obtained by terrestrial laser scanning was combined with a design three-dimensional model to identify deviations from design documentation. For other projects, BIM of existing structures and communications were developed based on point cloud. Then, BIM based on point cloud were combined with BIM based on design documentation for clash detection between structures and communications. The detected clashes allowed making changes to the design documentation before the start of installation work at the facility. The results showed the effectiveness of the joint use the TLS and CAD systems and identified the causes that affect the accuracy of the results at each stage of the work carried out.

Keywords Terrestrial laser scanning · BIM · Clash detection · Control results

1 Introduction

During the reconstruction of engineering structures, located in cold regions, special attention should be paid to the technical requirements for observing the durability and safety of operation of structures after reconstruction. An important condition for solving this problem is to obtain relevant data on the geometric parameters and technical characteristics of structures and equipment at the reconstruction site. One of the common problems during reconstruction is the lack of reliable information

A. A. Kuznetsova (✉)

Limited Liability Company IBCON, Saint-Petersburg, Russia
e-mail: anzhelikaalexeevna@gmail.com

© Springer Nature Singapore Pte Ltd. 2020

A. Petriaev and A. Konon (eds.), *Transportation Soil Engineering in Cold Regions*,
Volume 2, Lecture Notes in Civil Engineering 50,
https://doi.org/10.1007/978-981-15-0454-9_18

about existing construction in the as-built documentation. Recently, in connection with the transition to three-dimensional design in CAD systems [1, 2], it becomes a topical task to obtain data on existing construction in three-dimensional form.

A modern method of obtaining these source data is TLS. The main advantages of TLS are high detail and speed of shooting compared to traditional measurement methods [3]. TLS data can be further exported to CAD. The combined use of these technologies allows the analysis of design solutions to clash detection with existing structures and provides adjustments to design documentation in time.

This article provides an analysis of the results of four projects for objects located in cold regions. The main task was clash detection between the designed and existing engineering structures. On the basis of the obtained results, it was possible to show the effectiveness of the joint use of TLS and CAD technologies and to identify the causes affecting the accuracy of the results at each stage of the work.

2 Methodology

To carry out the projects, two methods were used to clash detection between the designed and existing structures. In the first method, the following work was carried out:

- Step 1. Terrestrial laser scanning;
- Step 2. Cloud registration and export to CAD;
- Step 3. Create BIM based on design documentation;
- Step 4. Create BIM based on point cloud;
- Step 5. Clash detection between BIM.

In the first method, clash detection was carried out between BIM, and in the second method, clash detection was carried out between BIM based on design documentation and a cloud of points.

It should also be noted that in all projects, the laser scanning, registration and alignment of the point cloud were carried out in the same methodological way and the same settings in the laser scanner measurement program.

Accuracy control of the laser scanning results, the registration results and alignment of the point cloud, and the results of creating BIM based on point cloud were carried out in all projects.

3 Construction Characteristics

Engineering construction differed in their size, purpose, and industrial environment. These factors influenced the performance of TLS and create BIM based on point cloud. In the first project, work was carried out on open technological site, with a three-tier shelf consisting of technological equipment, pipelines, and metal structures.

Table 1 Characteristics of the studied objects

Object name	EAVT		AD	GSP	UGS
Climatic conditions	-5		15	15	15
Object location	54°38'25" North 39°42'18" East		69°21'12" North 88°12'09" East		
Industrial environment	Vibration		Gas content	Vibration	Dust
Dimensions	X (m)	81	63	161	91
	Y (m)	24	102	63	80
	Z (m)	17	47	20	38

In other projects, the work was carried out in closed industrial buildings with large equipment and high spans between tiers of the shelves. Characteristics of the studied objects are shown in Table 1.

4 Measurements with TLS

Measurements at all sites were performed using a Leica ScanStation P20 terrestrial laser scanner (see Fig. 1). Measurements were carried out in an industrial environment during operation of the facility without stopping production with operating

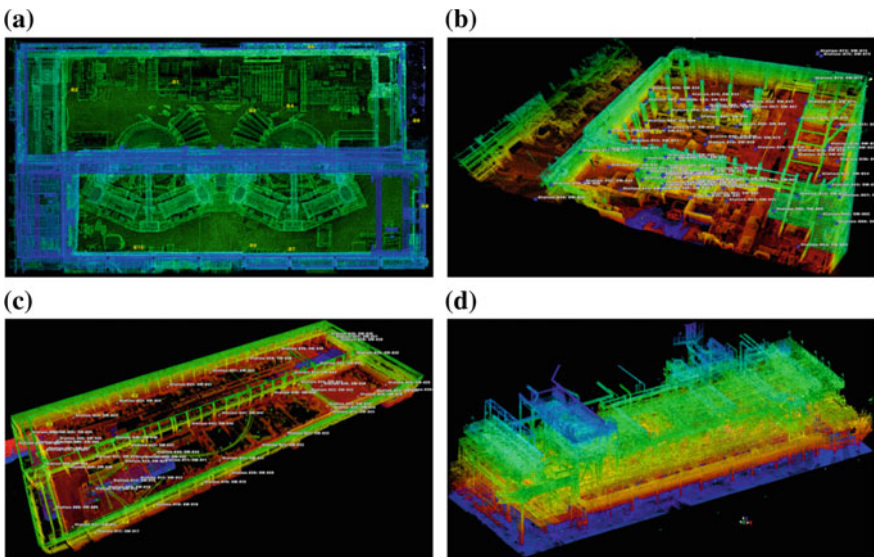


Fig. 1 View of object point cloud: AD (top left), UGS (top right), GSP (bottom left), and EAVT (bottom right)

equipment. Scanning was performed with maximum measurement overlap from two neighboring stations to exclude shadow zones. Considering the high density of structures and equipment at sites of construction, as well as the unfavorable industrial environment, all scans were taken with 5–10 m spacing at 6.3 mm/10 m resolution [4].

With such a resolution and large overlap of the point cloud, objects surfaces were covered with a 3 mm measurement grid, and this allowed as accurately as possible to identify small objects in the point cloud when creating BIM. To set a cloud of points to the coordinate system, targets were fixed on the reconstruction sites, the coordinates of which were determined using a Leica TS06 2'' total station.

5 Experimental Results

5.1 Cloud Registration

Registration of point clouds was carried out in Cyclone software using the «Visual Registration» tool [5–8]. In the case of using this tool, the software provides two parameters: «Error» and «Error vector» that give an indication of the registration accuracy [9]. The «Error» value for cloud connections represents the value of the variation connection between the clouds relatively to the global alignment and local alignment of two stations. Table 2 illustrates that in all the objects studied the mean «Error» does not exceed 3 mm, given the large number of connections between stations, possible to talk that the registration was done very accurately. The «Error vector» value for cloud connections represents the RMSE alignment of two individual scans. Table 2 illustrates that all the objects studied «Error vector» for is close to 1 cm. The increase in the value of the «Error vector» may involve to measurements in an industrial environment. High dust, gas content, and vibration could affect the accuracy of measurements.

Table 2 Registration diagnostics

Object name	Point clouds	Cloud constraints	Mean error (m) ^a	Mean error vector (m) ^b
EAVT	197	196	0.003	0.008
AD	238	6421	0.002	0.011
GSP	57	541	0.001	0.010
UGS	87	1031	0.001	0.011

^aMean «Error» for all connections

^bMean «Error vector» for all connections

5.2 Control Laser Scan Results

To control the accuracy of laser scanning results, the coordinates of the centers of the targets, determined using a total station, were taken as the standard. The coordinates of the same centers of the targets were obtained from the registered cloud of points. The results of the comparison of the obtained coordinates are presented in Fig. 2 which shows that the errors of the height (z) values are small, while the errors of the values of the coordinates (xy) increase and are scattered. In projects EAVT, GSP, and UGS, error in coordinates does not exceed 10 mm. In the AD project, the high gas content of the reconstruction site could affect the measurement accuracy of the target centers. This factor could affect both the measurements of laser scanning and the measurements of the total station. Therefore, these measurements require additional control.

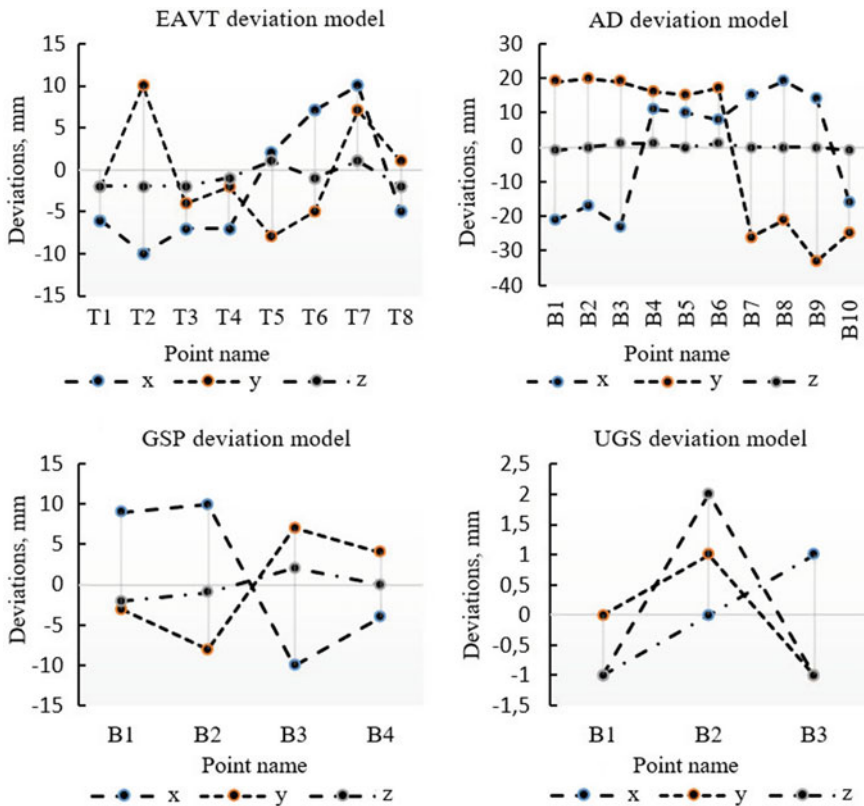


Fig. 2 Comparison of coordinate values: EAVT (top left), AD (top right), GSP (bottom left), and UGS (bottom right)

5.3 *Creating BIM*

To create a BIM in CAD, catalogs of structures were developed based on the specifications of design documentation. In the further, the structures of the catalogs were located in space in accordance with the data specified in the drawings of the design documentation. Thus, as-designed BIM was created for design documentation. To create as-built BIM using a point cloud, TLS data were imported into CAD. Subsequently, a group of points in a cloud of points describing structures and communications (reinforced concrete foundations, metal columns and beams, pipelines, equipment, elements of electrical networks, etc.) were identified in CAD. Three-dimensional solid-state structures from CAD catalogs were aligned by the identified groups of points [10].

Taking into account the technology of creating a three-dimensional model over a point cloud, an additional control of the accuracy of the three-dimensional model was carried out. For this, a number of areas in the three-dimensional model were defined, which are clearly defined edges and corners of building structures. At each site, five points were randomly selected, and a comparison was made of the coordinates of these points with the coordinates of similar points in the point cloud. In each three-dimensional model, points located on 20 different building structures were tested. The analysis of the obtained results showed that the average value of the modeling error was 12 mm.

5.4 *BIM Clash Detection*

For projects AD, GSP, and UGS, clash detection was carried out between the as-designed BIM and the as-built BIM. The algorithm of the automated clash detection implied the search for intersections between the elements of the BIM. For the EAVT project, clash detection was carried out sequentially between different types of structures of the as-designed BIM and a cloud of points. In this case, the algorithm of the automated clash detection tool analyzed the intersection of three-dimensional model objects with each point of cloud data.

As a result, reports were generated containing data on the number of detected clashes, their locations and the structures involved in clash. Based on the obtained results, an analysis of the identified design errors was carried out. The main errors were the discrepancy between the design heights of metal structures relative to the existing foundations and the intersection of the designed pipelines and metal bonds, ensuring the stability of the supporting structures. Table 3 shows the results of the clash detection.

From the data in the table, it can be seen that the number of clashes is directly proportional to the square of objects. However, for the GSP object, this dependence is broken in relation to the low saturation of the object with building structures.

Table 3 Results of clash detection

Object name	EAVT	AD	GSP	UGS
Object square (m ²)	1944	6426	10,143	7280
Number of clashes	64	211	56	239

6 Discussion and Future Work

Analyzing the results of work, we can say that at each stage of the work there are errors, and the total error can be expressed through the formula:

$$M = m_{ts} + m_{hds} + m_{reg} + m_{xyz} + m_{bim} \tag{1}$$

where

- m_{ts} the measurement error of the total station to determine the coordinates of control points taken as a standard;
- m_{hds} the measurement error of the terrestrial laser scanner;
- m_{reg} point cloud registration error;
- m_{xyz} the error of set of a cloud of points in a coordinate system;
- m_{bim} BIM creation error

To reduce these errors, restrictions should be placed on the technology and algorithms for carrying out work when implementing such projects:

- When conducting a laser scan on engineering construction with an unfavorable industrial environment, it is recommended to introduce a limit on the scan range. This will help reduce the number of inaccurate measurements of surfaces that are far from the station where the scanner is installed and whose visibility is hampered by heavy gas or dust.
- To reduce the error of set of a cloud of points in a coordinate system, it is recommended to increase the number of reference targets, the coordinates of which should be measured and equalized with the help of high-precision measuring systems. Their location on the object of work is also very important, it is a priority if the targets are located, evenly covering the entire area of the engineering construction.
- To control the accuracy of creating three-dimensional models, an urgent task is to create an algorithm in CAD for checking the conformity of the location of structures in the model and in the point cloud, since manual comparison is subject to human error.

7 Conclusion

As the results of this work showed, the joint use of TLS and BIM technologies makes it possible to identify errors in the project of reconstruction. The identified clash makes it possible to change the design documentation before the start of reconstruction and reduce the risk of financial losses at the time of the reconstruction.






However, it should be borne in mind that the application of these technologies imposes a certain error on the final result. Therefore, further research is required to develop algorithms and methodology for reducing errors.

References

1. Smith DK, Tardiff M (2009) Building information modeling: a strategic implementation guide for architects, engineers, constructors, and real estate asset managers. Wiley, New Jersey
2. Abdul Shukor SA (2015) 3D terrestrial laser scanner for managing existing building. *J Technol Sci Eng* 76(12):133–139
3. Muszynski Z, Milczarek W (2017) Application of terrestrial laser scanning to study the geometry of slender objects. *Earth Environ Sci* 95:2–7
4. Bosché F (2012) Plane-based registration of construction laser scans with 3D/4D building models. *Adv Eng Inf* 26(1):90–102
5. Besl PJ, McKay ND (1992) A method for registration of 3-D shapes. *IEEE Trans Pattern Anal Mach Intell* 14(2):239–256
6. Makovetskii AY, Voronin SM, Tihonkih DV, Alekseev MN (2017) Closed form solution of ICP Error minimization problem for affine transformations. *Chelyabinsk Phys Math J* 2(3):282–294 [in Russia]
7. Yang B, Zang Y (2014) Automated registration of dense terrestrial laser-scanning point clouds using curves. *ISPRS J Photogrammetry Remote Sens* 95:109–121
8. Akca D (2003) Full automatic registration of laser scanner point clouds. *Opt 3-D Measur Tech* 5:330–337
9. Bassier M, Vergauwen M, Van Genechten B (2016) Standalone terrestrial laser scanning for efficiently capturing AEC buildings for as-built BIM. *ISPRS Ann Photogrammetry Remote Sens Spat Inf Sci* 3(6):49–55
10. Tang P, Huber D, Akinci B, Lipman R, Lytle A (2010) Automatic reconstruction of as-built building information models from laser-scanned point clouds: a review of related techniques. *Autom Constr* 19(7):829–843

Three-Dimensional Laser Scanning for Safety of Transport Infrastructure with Application of Neural Network Algorithms and Methods of Artificial Intelligence



D. A. Gura , Y. V. Dubenko , G. G. Shevchenko , E. E. Dyshkant 
and N. I. Khusht 

Abstract Modern transport infrastructure is the most difficult and centralized system which influences all spheres of life. It can be divided into two broad categories: external (intercity) and internal (in-city). In this context, the importance of transfer hubs should be emphasized as they assist in redistribution of passenger flows in between different types of transport, thus optimizing the transportation process. It is worth mentioning that the safety of transport infrastructure is critical in preserving the stability of the transportation system as any disturbance to it might cause not only severe economic losses but most importantly deaths of civilians due to terrorist attacks, car crashes or other related accidents. Current paper focuses on description of methods to provide the safety of transport system utilizing technologies related to three-dimensional laser scanning that uses algorithms and artificial intelligence to process data and aid in decision making.

Keywords Safety of transport infrastructure · Neural network technologies · Three-dimensional laser scanning

1 Introduction

According to the Federal Law No. 16 “About Transport Safety,” stable and safe operation of transport network and the protection of citizens’ and society’s interests are the main objectives in terms of transport security.

There are several mechanisms to achieve the above-mentioned aims. It includes the creation of safety zones around the key transport infrastructure facilities (including development of security check systems that assist in identifying individuals and materials that are allowed in transport network as well as formation of laws) to engineering solutions that help prevent the disruption of normal passenger and cargo

D. A. Gura (✉) · Y. V. Dubenko · G. G. Shevchenko · E. E. Dyshkant · N. I. Khusht
Kuban State Technological University, Krasnodar, Russia
e-mail: gda-kuban@mail.ru

flows as well as provide safety of key infrastructure objects [1]. Although there are many preventative measures already in place, they still need to be perfected and improved in order to reduce risks associated with emergency situations in transport routes.

2 Intellectual Systems of Support and Decision-Making (ISPPR)

This paper presents alternative solutions to above-mentioned problems. These methods include development of intellectual systems of support and decision-making (ISPPR) that process digital information received from various sources such as video camera and laser scanner [2]. The analysis of data is executed by technologies that utilize artificial intelligence and neural networks [3]. Based on the results obtained from this analysis, the optimal decision is suggested.

It is also worth noting that in order to ensure adequate transport safety in cold climate, both additional time and human resources are required [4]. The proposed technologies aid in alleviating that problem as laser scanners and photo and video systems can function in low temperatures without requiring any personnel be exposed to severe weather conditions. To be more specific, the control of these systems can be performed remotely from any location allowing to receive data about the object in excess saving time and avoiding unnecessary field trips to the object [5].

As it was already explained above, the solution to the problem of transport safety is the development of intellectual systems of support and decision-making (ISPPR) that will manage the flow of information from various data collecting sources and provide the practical recommendations to reduce the risks associated with transportation and normalize normal traffic flow [6].

However, before the detailed description of the model is presented, it is necessary to consider a number of important aspects that are listed below [1].

- classification of objects: the principle and method by which the system will distinguish objects (people, freights, transport and engineering constructions);
- principle system's operation;
- system class (open, close and etc.);
- borders within which the system will operate (within municipality, region or the whole country in general);
- risks (assessment of possible risks on system's failure and determination of system's reliability—management of risks).

3 The Design of the Offered System

As one of the important features of the proposed model is the use of neural network technologies and artificial intelligence to process point cloud received as a result of laser scanning of objects and construct 3D models of objects of interest [7]. Furthermore, the systems of photo and video observations are also used to identify and classify the object with great precision [8].

The block diagram of the offered system is presented in Fig. 1.

In Fig. 1, the following elements are presented [9, 10]:

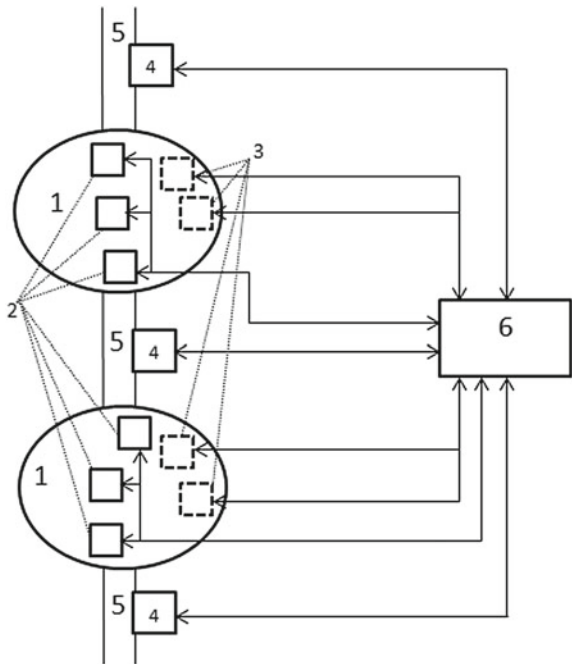
1. difficult engineering constructions (e.g., bridges or tunnels);
2. the cameras of photo and video recording, scanning systems installed on objects 1;
3. the sensors that detect slightest changes in conditions of load-carrying structures of objects 1;
4. the cameras of photo and video recording, scanning systems installed on the roads leading to objects 1;
5. road;
6. server part of a system.

The structure of a server part of a system is presented in Fig. 2.

In Fig. 2, the following elements are presented:

2, 3, 4—see Fig. 1;

Fig. 1 Skeleton diagram of a system



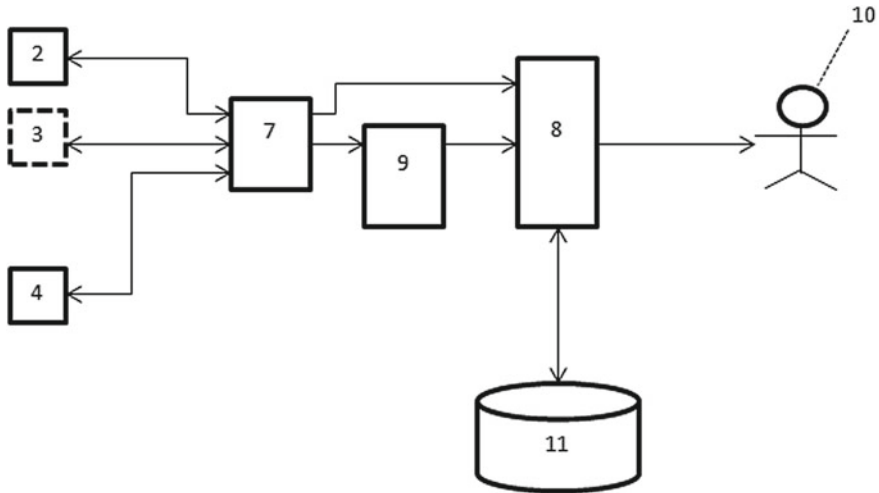


Fig. 2 Structure of a server part of a system

- 7. block of collecting and processing data;
- 8. decision-making block;
- 9. object recognition block;
- 10. operator;
- 11. data base.

The algorithm of the offered system includes the following stages:

1. The system in real-time mode receives images from cameras 2 and 4 and also from sensors 3.
2. Block 7 carries out processing of the acquired information and redistributes it between blocks 8 and 9.
3. Block 8 performs analysis of data that describes the basic elements of objects 1 and formulates recommendations that are transferred to the operator of system 10.
4. Block 9 carries out recognition and classification of the objects recorded by cameras 2 and 4 and transfers the results to block 8.
5. Block 8 performs analysis of potential dangers emanating from the recognized objects and transfers relevant information to the operator of system 10.

Camera 4 is placed on the roads that lead objects 1 to identify potentially dangerous objects in advance.

Examples of situations when block 10 develops warning signal are the unauthorized stop of the vehicle and recognition of vehicles that have inadmissible dimensions [10].

The most important component of a system is the decision-making block (8) based on INS (Fig. 3).

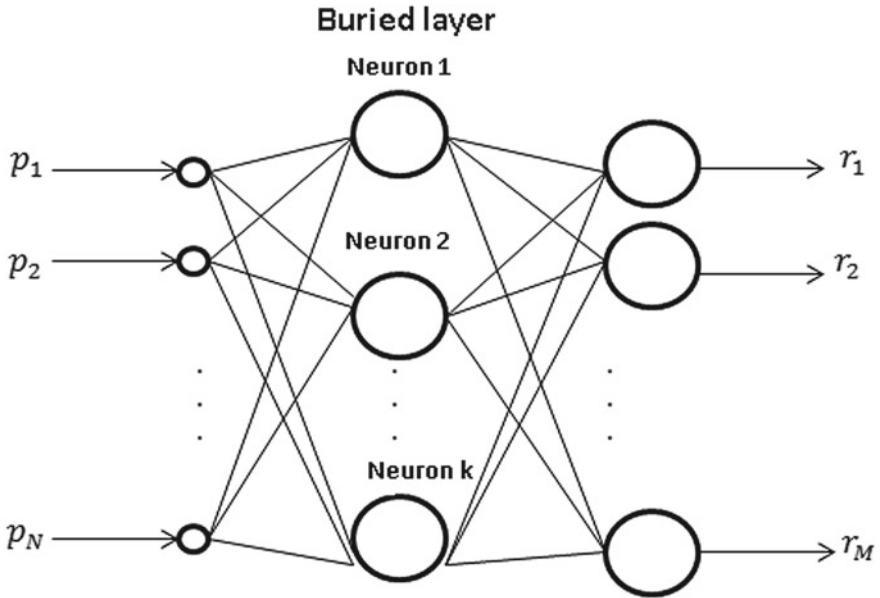


Fig. 3 Structure of INS for implementation of the block of decision making

p_1, p_2, \dots, p_N the parameters describing a problem situation on object (indicators of sensors 3, results of operation of block 9);
 r_1, r_2, \dots, r_M assessment of proposed recommendations' efficiencies for elimination of the problem situation.

Thus, the procedure to set INS presented in Fig. 3 can be described by following expression:

$$p_i \rightarrow r_j \tag{1}$$

For optimization of decision-making block's operations, the component implementing decision making on the basis of the precedents can be added to its structure [11]. We define the precedent as the similar problem situation that took place in the past. In this case, the precedent can have the following structure:

$$\langle P = \{p_i\}, Rc = \{rc_j\}, R = \{r_j\} \rangle \tag{2}$$

where

$P = \{p_i\}$ a set of the parameters describing a problem situation ($i = 1, 2, \dots, N$),
 $Rc = \{rc_j\}$ a set of descriptions of the recommendations allowing to eliminate this problem situation ($j = 1, 2, \dots, M$),

$R = \{r_j\}$ a set of estimates of recommendations' efficiencies related to ($j = 1, 2, \dots, M$).

The recognition of objects can be performed on the basis of above-mentioned algorithm.

4 Conclusion

In conclusion, it is necessary to mention that only the complex analysis of transport infrastructure objects with the use of neural networks and artificial intelligence will enable significant improvement of transport system objects' safety. It should be noted that creation of similar decision-making systems will have applied relevance not only on safety of transport infrastructure, but also on optimization of the so-called situational centers—the special rooms intended to control and monitor transport ways, freight and passenger flows and also adopt necessary operational decisions for traffic regulation.

References

1. Kravchenko AE, Gura DA, Dernovoy AY (2017) Flexible approach to municipal route network optimization for regular bus transport of general use. *Int J Econ Perspect* 3
2. Zvonkov VB (2014) On artificial intelligence. Reshetnev readings
3. Mukhamadiev KB (2015) Design of production systems with artificial intelligence. *Progressive processes and technologies* 2
4. Kravchenko AE, Gura DA, Dernovoy AY (2017) Flexible approach to municipal route network optimizations for regular bus transport. *Int J Econ Perspect* 3
5. Gura DA, Shevchenko GG, Kirilchik LF, Petrenkov DV, Gura TA (2017) Application of inertial measuring unit in air navigation for ALS AND DAP. *J Fundam Appl Sci* 1S(9):732–741
6. Kravchenko AE, Gura DA, Dernovoy AY (2018) Passenger transport service market functioning and development management in urban agglomerations based on integrated approach. *Amaz Investig* 13:331–350
7. Shevchenko GG, Gura DA, Eyes RE (2016) The analysis of the software for data processing of land laser scanning. *Mod Ind Civ Eng* 3(12):127–140
8. Gura DA, Shevchenko GG, Karslyan AM, Petrenkov DV (2016) Features of air laser scanning in the theory and in practice on the example of linear objects. *Scientific works of the Kuban State Technological University* 8:109–116
9. Dubenko YV, Dyshkant EE, Vandina AI (2018) Development of the block of decision-making of a self-training system of adaptive control by a complex technical system. *Electron Netw Polythematic J “Scientific Work KUBGTU”* 3:544–554
10. Dubenko YV, Dyshkant EE, Vandina AI (2018) Application of artificial neural networks to object recognition on the image. *Electron Netw Polythematic J “Scientific Work KUBGTU”* 3:544–554
11. Karpushin ES (2012) Formation of mathematical operations in artificial intelligence. *Intellectual property exchange* 5

Use of Geoinformatics for Landslide Susceptibility Mapping: A Case Study of Murree, Northern Area, Pakistan



Menal Zaheer, Anoosh Zaheer and Ali Hamza

Abstract Landsliding is considered as one of the major natural hazards that endanger human life and property, particularly in mountainous regions which have high precipitation rate and are seismically active. This paper identifies landslide-prone areas in Murree, a northern area of Pakistan and presents landslide susceptibility mapping technique using Geographic Information System (GIS) and Remote Sensing. The landslide triggering factors considered in this study are elevation, slope, geology (lithology), land use and land cover, seismotectonic settings and vegetation index. A spatial database using Geographic Information System (GIS) was developed. Slope was derived from topographical datasets; lithology and land use/land cover from geological datasets and vegetation index are from Landsat 8 imagery. Then finally, by using weight of evidence (WoE) method, landslide susceptibility map was developed. The final landslide susceptibility map has five classes from very low to very high landslide susceptibility. The results indicate that though only 8% of the study area falls in very high susceptible zone, it has a high land use percentage. This poses a serious threat to infrastructure and human life. Results of this study would be helpful in disaster risk management, geohazard studies and construction and regional planning.

Keywords Landslide susceptibility · GIS · Geohazard · Slope failure

M. Zaheer (✉)

National Engineering Services Pakistan (NESPAK), Lahore, Pakistan
e-mail: menal.zaheer@hotmail.com

A. Zaheer

Department of Geography, University of Punjab, Lahore, Pakistan

A. Hamza

Imperial College of Business Studies, Lahore, Pakistan

© Springer Nature Singapore Pte Ltd. 2020

A. Petriaev and A. Konon (eds.), *Transportation Soil Engineering in Cold Regions*,
Volume 2, Lecture Notes in Civil Engineering 50,
https://doi.org/10.1007/978-981-15-0454-9_20

1 Introduction

Landsliding is a phenomenon of downslope movement of rock or soil. A landslide susceptibility map is a cartographic representation of areas that are likely to encounter landslide hazard in the future by correlating the key parameters that trigger landslides with the historical pattern of landslide occurrences in that area [1]. There are several qualitative and quantitative techniques to develop landslide susceptibility maps. The accuracy of landslide susceptibility maps depends on the quality and amount of data available and the selection of suitable method of analysis.

Quantitative approaches depend on the relationship between triggering/controlling factors and landslides expressed numerically. Statistical and deterministic are the two types of quantitative approaches [2]. Weight of evidence (WoE) is a quantitative ‘data-driven’ statistical method which is used to combine datasets [3]. Originally, WoE method was developed to identify the mineral deposits. Recently, this method has been applied for landslide susceptibility mapping [4–6].

According to Bonham-Carter definition of positive and negative weights,

$$W^+ = \log_e \frac{P\{B|D\}}{P\{B|\bar{D}\}} \quad (1)$$

$$W^- = \log_e \frac{P\{\bar{B}|D\}}{P\{\bar{B}|\bar{D}\}} \quad (2)$$

where

- P Probability of landslide occurrence
- B Presence of landslide predictive factor
- \bar{B} Absence of landslide predictive factor
- D Presence of landslide
- \bar{D} Absence of landslide

W^+ (positive weight) and W^- (negative weight) indicate a positive and negative relationship between the presence of the predictive variable and the landslides, respectively [2]. A detailed description of this modeling is mentioned by Bonham-Carter.

2 Study Area

Himalayas are vulnerable with reference to their geology, seismic activities and climatic conditions. Murree, a hilly northern area of Pakistan having Himalayan hill range, due to its geography and geotectonic settings, is prone to earthquake activity and rainfall. Also, anthropogenic activities like deforestation, construction of roads and infrastructure development make the slopes unstable, thus triggering landsliding. The town of Murree lies 50 km to the northeast of Islamabad, the capital city of Pakistan. Area of interest (AoI) in this study is a part of Murree town having

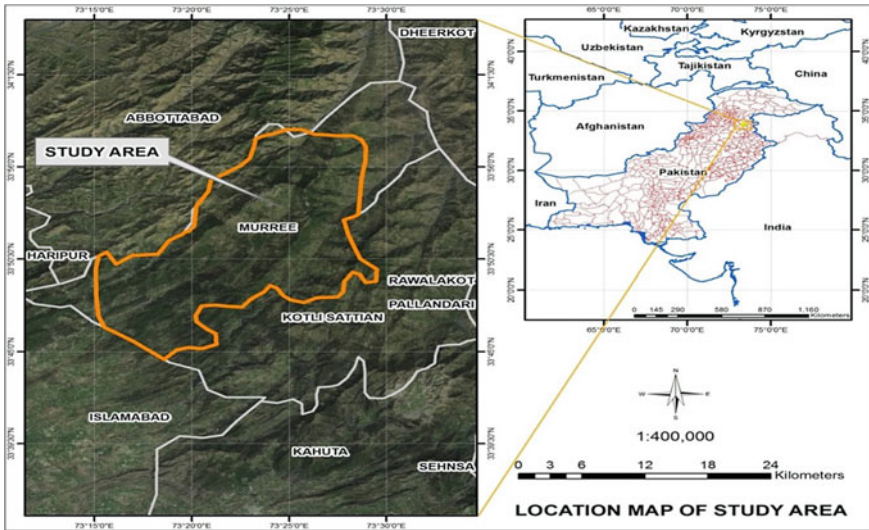


Fig. 1 Location map of the study area

an area of 300 km². Figure 1 shows the study area and stretch of its boundaries from 73° 20' 22.32" East and 33° 53' 53.80" to the North. The study area mainly consists of sandstone, shales and loosely bound slope forming material (locally called Murree and Chorgali Formation), thus providing a favorable zone for the geological faults to traverse and cause failure. Owing to the tectonic stresses and active geological faults, sedimentary rocks of this region are highly deformed, thus causing excessive landsliding activities in the study area. Murree also lies in the seismically active zone due to the presence of active Murree Boundary Thrust (MBT), and the slopes are moderately steep to highly steep, varying up to 75°.

Many studies have been performed to predict the movement and failure of slopes in advance and adopt remedial measures to avoid the loss of human life and destruction of infrastructure. Upper/Lower Dewal Landslide and Jhika Gali Landslide are considered as some of the major historical landslides in Murree.

3 Objective

The objective of this study is to identify and categorize zones that are prone to slope failure (landsliding) using Geoinformatics. Study also aims to develop a correlation between landslide and several triggering factors in Murree area using Geoinformatics, i.e., GIS-based weight of evidence (WoE) method.

4 Datasets and Methodology

The evidential themes considered for landslide occurrence in this study are digital elevation model (DEM), slope, aspect and lithology which were modeled in GIS environment, and then analyzed. Thirty m Shuttle Radar Topography Mission (SRTM) DEM was used to extract slope gradient and slope aspect patterns; SPOT-5 (2.5 m spatial resolution) was used as high-resolution satellite imagery to develop 3D model. Geological map from geological survey of Pakistan (GSP) was used as base map to digitize lithology. General locations, topology and settlement data were digitized from survey of Pakistan GT sheet. All these thematic maps were made digital using GIS advance techniques.

5 Results

5.1 Slope Angle Map

The slope is directly related to the landslides and is one of the major contributing factors in triggering landslides. The study area was categorized into nine (9) slope angle classes. The analysis was performed in the ArcGIS to know in which class of the slope angle most landslides happen. The results showed that those areas which have slope higher than 45° are more susceptible to failure. Hence, slopes less than 20° are stable and less likely to fail (Fig. 2). The results also concluded that areas, which are in the vicinity of Main Boundary Thrust (MBT)/Murree Thrust, are prone to landsliding.

5.2 Geological Map

As per the stratigraphy, the study area was divided into eight (8) geological formations groups. GIS-based geological map showed that a major contributing factor of landsliding in the study area is the weak rocks of Murree and Chorgali formation (maroon shale rock in higher percentage and sandstone), located on steep slope areas in the vicinity of active geological faults. Figure 3 shows the geological map of the study area.

5.3 NDVI

NDVI indicates the areas that have vegetation. The values of NDVI range from -1 to $+1$. -1 is assigned to water bodies while $+1$ is assigned to vegetated areas.

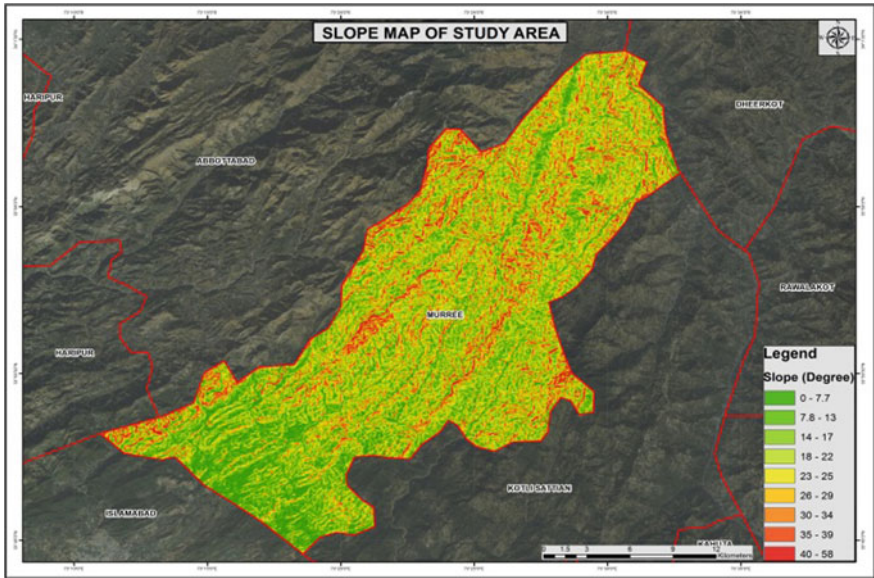


Fig. 2 Slope map of the study area

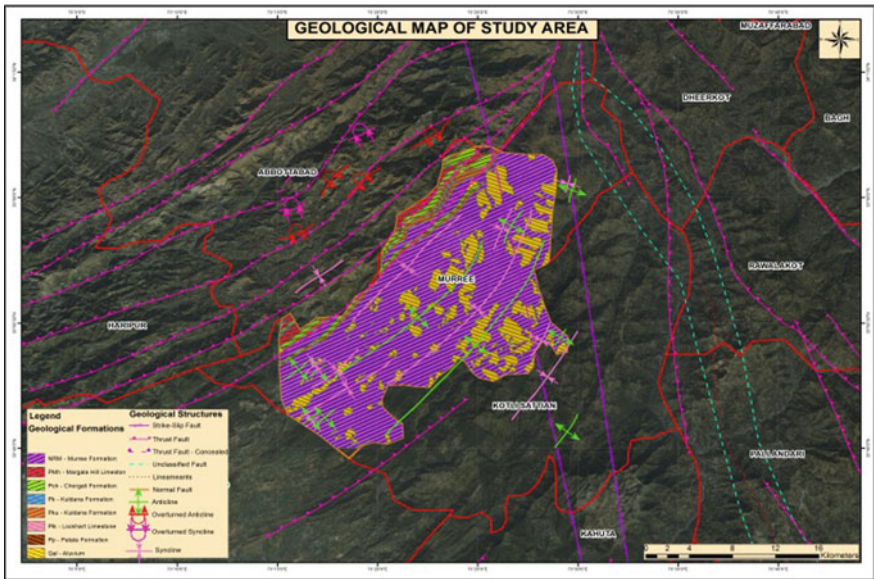


Fig. 3 Geological map of the study area

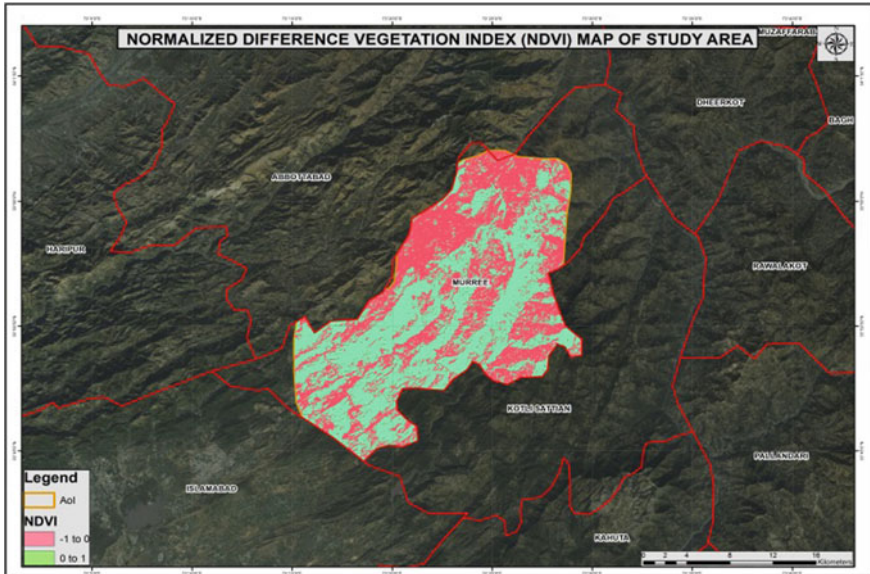


Fig. 4 NDVI map of the study area

NDVI map showed that the study area is partly vegetated, thus providing resistance to erosion and maintaining stability (Fig. 4). The vegetation can be seen mostly in the southern part of the study having slope range of 0–25°.

5.4 Land Use and Land Cover

The land use and land cover map were divided into four (4) groups, i.e., built-up area, vegetation, roads and waterways. For the analysis, the maximum weight was assigned to built-up area as anthropogenic activities (infrastructure and road construction) destabilize the slopes, thus causing landslides. The results depicted that the built-up area is in larger fraction in the north of the study area which has steep slopes and is prone to landsliding (Fig. 5).

5.5 Landslide Susceptibility Map

All the weighted value maps of the factors considered in this study were combined to get the final landslide susceptibility map. The final map shows five landslide susceptibility classes, i.e., very low, low, moderate, high and very high, and these classes cover 15%, 27%, 29%, 21% and 8% of the study area, respectively (Fig. 6).

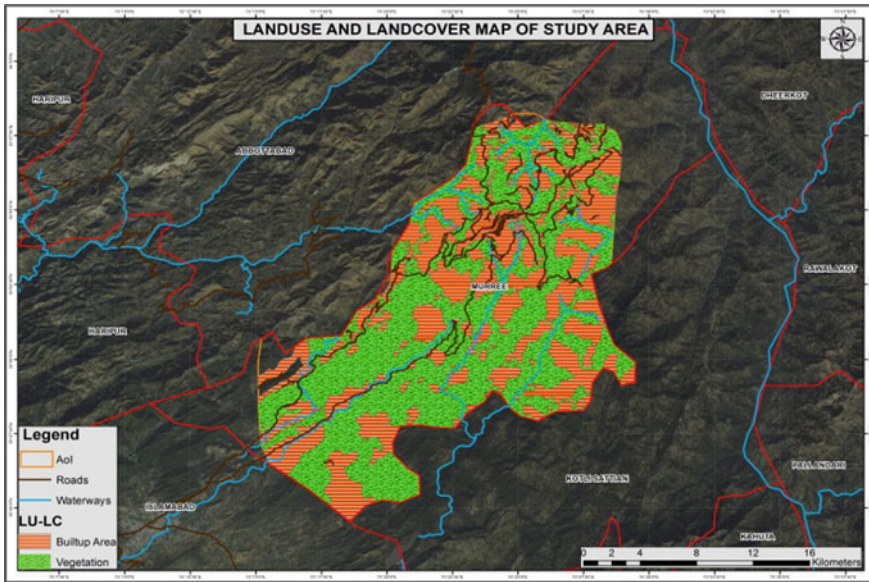


Fig. 5 Land use and land cover map of the study area

6 Conclusion

The results concluded that though, only a small area of 8% falls in highly susceptible landslide class but, it has the high land use percentage which is a serious threat to human life and infrastructure.

The final map indicated that the landslide areas that were predicted as hazardous in the GIS Software are almost the same as observed during the field check (Figs. 7 and 8). These areas have varying slope, geological, vegetation and weathering conditions.

7 Recommendations

GIS and Remote Sensing techniques are the latest analytical tool for feasibility studies and design of a project, and this technique has proved to be highly accurate for landslide hazard mapping, ground surveys, topography and terrain assessment. Moreover, it also endures much less cost as compared to extensive field surveys.

Thus, GIS-based baseline maps and satellite images are capable of undertaking the engineering, social and resettlement and environmental studies. These studies should be part of the survey and investigations for every project.

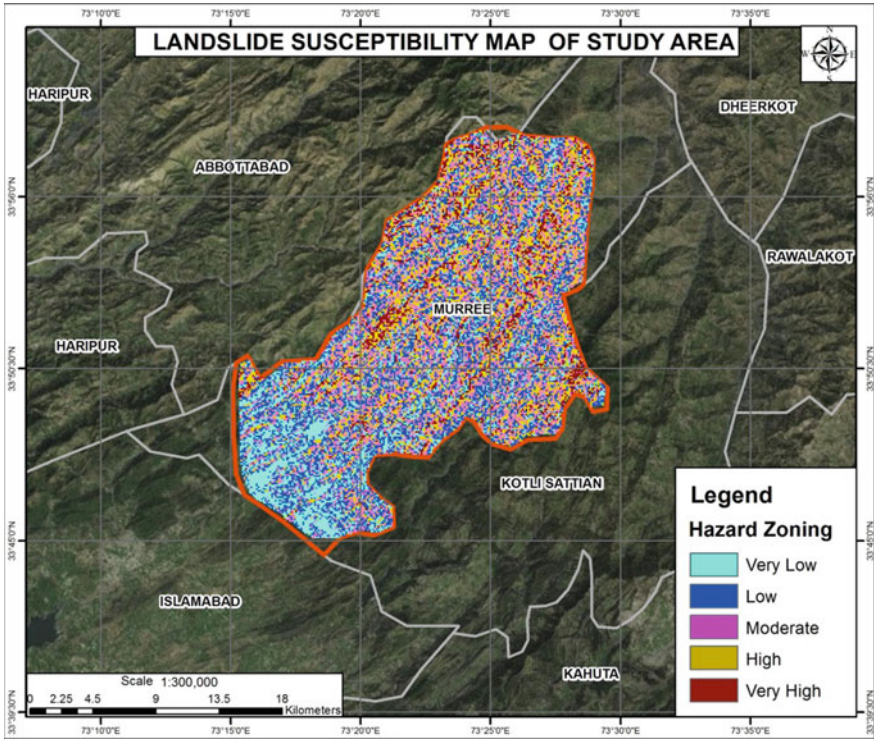


Fig. 6 Landslide susceptibility map of the study area



Fig. 7 View of landslide along the road in Murree, Pakistan



Fig. 8 Landslide due to erosion and reactivates after every rainy season in Murree, Pakistan

References

1. Yalcin A (2008) GIS-based landslide susceptibility mapping using analytical hierarchy process and bivariate statistics in Ardesen comparisons of results and confirmations. *CATENA* 72(1):1–12
2. Aleotti P, Chowdhury R (1999) Landslide hazard assessment: summary review and new perspectives. *Bull Eng Geol Env* 58:21–44
3. Pradhan AMS, Dawadi A, Kim YT (2012) Use of different bivariate statistical landslide susceptibility methods: a case study of Kulekhani watershed. *Nepal J Nepal Geol Soc* 44:1–12
4. Bui HB, Nguyen Q, Nguyen VT (2008) GIS-based weight of evidence modeling for landslide susceptibility mapping at Jaechon area, Korea. In: *International symposium on geoinformatics for spatial infrastructure development in earth and allied sciences*. p 4
5. Bonham-Carter GF (2002) Geographical information systems for geoscientist: modelling with GIS. In: Merriam DF (ed) *Computer methods in the geosciences*, vol 13. Pergamon/Elsevier, New York, pp 302–334
6. Lee S, Choi J, Min K (2002) Landslide susceptibility analysis and verification using the Bayesian probability model. *Environ Geol* 43:120–131

Bridge Leveling Network Monitoring in Construction on Highly Heaving Soils



Dmitry Afonin , Nikolay Kanashin  and Andrey Nikitchin 

Abstract Sometimes, there are deformations of the points of the geodetic network, which are placed on the construction site, in the process of bridges construction on heaving soils. Moreover, most points of the geodetic network are often removed due to heaving soils that make monitoring of such geodetic network more difficult. This article contains comparing and studying the results of the monitoring of the vertical geodetic control network in constructing the bridge over the Verebushka River, obtained by A. Kostechel method and by leveling relative to the bridge under-truss sites. It is proved that the traditional A. Kostechel method in these conditions does not fit because of false results. Consequently, it is suggested for geodetic network monitoring to fasten additional reference marks on the stable elements of the structure in constructing bridges in similar conditions. Then, it is necessary to level their marks regarding the existing benchmarks. It is also suggested to use the heights of these points as control heights to save the common system of heights during constructing in such conditions when traditional monitoring methods are giving false results.

Keywords Heaving soils · Network monitoring · Kostechel method

1 Introduction

Leveling network monitoring methods are sufficiently researched and described in specialized literature nowadays [1].

It is shown in these scientific researches that the more unstable points of the network we have the more difficult it is to identify these points.

In this research [2], a rare case was considered and it was noted that when half or more network points were displaced, the task of identifying them unequivocally was not solved by any of the existing control methods, therefore when using the methods considered in [1] proceed from the assumption that such an event is insignificant,

D. Afonin · N. Kanashin · A. Nikitchin (✉)

Alexander I Petersburg State Transport University, Moskovsky Pr., 9, 190031 Saint-Petersburg, Russia

e-mail: anikitchin@gmail.com

© Springer Nature Singapore Pte Ltd. 2020

A. Petriaev and A. Konon (eds.), *Transportation Soil Engineering in Cold Regions*,

Volume 2, Lecture Notes in Civil Engineering 50,

https://doi.org/10.1007/978-981-15-0454-9_21

especially if the network consists of a large number of points. Such an assumption [3–10], as a rule, is justified, taking into account the requirement of laying the points, taking into account their long-term preservation. However, in practice, there are cases of construction on unstable foundations where the task of monitoring the control network stability becomes uncertain. For example, let us take the geodetic control network of the construction object “The bridge over the Verebushka River”.

2 General Information on the Construction Object

The bridge over the Verebushka River (hereinafter bridge) is a civil-engineering work as a part of the high-speed toll road Moscow-Saint-Petersburg at 451–472.8 km and is located in the Okulovsky district of the Novgorod region. The bridge is classified as a big out-of-class bridge about 270 m long. Bridge pillars are of pile and raft slabs. The height of the pillars reaches 20 m. The static scheme of the bridge is a temperature-continuous system with ferro-concrete beams 21 m long for extreme spans and 33 m for intermediate spans. Engineering and geological conditions of the construction site are of II complexity level. The soils at the depth of freezing: semi-hard loam and sandy loam, hard loam and sandy loam, soft sandy loam, hard clay, dusty sand and fine sand. Standard depth of seasonal freezing for these soils is 1.6–1.95 m. The waters of the first aquifer from the surface are opened at a depth of 0.3–1.6 m. Maximum levels during unfavorable periods of the year (periods of rain and snowmelt) are 0.00–0.05 m.

The geodetic center network consists of eight points of forced centering, made of metal pipes, equipped with centering devices, in which the centers of planned coordinates and heights are combined (Fig. 1). The depth of the point and the design of its anchor is unknown. Figure 2 presents the layout of the network points.

3 Geodetic Control Network Stability Monitoring

The significant mismatches of the reference mark location with their catalog heights were noted during the construction of the object. To control the stability of benchmarks, the method used by A. Kostehel was used, which is based on the principle of the unchanged mark of the most stable network reference [2], which was derived from the adjustment of a closed leveling route laid out by the Sokkia C330 level reference frames. The results of determining the most stable reference by the method of A. Kostehel are given in Table 1.

As can be seen from Table 1, the most stable point of the network can be considered the benchmark RM47511, for which $[vv] = \min$ and it is possible to take its mark as the starting point when calculating the heights of the other benchmarks to determine their displacements by the method of A. Kostehel (Table 2).



Fig. 1 Point RM47512 geodesic center network for the construction of a bridge across the river Verebushka on PK4751 + 14 highway Moscow—St. Petersburg

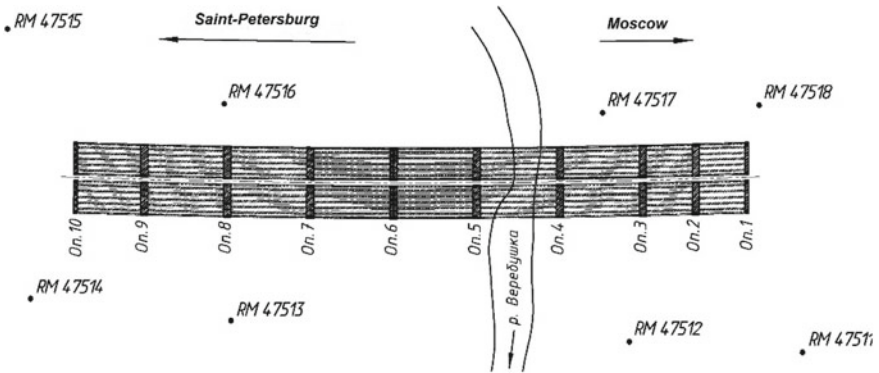


Fig. 2 Layout of the geodesic control network for the bridge construction

If the value of the vertical displacement is less than or equal to the limiting error of its determination, then the change in the height of the reference does not exceed the leveling error, and it is considered stable. Otherwise, it is assumed that the benchmark is unstable. The marginal error of determining the offset is calculated by the formula.

$$m_{\Delta H'(\text{пред})} = t \sqrt{m_H^2 + m_{H'}^2},$$

Table 2 Determination of benchmark offsets by the method of A. Kostehel

Name	H , m	H' ,m	$\Delta H' = H' - H$,mm	$m_{\Delta H'(\text{nped})}^2, \text{mm}^2$	Benchmark status
RM47511	77.484	77.484	0	–	Control
RM47512	70.760	70.773	13	3	Unstable
RM47513	69.773	69.776	3	4	Stable
RM47514	81.507	81.506	–1	4	Stable
RM47515	74.767	74.772	5	4	Unstable
RM47516	67.174	67.176	2	4	Stable
RM47517	72.343	72.332	–11	3	Unstable
RM47518	79.922	79.912	–10	2	Unstable

where t —is the normalized factor taken to be 2; 2.5 or 3; $m_H, m_{H'}$ —the mean square errors of the heights of the frames determined from the adjustment, respectively, cataloged and obtained after controlling the stability of the high-rise network.

As can be seen from Table 2, four out of eight benchmarks, i.e., half of the height network points, may be classified as unstable, with two reference points characterized by pro-landing in the period of frost heaving of the ground, which is beyond logical explanation. This raises doubts regarding the compliance of the obtained reference marks' heights with their real location.

Then, based on the assumption that most of the benchmarks are biased, and not one of the existing methods for monitoring, the height geodetic network will allow obtaining reliable results, it was decided to use the points located on the structural elements of the bridge itself as stable control benchmarks. As such elements, three-support platforms were used (Op. 3, Op. 5, Op. 6), which at the time of monitoring, the network were free of beams and, accordingly, were open for geodetic measurements. Such a choice was justified by the following considerations: sub-platform sites refer to the critical structures of the bridge, their heights are known, as reflected in the executive diagrams and were determined during the stable network with high accuracy, and for different supports executive surveys were carried out with various combinations of frames; the bridge supports, on which sub-farm platforms are located, from the moment of the performance survey and up to the moment of monitoring the stability of the high-rise network theoretically remained motionless, since they are located on the pile foundation and were not loaded with beams.

On each pillar, there are 12 bridge under-truss sites. Consequently, as control points, we used 36 points. To each of these points independently though one of the reference marks (RM47511), we tied the leveling line run through the reference marks, adjusted as free. Assuming that the heights of the under-truss sites taken from the executive diagrams are equal-accuracy results, the arithmetic mean value $H^* = 77.502$ m was taken as the final height of the RM47511 while its mean square error was less than 1 mm. Then, relative to the benchmark RM47511, the heights H^* of the other reference points were determined (Table 3).

Table 3 Comparing vertical displacements of the reference marks measured by Kostechel method and determined relative to the bridge elements

Name	H , m	H' , m	H^* , m	$\Delta H' = H' - H$, mm	$\Delta H^* = H^* - H$, mm
RM47511	77.484	77.484	77.502	0	18
RM47512	70.760	70.773	70.791	13	31
RM47513	69.773	69.776	69.794	3	21
RM47514	81.507	81.506	81.524	-1	17
RM47515	74.767	74.772	74.790	5	23
RM47516	67.174	67.176	67.194	2	20
RM47517	72.343	72.332	72.350	-11	7
RM47518	79.922	79.912	79.930	-10	8

Table 3 presents comparing vertical displacements of the reference marks measured by A. Kostechel method $\Delta H'$ and determined relative to the bridge under-truss sites ΔH^* . The table shows that the network stability monitoring, carried out relative to the bridge under-truss sites, gave a completely different result than that of A. Kostechel method and confirmed the assumption of the displacement of the most reference marks.

This displacement can be explained by the fact that the soils, where the points are placed, are classified as heaving ones. The force of frost heaving depends on many factors [2], including those that took place during the construction: high level of groundwater; temperature extremes; lack of snow cover in season of frosts.

The similar situation with reference to networks at the same period was found on the other bridges nearby, which indirectly confirms the reliability of the findings. After remeasuring the heights of “the bridge” points, they can be used as control ones for checking heights of the “road” points located between them.

4 Conclusion

According to this research, it appears to be possible to recommend in construction of engineering facilities to set auxiliary points on their conditionally stable structural elements and measure their heights relative to the existing benchmarks.

In case of not having unambiguous results by using existing methods, one should use them as control ones.

This approach provides the continuity of the height system of the object during its construction and the link of the position of the construction parts built before and after network monitoring.

References

1. Levchuk GP, Novak VE, Konusov VG (1991) Applied geodesy: main methods and principals of engineering-geodetic works: training manual. Nedra, Moscow
2. Saitsev AK, Marfenko SV, Michelev DS (1991) Geodetic methods of studying deformations of engineering facilities. Nedra, Moscow
3. Bitelli G, Bonsignore F, Unguendoli M (2000) Levelling and GPS networks to monitor ground subsidence in the Southern Po Valley. *J Geodyn* 30:355–369
4. Scaioni M, Barazzetti L, Giussani A, Previtali M, Roncoroni F, Alba MI (2014) Photogrammetric techniques for monitoring tunnel deformation. *Earth Sci Inf* 7(2):83–95
5. Duchnowski R (2009) Geodetic application of r-estimation—levelling network examples. *Tech Sci* 12:135–144
6. Chen Ch (2001) Rank estimating equations for random effects models. *Statist Probab Lett* 54:5–12
7. Dionne L (1981) Efficient nonparametric estimators of parameters in the general linear hypothesis. *Ann Stat* 8(2):457–460
8. Zheng-Lin YU, Zong-Chou YU (1983) Dynamic adjustment of repeatedly observed levelling networks used in crustal vertical deformation monitoring. *Dev Geotecton* 20:279–291
9. Xu P (1989) On robust estimation with correlated observations. *Bull Geod* 63:237–252
10. Yang Y (1994) Robust estimation for dependent observations. *Manuscripta Geod* 19:10–17

Determining the Refraction Coefficient Based on the Differences of the Measured and Known Zenith Distances in Short-Distance Trigonometric Leveling



Yulia Lobanowa , Mikhail Bryn  and Evgeniy Svintsov 

Abstract This article provides a systematization of the main errors affecting the results of determining relative heights by unilateral trigonometric leveling. The zenith distance determination accuracy vs the height of the instrument, the known elevation and the distance between stations has been pre-calculated. Refraction is the main factor preventing the use of the accuracy capabilities of modern electronic tacheometers. The results of daily experimental studies to determine the refraction coefficient are presented, and the results obtained have been analyzed.

Keywords Vertical refraction · Refraction coefficient · Trigonometric leveling · Electronic tacheometer

1 Introduction

At this stage, influence of the environment significantly limits the accuracy of angular and linear measurements. Very low air temperatures (i.e., while working in cold regions) result in instruments deformation and distortion of measurement results [2, 4]. In these cases, it is necessary to introduce the temperature corrections to the calculation during high-precision geodesic measurements. Violent temperature changes lead to undesirable optical phenomena (e.g., increased refraction). In view of this, we can conclude that it is very important to study the nature of refraction occurrence, as well as to determine the correction for refraction and to introduce it into the results of geodesic measurements.

Y. Lobanowa (✉) · M. Bryn · E. Svintsov
Alexander I Petersburg State Transport University, Moskovsky Pr., 9, 190031 Saint-Petersburg,
Russia
e-mail: lobanowa_@mail.ru

© Springer Nature Singapore Pte Ltd. 2020
A. Petriaev and A. Konon (eds.), *Transportation Soil Engineering in Cold Regions*,
Volume 2, Lecture Notes in Civil Engineering 50,
https://doi.org/10.1007/978-981-15-0454-9_22

209

2 Determination of Refractive Indexes

Nowadays, electronic tacheometers are mainly used for geodetic surveys for construction. Refraction—atmospheric density inhomogeneity—is the main factor preventing the use of the accuracy capabilities of modern electronic tacheometers [9–12]. In modern tacheometers, the refraction is taken account of by introducing the refraction coefficient k in the instrument memory, and therefore, the calculation of k remains a pressing issue [6].

This article provides a systematization of the main errors that affect the results of determining relative heights by unilateral trigonometric leveling; the accuracy of the effect of different arguments on the final result has been pre-calculated, and the results of the field experiment to determine the refraction coefficient have been analyzed.

In trigonometric leveling, the relative heights between geodetic stations are calculated using formula [1, 5]:

$$h = d \cdot \operatorname{ctgz} + i - l + f, \quad (1)$$

where d is the horizontal distance between stations; z is the zenith distance; i is the height of the instrument; l is the height of the sighting target; f is the correction for the combined effect of the Earth curvature and refraction. It is expressed using formula [3]:

$$f = \frac{1 - k}{2R} \cdot d^2, \quad (2)$$

where R is the Earth's radius; k is the refraction coefficient. It is calculated using formula [7]:

$$k = \frac{R}{R_c},$$

where R_c is the radius of the light curve.

The analysis of formula (1) shows that several arguments—one of which is the zenith distance—influence the relative height determination accuracies. The zenith distance measurement errors, in turn, are divided into errors of non-refractive and refractive origin [3, 10].

The value of non-refractive errors depends on the instruments and the measurement methods used. This group is fairly easy to study. The main sources of errors of non-refractive origin are sighting errors, pipe horizontal axis inclination errors, instrument rotation vertical axis inclination errors, zenith position changes due to temperature effects, etc.

The values of refractive errors depend on the conditions in which measurements are conducted and are usually calculated indirectly using arguments measured (temperature, pressure, humidity, geodetic measurements, etc.) [8].

The following describes an experiment that aims to determine errors of refractive origin based on geodetic measurement results.

3 Field Survey and Pre-Calculation of the Accuracy of Measurement Results

For field studies, an experimental polygon has been formed which included the observation point and the selected point on the building (a reflective film RF has been glued onto it at a height of 11.990 m).

Field experimental studies have been carried out during one day from August 10 to August 11, 2018. The territory, where the research was conducted, is a construction site; the sighting beam was partially above the construction site fencing in a flat area with asphalt for an underlying surface. Field studies included zenith distance measurements and linear measurements from the observation point to the selected point.

Studies of the instrument (Sokkia SET 5 electronic tacheometer) were carried out prior to the field survey.

To identify the value and the nature of the effect of vertical refraction on measured zenith distances, it is necessary to know their theoretical values that can be obtained from formula (1) with $l = 0$:

$$\tilde{n}tgz = \frac{h - i}{d} - \frac{d}{2R},$$

The distance between the observation point and the RF was measured multiple times (23 times) with an electronic tacheometer. The intrinsic convergence root-mean-square error (RMSE) of the distance measurement was $m_d = 2.8$ mm, and the relative error was 1/57,000. The relative height between the observation point and a point at the wall of the building was determined from double geometric leveling with a root-mean-square error of $m_h = 1 \text{ mm} \cdot \sqrt{2} = 1.4$ mm using a Sokkia B30 level. The height of the sighting beam to the selected point on the surface of the building was determined multiple times (11 times) using a DISTO electronic tape measure with an RMS of 1.7 mm. The height of the instrument was measured with a tape measure (3 times) with an RMS of 1 mm. The RMS of the sighting target (m_l) is not considered because the measurements were conducted on the RF.

Thus, the total zenith distance measurement error was obtained taking into account instrument errors (m_h, m_i, m_d), for $d = 161.290$ m, $z = 87^\circ 17' 44''$):

$$m_z = \rho'' \cdot \sqrt{\frac{m_h^2 + m_i^2}{(1 + ctg^2z)^2 \cdot d^2} + \frac{(2R(h - i) + d^2)^2 m_d^2}{4R^2 d^4 (1 + ctg^2z)^2}} = 2.9'' \tag{3}$$

Consider the effect of m_h, m_i, m_d errors on the m_z value by inserting the values of all errors.

1. m_z as a function of m_h :

$$m_z = \rho'' \frac{m_h}{(1 + ctg^2z) \cdot d} = 2.5''$$

2. m_z as a function of m_i :

$$m_z = \rho'' \frac{m_i}{(1 + ctg^2z) \cdot d} = 1.3''$$

3. m_z as a function of m_d :

$$m_z = \rho'' \frac{(2R(h - i) + d^2) \cdot m_d}{2Rd^2(1 + ctg^2z)} = 0.1''$$

By analyzing the results obtained under these conditions, it can be concluded that under these conditions, m_z and m_d may be neglected.

One of the research objectives was to determine the effect of vertical refraction on the accuracy of measuring zenith distances as a function of time. CL and CR measurements of zenith distances were conducted for each measurement cycle, after which the average values of zenith distances were determined. To determine the values of the errors caused by the effect of vertical refraction (refractive errors), Δz differences were formed from the mean $z_{\bar{n}\bar{o}}$ and theoretical $z_{\bar{o}\bar{a}\bar{i}\bar{d}}$ values of the zenith distances.

The Δz differences formed include more errors of refractive origin.

A diagram was built (Fig. 1) based on the Δz differences for the observed point to determine the nature of the daily variation of refractive errors.

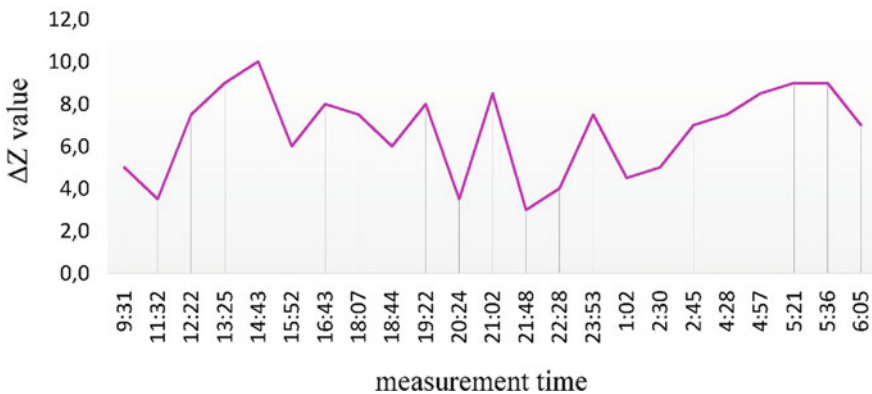


Fig. 1 Nature of daily variation of refraction

A diagram of fluctuations in the errors of refractive origin calculated based on the refraction coefficients was built for comparison (Fig. 2).

The formula for the calculation of refraction coefficients is derived from (2) through the $\Delta z''$ differences:

$$k = \frac{2R \cdot \Delta z}{d \cdot \rho},$$

where ρ is one radian in seconds.

During refraction coefficient calculations, it was assumed that the Δz differences are only caused by errors of refractive origin.

4 Conclusion

The diagram (Fig. 1) shows that there is no period during the day when the measured zenith distances are not distorted by refraction and when the effect of refraction has a pronounced daily variation.

During the day, the measured zenith distances are closer to the true values for all points in the morning and in the evening and greater than the true values for the rest—the greater—part of the day.

Refractive errors close to zero occur at sunrise and sunset, and the greatest values occur around midday. The fluctuation amplitude of the errors of refractive origin is $+3''$ to $+10''$.

The diagram (Fig. 2) shows the refraction coefficients have positive values and change over time within a wide range (from $+0.38$ to $+2.67$) throughout the day.

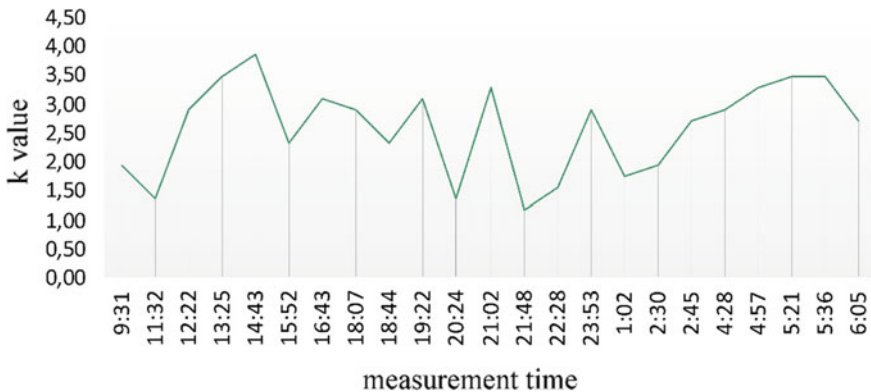


Fig. 2 Nature of the daily variation of the refraction coefficients k

References

1. Carlson AA (1993) Classification of accurate short-beam leveling. *Surveying Mapp* 6:11–13
2. Chrzanowski A (1989) Implementation of trigonometric height traversing in geodetic leveling of high precision. Technical report No. 142. University of New Brunswick, Canada
3. Drok MK (1962) Issue of the relative height correction for the combined effect of the earth's curvature and vertical refraction in short-distance geodesic leveling. In: *Proceedings of the Lviv Polytechnic National University, Surveying Series*. Issue 82, 7 pp 3–30
4. Khalil R (2007) Enlargement the sighting distance of sakkia digital level SDL30. *Strateg Integr Surveying Serv* 7:11–13
5. Kratzsch H (1979) Motorisierte Hohenzugmessung mit elektrooptischen Tachymetern. *Vermessungswesen und Raumordnung* 41:139–150
6. Milev G, Stoev G, Wassilewa K (1984) Experimentelle Untersuchungen zur Verfeinerung der trigonometrischen Höhenmessung in lokalen dreidimensionalen Netzen. *Fachricht Vermessungsw* 133:225–232
7. Moroz OI (2003) Determining and calculating the vertical refraction during geodetic measurements, vol 2. Polytechnic National University Publishers, pp 223–224
8. Nikonov AV (2013) Application features of modern geodesic survey instruments in the observation of settlements and deformations of buildings and structures of power engineering facilities. *SGGA Bull* 4(24):12–18
9. Piskunov ME (1980) Methodology for geodetic observations of structure deformations. Nedra Publishers, Moscow
10. Rueger JM (1995) EDM-height traversing refraction correction and experiences. *Trans Tasman Surveyor* 1:48–56
11. Vshivkova OV (2010) Integrated approach to solving the refraction problem. *Geodetic Airborne Photographic Surveying Ser* 3:3–9
12. Whalen CT (1985) Trigonometric motorized leveling at national geodetic survey. *North Am Vertical Datum* 1:65–80

Features of Engineering Surveys in Areas of Permafrost Prevalence by the Example of the Project “Northern Latitudinal Way”



Natalia Bogomolova , Yuriy Milyushkan , Sergey Shkurnikov , Nikolay Bushuev , Evgeniy Svintsov  and Vladimir Anisimov 

Abstract The Northern latitudinal way is a set of measures for the reconstruction and strengthening of the existing and the construction of new sections of the railway infrastructure “Obskaya–Salekhard–Nadym.” The construction of the railway is associated with the natural and climatic features of the region: permafrost soils, mainly sandstone and sandy loam unsuitable for the construction, losing bearing capacity during thawing. For a rational design and construction of the transport complex in permafrost conditions, detailed engineering and technical surveys have been carried out. On the basis of the results of exploration work, the area grounds with the most favorable engineering-geological and hydrogeological conditions as well as heaving and snow-dumping sites were identified.

Keywords Permafrost conditions · Engineering survey · Northern latitudinal way

1 Introduction

The Northern latitudinal way (hereinafter NLW) is a set of measures for the reconstruction and improvement of the existing sections of the Obskaya—Salekhard—Nadym railway infrastructure, as well as the construction of new sections. The feasibility of the project is due to the need to export oil and gas cargo; the Trans-Siberian line cannot cope with, though operating at the maximum output.

Three participants are to implement the project, namely OAO Russian Railways, OAO Gazprom, and PAO YaNAO [1].

For the first time in Russian railway construction, the new Obskaya—Salekhard—Nadym section will be engineered as part of a concession agreement.

The NLW will extend to about 1,255 km of railway infrastructure, of which 395 km is new construction. The total cost of the project is estimated at 471.9 billion rubles, and the project implementation period is 2018–2022.

N. Bogomolova (✉) · Y. Milyushkan · S. Shkurnikov · N. Bushuev · E. Svintsov · V. Anisimov
Alexander I Petersburg State Transport University, Moskovsky Pr., 9, 190031 Saint-Petersburg,
Russia
e-mail: bogomolova.n.n@yandex.ru

© Springer Nature Singapore Pte Ltd. 2020

A. Petriaev and A. Konon (eds.), *Transportation Soil Engineering in Cold Regions*,
Volume 2, Lecture Notes in Civil Engineering 50,
https://doi.org/10.1007/978-981-15-0454-9_23

215

The project “Northern Latitudinal Way” dates back to the 70s of the last century. It was then that OAO LENGIPROTRANS performed a complex of design and exploration work under the title “Restoration of Railways. Labytnangi—Salekhard—Igarka lines. The Labytnangi—Salekhard—Nadym section for the exploration of the gas field Medvezhy, the construction and operation of the Northern Lights gas pipeline (Medvezhye—Nadym—Salekhard—Chum—Ukhta). In 1985, construction began on the world’s northernmost railway Labytnagi—Bovanenkovo. Since 2003, the need has arisen to create a fully featured highway; at the same time, the Yamal Railway Company was established on the basis of Russian Railways and the Yamal-Nenets Autonomous Area.

To date, there are two current approaches to the NLW, to be strengthened, Konosha—Labytnangi and Korotchaevo—Tyumen; and two poorly functioning sections: Nadym—Pangody and Pangody—Novy Urengoy—Korotchaevo, which need reconstruction [2]. The construction of the Obskaya—Salekhard—Nadym section is unique because the available experience cannot be applied to the severe conditions in the natural areas of Western Siberia. The NLW route extends in the latitudinal direction and runs along the northern Arctic Circle, mainly from its southern side. The climate of the territory considered is sharply continental, with a harsh long winter (180 days) and short transitional seasons. The severity of the climate is complicated by the proximity of the Kara Sea. The period with a steady snow cover lasts for more than 220 days. Climatic conditions, an extremely extensive hydrographic network of full-flowing rivers, numerous lakes and marshes showing their worth during snowmelt season, while widespread permafrost and finely dispersed sediments predetermine unfavorable engineering and geological conditions for any type of construction.

For efficient design and construction of the transport complex in permafrost conditions, detailed engineering and technical surveys have been carried out.

2 Geodetic Measurements

Engineering geodesic surveys were carried out in order to obtain information about the topography of the NLW construction area, its geomorphological characteristics, outlines of water bodies, and availability of existing engineering services, roads, and other utilities.

The large-scale complex of geodetic works included ground reconnaissance; survey of the starting points of the State Geodetic Network (SGN) and State Leveling Network (SLN); laying out the points of the geodetic control network (GCN) and the points of the control network; satellite observations at the points of SGN, GCN, and control network points; laying of leveling lines according to the class III method between the points of SGN, GCN, and control network; laying out tachometric and leveling lines to create geodetic control from the GCN and control network points; topographic survey at a scale of 1 in 500 with a cross section of the relief every 0.5 m; survey morphometric profiles; and cameral work.

The area under consideration is located in the tundra and forest-tundra zones. Since the study area is primarily swampy, the GCN points were fixed in pairs in year-round access points outside the construction site. To perform engineering and geodetic works on laying polygonometric and tachometric lines, and on creating a linear-angular network, the nearest GCN points and points of the control network were used as starting points.

As part of the performance of geodetic surveys, the maximum depth of thawing in the field of permafrost was determined, using drilling and boring. The stability of geodetic points was ensured by securing the lower part of the center of the points with an anchor in permafrost. Places for laying the points were selected on elevated landforms with a shallow melting depth.

A topographical survey of the territory was carried out using a combination of methods of tachometric, horizontal, and vertical survey from the control network points [3].

In the survey area, there are more than 400 rivers with a length of 10 km and above. The Ob River holds a special place in the river system of the region—the largest Russian basin. During the construction of the NLW infrastructure, it is planned to build nine bridges. In order to compile morphometric profiles for the design of bridges, field tracing on the terrain with bringing the picket points of morphometric sections was performed. The coordinates and heights of the points of the morphometric profiles of the bottom of the river, water bodies, flooded areas, and land areas were determined in 30 m increments using water transport in the summer period [3]. The main hydrological characteristics in the design of bridges are the highest water levels, which are most difficult to determine in the conditions of the studied area because their dependence on the design expenses during the spring flood is broken. During the flood period, up to 90% of the annual runoff occurs, and maximum water levels are recorded, which results in rather restricted methods of determination of high water levels in the territory under consideration, i.e., only on the rivers with a catchment area of more than 100 km². To establish reliable parameters in determining the maximum runoff from unexplored catchments will need any, even short-term observations on the rivers of the region [4].

Following the results of engineering and geodetic surveys, topographic plans at a scale of 1 in 500 with a vertical interval of 0.5 m, and morphometric profiles were drawn up, a survey was carried out and the location was agreed with the owners of utilities and artificial structures.

3 Geological Measurements

Engineering-geological surveys of the area were carried out in order to obtain a comprehensive assessment of the natural and man-made conditions of the work site, necessary for the development of optimal, reasonable, cost-effective, constructive, and engineering solutions.

The fieldwork was started with the reconnaissance survey of the study area and drilling of wells to determine the lithological composition and mode of occurrence of the soils. In total, more than 1,500 wells were drilled during the survey period. At the laboratories, a comprehensive analysis was performed to determine the physical and mechanical characteristics of the soil, the chemical composition of the soil and groundwater. Their aggressiveness toward structures made of concrete, reinforced concrete, and carbon steel was determined.

On the bridge crossing sections, with the base of the approach fills composed of thawed soils, static sounding was carried out to the depth of the studied section in order to assess the bearing capacity of the soils.

The wells that have exposed permafrost soils were subjected to thermometric work to study the natural temperature behavior of the soils.

According to [5], the survey area represents the area of the noncontinuous permafrost occurrence. Permafrost is of island nature and has a heterogeneous structure, both in plan and in section. The surveys have established that the exposed thickness of permafrost within the site reaches 39.5 m [4]. Throughout the studied area, the negative soil temperatures are rather low in absolute value. This suggests that any slight change in temperature resulted from the construction can contribute to the degradation of permafrost and the development of frost-thaw processes [4].

The territory features a large number of swamps. According to the results of surveys, heaving areas were revealed in the extensive frost-thaw depressions and in the areas of high bogs. Peat occurs on the mineral base of lithological composition that varies, often on the clayey low-permeable soils [6]. Field studies showed that if it is impossible to remove or replace peat at the base of the structure completely, it can be used only if the piles of the peat stratum are cut through to full capacity and peat remains in the hard rock condition during the entire period of operation of the structure.

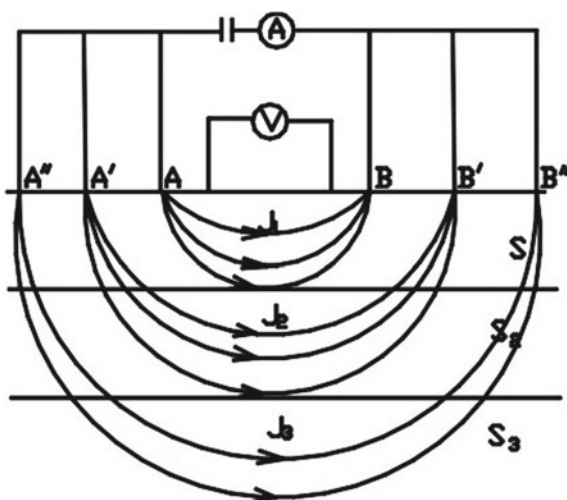
4 Geophysical Measurements

Geophysical studies at the facility were performed to study the parameters of geoelectric sections and their homogeneity for design, determine the specific electrical resistance of soils in natural occurrence and assess their corrosive aggressiveness with respect to carbon steel, determine the presence and magnitude of the potential difference created by “stray” currents in the ground.

The presence of “stray” currents in the earth at the object under study was determined by measuring the potential difference between two points of the earth. The observations were carried out in two mutually perpendicular directions with the spacing of the measuring lines of 100 m (58 measurements).

Cameral processing of the results of determining the presence of stray currents was reduced to the determination of the difference between the minimum and maximum readings of the natural electric field strength in soils at each measurement point.

Fig. 1 Electrical resistivity measurement circuit by the method of vertical electrical sensing



According to the results of work at the facility, no stray currents were detected in the earth of a dangerous size.

To study the geological features of soils, geophysical surveys were conducted on the object using the method of vertical electrical sounding.

In the course of the work, a Schlumberger symmetrical four-electrode installation was used according to the AMNB scheme (Fig. 1) with the line length AB max equal to 300 m, MN equal to 1.0 and 5.0 m at the “gate” transition. The choice of such spacing allowed us to explore the geological section to a depth of 40 m. In the further construction of geoelectric sections, surface heterogeneities and deviations from the logical distribution of the curves were taken into account.

The equivalence principle was evaluated to determine the minimum number of geoelectric layers. The obtained quantitative dependences were used to build the depths of changes in the specific resistances taking into account the principle of equivalence of the number of geoelectric layers. Cameral processing of electrical resistivity measurements consisted in the calculation of numerical values with the subsequent determination of the corrosiveness of soils with respect to carbon steel.

Geoelectric sections, constructed as a result of interpretation, have a two-layer, three-layer, and four-layer character since geological sections are represented by seasonally frozen and thawed soils, as well as by permafrost soils.

5 Conclusion

As a result of the work performed in the construction area, 76 engineering-geological elements were identified, a chemical analysis of groundwater was performed, the degree of corrosive soil was established, an analysis of the temperature condition of

the soils of the bridge bases was carried out, and geophysical works made it possible to refine the data on the engineering-geological and geocryological structure of the route. Calculations and experience of field surveys showed that under the conditions of the region under consideration, it is possible to ensure the formation of permafrost. Integrated engineering surveys carried out on the territory of the NLW construction will form the basis for the design of a unique railway line. Identified important aspects of the design: the presence of permafrost, the spread of karst, poor hydrological study of the area, prolonged freeze-up, peat formation and much more. Created a digital terrain model. The results of the engineering surveys allow us to make recommendations for ensuring the stability of the subgrade base, predict the magnitude of the expected vertical deformations, and also prevent the occurrence of unacceptable elastic deformations of the embankment during rolling stock movement [7–14]. The survey materials will allow organizing effective geotechnical supervision and deformation monitoring during the construction and operation of the infrastructure.

References

1. The business plan of the project (2017) “Creating the northern latitudinal railway Obskaya-Salekhard-Nadym-Pangody-Novy Urengoy-Korotchaevo” and railway approaches to it” (Russian Railways, Moscow), 190
2. Data from the site of the company Vostock Capital—Key Yamal deposits [Electronic resource]. <https://www.vostockcapital.com/geologorazvedka/klyuchevyie-mestorozhdeniya-yamala/>. Accessed 27 Jan 2017
3. “Technical report on the results of engineering and geodetic surveys”, LLC “Geoaspect”, 12–13 (2018)
4. “Technical report on the results of engineering and geological surveys of the Salekhard-Nadym site”, Transproject LLC, 22–23 (2018)
5. SP 11–105-97 (1999) “Engineering and geological surveys for construction, part 4 of the Rules of work in areas of permafrost,” Gosstroy of Russia, Moscow
6. Zhinkin GN (2000) Features of the construction of railways in areas of permafrost and swamps [Electronic resource]. ZHDT, Moscow. ISBN 5-89035-038-2
7. Emond AM, Graham GRC, Janssen KA (2019) Geophysics in Alaska: Alaska division of geological & geophysical surveys information circular 78
8. Lewkowicz AG, Etzelmüller B, Smith SL (2011) Characteristics of discontinuous permafrost based on ground temperature measurements and electrical resistivity tomography, Southern Yukon, Canada. *Permafrost Periglac Process* 22(4):320–342
9. Murton JB (2001) Thermokarst sediments and sedimentary structures, Tuktoyaktuk coastlands, western arctic Canada. *Glob Planet Change* 28:175–192
10. Lautala P, Oommen T, Addison P (2016) Utilizing vegetation indices as a proxy to characterize the stability of a railway embankment in a permafrost region. *AIMS Geosci* 2(4):329–344. <https://doi.org/10.3934/geosci.2016.4.329>
11. Douglas TA, Jorgenson MT, Dana RN, Brown, Campbell S W, Hiemstra CA, Saari SP, Bjella K and Liljedahl AK (2016) Degrading permafrost mapped with electrical resistivity tomography, airborne imagery and LiDAR, and seasonal thaw measurements, *GEOPHYSICS*, 81(1), (WA71-WA85) <https://doi.org/10.1190/geo2015-0149.1>
12. Voytek EB, Rushlow CR, Godsey SE, Singha K (2016) Identifying hydrologic flowpaths on arctic hillslopes using electrical resistivity and self potential. *Geophysics* 81(1):WA225–WA232. <https://doi.org/10.1190/geo2015-0172.1>

13. Trochim ED, Schnabel WE, Kanevskiy M, Munk J, Shur Y (2016) Geophysical and cryostratigraphic investigations for road design in northern Alaska. *Cold Reg Sci Technol* 131:24–38. <https://doi.org/10.1016/j.coldregions.2016.08.004>
14. Magnin F, Krautblatter M, Deline P, Ravanel L, Malet E, Bevington A (2015) Determination of warm, sensitive permafrost areas in near-vertical rockwalls and evaluation of distributed models by electrical resistivity tomography. *J Geophys Res Earth Surf* 120(5):745–762

The Study of Railway Embankment Deformations in Cold Regions



Natalia Bogomolova , Mikhail Bryn , Andrey Nikitchin ,
Alexey Kolos  and Andrey Romanov 

Abstract Concerning the need for railway capacity increase, the trains marshaled of innovative cars with 27 t axle load are being tested at the test sites. At one of the sites of Sverdlovsk Railway, 100 km Kachkanar—Smychka, the works have been organized to provide geodetic monitoring of the permanent way and the high embankment formation deformations. The geodetic surveys were carried out for eight months from December 2017 to July 2018 at four test sites. The analysis of the measurements shows an intensive frost heaving of the soils at two test sites in winter period. The permanent deformations of the main site of the formation were observed at these sites in summer period.

Keywords Permafrost conditions · Geodetic monitoring

1 Introduction

Growing exports of minerals of the Russian Federation necessitates the development of railway transport infrastructure, which is the major land carrier of the extracted raw materials. Promising Asian markets cannot be provided with Russian minerals without increasing the capacity of the railways of the Eastern Polygon, which operational length is more than 17 thousand km. To remove the restraints of JCS Russian Railways infrastructure, since 2013, a program has been implementing for the development of the Trans-Siberian and Baikal–Amur Highways (Eastern Polygon).

One of the possible alternatives for improving the efficiency of the transportation process in the transport corridor allowing for cargo traffic to the Asia-Pacific region is to increase the axial load to 27 ton-force [1]. The experience of introducing heavy-weight traffic to the world practice shows a significant economic effect. However, the use of innovative cars with increased carrying capacity is expected to increase the vibration dynamic effect on the subgrade and result in greater deformations. At

N. Bogomolova (✉) · M. Bryn · A. Nikitchin · A. Kolos · A. Romanov
Alexander I Petersburg State Transport University, Moskovsky pr., 9,
Saint-Petersburg 190031, Russia
e-mail: bogomolova.n.n@yandex.ru

the same time, high railway embankments employed for a long time (with levels of at least 6 m) are the most susceptible to the development of deformation processes (washouts, slope failures). It should be noted that the Eastern Polygon of the railway network is located in the Siberian and Far Eastern Federal Districts, where harsh climatic conditions contribute to the deformation process.

2 Evaluation of the Impact of Heavy Traffic on the State of High Railway Embankments

To assess the effect of the passage of trains formed by the cars with an axle load of 27 ton-force on the state of high railway embankments, a research work was organized on monitoring the condition of the superstructure and the roadbed on the Kachkanar—Smychka railway line [2].

In accordance with the technical design assignment and the test program, three experimental sites and one control site were selected that qualify for the following criteria: at the experimental sites, the railway embankments height is 6.0 m and more; each experimental site is located on a double-track running line; at each experimental site, two section lines were selected, with the first one in the middle part of the string (link), the second one at the rail joint; geotechnical conditions within the same range are of the same type (according to the data of the geotechnical survey of the site).

At each site, one of the tracks is a continuous welded rail on reinforced concrete cross ties, and the other is a link rail on wooden cross ties. All sections are characterized by a stable condition of the rail track according to the data of the geometry car passages.

The area where the objects of study are located is described by a moderately continental climate with hot summers and cold frosty winters. Temperature in different seasons varies from $+28^{\circ}$ to -25° , with high humidity.

Climatic conditions of operation of the railway track contribute to the deformation of the subgrade. The reasons for the development of deformations are associated with excessive wetting of the subgrade in the autumn, heaving (raising the subgrade as a result of freezing of water in the pores of the soil) and its lowering accompanied by destruction, during thawing in spring.

To identify the geotechnical conditions at survey sites, it is necessary to know the nature of the bedding of the subgrade soil and its foundation and their physico-mechanical characteristics. Considering the depth of pro-freezing in this region, the minimum depth of excavation was not less than 3.0 m. In terms of age and genesis, two types of soils were distinguished at survey sites: modern quaternary technogenic undifferentiated mid-upper quaternary deposits. According to the composition and physico-mechanical properties, five engineering-geological elements are distinguished in the studied areas.

Engineering-geological element number 1: It is represented by bulk soil, followed, in the form of crushed granite rocks. Crushed stone is a ballast material of a railway track. The dimension of rubble is from 50 to 70 mm.

Engineering-geological element number 2: It is represented by bulk soil, followed, in the form of crushed granite rocks. Crushed stone is a material of ball-prism of a railway track. The dimension of crushed stone is from 10 to 30 mm.

Engineering-geological element number 3: It is represented by loose soil, followed by, in the form of sandy brownish-yellow sandy solids with plastic layers with rare gravel.

Engineering-geological element number 4: It is represented by sandy loams brownish-yellow sandy hard with gravel up to 25%, with rare pebbles, in the upper part with rare plant residues.

Engineering-geological element number 5: It is represented by heavy, silty, soft-plastic loam with an admixture of organic matter up to 4%.

No groundwater was found while drilling.

To determine the residual deformations of the subgrade, the experts of the FSBEI of HE Petersburg State Railway Engineering University designed a geodetic standard elevation by laying a closed leveling line along ground with reference marks. Leveling was carried out using the Trimble Dini 03 level and Inv 12 LD12 control rod according to the program of class I high-precision leveling according to [1]. Ground reference marks (three marks per each section) were laid at a distance of at least 50 m from the axis of the track within the railroad precincts.

The main areas of the subgrade of the studied areas were equipped with soil marks, which serve to assess deformations.

The marks were fixed in the directions along and across the rail axis (Fig. 1).

In the transverse direction, the marks were fixed in two sections corresponding to the zone of the rail joint and the middle part of the link. The leveling technique for determining the grade of ground marks was focused on maximizing the effect of various sources of error. Leveling was carried out according to the program of class III high-precision leveling according to [1]. To determine the soil marks, a closed leveling line was laid at each experimental site from the initial benchmark; each soil mark was determined with two instrument horizons; the deviations in the resulting values did not exceed 0.8 mm.

Geodetic observations were made for eight months, from December 2017 to July 2018. The dynamics of the deformation processes is reflected in Figs. 2, 3, 4, and 5.

Dynamics of deformation processes is presented in Fig. 6.

Analysis of the geodetic observations findings indicates intense frost heaving of soils in two experimental sites in winter (sites No. 1, No. 2). During the summer period, residual deformations of the main subgrade area were revealed at these sites.

At experimental site No. 3, intensively growing residual deformations were recorded, which accelerated during the period of subgrade thawing.

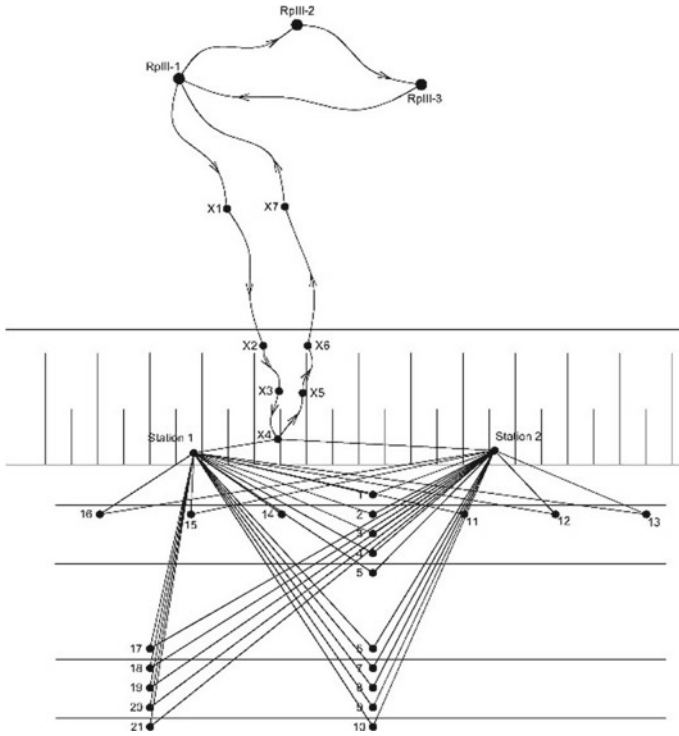


Fig. 1 Marks scheme

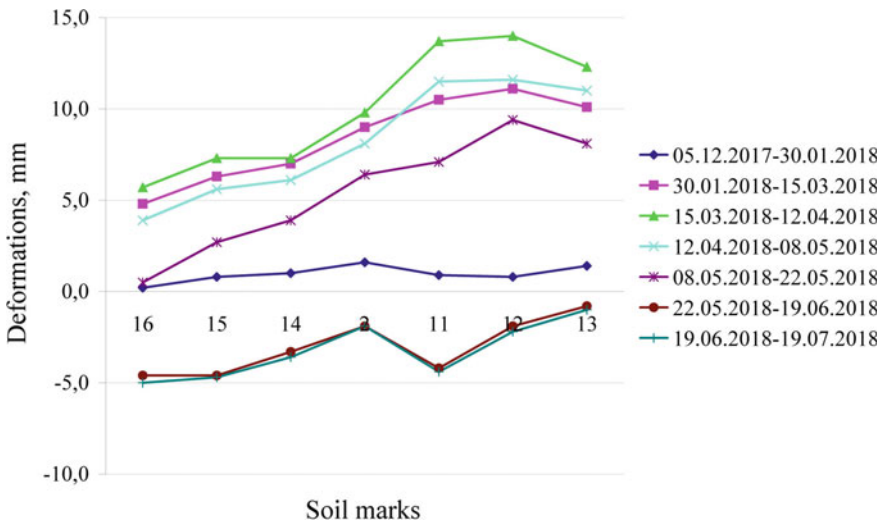


Fig. 2 Deformations along the axis of the track in Sect. 2

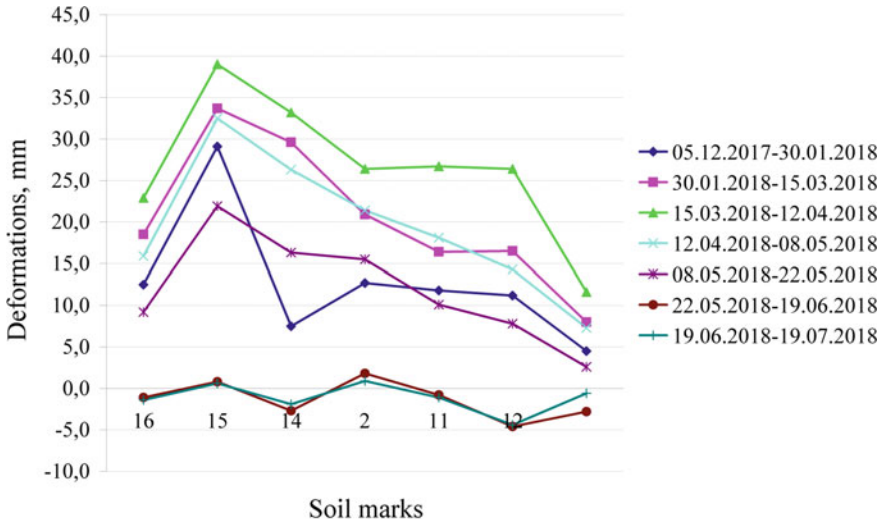


Fig. 3 Deformations along the axis of the track in Sect. 2

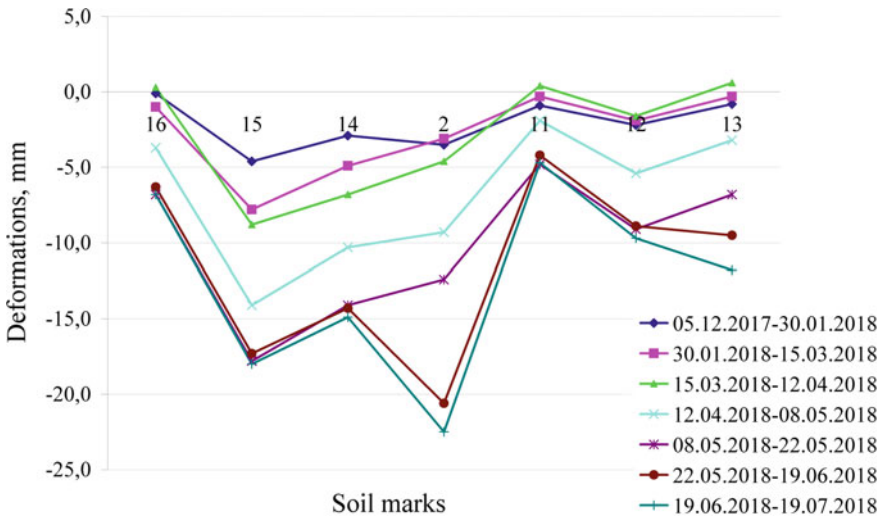


Fig. 4 Deformations along the axis of the track in Sect. 2

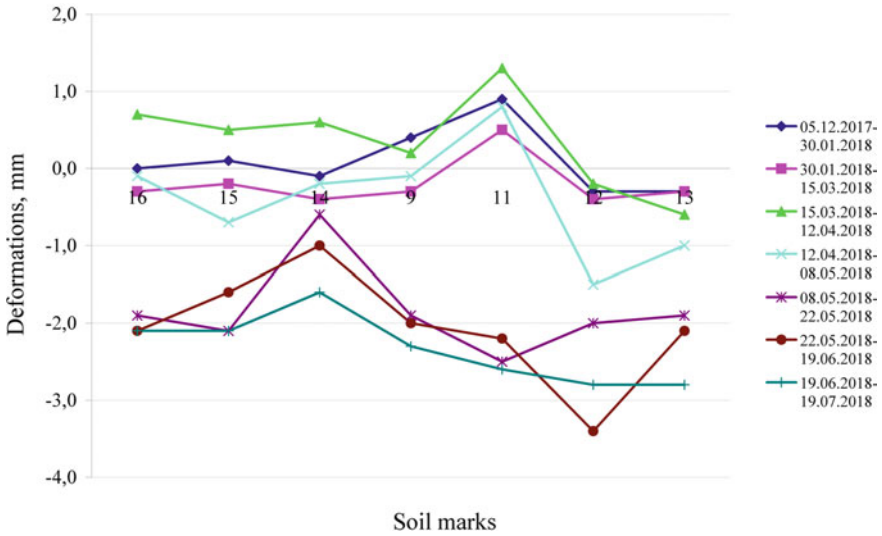


Fig. 5 Deformations along the axis of the track in Sect. 2

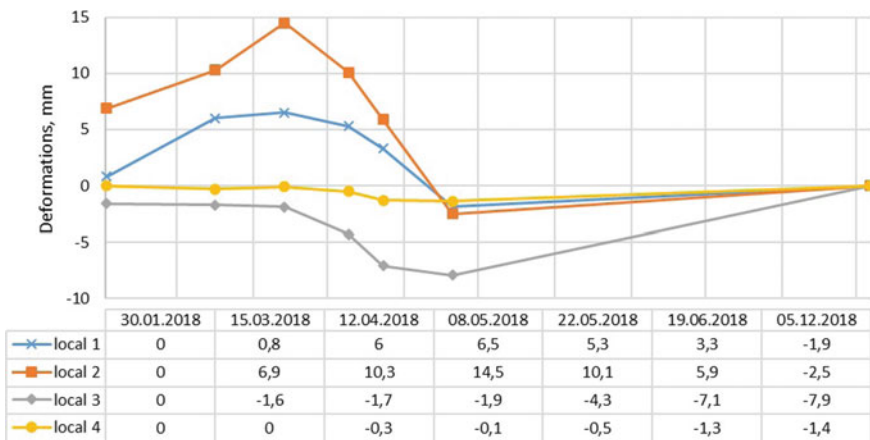


Fig. 6 Dynamics of deformation processes of the subgrade for the period December 2017–July 2018

3 Conclusion

As a result of evaluating the impact of rolling stock on the way, it was experimentally established that during soil freezing and thawing of the main site of the subgrade, and partial soil freezing and thawing of the working area of the subgrade, increased axial loads do not have a significant effect on the development of subgrade deformations. At the same time, the results of geodetic survey confirm the relevance of

the research activities related to the development of geotechnologies that contribute to the stabilization of soil deformations of the railway fill and its base in northern latitudes [3–10]. Effective control of frost heaving in cold regions will reduce the cost of maintaining and repairing railways, as well as ensure their safe operation.

References

1. Kolos AF, Romanov AV (2018) The impact of innovative cars with a load on the axle of 27 tf on the condition of the road bed of railways. In: Rolling stock of the XXI century: ideas, requirements, projects. Proceedings of the XIII international scientific and technical conference. PGUPS
2. Interstate Standart 24846-2012 (2013) Soils. Methods of measuring the strains of structure and building bases
3. Barzaghi R, Cazzaniga NE, De Gaetani CI, Pinto L, Tornatore V (2018) Estimating and comparing dam deformation using classical and GNSS techniques. *Sensors* 18(3):756
4. Dardanelli G, Pipitone C (2017) Hydraulic models and finite elements for monitoring of an earth dam, by using GNSS techniques. *Periodica Polytech Civil Eng* 61(3):421–433
5. Ghorbani M, Sharifzadeh M, Yasrobi S, Daiyan M (2012) Geotechnical, structural and geodetic measurements for conventional tunnelling hazards in urban areas—the case of Niayesh road tunnel project. *Tunn Undergr Space Technol* 31:1–8
6. Hwang C, Hung W-C, Liu C-H (2008) Results of geodetic and geotechnical monitoring of subsidence for Taiwan High Speed Rail operation. *Nat Hazards* 47(1):1–16
7. Kalkan Y (2014) Geodetic deformation monitoring of Ataturk dam in Turkey. *Arab J Geosci* 7(1):397–405
8. Sekuła K, Borecka A, Kessler D, Majerski P (2017) Smart levee in Poland. Full-scale monitoring experimental study of levees by different methods. *Comput Sci* 18:357–384
9. Tedd P, Charles J, Holton R, Robertshaw A (1994) Deformation of embankment dams due to changes in reservoir level. *Proc XIII Int Conf Soil Mech Found Eng* 3:951
10. Yavaşoğlu HH, Kalkan Y, Tiryakioğlu İ, Yigit CO, Özbey V, Alkan MN, Bilgi S, Alkan RM (2018) Monitoring the deformation and strain analysis on the Ataturk Dam, Turkey. *Geomatics, Natural Hazards Risk* 9(1):94–107

Laboratory Soil Testing

Compression Curves' Extrapolation to High Pressures for Soft Clay Soils



Peter Klemysionok , Svetlana Kolmogorova  and Sergey Kolmogorov 

Abstract One of the features of modern construction is the increase of loads on foundations and basements of buildings. Therefore, high-pressure soil compressibility has become a topical issue. However in production conditions tests have been performed at pressure no more than 0.4 ... 0.5 MPa. The article deals with compression curves extrapolation to high pressures for different genetic types of clay soils. The dependence of coefficient of compression B_k and pressure of void ratio at plasticity limit (p_p) on the soil condition was analyzed. Two segments are displayed on compression curve: initial segment and the main segment.

Keywords Compression · Clay soils · High pressures

1 Introduction

One of the features of modern construction is the increase of loads on foundations and basements of buildings [1–3]. Therefore, high-pressure soil compressibility has become a topical issue. However in production conditions, soils have been tested at pressure no more than 0.4 ... 0.5 MPa. The article deals with compression curves' extrapolation to high pressures for several genetic types of clay soils.

Compressive tests were tested according to standard methods under water at pressures 0.125; 0.25; 0.5; 1; 2; 3; and 4 kg/cm². The object of the research is fluid loam of marine and lake glacial deposits. The similar character of compressibility of these genetic types of clay soils made it possible to analyze them together [1, 2, 4–7].

P. Klemysionok · S. Kolmogorova
Emperor Alexander I State Transport University, 9 Moskovsky ave., St. Petersburg 190031, Russia

S. Kolmogorov (✉)
Saint-Petersburg State Agrarian University, 2, sh. Petersburg, Pushkin, Saint Petersburg 196601, Russia
e-mail: kolmogorovsg@list.ru

2 Main Part

Physical properties of soils are presented in Table 1.

The average compression curves for marine loam and lake glacial loam are shown in Fig. 1. Two segments are displayed on compression curve: initial segment and the main segment. The initial segment is characterized by the influence of structural bonds. On the main segment, there are the following factors: mineralogical and granulometric compositions and the destruction of structural bonds, but this is offset by the increase of the initial soil adhesion due to compaction. On the both segments, the influence of natural location indicators is shown. The boundary between the segments can be taken (for researched soils) as $P = 0.5 \dots 1 \text{ kg/cm}^2$.

Compression curve at pressure, higher than some initial pressure, often can be described as the following ratio [8]:

$$e_i = e_H - \frac{\lg\left(\frac{P_i}{P_H}\right)}{B_k} \quad (1)$$

where $p_H = 1 \text{ kg/cm}^2$ is initial pressure, e_H is air-void ratio at initial pressure, and B_k is coefficient of compression.

The values of coefficient of compression (B_k) were calculated at pressures higher than initial pressure and respective values of air-void ratio using formula (1). The results of calculations are given in Table 2.

Figure 2 shows the results of compressive tests which are presented in semi-log coordinates, where the test data is solid curve and extrapolation data is dashed curve.

Table 1 Physical properties of soils

Sample №	Clay particles Mc, %	Particle density ρ_s , g/cm ³	Soil density ρ , g/cm ³	Water content w, %	Lower liquid limit w_L , %	Plasticity limit w_p , %	Degree of water saturation Sr	Void ratio e_0
<i>Loam, mQIV</i>								
1	37	2.70	1.83	38	30	19	1.00	1.030
2	41	2.70	1.87	35	31	20	1.00	0.942
3	48	2.72	1.88	35	31	20	1.00	0.957
4	32	2.72	1.88	34	30	19	0.97	0.943
5	46	2.73	1.82	39	34	21	0.98	1.084
6	44	2.72	1.85	36	32	20	0.97	1.001
<i>Loam, lgQIII</i>								
1	43	2.72	1.89	34	28	18	1.00	0.929
2	44	2.73	1.85	37	34	21	1.00	1.022
3	51	2.73	1.82	41	35	21	1.00	1.116
4	45	2.72	1.85	36	31	19	0.98	1.000
5	44	2.71	1.84	38	33	21	0.99	1.038

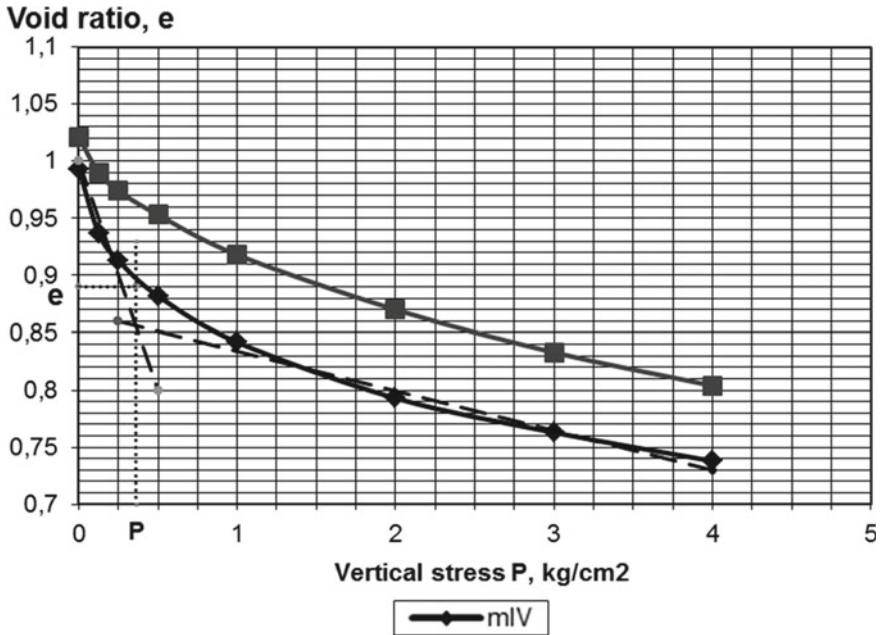


Fig. 1 Compression curves for marine loam and lake glacial loam

The compression curves' extrapolation makes it possible to determine pressure at water content of soil $w_i = w_p$, when the soil turns into solid form. At water saturation of soil $e_p = \rho_s \cdot w_p$ and using formula (1), p_p was calculated:

- lake glacial loam $p_p = 74.1 \frac{\text{kg}}{\text{cm}^2} = 7.41 \text{ MPa}$
- marine loam $p_p = 56.0 \frac{\text{kg}}{\text{cm}^2} = 5.6 \text{ MPa}$

The pressure p_L at water content of soil $w_i = w_L$ is of interest for fluid soils. This pressure reflects the impact of structural strength—soil cohesion. It is determined by calculation of void ratio e_L and compression curves.

For the average compression curve, pressure P_L is:

- lake glacial loam $p_L = 1.78 \frac{\text{kg}}{\text{cm}^2} = 0.178 \text{ MPa}$
- marine loam $p_L = 0.86 \frac{\text{kg}}{\text{cm}^2} = 0.086 \text{ MPa}$

The results of the same calculations of p_p and p_L values for the researched soils are given in Table 2.

In this paper, the dependence of coefficient of compression B_k and pressure p_p on the soil condition was analyzed. The dependence on water content (Fig. 3), content of clay particles, plasticity index, lower liquid limit was established for to coefficient of compression B_k and pressure p_p .

According to Fig. 3, the dependence of B_k on water content is observed quite clearly. The regression equation was found as $B_k = 20.4 - 0.41 w$ at the correlation

Table 2 Calculation results

Sample №	Void ratio at initial pressure e_H	Void ratio at lower liquid limit e_L	Void ratio at plasticity limit e_p	e_L pressure P_L , kg/cm ²	Coefficient of compression B_k	e_p pressure P_p , kg/cm ²
<i>Loam, mQ_{IV}</i>						
1	0.855	0.810	0.513	2.0	5.5	76
2	0.827	0.837	0.540	0.8	6.3	64
3	0.850	0.843	0.544	1.2	6.0	69
4	0.798	0.816	0.517	0.63	7.4	120
5	0.928	0.928	0.573	1.0	4.1	28.5
6	0.796	0.970	0.544	0.32	5.2	20.4
<i>Indices of the average compression curve, m_{IV}</i>						
	0.842	0.851	0.538	0.86	6.0	56
<i>Loam, lgQ_{III}</i>						
1	0.796	0.762	0.49	1.7	6.0	69
2	0.934	0.928	0.573	1.2	5.5	97
3	1.024	0.956	0.573	2.4	3.7	47
4	0.910	0.843	0.517	2.6	5.0	92
5	0.928	0.894	0.569	1.5	5.0	62
<i>Indices of the average compression curve, lg_{III}</i>						
	0.918	0.877	0.544	1.78	5.7	74.1

index $r = -0.88$. However, the dependence of pressure p_p on water content is lower, with the regression equation $P_p = 287.7 - 6w$ at the correlation coefficient $r = -0.68$. The reason of data variability is the influence of other factors; one of them is the method of calculation of the pressure p_p using the formula (1). Therefore, the pressure p_p depends not only on B_k , but also on the void ratio e_H and e_p , which in turn depends on soil compressibility.

The dependence on content of clay particles, plasticity index, lower liquid limit shows the similar character of relations with the increase of data variability for pressure p_p .

The dependence of pressure p_L on relative water content w/w_L and structural bonds ΔC_B is clearly observed (Fig. 4). Structural bonds ΔC_B were evaluated by the method [9].

3 Conclusions

Two segments are displayed on compression curve: the initial segment and the main segment. The initial and main segments are different in intensity and character of

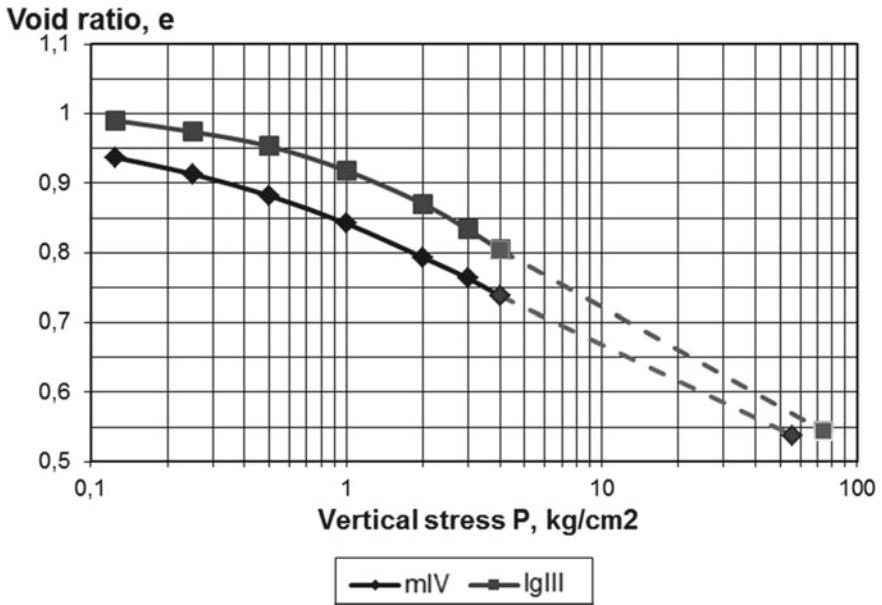


Fig. 2 Compression curves' extrapolation

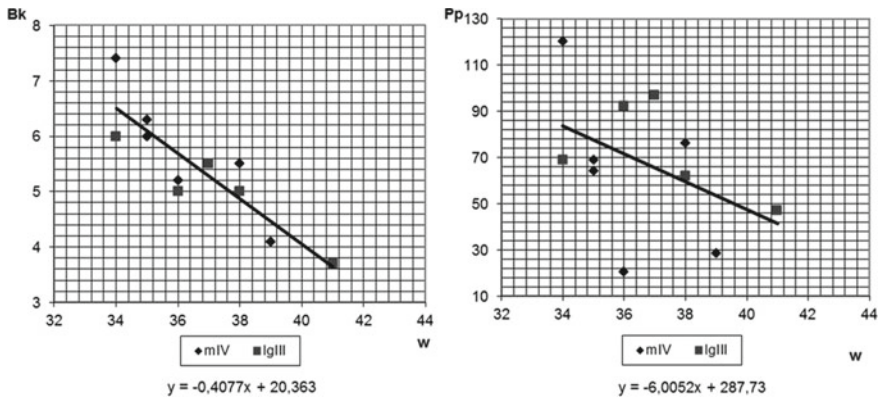


Fig. 3 Dependence of coefficient of compression B_k and pressure p_p on water content

deformations: structural deformations at the initial segment and structural adsorption ones in the second segment.

The dependence of coefficient of compression B_k and pressure of void ratio at plasticity limit p_p on the soil condition was analyzed. The dependence on water content, content of clay particles, plasticity index, lower liquid limit was established for coefficient of compression B_k and pressure p_p .

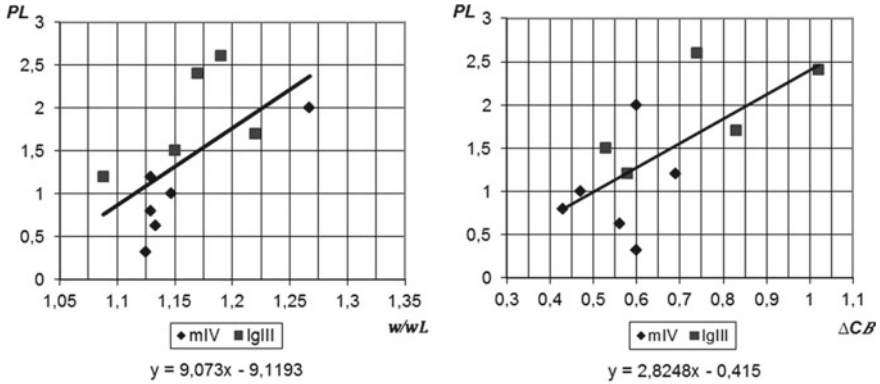


Fig. 4 Dependence of pressure p_L on w/w_L and structural bonds ΔC_B

References

1. Lysenko MP (1980) Composition and physical-mechanical properties of soil. M.: Izd. Nedra
2. Holtz W, Gibbs H (1954) Engineering properties of expansive clays. In: proceedings of the American society of civil engineers, vol 80
3. Flaate K, Preber T (1974) Stability of road embankments in soil clay. Canadian Geotech J 11(1)
4. Priklnsky VA (1955) Soil science. Ed.3. Gosgeoltekhizdat M (1955)
5. Denisov NI (1951) About the nature of the deformation of clay rocks. Minrechflot
6. Kagan AA (1974) Physical and mechanical properties of varve clays of late-glacial lakes. Woks of Hydroproject No. 37
7. Fursa VM (1975) Structural properties of soils in Leningrad area. L.: Izd. LO
8. Goldstein MN (1979) Mechanical properties of soils. Mmm., Sroyizdat
9. ZAO Lentisiz (2004) Leningrad trust of engineering-geological surveys. Technical report on engineering-geological surveys. SPb

Experimental Study on Pore Water Pressure and Microstructures of Silty Clay Under Freeze-Thaw Cycles



Dan Wang , Chengsong Yang , Guodong Cheng, Wei Ma and Lianhai Zhang

Abstract The variations on physical properties and microstructures of soils are essential to explore the freeze-thaw mechanisms. We do some experiments on freeze-thaw test of Qinghai-Tibet silty clay and cryo-scanning electron microscope (cryo-SEM) observing after freeze-thaw test and monitoring the changes of temperature, pore water pressure, and displacement. The results showed that the change of pore water pressure was closely related to soil particles rearrange, particle size redistributing, and then develop a new arranging tendency of soil pores during freeze-thaw cycles. During the period of soil freezing, the pore water pressure decreased gradually, and the particles became more gathering from point to point ($P-P$) form along with freezing rate decreasing, the relevant microstructures had changed from the matrix structure to gel structure, and pores became more simplex. During soil melting, the pore water pressure rose to stability, and the soil mainly experienced a consolidation process. In our study, we also quantify cryo-SEM images by Imagepro Plus (IPP) software. The results reflect the change of pore water pressure had a certain correlation with structural parameters under freeze-thaw cycles. These findings substantially contribute to understand the freeze-thaw mechanism and assist in upscale the microscale physical characteristic of frozen soil.

Keywords Frozen soil · Freeze-thaw mechanism · Cryo-scanning electron microscope · Microstructure · Pore water pressure · Structural parameters

D. Wang · C. Yang (✉) · G. Cheng · W. Ma · L. Zhang
State Key Laboratory of Frozen Soil Engineering, Northwest Institute of Eco-Environment and Resources, Chinese Academy of Sciences, Lanzhou, China
e-mail: ychsong@lzb.ac.cn

D. Wang
e-mail: dwang1922@lzb.ac.cn

D. Wang
University of Chinese Academy of Sciences, Beijing, China

© Springer Nature Singapore Pte Ltd. 2020
A. Petriaev and A. Konon (eds.), *Transportation Soil Engineering in Cold Regions*,
Volume 2, Lecture Notes in Civil Engineering 50,
https://doi.org/10.1007/978-981-15-0454-9_26

1 Introduction

In cold regions, soils are commonly exposed to freeze-thaw cycle every year [1]. This phenomenon has a significant effect on the service performance of engineering facilities [2, 3]. As a specific form of temperature change, the freeze-thaw cycle is a strong weathering process that can remarkably change the physical properties and microstructure of soil [4]. During freezing, soil typically subjected to frost heave which involves the phase change of water, water migration, and ice segregation. Also, consolidation of soil typically develops in the thawing process [5]. Fine-grained soils influenced by freezing and thawing show changes in volume [6], in strength and compressibility, dry density, densification, unfrozen water content, pore water pressure, bearing capacity, and microstructure [7–11]. Virtually, when considering soil physical behaviors and microstructural transformations due to freezing and thawing, the balance of pore water pressure in the soil had a significantly affects to reveal these phenomena [12].

Investigation of the pore water pressure during soil freezing and thawing is essential when exploring the mechanisms of freeze-thaw cycle, which revealing the driving force of water migration, the mechanisms of frost heave, the validity of the Clausius-Clapeyron equation, and the consolidation phenomenon of soil [13]. In particular, the consolidation phenomenon in the freeze-thaw cycle is a result of an increase in effective stress due to a decrease in pore water pressure [14, 15]. And in an attempt to reveal this variation, researcher focuses on the consolidation pattern in the different stages of soil freezing based on the observed pore water pressure and its numerical simulations, proposes that consolidation in the unfrozen zone during soil freezing includes compression-induced consolidation which results from an increase in frost heaving stress, also vacuum induced consolidation which results from a decrease in pore water pressure [12]. Typically, the growth of ice lenses results in substantial decreases in pore pressure and ultimately dewatering and unsaturation in the unfrozen zone during closed system tests without an external water supply [16]. Moreover, pore water pressure during freezing was measured and could be correlated to the subsequently observed volume and water changes [17]. The changing of pore water pressure shows that the water moving is an important influencing factor on soils by its action on structure development, deformation, particle translocation, and consolidation under the freeze-thaw cycle.

Meanwhile, the frozen soil microstructure analysis has been more important [18, 19]. During the freeze-thaw consolidation, the soil became fissured and jointed [20], and ices in various sizes and shapes tend to segregate in soils resulting in the formation of a characteristic in micro- and macroscales [21]. After the melting of soil or thaw consolidation, the inter-fissures are still open, leading to gel or closed-cell macroscopic soil structure [22]. In the condition of alternating freezing and thawing, the frost heave and consolidation occur together with more or less developed particles and aggregate broken, leaded to compaction, displacement, rotation, and formation of the soil microstructure, further affect the shape and size of the aggregates and pore distribution [23–26], giving rise to different types of microstructure formation

Table 1 Physical properties of silty clay

Soil property	Liquid limit, L_L (%)	Plastic limit, L_P (%)	Plasticity index, P_I
Value	24.8	15.0	9.8

[10, 27, 28]. The resulting change in a microstructure, in turn, affects the water moving on soil during frozen frost and thaw consolidation.

Although the significance of pore water pressure and microstructure change during freeze-thaw cycle has been widely acknowledged, few information has been reported on the relationship between pore water pressure and microstructure under the freeze-thaw cycle. Therefore, we examined the pore water pressure during freeze-thaw cycles of the silty clay in the Qinghai-Tibet of China, after that, investigated the microstructure of each layer of soil. By clarifying the variation in the pore water pressure and microstructure under freeze-thaw cycles, we expect to found a certain relationship to provide a reference to understanding freezing and thawing mechanism.

2 Experimental Study

2.1 Materials and Specimen Preparation

In this study, silty clay obtained from Qinghai-Tibet Plateau is subjected to do freeze-thaw tests. The main physical properties of this type of silty soil are given in Table 1. It was classified as CL (Low liquid limit Clay) per Unified Soil Classification System. The grain size distributions of the silty clay are presented in Fig. 1. The uniformity coefficient and the coefficient of curvature of the silty clay is 1.24.

The soil samples were prepared and tested at the State Key Laboratory of Frozen Soil Engineering CAS. Before making soil specimens, the soils were air-dried, sieved with an aperture of 2 mm. And then, the soils were slurry mixed with certain water content (21.4%) and left 24 h in a sealed plastic bag to ensure adequate water redistribution. The samples were compressed into a cylindrical Perspex cell with an inner diameter of 101 mm and a height of 140 mm, witch initial density was 1.69 g/cm^3 .

2.2 One-Dimensional Freeze-Thaw Test

The one-dimensional freeze-thaw test system consists of an insulated environmental chamber, a specimen cell, two cryostats with the temperature accuracy of $\pm 0.1 \text{ }^\circ\text{C}$, and various sensors necessary for measuring soil temperature, pore water pressure, displacement, and water intake (Fig. 2). A cylindrical Perspex cell with lateral thermal insulation was placed in the test machine box. Two columns of holes were drilled in the wall of the cell. One column contained night holes for installing the temperature

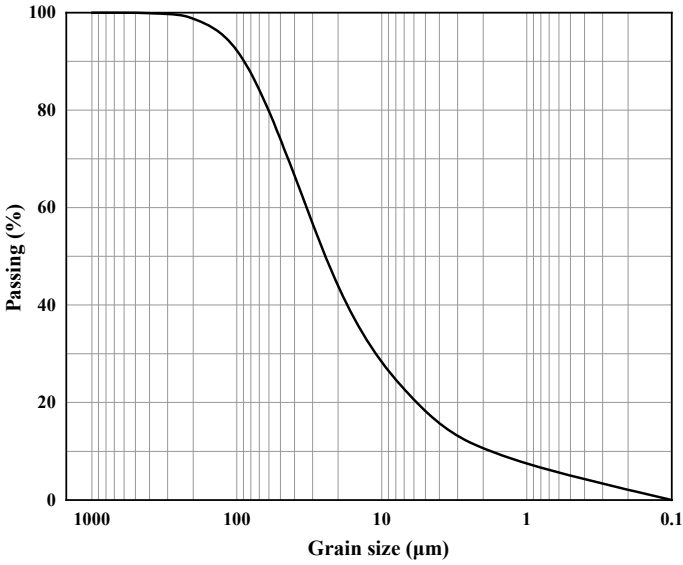


Fig. 1 Grain size distribution of silty clay

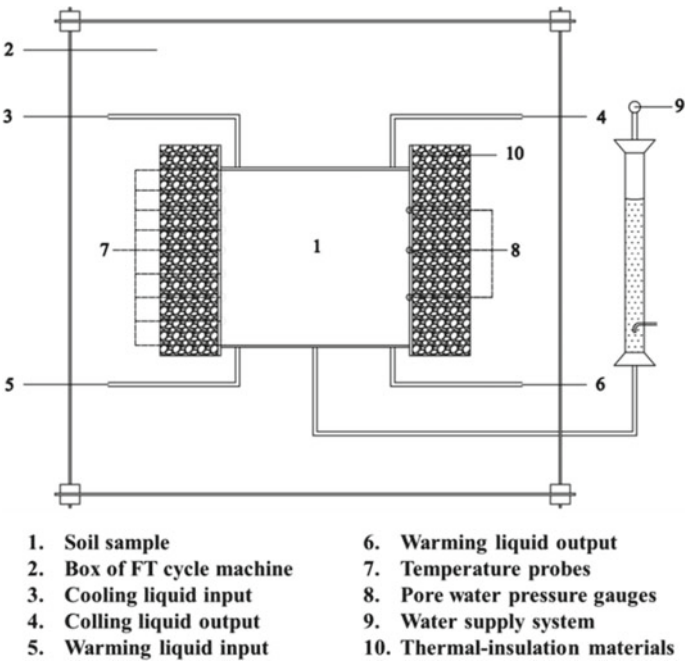


Fig. 2 Sketch of the one-dimensional freeze-thaw test system

probes at intervals of 15 mm, the high-sensitivity temperature probes with a precision of 0.05 °C and a valid temperature range of ±30 °C, and was manufactured by the State Key Laboratory of Frozen Soil Engineering [29]. Meanwhile, the other side’s holes of the specimen cell for inserting the pore water pressure transducer into the soil at different depths (see Fig. 3), which has a measuring range of ±100 kPa with a reference pressure point and an accuracy of ±0.1% full scale [12]. Moreover, the freeze-thaw tests were performed in the open soil-water system, using a Marriot bottle that monitored changes in water volume in real time.

To obtain conventional laboratory testing data, the specimens with test conditions were set for the freeze-thaw cycle. First, the prepared sample was placed into the cylindrical Perspex cell of the freeze-thaw cycling test machine. Next, the sensor of the temperatures, pore water pressure gauges, and water supply gauge were installed. And, all installed sensors were set to take measurements at 30 s intervals. Finally, the freeze-thaw experiment was conducted by controlling the top and bottom plate temperatures, as shown in Table 2.

Fig. 3 Holes arrangement of the sample

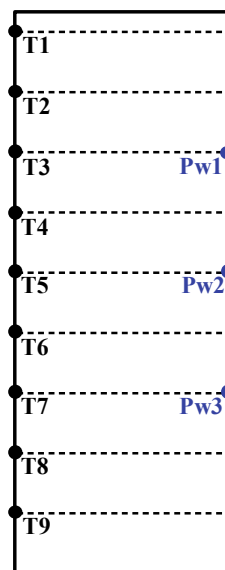


Table 2 A single freeze-thaw cycle test conditions

Soil type	Temperature at the cold end, °C	Temperature at the warm end, °C	Duration of freezing, h	Thawing temperature, °C	Duration of thawing, h	Water supply
Silty clay	-5	1	13	Room temperature	13	Yes

2.3 *Cryo-SEM Technique and the Microstructure Observation*

Cryo-SEM technique makes it possible to examine wet samples and to preserve their natural characteristics for further testing, which is an obvious advantage compared to conventional SEM [30]. Such direct imaging, in which, can transform the water into ice whose crystalline domain dimensions do not exceed those of the finest details that can be observed, and thus do not modify the morphology of the samples at the observation scale.

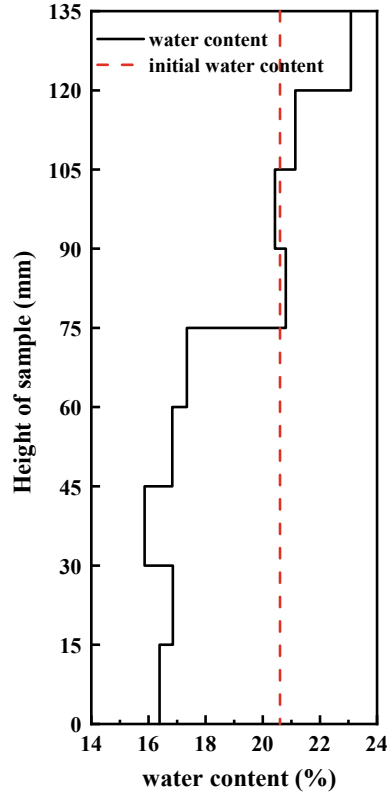
The samples of microstructure observation from laboratory tested specimen subjected to freeze-thaw cycle, which was layered every 15 mm. Given that the specific samples of cryo-SEM observation were stuck to a 5 mm hollow copper column. The sample was then hand-plunged into a nitrogen slush using sample holder. The plunge-frozen sample was then retrieved with a pre-cooled vacuum-cryo-transfer shuttle and transferred to a freeze-fracture system, where it was maintained at $-140\text{ }^{\circ}\text{C}$ and a pressure of 1.7×10^{-5} Pa. A layer of surface ice was removed by allowing the sample temperature to rise to $-90\text{ }^{\circ}\text{C}$ and holding the temperature at $-90\text{ }^{\circ}\text{C}$ for 5 min before returning the sample to $-140\text{ }^{\circ}\text{C}$. Finally, the sample was coated with gold under cryogenic conditions, and transferred sample to a cryo-SEM using sample holder. Then, the sample was imaged at $-140\text{ }^{\circ}\text{C}$ using an accelerating voltage of 10 kV and secondary electron detector.

3 Typical Results and Analysis

3.1 *Redistribution of Water*

There are some evidences that moisture redistribution continues within the frozen soil in the open soil-water system. Figure 4 presents the water content profiles of silty clay after the freeze-thaw cycle. It is apparent that the moisture significantly redistributed during freeze-thaw cycle. For example, water content at the bottom of the soil sample was 16.4% and at the top was 23.1%. Especially, it can be noticed that the gap at the height of 75 mm became bigger and with much higher moisture content than initial water content. It can be recognized that movement of water during freezing of this region soils causes the development of channels with provided water to the frozen regions and the system of channels benefits to remove water from the soil during the thawing process. In general, when a sudden negative temperature was applied to the top surface of the soil sample, unsteady heat flow is initiated. The freezing front progresses into the soil as a function of the imbalance of the heat and pore water freezes in situ. At the same time, a suction gradient develops in the frozen zone in response to any temperature gradient and water migrates from the unfrozen soil into the frozen zone. And the freezing-induced suctions further consolidate the unfrozen soil since its water content decreased from 21.4 to 16.4%. With the increase of sample

Fig. 4 Water content profiles after freeze-thaw cycle



temperature, the ice of soil was melting, and the pore volume decreased as the self-weight of overlying soil, thus also caused water migration and the consolidation of the sample.

3.2 The Change of Pore Water Pressure

Figure 5 illustrates the changes in the relationships among the pore water pressure, temperature, and time during the freeze-thaw cycle. Similar variation trends of pore water pressure with different soil sectors may be found in the silty clay at the same moment. When considering the freezing process, pore water pressure was generally divided into three stages: during the first stage, the pore water pressure increased as the temperature decreases. During the second stage, the pore water pressure decreased at first and then increased. During the third stage, the temperature quickly decreased from 5.65 to $-2.26\text{ }^{\circ}\text{C}$, the pore water pressure became to the negative value. It was also noted from Fig. 5 that the pore water pressure tended to 0 kPa from negative value as the temperature increased during thawing process. Based on the results, we

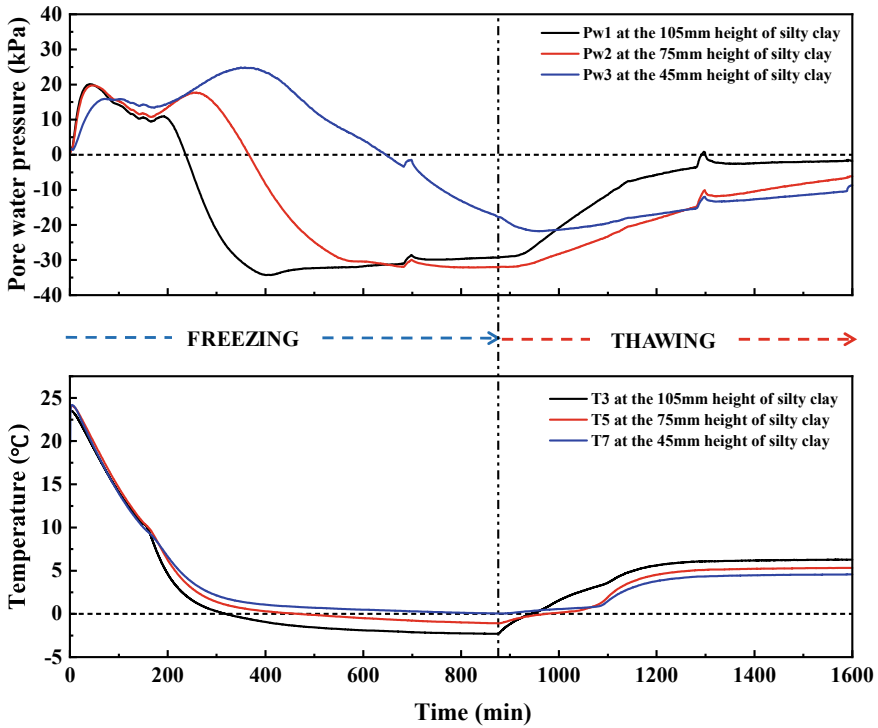


Fig. 5 Variation of the pore water pressure of silty clay during freeze-thaw cycle

concluded that the changes in pore water pressure were attributed to the influence of the phase change of water. At the beginning of experiments of silty clay, the lower temperature made the capillary water first turned into ice, causing a change in the capillary hydrostatic pressure. And then, the thickness of the unfrozen water film and adsorption potential in the soil sample changes because of adsorbed water is transformed into ice. During the process of ice melting, the radius of curvature of the ice–water interface increased, which changed the capillary and adsorption potential causing the pore water pressure increases.

The Pw1, Pw2, and Pw3 pore water pressure probes were located at different soil heights during the freeze-thaw experiment of the silty clay samples, as shown in Fig. 5. Although the pore water pressure at different heights presented similar tendency, it was clearly found that the dissipation of the Pw1 pore water pressure occurred earlier and faster than that of Pw2 and Pw3 pore water pressure. For example, the Pw1 pore water pressure decreased to -34.2 kPa from 19.7 kPa during the freezing process and then increased to -2.7 kPa along with temperature increased. While the Pw3 pore water pressure changed from 24.7 kPa to -21 kPa, and finally increased to -9.1 kPa. So, we concluded that the more rapid dissipation of the pore water pressure occurred near the freezing front, and the dissipation of the pore water

pressure proceeded from the top to bottom as the water migrated from the unfrozen to frozen zone.

Therefore, the differences in the pore water pressures may result from a combination of two factors. First, the change of pore water pressure during the freeze-thaw cycle due to the transformation of the ice–water phase. Second, the dissipation of the pore water pressure resulted from the migration of water in the soil sample.

3.3 Analysis of Microstructure

Freeze-thaw cycles also have been shown significant influence on soil microstructural transformations. Commonly, the change in soil structure due to freezing and thawing is basically caused by the phase transformation of pore water and water distribution. Therefore, structural form following freeze-thaw was dependent on both temperatures of the top sample and the water migrating at the time of the freeze-thaw cycle. Indeed, when considering soil deformation, soil samples that have been subjected to unidirectional freezing are generally divided into three zones: the frozen zone, the frozen fringe, and the unfrozen zone [12]. And according to the tested temperature and pore water pressure, such zones correspond to the 105, 75, and 45 mm heights of the specimens.

At the top of the specimen subjected to fast freezing conditions, the restricted water flow and resultant in situ growth of ice crystals are usually considered to be structurally destructive, can strongly affect the type of ice forms and structure in the soil. Besides that, the water content at the time of freezing is also an important control in determining the effects of pore ice formation, shown in Fig. 6, which was the cryo-SEM image at the 105 mm height of silty clay after freeze-thaw cycles.

In this region, because of the strong temperature gradients, upward moisture flow is minimized as the rapid advancement of the freezing front does not have sufficient time for appreciable pore water moving, leading to frozen in situ. As such, the approximately 9% volumetric expansion resulting from ice formation has been credited with rupturing existing aggregates and increasing the proportion of fine

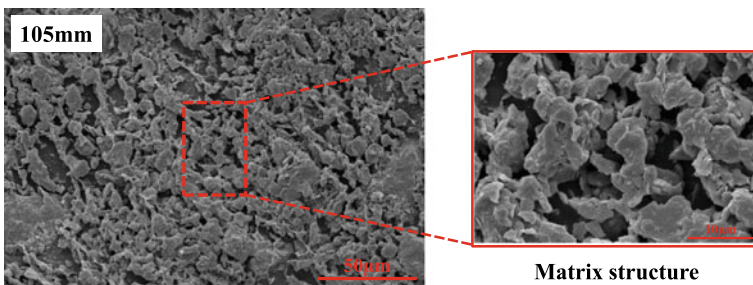


Fig. 6 Cryo-SEM image at the 105 mm height of silty clay

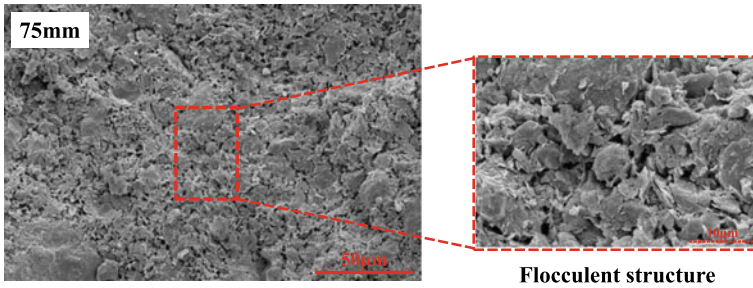


Fig. 7 Cryo-SEM image at the 75 mm height of silty clay

material [17]. Meanwhile, the ice crystal growth would tend to shatter aggregates into smaller particles and increase the size of inter-aggregate pores, resulting in the formation of a loose structure on the soil. With the further dropping of temperature, ice would eventually invade the successively smaller intra-aggregate micro-pores. Immediately the following thaw, large decreases in pore ice alter the pores on soil through an alteration of the particle connection, and leading pores between particles have good connectivity. Cryo-SEM shows that the volumetric expansion due to the phase change of water increased the pore volume on the soil.

Under these conditions, analyses of the frozen zone have noted a typical matrix structure. In which, the freeze-thaw cycle commonly results in point–point ($P-P$) form mostly consisting of smaller aggregates and particles. And, less continuous intra-aggregate micro-pores are separated by inter-aggregated macro-pores developed more complex pore system.

As the moving of the freezing front to higher temperature bottom, a weaker temperature gradient usually occurs at deeper levels within the sample. It is thus highly likely that consolidation occurs in front of the $0\text{ }^{\circ}\text{C}$ isotherm and in the unfrozen or partly frozen regions between ice accumulations in freezing clay [31]. So, the mineral skeleton adjacent near this area underwent appreciable compression, shown in Fig. 7, which was close to freezing front, represents the structural characteristics of the frozen fringe regions. The whole system shows the flocculent structure of this area which were more complicated, individual particles and smaller aggregates arrange in a random orientation rather than matrix structure by face–face ($F-F$) and face–edge ($F-E$) contacts. These results indicate that the presence of a pre-existing soil structure provides intra-aggregate and inter-aggregate pathways for thermally induced water flow and zones of weakness in which ice can form. At the boundary of freezing on soil of this region, coupled heat and moisture flow generate a tension to draw pore water toward the point of ice nucleation, resulting in a drastic phase change of water, as the inter-aggregate pore plays an important role in the water migration. As the films of bound water around the particles become thinner, the particles draw closer and their interaction increasing, their structural bonds become stronger, resulting in bigger aggregate happens. Meanwhile, if unfrozen pore water can continue to slowly migrate toward frozen zone through this area, it may contribute to weak the

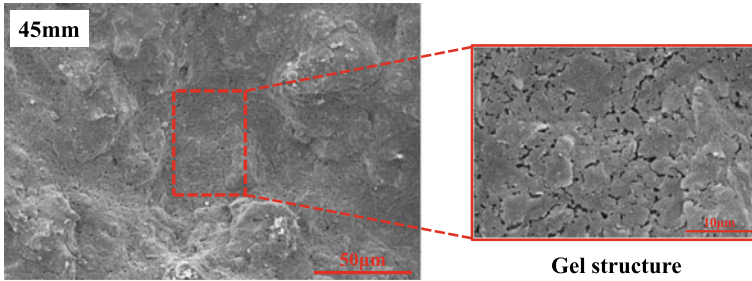


Fig. 8 Cryo-SEM image at the 45 mm height of silty clay

connection between particles. As Leo [32] noted that as a dramatic region of ice and water phase transition, many small crystals associated with pore ice destroyed the microstructure of the soil by destroying the micro-pores and increased aggregation through compression.

Figure 8 shows the gel structure at the 45 mm height of silty clay, which typically represents the unfrozen region after freeze-thaw cycles. The structure on unfrozen region commonly subjected to compaction because of overburden pressure and pressures induced by growing ice crystals, which have been characterized as hardening and curing. At the hardening and curing, the water migration is thought to be a major controlling factor through its influence on particle rearrangement. During rearrangement, this close proximity between soil particles is also thought to promote the colloids and face-face ($F-F$) form development. In the freezing process, pore water is drawn toward growing ice crystals, leading particles gathering and stacking on unfrozen zones. While water transfers from the unfrozen to the freezing region, the mineral skeleton of the unfrozen part becomes shrunken irrespective of the rate of water inflow to the soil sample. Desiccation by the removal of moisture from within the clay inter-layer during the growth of pore ice which stable aggregates may be formed during the freezing and thawing process. Moreover, on unfrozen regions lying rather far from the freezing boundary, the pore characteristic does not change much, and inter-granular pore most development.

3.4 Relationship Between Macroscopic Phenomena and Microstructure

It is commonly hypothesized that the freezing-induced volumetric expansion of pore water is responsible for aggregate breakdown [31] and it has also been confirmed that the freeze-thaw cycles had a significant effect on microstructure on soils. We further provided a quantitative analysis of microstructure to explore the relationship between pore water pressure and structural parameters, to understand the freeze-thaw cycle mechanism.

Cryo-SEM images of different heights of sample were presented in Figs. 6, 7 and 8. A view magnification of $\times 1000$ was selected, and the image was employed to quantitative analysis using Photoshop and Image-pro Plus(IPP) software. Images were all converted a 2-bit, a black-and-white image format for examination of particle distribution and pore characteristics in the soil sample (shown, e.g., as Fig. 9). Particles were turned white, and the pores were colored black. After that, the structural parameters were extracted, and the pore areas also be calculated.

Figure 10 shows the particle properties, including clay content and accumulated fractal dimension of particle distribution. Generally, the higher fractal dimension means the more dispersed of particle distribution, the lower gathering of particles, and the more complex of distribution pattern, which reveals the particle distribution in the plane. For the height of 75 mm on specimen which has higher fractal dimension and the highest clay content. For example, the fractal dimension of the particles was 1.24, and the clay content was 30.33% of this region. Obviously, the effect of freeze-thaw cycle on the behavior of the particle is very significant. Comparing the

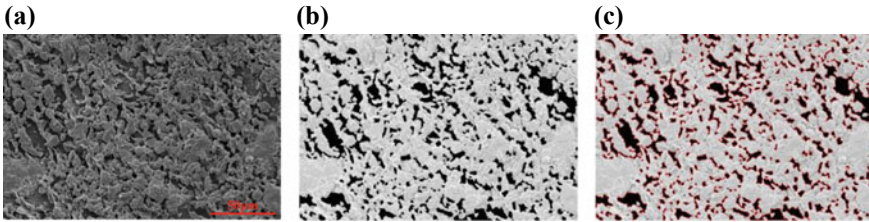


Fig. 9 A cryo-SEM image of the 105 mm height that was used for the analysis of example section **a** cryo-SEM image; **b** cryo-SEM image after thresholding by the Photoshop; **c** quantitative analysis using by IPP

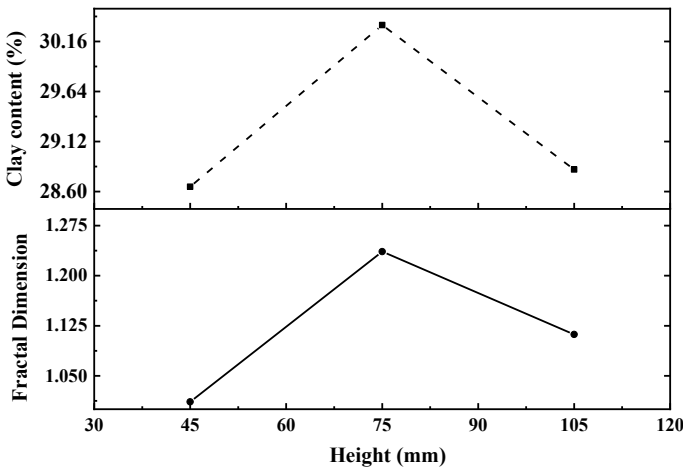


Fig. 10 Particle properties analysis at different heights of sample

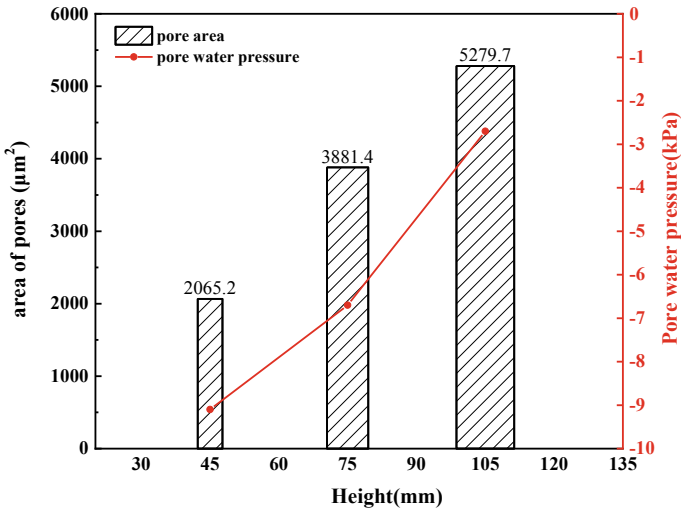


Fig. 11 Area of pores at different heights of sample

change of pore water pressure in this region during the freeze-thaw cycle, a positive relationship between structural parameters of particles and pore water pressure can be defined. More specifically, when there is a bigger gap variation of pore water pressure in this region during the freeze-thaw cycle, the structure is more chaotic and the structural parameters become larger. It is quite obvious that the clay content and fractal dimension present lower and the variation amplitude of pore water pressure is smaller on the else height of soil.

The change of pore has reflected an alteration of the arrangement of mineral particles within the soil. Figure 11 shows the pore area and pore water pressure values at the different height of silty clay after freeze-thaw cycles. The change of the pore area after the freeze-thaw cycles is discussed and a certain relationship between pore water pressure values is also determined. As can be seen from the histogram, the frozen zone of the sample corresponds to a much more pore distribution. Meanwhile, the area of pores decreases at the lower height of the specimen, in which has a positive correlation with changes in pore water pressure. Such as at the 105 mm height of silty clay, the pore water pressure value was -2.7 kPa. While at the 45 mm height of soil, the pore water pressure value was -9.1 kPa.

4 Conclusions

In this paper, the pore water pressure and microstructure under freeze-thaw cycle was tested. Through the information obtained from the laboratory data and cryo-SEM

images, the relationship between pore water pore pressure and structural parameters is preliminary analysis. The following points are drawn based on this study:

- (1) During freezing and thawing periods, the pore water pressure changes are complicated along with temperature first decreased and then increased. Meanwhile, the microstructure has a significant change at the different height of the specimen. Typically, the bigger gap of pore water pressure values variation, more complex structure, higher clay content and fractal dimension of the particle were more sensitive at the 75 mm height on soil to freeze-thaw cycle than other regions.
- (2) In the process of soil freezing and thawing period, there was a certain relationship among particle properties, pore area, and pore water pressure of soil. The magnitude of the change in pore water pressure is positively correlated with the structural parameters of the particles during the freeze-thaw cycle on the timescale. While, the pore water pressure value is positively correlated with the pore area after the freeze-thaw cycle on the spatial scale.

Acknowledgements This research was supported by the National Natural Science Foundation of China (No. 41501072; No. 41271087; No. 40701030; No. 41630636) and the National Key R&D Program of China (No. 2017YFC0405101). And, the authors would like to thank our colleagues in the laboratory Guoji Zheng and Shuguang Yang, for many helpful discussions and the testing methods. The discussion and conclusion presented in this work reflect the opinions of the authors only.

References

1. Edwards L (2006) The effect of alternate freezing and thawing on aggregate stability and aggregate size distribution of some Prince Edward Island soils. *Eur J Soil Sci* 42:193–204. <https://doi.org/10.1111/j.1365-2389.1991.tb00401.x>
2. ASCE, Andersland, OB, Ladanyi B (2003) *Frozen ground engineering*, 2nd edn. Wiley
3. Stewart M, Val D, Bastidas E (2014) Climate adaptation engineering and risk-based design and management of infrastructure. In: *Maintenance and safety of aging infrastructure*. CRC Press, pp 641–684
4. Zhang Z, Ma W, Qi J (2014) Structure evolution and mechanism of engineering properties change of soil under effect of freeze-thaw cycle. *J Jilin University (Earth Science Edition)* 43(6):1904–1914 (in Chinese)
5. Edwin JC, Anthony JG (1979) Effect of freezing and thawing on the permeability and structure of soils. *Eng Geol* 13:73–92. <https://doi.org/10.1016/B978-0-444-41782-4.50012-9>
6. Leroueil S, Tardif J, Roy M (1991) Effects of frost on the mechanical behavior of champlain Sea clays. *Can Geotech J* 28:690–697. <https://doi.org/10.1139/t91-083>
7. Yang C, He P, Cheng G (2004) Freeze-thaw experiment influence on moisture content distribution of soil. *J Glaciol Geocryology* 26(suppl):50–55 (in Chinese)
8. Qi J, Ma W, Song C (2008) Influence of freeze-thaw on engineering properties of a silty clay. *Cold Reg Sci Technol* 53(3):397–404. <https://doi.org/10.1016/j.coldregions.2007.05.010>
9. Zhang L, Ma W, Yang C (2014) Investigation of the pore pressure of coarse grained sandy soil during open system step-freezing and thawing tests. *Eng Geol* 181:233–248 (in Chinese)

10. Hendry MT, Onwude LU (2016) A laboratory investigation of the frost heave susceptibility of fine-grained soil generated from the abrasion of a diorite aggregate. *Cold Reg Sci Technol* 123:91–98. <https://doi.org/10.1016/j.coldregions.2015.11.016>
11. Fu Q, Hou R, Li T (2018) Effects of soil water and heat relationship under various snow cover during freezing-thawing periods in Songnen Plain China. *Sci Rep* 8:1325
12. Zhang L, Ma W, Yang C (2016) An investigation of pore water pressure and consolidation phenomenon in the unfrozen during soil freezing. *Cold Reg Sci Technol* 130:21–32. <https://doi.org/10.1016/j.coldregions.2016.07.007>
13. Ma W, Zhang L, Yang C (2015) Discussion on applicability of the generalized Clausius-Clapeyron equation and the frozen fringe process. *Earth Sci Rev* 142:47–59
14. Akagawa S (1988) Experimental study of frozen fringe characteristics. *Cold Reg Sci Technol* 15:209–223. [https://doi.org/10.1016/0165-232X\(88\)90068-7](https://doi.org/10.1016/0165-232X(88)90068-7)
15. Akagawa S, Hiass S, Kanie S (2008) Pore water and effective pressure in the frozen fringe during soil freezing. In: Proceedings of the 9th international conference on Permafrost. University of Alaska Fairbanks, Fairbanks, Alaska, USA, pp 13–18
16. Tiedje EW, Guo P (2011) Dewatering induced by frost heave in a closed system. In: Pan-Am CGS Geotechnical Conference. <http://geoserver.ing.puc.cl/info/conferences/PanAm2011/panam2011/pdfs/GEO11Paper559.pdf>
17. Eigenbrod K (1996) Effects of cyclic freezing and thawing on volume changes and permeabilities of soft fine-grained soils. *Can Geotech J* 33:529–537. <https://doi.org/10.1139/cjce-2016-0052>
18. Daryl DF (2006) Effect of the freeze/thaw process on the structural stability of soil aggregates. The University of Guelph, Canada.[Ph.d.]
19. Wang E, Richard M, Chen X (2012) Effects of moisture condition and freeze-thaw cycles on surface soil aggregate size distribution and stability. *Can Geotech J* 92:529–536. <https://doi.org/10.4141/cjss2010-044>
20. Eigenbrod K, Knutsson S, Sheng D (1996) Pore water pressure in freezing and thawing fine grained soils. *J Cold Regions Eng ASCE*. In press. [https://doi.org/10.1061/\(asce\)0887-381x\(1996\)10:2\(77\)](https://doi.org/10.1061/(asce)0887-381x(1996)10:2(77))
21. Hoham PM (2002) Microfabric effects in frozen clays in relation to geotechnical parameters. *Appl Clay Sci* 21(1–2):77–87. [https://doi.org/10.1016/S0169-1317\(01\)00094-1](https://doi.org/10.1016/S0169-1317(01)00094-1)
22. Tang Y, Li J (2018) Test method and application for microstructure of undisturbed silty sand and sandy silt. *Environ Earth Sci* 77:657
23. Konrad J, Morgenstern N (1981) The segregation potential of a freezing soil. *Canadian Geotech J* 482–491. <https://doi.org/10.1139/cgj-2016-0150>
24. Dagesse DF (2015) Cyclic freezing and thawing effects on atterberg limits of clay soils. In: Proceedings of GeoQuebec 2015 68th Canadian geotechnical conference and 7th Canadian Permafrost conference
25. Wang T, Liu Y, Yan H (2015) An experimental study on the mechanical properties of silty soils under repeated freeze-thaw cycles. *Cold Reg Sci Technol* 112:51–65. <https://doi.org/10.1016/j.coldregions.2015.01.004>
26. Wang S, Yang P, Yang Z (2018) Characterization of freeze-thaw effects within clay by 3D X-ray computed tomography. *Cold Reg Sci Technol* 148:13–21. <https://doi.org/10.1016/j.coldregions.2018.01.001>
27. Cui Z, He P, Yang W (2014) Mechanical properties of a silty clay subjected to freezing-thawing. *Cold Reg Sci Technol* 98(3):26–34. <https://doi.org/10.1016/j.coldregions.2013.10.009>
28. Ding Z, Zhang M, Wei X (2016) Study on pore pressure and microstructure of frozen and thawed soft soil under subway cyclic loading. *Chinese J Underground Space Eng* 35(11):2328–2336 (in Chinese)
29. Liu J, Shen Y, Zhao S (2011) High-precision thermistor temperature sensor: technological improvement and application. *J Glaciol Geocryology* 33(4):765–771 (in Chinese)
30. Negrea M, Leonea P (2004) Characterization of model soil colloids by cryo-scanning electron microscopy. *Geoderma* 121:1–16. <https://doi.org/10.1016/j.geoderma.2003.09.011>

31. Knocke W, Trahern P (1989) Freeze-thaw conditioning of chemical and biological sludges. *Water Res* 23:35–42. [https://doi.org/10.1016/0043-1354\(89\)90058-4](https://doi.org/10.1016/0043-1354(89)90058-4)
32. Leo M (1963) Effect of freezing and thawing on some physical properties of soils as related to tomato and barley plants. *Soil Sci* 96:267–274

Technical Improvements in Testing Small-Strain Deformation Behaviour of Frozen Soil



Jinyuan Wang, Satoshi Nishimura , Bhakta Raj Joshi and Shota Okajima

Abstract Small-strain modulus is an important parameter in engineering constructions such as tunneling employing artificial ground freezing method. Temperature and strain rate are two main factors influencing the small-strain deformation behaviour of frozen soil. Testing conditions and some technical cautions are crucial to the accurate measurement of the small-strain modulus. This paper reports an experimental study on small-deformation behaviour of clay frozen directly under confining pressure after being consolidated to different isotropic effective stresses. The loading probes were then conducted at three different axial strain rates (0.001, 0.01 and 0.1%/min) and three different temperatures (-10 , -5 and -2 °C). The freezing method, calibrating factor of local displacement sensor against temperature and loading approach with load cell outside the freezing chamber, was specially considered. The clay specimen was frozen under confining pressure to fully imitate the in situ freezing process. The adopted local gap sensor functioned well under different temperatures in the refrigerant, and the temperature effect on the calibration factor is negligible. After overcoming the error brought about by the external load cell, it is found that the small-strain modulus of frozen clay appears to be independent of strain rate. The samples frozen from higher effective mean stress state exhibited smaller initial stiffness.

Keywords Frozen soils · Laboratory tests · Stiffness

J. Wang (✉)

State Key Laboratory of Water Resources and Hydropower Engineering Science,
Wuhan University, Wuhan, Hubei, PR China
e-mail: jinyuan2011@whu.edu.cn

S. Nishimura

Faculty of Engineering, Hokkaido University, Sapporo, Hokkaido, Japan

B. R. Joshi · S. Okajima

Graduate School of Engineering, Hokkaido University, Sapporo, Japan

© Springer Nature Singapore Pte Ltd. 2020

A. Petriaev and A. Konon (eds.), *Transportation Soil Engineering in Cold Regions*,
Volume 2, Lecture Notes in Civil Engineering 50,
https://doi.org/10.1007/978-981-15-0454-9_27

1 Introduction

Initial stiffness is a vital parameter in frozen soil engineering, especially for projects such as excavation and tunneling employing artificial ground freezing with small-deformation tolerance. For static testing, the initial stiffness needs to be obtained in very small strain range [1]. The accuracy in measurement of this small strain tends to make a great difference. For high accuracy of strain measurement, on-specimen measurement method was developed with the help of high-precision LVDTs [2] or some proximity transducer such as gap sensors [3]. This turns out to dramatically improve the quality of measurement compared to the traditional external displacement transducer.

As well as strain measurement, the accuracy of load outputs is equally significant to determine the small-strain stiffness. Internal load cell (load cell inside chamber) can directly measure the contact force on the specimen [4]. However, the authors have experienced occasional malfunction of the load cell under extreme temperature changes. Alternatively, load cell may be installed outside the chamber [5, 6] to avoid the temperature effect. This arrangement has been known to cause significant errors in measuring unfrozen soils' stiffness due to the ram-bush friction. However, it has not been explored whether this factor plays a significant role in frozen soil testing, in which the stiffness and hence the involved stress increments are much greater.

This paper reports a test programme employing apparatus equipped with gap sensors and external load cell. Accurate measurement of on-specimen strain below 0.01% and eliminating impact of ram-bush friction were realized in this study. Meanwhile, the carefully controlled soil state before freezing and freezing directly under confining pressure make frozen specimen close to in situ freezing soil. The effects of strain rate and temperature on initial stiffness were investigated through non-destructive loading probes on a single unique specimen at different strain rates and temperatures.

2 Material and Test Method

2.1 Tested Material and Triaxial Apparatus

Kasaoka clay having high plasticity was selected in this laboratory study. The liquid limit and plastic limits are 59.6% and 22.5%, respectively. Its specific gravity is 2.70. We prepared the samples by using a consolidometer through applying vertical pressures, $\sigma_{v0}' = 50, 100$ or 200 kPa, on slurry with a water content of 100%. The reconstituted samples under these three pre-consolidation pressures have initial density of 1.76, 1.81 and 1.87 g/cm^3 , respectively, and corresponding initial water content of 46.1%, 40.9% and 35.6%, respectively. The specimen size in this study is 30 mm in diameter and 60 mm in height.

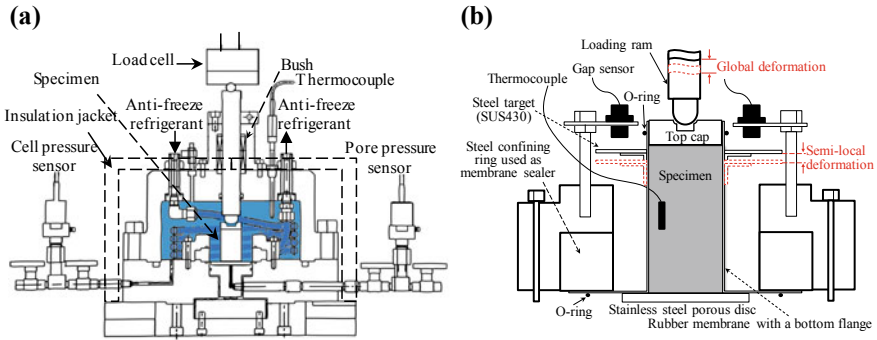


Fig. 1 Triaxial apparatus for frozen specimen **a** schematic diagram of the apparatus; **b** close-up diagram of the gap sensor set-up

We conducted the frozen soil experiments in a temperature-controlled triaxial apparatus shown in Fig. 1a. An external load cell was used to measure the vertical force on the top cap of the specimen. A pair of gap sensors with measuring range of 4 mm was employed to measure on-specimen local deformation, as shown in Fig. 1b. In addition, considering that the sensors were immersed in low-temperature refrigerant rather than the usual medium of water, we investigated the effect of temperature and medium on the performance of gap sensors. Through calibration, we obtained the calculation factors which are parameters to transform the output voltage of gap sensor to the measured displacement. The calculation factors of gap sensor immersed in the refrigerant at temperatures of 25, -2 and -10 °C are 0.206, 0.207 and 0.210, respectively. It proves that the temperature effect when immersed in low-temperature refrigerant is negligible.

2.2 Testing Conditions and Procedures

To test the small-strain deformation behaviour of frozen soil, the test procedures with various testing conditions were implemented by steps as followed: (1) The specimen was set-up in the apparatus and subjected to isotropic consolidation to $p_c' = 100, 200$ or 400 kPa (represented by F100, F200 and F400). In order to erase the inherent K_0 -consolidation history developed in the sample preparation by consolidometer, we subjected the specimen to isotropical consolidation under effective mean stress of $2\sigma_{v0}'$. (2) After sufficient consolidation, a freezing process was conducted on the specimen. While keeping the cell (confining) pressure, we drained off the cell water and inserted pre-cooled antifreeze refrigerant instead. The specimen was quickly frozen in this way. By circulating the refrigerant from a refrigeration bath, the specimen was then cooled to -15 °C and sustained for 12 h. (3) There are three testing temperatures ($-10, -5$ and -2 °C) in this study. The temperature of specimen was firstly increased to -10 °C and kept for 24 h for equilibrium. (4) Probes of three

testing strain rate were conducted in this step. Take probe of 0.01%/min, for example, we deformed the specimen axially at a strain rate of 0.01%/min until an axial strain increment of 0.025% measured from an external displacement transducer. The specimen was then unloaded by retracting the loading ram to initial position, which forms a cycle of probe. Three cycles of loading and un-loading on the frozen specimen were implemented for each testing strain rate in an order of 0.01, 0.1 and then 0.001%/min. After these probes for three testing strain rates at $-10\text{ }^{\circ}\text{C}$ were performed, a new testing temperature ($-5\text{ }^{\circ}\text{C}$ followed by $-2\text{ }^{\circ}\text{C}$) was set for this frozen specimen in the chamber and kept for 24 h. The 0.025%-strain probes for various strain rates were repeated for the two new temperatures.

The freezing process in the tests involved draining off the cell water and replacing with pre-cooled refrigerant with constant cell pressure in the chamber as illustrated in Fig. 2. After prescribed consolidation of the unfrozen specimen was reached, the temperature of chamber was decreased to around $+1\text{ }^{\circ}\text{C}$ by circulating a certain-temperature refrigerant through the spiral copper tube inside the confining chamber. This pre-cooling operation reduced the actual temperature difference and boosted the freezing. We then drained out the cell water slowly by slightly opening the valve so that same cell pressure could be ensured as before draining. As shown in Fig. 2, a tank filled with pre-cooled refrigerant at $-18\text{ }^{\circ}\text{C}$ was to be transferred into the chamber. A pressure of $210\text{ kPa} + p_c'$ having an excess of 10 kPa compared to cell pressure was applied to pump the refrigerant into the chamber. Addition of refrigerant in the $+1\text{ }^{\circ}\text{C}$ chamber environment made swift freezing of the specimen. Meanwhile, the cooling bath began to circulate the refrigerant at $-25\text{ }^{\circ}\text{C}$ along the spiral copper tube inside the chamber. This method could decrease the cell temperature till $-15\text{ }^{\circ}\text{C}$ within one hour.

The above efforts succeeded in freezing the specimen quickly under unchanged confining pressure and preventing the formation of ice lensing. This quick freezing under confining pressure as well as the low-permeability property of clay yielded a relatively uniform specimen, which can be confirmed by observing the cross-section of the frozen specimen after test as shown in Fig. 3a. But we still observed slight

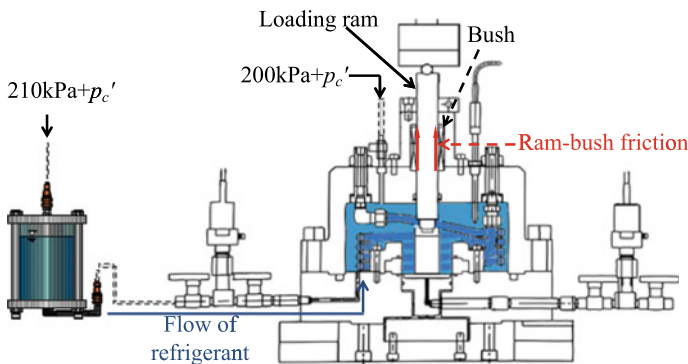


Fig. 2 Illustration of injection of pre-cooled refrigerant into cell and ram-bush friction

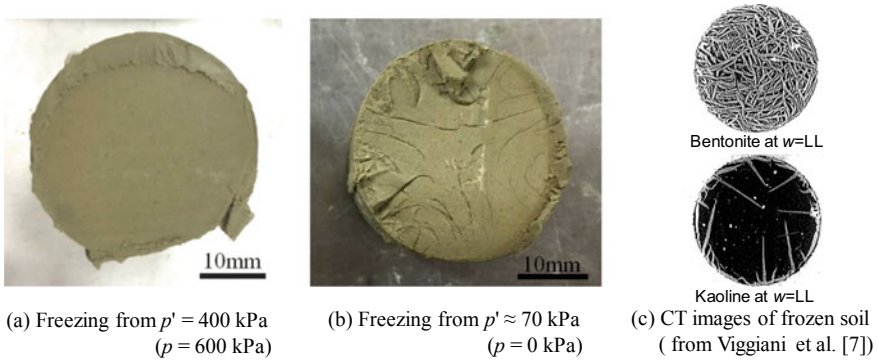


Fig. 3 Cross-section of frozen soil sample

water migration from the core to the rim of the specimen based on local water content measurements as shown in Fig. 4. Figure 3b shows obvious cracking caused by internal water migration when specimen was frozen in the cooling bath directly with no confining pressure. Slow freezing at atmosphere pressure would lead to formation of minute ice lenses even in clays, as revealed by Viggiani et al. [7] through CT images of frozen sample shown in Fig. 3c. The nonuniformity of the frozen specimen is not appropriate for element test.

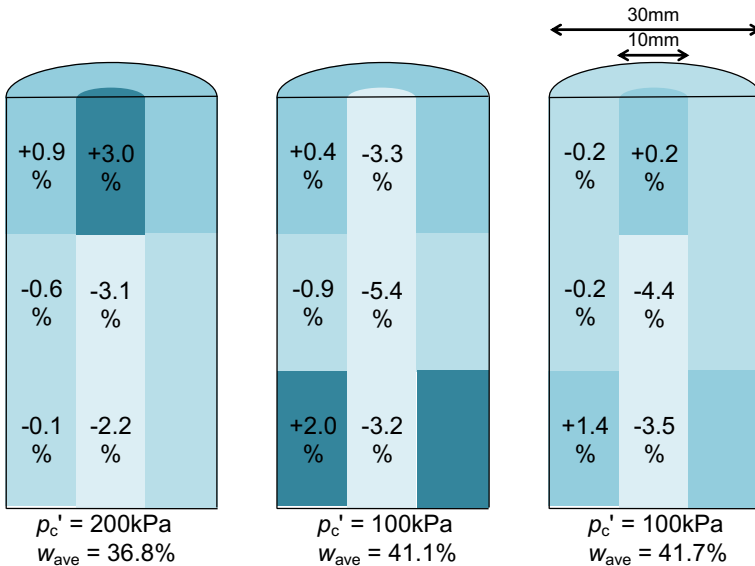


Fig. 4 Water content distribution of frozen sample

3 Test Results and Discussions

3.1 Comparison of Two Loading Approaches to Deal with Effect of Ram-Bush Friction

A load cell installed outside chamber was adopted in this study. Being unaware of problems brought by this arrangement, loadings at constant strain rate was initiated directly from the stationary state of ram contacting the specimen top cap which was kept during consolidation and freezing. Existence of axial load measurement errors due to ram-bush friction triggered by stationary ram-platen contact between the two consecutive probes was discovered and paid attention to afterwards, as illustrated in Fig. 2. To cope with the ram-bush friction, the loading ram was lifted up in advance to leave an enough space between the top cap and ram. The specimen was then loaded at constant strain rate with some free-running of the ram before contacting the top cap. This approach turned out very effective in eliminating the ram-bush friction effect on the axial force measurements and was adopted in all the rest of tests.

Figure 5 shows incremental axial stress-strain relationships at $-10\text{ }^{\circ}\text{C}$ for the specimen frozen from $p' = 200\text{ kPa}$ (Test F200). The stress-strain curves with hollow square markers representing 3 trials of constant strain-rate loadings initiated from a stationary state of ram exhibited significant curvature at the beginning. In contrast, the stress-strain curves of three trial loadings from detached state of ram were linear from the very beginning. Ignoring the initial nonlinearity in stress-strain of loading with stationary state, a clear offset between the parallel stress-strain was observed and attributable to the ram-bush friction. Being unaware of the friction may lead to overestimation of initial stiffness at very small strains. In addition, the friction-induced stress-strain nonlinearity did not stick to the same curvature at slower strain rates, as seen in Fig. 5a in case of strain rate with $0.01\%/min$. Therefore, the friction-induced error needs to be specially noticed in measuring the small-strain stiffness. The problem brought by external load cell was solved by slightly changing the initial loading approach.

3.2 Small-Strain Deformation Characteristics of Frozen Clay

A series of triaxial tests on the frozen Kasaoka clay samples was performed to observe the small-strain stiffness behaviour of the frozen soil. Figure 6 shows the incremental stress-strain relationships of clay frozen from $p' = 400\text{ kPa}$ (Test F400) in small axial strain increment at three different axial strain rates and three different freezing temperatures. The stress-strain curve is observed clearly linear and corresponding well-defined initial modulus E_0 is shown in Fig. 6. The initial modulus E_0 is determined by the secant stiffness to 0.002% axial strain increment. For the three freezing temperatures, the initial modulus E_0 is independent of the strain rate. The

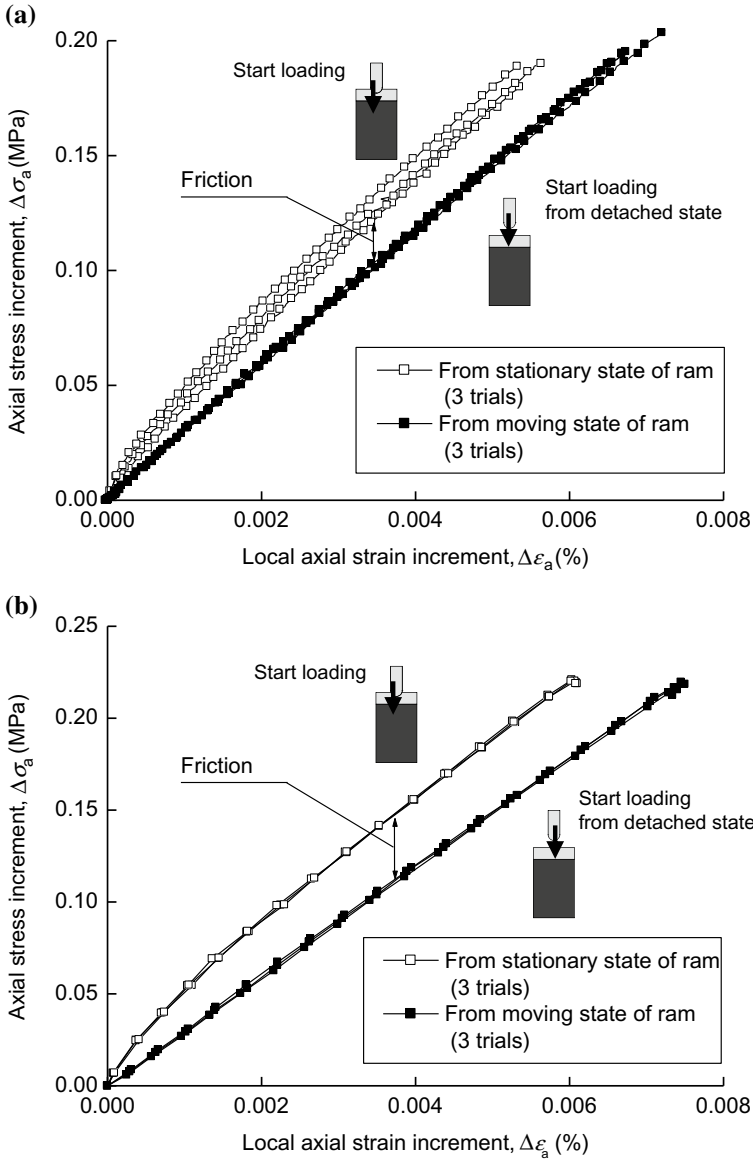


Fig. 5 Axial stress increment—axial strain increment relationships at -10°C for the sample frozen from $p' = 200\text{ kPa}$ (Test F200): **a** $0.01\%/min$, **b** $0.1\%/min$

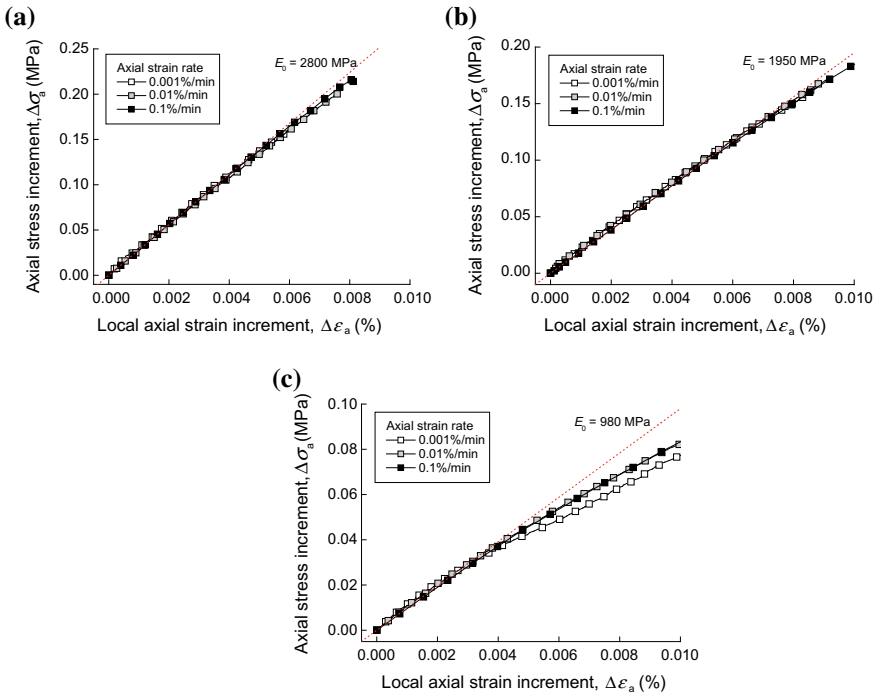


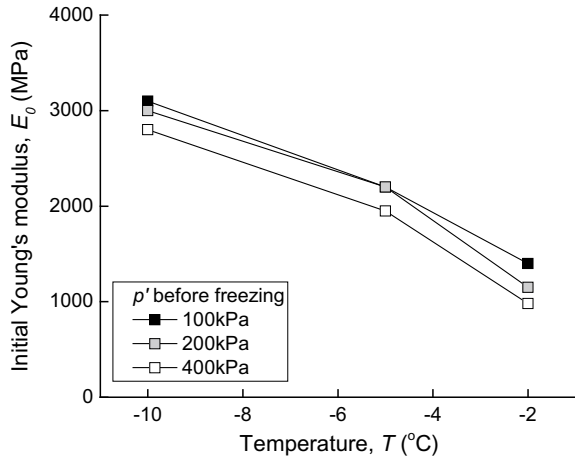
Fig. 6 Axial stress increment—axial strain increment relationships for sample frozen from $p' = 400$ kPa (Test F400): **a** -10 °C, **b** -5 °C, **c** -2 °C

stress–strain nonlinearity appears at smaller strains at slower strain rate. The incremental stress–strain curves are affected by the loading rate only after the nonlinearity starts. This behaviour resembles remarkably that of unfrozen geomaterials found by Tatsuoka et al. [8]. We also observed that onset of nonlinearity started at smaller strains for lower loading rate. For stress–strain of samples at -10 °C and 0.1%/min, nonlinearity even did not appear for the tested strain range.

The $p' = 100$ kPa and 200 kPa cases are not shown here. The results were generally consistent with that of $p' = 400$ kPa case. Frozen soil is basically regarded as highly viscous. But the test results suggest that frozen specimen subjected to very small strain from a very stable condition does not exhibit viscosity. Swan [9] and Andersen et al. [4] had very similar findings. They found that Young’s modulus of frozen Manchester fine sand (measured by LVDTs) was independent of strain rate.

It can be seen from Fig. 7, initial Young’s modulus E_0 decreased with the increase of temperature. The interesting point is that the frozen samples with lower p' (i.e., having greater void ratio, e) exhibited greater E_0 . This abnormal trend happens probably with a mechanism. The possible explanation is that samples frozen from lower p' have larger ice content than that of samples frozen from higher p' , and the ice inclusions play a dominant role relative to soil skeleton in determining the stiffness of frozen soil. Wang et al. [10] demonstrated a simple mechanism to explain this.

Fig. 7 Variation of initial young's modulus E_0 with temperature: frozen from different mean effective stress p'



4 Summary and Conclusions

This paper reported an original testing method on frozen clay's initial stiffness with detail. The carefully controlled soil state before freezing and freezing directly under confining pressure make frozen specimen close to in situ freezing soil. Measurement of on-specimen local strain ensures the accuracy of obtained initial stiffness. Non-destructive loading probes on an identical specimen under different strain rates and temperatures ensure the uniqueness of specimen and allow interpretation of the effect of strain rate and temperature exclusively on initial stiffness of frozen soil. The following summary and conclusions can be made:

1. A quick freezing of soil sample under confining pressure turned out to give a uniform frozen sample avoiding ice lensing.
2. In case of load cell installed outside the chamber, loadings from a free-running, moving state of ram that had been detached from the top cap are effective in removing the influence of ram-bush friction and freeze-adhesion on the axial stress measurements.
3. The initial stiffness of frozen clay turned out independent of strain rate. The onset of stress-strain nonlinearity (or yielding) started at smaller strains for slower loading. The lower the temperature was, the greater the initial stiffness of frozen clay.
4. The samples frozen from higher effective mean stress state (and hence denser, having smaller void ratio, e) exhibited smaller initial stiffness. These samples tended to have lower ice content that may be the major contributor to frozen soil stiffness, which may explain the counter-intuitive observation.

References

1. Viggiani G, Atkinson JH (1995) Stiffness of fine-grained soil at very small strains. *Géotechnique* 45(2):249–265
2. Cuccovillo T, Coop MR (1997) The measurement of local axial strains in triaxial tests using LVDTs. *Géotechnique* 47(1):167–171
3. Kokusho T (1980) Cyclic triaxial test of dynamic soil properties for wide strain range. *Jpn Geotech Soc Spec Publ* 20(2):45–60
4. Andersen GR, Swan CW, Ladd CC, Germaine JT (1995) Small-strain behavior of frozen sand in triaxial compression. *Can Geotech J* 32(3):428–451
5. Wang D, Ma W, Wen Z, Wu Z (2007) Stiffness of frozen soils subjected to K0 consolidation before freezing. *Soils Found* 47(5):991–997
6. Li Q, Ling X, Hu J, Zhou Z (2018) Residual deformation and stiffness changes of frozen soils subjected to high-and low-amplitude cyclic loading. *Can Geotech J*. <https://doi.org/10.1139/cgj-2017-0720>
7. Viggiani G, Andò E, Takano D, Santamarina JC (2015) Laboratory X-ray tomography: a valuable experimental tool for revealing processes in soils. *Geotech Test J* 38(1):61–71
8. Tatsuoka F, Jardine RJ, Lo Presti D, Di Benedetto H and Kodaka T (1999) Characterising the pre-failure deformation properties of geomaterials. In: 14th international conference on soil mechanics and foundation engineering, Hamburg, Germany, pp 2129–2164
9. Swan C (1994) Physical mechanisms controlling the deformation and strength behavior of unfrozen and frozen manchester fine sand. Sc.D. thesis, Department of Civil and Environmental Engineering, MIT, Cambridge, MA
10. Wang J, Nishimura S, Okajima S, Joshi BR (2018) Small-strain deformation characteristics of frozen clay from static testing. *Géotech press*. <https://doi.org/10.1680/jgeot.18.p.115>

Experimental Study on Induced Anisotropies of Remolded Loess in Cold Region



Yongzhen Feng, Lingxiao Liu, Wuyu Zhang and Yanxia Ma

Abstract To improve the understanding of the influence of induced anisotropy on the strength and deformation characteristics of loess, a series of directional HCA tests under consolidated-drained condition were conducted. The test results indicated that the remolded loess showed a pronounced anisotropy in stress–strain relationship, strength, and deformation. The maximum difference in shear strength due to directional effect was 25% in the range of major principal stress orientation. Induced anisotropy has a great influence on the stress–strain relationship of soil, which is the essence of soil properties. In some engineering practices, the results of stress–strain analysis of soil have great influences. Approximately, isotropic remolded loess substantially eliminates its inherent anisotropy. The soil studied in this experiment is from the permafrost region of Qinghai. With the increase of engineering constructions, the geotechnical engineering problems here are becoming more and more significant. Therefore, this experiment will provide a good reference for the further study of soil anisotropy under complicated stress paths such as principal stress axis rotation.

Keywords Induced anisotropy · Hollow cylinder apparatus · Remolded loess · Complex stress path · Strength and deformation characteristics

1 Introduction

Anisotropy is one of the fundamental properties of soils. It is generally divided into inherent anisotropy and induced anisotropy [1]. The inherent anisotropy is developed over the course of soil deposit, whereas the induced anisotropy is due to changes in applied stress (e.g., varied stress direction and magnitude) [2].

The importance of the induced anisotropy of soils has been recognized by researchers and engineers in geotechnical engineering for a long time. Bjerrum [3]

Y. Feng · L. Liu · W. Zhang (✉) · Y. Ma
School of Civil Engineering, Qinghai University, 251, Ningda Road,
Xining 810016, Qinghai, China
e-mail: qdzwy@163.com

© Springer Nature Singapore Pte Ltd. 2020
A. Petriaev and A. Konon (eds.), *Transportation Soil Engineering in Cold Regions*,
Volume 2, Lecture Notes in Civil Engineering 50,
https://doi.org/10.1007/978-981-15-0454-9_28

265

and Jardine and Smith [4] observed the occurrence of rotation in principal stresses in soft clays under embankment loading, highlighting the important role of strength anisotropy. Zdravkovic et al. [5] successfully applied a calibrated anisotropic constitutive model to examine factors which influence the stability of embankment, including strength anisotropy, embankment geometry, and ground movements.

Experimentally, soil anisotropy has been researched on conventional triaxial apparatus or plane-strain apparatus in earlier times. However, these tests were unable to replicate the soil anisotropy reasonably. In 1970s, Saada [6] pioneered the first anisotropic device to measure rotation in the direction of principal stresses. Since the 1980s, the hollow cylinder apparatus (HCA) has been evolved to be the main tool to investigate soil anisotropy [7–9].

Theoretically, many anisotropic constitutive models were proposed with growing data available from HCA tests. Miura [10] proposed a constitutive model to predict deformation of an anisotropic sand under the varying stress conditions including arbitrary directions of principal stress. The model was verified through HCA tests on anisotropic dense sands. The calculated deformation pattern was also found in a cross-anisotropic elastic material symmetric in z -direction. Nishimura [11] estimated the effective stress-path inclinations, $d(\sigma_z - \sigma_\theta)/d(2p')$, using cross-anisotropic elastic theory and small-strain stiffness parameters obtained experimentally by Gasparre [12]. The calculated inclinations were found to generally agree with the observed one.

Most of researches concerning anisotropy have been directed to conventional sands and clays; however, very limited results have been reported about the anisotropy of loess [13]. The loess shows strong deformation and strength anisotropy, but it has not been well studied. To this end, the purpose of this study was to experimentally investigate the anisotropic behavior of remolded loess based on a series of HCA tests. The induced anisotropy is generated by varying the orientation of major principal stress. The effect of induced anisotropy in loess on deformation and strength behavior of loess was discussed.

2 Materials and Methods

2.1 Test Materials

The material used in this study was loess retrieved from a foundation pit in Qinghai, a northern province in China. Qinghai province is located in the eastern part of the Qinghai–Tibet Plateau, where there are permafrost regions. Basic properties of the loess including maximum dry density, liquid limit, and plastic limit were measured, as tabulated in Table 1.

The hollow specimen had a dimension of 200 mm (height) * 100 mm (outer diameter) * 60 mm (inner diameter). The detailed procedures to prepare the test specimen are as follows: (1) The loess was screened by removing large size particles

Table 1 Basic parameters of Qinghai loess samples

Maximum dry density (g/cm ³)	Liquid limit (%)	Plastic limit (%)	Dry density (g/cm ³)	Relative density	Water content (%)
1.76	25.0	16.1	1.55	2.72	15

(>2 mm). (2) The loess after screening was dried at 105 °C for eight hours. (3) The dried loess was moistened to a moisture content of 15%. (4) The moist loess was compacted in ten layers in the mold to a dried density of 1.55 (or moisture density 1.8 g/cm³).

2.2 The Instrument Used in the Test

The instrument used in this paper is the hollow cylinder apparatus (HCA) of Zhejiang University. The instrument allows several parameters to be changed at the same time or separately, including the principal stress rotation angle (α), the intermediate principal stress coefficient (b), the deviatoric stress (q), and the effective average principal stress (p). The process of stress variation of the soil is a very complicated, process as the foundation soil is subjected to external loads. The complex stress paths were simulated by changing the above parameters.

These four parameters are effective mean principal stress ($p, p = 1/3(\sigma_1 + \sigma_2 + \sigma_3)$), intermediate principal stress coefficient (b), deviatoric stress ($q, q = 1/2(\sigma_1 - \sigma_3)$), and principal stress direction (α).

2.3 Test Plan

The test procedures included isotopically consolidating the test specimens in the hollow cylinder shear pressure chamber under a confining pressure of 200 kPa. After consolidation, the specimen was subjected to a variety of anisotropic shearing. A total of five HCA tests was carried out by varying α value (0°, 30°, 45°, 60°, and 90°) and maintaining constant $p = 200$ kPa and $b = 0.5$. The η was kept between 0 and η_{max} .

3 Results

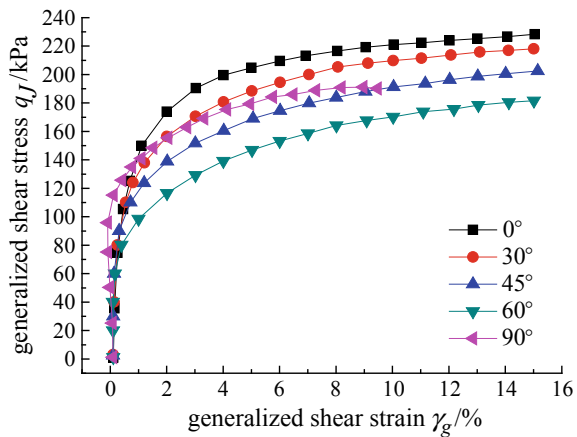
3.1 Stress and Strain Relationship

Figure 1 shows the relationships between generalized shear stress and generalized shear strain when the principal stress coefficient $b = 0.5$.

As expected, the stress–strain curves appeared to vary with the orientation of major principal stress. However, at the small strain, the stress–strain response seemed to be independent of the induced anisotropy, indicating the same initial shear modulus. With the increase of shear strain, the stress–strain anisotropy is increasingly pronounced. The peak shear strength declined as α rose for $\alpha \leq 60^\circ$ but it bounced back slightly when $\alpha = 90^\circ$. This result might be attributed to variation of particle fabric with different strain levels. At a small shear strain, the degree of soil particle rearrangement was trivial in responding to applied stress.

In other words, the soil fabric remained isotropic at small strain, leading to the isotropic initial modulus. At a higher shear strain, the soil particles started to slip and rotate, until reaching equilibrium under the new major principal stress. However, the increase in α caused the decrease in the angle between the failure plane and the horizontal plane where the resistance to particle sliding was minimum. As the shear plane approached the direction of the plane, the soil particles were more likely to slip, resulting in an increased deformation or decreased peak shear stress of the specimen. The similar result was reported by Wang [14] on cohesive soils. When $\alpha = 90^\circ$, the peak shear stress increased because the angle between the failure plane and the horizontal plane began to increase.

Fig. 1 Stress–strain curves at different α



3.2 Soil Strength

The peak stress (or strength) in the stress–strain curves in Fig. 1 was normalized by mean principal stress. The normalized strength (q_{\max}/p) was plotted to be a function of orientation of major principal stress as shown in Fig. 2.

The relationship between the normalized strength and the principal stress direction angle of the remolded loess under different principal stress directions can be fitted by a quadratic polynomial. In order to facilitate the expression, the normalized strength Q was defined as the ratio of the generalized shear stress q_{\max} to the average principal stress p in the remolding of the loess.

The expression of Q is

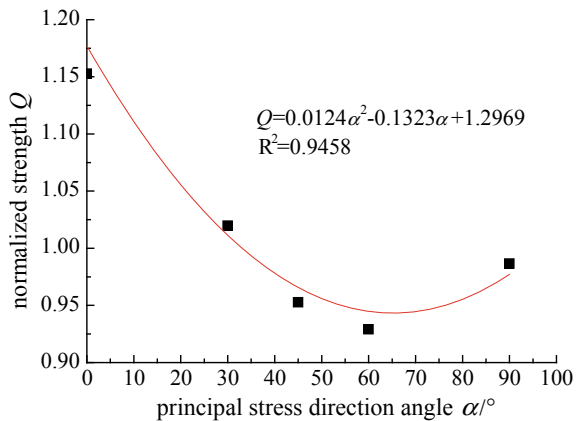
$$Q = q_{\max} / p \tag{1}$$

In the stress path of directional shear tests, the fitting formula for the relationship between the strength and the principal stress orientation angle of the remolded loess in the Xining region is as follows:

$$Q = 0.0124\alpha^2 - 0.1323\alpha + 1.2969 \tag{2}$$

The relationship can be curve fitted in a quadratic function which is $R^2 = 0.946$. The functional relationship between the strength of the remolded loess soil and the direction angle of the principal stress presents a quadratic function, and the curve shape is close to the scoop shape. R^2 is the parameter index of trend line fitting degree in Eq. (2). The numerical value of R^2 can reflect the fitting degree between the estimated value of the trend line and the corresponding actual data, and the higher the fitting degree, the higher the reliability of the trend line. The value of R^2 ranges from 0 to 1, and the reliability is highest when the numerical value of R^2 of trend is 1 or close to 1, otherwise, the reliability is lower. As it can be seen from the Eq. (2),

Fig. 2 Variation of normalized strength with the orientation of major principal stress



when R^2 is close to 1, the degree of fit between the estimated value of the curve fitting and the corresponding actual data is high, and the reliability of the fitted line is high.

Within the range of $\alpha = 0^\circ\text{--}90^\circ$, the normalized strength varied from 1.17 to 0.92 with a maximum difference of 25%.

3.3 Deformation

Figure 3 presents the results of major principal strain (ε_z), minor principal strain (ε_θ), and intermediate principal strain (ε_r) at different shear stress under different directional angle of major principal stress.

The major principal strain and minor principal strain showed opposite trends as shear stress increased. The former decreased with q but the latter increased with q . The intermediate principal strain showed mixed compression and tension when $\alpha \geq$

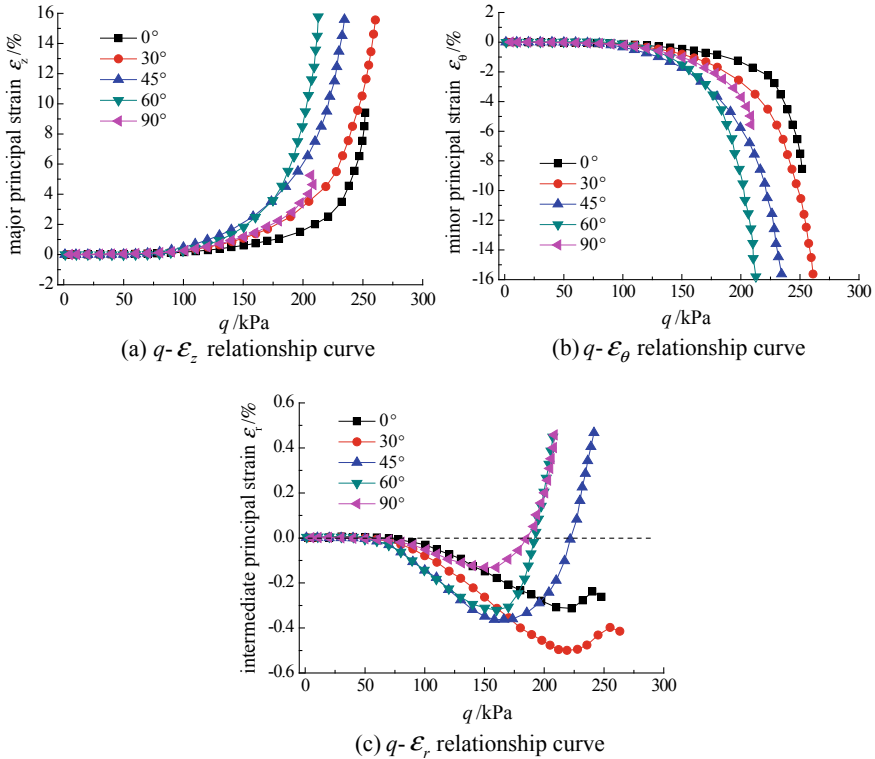


Fig. 3 Strains under different directional angle of major principal stress **a** $q\text{--}\varepsilon_z$ relationship curve, **b** $q\text{--}\varepsilon_\theta$ relationship curve, **c** $q\text{--}\varepsilon_r$ relationship curve

45°, but only tension when $\alpha < 45^\circ$. It seemed that $\alpha = 45^\circ$ is a threshold greater than which the strain pattern commenced to change with q .

4 Conclusions

A series of HCA tests were conducted to investigate the strength and deformation anisotropies of loess obtained in Qinghai, China. Based on the test results, the following conclusions can be obtained.

- (1) The anisotropy of stress–strain relationship in loess was evidently a consequence of changes in the orientation of the major principal stress (α). However, the initial shear modulus remained isotropic, which is not related to the change of α . The strength anisotropy was pronounced, and it decreased with α when α changed from 0° to 60° but increased with α when α ranged from 60° to 90°. The relationship between normalized strength and α could be fitted into a quadratic equation. The maximum difference in normalized strength due to the change of α was 25%.
- (2) The major principal strain consistently increased as the shear stress (q) increased whereas the minor principal strain decreased with q . The intermediate principal strain showed mixed compression and tension as $\alpha \geq 45^\circ$ but only tension as $\alpha < 45^\circ$.

Acknowledgements This study was supported by the National Natural Science Foundation of China (Grants No. 51768060), the Fundamental Research Program and the Cooperation Program of Qinghai Province (Grants No. 2017-ZJ-792 and No. 2017-HZ-804), and the Technological Innovation Service Platform of Qinghai Province (Grants No. 2018-ZJ-T01). The authors would like thank all the supports.

References

1. Li GX (2004) Advanced soil mechanics. Tsinghua University Press, Beijing
2. Liu ZhY (2014) Study on yield characteristics and anisotropic yield surface equation of soft clay. Zhejiang University
3. Bjerrum L (1973) Problems of soil mechanics and construction on soft clays and structurally unstable soils (collapsible, expansive and others). In: Proceedings 8th international conference on Soil Mechanics and Foundation vol 3. Moscow, pp 111–159
4. Jardine RJ, and Smith PR (1991) Evaluating design parameters for multi-stage construction. In: Proceedings international conference on Geotechnical Engineering for Coastal Development, Geo-coast'91, vol 1. Yokosuka, pp 197–202
5. Zdravkovic L, Potts DM, Hight DW (2002) The effect of strength anisotropy on the behaviour of embankments on soft ground. *Geotechnique* 52(6):447–457
6. Saada AS (1970) Testing of Anisotropic clay soils. *J Soil Mech sand Found Div, ASCE*, 96(5)
7. Towhata I, Ishihara K (1985) Undrained strength of sand undergoing cyclic rotation of principal stress axes. *Soils Found* 25(2):135–147
8. Nakai T, Ftljii J, Taki H (1991) Kinematic of anisotropic hardening model for sand. In: Nakai T (ed) Proceedings 3rd international conference on Constitutive Laws for Engineering Materials, pp 36–45

9. Shen Y, Zhou J, Zhang JL (2008) Influence of cyclic rotation of principal stress axis with low shear stress on undisturbed clay. *Chin J Rock Mech Eng* S1:123–126
10. Miura K, Toki S, Miura S (1986) Deformation prediction for anisotropic sand during the rotation of principal stress axes. *Soils Found* 26(3):42–56
11. Nishimura, Satoshi (2006) Laboratory study on anisotropy of natural London Clay. Ph.D. thesis, (Doctoral dissertation, Imperial College London (University of London))
12. Gasparre, Apollonia (2005) Advanced laboratory characterization of London clay. Ph.D. thesis, Imperial College London (downloadable from www.imperial.ac.uk/geotechnics)
13. Chen W, Zhang WY, Chang LJ (2015) Experimental study of anisotropy of compacted loess under directional shear stress path. *Chin. J. Rock Mech. and Eng* 09:4320–4324
14. Wang H J, Zhang G P, Zhou K B. Influence of Intrinsic and Induced Anisotropy on Strength and Deformation Properties of Compacted Clay. *Chin. J. Rock Mech. and Eng*, 1–10(1996)

Investigation of Frost Heave Considering the Boundary Conditions of Artificial Ground Freezing



Katharina Niggemann 

Abstract The construction of traffic routes in the subsoil is increasingly been carried out by artificial ground freezing. Due to artificial heat removal, a load-bearing frost body arises, which becomes water-impermeable in its closed form. However, frost heave at the ground surface may lead to damage buildings. In fine-grained soils, the frost heave is caused by the 9% volume expansion of the pore water during freezing and, in particular, by the formation of ice lenses. For the formation of ice lenses, water from unfrozen zones is suctioned to the frost line and freezes to continuous ice lenses. Based on horizontal freezing pipes in the subsoil, the decisive heaves at the ground surface result from the frost penetration direction to the ground surface and in the opposite direction. In this case, the ice lenses grow parallel to the ground surface. In order to investigate the frost heave due to ground freezing boundary conditions, a test device was designed to carry out one-dimensional frost heave tests taking into account the upward and downward freezing directions.

Keywords Frost heave · Ice lens formation · Artificial ground freezing

1 Introduction

The increasing demand of efficient infrastructure requires the development of underground traffic routes. Artificial ground freezing is used particularly in inner-city areas. The frost body has a static and, in its closed form, a waterproofing function. However, the frost body expansion may cause soil deformations and undesirable frost heaves at the ground surface. Especially in fine-grained soils, frost heave can become very large depending on the existing boundary conditions. This is caused by the formation of ice lenses and occurs additionally to the 9% volumetric expansion of the pore water during phase change. Ice lenses are formed near the freezing front by accumulation of sucked water.

K. Niggemann (✉)
RWTH Aachen University, Aachen, Germany
e-mail: niggemann@geotechnik.rwth-aachen.de

© Springer Nature Singapore Pte Ltd. 2020
A. Petriaev and A. Konon (eds.), *Transportation Soil Engineering in Cold Regions*,
Volume 2, Lecture Notes in Civil Engineering 50,
https://doi.org/10.1007/978-981-15-0454-9_29

In the past, various experiments were carried out to determine frost heave with ice lens formation. In addition to grain size distribution and plastic properties, the influence of overburden pressure (e.g. [1, 2]) as well as the influence of mineralogy and ion concentration (e.g. [3, 4]) was investigated. In these experiments, the soil samples were always frozen from the top, with a frost penetration downwards, so that the sucked water for the formation of ice lenses had to flow against gravity. For the determination of frost heave due to artificial ground freezing, the different freezing directions (radial around the freezing pipes) must be considered. The following section explains the model assumptions, which are the basis for the practical tests. The different freezing directions were considered in order to investigate the influence on the formation of ice lenses.

1.1 Model Assumptions

Ice lenses are formed parallel to the isotherms and thus theoretically radial around a freezing pipe. The following Fig. 1 exemplarily illustrates soil freezing of a tunnel cross-section with horizontal freezing pipes. The material is a clayey silt with an initial soil temperature of $10\text{ }^{\circ}\text{C}$. The temperature of the freezing pipes is $-35\text{ }^{\circ}\text{C}$, and the distance between the freezing pipes was chosen to 1.2 m . The calculation shows that the area between the single pipes freezes quickly due to the steep temperature gradient. After four days (Fig. 1, left), the cross section is completely closed. Since ice lenses only form during slow frost penetration, it is assumed that no ice lenses form between the freezing pipes.

Frost deformations in the vertical axis are decisive for the maximum frost heave at the ground surface. The maximum frost heave at the ground surface results from the formation of ice lenses at the tunnel roof, with a frost penetration towards the ground surface and in the opposite direction (Fig. 1, right).

Therefore, the two defined freezing directions are investigated and compared with each other with the use of one-dimensional frost heave tests. The results are applied to clarify differences in the formation of ice lenses and to determine whether factors

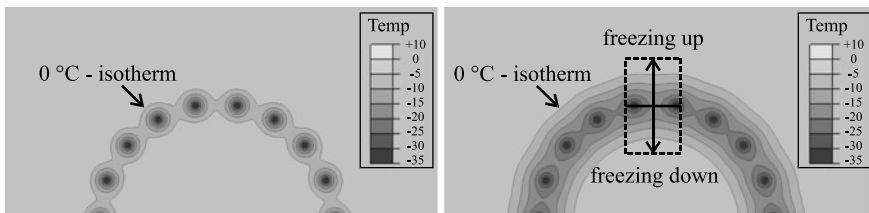


Fig. 1 Thermal simulation of a freezing tunnel cross-section, left: $t = 4\text{ d}$, right: $t = 15\text{ d}$

such as gravity have an influence on them. Prospectively, it will be examined if already existing theories and approaches for the calculation of frost heave are valid for both freezing directions.

2 Mechanism of Frost Heave

Frost heave occurs as a result of frost penetration into the soil. The size of the temperature gradient affects the penetration velocity of the frost front. With increasing frost penetration, the temperature gradient and thus the penetration velocity decrease until the frost line does not migrate further. Under these conditions, the last ice lens is formed. This state, without further local changes of the frost line but slight thermal changes due to the formation of the ice lens, is described in the text as the quasi-stationary state.

In fine-grained soils, the pore water freezes at different negative temperatures depending on the appearance of water (bound/unbound). Therefore, water can occur in different aggregate states at the same temperature. This partially frozen zone is also called frozen fringe. During freezing, only pure water freezes without ions, and thus, the frozen pore water has a lower ion concentration as the unfrozen water. A chemical gradient occurs and causes the water to migrate towards the lower potential. The water migrates to the partially frozen zone and accumulates at the base of the ice lens. For the ice lens initiation, the effective stresses in the soil at the level of the formed ice lens must first be exceeded. The separation pressure is described as a force, acting between the adsorbed films of the mineral grains. In the state of equilibrium, these forces maintain the film thickness between two solid bodies (e.g. ice and grain). The mean separation pressure along the isotherm corresponds to the effective stresses at this interface [5, 6].

Konrad and Morgenstern [7] divide the freezing ground into a passive, frozen zone and an active, partially frozen and unfrozen zone. The unfrozen water in the negative temperature range, which exists at the same temperature as ice, interrupts the thermodynamic equilibrium due to different energy levels. The equilibrium has to be restored by freezing further water, which is sucked from the active zone. Konrad and Morgenstern [7] explain the end of ice lens formation by the fact that at quasi-stationary temperature conditions, the warm side of the ice lens approaches 0 °C with time. This leads to a decreasing suction and thus to an end of the water flow.

Unold [3] examines the development of suction in freezing soils as a result of osmotic rejection of the ice and mineral surface. The osmotic pressure depends on the ion concentration at the mineral surface and causes an increasing surface distance between the mineral and ice. As a result, water can flow into and the ion concentration decreases. This leads to an increasing freezing point so the water freezes faster. Unold [3] explains the end of ice lens formation by the compression of the area below the ice lens, which reduces water permeability in the unfrozen zone. If no water can accumulate to maintain the water film thickness, no further phase change occurs, and thus, no released thermal energy is available for the transport

of water. At the beginning of a freezing test with a high-temperature gradient, no or only very thin ice lenses form due to the rapidly decreasing permeability. The smaller the temperature gradient becomes over time, the slower the frost penetrates the soil, and the individual ice lenses become thicker. The thickest ice lens results at quasi-stationary temperature conditions.

3 Test Device and Soil Properties

Figure 2 shows the test device for the frost heave tests with different freezing directions. The dimensions of the cylindrical specimens are $d = 25$ cm and $h = 20$ cm. Each specimen is placed in a test cylinder consisting of eight ring elements with a 2.5 cm thickness. During the frost heave tests, the individual rings are pulled apart so that the soil sample does not have to overcome any frictional resistance while heaving. The top and the bottom of the sample, respectively, are cooled by a freezing element (1), which is connected to a circulation thermostat. For the formation of ice lenses, sufficient water must be available. This is achieved by a water-saturated porous plate (2), which is connected to an external water supply. The porous plate is placed on the warm side of the soil sample. The soil sample is additionally heated on the warm side to avoid freezing of the total sample. This is done by using a heating plate (3) which is placed above or below the porous plate, respectively. All tests are carried out in a climatic chamber with a constant temperature and humidity. Consequently, external influences, such as seasonal fluctuations, can be excluded.

For data recording, temperature sensors (6) are distributed over the sample height. In order to calculate the temperature profile over time, the displacements of the temperature sensors as a result of frost heave are recorded by using displacement sensors. The displacement measurement of the temperature sensors is not shown in Fig. 2. The uniaxial deformations on the top of the specimen are recorded by displacement transducers (5). To determine the water inflow into the sample due to the increasing suction, the water mass is recorded by a load cell (4).

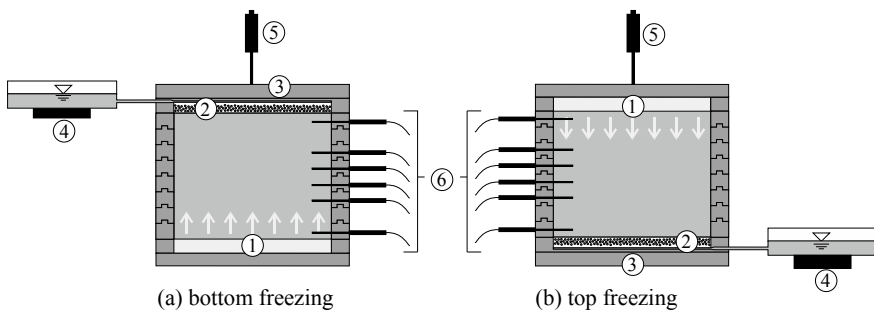


Fig. 2 Schematic structure of freezing cell: 1 freezing element, 2 porous plate with water supply, 3 heating plate, 4 load cell, 5 displacement transducer, 6 temperature sensors

Table 1 Soil properties

Grain density ρ_s [g/cm ³]	Liquid limit w_l [%]	Plastic limit w_p [%]	Hydraulic conduct. k_f [m/s]
2.683	32.9	18.4	$1.2 \cdot 10^{-10}$

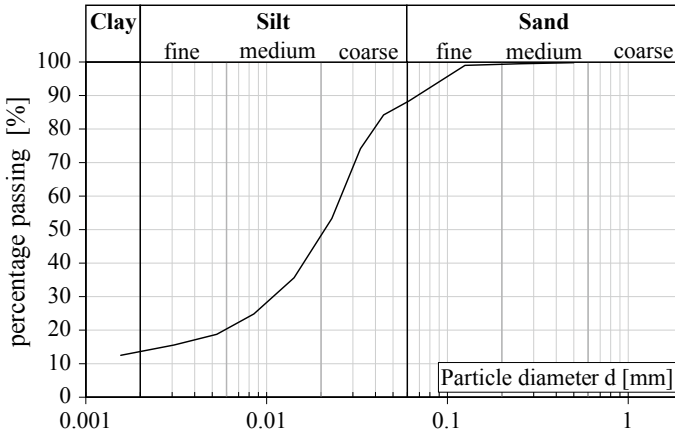


Fig. 3 Particle size distribution

For the experiments, a silt is used which also contains fine sand and clay. The material is produced artificially to ensure an equal composition for all tests and thus improved comparability of the results. The essential soil properties and particle size distribution are shown below (Table 1) (Fig. 3).

4 Testing Program

The soil samples prepared with a water content of 20% ($S_r \sim 0.9$) are frozen one-dimensionally from the cold side. During the entire experiment, water can be sucked from the external supply. The environmental conditions are controlled by the climatic chamber. The ambient temperature for the test series presented here is $T_0 = 15^\circ\text{C}$. This is also the initial temperature of the soil sample. The following presented test series are categorized into Tables 2 and 3 depending on the freezing direction (top freezing—TF/bottom freezing—BF).

In the first presented test series 1 (TF1/BF1), no external water source was provided, so the sucked water for ice lens formation only came out of the soil sample. For test series 2 – 4, a water source was provided. The temperatures T_c (cold side) and T_w (warm side) are the measured temperatures 1.25 cm below or above the edge of the cold side, respectively, at the quasi-stationary temperature state. Furthermore,

Table 2 Test series: top freezing (TF)

	Cold side T_c [°C]	Warm side T_w [°C]	Grad T_f [°C/cm]	Surcharge p [kN/m ²]	Saturation S_r [-]	Porosity n [-]
TF1	-9.2	8.1	0.911	1.75	0.832	0.392
TF2	-8.3	8.1	0.868	3.75	0.890	0.376
TF3	-13.9	5.0	0.999	3.75	0.881	0.379
TF4	-4.2	10.6	0.929	3.75	0.928	0.366

Table 3 Test series: bottom freezing (BF)

	Cold side T_c [°C]	Warm side T_w [°C]	Grad T_f [°C/cm]	Surcharge p [kN/m ²]	Saturation S_r [-]	Porosity n [-]
BF1	-9.2	5.9	0.831	1.73	0.807	0.399
BF2	-9.2	7.4	0.881	3.73	0.897	0.374
BF3	-14.0	4.6	0.992	3.73	0.875	0.380
BF4	-4.5	10.6	0.908	3.73	0.896	0.375

the temperature gradient $\text{grad } T_f$ across the frozen zone (up to 0 °C—isotherm) at the quasi-stationary state, the load p , the degree of saturation S_r and the porosity n are given.

5 Test Results

For the evaluation of the test results, it should be noted that the frost penetration into the soil sample depends on the temperature boundary conditions. The larger the frozen zone, the more heaves caused by volumetric expansion of the pore water can occur during freezing. The courses of the 0 °C—isotherm for the test series 1 – 4 are pictured in Fig. 4. They result from the temperature measurements at the sample, which are interpolated over the sample height as a function of time. The 0 °C—isotherm due to top freezing runs downwards from the upper edge of the soil sample. For better comparability, the 0 °C—isotherm due to bottom freezing was converted to a downward coursed curve. The comparison of both freezing directions gives an approximately good agreement of the 0 °C—isotherms, and thus, a comparison of the further results is possible. For the following evaluation, it is assumed that quasi-stationary temperature conditions start at the time $t \sim 50$ h for the test series 1 – 3. In test series 4, the quasi-stationary temperature conditions are reached earlier at $t \sim 25$ h.

The temperature gradient in the frozen zone decreases with the frost penetration, which leads to better conditions for the ice lens formation. Especially because the pore channels, which are necessary for the water supply to the ice lens, freeze more slowly. The smaller the temperature gradient along the frozen zone during freezing,

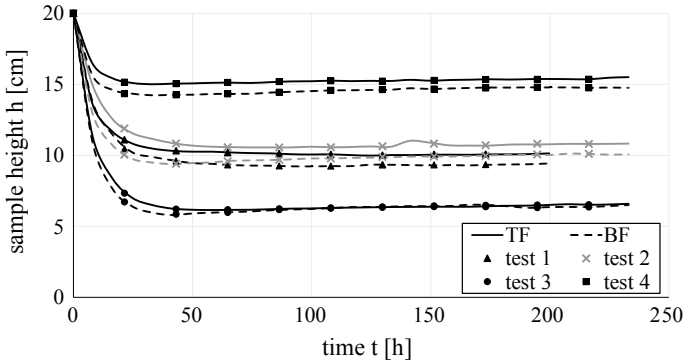


Fig. 4 Courses of 0 °C— isotherms

the more time is left for water accumulation. For this reason, the ice lens formation may already take place during the thermal transient state. The temperature gradients determined for the frozen zone in the quasi-stationary state are between 0.83 °C/cm and 1.0 °C/cm. Under these thermal conditions, the last ice lens is formed. The temperature gradients of both test variants (TF/BF) of the test series essentially agree well.

The heave results of the tests are shown in Figs. 5, 6, divided in total heave and heave due to the formation of the final ice lens ($h_{ice\ lens}$). The comparison of the test series 1 and 4 shows that the total heaves of the test series 1 are significantly higher, but the heaves due to the formation of the final ice lens correspond approximately to test series 4. In test series 1, the final frozen zone is greater, which enables more ice lenses to form in the thermal transient state. In both cases, the heave rate during the formation of the final ice lens decreases over time. Test series 1 is not connected to an external water source and only sucks water out of the unfrozen zone of the sample. The entire unfrozen zone of the soil sample has an approximately 5% lower

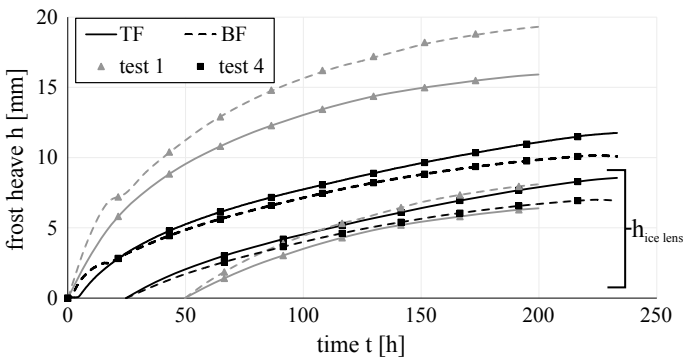


Fig. 5 Frost heave of the test series 1 and 4

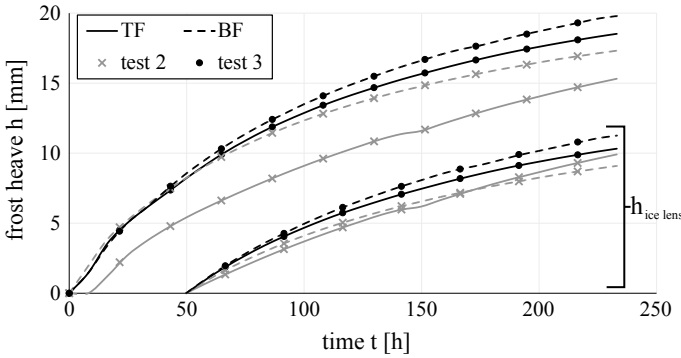


Fig. 6 Frost heave of the test series 2 and 3

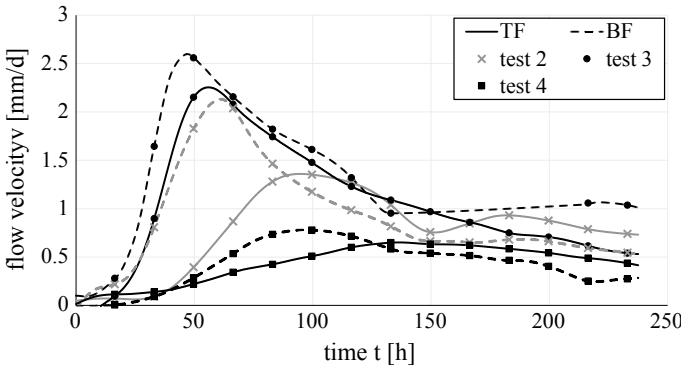


Fig. 7 Flow velocity of sucked water

water content at the end of the test. In test series 4, the flow velocity of the sucked water is comparatively low (Fig. 7), so that a smaller magnitude of suction at the ice lens can be assumed. An increased draining of the unfrozen area according to test series 1 could not be determined. The largest ice lens is formed in test series 3 (Fig. 6) with a cold side temperature of $T_c \sim -14 \text{ }^\circ\text{C}$ and a temperature gradient at quasi-stationary conditions of $\text{grad } T_f \sim 1.0 \text{ }^\circ\text{C/cm}$. Under these conditions, the water freezes faster compared to the other test series, and more conversion energy is released. The conversion energy is significant for the magnitude of suction, which causes the water transport to the ice lens. The same result can be seen in Fig. 7 by comparing the velocities of sucked water from the external water source. The highest flow velocities are at test series 3. The maximum value of the sucked water occurs approximately with the formation of the final ice lens.

Comparing the test variants top and bottom freezing, it can be seen that the heaves resulting from bottom freezing are generally greater than those resulting from top freezing (Figs. 5, 6). The tests TF3 and BF3 can be compared very well due to the

almost equal thermal boundary conditions. The heaves up to the quasi-stationary state, which is reached after 50 h, are almost the same. Afterwards, the heaves of BF3 increase faster as a result of the final ice lens formation. Considering Fig. 7, the same trend is recognized.

The investigation of the soil samples after the freezing tests indicates that longitudinal cracks along the sample height occurred during freezing (Fig. 8, right). In addition, horizontal areas with polygonal-shaped cracks were formed directly below the ice lens (Fig. 8, left; see also [5]). During bottom freezing, where the water inflow is affected by gravity, these cracks allow an increasing water flow to the frost line and thus improve the formation of ice lenses.

Investigations of the water content over the sample height show that the water content in the unfrozen zone of the soil sample is clearly below the initial water content, especially close to the ice lens. The lower water content may cause soil shrinking at the ice lens and thus cracks, which improve the water supply during bottom freezing. Figure 9 shows an example of the water content profile of test series 3 after the freezing test.

The obtained results of top and bottom freezing show qualitatively similar results. In the frozen zone, the water content after freezing is higher than the initial water

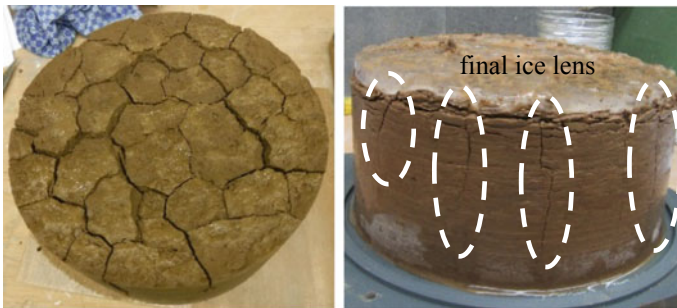
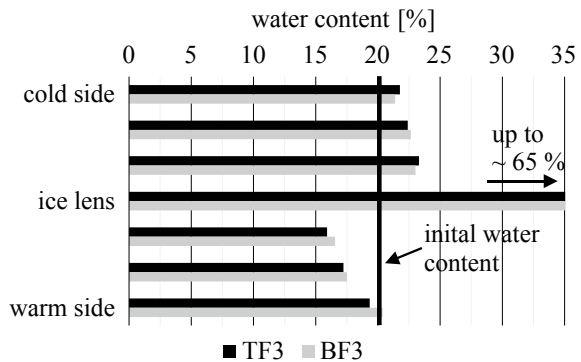


Fig. 8 Left: horizontal soil sections at the soil-ice lens interface, right: longitudinal cracks along a half soil sample

Fig. 9 Water content profile



content. This is related to the formation of ice lenses during the thermal transient state. The unfrozen zone has a significantly lower water content in comparison with the initial water content. Especially close to the final ice lens, the water content is about 4% below the initial water content. Kellner [2] carried out experimental investigations of ice lens formation at different soils and also found out that the water content in the unfrozen area drops towards the frost line. A comparison of the test variants top freezing and bottom freezing shows that the water content in the unfrozen area is slightly higher at bottom freezing. This gives the impression that the natural flow of water ensures a higher saturation, especially under consideration of the vertical cracks.

6 Conclusion

A test device was presented to investigate the influence of the freezing direction at artificial ground freezing. For this purpose, one-dimensional frost heave tests were carried out considering the freezing direction (top freezing/bottom freezing). The experimental results of both test variants (TF/BF) were compared to work out differences at the ice lens formation. For the experimental investigations, a frost susceptible silt was frozen one-dimensionally under defined boundary conditions. The obtained results indicate that bottom freezing basically produces larger frost heaves due to ice lens formation. A reason is the formed cracks during freezing, which improve the water supply to the frost line. The water content profile shows a redistribution of water in the soil after freezing. Top freezing as well as bottom freezing show similar water distributions after freezing, whereas the saturation of the unfrozen zone at bottom freezing is slightly higher. Particularly, noticeable is the increased reduction of the water content at the ice lens (in the unfrozen zone), which probably causes the crack formation.

Within the framework of further experimental investigations, an extensive parameter study is planned. The aim is to examine whether existing theories and approaches for the calculation of frost heaves are valid for both freezing directions.

Acknowledgements The author would like to thank the Deutsche Forschungsgemeinschaft (DFG, German Research Foundation) for supporting this research project-Project-No. 409760547.

References

1. Konrad JM, Morgenstern NR (1982) Effects of applied pressure on freezing soils. *Can Geotech J* 19(4):494–505
2. Kellner C (2008) Frosthebungsverhalten von Böden infolge tief liegender Vereisungskörper. Dissertation, Chair and Testing Office for Foundation Engineering, Soil Mechanics, Rock Mechanics and Tunneling, Technical University Munich (in German)

3. Unold F (2006) Der Gefriersog bei der Bodenfrostung und das Kompressionsverhalten des wieder aufgetauten Bodens. Dissertation, Institute for Soil Mechanics and Foundation Engineering University of the Federal Armed Forces Munich (in German)
4. Herzog F, Boley C (2013) Mechanism during formation of ice lenses and suction in freezing soils. In: Proceedings of the 18th international conference on Soil Mechanics and Geotechnical Engineering, Paris, pp 337–340
5. Chamberlain EJ (1989) Physical changes in clays due to frost action and their effect on engineering structures. In: International symposium frost in Geotechnical Engineering, Saariselka, Finland, pp 863–893
6. Henry B (1988) Chemical aspects of soil freezing. Cold Regions Research and Engineering Laboratory Report, USA, pp 88–17
7. Konrad J-M, Morgenstern NR (1980) A mechanistic theory of ice lens formation in fine-grained soils. *Can Geotech J* 17(4):473–486

Frost-Heaving Pressure and Stiffness of Compacted Roadbed Material by Laboratory Model Test



Eun Chul Shin, Byung Hyun Ryu and Hee-Mun Lee

Abstract The laboratory model test was carried out in the freezing chamber and the size of insulated steel box is $0.9\text{ m}(L) \times 0.9\text{ m}(B) \times 0.9\text{ m}(H)$ which simulated actual roadbed structure. Data logger was used to measure the variation of temperature. The variation of heaving pressure with elapsed time for various roadbed conditions was determined through the laboratory model test. The influence of crushed natural aggregate to the freezing of the subgrade soil was studied to verify the function and effectiveness of the anti-freezing layer. The thermal gradient is greatly influenced prior to reach the soil temperature of $0\text{ }^{\circ}\text{C}$ or below $0\text{ }^{\circ}\text{C}$. The heat transfer rate is greater at the roadbed surface and then slightly decreases with the depth of roadbed. The degree of air temperature and the type of soil layer are also influenced on the freezing temperature ($0\text{ }^{\circ}\text{C}$) at the roadbed depth. On the other hands, the anti-freezing materials like crushed natural aggregates can reduce the event of frost heaving of subgrade soil at the same condition of soil density, temperature, and moisture content. The loading pressure and deflection for the compacted roadbed materials prior to freezing and after thawing and hence, the modulus of elasticity were determined by the application of the light falling weight deflectometer (LFWD).

Keywords Compacted roadbed material · Freezing and thawing · LFWD · Heaving pressure · Modulus of elasticity

1 Introduction

The pavement structures are subject to freezing and weakening during the spring season. Consequently, the mechanical properties of pavement structures can be greatly affected by the seasonal changes in temperature and soil moisture. During the winter

E. C. Shin (✉) · H.-M. Lee
Incheon National University, Incheon, Republic of Korea
e-mail: ecshin@inu.ac.kr

B. H. Ryu
Korea Institute of Civil Engineering and Building Technology, Goyang-Si, Republic of Korea

© Springer Nature Singapore Pte Ltd. 2020
A. Petriaev and A. Konon (eds.), *Transportation Soil Engineering in Cold Regions*,
Volume 2, Lecture Notes in Civil Engineering 50,
https://doi.org/10.1007/978-981-15-0454-9_30

season, the stiffness of unbound layers generally increases because of ice bonding of soil particles in the base and subbase, and ice lens formed in the subgrade.

In contrast, the pavement structure during the spring season may become saturated from thawing ice, and the stiffness can be substantially reduced. Under such conditions, substantial settlements can occur if the structure is exposed to the loading of heavy freight vehicles.

The contribution of infiltrating melt water can further decrease the bearing capacity and extend the thaw-weakening period. During the freezing season, intermittent freeze–thaw cycles can also affect to the structural adequacy.

The soil begins to be gradually frozen if the external temperature is maintained less than 0 °C. At this time, while the moisture of the underground which is not frozen by the capillary phenomena moves to the freeze direction and the ice lense is generated, this ratio and size increases gradually, the ground protrudes. The ice lense is not frozen in the temperature of the soil, then the floating moisture is formed. It can be the phenomenon that accordingly the ground inflates and it rises the in-phase [1]. This phenomenon is called as the frost heaving [2].

In the winter season, the surface of paved road is frequently damaged due to the freezing of the pavement structures. The repairing cost of damaged paved road is a great amount nationwide. Therefore, in this study, the large-scale laboratory test was performed inside the large freezer and the stiffness characteristics for the roadbed materials prior to freezing and thawing of the roadbed material were analyzed by conducting the LFWD test. The loading pressure and the variation of vertical deflection were measured during the process of freezing and thawing. Reference [3] reported that the rigidity of clay soil reduced by the volume change because of freezing and thawing of the soil. The influence of crushed natural aggregate to the freezing of the subgrade soil was studied to verify the function and effectiveness of the anti-freezing layer.

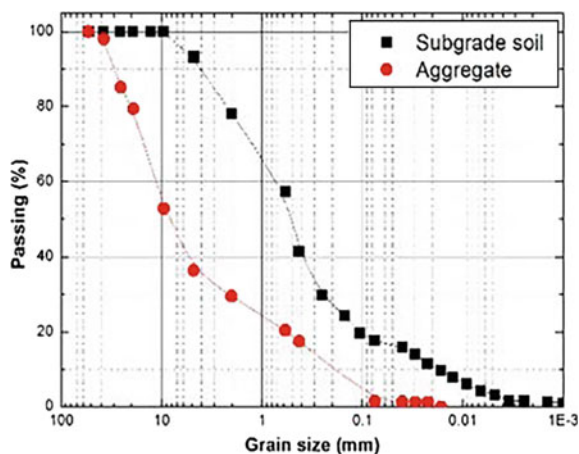
2 Laboratory Model Test in the Freezing Chamber

For laboratory model test, the subgrade soil and aggregate were collected from the road construction site. The geotechnical properties of subgrade soil were determined in the laboratory by following the KS F test methods (Korean standard for soil testing) and tabulated in Table 1.

Table 1 Geotechnical properties of subgrade soil

Specific gravity (G_s)	Plastic index (PI)	D-Compaction		(USCS)	Uniformity coefficient (C_u)	Coefficient of gradation (C_g)	No. 200 passing (%)
		r_{dmax} (tf/m ³)	w_{Opt} (%)				
2.63	N.P	2.04	7.95	SM	45.6	5.3	17.6

Fig. 1 Grain-size distribution curves of subgrade soil and aggregate



Laboratory test on the subgrade soil samples consisted of determining the grain-size distribution, specific gravity, Atterberg limits, and *D*-Type compaction tests. The results of the sieve analysis and hydrometer test show that the soil had about 17.6% finer than No. 200 U.S sieve (0.075 mm opening). The coefficient of uniformity (C_u) and gradation (C_g) is 45.6 and 5.3, respectively. Figure 1 shows the grain-size distribution curves of subgrade soil and aggregate. The specific gravity of subgrade soil was determined as 2.63 by following the ASTM test designation D-854. The plasticity index was determined and it is turned out to be non-plastic.

D-Type compaction test was performed by using the modified proctor compaction mold by following the procedure recommended in KS F to determine the maximum dry unit weight and the optimum moisture content. The inner diameter of the mold is 152.4 mm with the height of 116.4 mm. The subgrade soil is compacted in five layers by a hammer that weights 4.54 kg. The drop height of the hammer is 457.2 mm. The number of hammer blows for each layer is kept at 55 blows. The *D*-Type compaction test for the subgrade soil gives a maximum dry unit weight of 2.04 t/m^3 at an optimum moisture content of about 7.95%. On the basis of geotechnical properties [4], the subgrade soil can be classified by the Unified Soil Classification System as silty sand (SM).

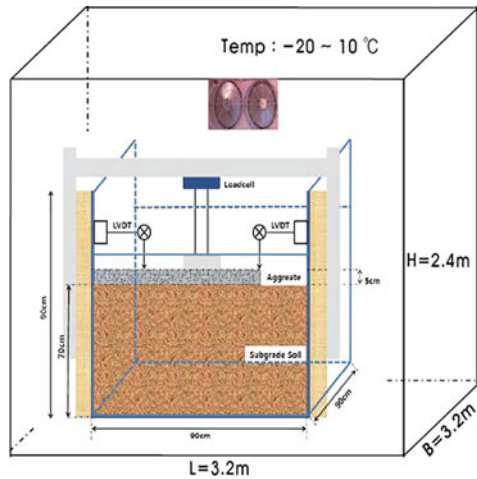
The aggregate used in the test is frost unsusceptible. The specific gravity and the percentage of #200 passing (0.075 mm opening) are 2.75 and 1.5%, respectively. The absorption ratio of moisture was determined as 0.71% by following the KS F. The *E*-Type compaction effort was made for the aggregate layer which gives a maximum dry unit weight of 2.26 t/m^3 at an optimum moisture content of 5.8%. The volume of *E*-type compaction mold and the weight of hammer are the same as the *D*-Type compaction. However, the number of hammer blows for each layer is kept at 92 blows and compacted in three layers.

The laboratory model test condition was classified according to the freezing temperature and roadbed section as tabulated in Table 2. The laboratory model test was performed in order to measure the heaving pressure of the subgrade soil with elapsed

Table 2 Sequence of laboratory model test condition

Temperature		CASE 1_(T20-A0)	CASE 2_(T15-A0)	CASE 3_(T15-A5)
		-20 °C	-15 °C	-15 °C
Roadbed section	Subgrade soil layer	30 cm	30 cm	30 cm
	Aggregate layer	0 cm	0 cm	5 cm
Moisture content (%)	Subgrade soil layer	15.3	15.2	15.2
	Aggregate layer	0	0	2.1

Fig. 2 Freezing chamber physical dimension of model test box



time due to freezing. As shown in Fig. 2, the temperature of the freezing chamber can be varied from -20 °C to +10 °C. The size of freezing chamber is 3.2 m(width) × 3.2 m(length) × 2.4 m(height).

The laboratory model tests were conducted in a steel box measuring 90 cm(width) × 90 cm(length) × 90 cm(height). The model test box was fabricated by using steel panel and braced with angle irons to avoid yielding during soil placement and LFWD loading on the soil. The subgrade soil was placed in the model test box and compacted in 20 cm thick layer using a flat-bottomed vibratory rammer to meet the required relative density, 95% of rd(max).

The load-bearing capacity of compacted roadbed material was determined by using the light falling weight deflectometer(LFWD). The elastic modulus and deflection for the unbound roadbed materials have been used for pavement design [5]. These design parameters are normally verified during the construction of roadbed using the LFWD. The free drop sinker load is applied on the surface of roadbed, then vertical impact peak force and peak elastic deflection are measured by using the geophone on the LFWD as shown in Fig. 3. The modulus of elasticity can be obtained with the

Fig. 3 View of LFWD



measured elastic deflection and applied peak force through the elasticity theory [6] as in Eq. (1).

$$E_{LFWD} = \frac{q_d}{w_d} r \frac{\pi}{2} (1 - \nu^2) \tag{1}$$

where E_{LFWD} is the modulus of elasticity by the LFWD test, q_d is the peak force per unit area, w_d is the elastic deflection, ν is the Poisson’s ratio of soil, and r is a radius of plate. A diameter of plate used in the LFWD is 300 mm and the Poisson’s ratio of subgrade soil is assumed to be 0.35.

3 Laboratory Model Test Results

The freezing rate is depending upon the depth of soil, the type of soil, and moisture content of soil. The thermal gradient of roadbed is greatly influenced prior to reach the soil temperature of 0 °C or below 0 °C. The heat transfer rate is greater at the roadbed surface and then slightly decreases with the depth of roadbed. The degree of air temperature and the type of soil layer are also influenced on the freezing temperature (0 °C) at the roadbed depth. The elapsed times to reach the temperature of 0 °C at the roadbed depth are described in Table 3 for three different cases. With comparison between Case 2 and Case 3, the covering with an aggregate layer over the subgrade soil is greatly extended the time of reaching 0 °C.

The variation of heaving pressure with the elapsed time for three different roadbed conditions is shown in Fig. 4. This figure indicates that the colder air temperature gives the higher rate of heaving pressure and reached the maximum heaving pressure at the much shorter time period with comparing other two roadbed conditions. The

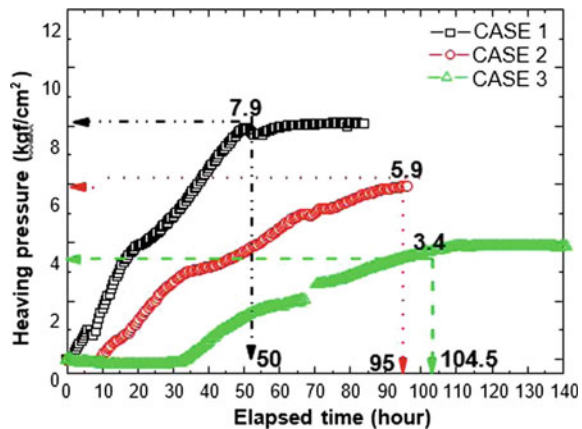
Table 3 Elapsed time for reaching 0 °C at the different depths of roadbed

Roadbed depth mm	CASE 1_(T20-A0) (Hour)	CASE 2_(T15-A0) (Hour)	CASE 3_(T15-A5) (Hour)
0	6	10	25
25	10.5	20	33.5
50	19.5	30	42

Table 4 Variation of elastic moduli and SDR for compacted roadbed materials

	E Before freezing (kgf/cm ²)	E After thawing (kgf/cm ²)	SDR (%)
CASE 1_(T20-A0)	190	120	36.8
CASE 2_(T15-A0)	170	150	11.7
CASE 3_(T15-A5)	210	160	23.8

Fig. 4 Variation of heaving pressure with elapsed time for various roadbed conditions



aggregate layer over the subgrade soil (Case 3) induces much lower heaving pressure at the longer period of elapsed time.

The stiffness of compacted roadbed material was determined by the application of the light falling weight deflectometer (LFWD). The LFWD tests were performed for the compacted roadbed material prior to freezing and after thawing. The loading pressure and deflection were measured during the LFWD test. The test conditions of the compacted roadbed material and temperature are described in Table 2. The measured vertical loading pressures and the elastic vertical deflections for Case 1–Case 3 are shown in Figs. 5, 6 and 7. From the test results shown in the figures, the elastic moduli of compacted roadbed material (E_{LFWD}) were determined by Eq. (1). On the other hand, the stiffness decrease rate (SDR) by using the modulus of elasticity

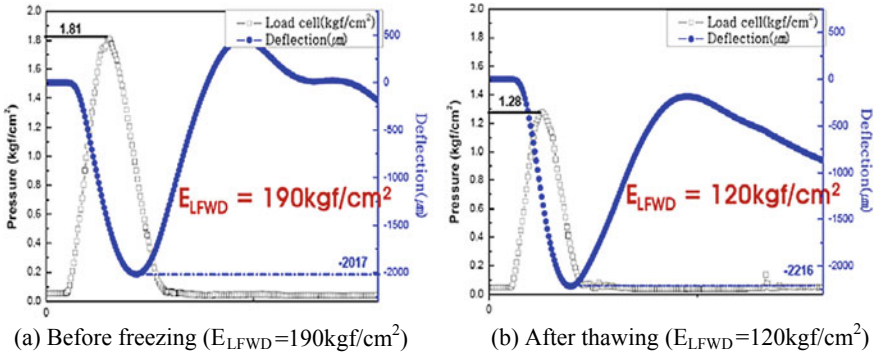


Fig. 5 CASE 1_(T20-A0), stiffness of roadbed

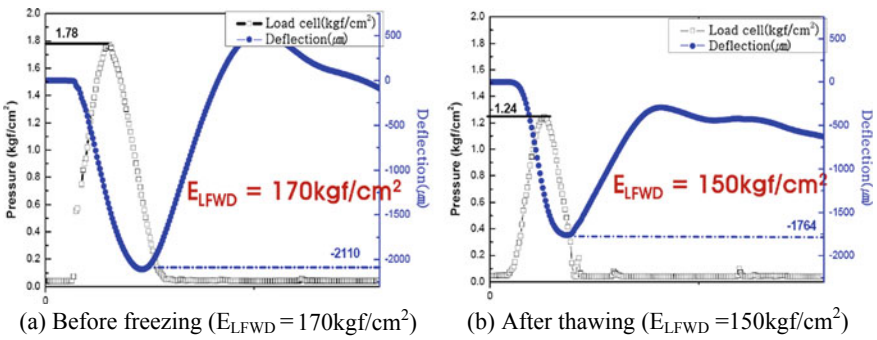


Fig. 6 CASE 2_(T15-A0), stiffness of roadbed

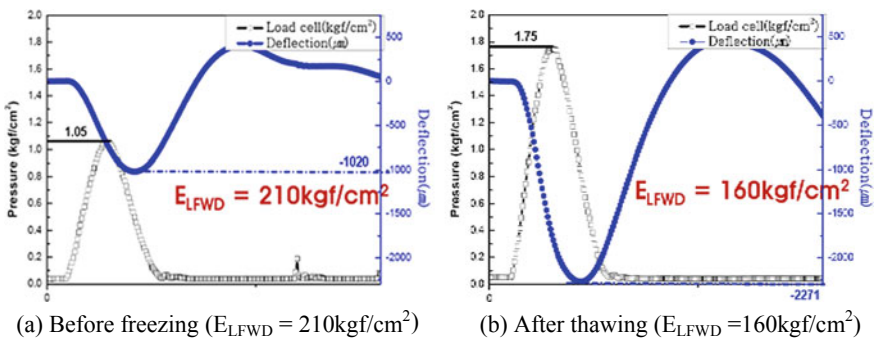


Fig. 7 CASE 3_(T15-A5), stiffness of roadbed

on the roadbed material prior to freezing and after thawing can be calculated by Eq. (2).

$$\text{SDR}(\%) = \frac{E_{\text{Before freezing}} - E_{\text{After thawing}}}{E_{\text{Before freezing}}} \quad (2)$$

The elastic moduli for both before freezing and after thawing of the compacted roadbed materials and SDR(%) are described in Table 4.

Based on the LFWD test results in Figs. 5 and 6 and Table 4, the freezing temperature for Case 1(−20 °C) gives the highest stiffness decrease rate, 36.8%, comparing with the test results of Case 2(−15 °C) and Case 3(−15 °C) with additional aggregate layer. This is the simple evidence of shear strength reduction and hence, the highway slope and the bearing capacity failure of roadbed could be occurred during the early spring season. In the case of Case 3, the modulus of elasticity before freezing is much higher than those of other two cases due to an additional layer of aggregate. However, the modulus of elasticity after thawing is greatly reduced because the moisture was migrated to the boundary between aggregate layer soil and top of subgrade during the freezing.

4 Conclusion

In this study, the laboratory model test which simulated the roadbed structure was conducted in the freezing chamber. The variation of heaving pressure with elapsed time for various roadbed conditions was determined through the laboratory model test. The loading pressure and deflection for the compacted roadbed materials prior to freezing and after thawing were determined by the application of LFWD. Based on the laboratory model test results, the following conclusions can be made.

1. The degree of air temperature, types of soil, and moisture content of soil are greatly influenced to the freezing temperature with respect to the compacted roadbed materials.
2. The heat transfer rate is greater at the roadbed surface and then slightly decreases with the depth of roadbed.
3. An additional thin layer of aggregate can reduce the heaving pressure greatly, can delay the time to reach the maximum heaving pressure.
4. The LFWD test is an efficient method to determine the loading pressure and deflection for the compacted roadbed materials and hence the modulus of elasticity can be obtained. The modulus of elasticity for the compacted roadbed material could be reduced in the range of 11.7–36.8% after one cycle of freezing and thawing process.

References

1. Ohrai T (1986) Experimental studies on the effect of ice and unfrozen water on the compressive strength of frozen soil. Ph.D. Dissertation, Hokkaido University, Sapporo, Japan
2. Takagi S (1965) Principles of frost heaving. US Army CRREL Res Rep 140:24
3. Olhoeft FR (1977) Electric prosperities of clay permafrost. *Can J Earth Sci* 14:16–21
4. Yong RN, Warkentin BP (1975) Soil properties and behaviour, Elsevier Scientific Publishing Company, 383–419
5. Yoder EJ, Witczak MW (1973) Principles of pavement design, 2nd edn. Wiley, New York
6. Goodier JN, Timoshenko SP (1982) Theory of elasticity, 3rd edn. McGraw-Hill, New York

The Effect of Different Additives on the Swelling Process of Heavy Clays



Alexey Kolos, Vera Alpysova, Grigoriy Osipov and Irina Levit

Abstract In areas where heavy clays predominate (clays with plasticity index of more than 27), engineers always face the problem of replacing soils when constructing a roadbed for railroads and highways. Transportation of suitable construction material, as a rule, is very expensive. Construction of the roadbed of railroads and highways, especially in the cold regions of the Russian Federation, is almost always accompanied by a shortage of soils with good physical and mechanical properties. As a rule, these areas are characterized by clay deposits with unfavorable properties: high degree of swelling, low hydration strength, poor compaction, etc. Such properties are also characteristic of heavy clays which are widespread not only in Russia but also abroad. These features of heavy clays do not allow them to be used in the construction of the roadbed of railroads and highways without taking measures to improve their properties. The same problem has been faced by the engineers involved in the construction of the railroad track on the Taman Peninsula. Heavy swelling clays are common for this area. In the summer of 2017, soil samples were taken from the Taman Peninsula and tested in the laboratories of St. Petersburg State Transport University (PGUPS). Physical and mechanical properties of heavy clays were studied as well as properties of reinforced clays. The research shows that the optimal method for improving physical and mechanical properties of heavy clays (swelling, deformability) is the creation of a composite material consisting of heavy clay with the addition of dust filled sand (10% of the mass) and grade M400 cement (3% of the weight). This technique is applicable to all areas where heavy clays are common.

Keywords Roadbed · Engineering material · Heavy clay · Clay swelling

A. Kolos (✉) · V. Alpysova · G. Osipov · I. Levit
Emperor Alexander I St. Petersburg State Transport University, Saint Petersburg, Russia
e-mail: kolos2004@inbox.ru

I. Levit
e-mail: alfanova.irina@gmail.com

© Springer Nature Singapore Pte Ltd. 2020
A. Petriaev and A. Konon (eds.), *Transportation Soil Engineering in Cold Regions*,
Volume 2, Lecture Notes in Civil Engineering 50,
https://doi.org/10.1007/978-981-15-0454-9_31

1 Introduction

A great amount of soil building materials is needed during the construction of railroad tracks and highways. In the regions of Russia with a long period of cold weather, which are the most suitable from the point of view of their transport development, there is a well-known problem of the lack of suitable soils for the construction of the roadbed. The most optimal scheme for soil transportation is the use of soil excavated from cuts or open pits to be further used in making fills. For cold regions, this is not always possible, as applied soil material often does not meet regulatory requirements, since it is characterized by high humidity, swelling and a significant decrease in strength during thawing. In this case, all additional amounts of soil material that complies with the standard requirements must be supplied from the deposits located in other regions with more favorable climatic conditions. Such organizational decision will result in longer construction period, significant increase in costs and additional traffic load for the existing railroad and highway network.

Such unfavorable construction properties are also characteristic of heavy clays widely distributed not only in Russia but also abroad. Their high plasticity, poor compaction, high degree of swelling and sharp decrease in hydration strength do not allow the use of heavy clays in the construction of roads and railroads without taking measures to improve their properties. At the same time, the source of heavy clays in the areas of construction work is sometimes significant, which dictates the urgency of finding methods to improve the properties of heavy clays for use in the construction of fills.

Heavy clays (with the plasticity index exceeding 27) have a number of negative physical and mechanical (construction) properties: high degree of swelling, increased plasticity, high adhesiveness, poor compaction, dramatic loss of strength and compaction at hydration, etc. That is why the use of heavy clays for the construction of fills is prohibited by the Russian and foreign standards [1–3]. In such cases, the delivered materials, complying with the regulatory requirements, are traditionally used for construction of the tracks.

This decision is the simplest but at the same time results in a number of significant problems. Availability of suitable local soil materials in the region of construction involves the need for developing new deposits and contributes to disturbing natural landscapes and hydro-geological conditions. If suitable local soil materials in the region of construction are unavailable, then they must be delivered from the sites, located tens or even hundreds kilometers away. Under such circumstances, the transportation scheme for the material deliveries to the construction site usually requires arranging temporary storage grounds for the soil materials (the so-called makeshift open pits), for accumulation of the necessary primary supplies of soil [4].

Arranging temporary storage grounds is associated with the need for additional temporary land acquisition and consequently with cultivation of occupied territories. In both cases we have one more problem, namely transportation and storage of the previously excavated heavy clays on specially allocated grounds.

Thus, the application of delivered materials for construction of fills, as well as storage of heavy clays on special landfills, leads to the essential growth of additional costs. The development and implementation of low-cost construction technologies for improvement of physical and mechanical properties of the heavy clays that permit the use of large amounts of such materials for railroad fills becomes an important scientific problem for construction and reconstruction of transport objects in case of limited financial resources.

2 Construction Properties of Heavy Clays—Research Findings

The efficiency of various construction technologies aimed at improvement of heavy clay characteristics greatly depends on the initial (natural) properties. Considering a large amount of excavated soils (exceeding 100 samples of undisturbed composition) from various bore holes and from various depths on the construction sites of the transport objects in the southern regions of Russia, research was conducted to determine physical and mechanical properties of initial heavy clays. The aim of the tests was to select individual varieties of soil masses possessing the same physical and mechanical properties. The data obtained during this research were compared with the results already published in [5–12]. Comparative analysis of experimental data gave a good correlation between the findings of performed investigations and the data, obtained by other authors. Elaboration of reinforcement methods (technologies) in order to improve physical and mechanical properties of heavy clays was the next stage, aimed at their further use during the construction of fills for the railroad tracks and highways.

On the basis of performed investigations, we can state that in the whole set of monoliths of undisturbed composition, the soils under consideration are represented by heavy, semi-solid, mid-swelling clays according to [13]. At the same time, two kinds of soils may be selected that possess other physical and mechanical properties. For the convenience of comparative analysis, they are conventionally designated as soil №1 and soil №2 (See Table 1).

According to Table 1, soil №1 differs from №2 in the following:

density of dry soil, and as a result, porosity factor. Soil №2 has porosity factor exceeding 1.0 (mean value-1.43), and therefore, these clays may be characterized as macro-porous soils.

plasticity index. Soil №1 has plasticity index equal to 29, close to the maximum value of 27, and therefore, it is classified according to [13], as heavy clay. At the same time, plasticity index of clay represented by soil №2 is 1.6 times as high. Therefore, one can expect that it is more subject to swelling, and this was confirmed by the test findings.

relative deformation of free swelling. Soil №1 has a mean value of relative deformation of free swelling equal to 0.105. According to [13], we can classify such clays

Table 1 Main mean values for physical and mechanical characteristics of the selected varieties of heavy clays with undisturbed composition

Parameter	Variety of soil	
	Soil №1	Soil №1
	Heavy, semi-solid, mid-swelling clay	Heavy, semi-solid, mid-swelling clay
Density, ρ , g/cm ³	1.81	1.68
Density of dry soil, g/cm ³	1.41	1.13
Porosity factor, e	0.94	1.42
Plasticity index, I_P , %	29	46
Fluidity index, I_L	0.02	0.23
Relative deformation of free swelling, ε_{SWO}	0.105	0.113
Maximum density under standard compaction, ρ_{d-max} , g/cm ³	1.47	1.30
Optimum moisture content, W_{opt} , %	29	34
Specific adhesion, C, kPa	71	45
The angle of internal friction, φ , deg.	28	16

as mid-swelling. Soil №2 has this value equal to 0.113, so we can also classify this clay as mid-swelling. However, the mean value of this parameter is very close to the limit value of 0.120. At this value, clays belong to the category of high swelling soils.

- in natural water content, the difference between soil №1 (28%) and soil №2 (48%) is by 1.7 times.
- strength properties: specific adhesion and angle of internal friction. Because of the lower porosity and lower natural water content, soil №1 has much higher strength properties. For example, specific adhesion values of soil №1 are 1.6 times as high, and values of angle of internal friction are 1.7 times as high compared to soil №2.

Based on this difference, these soils were subdivided into two main varieties in order to develop methods for improvement of physical and mechanical properties.

Soils №1 and №2 have such common features, as low density of dry soil and heterogeneity in depth, as well as poor compaction. The findings of standard compaction test showed that even 150 impacts in the installation for standard compaction result in non-uniform macro-porous structure, and the resulting maximum of density does not exceed 1.47 g/cm³.

One of the peculiarities of heavy clays is the significant influence of soaking process on physical and mechanical properties changes (degradation). Table 2 illustrates soil's physical and mechanical properties after testing free swelling of soils №1 and №2.

Table 2 Comparison of main physical and mechanical properties of soil following their saturation in the process of testing soil swelling

Parameter	Variety of soil			
	Soil №1		Soil №2	
	Before the free swelling test	After the free swelling test	Before the free swelling test	After the free swelling test
Density, ρ , g/cm ³	1.81	1.86	1.68	1.74
Natural water content, w , unit parts	0.28	0.39	0.48	0.59
Density of dry soil, ρ_d , g/cm ³	1.41	1.34	1.13	1.10
Porosity factor, e	0.94	1.06	1.42	1.52
Fluidity index, I_L	0.02	0.41	0.23	0.46
Specific adhesion, C , kPa	71	20	45	15
The angle of internal friction, φ , deg.	28	6	16	11

In Table 2, data analysis shows that under the saturation conditions, the soil hydration increases and swelling process occurs. This results in the loss of soil compaction—density of dry soil decreases while porosity increases. The main peculiarity of the saturation process is sufficient decrease in strength characteristics for both soils №1 and №2. In spite of the fact that after the swelling test, clays acquire tight plastic consistency their values of specific adhesion, and especially, the angle of internal friction become lower. The value of specific adhesion for the soil №1 decreased from 71 to 20 kPa, and for the soil №2—from 45 to 15 kPa. The angle of internal friction for soil №1 after the saturation was 6° in comparison with that of 28° under natural water content. For soil №2, these values are equal to 16° and 11°, respectively. Such low values for the angle of internal friction are characteristic of weak clay soils with fluid-plastic and fluid consistency and rarely occur in case of ordinary clay soils with tight plastic consistency, the latter being characteristic of heavy clays. Therefore, we can state that heavy clays selected for the tests are extremely sensitive toward increased water content, resulting in significant reduction of their strength properties. That is why they cannot be used in the constructions of fills for the railroad tracks and highways without additional measures for the improvement of their properties.

3 Methods for Improvement of Physical and Mechanical Properties of Heavy Clays

Measures for improvement of physical and mechanical properties of heavy clays intended for use in the roadway construction must provide: the uniform soil structure during compaction; high dry soil density during compaction; elimination of swelling during hydration; and elimination of significant decrease in strength and deformation characteristics under the increased hydration. Besides, it is recommended to reduce soil adhesiveness in order to avoid soil clinging to the roller of the soil-packing machine.

Elaboration of the reinforcement formula was aimed at meeting the following requirements: maximum use of local soil materials; selection of only domestic reinforcing materials; and mutual compatibility of all the materials used. All the materials and soils, used as additives, must be environmentally safe for the local area; the resulting material must be non-aggressive toward concrete, reinforced concrete and metal parts and constructions, aluminum and lead cable coatings. The costs of the additives used for reinforcement must be low. The preliminary experiments as well as the complex analysis [14–21] showed that cement and dust sands would be the optimal additives to heavy clays.

Sand and cement have different influence on the construction properties changes of heavy clays. Addition of sand to the mixture composition would change the particle-size distribution of heavy clays. The increase in the sand-particle percentage in the clay-sand mixture decreases its dispersion, total specific area and total surface activity of clay particles [22]. Table 3 provides six samples of local dust sand grain distribution.

Specific area of local dust sands (m^2/kg) was determined according to the Ladinsky formula [23]:

$$S = B \cdot K(a + 2b + 4c + 8d + 16e + 36d)/1000 \quad (1)$$

where B is empirical factor, assumed to be equal to 6.35 where specific area is designated in m^2/kg ; K —coefficient showing the shape and surface roughness of sand grains, taken as equal to 1.00; and a, b, c, d, e, f —individual remainder on the sieves (Table 3).

Therefore, the total specific area of the experimentally used dust sand was $0.115 \text{ m}^2/\text{g}$.

Table 3 Mean values of local dust sand grain distribution

Grain size, mm	5.0–2.5	2.5–1.25	1.25–0.63	0.63–0.315	0.315–0.16	<0.16
Particle remainder, %	1.1	50.9	114.2	265.6	271.8	296.4

An approximate assessment of surface activity of clay soils is based on the granulometric and mineralogical composition analysis [15]. Based on six sets of micro-aggregate analysis, clay soils contain: sand fraction (2–0.05)-10%; dust fraction (0.05–0.005)-28%; and clay fraction (<0.005)-6.25%. The mineralogical composition of sand particles includes minerals of quartz, feldspar and mica over 0.05 mm in size. These are the products of mechanical weathering. They have rigid crystal lattice, without any physical and chemical activity. The dust fraction is an intermediate one between sand and clay fractions. It includes quartz and feldspar, which retain their rigid crystal lattices because they are not affected by chemical weathering due to particle size over 0.001 mm. Mica's minerals, i.e., biotite, having particles 0.01 mm in size, do not resist chemical weathering. Because of chemical weathering of mica's minerals, dust fraction contains surface-active particles and possesses physical and chemical absorption ability.

The whole set of investigated soil materials consisting on average of 30% of montmorillonite minerals, 47% of hydro-micas and 23% of quartz, feldspars and micas had mean specific area of 428 m²/g. Addition of 10% of the dust sand into the mixture results in reduction in specific area by approximately 14% (the specific area of the mixture is 368 m²/g), which improves construction properties of heavy clays.

Mixture of dust sand and heavy clay has an ambiguous influence on the swelling process. With the plasticity index of the clay soil being less than 30, the addition of sand leads to increased swelling. The increased plasticity index (exceeding 30) and increased montmorillonite's content in clay soil result in the negligible increase in swelling [14]. At the same time, dust sand addition decreases soil's adhesiveness and provides much higher dry soil density during compaction.

The cement, being the hydraulic binder and during interaction with the highly dispersed montmorillonite's particles, provides the reinforcement of the clay soil coagulation structure [12, 14]. The cement blocks almost completely the swelling process and decreases the adhesiveness.

Affected by adverse hydro-meteorological conditions, cement and sand components of the mixture provide: formation of the uniform soil structure during compaction; increase in dry soil density of mixture; and increase in mechanical parameters stability (namely—the angle of internal friction, specific adhesiveness and deformation modulus).

During this investigation, the following methods for improvement of physical and mechanical properties of the heavy clays were considered:

- reinforcement of soil material by means of mixing it with cement grade M400 (3% of mass);
- addition of dust sand to the soil (10% of mass) in order to decrease material adhesiveness;
- simultaneous addition of dust sand (10% of mass) and cement grade M400 (3% of mass).

4 Reinforced Soils Properties Investigation Findings

Samples for the investigations were prepared from the mixtures with the compositions complying with the methods for improvement of physical and mechanical properties, mentioned above. Investigation of each method included finding a similar set of physical and mechanical characteristics for the purpose of comparative analysis. The results obtained made it possible to prove the optimum formula for soil mixtures and various additives aimed at their use in the fills construction.

The comparative data of the main soil characteristics are listed in Tables 4 and 5.

The following designations are used in Tables 4 and 5: G —initial ground soil (heavy clay) of undisturbed composition characterized by natural water content and porosity; $G(W)$ —initial soil (heavy clay) with water content after free swelling test;

Table 4 Comparative data on physical and mechanical properties for soil №1 and for mixture of soil №1, sand and cement

Soil property	Soil № 1 ($G1$)				
	$G1$	Water content after the free swelling test			
		$G1(W)$	$G1(S)$	$G1(C)$	$G1(CS)$
Density of dry soil, ρ_d , g/cm ³	1.41	1.34	1.39	1.46	1.41
Natural water content, w , unit parts	0.28	0.39	0.42	0.31	0.35
Porosity factor, e	0.94	1.06	0.97	0.88	0.95
Plasticity index, I_p , %	29	29	26	26	22
Relative deformation of free swelling, ε_{SWO}	0.105	–	0.049	0.027	0.009
Specific adhesion, C , kPa	71	20	20	56	94
The angle of internal friction, φ , deg.	28.0	6.0	6.4	20.4	15.5

Table 5 Comparative data on physical and mechanical properties for soil №2 and for mixture of soil №2, sand and cement

Soil property	Soil № 2 ($G2$)				
	$G2$	Water content after the free swelling test			
		$G2(W)$	$G2(S)$	$G2(C)$	$G2(CS)$
Density of dry soil, ρ_d , g/cm ³	1.13	1.10	1.23	1.21	1.29
Natural water content, w , unit parts	0.48	0.59	0.52	0.52	0.42
Porosity factor, e	1.42	1.52	1.23	1.28	1.13
Plasticity index, I_p , %	46	46	36	46	40
Relative deformation of free swelling, ε_{SWO}	0.113	–	0.060	0.057	0.039
Specific adhesion, C , kPa	45	15	31	85	90
The angle of internal friction, φ , deg.	15.8	11.2	8.3	14.1	25.6

$G(S)$ —heavy clay with addition of dust sand (10% of mass) whose density is close to an optimum; $G(C)$ —heavy clay with addition of cement grade M400 (3% of mass) whose density is close to an optimum; and $G(CS)$ —mixture of heavy clay, dust sand (10% of mass) and cement grade M400 addition (3% of mass) whose density is close to an optimum. G designates the selected kind of ground soil: for soil №1- $G1$ and for soil №2- $G2$, respectively.

The analysis of data from Tables 4 and 5 shows that the use of technologies for improvement of soil's characteristics results in increased density for reinforced soils achieved even after their saturation. For the mixtures of soils №1 and №2, the density of dry soil after free swelling tests (after saturation for 3 days) appeared to be higher than that for non-reinforced soils under similar conditions. This means that addition of cement or dust sand or their mixtures with heavy clay decreases decompaction of the samples during saturation because of their lower sensitivity toward free swelling. This fact was proved during determination of the relative strain index for free swelling (fifth parameter in the first column, Tables 4 and 5). The best results are achieved by the mixture of soil with additives of dust sand (10% of mass) and of cement grade M400 (3% of mass).

The investigation of plasticity properties of heavy clays showed that plasticity index for various methods of reinforcement generally decreases (Tables 4 and 5), but does not change significantly. In soils reinforced by means of dust sand (10% of mass) plasticity index decreased for soil №1 from 29 to 26, and for soil №2—from 46 to 36, respectively. It should be mentioned that for clays reinforced with cement additive, this value was determined only at the moment of mixture preparation. As the time passed, it was impossible to determine the plasticity index because soil strength increased sharply so this value could not be considered as the defining one from the point of view of fill construction.

For the development of methods improving physical and mechanical properties, it would be important to select the one that minimizes or even completely eliminates deformations due to soil swelling. Non-swelling soils are recommended for use in construction of fills, i.e., the soils, having the index of relative deformation for free swelling process not more than 0.04 [1]. The results of studies of the swelling properties of the reinforced soils are given in Tables 4 and 5. These data show that such values can be achieved for soils, reinforced through simultaneous addition of the dust sand (10% of mass) and of cement grade M400 (3% of mass). This method appears to be the basic one, as it solves the problem of heavy clays swelling.

The main characteristics that provide strength and stability of fills comprise the strength properties of soils: specific adhesion and angle of internal friction. Maintaining these properties in soil material affected by adverse factors, i.e., increased water content, is very important.

As a result of studies, it became evident that the soils, remaining in undisturbed state and possessing natural density and water content show sufficiently high strength characteristics, but their hydration would lead to the decrease in both the specific adhesion and the angle of internal friction. In this case, the above-mentioned soils in

Table 6 Shear resistance of soils, τ , kPa under the normal load, $\sigma_n = 15$ kPa

The reinforcement method	Shear resistance, τ kPa, under the normal load, $\sigma_n = 15$ kPa, for the sample	
	Soil №1	Soil №2
Non-reinforced soil	79.0	49.7
Non-reinforced soil after saturation under the swelling test	21.2	17.7
Soil, reinforced with addition of dusty sand (10% of mass)	21.7	32.7
Soil, reinforced with addition of cement grade M400 (3% of mass)	61.9	88.8
The ground soil, reinforced with additives of dusty sand (10% of mass) and of cement grade M400 (3% of mass)	97.8	97.2

hydrated state and after the swelling test may be classified as weak clay soils, due to extremely low value of the internal friction angle. That is why the development of a technology for reinforcement of soils in order to eliminate humidifying effect on the strength properties of clays was one of the main purposes of this study.

The results of shear resistance tests (the last two lines in Tables 4 and 5) clearly showed the increase in the strength properties of reinforced soils following water content growth. The largest reinforcement effect for the soils is achieved by means of dust sand (10% of mass) and cement grade M400 (3% of mass) additives. This conclusion is proved in Table 6, where shear resistance for reinforced soils under the vertical load of 15 kPa is given.

5 Conclusion

The results of the studies proved that the best values of physical and mechanical properties improvement for heavy clays were achieved by means of simultaneous addition of the dusty sand (10% of mass) and of cement grade M400 (3% of mass). Such soils are classified according to [13] as non-swelling. This technical solution decreases soil adhesiveness, thus reducing clinging of clay to the rollers of the soil compacting machine. The shear resistance of reinforced soil under the normal load of 15 kPa and after 3 days of saturation gives the mean value of 97 kPa, providing the stability of roadbed slopes and their bearing strength.

On the basis of performed studies, formulas of composite mixtures are recommended depending on plasticity index for heavy clay used (see Table 7).

Table 7 Recommended formulas of composite mixtures

№ of composition	Composition	Content % of mass
1	Heavy clays, $30 < I_p \leq 35$	90.0–93.0
	Dust sand	5.0–7.5
	Cement M400	2.0–2.5
2	Heavy clays, IP > 35	87.0–90.0
	Dust sand	7.5–10.0
	Cement M400	2.5–3.0

References

1. Set of rules (2015) SP 238.1326000.2015 Railway Track. Ministry of Transport of the Russian Federation. Moscow. p 71
2. Directive Deutsche Bahn Gruppe Ril 836.0501 Earthworks. Mound Principles
3. Standards of the International Union of Railways (UIC) UIC 719R (2008) Earthworks and ballast section for railway tracks
4. Prokudin IV, Spiridonov ES, Grachev IA, Kolos AF (2008) Organization of the construction and reconstruction of railways. Under the editorship of Prokudin IV, Educational and methodological center for education on the railway transport, p 736
5. Dashko RE, Shidlovskaya AV Physico-chemical nature of swelling and osmotic shrinkage of clay rocks at the base of structures based on the results of experimental studies. Zapiski Mining Institute, vol 200. pp 193–200
6. Osipov VI (1979) The nature of the strength and deformation properties of clay rocks. Publishing House of Moscow State University, Moscow, p 235
7. Zvereva IA, Lbova DS, Kachenov VI (2016) Study of the swelling of clay soils as the foundations of structures. Modern technologies in construction. Theory and practice pp 420–423
8. Danilov VI et al. (1988) On soil softening under the influence of the processes of swelling—shrinkage. Soil Sci J 6:59–70
9. Egorov YK, Pakhomov SI, Kail EV (1988) Investigation of the properties of swelling soils, No. 88–5. TSNTI, Stavropol, p 3
10. Christodoulis J (2015) Engineering properties and shrinkage limit of swelling soils in Greece. J Earth Sci Climatic Chang 6(5):1–6
11. Osipov VI, Nguen NB, Rumjantseva NA (1987) Cyclic swelling of clays. Appl Clay Sci, Amsterdam pp 363–374 Elsevier Science Publishers B. V.
12. Hashim R, Muntohar A, Al-Rawas AA, Goosen MFA (2006) Swelling rate of expansive clay soils. Expansive soils: recent advances in characterization and treatment, pp. 139–148
13. GOST 25100-2011 (2018) Soils Classification. Standardinform, Moscow p 38
14. Lazorenko GI (2011) Theoretical study of the effect of nano-additives on the physical properties of montmorillonite clays. Don. Eng J, Rostov-on-Don pp 100–103
15. Omar M, Shanableh A, Al Zaylaie M (2016) Modification of the swelling characteristics and phosphorus retention of bentonite clay using alum. Soils Found 56(5):861–868
16. Mirzababaeia M, Arulrajahb A, Oustonc M (2017) Polymers for stabilization of soft clay soils. Procedia Eng 189:25–32
17. Estabragh AR, Moghadam M, Javadi AA (2013) Effect of different types of wetting fluids on the behaviour of expansive soil during wetting and drying. Soils Found 53(5):617–627
18. Phanikumara BR, Singlab R (2016) Swell-consolidation characteristics of fibre-reinforced expansive soils. Soils Found 56(1):138–143
19. Sasaniana S, Newsonb TA (2014) Basic parameters governing the behaviour of cement-treated clays. Soils Found 54(2):209–224

20. Kamei T, Ahmedb A, Ugai K (2013) Durability of soft clay soil stabilized with recycled Bassanite and furnace cement mixtures. *Soils Found* 53(1):155–165
21. Ma C, Qin Z, Zhuang Y, Chen L, Chen B (2015) Influence of sodium silicate and promoters on unconfined compressive strength of Portland cement-stabilized clay. *Soils Found* 55(5):1222–1232
22. Kotelnikov DD, Konyukhov AI (1986) Clay minerals of sedimentary rocks. Nedra, Moscow, p 247
23. Ladinsky AS (1932) Standard case/Ing. A. Ladinsky. East Inst. – Sverdlovsk Uralogiz, Moscow

Geocoprotective Materials, Structures and Technologies for Transportation

The Method of Estimation of the Technical Conditions of Transport Facilities Used in Cold Regions After the Accidents Caused by Temperature Anomalies



Nikolay Gusev, Larisa Svatovskaya and Alexandr Kucherenko

Abstract The object of the research is the load-bearing structures of transport facilities used in cold regions. The subject of the research is the method and means of assessing the technical conditions of load-bearing structures of transport facilities at the extremely low temperatures. The aim of the research is to ensure the recording and retaining the transport facilities state parameters at the temperatures below -40 °C. The analysis of the specific use of transport facilities in cold regions and the systems employed for technical conditions control has been carried out. The results obtained gave the possibility to propose some technical designs for transducers capable of recording both current and maximum/minimum values of the transport facilities state parameters caused by the extremely low temperatures. A method for estimating the parameters of the stress-strain state of the load-bearing structures of transport facilities at the moment of accidents caused by temperature anomalies is proposed. The method can be used even in the conditions of the monitoring systems secondary equipment failure.

Keywords Temperature anomalies · Negative temperatures · Monitoring of technical condition of transport facilities · Stress-strain state · Primary string converters · Intelligent sensors · Secondary equipment · Cable network

1 Introduction

Modern transport facilities in most cases are potentially dangerous, technically complex and unique objects [1–3]. There exist wide experiences of building technical condition control of this class [4–26] by means of monitoring systems. In transport systems such as bridges, they are called bridge monitoring systems of continuous operation (SCMB) [5, 6]. SCMB systems are usually developed on the basis of

N. Gusev · A. Kucherenko (✉)

Military Space Academy Named After A.F. Mozhaysky, St. Petersburg 197198, Russia
e-mail: kucher_90@bk.ru

L. Svatovskaya

Emperor Alexander I St. Petersburg State Transport University, St. Petersburg 190031, Russia

© Springer Nature Singapore Pte Ltd. 2020

A. Petriaev and A. Konon (eds.), *Transportation Soil Engineering in Cold Regions*,

Volume 2, Lecture Notes in Civil Engineering 50,

https://doi.org/10.1007/978-981-15-0454-9_32

string measuring transducers with pulse excitation (SMTI) [1–3] allowing to control a wide range of parameters P of the stress-strain state (SSS) of building structures (stress, deformation and displacement, efforts in the reinforcement, etc.) in different measurement ranges [1–3]. Each SMTI has an individual calibration produced at the expense of the string vibration excitation by means of standard pulses. The pulses parameters provide the value of the damped string oscillations amplitude in the range from y_{\max} to y_{\min} during the entire measurement interval. To measure the relative linear compression or tension strains of concrete structures as well as non-bending metal structures linear strain SMTI measuring string (CLDS) are designed, the range of operating temperatures being -30 to $+40$ °C. The SCMB systems also include commuting and secondary equipment (specialized period more) and cable network [3].

Methods of measurement by means of SMIT are based on the dependence of the frequency f (or period T) of the frequency resonator (string) oscillation on the string tension σ (the first method) or its length l (the second method) which in each particular string converter is proportional to the measured parameter P SSS.

In the practice of creating SCMB systems, the first method of measurement became especially widespread. However, when it is implemented in case of a change in ambient temperature, there appears a change in the linear dimensions of the SMTI body and the string itself, as well as a change in the modulus of elasticity of the materials they are made of, which results in a temperature error in the physical quantity measurement P [1–3].

The expression for the relative error in determining the frequency f caused by the changes in ambient temperature is [1]:

$$\delta_t^0 = (\alpha_c - \alpha_s)l \frac{\Delta t^\circ}{2} \Delta l_0 \quad (1)$$

where α_c , α_s —temperature coefficients of the body and string elongation; Δl_0 —maximum working extension of the string caused by the measured physical quantity P ; Δt° —the increment of temperature; l —the length of the string.

Analysis of the expression (1) suggests that:

First, the string oscillation frequency depends on both the Δt° and Δl_0 parameters.

Secondly, the relative error in determining the frequency f depends on the difference $(\alpha_c - \alpha_s)$ between the temperature coefficients of the body and the string elongation of the SMTI which depend on the temperature themselves. So the value of the coefficient α_s for the string material (steel grade 45G2) in the range of SMTI operating temperatures varies—11.3 to 11.6 mkK⁻¹ (i.e., 1.7%), and the value of the coefficient α_c for the body material (steel grade 40H) in the range of operating temperatures of SMTI varies—11.8 to 12.0 mkK⁻¹ (i.e., 2.7%). In this case, the temperature elongation of the CLDS-150 SMTI string up to 0.11 mm, and the body—0.14 mm takes place, which is commensurate with the maximum SMTI string elongation in the operating range of the physical quantity P measurement ($\Delta l_0 = 0.24$ mm) [1].

Thirdly, the expression (1) does not take into account the rate of the temperature change of the SMTI during the measurement in extreme situations which can be tens or even hundreds of deg/sec.

The negative outdoor temperature in the northern climatic zone of Russia with the most severe conditions can be -54 to -71 °C [12, 26]. For example, in the area of construction of the bridge across the river Lena in the Tabaginsky alignment the air temperature reaches -65 °C in winter and $+35$ °C in summer.

Analysis of the operating temperature range of the SMTI (-30 to $+40$ °C) shows that it is much more narrow than the climatic temperature range in cold regions (-70 to $+35$ °C) and the range of the possible temperatures in extreme situations. Besides that SMTI are designed to operate in the conditions of a relatively slow daily change of air temperature. In case of an accident at a transport facility, which may be accompanied by a sudden change in temperature the performance of the SCMB systems based on SMTI has not been studied either theoretically or experimentally.

The purpose of this investigation is to analyze the influence a sharp change in temperature at the transport facilities both in a larger side (at an explosion or fire) and in a smaller one (in cryogenic emissions) on the metrological properties of SMTI.

2 Materials and Methods

The investigations were carried out according to the standard method [1] on the SMTI of the CLDS-150 type with the parameters provided by the standards (string length—150 mm, constructive gap $\delta=0,4$ mm, the range of output signal periods—450 to 1250 mks, operating temperature range -30 to $+40$ °C [1]).

The experimental installation consisted of the following devices and equipment: specialized periodometer (PCP-1); electronic thermometer Rexant 70-0501 (temperature measurement range -50 to $+120$ °C); cryogenic installation DFC-84EC (minimum temperature -86 °C); heating element THERMOWATT RCA PA (power 1500 W); laboratory capacity (volume 20 l) with the antifreeze Aga Z42 (temperature range -42 to $+123$ °C).

During the experiment, we have determined:

- The dependence of the output signal period of the SMTI on the temperature difference of the medium in which it was placed and the rate of its change;
- The temperature stabilization time of SMTI.

The experiment was conducted in four stages.

During the first three stages, SMTI was immersed into a laboratory container with antifreeze AgaZ42 at the initial t_{init}° and the final t_{fin}° temperature values -40 to $+80$ °C, the values t_{init}° and t_{fin}° being given with increments of 20 °C. The temperature difference was given with a span $\Delta t^{\circ}=20$ to 120 °C: at the first stage from smaller values to larger ($\uparrow \Delta t^{\circ}$); at the second one—from larger values to smaller ($\downarrow \Delta t^{\circ}$). At the same time, at the each stage the SMTI was maintained up to the complete stabilization (during 30 min).

At the third stage, the temperature of the working fluid was being increased monotonically at the rate of $-2.3-2.5$ °C/min.

At the fourth stage, the time of temperature stabilization of SMTI depending on t_{init}° and t_{fin}° of the antifreeze was determined. The values of t_{init}° and t_{fin}° were given with the increments of 20 °C. The temperature difference of $\uparrow\Delta t^{\circ}$ and $\downarrow\Delta t^{\circ}$ was given with the span of $\Delta t^{\circ}-20$ to 120 °C.

3 Results

The results of the experiment (See Figs. 1, 2, 3 and 4).

The results of the investigation presented in Figs. 1, 2, 3 and 4 show that:

1. At abrupt change of SMTI temperature both at $\uparrow\Delta t^{\circ}$ (see Figs. 1.1, 1.2, 3.2) and at $\downarrow\Delta t^{\circ}$ (see Figs. 1.3, 1.4, 1.5, 3.1) the T value of the output signal of the SMTI changes abruptly during the first 3–7 s. Then a smooth recovery (stabilization) in the range of 20–30 min takes place.
2. With a sudden change in SMTI temperature at $\uparrow\Delta t^{\circ}$ (see Figs. 1.1, 1.2, 3.2) the value of T decreases and when the temperature changes at $\downarrow\Delta t^{\circ}$ (see Figs. 1.3, 1.4, 1.5, 3.1)—increases.
3. In case of a sudden change in the SMTI temperature, both at $\downarrow\Delta t^{\circ}$ and $\uparrow\Delta t^{\circ}$ in the operating temperature range of the SMTI (-30 to $+40$ °C) the relative measurement error of the SMTI during the first 3–7 s exceeds 22% (see Figs. 1, 3).

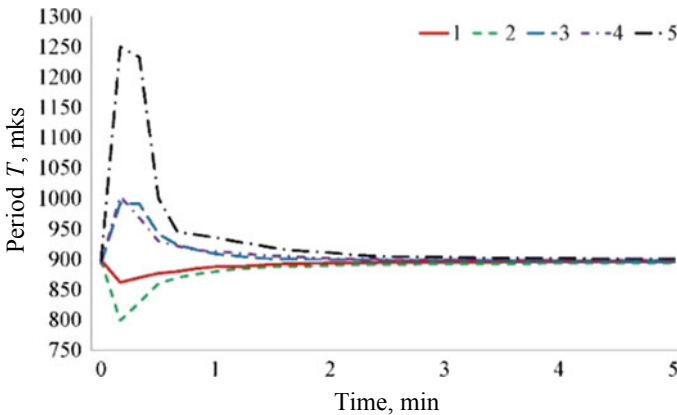


Fig. 1 Experimental dependences of $T(t)$ for SMTI circuit at an abrupt change in temperature: (1) from $t_{\text{init}}^{\circ} = +20$ °C to $t_{\text{fin}}^{\circ} = +40$ °C, (2) from $t_{\text{init}}^{\circ} = +20$ °C to $t_{\text{fin}}^{\circ} = +80$ °C, (3) from $t_{\text{init}}^{\circ} = +60$ °C to $t_{\text{fin}}^{\circ} = +20$ °C, (4) from $t_{\text{init}}^{\circ} = +80$ °C to $t_{\text{fin}}^{\circ} = +20$ °C; (6) from $t_{\text{init}}^{\circ} = +20$ °C to $t_{\text{fin}}^{\circ} = -40$ °C

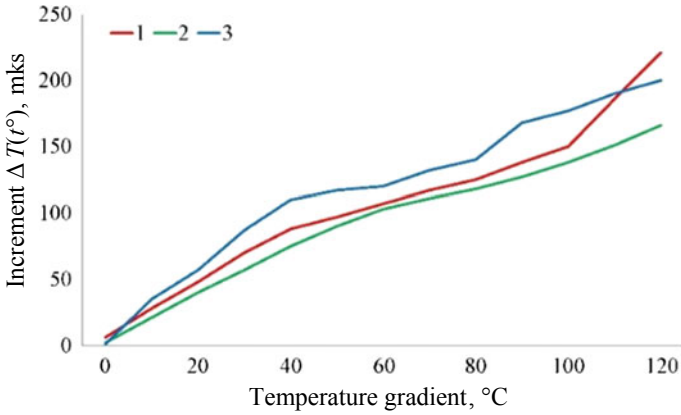


Fig. 2 Experimental dependences $\Delta T(t^\circ)$ at an abrupt change in temperature with increments of 20 °C at: (1) $t_{init}^\circ = -40$ °C; (2) $t_{init}^\circ = -20$ °C; (3) $t_{init}^\circ = +80$ °C

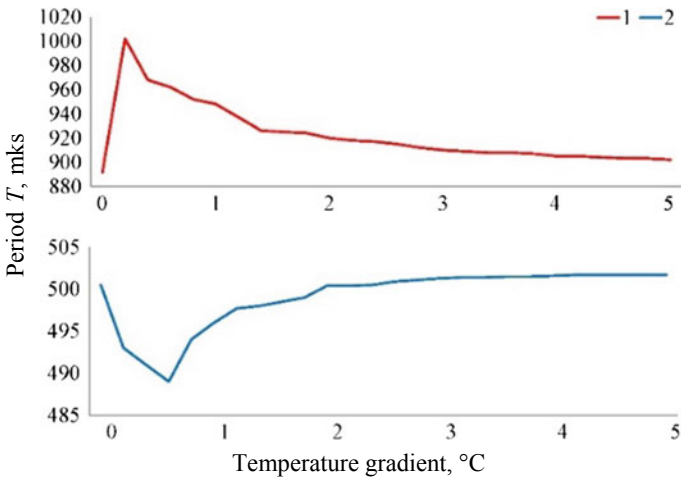


Fig. 3 Experimental dependences of $T(t)$: (1) at an abrupt temperature change +80 to +20 °C for CLDS-150; (2) at an abrupt change of temperature from $t_{init}^\circ = +20$ °C to $t_{fin}^\circ = +60$ °C for CDS-3

4. At a slow monotonic temperature change in the working temperature range at a rate of 2.3–2.5 °C/min from $t_{init}^\circ = -30$ °C to $t_{fin}^\circ = +40$ °C relative measurement error remains within the certified values of SMTI and does not exceed 0.4%. However, when the t_{fin}° value exceeds +40 °C, the relative measurement error increases sharply (see Fig. 4).
5. The relative error of the first method of measurement depends on the difference between the values of $t_{init}^\circ - t_{fin}^\circ$ (see Figs. 1, 2, 3), the rate of temperature change (see Fig. 4) and the design features of SMTI (see Fig. 3).

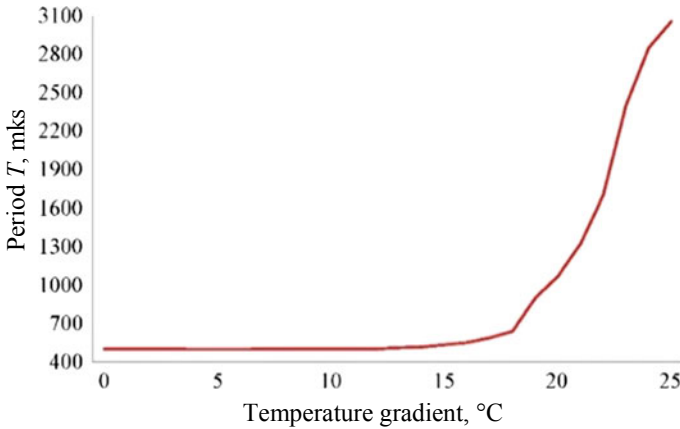


Fig. 4 Experimental dependences of $T(t)$ at a monotonic temperature change at a rate of 2.3–2.5 °C/min from $t_{\text{init}}^{\circ} = +20$ °C to $t_{\text{fin}}^{\circ} = +80$ °C for CLDS-150

6. With a slow monotonic temperature change at the rate of 2.3–2.5 °C/min when the temperature exceeds the value of +60 °C, the SMTI (CLDS-150) (see Fig. 4) loses its efficiency due to the amplitude increase of the string y_{max} more than the value of the constructive gap δ of the SMTI.
7. Temperature stabilization of the SMTI after a sudden change in temperature occurs within 20–30 min, depending on the values of t_{init}° and t_{fin}° and the design features of SMTI.

4 Discussion

Accidents at transport facilities in cold regions may be accompanied by:

- (a) A sudden change in the SSS of load-bearing structures with a random change in time;
- (b) An abrupt change of the ambient temperature and load-bearing structures;
- (c) A breakage or damage of the cable network between the components of the SCMB systems or emergency power disconnection of the SCMB systems.

In case of accidents at transport facilities accompanied by temperature anomalies, the first method of the measurement by means of SMTI is not applicable on the following grounds:

1. The events pointed out in the items (a) and (b) exclude the possibility of the SSS control parameters of the transport construction directly at the moment of accident as there is no possibility of the SSS parameters component division caused by the simultaneous change of parameters Δt° and Δl_0 .

2. The event pointed out in the item (c) exclude the possibility the SSS parameters control of the transport construction directly at the moment of the accident because of the termination of the power supply of the secondary equipment of the SCMB systems.

5 Conclusions

The determining parameters in assessing the operational suitability of the load-bearing structures of transport facilities after the accidents, including those caused by temperature anomalies, are the maximum and minimum values of the SSS parameters directly at the moment of the accidents.

A significant disadvantage of the SMTI implementing the first method of the measurement is that the registration of the measured parameters is possible only when the secondary equipment is turned on. In the time intervals, when the secondary equipment is switched off or damaged the information from the sensor are stopped. However, in these time intervals the excess of the maximum values of the building structures stress-strain state parameters, i.e., their maximum permissible values, is possible.

To eliminate the disadvantages of SMTI implementing the first method of measurement, the authors have developed the theoretical basis and proposed technical solutions for SMTI, implementing the second method of measurement. They are capable of registering at least the maximum and minimum values of the transport facilities structures state parameters at the moment of the accidents, and the current values of these parameters after the temperature stabilization of the SMTI. The authors have proposed a method for estimating the stress-strain state parameters of load-bearing structures of transport structures directly at the moment of accidents caused by temperature anomalies, even if the failure of the secondary equipment systems of SCMB takes place. The essence of the method consists in the use of intelligent primary converters with mechanical memorization of the maximum and minimum values of the controlled parameters of SSS with time-spaced processes of fixing these parameters and the results of their measurements (see Fig. 5).

The operation of SMTI of SCMB systems, implementing the method of measurement based on the dependence of the frequency f (or period T) oscillations of the frequency resonator (string) on the tension of the string σ (see Fig. 6).



Fig. 5 Intelligent SMTI with mechanical memorization of the maximum and minimum values of the controlled SSS parameter

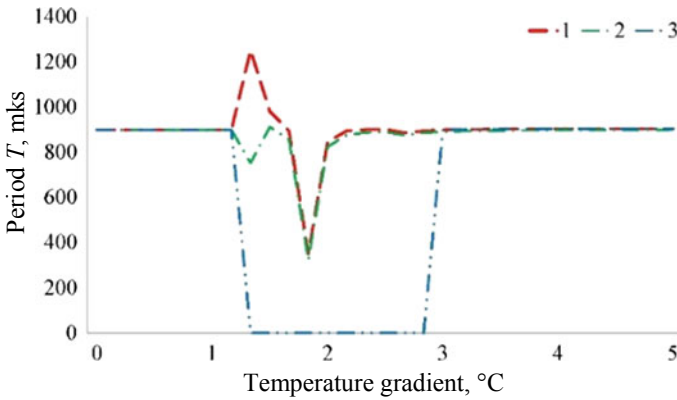


Fig. 6 Diagrams operation of SMTI of SCMB systems, implementing the first method of measurement: (1) the dependence of the informative parameter $T(t)$ at the output of the SMTI in the absence of a sudden change in temperature; (2) the dependence of the informative parameter $T(t)$ at the output of the SMTI at a sudden change in temperature from $t_{init}^{\circ} = +80^{\circ}\text{C}$ to $t_{fin}^{\circ} = -40^{\circ}\text{C}$; (3) the dependence of the informative parameter $T(t)$ at the output of the SMTI in case of an emergency power disconnection

The method proposed allows (see Fig. 7) to estimate, at least, the maximum and minimum parameter values of a transport structure design state at the moment of the accident, and the current values of these parameters after temperature stabilization of SMTI, which is reached by separation the processes of fixing these parameters and their measurement in time.

The method proposed by our group makes it possible to estimate the maximum and minimum values of the parameters of a transport construction design state, even

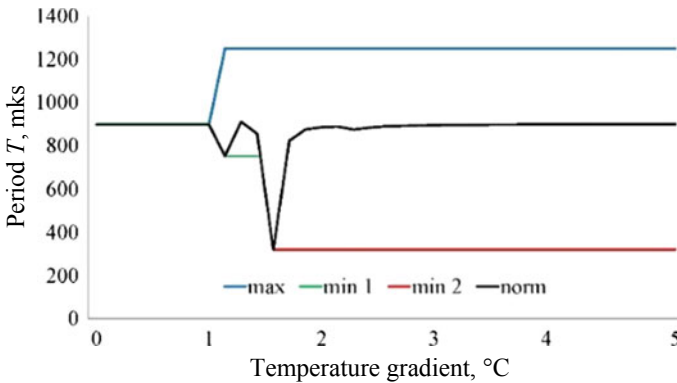


Fig. 7 Intelligent SMTI operation diagrams: the dependence of the informative parameter $T(t)$ at the SMTI outputs after a sudden temperature change from $t_{init}^{\circ} = +80^{\circ}\text{C}$ to $t_{fin}^{\circ} = -40^{\circ}\text{C}$

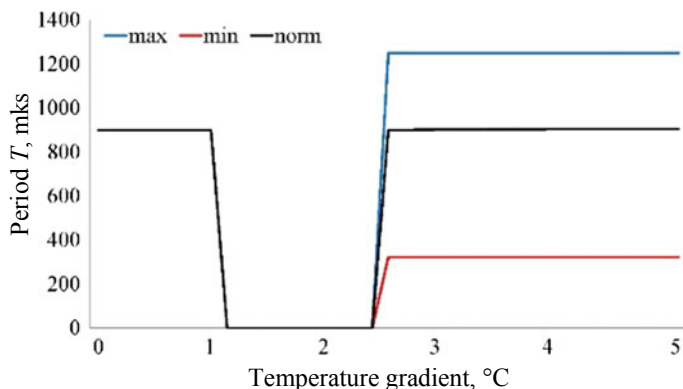


Fig. 8 Intelligent SMTI operation diagram: the dependence of the informative parameter $T(t)$ at the SIPI outputs when power supply is lost

in case when the secondary equipment of the SCMB system will be de-energized at the moment of the accident (see Fig. 8).

References

1. Gusev N, Svatovskaya L, Kucherenko A (2018) Effect of changing of the parameters of the cable network of monitoring systems of high-rise buildings on the basis of string converters on their operability. In: E3S web of conferences, vol 33, pp 02069. <https://doi.org/10.1051/e3sconf/20183302069>
2. Gusev NN (2007) Method and means of restoration of operability of monitoring systems of safety of buildings and constructions of hazardous production facilities and hydraulic engineering structures at liquidation of consequences of emergency situations. In: XXI century: man society science. Collection of scientific articles. Military Academy of communications. NWB RRI MIA of Russia, Saint-Petersburg, pp 31–34
3. Gusev NN (2006) Problems of creation and operation of the information system for monitoring the safety of buildings and structures of hazardous production facilities and hydraulic structures. In: Regional informatics—2006. Proceedings of the anniversary X international conference. Saint-Petersburg Institute of Informatics and automation of the RAS, Saint-Petersburg, 24–26 October 2006
4. Federal law of the Russian Federation of 30 December 2009 No 384-FL (2009) “Technical regulations on the safety of buildings and structures”. Moscow, 22 p
5. Industry road regulations ODN 218.017-03 (2004) Guidelines for the assessment of transport and operational status of bridge structures. Federal Road Agency, Moscow, 47 p
6. Branch road of the methodological document ODM 218.4.002-2008 (2008) Guidelines for monitoring the state of the bridge structures in operation. Federal Road Agency, Moscow, 46 p
7. Bazarov AD (2014) Development of hardware-software complex for control of dynamic characteristics of engineering structures. In: Bazarov AD (ed) Thesis for the degree of candidate of technical sciences: 05.11.13. Tomsk, 134 p
8. Korgina MA (2008) Assessment of stress-strain state of bearing structures of buildings and structures in the course of monitoring their technical condition. In: Korgina MA (ed) Thesis for the degree of candidate of technical sciences: 05.23.01. Moscow, 225 p

9. Lisov DA Ensuring structural safety of buildings and structures with long-span structures. In: PFUR. Moscow city conference of young scientists "Modern problems of engineering research", Moscow, 24 p
10. Hiller B, Yamaev CK (2016) Development and full-scale testing of automated deformation control system. Bulletin SSUG and T, Novosibirsk, pp 48–61
11. Lisov DA (2011) Automated control of structural safety of unique objects, including high-rise and long-span. In: Gurev VV, Dorofeev VM, Lisov DA, Nazmov NV (eds) Structural mechanics of engineering constructions and buildings. PFUR, Moscow, pp. 55–61
12. Kiseleva LV (2002) Climatology and meteorology on a railway transportation. In: Kiseleva LV, Vasilev SV, Garanina TV (eds) EMS MPS, Moscow, 189 p
13. Peeters B (2000) System Identification and damage detection in civil engineering. In: Peeters B (ed). Katholieke Universiteit Leuven, Belgium, 256 p
14. Olson LD (2005) Dynamic bridge substructure evaluation and monitoring. In: Olson LD (ed) US Department of Transportation, Federal Highway Administration, USA, 219 p
15. Zinovev RK (2005) Modernization of string measuring instruments for monitoring the safety of power facilities. Bulletin PFUR. Series "Engineering research", Moscow, pp 64–66
16. Glisic B, Inaudi D, Nan C (2002) Piles monitoring during the axial compression, pullout and flexure test using fiber optic sensors. In: 81st Annual Meeting of the Transportation Research Board (TRB), on CD paper number 02-2701, Washington DC, 13–17 Jan 2002
17. Lynch JP (2007) An overview of wireless structural health monitoring for civil structures. R Soc. <https://doi.org/10.1098/rsta.2006.1932>
18. Maeck J (2003) Damage assessment of civil engineering structures by vibration monitoring. In: Maeck J (ed). Katholieke Universiteit Leuven, Belgium, 224 p
19. Rades M (2010) Mechanical vibrations II. Structural dynamic modeling. In: Rades M (ed). University Politehnica Bucharest, Rumania, 354 p
20. Swartz RA (2008) Damage characterization of the Z24 bridge by transfer function pole migration. In: Swartz RA, Lynch JP (eds) Proceedings of the international modal analysis conference (IMAC) Orlando, Florida, 4–6 Feb 2008, vol XXVI, 13 p
21. Wenzel H (2005) Ambient vibration monitoring. In: Wenzel H, Pichler D (eds). John Wiley & Sons Ltd, Chichester, England, 291 p
22. Mechanical properties of structural materials. In: Fridlyander IN (ed) Collection of proceedings. Metallurgy, Moscow, 432 p
23. Wiberg J (2006) Bridge monitoring to allow for reliable dynamic FE modeling. In: Wiberg J (ed). Stockholm, Sweden, 175 p
24. Straser EG, Kiremidjian AS (1998) A modular, wireless damage monitoring system for structures. In: Report no 128, John A. Blume Earthquake Engineering Center, Department of Civil and Environmental Engineering, Stanford University, Stanford, CA
25. Mary TA, Evans JSO, Vogt T, Sleight AW (1996) Negative thermal expansion from 0.3 to 1050 Kelvin in ZrW₂O₈/. vol 272, pp 90–92. <https://doi.org/10.1126/science.272.5258.90>
26. Construction Regulations SP 52-105-2009. Reinforced concrete structures in cold climates and on permafrost soils, PC "CDP", Moscow, 36 p

Geocoprotective Building Structures for Transport Construction Using Mineral Technogenic Silicates and Their Properties



Maria Shershneva , Ivan Kozlov , Galina Pankrateva 
and Ivan Drobyshev 

Abstract The relevance of the problem is due to the formation and storage of multi-tonnage mineral technogenic silicates obtained as a result of the construction and mining industry. The aim of this work is to identify useful research geocoprotective properties of technogenic silicates, as well as in the development of technological solutions for their application in cold regions. The objects of study selected waste of heavy concrete and chlorine-containing crushed stone. The study used methods to identify geocoprotective properties and iodometric method for determining microbial numbers. Discovered and investigated the properties of the waste heavy concrete and rubble floristerias determine the possibility of their use in geocoprotective structures. In this case, such structures as the railway embankment may have geocoprotective function. The article is aimed at studying the possibility of using mineral technogenic silicates in the body of the railway to reduce the negative impact of pollution of different nature. The article presents technological solutions for the use of heavy concrete and rubble floristerias having geocoprotective properties. The article gives formulas for calculating the required number of mineral technogenic silicates, to make the structures geocoprotective properties, and the calculation results. The materials of the article can be used to develop technological solutions for the utilization of mineral technogenic silicates in their useful application in transport construction to protect soils and surface runoff of the railway from pollution of various natures.

Keywords Geocoprotective properties · Chlorite-containing crushed stone · Waste of heavy concrete

M. Shershneva · I. Kozlov (✉) · G. Pankrateva · I. Drobyshev
Emperor Alexander I State Transport University, St. Petersburg, Russia
e-mail: kis-84@list.ru

© Springer Nature Singapore Pte Ltd. 2020
A. Petriaev and A. Konon (eds.), *Transportation Soil Engineering in Cold Regions*,
Volume 2, Lecture Notes in Civil Engineering 50,
https://doi.org/10.1007/978-981-15-0454-9_33

1 Introduction

Today, the problem of the formation of solid mineral waste from various industries is widely known and relevant [1–5]. At the same time, the work of many scientists is aimed at developing technological solutions to minimize the negative impact on the environment of various types of pollution during the operation of transport construction facilities [6–11]. As a rule, such solutions involve the use of geocoprotective structures in the form of embankments, screens or barriers [12–16] and involve the use of a large number of mineral substances active with respect to pollution. If such substances belong to industrial waste, then problems can be solved in a complex.

Sources of pollution can be a variety of industries, including railway transport. The soils around large industrial facilities at a distance of several tens of kilometers are contaminated with heavy metals, and up to 200 thousand tons of heavy metals per year are transported from the railroad transport as a result of brake pad wear. One of the components of the activities of JSC “Russian Railways” is to ensure the environmental safety of the entire transport complex, which is carried out in accordance with the Environmental Strategy of JSC “Russian Railways” until 2030. According to the report of Russian Railways, it is noted that continuing wastewater discharges without treatment into surface water bodies and on the terrain (up to 30 million cubic meters annually) are the most acute problem of the negative impact of transport on water resources. A significant part of these discharges leads to bacterial contamination of the tracks and adjacent territories due to the use of old types of toilets in passenger cars. The detected fecal contamination of the ballast of railway lines, as well as the account of the excess of the infestation rate by the helminths of road fitters and the high probability of secondary bacterial contamination of drinking water in passenger cars, has led to the need to introduce new life support technologies in passenger trains. The solution of this problem led to the substantiation and introduction of new hygienic requirements, which, in turn, provide for the equipment of wagons with environmentally friendly closed systems for the collection and disposal of sewage; comprehensive collection and disposal of solid household waste from passenger trains; provision of cars with small-sized devices for additional disinfection and purification of drinking water.

One of the solutions to the problem of cleaning surface water from railways from heavy metal ions (HMI) and bacterial contamination can be the creation of a geocoprotective embankment of materials active in relation to these contaminants.

The article presents the results of a study of the possibility of using some mineral technogenic silicates in geo-ecological embankments in the body of a railroad bed to minimize the negative impact of heavy metal ions and bacterial contamination.

2 Research Objects and Methods

The objects of the study were selected concrete and chlorite-containing crushed stone, having a silicate nature, which predicts their activity with respect to heavy metal ions [17–20]. The battle of concrete is formed by the destruction or disassembly of industrial and civil structures. About 2.5 billion tons of construction mineral waste is generated on the planet every year. More than half of them are destroyed concrete and reinforced concrete, which, unlike other construction debris, does not rot and does not decay.

Chlorite-containing crushed stone is a by-product in shungite mining. In appearance, crushed stone is a solid material of dark gray color with a greenish tint. According to the petrographic composition, it is quartz-albite-chlorite slate (Table 1). The structure of the rock is fine-grained, the texture is schist.

According to the mineral composition, the main phase of chlorite-containing crushed stone are chlorite and plagioclase minerals, which belong to silicate-containing minerals and determine the ability of crushed stone to absorb heavy metal ions [18–21], as well as up to 3% of shungite (carbon), whose presence causes its ability to absorb dissolved petroleum products [20] and suggests the presence of antiseptic properties.

To determine the concentrations of heavy metal ions in solutions, the ionometric method was used using appropriate ion-selective electrodes.

Activity in relation to HMI was determined in static and dynamic conditions and was calculated by the formula (1):

$$a = (C_{\text{ini}} - C_{\text{fin}}) \cdot V / m \quad (1)$$

where

a the activity, mg/g;

C_{ini} the initial concentration of HMI in the model solution, mg/l;

C_{fin} the final concentration of HMI in the model solution, mg/l;

V the volume of solution, l;

M the mass of waste.

To determine the concentration of bacterial contamination was used analysis to determine the microbial number (DMN). This analysis as a criterion for biological

Table 1 Mineral composition of chlorite-containing crushed stone

Mineral composition	Content, volume %
Quartz	15–20
Plagioclase (albite)	35–40
Chlorite	40–45
Carbonate (calcite)	1–3
Schungite substance	1–2

contamination estimates the total number of bacterial colonies in one ml of water. This indicator allows to take into account not all microorganisms, but only those capable of growing on simple media at a temperature of 37 °C (mesophilic, saprotrophic). However, the number of saprotrophic microorganisms, usually corresponds to the degree of contamination of water with organic substances, and, thus, indirectly characterizes its sanitary state.

3 Research Results

In determining the activity of concrete combat with respect to HMI, images of various classes B20, B22.5, B25 were used, having an initial compressive strength of 200, 300, 350 MPa.

The results of determining the activity of concrete combat in static conditions are presented in Table 2.

According to Table 2, it can be seen that there is no significant difference in the tanks for concrete of various classes. Therefore, the activity of the battle of concrete in dynamic conditions was determined for class B20. The research results are presented in Table 3.

The activity of concrete combat in relation to such dangerous contaminants as heavy metal ions allows its use in technological solutions for transport construction. The proposed technological solution involves the current or major overhaul of the railway embankment, when they carry out a full or partial replacement of ballast to use not natural materials, but concrete. In this case, the ions of heavy metals contained in the surface drains of the railway bed will be neutralized, the railway embankment will acquire geocoprotective functions.

In terms of its physico-mechanical characteristics, the battle of concrete (secondary crushed stone) complies with the requirements for materials used in such construction.

In determining the antiseptic properties of chlorite-containing rubble, sampling was carried out on a section of a railway track 500 m long in a drainage tray. Chlorite-containing crushed stone was sieved through a number of sieves and the following fractions <0.114, 0.114–0.315, 0.315–0.630, 0.630–1.250, 1.250–2.50, 2.50–5.00, >5.00 mm were isolated. For research, a fraction with a grain size of more than 5 mm was used. Samples of water were placed in a measuring cup in an amount of 50 ml, 2 mg of crushed stone was added to the samples, the volume was thoroughly mixed and infused for 20 min, and then the sample was filtered through a paper filter. The water treatment time was 12 and 24 h. The samples determined the value of DMN. During the analysis, all bacteriological dishes before sterilization were washed and sterilized in a drying cabinet at a temperature of 160 °C for 1 h, counting from the moment the temperature was reached. The research results are presented in Table 4.

The results showed that when treating natural water with chlorite-containing rubble, the number of colonies decreased compared with the initial water. According

Table 2 Concrete combat activity (static conditions)

Metal ion	The density of concrete combat											
	B20				B22.5				B25			
	0.114–0.315 (mm)	0.315–0.63 (mm)	0.63–1.25 (mm)	>1.25 (mm)	0.114–0.315 (mm)	0.315–0.63 (mm)	0.63–1.25 (mm)	>1.25 (mm)	0.114–0.315 (mm)	0.315–0.63 (mm)	0.63–1.25 (mm)	>1.25 (mm)
Mn ²⁺	1.15	1.15	1.15	0.96	1.25	1.15	1.10	1.00	1.15	1.00	1.00	0.96
Fe ³⁺	1.35	1.20	1.20	1.15	1.35	1.25	1.10	1.10	1.35	1.30	1.25	1.00
Ni ²⁺	1.10	1.12	1.10	1.10	1.12	1.12	1.11	1.14	1.10	1.12	1.10	1.10
Cu ²⁺	1.10	1.10	1.00	0.95	1.10	1.10	0.95	0.95	1.10	1.10	1.10	1.00
Cr ³⁺	1.25	1.25	1.06	0.96	1.24	1.10	1.05	1.05	1.25	1.25	1.15	1.05
Cd ²⁺	1.25	1.24	1.22	1.01	1.24	1.25	1.15	1.13	1.25	1.25	1.13	1.02

Table 3 Concrete combat activity (dynamic conditions) (mg/g)

Mn ²⁺	Fe ³⁺	Ni ²⁺	Cu ²⁺	Cd ²⁺	Cr ³⁺
0.78	0.45	0.98	0.60	0.79	0.98

Table 4 Results of determination of total microbial number

Nº	Water sample/contact time	DMN
1	Source contaminated water	290
2	Initial water infused with chlorite-containing rubble/12 h	6
3	Initial water infused with chlorite-containing rubble/24 h	6

to the research results, a patent of the Russian Federation No. 2497757 “Antiseptic agent for water treatment” was obtained.

Thus, chlorite-containing crushed stone is a promising mineral technogenic silicate with antiseptic properties. It can be used in the technological solution for the construction and reconstruction of transport routes in order to reduce bacterial contamination of man-made embankment soils, adjacent soils and surface runoff from the railroad tracks.

To recommend crushed stone as a ballast or sub-ballast layer of a railroad bed, it is necessary to analyze its physico-mechanical properties for compliance with the requirements for crushed stones of such purpose [22–27]. Average data on the physico-mechanical properties of chlorite-containing crushed stone are given in Table 5.

In the case of the use of concrete and chlorite-containing rubble in geocoprotective embankments, the question arises as to the necessary amount of waste that provides the geocoprotective functions of the embankment. There is no doubt that the amount of material will depend on the degree of contamination of surface runoff, on the activity of the waste, to absorb these contaminants and the time of its operation.

The required waste mass can be calculated by the formula (2):

$$M_{\text{waste}} = T \cdot (10 \cdot h_r \cdot \Psi_r \cdot F \cdot C_r + 10 \cdot h_m \cdot \Psi_m \cdot F \cdot C_m) / a \quad (2)$$

where

- T the lifetime of the geocoprotective structure (years);
- h_r precipitation layer (mm), for the warm period of the year;
- Ψ_r and Ψ_m the total coefficient of flow of rain and melt waters;
- F the total area of pollution runoff (ha);
- C_r the concentration of the pollutant in rainwater (g/m³);
- h_m sediment layer, (mm), for the cold period of the year;
- C_m the concentration of the pollutant in the melt waters (g/m³);
- a concrete combat activity (g/kg).

Table 5 Physico-mechanical properties of crust-containing crushed stone

№	Measured indicator	Regulatory value	Test results
1	The content of grains of lamellar (flap) and needle shape, %	Group of rubble 3 15–25% inclusions	24.5
2	Grade of crushed stone by crushability (mass loss, %)	Mark 1200 up to 11	5.3
3	Grade of rubble by abrasion (mass loss during testing, %)	Mark I-1 (up to 25)	I-1 (16.7)
4	The content of grains of weak rocks, % by weight, not more	5	Not found
5	Grade of crushed stone by frost resistance (mass loss after 15 cycles of saturation-drying in sodium sulfate solution, %, not more)	F 200 (3)	F 200 (2.8)
6	Content of dust and clay particles, % by weight	1	0.01
7	Content of clay in lumps, % by weight, not more	0.25	Not found
8	Stability of crushed stone structure against all types of decay—mass loss during decay, %	3	1.0

The approximate life of ballast rubble prior to its replacement with current and capital repairs is 15 years; for the North-West region of Russia, the precipitation during the warm and cold periods is 0.7 and 0.6 mm, respectively. The total coefficient of flow of rain and melt waters is 0.5. The concentration of iron ions in rain and thawed waters of surface runoff of railway tracks reaches 5 g/m³. Taking into account the activity of concrete combat with respect to iron ions (Table 3), it is possible to calculate the required waste mass per 1 ha of the railway embankment:

$$M_{\text{waste}} = 15 \cdot (10 \cdot 0.7 \cdot 0.5 \cdot 1 \cdot 5 + 10 \cdot 0.6 \cdot 0.5 \cdot 1 \cdot 5) / 0.45 = 1083(\text{kg})$$

Thus, in order to neutralize iron ions in the surface runoff of a railway bed on an area of 1 ha, it is necessary to use about 1 ton of concrete battle. In practical application, it should be borne in mind that the presence of other heavy metal ions will reduce the activity of concrete breakdown, and the presence of other pollutants, such as oil products, will not affect the activity of concrete breakdown.

4 Findings

1. Geocoprotective properties of some technogenic silicates were discovered and investigated. Concrete fights are capable of neutralizing heavy metal ions, chlorite-containing rubble has antiseptic properties.
2. The discovered and investigated properties of technogenic silicates determine the possibility of their use in geocoprotective structures.
3. It is proposed to use concrete and chlorite-containing crushed stone in the construction or reconstruction of a railway embankment, which at the same time acquires geocoprotective functions.
4. Formulas for calculating the required mass of mineral technogenic silicates, for giving geocoprotective properties to structures, and calculation results are proposed.

References

1. Yang Y, Chen B (2016) Potential use of soil in lightweight foamed concrete. *KSCE J Civ Eng* 20(6):2420–2427
2. Kuzielová E, Pach L, Palou M (2016) Effect of activated foaming agent on the foam concrete properties. *Constr Build Mater* 125:998–1004
3. Mugahed Amran YH, Abang Ali AA, Rashid RSM, Hejazi F, Safiee NA (2016) Structural behavior of axially loaded precast foamed concrete sandwich panels. *Constr Build Mater* 107:307–320
4. Krämer C, Schauerte M, Müller T, Gebhard S, Trettin R (2017) Application of reinforced three-phase-foams in UHPC foam concrete. *Constr Build Mater* 131:746–757
5. Namsone E, Šahmenko G, Korjakins A (2017) Durability properties of high performance foamed concrete. In: *Procedia Engineering* 12. “Modern building materials, structures and techniques”, pp 760–767
6. Wan K, Li G, Wang S, Pang C (2017) 3d full field study of drying shrinkage of foam concrete. *Cement Concr Compos* 82:217–226
7. Sahu SS, Gandhi ISR, Khwairakpam S (2018) State-of-the-art review on the characteristics of surfactants and foam from foam concrete perspective. *J Inst Eng (India) Ser A* 99(2):391–405
8. Pedro R, Tubino RMC, Anversa J, De Col D, Lermen RT, Silva RA (2017) Production of aerated foamed concrete with industrial waste from the gems and jewels sector of rio grande do sul-brazil. *Appl Sci (Switzerland)* 7(100):985
9. Tao C, Dong S (2017) Effects of different fly ash proportion on the physical and mechanical performance and pore structure of foam concrete. *Chem Eng Trans* 62:1021–1026
10. Svatovskaya LB, Kabanov AA, Sychov MM (2017) The improvement of foam concrete geocoprotective properties in transport construction. In: *IOP conference series: earth and environmental science*, 1755-1315 90 012010, p 90
11. Svatovskaya LB, Kabanov AA, Sychov MM (2017) Lithosynthesis of the properties in the transport construction on the cement base. In: *IOP conference series: earth and environmental science*, 1755-1315 90 012009, p 90
12. Svatovskaya LB, Kabanov AA, Sychov MM (2017) Soling, aerating and phosphating for soil strengthening and detoxication. *Procedia Eng* 189:398–403
13. Svatovskaya LB, Shershneva MV, Baidarashvili MM, Yakimova NI, Khitrov AV (2004) Foam concrete construction demolished waste. In: *Proceedings of the international conference on*

- sustainable waste management and recycling: construction demolition waste. London, pp 199–203
14. Svatovskaya LB, Sakharova AS, Baidarashvilly MM, Petriaev AV (2014) Building wastes and cement clinker using in the geocoprotective technologies in transport construction. In: Proceedings of the 14th international conference of international association for computer methods and recent advances in geomechanics. Kyoto, pp 152
 15. Sychova AM, Svatovskaya LB, Mjakin SV, Vasiljeva IV (2009) Modification of fillers for cements. In: Electron beam modification of solids: mechanisms, common features and promising applications, pp 35–37
 16. Sychova AM, Svatovskaya LB, Mjakin SV, Vasiljeva IV (2009) Activation of aqueous phase at cement and concrete solidification. In: Electron beam modification of solids: mechanisms, common features and promising applications, pp 39–47
 17. Maslennikova LL, Svatovskaya LB, Mjakin SV, Vasiljeva IV (2009) Activation of reactions at solid-solid interfaces. Improvement of ceramics materials. In: Electron beam modification of solids: mechanisms, common features and promising applications, pp 57–61
 18. Shershneva MV, Makarova EI (2017) Minimization of negative impact from solid waste landfills with use of mineral geoantidotes. In: Procedia engineering transportation geotechnics and geoecology, TGG 2017. Saint Petersburg, pp 315–319
 19. Svatovskaya LB, Shershneva MV (2017) Geocoprotective technologies of storage of used wooden sleepers. In: Procedia engineering transportation geotechnics and geoecology, TGG 2017. Saint Petersburg, pp 605–609
 20. Shershneva MV, Makarova EI (2017) Oil products absorbing properties of foam concretes. In: Procedia engineering transportation geotechnics and geoecology, TGG 2017. Saint Petersburg, pp 320–324
 21. Svatovskaya LB, Shershneva MV (2017) Geocoprotective properties of binders for transport systems In: Procedia engineering transportation geotechnics and geoecology, TGG. Saint Petersburg, pp 440–445. <https://doi.org/10.1016/j.proeng.2017.05.071>
 22. Komokhov PG, Maslennikova LL, Makhmud A (2003) Control of strength of ceramic materials by forming the contact zone between clay matrix and leaning agent. *Stroitel'nye Mat* 12:44–46
 23. Maslennikova LL, Abu-Khasan MS, Babak NA (2017) The use of oil-contaminated crushed stone screenings in construction ceramics. *Procedia Eng* 189:59–64
 24. Abu-Khasan M, Solovyova V, Solovyov D (2018) High-strength concrete with new organic mineral complex admixture. *MATEC Web Conf Proc* 193:03019
 25. Maslennikova LL, Naginskii IA, Troshev AN (2017) Use of waste from aluminothermic welding of railroad tracks in structural materials science. *Procedia Eng* 189:94–98
 26. Svatovskaya LB, Sychova AM, Soloviova VY, Maslennikova LL, Sychov MM (2016) Absorptive properties of hydrate silicate building materials and products for quality and geocoprotection improvement. *Indian J Sci Technol* 9(42):104231
 27. Svatovskaya LB, Sychova AM, Soloviova VY, Maslennikova LL, Sychov MM (2016) Obtaining foam concrete applying stabilized foam. *Indian J Sci Technol* 9(42):104304

Geocoprotective Technologies from Heavy Metal Ions Pollution for Transport Construction in Permafrost Regions



Maria Shershneva , Yuliya Puzanova and Antonina Sakharova 

Abstract Every year, 15–17 million tons mineral wastes are generated in Russia including permafrost regions. A large amount of these wastes contain minerals such as silicates and sulfates. Different industries leading to geosystem pollution by heavy metals, including lead, cadmium, copper, zinc, manganese, and iron compounds. Such pollution must be prevented. The purpose of the work was to study geocoprotective properties of mineral wastes of silicate and sulfate nature and how they can be used to create geocoprotective technologies against heavy metal ions pollution in permafrost regions. The silicate and sulfate mineral wastes were selected as objects of study in the form of phosphogypsum, foamed gypsum, calcium sulfate anhydrous, hemihydrate gypsum and calcium sulfate dihydrate, asbestos- and chlorite-containing crushed stone, and talc. A potentiometric method for determination of concentrations in solutions was used to define the absorptive capacity of mineral wastes against heavy metal ions. The detected absorptive capacities of aforementioned mineral wastes for such heavy metals as cadmium, copper, lead, and barium are presented in the article. The dependences of the absorptive capacity of the mineral waste on the initial concentration of heavy metal ions, on the interaction time with the solution and on the fraction size are also given in the article. The experimental results showed that the selected mineral wastes can be used in technological solutions for soil cleanup and surface runoff purification from heavy metal ions.

Keywords Geosystem pollution · Mineral wastes · Geocoprotective technologies · Heavy metal ions

M. Shershneva · Y. Puzanova · A. Sakharova (✉)
Emperor Alexander I St. Petersburg State Transport University (PGUPS), St. Petersburg 190031,
Russia
e-mail: assakharova@list.ru

© Springer Nature Singapore Pte Ltd. 2020
A. Petriaev and A. Konon (eds.), *Transportation Soil Engineering in Cold Regions*,
Volume 2, Lecture Notes in Civil Engineering 50,
https://doi.org/10.1007/978-981-15-0454-9_34

1 Introduction

According to the European Association for the Demolition of Buildings, about 2.5 billion tons of construction waste is generated annually on the planet as a result of human activity. Construction wastes resulting from natural and man-made disasters not included in this amount. Every year, 15–17 million tons mineral wastes are generated in Russia including permafrost regions. A large amount of these wastes contain minerals such as silicates and sulfates [1–4]. There are now also underway for the construction and reconstruction activities in the transport sector in permafrost regions. Also currently works on construction and reconstruction of the transport sector in permafrost regions. The construction and operation of facilities located in permafrost regions lead to the pollution of lithosphere by heavy metals, including lead, cadmium, copper, zinc, manganese, and iron compounds.

Heavy metal ions of (HMI) are supertoxicants the XXI century [5, 6]. Therefore, the development of technological solutions for the lithosphere protection from their negative impact is an urgent task of geoecology [7–11]. The authors propose to develop technological solutions for soil and surface waters protection from HMI pollution using mineral wastes. These mineral wastes can absorb and neutralize pollutants due to the formation of low-solubility compounds. For the application of such technological solutions, it is necessary [12–16]:

- To research and evaluate the mineral waste ability to neutralize heavy metal ions;
- To develop technological solutions for soil and surface water protection in permafrost regions from heavy metal ions through the use of mineral wastes.

2 Materials and Methods

The silicate and sulfate mineral wastes were selected as objects of study in the form of phosphogypsum, foamed gypsum, calcium sulfate anhydrous, gypsum hemihydrate and dihydrate, asbestos- and chlorite-containing crushed stone, and talc [17, 18]. They were chosen because a large amount of waste with a similar composition is formed in various industries.

Capacity was calculated by the use of this formula:

$$a = ((C_i - C_r)V)/m \quad (1)$$

where

a absorptive capacity, mg g^{-1} ;

C_i initial concentration of heavy metal ions in model solution, mg l^{-1} ;

C_r residual concentration of heavy metal ions in model solution, mg l^{-1} ;

V solution volume, l;

M mineral waste mass, g.

A potentiometric method for determination of concentration of heavy metal ions in solutions was used to define the absorptive capacity of mineral wastes. Determination of the concentration in the solution before and after interaction with the mineral wastes was performed on an electronic analyzer «Expert- 001» and ion-selective electrodes [Cd (II), Cu (II), Pb (II), Ba (II)].

3 Research Results

Table 1 demonstrates the results of experiments to determine the dependence of the static capacity of sulfate-containing mineral wastes on the initial concentration of the solution for phosphogypsum as an example.

According to the data obtained, a concentration of 10^{-4} mol l⁻¹ has been chosen to determine the static capacity. The residual concentration under the chosen conditions was 2.195 mg l⁻¹ for phosphogypsum, 2.935 mg l⁻¹ for foamed gypsum, 4.783 mg l⁻¹ for calcium sulfate anhydrous, 1.195 mg l⁻¹ for gypsum hemihydrate, and 6.207 mg l⁻¹ for gypsum dihydrate. The purification rate was 52–91%.

Tables 2, 3, 4, 5 and 6 present the results of experiments to determine the dependence of the static capacity of sulfate-containing mineral wastes on the contact time with the solution.

Table 1 Dependence of the static capacity of phosphogypsum on the initial concentration of a solution containing cadmium ions

Mass (g)	Solution concentration Cd(NO ₃) ₂ (mol l ⁻¹)	Initial concentration (mg l ⁻¹)	Residual concentration (mg l ⁻¹)	Capacity (mg g ⁻¹)
1	10 ⁻⁶	0.042	0.011	0.003
1	10 ⁻⁵	1.620	1.367	0.025
1	10 ⁻⁴	12.786	2.195	1.059
1	10 ⁻³	162.817	57.102	10.570
1	10 ⁻²	1537.309	663.379	87.393

Table 2 Dependence of the static capacity of phosphogypsum on the contact time with the Cd(NO₃)₂ solution

Contact time (h)	Initial concentration (mg l ⁻¹)	Residual concentration (mg l ⁻¹)	Capacity (mg g ⁻¹)
0.25	12.786	2.195	1.059
2	12.786	2.170	1.062
6	12.786	2.573	1.021
24	12.786	2.322	1.046

Table 3 Dependence of the static capacity of foamed gypsum on the contact time with the $\text{Cd}(\text{NO}_3)_2$ solution

Contact time (h)	Initial concentration (mg l^{-1})	Residual concentration (mg l^{-1})	Capacity (mg g^{-1})
0.25	12.786	2.935	0.985
2	12.786	2.661	1.062
6	12.786	2.573	1.013
24	12.786	2.651	1.014

Table 4 Dependence of the static capacity of calcium sulfate anhydrous on the contact time with the $\text{Cd}(\text{NO}_3)_2$ solution

Contact time (h)	Initial concentration (mg l^{-1})	Residual concentration (mg l^{-1})	Capacity (mg g^{-1})
0.25	12.786	4.783	0.800
2	12.786	3.332	0.945
6	12.786	3.011	0.978
24	12.786	2.339	1.045

Table 5 Dependence of the static capacity of gypsum hemihydrate on the contact time with the $\text{Cd}(\text{NO}_3)_2$ solution

Contact time (h)	Initial concentration (mg l^{-1})	Residual concentration (mg l^{-1})	Capacity (mg g^{-1})
0.25	12.786	1.935	1.085
2	12.786	1.324	1.146
6	12.786	0.678	1.211
24	12.786	0.513	1.227

Table 6 Dependence of the static capacity of gypsum dihydrate on the contact time with the $\text{Cd}(\text{NO}_3)_2$ solution

Contact time (h)	Initial concentration (mg l^{-1})	Residual concentration (mg l^{-1})	Capacity (mg g^{-1})
0.25	12.786	6.207	0.658
2	12.786	4.850	0.794
6	12.786	4.423	0.836
24	12.786	4.137	0.865

Table 7 Static capacity of sulfate-containing construction and industrial mineral wastes

Mineral wastes	Static capacity (mg g ⁻¹)			
	Cd ²⁺	Cu ²⁺	Pb ²⁺	Ba ²⁺
Phosphogypsum	1.06	1.28	1.51	1.29
Foamed gypsum	0.99	1.21	0.85	1.33
Calcium sulfate anhydrous	0.80	1.09	1.17	1.30
Gypsum hemihydrate	1.26	1.34	1.52	1.31
Gypsum dihydrate	0.66	0.88	0.86	1.33

The data from Tables 2, 3, 4, 5 and 6 illustrate that for every contact time the difference in residual concentrations is 0.4 mg l⁻¹ for phosphogypsum and 0.36 mg l⁻¹ for foamed gypsum. Therefore, the increase of contact time more 15 min is impractical.

Additional studies have carried out for such heavy metal ions as copper, lead, and barium for selected conditions. Table 7 demonstrates the results.

Tables 8, 9 and 10 present the results of experiments to determine the dependence of the static capacity of magnesium silicate-containing mineral waste on the initial concentration of the solution.

Table 8 Dependence of the static capacity of chlorite-containing crushed stone on the initial concentration of the cadmium ions solution

Mass (g)	Solution concentration Cd(NO ₃) ₂ (mol l ⁻¹)	Initial concentration (mg l ⁻¹)	Residual concentration (mg l ⁻¹)	Capacity (mg g ⁻¹)
1	10 ⁻⁶	0.042	0.000	0.004
1	10 ⁻⁵	1.620	0.097	0.152
1	10 ⁻⁴	12.786	1.335	1.145
1	10 ⁻³	162.817	142.396	2.042
1	10 ⁻²	1537.309	1431.389	10.592

Table 9 Dependence of the static capacity of asbestos-containing crushed stone on the initial concentration of the cadmium ions solution

Mass (g)	Cd(NO ₃) ₂ solution concentration (mol l ⁻¹)	Initial concentration (mg l ⁻¹)	Residual concentration (mg l ⁻¹)	Capacity (mg g ⁻¹)
1	10 ⁻⁶	0.042	0.000	0.004
1	10 ⁻⁵	1.620	0.072	0.155
1	10 ⁻⁴	12.786	1.488	1.130
1	10 ⁻³	162.817	142.066	2.075
1	10 ⁻²	1537.309	1408.498	12.931

Table 10 Dependence of the static capacity of talc on the initial concentration of the cadmium ions solution

Mass (g)	Cd(NO ₃) ₂ solution concentration (mol l ⁻¹)	Initial concentration (mg l ⁻¹)	Residual concentration (mg l ⁻¹)	Capacity (mg g ⁻¹)
1	10 ⁻⁶	0.042	0.000	0.004
1	10 ⁻⁵	1.620	0.043	0.158
1	10 ⁻⁴	12.786	0.528	1.226
1	10 ⁻³	162.817	137.848	2.497
1	10 ⁻²	1537.309	1424.811	11.250

Table 11 Dependence of the static capacity of chlorite-containing crushed stone on the contact time with the Cd(NO₃)₂ solution

Contact time (h)	Initial concentration (mg l ⁻¹)	Residual concentration (mg l ⁻¹)	Capacity (mg g ⁻¹)
0.25	12.786	1.335	1.145
2	12.786	0.499	1.229
6	12.786	0.196	1.259
24	12.786	0.008	1.278

According to the received data a concentration of 10⁻⁴ mol l⁻¹ was chosen to determine the static capacity. At the same time, the residual concentration for selected conditions was 1.335 mg l⁻¹ for chlorite-containing crushed stone, 1.488 mg l⁻¹ for asbestos-containing crushed stone, and 0.528 mg l⁻¹ for talc. The purification rate was 88–96%.

Tables 11, 12 and 13 demonstrate the results of experiments to determine the dependence of the static capacity of magnesium silicate-containing mineral wastes on the contact time with the solution.

The results showed that the increase of contact time increases of the purification rate. This means that the tested materials have «reserve» of the absorptive capacity.

Table 12 Dependence of the static capacity of asbestos-containing crushed stone on the contact time with the Cd(NO₃)₂ solution

Contact time (h)	Initial concentration (mg l ⁻¹)	Residual concentration (mg l ⁻¹)	Capacity (mg g ⁻¹)
0.25	12.786	1.488	1.130
2	12.786	0.253	1.253
6	12.786	0.080	1.271
24	12.786	0.000	1.279

Table 13 Dependence of the static capacity of talc on the contact time with the $\text{Cd}(\text{NO}_3)_2$ solution

Contact time (h)	Initial concentration (mg l^{-1})	Residual concentration (mg l^{-1})	Capacity (mg g^{-1})
0.25	12.786	0.528	1.226
2	12.786	0.406	1.238
6	12.786	0.672	1.211
24	12.786	0.568	1.222

Table 14 Static capacity of mineral wastes

Mineral wastes	Static capacity (mg g^{-1})			
	Cd^{2+}	Cu^{2+}	Pb^{2+}	Ba^{2+}
Asbestos-containing crushed stone	1.13	1.30	1.46	0.47
Chlorite-containing crushed stone	1.15	1.11	1.26	0.47
Talc	1.23	1.33	1.51	0.50

However, taking into account received data from other mineral wastes the contact time for chlorite-containing and asbestos-containing crushed stone was taken 0.25 h.

The data from Table 13 shows that for every contact time the difference in the residual concentrations is 0.27 mg l^{-1} . Therefore, it is not necessary to increase the contact time more than 15 min. Additional studies were carried out for such heavy metal ions as copper, lead, and barium in the same conditions. Table 14 presents the analysis results.

The authors suggest using of the construction and industrial mineral wastes as an additional drainage fills in areas polluted by heavy metal in permafrost regions. It will be geocoprotective screens for the highways construction and repair.

One of the most frequently used ways to reinforcement of ramps from subgrade deformation erosion is mechanized grass cultivation. It is possible to build the geocoprotective screen for this operation at the same time strengthening the ramps using mechanisms for grass cultivation. Experimental testing of some investigated mineral wastes in a model experiment was carried out on a test site in the zone of highway and railway. Tests showed the possibility of the use them to create geocoprotective screen in permafrost regions (Table 15).

The use of construction and industrial mineral waste as a drainage material directly in the drainage trays of highways is considered. Such a solution will help to prevent soil contamination by surface wastewater containing HMI during the construction of transport networks. Preventive protection of soil and groundwater during the surface runoff treatment can be achieved through the use of construction and industrial mineral waste as a filtering material [19–21]. The experimental operation of stormwater runoff purification from lead ions and oil products was carried out using a combined filter cartridge on the gas station territory. The upper part of the combined filter cartridge on one-third the height was filled by phosphogypsum. He was placed instead of a part of the non-woven fabric. The concentration of lead ions in the purified

Table 15 Results of soil cleanup through the use of mineral wastes

Materials	pH	Initial concentration of lead ions (mg l^{-1})	Residual concentration of lead ions (mg l^{-1})	Purification rate (%)
Sand clay	6.3	235.875	43.441	81.58
Sand clay + phosphogypsum	7.1	235.875	0.760	99.68
Sand clay + foamed gypsum	7.20	235.875	0.075	99.97
Sand clay + chlorite-containing crushed stone	7.2	235.875	0.012	99.99
Sand loam	5.2	235.875	155.674	34.00
Sand loam + phosphogypsum	6.9	235.875	0.413	99.82
Sand loam + foamed gypsum	7.2	235.875	0.438	99.81
Sand loam + chlorite-containing crushed stone	7.1	235.875	0.060	99.97
Bog peat	5.0	235.875	152.375	35.40
Bog peat + phosphogypsum	5.5	235.875	10.216	95.67
Bog peat + foamed gypsum	5.9	235.875	10.821	95.41
Bog peat + chlorite-containing crushed stone	6.4	235.875	0.584	99.75

surface runoff has decreased by ten times (from 0.1 to 0.01 mg l^{-1}) during the entire test period. The purification level has reached the admissible concentration limit.

4 Conclusions

1. The dependences of the absorption capacity of calcium sulfate and hydrosilicate systems on the initial concentration of the solution containing heavy metal ions on the contact time with the solution and on the fraction size were determined.
2. The absorption capacity of sulfate-containing calcium mineral wastes was determined. It corresponds to the values in the intervals: 0.66–1.26 mg g^{-1} for cadmium ions; 0.88–1.34 mg g^{-1} for copper ions; 0.85–1.52 mg g^{-1} for lead ions; 1.29–1.33 mg g^{-1} for barium ions.

3. The absorptive capacity of silicate-containing magnesium mineral wastes was determined, which corresponds to values: 1.26–1.52 mg g⁻¹ for lead ions and 0.47–0.88 mg g⁻¹ for barium ions.
4. Construction and industrial mineral wastes that are wastes of hazard class IV spontaneously interact with heavy metals ions of hazard classes I and II. They bind and neutralize them. In the resulting compounds with a low solubility are produced in the form of salts and hydroxides of heavy metals of hazard class IV.
5. Technological solutions were proposed to protect the lithosphere during transport construction using construction and industrial mineral waste. These solutions include steps:
 - The creation of geocoprotective screen for highways and railways construction for the preventive protection of roadside land from HMI;
 - Preventive protection of soils and groundwater by using of the surface runoff purification from the HMI in the drainage tray during the transport highway construction, and in the gas station during the highway reconstruction.
6. Aforecited technological solutions can be applied in permafrost regions under positive temperatures conditions.

References

1. Svatovskaya LB, Kabanov AA, Sychov MM (2017) The improvement of foam concrete geocoprotective properties in transport construction. *IOP Conf Ser Earth Environ Sci* 90:012010
2. Svatovskaya LB, Kabanov AA, Sychov MM (2017) Lithosynthesis of the properties in the transport construction on the cement base. *IOP Conf Ser Earth Environ Sci* 90:012009
3. Svatovskaya LB, Kabanov AA, Sychov MM (2017) Soling, aerating and phosphating for soil strengthening and detoxication. *Procedia Eng* 189:398–403
4. Svatovskaya LB, Shershneva MV, Baidarashvili MM, Yakimova NI, Khitrov AV (2004) Foam concrete construction demolished waste. In: *Proceedings of the international conference on sustainable waste management and recycling: construction demolition waste*. London, pp 199–203
5. Zhang Y, Li S, Lai Y, Wang L, Wang F, Chen Z (2019) Predicting future contents of soil heavy metals and related health risks by combining the models of source apportionment, soil metal accumulation and industrial economic theory. *Ecotoxicol Environ Saf* 171:211–221
6. Qiao P, Yang S, Lei M, Chen T, Dong N (2019) Quantitative analysis of the factors influencing spatial distribution of soil heavy metals based on geographical detector. *Sci Total Environ* 664:392–413
7. Svatovskaya LB, Sakharova AS, Baidarashvilly MM, Petriaev AV (2015) Building wastes and cement clinker using in the geocoprotective technologies in transport construction. In: *Proceedings of the 14th international conference of international association for computer methods and recent advances in geomechanics, IACMAG*. Taylor and Francis—Balkema, Netherlands, pp 619–622
8. Shershneva MV, Makarova EI, Efimova NN (2017) Minimization of negative impact from solid waste landfills with use of mineral geoantidotes. *Procedia Eng* 189:315–319
9. Svatovskaya LB, Shershneva MV, Savelyeva MY (2017) Geocoprotective technologies of storage of used wooden sleepers. *Procedia Eng* 189:605–609

10. Shershneva MV, Makarova EI, Savelyeva MY (2017) Oil products absorbing properties of foam concretes. *Procedia Eng* 189:320–324
11. Svatovskaya LB, Shershneva MV, Bobrovnik AB (2017) Geocoprotective properties of binders for transport systems. *Procedia Eng* 189:440–445
12. Sakharova A, Baidarashvili M, Petriaev A (2017) Transportation structures and constructions with geocoprotective properties. *Procedia Eng* 189:569–575
13. Sakharova AS, Svatovskaya LB, Baidarashvili MM, Petriaev AV (2018) Construction wastes application for environmental protection. In: *WASTES—solutions, treatments and opportunities II—selected papers from the 4th edition of the international conference wastes: solutions, treatments and opportunities*. Taylor and Francis—Balkema, Netherlands, pp 345–350
14. Trong Nhuan M, Thi Hoang Ha N, Hoai TT, Dang Quy T (2016) A review on the geoenvironmental and geocological integrated technology for environmental remediation in Vietnam: approaches, contributions, challenges and perspectives. *IOP Conf Ser Earth Environ Sci* 71(1):012012
15. Mohamed A-MO, Paleologos EK (2017) *Fundamentals of geoenvironmental engineering: understanding soil, water, and pollutant interaction and transport*. Elsevier Inc., Netherlands
16. Baidarashvili M, Sakharova A, Petriaev A (2017) The modern structure for storm sewage purification of roads. *Procedia Eng* 189:576–581
17. Svatovskaya LB, Sychova AM, Soloviova VY, Maslennikova LL, Sychov MM (2016) Absorptive properties of hydrate silicate building materials and products for quality and geocoprotection improvement. *Indian J Sci Technol* 9(42):104231
18. Maslennikova LL, Abu-Khasan MS, Babak NA (2017) The use of oil-contaminated crushed stone screenings in construction ceramics. *Procedia Eng* 189:59–64
19. Gong Y, Zhao D, Wang Q (2018) An overview of field-scale studies on remediation of soil contaminated with heavy metals and metalloids: technical progress over the last decade. *Water Res* 147:440–460
20. Carvalho FM, Tavares TM, Lins L (2018) Soil contamination by a lead smelter in Brazil in the view of the local residents. *Int J Environ Res Public Health* 15(10):2166
21. Nicolova M, Spasova I, Georgiev P, Groudev S (2017) Microbial removal of toxic metals from a heavily polluted soil. *J Geochem Explor* 182:242–246

High-Strength Concrete with Improved Deformation Characteristics for Road Surfaces



Valentina Solovieva, Irina Stepanova and Dmitriy Soloviev

Abstract The research area is construction in cold regions. The paper demonstrates that highly effective chemical activation of the cement-containing composite system with the use of a new generation of nanostructural additive ensures the creation of high-strength concretes having improved strength and deformation characteristics which are most effective for road surfaces. The recommended nanostructural additive has an increased effect of triple action: reaction, catalytic and plasticizing effects. The application of the proposed additive increases the hydration activity of the hardening system having chemical and thermal energy effects on it. The heat impact is due to the use of heat released as a result of enhanced hydration processes. This contributes to the creation of high-strength concrete with a new level of physical and mechanical properties.

Keywords High-strength concrete · Hydration activity · Nanostructural additive · Strength · Crack resistance · Frost resistance · Durability · Deformation characteristics · Density

1 Introduction

It is necessary to use concrete with increased strength and reduced abrasion for road surfaces because of the heavier traffic. In addition, in cold regions, the base of the road surface, as a rule, is presented in the form of frozen soils which thaw unevenly in summer. This fact must be taken into account and, as a consequence, one should use concrete with increased crack resistance for such objects [1–8].

Concretes having high compressive strength are brittle materials and to increase the crack resistance of the stone they are reinforced by armature of different nature [9–12].

V. Solovieva · I. Stepanova (✉) · D. Soloviev
Emperor Alexander I St. Petersburg State Transport University (PGUPS), St. Petersburg 190031,
Russia
e-mail: ivstepanova88@mail.ru

© Springer Nature Singapore Pte Ltd. 2020
A. Petriaev and A. Konon (eds.), *Transportation Soil Engineering in Cold Regions*,
Volume 2, Lecture Notes in Civil Engineering 50,
https://doi.org/10.1007/978-981-15-0454-9_35

339

The use of metal reinforcement is not very favorable in cold regions since the metal is subjected to corrosion quite intensively at low temperatures. Other types of reinforcement, for example, basalt one, require special engineering solutions for its use which are currently at an early stage of development [13, 14].

In permafrost regions, it is effective to perform micro-reinforcement of high-strength concrete by producing sparingly soluble complex hydrate compounds. Their structure is in the form of elongated prisms or fibers, as well as felted masses. Mainly, low-basic hydrosilicates which are presented, for example, by gyrolite (1), okenite (2), nekoite (3), have such structures. These hydrate compounds have a high hardness which varies from 4 to 5 points on the Mohs scale.



This should give a special hardness to the road surface and reduce its abrasion [15, 16].

The formation of this kind of hydrate compounds is possible in the presence of an increased number of reactive SiO_2 dispersions in the hardening system, but, in this case, it is preferable to provide a temperature of 80–85 °C into the hardening system. This becomes possible when forming a sufficiently dense structure which at the same time should have an increased reactivity to ensure the release of an increased amount of heat in the process of hydration reactions. It should be fully accumulated inside the hardening system [17–21].

2 Results and Discussion

Studies have shown that the use of complex chemical additives, which are based on polycarboxylate polymers combined with high-molecular compounds that form long and branched polymer chains modified by nanostructural elements, $\text{SiO}_2 \cdot n\text{H}_2\text{O}$, provide the formation of high-strength concrete.

It is experimentally established that the rational amount of the complex additive is 1.0 m. % by mass of cement.

Research results (Table 1) showed that the concrete of normal hardening, regardless of compressive strength class, is characterized by an increased strength gain at an early age, i.e., up to 7 days from the time of its manufacture. At the age of 7 days, the strength value is 85–90% of its design value. It should be noted that the rate of the gain in tensile strength in bending increases to a greater extent only to the design age when there is a formation of the structure of the produced hydrate compounds

Table 1 Evaluation of the effectiveness of the developed complex nanostructured additive

№	Concrete class, B	Required compressive strength, MPa, according to GOST 18105-2010	Additive		Strength (MPa)				Crack resistance coefficient	
			Control composition without the additive	Developed complex nanostructural additive	Compressive strength	Tensile strength in bending		Crack resistance coefficient		
						Age, days	Age, days	Age, days	Age, days	
1	B25	32.0	+	-	21.8	32.4	2.5	3.9	0.116	0.119
					7	28	7	28	7	28
2		32.0	-	+	27.2	41.4	3.5	5.9	0.129	0.142
					7	28	7	28	7	28
3	B30	38.4	+	-	26.5	39.0	3.0	4.6	0.114	0.117
					7	28	7	28	7	28
4		38.4	-	+	33.4	50.3	4.2	6.9	0.126	0.138
					7	28	7	28	7	28
5	B40	51.2	+	-	35.8	51.7	4.0	5.8	0.111	0.113
					7	28	7	28	7	28
6		51.2	-	+	46.1	68.8	5.7	8.9	0.123	0.130
					7	28	7	28	7	28

and, as a consequence, there is a greater degree of increased crack resistance of the material.

Analysis of the data presented in Table 1 shows that the crack resistance of the material, determined by the crack resistance coefficient (4), changes as follows: it exceeds the crack resistance of the control composition by 11% at the age of 7 days, and the crack resistance increases by 18% at the age of 28 days.

$$C_{cr.} = \frac{R_{b.t.}}{R_{com}}. \quad (4)$$

According to the data of physical and chemical studies, carried out by means of x-ray phase and differential thermal methods of analysis, it is established that at the age of 28 days, in addition to hydrosilicates, like CSH(I), low-basic hydrate compounds, such as nekoite (4), are found as the main products of hydration, the *d*-spacing for nekoite being (*d*/*n* = (9.25; 3.36; 2.82) 10⁻¹⁰ m). Crystals of nekoite are presented by elongated fibers which have a positive effect on raising the tensile strength in bending and, as a result, they increase the crack resistance of concrete. Besides, the complex composition of hydrosilicate, such as afwillite 3CaO 2SiO₂ 3H₂O (*d*/*n* = (6.46; 5.74; 4.73; 3.19; 2.84) 10⁻¹⁰ m), are found. It is characterized by high hardness which corresponds to 4 points on the Mohs scale. This contributes to an increase in the hardness of the material.

The formation of these complex hydrate compounds is confirmed by the data of differential thermal studies.

The formation of nekoite is proved by the presence of an endothermic effect at a temperature of 720 °C.

The presence of afwillite supports a broad endothermic effect in the temperature range 385–395 °C, as well as a small exothermic effect at a temperature of 315 °C.

The conducted complex physical and mechanical studies demonstrated that the concrete with the developed complex nanostructural additive is characterized by a complex of improved physical and mechanical characteristics. The results of this research are given in Table 2.

Frost resistance of concrete, regardless of its design class, is increased by more than 30%; water absorption of concrete is reduced by 33–37%, thus increasing the density of the forming structure of concrete and, as much as possible, preserving the heat, released during hydration reactions, inside the hardening concrete. This results in further increasing the hydration activity of the hardening system ensuring a raise in the level of concrete properties.

The physical and mechanical characteristics presented in Table 2 prove that the concrete with the developed nanostructural additive is characterized by increased reliability and durability.

Table 2 Comparative physico-mechanical characteristics of the control and nano-modified concrete

№	Concrete class, B	Additive		Physical and mechanical characteristics of concrete at the design age				
		Control composition without the additive	Developed complex nanostructural additive	Strength (MPa/%)	Tensile strength in bending	Crack resistance coefficient	Water absorption, Wm, % according to GOST 12730.2	Grade of frost resistance, F ₂
1	B25	+	-	32.4/100	3.9/100	0.119	4.8	150
2		-	+	41.4/128	5.9/151	0.142	3.2	200
3	B30	+	-	39.0/100	4.6/100	0.117	4.6	200
4		-	+	50.3/129	6.9/150	0.138	3.0	300
5	B40	+	-	51.7/100	5.8/100	0.113	4.4	300
6		-	+	68.8/133	8.9/153	0.130	2.8	400

3 Conclusions

It is effective for cold regions to use a complex chemical additive which is based on polycarboxylate and modified by nanostructural elements.

The chemical additive ensures the formation of a particularly dense concrete. This contributes to the preservation of heat inside the hardening system which is effectively used later to increase the rate of hydration processes occurring during the formation of artificial stone.

The formation of complex hydrate compounds characterized by fibrous or needle-like structure gives a set of such positive properties like high compressive strength, tensile strength in bending, crack resistance and increased frost resistance to hardened activated concrete.

References

1. Solovieva VY, Kozin PA, Stepanova IV, Smirnova TV (2014) High-strength concrete bonets of improved durability modified by nanopolymer additive. *Sci Technol* 2(70):296–298
2. Solovieva VY, Kozin PA, Stepanova IV, Smirnova TV (2014) Features of hardening of concrete modified by nanopolymer additive under conditions of negative temperatures. *Sci Technol* 2(70):299–301
3. Svatovsaya L, Solovieva V, Sychova A, Maslennikova L, Sychov M (2016) Obtaining foam concrete applying stabilized foam. *Indian J Sci Technol* 9(42):104304
4. Svatovsaya L, Solovieva V, Sychova A, Maslennikova L, Sychov M (2016) Absorptive properties of hydrate silicate building materials and products for quality and geoection improvement. *Indian J Sci Technol* 9(42):104304
5. Solovieva VY, Abu-Khasan M, Ershikov NV, Soloviev DV, Miraev GA (2017) Concrete with improved corrosion resistance for road pavements. *Transport construction* 12 с:12
6. Ageev VD, Fedulov VK (1996) Prefabricated road and airfield covers: highways. In: Survey information. M-F 6, p 64
7. Babkov VF (1998) Ways to improve the transport and operational qualities of highways in Russia. The issues of the design of highways: sat. In: Scientific proceedings, MADI-TU, Moscow, pp 4–14
8. Glushkov GI, Babkov VF (1994) Hard cover airfields and highways. Textbook for High Schools. Transport, Moscow
9. Sheinin AM, Ekkel SV (2005) Use of silica fume in road concrete. *Sci Technol Road Ind* 2:28–33
10. Sheinin AM, Ekkel SV (2003) High-strength containers for road construction. *Sci Technol Road Ind* 2:18–21
11. Kuntsevich OV (1983) Concrete of high frost resistance for constructions of the Far North. Stroyizdat, Leningrad
12. Gamaliy EA (2009) Complex modifiers based on polycarboxylate ethers and active mineral additives for heavy structural concrete. In: Abstract thesis for the degree of candidate of technical sciences Chelyabinsk 18
13. Solovieva V, Kondratov V, Stepanova I (2017) The development of a high performance material for a ballast layer of a railway track. *Procedia Eng* 189:823–828
14. Solovieva VY, Stepanova IV, Smirnova TV (2014) Innovations in new generation of cement-based products. In: Materials of 1st international scientific-practical conference, innovative technologies in engineering and geoeology, Sputnik+, Moscow, pp 28–32

15. Maslennikova LL, Svatovskaya LB, Mjakin SV, Vasiljeva IV (2009) Electron beam modification of solids. In: Mechanisms, common features and promising applications, pp 57–61
16. Sychova A, Solomahin A, Kotovich V, Svatovskaya L, Kamenev Y (2018) Improving of the monolithic foamconcrete quality for used in the high-rise constructions. E3S Web Conf 33:02058
17. Soloviova VY, Abu-Khasan M, Kasatkin SP, Ershikov NV, Soloviov, DV (2017) Innovative high-strength concrete for high-voltage lines. In: Materials of IV international scientific-practical conference, innovative technologies in engineering and geoecology. Sputnik+, Moscow
18. Svatovskaya LB, Sakharova AS, Baidarashvilly MM, Petriaev AV (2015) Building wastes and cement clinker using in the geocoprotective technologies in transport construction. In: Proceedings of the 14th international conference, computer methods and recent advances in geomechanics, Taylor and Francis—Balkema, Netherlands, pp 619–622
19. Sychova AM, Svatovskaya LB, Mjakin SV, Vasiljeva IV (2009) The effect of electron beam treatment of the aqueous phase on the strength of cements: Electron beam modification of solids. In: Mechanisms, common features and promising applications, pp 35–37
20. Babaev ShT, Komar AA (1987) Energy-saving technology of reinforced concrete structures of high-strength concrete with chemical additives. Stroizdat, Moscow
21. Chan Tuan Mi, Korovyakov VF (2012) Self-laying concrete mixtures. Vestnik MGSU 3:131–137

Geocoprotective Screens for Road Construction and Operation in Cold Regions



Maria Shershneva , Antonina Sakharova  and Ivan Kozlov

Abstract The intensive development of highways leads to the natural system pollution by hazardous substances such as heavy metals and oil products. At the same time, wastes are accumulated and stored in the metallurgical industry, which has a negative impact on environment. The purpose of the work is to study the applicability of the metallurgy waste for transport construction to minimize the negative impact of polluted roads on the environment in cold regions. The task of the work is using of the metallurgical wastes properties in geocoprotective technological solutions in road construction and operation. Blast-furnace metallurgical slag was chosen as the object of study. IR spectrometry, atomic absorption photometry, and PQ analysis methods were used to study the properties of this slag. The article presents data on the degree of road pollution and on geocoprotective capacity of blast-furnace metallurgical slag against heavy metal ions. The authors have proposed the technological solutions for using of blast-furnace metallurgical slag in transport construction and reconstruction, including the effective life calculation during their operation. There are two geocological problems being solved for cold regions: utilization of metallurgical wastes and the use these wastes for soil cleanup and treatment of runoff containing heavy metal ions.

Keywords Geocoprotective screens · Road construction · Blast-Furnace metallurgical slag · Highways · Heavy metal ions · Local treatment plants

1 Introduction

Surface runoff is the most susceptible to pollution during the construction and operation of roads. It is formed by rain and snow melting. Surface runoff contamination in cold regions depends on many factors, which can be grouped into the following groups: climatic conditions, sanitary state of the drainage area and ground-level air, and hydrogeological regularities of surface runoff movement over the land topog-

M. Shershneva · A. Sakharova (✉) · I. Kozlov
Emperor Alexander I St. Petersburg State Transport University (PGUPS), St. Petersburg, Russia
e-mail: assakharova@list.ru

© Springer Nature Singapore Pte Ltd. 2020
A. Petriaev and A. Konon (eds.), *Transportation Soil Engineering in Cold Regions*,
Volume 2, Lecture Notes in Civil Engineering 50,
https://doi.org/10.1007/978-981-15-0454-9_36

Table 1 Pollutants concentrations in the surface runoff

Road category	Runoff type	Pollutants concentration (mg l ⁻¹)		
		Iron ions	Lead ions	Oil products
I	Rainfall runoff	0.90	0.28	24
	Snowmelt runoff	0.93	0.30	26
II	Rainfall runoff	0.78	0.22	19.2
	Snowmelt runoff	0.80	0.24	20.8
III	Rainfall runoff	0.56	0.16	14.4
	Snowmelt runoff	0.60	0.18	15.6
IV	Rainfall runoff	0.43	0.11	9.6
	Snowmelt runoff	0.45	0.12	10.4
V	Rainfall runoff	0.30	0.08	7.2
	Snowmelt runoff	0.33	0.09	7.8

raphy and in the catchment area [1–4]. The main pollutants of surface runoff from highways are dissolved oil products and heavy metal ions (HMI) [5–8]. Table 1 shows data on the pollution degree of surface runoff depending on the road category.

Many measures are performed for reducing pollutants concentrations in surface runoff. The main ones are as follows: the organization of regular mechanized site cleanup, timely repair of roads pavement, the fencing of landscaping zones by borders, etc. In cases, when stormwater treatment is necessary, the entire wastewater volume should be directed to local treatment plants. The efficiency of local treatment plants can be increased by applying cheap and effective materials for pollutants neutralization.

Polluted runoff from roads is collected in roadside trays, ditches and closed sewers, located in the lower roads sections. There are several methods of surface runoff diversion from road:

- runoff spontaneously flows from road surface and is discharged from the shoulders along slopes, side channels for drainage systems, or cuvettes;
- runoff flows from road pavement into special trays for water collection. A reinforced drainage ditch is a place for surface water collection and an intermediate point before the treatment plants or land topography;
- runoff is collected in open types of trays located along the curbs on opposite sides of the road in order to subsequently get into the drainage ditch;
- urban runoff flows into the municipal surface sewage collection system.

2 Objects and Research Methods

The object of the research was selected granulated blast-furnace slag, which is waste of metallurgical production in Russia including cold regions. About a ton of slag is formed for each ton of metal when smelting iron and steel. Rapid cooling (granulation) contributes to the detection of glass in the slag, the content of which is up to 80% by mass or more. The gellenite, monticellite, spinel and other silicates, aluminates, and aluminum silicates of Ca and Mg are in the crystalline component [9, 10]. The authors consider the blast-furnace granulated slag of the Cherepovet’s Metallurgical Combine. This slag has an amorphous structure. It contains C₂S and a small amount of iron and manganese compounds. Table 2 presents the approximate chemical composition of the slag.

Atomic absorption method was used for investigation of the sorption characteristics of blast-furnace slag against heavy metal ions. The control over the water treatment degree from heavy metal ions was carried out on an atomic absorption spectrometer (AAS) of the Perkin–Elmer company (USA), model PE-305. It is designed for concentration determination through the monochromatic light absorption by element steam. The wavelength of the light corresponds to the center of the absorption line. AAS PE-305 allows determining more than 30 elements in the analytical laboratories conditions for solving ecology, agrochemistry, biology, medicine, geology, metallurgy, chemistry problems, and scientific research.

Laboratory infrared Fourier spectrometer (FSM) was used for investigation of the sorption characteristics of slag against oil products. It is intended for recording and studying optical spectra in the infrared (IR) region, as well as for environmental control, forensic, and other types of examinations.

PQ method was used for quality assessment of the proposed technological solutions. The PQ method allows evaluating not only the geological aspects of technological solutions, but also the economic and operational aspects, which are summarized then. The results of this method are the higher the index value, the higher the quality of the proposed technological solution.

The capacity (mg g⁻¹) is the main value characterizing the geocoprotective properties of slag to absorb heavy metal ions. It shows the mass of pollutants (mg) absorbed by one gram of slag [11–14].

Capacity was determined against various HMI and was calculated by the formula 1:

$$a = \frac{(C_i - C_r)V}{m} \tag{1}$$

Table 2 Chemical composition of the slag, mass%

Oxides content (mass%)					
SiO ₂	Al ₂ O ₃	Fe ₂ O ₃	CaO	MnO	MgO
41.92	6.6	0.33	44.8	0.9	2.38

where

- a capacity, mg g^{-1} ;
 C_i, C_r initial and residual concentrations of HMI in specimen, mg l^{-1} ;
 V specimen volume, l; and
 M slag mass, g

The treatment degree corresponded to the level of maximum allowable concentration (MAC) (for fishery water) for each metal. The capacity was determined under dynamic conditions: the treatment was carried out by filtration through the slag layer.

3 Research Results

First of all, researches conducted on the choice of the optimal grain size of the slag and the filtration rate of polluted water. Table 3 presents the results.

According to the experiment results on determination of dynamic capacity of the slag, a filtration rate of 6 m h^{-1} and 0.315–0.63 mm fraction size was chosen. For such conditions, the dynamic capacity of the slag was determined against various HMI (Table 4).

The dynamic capacity of slag was determined for each metal in the presence of the other two for investigation of slag ability to sorb the several heavy metal ions simultaneously. Table 5 demonstrates the research results.

The data from Table 4 confirm that selective sorption is not observed for any selected metals during simultaneous presence of all metal ions in the solution. The capacity for each metal has significantly decreased.

Table 3 Data on the choice of slag grain size and filtration rate

Grain size, mm	Filtered solution volume before breakthrough at the MAC (l)			
	Filtration rate (m h^{-1})			
	1	3	6	9
0.114–0.315	23	22	22	–
0.315–0.630	23	22	22	21
0.630–1.25	10	6	5	5
1.25–2.5	8	5	4	3
2.5–5.0	5	3	3	2

Table 4 Dynamic capacity of the slag (mg g^{-1})

HMI					
Mn^{2+}	Fe^{3+}	Ni^{2+}	Pb^{2+}	Cd^{2+}	Cr^{3+}
0.65	0.9	0.5	0.75	0.85	1.10

Table 5 Absorption research results

Sorbent	Dynamic capacity for each metal in the presence of two other (mg g ⁻¹)		
	Mn ²⁺	Fe ³⁺	Cr ³⁺
Slag	0.23	0.44	0.52

Table 6 Study results of exchangeable ions in the filtrate

Sorbent	Concentration of exchangeable metal ions (mg l ⁻¹)					
	Background content			HMI filtration		
	Ca ²⁺	K ⁺	Na ⁺	Ca ²⁺	K ⁺	Na ⁺
Slag	2	2	0.5	9.8	2.0	0.5

These studies were conducted on identification of exchangeable ions in the filtrate to explain the sorption mechanism. It was found that during water passes through the slag, calcium ions are washed out to water (Table 6).

The strength of formed bonds between the sorbent and HMI can be determined by «washing out» the ions into the aquatic medium from its surface. For this purpose, the slag was previously saturated by iron ions. Then analysis of slag aqueous extract was carried out (Table 7).

The research results shown in Table 6 exclude the possibility of HMI elution from sorbent surface.

Study of the sorption process in the simultaneous presence of water pollutants of various nature (organic and inorganic) is important for practical purposes. Studies on determination of sorbents sorption capacity have been conducted during simultaneous presence of HMI and dissolved oil products in water, as previous experiments have shown that the tested sorbents do not have selectivity for HMI sorption. There for model solution contained ions only one metal (manganese ions) with a concentration of 10 MAC and dissolved oil products with a concentration of about 2 mg l⁻¹. The breakthrough was taken as the concentration of HMI and dissolved oil products at a level which corresponds to the MAC. The research results showed that sorbents capacity for manganese during the presence of dissolved oil products in model solution is not decreased. These results indicate that HMI sorption does not depend on presence of organic pollutants in water. The research results allow proposing technological solutions for the use of blast-furnace metallurgical slag during highway construction and reconstruction in cold regions [15–19]:

Table 7 Analysis results of aqueous extract

Waste name	Fe (III) concentration in the aqueous extract (mg l ⁻¹)	Ca (II) concentration in the aqueous extract (mg l ⁻¹)
Slag	–	0.5–0.8

- firstly, granulated blast-furnace slag can be part of earth roadbed. In this case, HMI entering through surface runoff from road pavement will be neutralized in the earth roadbed;
- secondly, blast-furnace granulated slag can be used in gabion construction, which is applied in road construction for slope reinforcement or in treatment facilities.

The calculation of granulated slag effective life in the earth roadbed or gabion constructions was made on 5 km of category I road for conditional pollution by HMI with 10 MAC concentration.

Average width of this category road is up to 22.5 m, taking into account shoulder width (3.75 m), which is also subject of HMI pollution. The total pollution area of 5 km of the road is calculated by the formula (2):

$$S_p = l \cdot m, \quad (2)$$

where

S_p pollution area, m^2 ;

L road segment length, m;

M road segment width, m; and

$$S_p = 5000 \cdot 30 = 150,000 \text{ m}^2$$

The average annual rainfall for the North-West region is 500 mm per year. The precipitation volume, discharged on average per year from the surface of road segment, can be calculated by the formula (3):

$$V = S_p \cdot 0.5, \quad (3)$$

where

S_p pollution area, m^2 ;

0.5 average annual rainfall, m/year

$$V = 150,000 \cdot 0.5 = 75,000 \text{ m}^3/\text{year}$$

It was chosen the MAC for lead (0.001 mg l^{-1}) for effective life calculation. Lead ions concentration in runoff was taken 0.28 mg l^{-1} (0.28 g m^{-3}) from Table 1.

The total mass of pollutants discharged from the estimated road segment per year is calculated by the formula (4):

$$m = V \cdot 0.28, \quad (4)$$

where m —the lead ions mass in runoff from the estimated road segment, g/year.

$$m = 75,000 \cdot 0.28 = 21,000 \text{ g/year}$$

Rains with an intensity of 7–12 l s⁻¹ per 1 ha for 20 min almost completely flush all pollutants from catchment surface. Also, taking into account the snow removal during the winter period, the mass of lead ions entering gabion constructions can be up to 10% of the calculated (2100 g/year).

The lead mass that can be neutralized by blast-furnace metallurgical slag is calculated by the formula (5):

$$m_{\text{Pb}^{2+}} = a \cdot m_{\text{III}}, \tag{5}$$

where

- $m_{\text{Pb}^{2+}}$ lead ions mass, g;
- a slag capacity, g kg⁻¹; and
- m_{III} slag mass, kg

The weight of the used slag per 5 km will be 45,000 kg with 900 kg m⁻³ average density using up to 1 m³ of blast-furnace metallurgical slag for every 100 m of road segment. The slag capacity for lead is 0.75 g kg⁻¹ (Table 4).

$$m_{\text{Pb}^{2+}} = 45,000 \cdot 0.75 = 33,750 \text{ g}$$

Geocoprotective material effective life can be calculated by the formula (6):

$$T = \frac{m_{\text{Pb}^{2+}}}{m}, \tag{6}$$

where T —geocoprotective material effective life, years

$$T = \frac{33,750}{2100} = 16 \text{ years.}$$

The following factors should be taken into account when calculating the effective life:

- first, the slag volume can be significantly increased (up to 10–20 m³ for every 100 m of the road). This can significantly increase geocoprotective material effective life;
- second, the presence of other HMI will be reducing slag capacity (Table 5), which can decrease material effective life;
- third, the presence of suspended solids and film oil products in the surface runoff will be reducing the slag filtering capacity.

Therefore, the real effective life can only be determined on the results of monitoring the HMI concentrations in the surface runoff from specific road segment.

PQ method was used [20–24] to compare the proposed technological solutions for the application of granulated blast-furnace slag for surface runoff treatment from

Table 8 PQ index calculation results

Technological solutions	PQ indexes
Surface runoff purification in local sewage treatment plants	0.58
Surface runoff treatment using the slag in gabion constructions of road	0.73
Surface runoff treatment using slag in the composition of the earth roadbed	0.88

highways. The assessment was carried out on such aspects as geocoprotective, technological, and operational. Technological solutions were compared with the applied technology for surface runoff purification in local sewage treatment plants. Table 8 presents the results.

A higher PQ index for the technological solution with the use of slag in the composition of earth roadbed is explained by the simplicity of this solution in the implementation. The low PQ index for the technological solution with the use of local sewage treatment plants is explained by the high cost of 1 m³ surface runoff purification.

4 Conclusions

1. The use of granulated blast-furnace slag having geocoprotective properties against heavy metal ions for highways construction in cold regions is proposed. It will allow simultaneously solving the problems of slag utilization and surface runoff treatment from highway.
2. Studies have shown that calcium ions are washed out from slag into the filtrate during HMI absorption. There is no leaching of absorbed metals into an aqueous solution from a saturated slag. There is no selectivity against various HMI, and there is no impact of organic pollutants on the slag capacity.
3. Granulated blast-furnace slag can be used for surface runoff treatment from the highway as part of the earth roadbed or in gabion constructions.
4. The approximate effective life of the blast-furnace granulated slag can be calculated using the formulas proposed in the article. The real effective life can be determined by monitoring the surface runoff composition near roads in cold regions.
5. The quality assessment of the proposed technological solutions using the PQ method has shown the advantage of using granulated blast-furnace slag as part of the earth roadbed.

References

1. Zhou QQ, Leng GY, Su JH, Ren Y (2019) Comparison of urbanization and climate change impacts on urban flood volumes: importance of urban planning and drainage adaptation. *Sci Total Environ* 658:24–33
2. Sanda M, Vitvar T, Jankovec J (2019) Seasonal subsurface water contributions to baseflow in the mountainous Uhlirská catchment (Czech Republic). *J Hydrol Hydromechanics* 67:41–48
3. Hou WJ, Gao JB (2019) Simulating runoff generation and its spatial correlation with environmental factors in Sancha River Basin: the southern source of the Wujiang River. *J Geog Sci* 29:432–448
4. Jepsen SM, Harmon TC, Sadro S, Reid B, Chandra S (2019) Water residence time (age) and flow path exert synchronous effects on annual characteristics of dissolved organic carbon in terrestrial runoff. *Sci Total Environ* 656:1223–1237
5. Dausmann V, Gutjahr M, Frank M, Kouzmanov K, Schaltegger U (2019) Experimental evidence for mineral-controlled release of radiogenic Nd, Hf and Pb isotopes from granitic rocks during progressive chemical weathering. *Chem Geol* 507:64–84
6. Pressl A, Pucher B, Scharf B, Langergraber G (2019) Treatment of de-icing contaminated surface water runoff along an airport runway using in-situ soil enriched with structural filter materials. *Sci Total Environ* 660:321–328
7. Lazareva EV, Myagkaya IN, Kirichenko IS, Gustaytis MA, Zhmodik SM (2019) Interaction of natural organic matter with acid mine drainage: in-situ accumulation of elements. *Sci Total Environ* 660:468–483
8. Kwaansa-Ansah EE, Nkrumah D, Nti SO, Opoku F (2019) Adsorption of Heavy Metals (Cu, Mn, Fe and Ni) from Surface Water using *Oreochromis Niloticus* Scales. *Pollution* 5:115–122
9. Rytvin VM, Perepelitsyn VA, Ponomarenko AA, Gil'varg SI (2017) Titanium-Alumina slag—semifunctional technogenic resource of high-alumina composition. Part 1. Substance composition and Titanium-Alumina slag properties. *Refract Ind Ceram* 58:130–135
10. Zhao ML, Wu SP, Chen ZW, Li C (2017) Production and application of steel slag coarse aggregate in asphalt mixture. *Emerg Mater Res* 6:219–222
11. Shershneva MV, Makarova EI, Efimova NN (2017) Minimization of negative impact from solid waste landfills with use of mineral geoadaptants. *Procedia Eng* 189:315–319
12. Svatovskaya LB, Shershneva MV, Savelyeva MY (2017) Geocoprotective technologies of storage of used wooden sleepers. *Procedia Eng* 189:605–609
13. Shershneva MV, Makarova EI, Savelyeva MY (2017) Oil products absorbing properties of foam concretes. *Procedia Eng* 189:320–324
14. Svatovskaya LB, Shershneva MV, Bobrovnik AB (2017) Geocoprotective properties of binders for transport systems. *Procedia Eng* 189:440–445
15. Baidarashvili M, Sakharova A, Petriaev A (2017) The modern structure for storm sewage purification of roads. *Procedia Eng* 189:576–581
16. Svatovskaya LB, Urov OV, Kabanov AA (2017) Geocoprotective technology of transport construction using silica sol absorption method. *Procedia Eng* 189:454–458
17. Maslennikova LL, Naginskii IA, Troshev AN (2017) Use of waste from aluminothermic welding of railroad tracks in structural materials science. *Procedia Eng* 189:94–98
18. Svatovskaya LB, Kabanov AA, Sychov MM (2017) The improvement of foam concrete geocoprotective properties in transport construction. *IOP Conf Ser Earth Environ Sci* 90:012010
19. Maslennikova LL, Abu-Khasan MS, Babak NA (2017) The use of oil-contaminated crushed stone screenings in construction ceramics. *Procedia Eng* 189:59–64
20. Komokhov PG, Maslennikova LL, Makhmud A (2003) Control of strength of ceramic materials by forming the contact zone between clay matrix and leaning agent. *Stroitel'nye Mat* 12:44–46
21. Abu-Khasan M, Solovyova V, Solovyov D (2018) High-strength concrete with new organic mineral complex admixture. *MATEC Web Conf Proc* 193:03019

22. Svatovskaya LB, Shershneva MV, Baidarashvili MM, Yakimova NI, Khitrov AV (2004) Foam concrete construction demolished waste. In: Proceedings of the international conference on sustainable waste management and recycling. Construction Demolition Waste, London, pp 199–203
23. Maslennikova LL, Svatovskaya LB, Mjakin SV, Vasiljeva IV (2009) Activation of reactions at solid-solid interfaces. Improvement of ceramics materials. In: Electron beam modification of solids: mechanisms, common features and promising applications, pp 57–61
24. Svatovskaya LB, Sychova AM, Soloviova VY, Maslennikova LL, Sychov MM (2016) Absorptive properties of hydrate silicate building materials and products for quality and geocopro-tection improvement. *Indian J Sci Technol* 9(42):104231

Efficiency Evaluation of the Use of Mineral Technogenic Substances in Geocoprotective Technologies of Transport Construction



Maria Shershneva , Antonina Sakharova , Denis Anpilov and Egor Ereemeev

Abstract Today, the evaluation of the proposed geocoprotective technologies, including the transport facilities construction at low temperatures conditions, is imperative and timely. The purpose of the work is quality evaluation of geocoprotective technological solutions in construction and operation of traffic arteries. The task of the work is to study the possibility of the use of the property quality method (PQ) for geocoprotective technological solution evaluation. The objects of research are technological solutions which can reduce heavy metal ions concentration in geosystems. PQ method was used as evaluation method. The calculation results of the geocoprotective technologies efficiency, using geosynthetic materials, gabions, and mineral geoantidotes have been presented. Mineral geoantidotes (MGa) are substances that can detoxify heavy metal ions. The geomembrane for waterproofing of railroad body and MGa in the form of crushed silicate brick were used in the first technology. The gabion construction and MGa in the form of clinker as filling were proposed in the second technology. The third technology involves the use of a drainage tray, in which MGa in the form of autoclaved foam concrete waste is used as a drainage material. The authors of the article give the values of PQ indexes for these technologies and compare them with the currently known technologies. The article materials can be used for the development of technological geocoprotective solutions and their evaluation in transport construction of Russia and other countries including cold regions.

Keywords Geocoprotective technologies · Property quality method · Mineral geoantidotes · Geomembrane · Gabion

M. Shershneva · A. Sakharova (✉) · D. Anpilov · E. Ereemeev
Emperor Alexander I St. Petersburg State Transport University (PGUPS), St. Petersburg 190031,
Russia
e-mail: assakharova@list.ru

© Springer Nature Singapore Pte Ltd. 2020
A. Petriaev and A. Konon (eds.), *Transportation Soil Engineering in Cold Regions*,
Volume 2, Lecture Notes in Civil Engineering 50,
https://doi.org/10.1007/978-981-15-0454-9_37

1 Introduction

Currently, a problem's list of the evaluation of anthropogenic impact on the environment is formed. Among these problems, we can identify the insufficiently effective economic mechanism of nature management, including the innovative technologies evaluation to reduce the negative impact on the environment. In 2015, the inter-state standard GOST 33570-2015 «Resources saving. Waste treatment. Identification methodology. International experience» was published. This standard introduces the concept of «best available technologies», which means «innovative technological solutions to reduce the negative anthropogenic impact on the environment». The best available technologies have a fixed time for practical application, including economic, technical, environmental, and social factors. The standard contains the basic principles of economic feasibility evaluation from implementation of the best available technologies. However, the problem of economic assessment, environmental and social efficiency of the best available technologies continues to be relevant [1–4].

One of the most widely accepted methods of ecoprotective measure evaluation [2, 5, 6] is the calculation of prevented environmental damage. This method allows in monetary terms to assess the environment damage. But it does not allow choosing a specific technology with the same damage but with different application costs.

Scientists of the Engineering Chemistry and Natural Sciences Department of Emperor Alexander I St. Petersburg State Transport University developed innovative technological solutions for environmental protection from various nature pollutants [7–10]. They proposed the property quality method (PQ) for their evaluation.

2 Methods and Objects of Research

The PQ method allows evaluating not only the environmental aspects of the technology but also the technological and operational aspects of the technology. The obtained values are summed after the aspect evaluation, which is performed using certain mathematical operations [11–16]. This approach allows making a comprehensive evaluation of technological solutions. The higher is the index value in the PQ method, the higher is the technology quality.

When we use the PQ method, we can choose the best available technologies with the same environmental effect as the objects of research. When calculating the PQ index, we can independently choose the aspects by which the best technologies are evaluated. Technological, operational, economic, environmental, and social can be attributed to such aspects taking into account the above GOST. The significance of all aspects may be equally or one of the aspects may be assigned more or less important regarding other aspects. The significance of each aspect is determined by the region's economic and environmental conditions for which the calculation is performed.

It is possible to choose properties by which the best technologies will be evaluated for each aspect. The cost of implementing and operating the best technology should be taken into account in the economic aspect. In the environmental aspect, it is necessary to take into account the danger of environmental pollution and the achieved ecoprotective effect. The properties of technological and operational aspects take into account the possibility of the use of this technology in a particular region, the need for additional equipment, etc. The social aspect is estimated by demographic factors: population growth and morbidity. The significance of the aspects properties may differ on the relevance of the economic, social, and environmental problems of the region.

Evaluation of technological solutions by the PQ method is carried out according to the following algorithm:

- Step 1. The choice of research objects (the best available technologies).
- Step 2. The choice of aspects (economic aspect, environmental aspect, technological aspect, operational aspect, social aspect).
- Step 3. The choice of the aspect properties describing the object.
- Step 4. Determination of the intervals of property values ($I_{right-i}$; I_{left-i}).
- Step 5. Entering of a quality degradation coefficient (QDC) for each interval.
- Step 6. The calculation of the interval valuation coefficient.

$$C_d = \sum QDC_i * (I_{right-i} + I_{left-i}) \quad (1)$$

- Step 7. The calculation of the valuation coefficient for each interval.

$$C_{id} = QDC_i - C_d \quad (2)$$

- Step 8. The calculation of the PQ index on the interval limits.

$$PQ_{right} = PQ_{left} - (I_{right-i} + I_{left-i}) * C_{id} \quad (3)$$

- Step 9. Graphing of quality degradation.

Execution of the algorithm allows you to obtain PQ value, which corresponds to specific property in the considered aspect. After calculation, the dimensionless PQ index from 0 to 1 will be obtained. The highest value of the PQ index will characterize the best technology in certain aspects and their properties for the considered region including cold regions.

The Engineering Chemistry and Natural Sciences Department of Emperor Alexander I St. Petersburg State Transport University has created three new technological solutions for environmental protection [17–19]:

1. The use of geomembrane for waterproofing of railroad body and such mineral geoantidote (MGa) as crushed silicate brick. MGa has the ability to absorb heavy metal ions (HMI).
2. The use of gabion construction partially filled by such MGa as clinker.

3. The use of drainage tray, where MGa (autoclaved foam concrete waste) is used as a drainage material.

These technological solutions have become the objects of research for their evaluation using PQ method.

The standard method of prevented environmental damage calculation does not allow considering simultaneously various aspects (geoecological, technological, operational, etc.) from the technological solution implementation. The PQ method allows making a comparative evaluation.

When using the PQ method, each new technological solution was compared with the known technology currently used in railway transport. The following aspects were chosen: geoecological, technological, and operational. The specific value (SV^1) of the environmental aspect was taken as 50%, SV^2 and SV^2 of the other two aspects were taken as 25%.

The following properties were chosen for geoecological aspect:

- the HMI presence in the surface runoff of the railway track ($SV_{1,1}$ of this property is 25%);
- the presence of film and dissolved oil products in the surface runoff of the railway track ($SV_{1,2}$ of this property is 25%);
- possibility of waste utilization ($SV_{1,3}$ of this property is 25%);
- possibility of release of the useful lands occupied for waste placement ($SV_{1,4}$ of this property is 25%).

The following properties were chosen for technological aspect:

- compliance of used materials with physicomechanical requirements ($SV_{2,1}$ of this property is 33%);
- filtering capacity of materials ($SV_{2,2}$ of this property is 33%);
- the need for additional operations ($SV_{2,3}$ of this property is 34%).

The following properties were chosen for operational aspect:

- the materials effective life ($SV_{3,1}$ of this property is 33%);
- the materials availability ($SV_{3,2}$ of this property is 33%);
- the materials cost ($SV_{3,3}$ of this property is 34%).

After the $PQ_{j,k}^n$ index calculation, data were obtained (Table 1) for the first technological solution (the use of geomembrane and crushed silicate bricks).

The next step of the calculation is to determine the PQ_j^n index on various objects and properties using the next formula:

$$PQ_j^n = \sum SV_{j,k} * PQ_{j,k}^n \quad (4)$$

Table 1 $PQ_{j,k}^n$ index of technological solution «The use of geomembrane and crushed silicate bricks» for all aspects

Aspect	Property	$PQ_{j,k}^n$ index (designation)	
		The use of geomembrane and crushed silicate bricks	The use of geomembrane
Geoecological	The HMI presence in the surface runoff of the railway track	0.8 ($PQ_{1,1}^1$)	0 ($PQ_{1,1}^2$)
	The presence of film and dissolved oil products in the surface runoff of the railway track	0.25 ($PQ_{1,2}^1$)	0 ($PQ_{1,2}^2$)
	Possibility of waste utilization	1 ($PQ_{1,3}^1$)	0 ($PQ_{1,3}^2$)
	Possibility of release of the useful lands occupied under waste placement	1 ($PQ_{1,4}^1$)	0 ($PQ_{1,4}^2$)
Technological	Compliance of used materials with physicochemical requirements	1 ($PQ_{2,1}^1$)	1 ($PQ_{2,1}^2$)
	Filtering capacity of materials	1 ($PQ_{2,2}^1$)	1 ($PQ_{2,2}^2$)
	The need for additional operations	0.665 ($PQ_{2,3}^1$)	1 ($PQ_{2,3}^2$)
Operational	The materials effective life	1 ($PQ_{3,1}^1$)	1 ($PQ_{3,1}^2$)
	The materials availability	0.35 ($PQ_{3,2}^1$)	0.9 ($PQ_{3,2}^2$)
	The materials cost	0.5 ($PQ_{3,3}^1$)	0.21 ($PQ_{3,3}^2$)

1. We have been obtained the following property values for the geoecological aspect ($j = 1$):

– the use of geomembrane and crushed silicate bricks (PQ_1^1)

$$PQ_1^1 = 0.25 \cdot 0.8 + 0.25 \cdot 0.25 + 0.25 \cdot 1 + 0.25 \cdot 1 = 0.7625$$

– The use of geomembrane (PQ_1^2)

$$PQ_1^2 = 0.25 \cdot 0 + 0.25 \cdot 0 + 0.25 \cdot 0 + 0.25 \cdot 0 = 0$$

2. We have been obtained the following property values for the technological aspect ($j = 2$):

- the use of geomembrane and crushed silicate bricks (PQ_2^1)

$$PQ_2^1 = 0.33 \cdot 1 + 0.33 \cdot 1 + 0.34 \cdot 0.665 = 0.8861$$

- the use of geomembrane (PQ_2^2)

$$PQ_2^2 = 0.33 \cdot 1 + 0.33 \cdot 1 + 0.34 \cdot 1 = 1$$

3. We have been obtained the following property values for the operational aspect ($j = 3$):

- the use of geomembrane and crushed silicate bricks (PQ_3^1)

$$PQ_3^1 = 0.33 \cdot 1 + 0.33 \cdot 0.35 + 0.34 \cdot 0.5 = 0.6155$$

- the use of geomembrane (PQ_3^2)

$$PQ_3^2 = 0.33 \cdot 1 + 0.33 \cdot 0.9 + 0.34 \cdot 0.21 = 0.6984$$

Similar calculations were made for two other technological solutions.

Table 2 presents data obtained for the second technological solution (the use of clinker in the gabion construction) after the $PQ_{nj \cdot k}$ index calculation.

1. We have been obtained the following property values for the geoeological aspect ($j = 1$):

- the use of clinker in the gabion construction (PQ_1^3)

$$PQ_1^3 = 0.25 \cdot 0.8 + 0.25 \cdot 1 + 0.25 \cdot 0 + 0.25 \cdot 0 = 0.45$$

- the use of gabion construction (PQ_1^4)

$$PQ_1^4 = 0.25 \cdot 0 + 0.25 \cdot 0 + 0.25 \cdot 0 + 0.25 \cdot 0 = 0$$

2. We have been obtained the following property values for the technological aspect ($j = 2$):

- the use of clinker in the gabion construction (PQ_2^3)

$$PQ_2^3 = 0.33 \cdot 1 + 0.33 \cdot 1 + 0.34 \cdot 0.665 = 0.8861$$

- the use of gabion construction (PQ_2^4)

$$PQ_2^4 = 0.33 \cdot 1 + 0.33 \cdot 1 + 0.34 \cdot 1 = 1$$

Table 2 $PQ_{j \bullet k}^n$ index of technological solution «The use of clinker in the gabion construction» for all aspects

Aspect	Property	$PQ_{j \bullet k}^n$ index (designation)	
		The use of clinker in the gabion construction	The use of gabion construction
Geoecological	The HMI presence in the surface runoff of the railway track	0.8 ($PQ_{1,1}^3$)	0 ($PQ_{1,1}^4$)
	The presence of film and dissolved oil products in the surface runoff of the railway track	1 ($PQ_{1,2}^3$)	0 ($PQ_{1,2}^4$)
	Possibility of waste utilization	0 ($PQ_{1,3}^3$)	0 ($PQ_{1,3}^4$)
	Possibility of release of the useful lands occupied under waste placement	0 ($PQ_{1,4}^3$)	0 ($PQ_{1,4}^4$)
Technological	Compliance of used materials with physicochemical requirements	1 ($PQ_{2,1}^3$)	1 ($PQ_{2,1}^4$)
	Filtering capacity of materials	1 ($PQ_{2,2}^3$)	1 ($PQ_{2,2}^4$)
	The need for additional operations	0.665 ($PQ_{2,3}^3$)	1 ($PQ_{2,3}^4$)
Operational	The materials effective life	1 ($PQ_{3,1}^3$)	1 ($PQ_{3,1}^4$)
	The materials availability	0.5 ($PQ_{3,2}^3$)	0.9 ($PQ_{3,2}^4$)
	The materials cost	0 ($PQ_{3,3}^3$)	0.95 ($PQ_{3,3}^4$)

3. We have been obtained the following property values for the operational aspect ($j = 3$):

– the use of clinker in the gabion construction (PQ_3^3)

$$PQ_3^3 = 0.33 \cdot 1 + 0.33 \cdot 0.5 + 0.34 \cdot 0 = 0.495$$

– the use of gabion construction (PQ_3^4)

$$PQ_3^4 = 0.33 \cdot 1 + 0.33 \cdot 0.9 + 0.34 \cdot 0.95 = 0.95$$

Table 3 illustrates data for the third technological solution (the use of autoclaved foam concrete waste in drainage tray) after the $PQ_{j,k}^n$ index calculation.

1. We have been obtained the following property values for the geoeological aspect ($j = 1$):

- the use of autoclaved foam concrete waste in drainage tray (PQ_1^5)

$$PQ_1^5 = 0.25 \cdot 0.95 + 0.25 \cdot 0.25 + 0.25 \cdot 1 + 0.25 \cdot 1 = 0.8$$

- the use of drainage tray (PQ_1^6)

Table 3 $PQ_{j,k}^n$ index of technological solution «The use of autoclaved foam concrete waste in drainage tray» for all aspects

Aspect	Property	$PQ_{j,k}^n$ index (designation)	
		The use of autoclaved foam concrete waste in drainage tray	The use of drainage tray
Geoeological	The HMI presence in the surface runoff of the railway track	0.95 ($PQ_{1,1}^5$)	0 ($PQ_{1,1}^6$)
	The presence of film and dissolved oil products in the surface runoff of the railway track	0.25 ($PQ_{1,2}^5$)	0 ($PQ_{1,2}^6$)
	Possibility of waste utilization	1 ($PQ_{1,3}^5$)	0 ($PQ_{1,3}^6$)
	Possibility of release of the useful lands occupied under waste placement	1 ($PQ_{1,4}^5$)	0 ($PQ_{1,4}^6$)
Technological	Compliance of used materials with physicochemical requirements	1 ($PQ_{2,1}^5$)	1 ($PQ_{2,1}^6$)
	Filtering capacity of materials	1 ($PQ_{2,2}^5$)	1 ($PQ_{2,2}^6$)
	The need for additional operations	1 ($PQ_{2,3}^5$)	1 ($PQ_{2,3}^6$)
Operational	The materials effective life	1 ($PQ_{3,1}^5$)	1 ($PQ_{3,1}^6$)
	The materials availability	0.15 ($PQ_{3,2}^5$)	0.9 ($PQ_{3,2}^6$)
	The materials cost	0.93 ($PQ_{3,3}^5$)	0.21 ($PQ_{3,3}^6$)

$$PQ_1^6 = 0.25 \cdot 0 + 0.25 \cdot 0 + 0.25 \cdot 0 + 0.25 \cdot 0 = 0$$

2. We have been obtained the following property values for the technological aspect ($j = 2$):

- the use of autoclaved foam concrete waste in drainage tray (PQ_2^5)

$$PQ_2^5 = 0.33 \cdot 1 + 0.33 \cdot 1 + 0.34 \cdot 1 = 1$$

- the use of drainage tray (PQ_2^6)

$$PQ_2^6 = 0.33 \cdot 1 + 0.33 \cdot 1 + 0.34 \cdot 1 = 1$$

3. We have been obtained the following property values for the operational aspect ($j = 3$):

- the use of autoclaved foam concrete waste in drainage tray (PQ_3^5)

$$PQ_3^5 = 0.33 \cdot 1 + 0.33 \cdot 0.15 + 0.34 \cdot 0.93 = 0.6957$$

- the use of drainage tray (PQ_3^6)

$$PQ_3^6 = 0.33 \cdot 1 + 0.33 \cdot 0.9 + 0.34 \cdot 0.21 = 0.6984$$

Next step, the PQ^n index was calculated for each technology using formula (5):

$$PQ^n = \sum SV^n * PQ_j^n \tag{5}$$

1. PQ^n index of technological solution «The use of geomembrane and crushed silicate bricks»:

$$PQ^1 = 0.5 \cdot 0.7625 + 0.25 \cdot 0.8861 + 0.25 \cdot 0.6155 = 0.7567$$

2. PQ^n index of technological solution «The use of geomembrane»:

$$PQ^2 = 0.5 \cdot 0 + 0.25 \cdot 1 + 0.25 \cdot 0.6984 = 0.4246$$

3. PQ^n index of technological solution «The use of clinker in the gabion structure»:

$$PQ^3 = 0.5 \cdot 0.45 + 0.25 \cdot 0.8861 + 0.25 \cdot 0.495 = 0.5703$$

4. PQ^n index of technological solution «The use of gabion structure»:

$$PQ^4 = 0.5 \cdot 0 + 0.25 \cdot 1 + 0.25 \cdot 0.95 = 0.4875$$

Table 4 Results of the PQ index calculation

Objects of research	PQ index
The use of geomembrane and crushed silicate bricks	0.7567
The use of geomembrane	0.4246
The use of clinker in the gabion structure	0.5703
The use of gabion construction	0.4875
The use of autoclaved foam concrete waste in drainage tray	0.8239
The use of drainage tray	0.4246

5. PQ^5 index of technological solution «The use of autoclaved foam concrete waste in drainage tray»:

$$PQ^5 = 0.5 \cdot 0.8 + 0.25 \cdot 1 + 0.25 \cdot 0.6957 = 0.8239$$

6. PQ^6 index of technological solution «The use of drainage tray»:

$$PQ^6 = 0.5 \cdot 0 + 0.25 \cdot 1 + 0.25 \cdot 0.6984 = 0.4246$$

Table 4 presents the results of PQ index calculation.

3 Conclusions

1. Using the PQ method to evaluate geocoprotective technology solutions allows you combining different evaluation aspects and choosing the best for a specific region including cold regions.
2. The PQ method allows for uniform rating scale to evaluate the quality of these various properties such as the material cost, decontamination, material availability, and physicomechanical characteristics.
3. Evaluation of the proposed technological solutions by PQ method taking into account geocological, technological, and operational aspects showed the advantage of these technological solutions. The use of these technologies will minimize the negative environmental impact of railway facilities.

References

1. Markiewicz A, Bjorklund K, Eriksson E, Kalmykova Y, Stromvall AM, Siopi A (2017) Emissions of organic pollutants from traffic and roads: priority pollutants selection and substance flow analysis. *Sci Total Environ* 580:1162–1174
2. Levashov SP, Yakimchuk NA, Korchagin IN (2018) Innovative geoelectric methods: multi-year experience of application for the practical problems of near-surface geophysics operative solution. *Geofizicheskiy Zhurnal-Geophys J* 40:97–128
3. Duong HT, Kadokami K, Trinh H, Phan TQ, Le GT, Nguyen DT, Nguyen TT (2019) Target screening analysis of 970 semi-volatile organic compounds adsorbed on atmospheric particulate matter in Hanoi Vietnam. *Chemosphere* 219:784–795
4. Svatovskaya LB, Urov OV, Kabanov AA (2017) Geoeoprotective technology of transport construction using silica sol absorption method. *Procedia Eng* 189:454–458
5. Kounetas K, Zervopoulos PD (2019) A cross-country evaluation of environmental performance: is there a convergence-divergence pattern in technology gaps? *Eur J Oper Res* 273:1136–1148
6. Korneeva TV, Yurkevich NV, Saeva OP (2018) Geochemical modeling of heavy metals behavior in technogenic systems. *Bull Tomsk Polytechnic University-Geo Assets Eng* 329:89–101
7. Shershneva MV, Makarova EI, Savelyeva MY (2017) Oil products absorbing properties of foam concretes. *Procedia Eng* 189:320–324
8. Svatovskaya LB, Shershneva MV, Bobrovnik AB (2017) Geoeoprotective properties of binders for transport systems. *Procedia Eng* 189:440–445
9. Maslennikova LL, Naginskii IA, Troshev AN (2017) Use of waste from aluminothermic welding of railroad tracks in structural materials science. *Procedia Eng* 189:94–98
10. Svatovskaya LB, Kabanov AA, Sychov MM (2017) Soling, aerating and phosphating for soil strengthening and detoxication. *Procedia Eng* 189:398–403
11. Balaman SY, Wright DG, Scott J, Matopoulos A (2018) Network design and technology management for waste to energy production: An integrated optimization framework under the principles of circular economy. *Energy* 143:911–933
12. Das Sharma S (2019) Risk Assessment and mitigation measures on the heavy metal polluted water and sediment of the Kolleru lake in Andhra Pradesh India. *Pollution* 5:161–178
13. Gonzalez-Castano A, Bandoni JA, Diaz MS (2018) Toward economically and environmentally optimal operations in natural gas based petrochemical sites. *Ind Eng Chem Res* 57:5999–6012
14. Kazaryan R (2018) Regarding some aspects of economic feasibility for the transport integrated use in favor of environmental security. In: Ilin I, Kalinina O (eds) International science conference Spbwosce-2017 business technologies for sustainable urban development
15. Leonzio G (2016) Upgrading of biogas to bio-methane with chemical absorption process: simulation and environmental impact. *J Clean Prod* 131:364–375
16. Matthes S, Grewe V, Dahlmann K, Fromming C, Irvine E, Lim L, Linke F, Luhrs B, Owen B, Shine K, Stromatas S, Yamashita H, Yin FJ (2017) A Concept for multi-criteria environmental assessment of aircraft trajectories. *Aerospace* 4:42
17. Svatovskaya LB, Sakharova AS, Baidarashvilly MM, Petriaev AV (2015) Building wastes and cement clinker using in the geoeoprotective technologies in transport construction. In: Proceedings of the 14th international conference of international association for computer methods and recent advances in geomechanics, IACMAG. Taylor and Francis, Balkema, Netherlands pp 619–622
18. Svatovskaya LB, Shershneva MV, Savelyeva MY (2017) Geoeoprotective technologies of storage of used wooden sleepers. *Procedia Eng* 189:605–609
19. Svatovskaya LB, Sychova AM, Soloviova VY, Maslennikova LL, Sychov MM (2016) Absorptive properties of hydrate silicate building materials and products for quality and geoeoprotection improvement. *Indian J Sci Technol* 9(42):104231

A High-Performance Repair Mixture to Restore and Protect Damaged Concrete Structures



Valentina Solovieva, Irina Stepanova, Dmitriy Soloviev and Anna Kasatkina

Abstract In cold regions, one of the major problems is frozen soils, which periodically thaw unevenly, which negatively affects the stability and integrity of concrete structures. The research area is the construction in cold regions. It is shown in the paper that modified repair solutions based on a modified repair mixture have a double effect: penetration effect and protective one. The penetration effect of the mortar mix ensures an increase in compressive strength by two classes, water resistance by two grades and frost resistance by 100 cycles to the loosen concrete base. Repair compositions used as a protective material have high crack resistance, and they are corrosion-resistant materials relative to carbon dioxide and magnesia corrosion. At the same time, they are characterized by high adhesive strength to the concrete base, creating the integrity of the restored base and protective repair composition. The modified repair mix possesses highly effective protective properties in relation to the concrete basis, due to high indicators of durability, crack resistance and corrosion resistance.

Keywords Repair mixture · Strength · Crack resistance · Integrity · Penetration effect · Protection · Water resistance · Modification · Activation · Corrosion resistance · Adhesive strength

1 Introduction

One of the problems of our time is the restoration of physical and mechanical properties of concrete structures loosened and damaged under the influence of external loads, the negative impact of the environment and their long-term operation.

V. Solovieva · I. Stepanova (✉) · D. Soloviev · A. Kasatkina
Emperor Alexander I St. Petersburg State Transport University (PGUPS), St. Petersburg 190031,
Russia
e-mail: ivstepanova88@mail.ru

© Springer Nature Singapore Pte Ltd. 2020
A. Petriaev and A. Konon (eds.), *Transportation Soil Engineering in Cold Regions*,
Volume 2, Lecture Notes in Civil Engineering 50,
https://doi.org/10.1007/978-981-15-0454-9_38

To solve the above problem, it requires the creation of a high-performance repair compound having double effects: restoring and protective ones. The developed mixture should have the ability to penetrate deep into the concrete base, having a positive effect on the restoration of its properties. And having improved quality indicators and increased adhesive strength, it would effectively protect the restored or reinforced base in the future [1–10].

The double effects of the repair mixture can be achieved by modifying it with additives of a certain nature which would have the ability to penetrate into the pores of the concrete base, and at the same time it would have the ability to produce an activation effect on the hydration processes of the mixture and base components [11–20].

The repair mixture of double effects requires high-performance chemical additives of a new generation, and so this scientific study is devoted to their creation.

2 Methods and Objects of Research

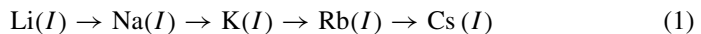
The basis for the creation of mortar mixes with a penetration effect of action is the idea about the possible intrinsic mobility of fine particles.

The penetration of fine particles from the mortar mix into the concrete base is based on the concept of transport mechanisms of ions or nanoparticles (size from 1 to 100 nm).

For example, nanoparticles of $\text{SiO}_2 \cdot n\text{H}_2\text{O}$, which are the basis of silica sol, have a developed surface and, as a consequence, high surface energy which enhances their ability to high mobility.

Due to high mobility, the nanoparticles are able to penetrate into the pores of the concrete base, carrying particles of the appropriate size, for example, new hydrate compounds formed from the mortar mix.

According to Samoilov O. Ya., cations of large radii also have increased mobility, but at the same time they have a small hydrate shell. The mobility of cations and their ability to penetrate as deep as possible into the concrete base are enhanced in the following sequence (1):



This fact was established experimentally and is consistent with the data of other scientists.

The penetration of hydrate compounds into the pores of the base and the formation of new hydrate compounds in the concrete base as a result of the involvement of unreacted cement minerals in the hydration processes result from the effective action of reactive additives.

The effectiveness of the protective effect of the modified solution is due to the physical and mechanical characteristics of the hardening mortar mix and the concrete base. The more hydrate compounds are produced in the protective coating, as well

as the more hydrate compounds are formed again in the concrete base, the more durable the contact is between the solution and the base, since at the time of their formation hydrate compounds have uncompensated bonds which are realized during the contact between the newly formed hydrate compounds of the protective solution and the concrete base.

To implement these theoretical assumptions, a high-performance complex chemical additive including the components of this effect is required.

It is effective to use polycarboxylate polymers as the basis of a complex additive [9, 10]. They are surfactants that have a positive effect on increasing the mobility of the components of the repair mix. In addition, as reactive components, it is advisable to consider the following:

- salts on the basis of the potassium cation having high mobility, such as potassium nitrite KNO_2 . They are able to increase the reactivity of the minerals of Portland cement without causing the corrosion of reinforcement.
- high mobility and reaction nanoparticles, for example, $\text{SiO}_2 \cdot n\text{H}_2\text{O}$, which are the basis of the colloidal solution of silicic acid. The addition of $\text{SiO}_2 \cdot n\text{H}_2\text{O}$ dispersions in a cement-containing system is useful because nanoparticles of $\text{SiO}_2 \cdot n\text{H}_2\text{O}$ have high mobility and high reaction activity. They are able to come into chemical interaction with various compounds of calcium, forming additional sparingly soluble complex hydrated compounds of calcium. This contributes to the improvement of the strength, density, crack resistance and corrosion resistance of the repair composition and the concrete base.

The evaluation of the effectiveness of the modified repair mixture was carried out by changing the compressive strength, tensile strength in bending and crack resistance of the repair material.

A comprehensive evaluation of the modified mortar mix effects was made by the change of the compressive strength, water resistance and frost resistance of the actual repair material and the concrete base.

For this purpose, cube samples of $10 \times 10 \times 10$ cm in size, made of concrete B25 and B30, were used as the most widely employed specimens in construction.

3 Results and Discussion

At the first stage of this study, the effectiveness of the developed complex chemical additive to change the strength of the repair mortar mix was assessed. The results of the research are presented in Table 1.

Analysis of the data given in Table 1 shows that the use of the complex chemical additive is most effective in an amount equal to 1.0% of the cement mass. In this case, the compressive strength of the hardened repair material is increased by 34–36% and the tensile strength in bending rises to a greater extent, by 43–45%. This increases the crack resistance of the repair material to 8.0%.

Table 1 Evaluation of the effectiveness of the developed complex chemical additive

№	Cement consumption per 1 m ³ of mortar mix (kg)	Consumption of the complex additive, % by cement mass	Strength (MPa %)				$C_{c.r.} = \frac{R_{b.t.}}{R_{com.}}$ (at the age of 28 days)
			Compressive strength		Tensile strength in bending		
			Age, days		Age, days		
			7	28	7	28	
1	2	3	4	5	6	7	8
1	300	–	17.5	26.0	2.0	3.0	0.115
2		0.8	23.6	34.5	2.6	4.2	0.122
3		1.0	23.8	34.8	2.7	4.3	0.124
4		1.2	23.7	34.6	2.6	4.2	0.121
5	350	–	22.0	32.7	2.6	3.9	0.119
6		0.8	30.0	43.9	3.5	5.5	0.125
7		1.0	30.2	44.1	3.6	5.6	0.126
8		1.2	30.1	44.0	3.5	5.5	0.125

One of the objectives of this study is to restore the physical and mechanical properties of damaged or loosened concrete structures.

The ability of the repair mixture to restore the concrete base is achieved not only by the reactivity of the components, but also by their ability to penetrate as deeply as possible into the concrete base.

The simultaneous presence of both surfactants on the basis of polycarboxylate and the modifier represented by potassium nitrite, KNO_2 , with the sol of silicic acid, $SiO_2 \cdot nH_2O$, is favorable. This contributes to the obtaining of a high effect of the penetration of particles into the concrete base, ensuring the formation of a maximum homogeneous structure along the height of the concrete structure.

When treating a concrete base with the modified mortar mix, the pore space of concrete is filled with fine particles that are part of the mortar mix. They are formed during the hardening of the mortar mix and move deep into the concrete base, resulting in an increase in the density of the pore structure of the concrete base.

According to microscopic studies conducted with the help of automatic image analyzer “Video Test,” it was found that the average pore size of the base is reduced by 13% of the diameter equal to 0.2954 mm to a value of 0.2586 mm. At the same time, the pore surface of the sample is reduced by 31% of the pore space area percentage, $S = 8.395\%$ to a value of $S = 5.86\%$.

As a result of the compaction of the base structure, the compressive strength parameters are improved. For concrete class B25 and B30, the strength is increased

by two classes: from class B25 to class B35 and from class B30 to class B40. The durability indicators such as water resistance and frost resistance give rise as well.

It is experimentally proved that the frost resistance is increased by 100 cycles, and the water resistance is increased by two grades.

In addition, the corrosion resistance of the modified repair solution was investigated relative to carbon dioxide and magnesia corrosion. 5% solution of sodium carbonate, Na_2CO_3 , and 5% solution of magnesium chloride, MgCl_2 , were used to assess corrosion resistance. The corrosion resistance of the repair solution modified by the complex additive consisting of potassium nitrite, KNO_2 , silicic acid sol, $\text{SiO}_2 \cdot n\text{H}_2\text{O}$, and a surfactant represented by polycarboxylate polymers increases by more than 15% relative to the control composition.

It was established that the coefficient of the chemical resistance of the modified repair mortar has the value $C_{\text{ch.r}} \approx 0.87$. Hence, the modified repair solution belongs to the category of chemically stable materials.

To assess the integrity of the composition, concrete base—repair material, the value of adhesive strength is used. It was experimentally determined that the adhesive strength to the surface of the concrete base varies in the range from 1.1 to 1.7 MPa depending on the strength of the concrete base. This is sufficient to ensure the integrity of the composition.

4 Conclusions

It was found that the repair mixture modified by the complex additive which is based on a surfactant on a polycarboxylate basis in combination with an electrolyte represented by potassium nitrite, KNO_2 , and silica sol, $\text{SiO}_2 \cdot n\text{H}_2\text{O}$, has an increased penetration effect which has a positive effect on an increase of as follows:

- compressive strength;
- adhesion strength;
- water resistance;
- frost resistance;
- corrosion resistance;
- ensuring the restoration of the specified quality parameters of loosened or damaged concrete base to the design value or above.

It was shown that the modified repair mixture has high-performance protective properties in relation to the concrete base, due to high indicators of strength, crack resistance and corrosion resistance.

References

1. Solovieva VY, Maslennikova LL, Abu-Khasan M, Stepanova IV, Smirnova TV, Boykova TI, Makarov VV, Kasatkin SP (2017) Thermodynamic basis for creating high-strength concrete and curing for pavements. *Sci. Technol.* 2(104):156–162
2. Solovieva VY, Kasatkina AS, Soloviev DV (2014) An innovative method of creating nanocomposite materials to restore and increase the level of physical and mechanical properties of concrete structures. In: *Materials of 1st international scientific-practical conference: innovative technologies in engineering and geoecology*, pp 42–46. Sputnik+, Moscow
3. Svatovskaya L, Solovieva V, Sychova A, Maslennikova L, Sychov M (2016) Absorptive properties of hydrate silicate building materials and products for quality and geoecoprotection improvement. *Indian J Sci Technol* 9(42):104304
4. Solovieva VY, Boykova TI, Kasatkin SP, Ershikov NV, Kasatkina AV (2016) Restoration and protection of building structures, as the preservation of the natural and man-made environment. *Materials of 2nd international scientific-practical conference: geoecology of lithosphere protection*, pp 33–36. Sputnik+, Moscow
5. Svatovskaya LB, Sakharova AS, Baidarashvily MM, Petriaev AV (2015) Building wastes and cement clinker using in the geoecoprotective technologies in transport construction. In: *Proceedings of the 14th international conference, computer methods and recent advances in geomechanics*, pp 619–622. Taylor and Francis—Balkema, Netherlands
6. Solovieva VY, Galanov EK (2015) The study of the electrical conductivity of cement M400 in the process of hydration and crystallization. *Proc Emp Alexander I Petersburg State Transp Univ* 4(45):101–107
7. Estemesov ZA, Soltambekov KT, Bondareva VM (2001) New in chemistry and technology of silicate and building materials. *Collect Art* 1:90–100. CELLSIM, Almaty
8. Korneev VI, Zozulya PV (2004) Dry building mixtures (composition, properties). SPSSS, St. Petersburg
9. Sultanbekov TK, Shayakhmetov TK, Soltambekov TK, Estemesov KT (2001) Modern dry building mixtures. Bastau, Almaty
10. Shangin VYu (2011) How and why are destroyed stone structures. IMEF, Ivanovo
11. Kondratov V, Solovyova V, Stepanova I (2017) The development of a high performance material for a ballast layer of a railway track название. *Procedia Engineering* 189:823–828
12. Boikova T, Solovyov D, Solovieva V (2017) Concrete for road pavements. *Proc Eng* 189:800–804
13. Boykova TI, Solovyova VY, Solovyov DV (2017) Effective repair and refurbishment compound for the strengthening of a road concrete pavements. *Proc Eng* 189:650–653
14. Sychov MM, Ogurtsov KA, Lebedev VT, Kulvelis Yu V, Török Gy, Sokolov AE, Trunov VA, Bakhmetyev VV, Kotomin AA, Dushenok SA, Kozlov AS (2012) *Semiconductors* 46–5: 696–700
15. Solovieva VY, Smirova TV, Stepanova IV, Shershneva MV (2014) *Methodological guidelines*. PGUPS, St. Petersburg
16. Solovieva VY, Surkov VN (2015) Concrete that does not require high quality raw materials. *Oil Gas* 4(13):239–243
17. Solovieva VY, Kasatkin SP, Stepanova IV, Ershikov NV (2015) Development of high strength concrete. In: *Materials of I international scientific-practical conference: innovative technologies in engineering and geoecology*, pp 23–27. Sputnik+, Moscow
18. Solovieva VY, Maslennikova LL, Abu-Khasan M, Stepanova IV, Ershikov NV, Boykova TI, Makarov VV, Kasatkin SP (2017) Physical and chemical bases of the processes of curing innovative concrete for pavements. *Sci Technol* 2(104):150–155

19. Medvedev PI (1957) Physical and colloidal chemistry. Gos. Publishing House of Agricultural Literature, Moscow
20. Pukhareno YuV, Shangina NN, Safonova TA (2011) Evaluation of the use of carbonate aggregates in the composition of dry mixes for restoration. Bull Civil Eng 1(26):98–103

Multifunctional Nanomodified Concrete of New Generation



Valentina Solovieva, Irina Stepanova, Dmitriy Soloviev
and Tatyana Kravchenko

Abstract The research area is construction in cold regions. It is shown in the paper that in order to create multifunctional concrete with a new level of physical and mechanical properties it is advisable to use two complex chemical additives on a polycarboxylate basis of a different nature simultaneously. They are modified by nanostructural elements of natural and synthetic origin. These chemical additives have the plasticization and reaction effects on cement-containing concrete mix, and they ensure the formation of new organic mineral chains, micro-reinforcing the structure of concrete from the moment of its manufacture to full hardening. The result of the combined effect of two complex chemical additives is the creation of the densest and the most durable concrete characterized by increased crack resistance, frost resistance and water resistance. It can be recommended for the manufacture of essential structures and for high-rise construction, including construction on problem soils in the regions of permafrost.

Keywords Chemical additive · High-strength concrete · Deformation characteristics · Crack resistance · Frost resistance · Durability · Improvement of physical and mechanical characteristics

1 Introduction

One of the directions of modern construction is high-rise construction, including construction in permafrost regions which are particularly unfavorable regions because of uneven thawing of soils in summer.

During the construction of high-rise buildings and structures, it is necessary to take into account two main factors:

V. Solovieva · I. Stepanova (✉) · D. Soloviev · T. Kravchenko
Emperor Alexander I St. Petersburg State Transport University (PGUPS), St. Petersburg 190031,
Russia
e-mail: ivstepanova88@mail.ru

© Springer Nature Singapore Pte Ltd. 2020
A. Petriaev and A. Konon (eds.), *Transportation Soil Engineering in Cold Regions*,
Volume 2, Lecture Notes in Civil Engineering 50,
https://doi.org/10.1007/978-981-15-0454-9_39

- The reduction of the structure weight to exert less pressure on the foundation of the structure. This can be achieved by the manufacture of concrete structures having reduced thickness through the use of high-strength concrete.
- The improvement of the deformation characteristics of concrete, such as tensile strength in bending and crack resistance, to avoid cracking in exploited structures even during uneven thawing of the soil [1–7, 19–21].

It is possible to create high-strength concrete with improved deformation characteristics when using chemical additives which have the plasticization effect of action and increased reactivity. At the same time, the additives used should have the micro-reinforcing effect on the forming structure of concrete as a result of the production of strong organic mineral chains and complex hydrate compounds of a certain structure [8–12, 22, 23].

To create concrete which has high compressive strength, tensile strength in bending, crack resistance, density, water resistance and frost resistance simultaneously, i.e., concrete having a new level of physical and mechanical properties, it is advisable at the same time to use two high-performance chemical additives:

- Liquid nanostructural additive based on polycarboxylate;
- Dry complex nanostructural additive based on polycarboxylate [13–18].

This scientific research is devoted to the creation of such multifunctional concrete of new generation.

2 Methods and Objects of Research

To create multifunctional concrete, that is particularly stable and effective for permafrost regions, the main problem of which is soils of reduced reliability, it is recommended to use two high-performance additives complementing each other in effect.

The basis of the used additives is polycarboxylate polymers of a different nature with a different length of side chains, which should produce the hyperplasticization effect together. Nanostructural elements of natural and synthetic origin are applied as reaction components in dry and liquid additives which, in addition to increasing the reactivity of the concrete mix components, are capable of forming new organic mineral chains having the micro-reinforcing effect on the structure of hardening concrete from the moment of its manufacture to the obtainment of the required physical and mechanical parameters.

The basis of the liquid additive is polycarboxylate polymers of the third generation which are represented by polypropylene polymers with copolymers of acrylic acid and ethyl methacrylate which have branched comb chains with short branches in each unit. Polycarboxylate polymers are modified by the synthesized nanostructural element, $\text{SiO}_2 \cdot n\text{H}_2\text{O}$, which is an aqueous solution of silica sol with a density of $\rho = 1,014 \text{ g/cm}^3$ and a pH value of $\text{pH} = 3.5$.

Silica sol is used to increase the reactivity of the components of concrete mix. Besides, nanodispersions of $\text{SiO}_2 \cdot n\text{H}_2\text{O}$ appear to be capable of interacting with

hydrosilicates and calcium hydroxides formed during the primary hydration of cement-containing concrete mix. This results in the formation of an additional number of new hydrate compounds, as well as the possible production of low-basic hydrate compounds having a fibrous structure. This has a positive effect on an increase of the compressive strength, including a rise of the tensile strength in bending, thereby enhancing the crack resistance of hardening concrete.

To enhance the plasticization effect of this additive action and to increase its reactivity, the second dry complex additive is applied. It consists of a superplasticizer based on polycarboxylate esters having a chain-like configuration of the molecule which is characterized by increased mobility and, as a consequence, by high adsorption capacity. Besides, the additive includes nanostructural elements of natural origin in the form of nanodispersions which are represented by montmorillonite $(Al, Mg)_2(OH)_2[Si_4O_{10}] \cdot H_2O$; kaolinite $Al_2O_3 \cdot 2SiO_2 \cdot 2H_2O$; and illite $K_{<1}Al_2[(Al, Si)_4O_{10}](OH)_2 \cdot nH_2O$ having the reaction effect on the components of the hardening system and contributing to the formation of magnesium aluminosilicates which produce a positive effect on an increase of the tensile strength in the bending of the hardened stone.

The simultaneous presence of different nature polycarboxylates which have a different structure should enhance the plasticization effect of their action. An increased number of nanostructural elements in the hardening system, which are characterized by the developed surface and, as a result, by increased surface energy, have a double effect on the forming artificial stone: First, they enhance the reactivity of the components of the system; second, they compact the forming artificial stone, thereby increasing the level of physical and mechanical properties of the material and its durability.

The evaluation of the plasticization effect of each additive separately and in their simultaneous presence was determined by the change of the water–cement ratio of concrete mix having the same flowability and by the value of compressive strength.

The reactivity of the additives used was determined by changing the toughness indexes at the age of 7 and 28 days of normal hardening. The compressive strength and tensile strength in bending were determined at the design and intermediate age. This allowed to estimate the crack resistance of the material. Then, it was compared with the test results of the control sample and the ratio of tensile strength in bending to compressive strength which are given in GOST 10180-2012, Appendix L.

The determination of the rational number of two complex additives is the basis for the creation of multifunctional concrete recommended for high-rise construction, including construction in permafrost regions. For this purpose, comprehensive physical and mechanical studies have been carried out and the durability indicators such as frost resistance and water resistance have been determined.

3 Results and Discussion

The rational amount of the liquid complex additive was established by the maximum value of the material strength with the maximum reduction of the water–cement ratio, i.e., with the maximum manifestation of the plasticization effect of the said additive. The results of the study are presented in Table 1.

Analysis of the data given in Table 1 shows that the rational amount of the liquid complex additive is $(1.0 \pm 0.2)\%$ by cement mass. The best results are obtained by using 1.0% of this additive by cement mass. The use of the liquid complex additive in the rational amount ensures a reduction in water consumption by more than 20% to achieve the same flowability of concrete mix. This proves the high plasticization effect of this additive, whereby the compressive strength increases by 32% at the design age, ensuring the production of B40 class concrete instead of the given concrete B30.

Further research was devoted to the determination of the rational consumption of the dry complex additive which was evaluated by the same way as in the case of the liquid additive: by the maximum reduction of water–cement ratio with the same flowability and by change in compressive strength. The results of the study are presented in Table 2.

The data given in Table 2 demonstrate that the best results in an increase of the flowability of concrete mix and a simultaneous increase of concrete strength occur when using the dry complex additive in an amount of 0.5% of cement mass. In this case, the effect of plasticization and gain in strength is several percents lower than that when using the liquid complex additive.

Next study was dedicated to the evaluation of the combined effectiveness of two complex additives. For this purpose, concrete B30P3 was used, and the compressive strength, tensile strength in bending and crack resistance of high-strength concrete were estimated. The results of the study are presented in Table 3.

The effect of the combined action of two complex additives proves the above-stated assumptions of the plasticization effect increase when plasticizers with a different nature and a different structure are present together. A significant increase in compressive strength and especially in tensile strength in bending appears to be caused by not only the production of an increased number of hydrate compounds having special composition which is characterized by fibrous or needlelike structure, but also the creation of a particularly dense structure of concrete, as well as the formation of new organic mineral chains that micro-reinforce the structure of concrete.

The complex physical and mechanical studies have shown that the combined use of two complex additives in the rational amount has a positive effect on the durability of concrete. This is confirmed by the results presented in Table 4.

Analysis of the data given in Table 4 shows that the combined use of two types of the complex additives on polycarboxylate basis of a different nature ensures a super cumulative effect which is expressed in reducing the water–cement ratio by

Table 1 Evaluation of the plasticization effect of the liquid complex additive

№	Concrete class, B	Cement consumption per 1 m ³ of concrete mix, kg	Consumption of the liquid complex additive, % by cement mass	Water consumption per 1 m ³ of concrete mix	W/C	Flowability grade of concrete, P	Compressive strengt, MPa	
							Age, days	7
1	B30	415	–	216	0.52	P3	26.5	39.0
2		415	0.6	191	0.46	P3	29.8	42.1
3		415	0.8	174	0.42	P3	32.7	47.4
4		415	1.0	170	0.41	P3	36.0	51.5
5		415	1.2	166	0.40	P3	33.4	48.2
6		415	1.4	166	0.40	P3	31.6	46.3

Table 3 Evaluation of the effectiveness of two complex additives having a different nature

№	Cement consumption per 1 m ³ of concrete mix, kg	Additive, % by cement mass		Water consumption per 1 m ³ of concrete mix	W/C	Strength, MPa (at the age of 28 days)		C _{c.r.} = $\frac{R_{b,t.}}{R_{b,em.}}$
		Liquid complex additive	Dry complex additive			Compressive strength	Tensile strength in bending	
1	415	-	-	216	0.52	39.0	4.6	0.118
2	415	1.0	-	170	0.41	51.5	6.6	0.128
3	415	-	0.5	174	0.42	50.3	6.3	0.125
4	415	1.0	0.5	147	0.35	67.0	11.4	0.170

Table 4 Physical and mechanical characteristics of complex modified concrete

№	Design class of concrete	Cement consumption per 1 m ³ of concrete mix, kg	Additive, % by cement mass		W/C	Flowability grade of concrete, P	Compressive strength, MPa at the age of 28 days	Actual concrete class	Tensile strength in bending, MPa at the age of 28 days	C.r.r. = $\frac{R_{bL}}{R_{com}}$		Water absorption, Wm, %	Frost resistance grade of concrete, F1	Water-resistant grade of concrete, W
			Liquid complex additive	Dry complex additive						Actual value	According to GOST 10180-2012			
1	B30	415	–	–	0.52	II3	39	B30	4.6	0.118	0.120	4.8	300	12
2	B30	415	1.0	0.5	0.35	II3	67	B50	11.4	0.170	0.120	3.1	600	16

33%; increasing the compressive strength by 72% and tensile strength in bending by 148%; and enhancing the crack resistance by 44%, frost resistance by 2 times and water resistance by 33%.

4 Conclusions

For high-rise construction, including construction in cold regions, it is advisable at the same time to use two complex chemical additives based on polycarboxylates of a different nature which are also modified by nanostructural elements of synthetic and natural origin.

The use of these additives contributes to the formation of new organic mineral chains which micro-reinforce the structure of the hardening concrete from the moment of its manufacture, improving its deformation characteristics and increasing the stability and crack resistance of concrete structures created on problem soils.

It is shown that the combined use of two complex additives of a different nature has the plasticization and reaction effects, ensuring the creation of multifunctional concrete with a new level of properties.

References

1. Soloviova VY, Kozin PA, Stepanova IV, Smirnova TV (2014) High-strength concrete bonets of improved durability modified by nanopolymer additive. *Sci Technol* 2(70):296–298
2. Soloviova VY, Maslennikova LL, Abu-Khasan M, Stepanova IV, Smirnova TV, Boykova TI, Makarov VV, Kasatkin SP (2017) Thermodynamic basis for creating high-strength concrete and curing for pavements. *Sci Technol* 2(104):156–162
3. Soloviova VY, Kozin PA, Stepanova IV, Smirnova TV (2014) Features of hardening of concrete modified by nanopolymer additive under conditions of negative temperatures. *Sci Technol* 2(70):299–301
4. Medvedev PI (1957) Physical and colloidal chemistry. Gos. Publishing House of Agricultural Literature, Moscow
5. Svatovskaya L, Soloviova V, Sychova A, Maslennikova L, Sychov M (2016) Absorptive properties of hydrate silicate building materials and products for quality and geocop-tection improvement. *Indian J Sci Technol* 9(42):104231
6. Svatovskaya LB, Sychova AM, Soloviova VY, Maslennikova LL, Sychov MM (2016) Obtaining foam concrete applying stabilized foam. *Indian J Sci Technol* 9(42):104304
7. Soloviova VY, Galanov EK (2015) The study of the electrical conductivity of cement M400 in the process of hydration and crystallization. *Proc Emperor Alexander I Petersburg State Transp Univ* 4(45):101–107
8. Soloviova VY, Surkov VN (2015) Concrete that does not require high quality raw materials. *Oil Gas* 4(13):239–243
9. Soloviova VY, Kasatkin SP, Stepanova IV, Ershikov NV (2015) Development of high strength concrete. In: *Materials of i international scientific-practical conference: innovative technologies in engineering and geocology, Sputnik+, Moscow*, pp 23–27
10. Svatovskaya LB, Sakharova AS, Baidarashvilly MM, Petriaev AV (2015) Building wastes and cement clinker using in the geocoprotective technologies in transport construction. In:

- Proceedings of the 14th international conference, computer methods and recent advances in geomechanics, Taylor and Francis—Balkema, Netherlands, pp 619–622
11. Sychova AM, Svatovskaya LB, Mjakin SV, Vasiljeva IV (2009) Modification of fillers for cements. Electron beam modification of solids: mechanisms, common features and promising applications, pp 35–37
 12. Sychova AM, Svatovskaya LB, Mjakin SV, Vasiljeva IV (2009) Activation of aqueous phase at cement and concrete solidification. Electron Beam Modification of Solids: Mechanisms, Common Features and promising Applications, pp 39–47
 13. Sychova A, Solomahin A, Khitrov A (2017) The increase of the durability and geoprotective properties of the railway subgrade. Proc Eng 189:688–694
 14. Solovieva V, Kondratov V, Stepanova I (2017) The development of a high performance material for a ballast layer of a railway track. Proc Eng 189:823–828
 15. Boikova T, Solovieva V, Solovyov D (2017) Concrete for road pavements. Proc Eng 189:800–804
 16. Boykova T, Solovieva V, Solovyov D (2017) Effective Repair and Refurbishment Compound for the Strengthening of a Road Concrete Pavements. Proc Eng 189:650–653
 17. Aitcin PC (1998) High Performance Concrete. E&FN SPON, London
 18. Gu C, Ye G, Sun W (2015) Ultrahigh performance concrete-properties, applications and perspectives. Sci China Technol Sci 58(4):587–599
 19. Kapielov SS, Travush VI, Karpenko NI (2008) Modified highly strong concretes of class b80 and b90 in monolithic structures. Build Mater 3:9–13
 20. Usherov-Marshak AV (2014) A look into the future of concrete. Constr Mater 3:4
 21. Kalashnikov VI (2016) Concrete present and future. Part 1. Changes in the composition and strength of concrete. Constr Mater 1:96–103
 22. Taylor HFW (1986) Models for prediction of microstructural development in cement-based materials. J Am Ceram Soc 69:464–467
 23. Jennings HM (2008) Refinements to colloid model of C–S–H in cement: CM-II.—Cem Concr Res 38(32):75–289

Increasing the Level of Properties of Composite Materials for Civil Engineering Geoconstruction with the Use of New Generation Additives



Valentina Solovieva, Irina Stepanova, Dmitriy Soloviev
and Nikolay Yorshikov

Abstract It is shown in the paper that the effective chemical activation of cement-containing composite mixture with the help of a new generation of a complex nanostructural additive ensures the creation of high-strength fine and heavy concretes with improved strength and deformation characteristics. The use of the proposed complex additive enormously increases the hydration activity of the hardening system, having the chemical and thermal effects on it resulting from the rational use of heat released in the process of hydration reactions and ensuring the creation of a composite building material with a new level of physical and mechanical properties. During the experiment it was found that the developed complex nanostructured additive has: highly plasticizing effect; increases the compressive strength, but to a greater extent, the tensile strength in bending (by 53–59)%, increases the crack resistance of the material by (16–17)%;—increases by 2 times the frost resistance of concrete and its water resistance by 50%. Nanomodified concrete with achieved physical and mechanical parameters is recommended for the manufacture of responsible structures, including cold regions, when using problem soils.

Keywords Composite mixture · Building material · High-performance concrete · Strength · Frost resistance · Water resistance · Durability · Deformation characteristics · Nanostructural additive · Hydration activity

1 Introduction

To create reliable and durable pavements, such as road or airfield pavements, as well as the creation of high-performance structures, it is advisable to use high-strength concretes which at the same time should have improved deformation characteristics and increased durability estimated by the parameters of frost resistance and corrosion resistance [1–6].

V. Solovieva · I. Stepanova (✉) · D. Soloviev · N. Yorshikov
Emperor Alexander I St. Petersburg State Transport University (PGUPS), St. Petersburg 190031,
Russia
e-mail: ivstepanova88@mail.ru

© Springer Nature Singapore Pte Ltd. 2020
A. Petriaev and A. Konon (eds.), *Transportation Soil Engineering in Cold Regions*,
Volume 2, Lecture Notes in Civil Engineering 50,
https://doi.org/10.1007/978-981-15-0454-9_40

Chemical activation with the help of effective chemical additives of a new generation should be one of the ways to create composite building materials with the specified set of physical and mechanical parameters. These additives would be most able to extract the internal energy reserve from Portland cement and other components of the composite mixture, maximally involving them in hydration processes and synthesis reactions [7–14].

For many decades, additives having the plasticization effect of action were mainly used as chemical additives for the production of precast concrete, ready-mixed concrete and reinforced concrete, since most researchers in the field of concrete science believed that, first of all, it is necessary to reduce the water–cement ratio for increasing the strength; i.e., it was assumed that an effective additive for concrete should basically have water-reducing properties [15–20].

Lignosulfonates (LSTs) have been applied as the first plasticizers.

In the middle of the twentieth century, the widespread use of more effective plasticizers based on naphthalenesulfonates began. The most well-known chemical additive among them is C-3 additive.

Recently, plasticizing additives on the polycarboxylate basis are considered and applied as plasticizing additives of new generation. Additives of this type ensure a significant reduction in water–cement ratio and, as a consequence, an increase in the strength and density of concrete. This allows to reduce the consumption of cement, as well as to decrease energy and labor costs.

The use of plasticizing additives ensures an increase in the density and compressive strength of concrete, and there is a little increase in frost resistance and water resistance of concrete.

It should be noted that the use of plasticizing additives does not imply the formation of new hydrate phases, which would have a positive effect on the deformation properties of the hardened stone and its corrosion resistance.

To create a new concrete of improved quality, new generation additives are required. They would not only have the plasticization effect, but would be also characterized by the reactivity or catalytic effect, having a positive influence on hydration processes. This contributes to the formation of new hydrated complex compounds, giving new properties to produced concrete [21–24].

The creation of additives having a new quality is considered in this study.

2 Methods and Objects of Research

To obtain a new type of additive, modern surfactants represented by polycarboxylate polymers were applied as a basis.

Nanostructural elements represented by nanodispersions of $\text{SiO}_2 \cdot n\text{H}_2\text{O}$ and potassium nitrite, KNO_2 , were used as modifiers.

Nanodispersions, due to the developed surface, have increased surface energy, and as a result, they have high mobility and reactivity.

Potassium nitrite also has high mobility and, as a consequence, has an increased effect on the enhancement of reactivity of Portland cement minerals. The increased activity of potassium nitrate is due to the high mobility of potassium cation, as a result of the increased size of the cation radius and, as a consequence, the formation of a very thin hydration shell.

Modifiers included in the chemical additive, due to their nature, should effectively contribute to increasing the hydration activity of Portland cement which will result in an increased number of new hydrate phases. At the moment of their formation, hydrate phases are of a nanosize, and therefore, they should compact the structure of the forming stone and fill its pores. At the same time, a large number of new and strong contacts between the components of the hardening stone are formed, which have a positive effect on the formation of improved quality parameters of hardened concrete.

Modifiers that are part of the chemical additive enormously contribute to the formation of a dense and durable structure of the artificial stone. Besides, nanodispersions of $\text{SiO}_2 \cdot n\text{H}_2\text{O}$, due to their reactivity, will enter into chemical interaction with $\text{Ca}(\text{OH})_2$ or with tobermorite-like hydrosilicates of CSH(I) type which are formed at the first stage of hydration of Portland cement minerals. They contribute to the formation of new phases which contain an increased amount of SiO_2 and belong to low-basic hydrosilicates having a fibrous or needle structure. This has the efficient micro-reinforcing effect on the structure of the composite material, and thereby the compressive strength increases. But the tensile strength in bending much more rises, and consequently the crack resistance of the hardened artificial stone is enhanced and its deformation characteristics are improved.

In the presence of the investigated complex chemical additive, the hardening system is subjected to a double energy effect: chemical and thermal effects.

Taking into account the above considerations, the chemical additive has an increased reactivity due to which the hydration activity of the components of the hardening system is significantly increased, resulting in a large amount of heat release.

One should also consider that in the presence of this additive a dense structure is formed, contributing to the preservation of the released heat inside the forming stone. This has the additional thermal energy effect on the hydration processes, increasing the activity of cement minerals.

In the presence of the complex chemical additive, as a result of double energy effect, the minerals of Portland cement will enter into the hydration processes at an earlier age. They are characterized by reduced activity, for example bicalcium silicate, $2\text{CaO} \cdot \text{SiO}_2$. Magnesium limestones consisting of calcium and magnesium carbonate, $\text{CaCO}_3 \cdot \text{MgCO}_3$, should also have the effective hydration activity in the presence of this additive. During the efficient hydration, they should form basic calcium and magnesium carbonates, which have a positive effect on improving the tensile strength in bending and increasing the corrosion resistance of the material.

The use of the investigated additive should have a positive effect on improving the water resistance, frost resistance and corrosion resistance of concrete. This increases the reliability and durability of concrete and, as a result, structures based on it.

The effectiveness of the complex chemical additive was assessed by the change of water–cement ratio of concrete mix having the same flowability, as well as by the change of the compressive strength and tensile strength in bending, and by the change in the density of concrete which was estimated by the amount of water absorption. For nanomodified concrete, the grade of water resistance, the grade of frost resistance and the coefficient of corrosion resistance were determined as the parameters of durability.

3 Results and Discussion

The studied complex chemical additive was presented in the form of an aqueous solution with a density of $\rho = 1.037 \text{ g/cm}^3$ and a pH value of $\text{pH} = 5.5$.

To assess the effectiveness of the additive, concrete B25 and concrete B30 were used as the most common classes of concrete for construction. The results of the studies are presented in Table 1.

The analysis of the data presented in Table 1 shows that the investigated complex additive should be added in an amount of $(1.0 \pm 0.2)\%$ by the mass of cement. This helps to reduce water consumption by $(22\text{--}23)\%$ that is necessary to ensure a given flowability. Therefore, this complex additive has the high plasticization effect. At that time, the compressive strength grows by $(32\text{--}34)\%$, and tensile strength in bending rises to a greater extent, by $(53\text{--}59)\%$, increasing the crack resistance of the material by $(16\text{--}17)\%$. As a result of increased hydration activity, the density of the hardened concrete, estimated by the water absorption parameter which decreases by $(27\text{--}31)\%$, rises.

During the research, approximately $(10\text{--}12)\%$ of sand were replaced by magnesium limestone. The main effect of the action was observed in an additional increase of the tensile strength in bending, by $(5\text{--}7)\%$, and in the total increase of the material crack resistance, by $(19\text{--}23)\%$.

According to the results of the research, it was found that the frost resistance of nanomodified concrete increases by 2 times and corresponds to F1600 grade, and water resistance rises by 50% and attains W18 grade. Corrosion resistance of concrete relative to carbon dioxide and magnesia corrosion reaches high levels which are estimated by the coefficient of corrosion resistance at the age of 1 year, $C_{c.r.} = 0.90\text{--}0.92$, that corresponds to corrosion-resistant concrete.

The developed nanomodified concrete with achieved physical and mechanical properties can be recommended for the production of road and airfield pavements, as well as for high-rise construction, including construction in cold regions, when using problem soils.

Table 1 Evaluation of the effectiveness of the complex additive consisting of polycarboxylate polymer, nanostructural element, SiO₂ nH₂O, and potassium nitrite, KNO₂

№	Concrete class	Cement, per 1 m ³ of concrete mix, kg	Complex additive, % by cement mass	Water, per 1 m ³ of concrete mix	W/C	Flowability grade, P	Strength, MPa, at the age of 28 day		C _{c.r.} = $\frac{R_{b,l.}}{R_{com.}}$	Water absorption, Wm, %
							Compressive strength	Tensile strength in bending		
1	B25	380	–	205	0.54	P3*	32.4	3.8	0.117	4.8
2		380	0.6	190	0.50	P3	38.0	4.6	0.121	4.4
3		380	0.8	171	0.45	P3	41.4	5.3	0.127	3.8
4		380	1.0	163	0.43	P3	42.8	5.8	0.136	3.5
5		380	1.2	160	0.42	P3	42.1	5.7	0.135	3.6
6		380	1.4	160	0.42	P3	41.6	5.5	0.132	3.7
7	B30	420	–	218	0.52	P3	38.7	4.6	0.120	4.6
8		420	0.6	197	0.47	P3	46.7	6.0	0.128	3.9
9		420	0.8	181	0.43	P3	51.3	7.0	0.137	3.4
10		420	1.0	172	0.41	P3	51.8	7.3	0.140	3.2
11		420	1.2	168	0.40	P3	51.4	7.1	0.138	3.3
12		420	1.4	168	0.40	P3	51.2	7.0	0.136	3.4

*Grade of flowability, P3, corresponds to (10–15) cm slump according to GOST 7473-2010

4 Conclusions

Studies conducted have shown that the developed complex chemical additive has the following increased effects:

- A plasticization effect;
- A reaction effect.

It is shown that the developed complex chemical additive is efficient in the combination with magnesium limestone. That is why it is advisable to apply them together.

It is established that nanomodified concrete which contains magnesium limestone instead of sand in its composition has a new level of physical and mechanical properties and can be recommended for particularly essential structures, including structures erected in the regions of permafrost.

References

1. Solovieva VY, Kozin PA, Stepanova IV, Smirnova TV (2014) Features of hardening of concrete modified by nanopolymer additive under conditions of negative temperatures. *Sci Technol* 2(70):299–301
2. Solovieva VY, Stepanova IV, Smirnova TV (2014) название. In: Materials of I international scientific-practical conference: innovative technologies in engineering and geocology, Sputnik+, Moscow, pp 28–32
3. Solovieva VY, Maslennikova LL, Ershikov NV, Boykova TI, Kasatkina AV, Kabanov AA, Kasatkin SP (2016) The mechanism of the protective effect of cement-based repair compounds in pavements. *Transp Constr* 10:13–15
4. Svatovskaya L, Solovieva V, Sychova A, Maslennikova L, Sychov M (2016) Absorptive properties of hydrate silicate building materials and products for quality and geocop-tection improvement. *Indian J Sci Technol* 9(42):104231
5. Kulchitsky VA, Makagonov VA, Vasilyev NB (2002) Airfield coverage. FizMatLit, Moscow
6. Smirnova GYe (2017) Technical regulation in the construction of airfield pavements. Collection of scientific papers: advances in chemistry and chemical technology 31(5):7–9. RHTU im. DI. Mendeleev, Moscow
7. Svatovskaya LB, Sychova AM, Solovieva VY, Maslennikova LL, Sychov MM (2016) Obtaining foam concrete applying stabilized foam. *Indian J Sci Technol* 9(42):104304
8. Solovieva VY, Boykova TI, Kasatkin SP, Ershikov NV, Kasatkina AV (2016) Restoration and protection of building structures, as the preservation of the natural and man-made environment. In: Materials of 2nd international scientific-practical conference: geoecology of lithosphere protection, pp 33–36, Sputnik+, Moscow
9. Solovieva VY, Abu-Khasan M, Ershikov NV, Soloviev DV, Miraev GA (2017) Concrete of the increased corrosion resistance for pavings. *Transp Constr* 12:28–32
10. Solovieva VY, Galanov EK (2015) The study of the electrical conductivity of cement M400 in the process of hydration and crystallization. *Proc Emperor Alexander I Petersburg State Transp Univ* 4(45):101–107
11. Solovieva VY, Surkov VN (2015) Concrete that does not require high quality raw materials. *Oil Gas* 4(13):239–243
12. Batrakov VG (1998) Modified concretes. Theory and practice. High School, Moscow
13. Kaprielov SS, Batrakov VG, Sheinfeld AV (1999) Modified concretes of new generations: reality and perspective. *Concr Reinf Concr* 6:6–10

14. Ramachandran VS, Feldman RF, Kollepari M (1988) *Concr Addit*. Stroizdat, Moscow
15. Soloviova VY, Kasatkin SP, Stepanova IV, Ershikov NV (2015) Development of high strength concrete. In: *Materials of I international scientific-practical conference: innovative technologies in engineering and geoecology*, Sputnik+, Moscow
16. Svatovskaya LB, Soloviova VY, Starchukov DS, Sychova AM, Solomakhin AS (2017) Increasing the durability of heavy concrete due to the anti-corrosion barrier. *Bull Constr Mach* 7:58–61
17. Soloviova VY, Smirova TV, Stepanova IV, Shershneva MV (2014) *Methodological guidelines*. PGUPS, St. Petersburg
18. Sychova AM, Svatovskaya LB, Mjakin SV, Vasiljeva IV (2009) Modification of fillers for cements. *Electron beam modification of solids: mechanisms, common features and promising applications*, 35–37
19. Sheinin AM, Ekkel SV (1998) High-strength concretes for road and airfield pavements. *Concr Reinf Concr* 6:7–9
20. Sheinin AM (2005) Use of microsilica in road concrete. *Sci Technol Road Ind* 2:28–33
21. Sychova AM, Svatovskaya LB, Mjakin SV, Vasiljeva IV (2009) Activation of aqueous phase at cement and concrete solidification. *Electron Beam Modif Solids Mech Common Featur Promis Appl* 39–47
22. Sychova A, Solomahin A, Kotovich V, Svatovskaya L, Kamenev Y (2018) Improving of the monolithic foamconcrete quality for used in the high-rise constructions. In: *E3S Web of conferences* 33, 02058
23. Soloviova V, Kondratov V, Stepanova I (2017) The development of a high performance material for a ballast layer of a railway track. *Proc Eng* 189:823–828
24. Baidarashvili M, Sakharova A, Petriaev A (2017) The modern structure for storm sewage purification of roads. *Proc Eng* 189:576–581

Geochemical Basis of Geoprotective Technologies



Larisa Svatovskaya , Kseniia Mikhailova, Tatyana Supeliuk
and Ivan Drobyshev

Abstract The area of the research is geosphere protection from heavy metal ion pollutions. Such types of pollution are typical for cold regions. Contaminants are military waste of metallic nature and heavy metal ions because of that. The aim of the work is the development of geochemical basis for new geoprotective technologies based on mineral geoantidotes (MGA) by calculating concentration values and detoxifying pollutions in certain geochemical reactions. The methods of the research were chemical, physical–chemical and mathematical ones. The concentrations of heavy metal ions (HMI) in saturated solutions were calculated and compared with the values of maximum permissible concentration (MPC) for HMI in the soils. The range of MGA effectiveness in HMI detoxification by their nature has been developed, and the formula of the effectiveness evaluation has been presented. The classification of MGA as disperse systems was made, which made it possible to distinguish the features of geochemical reactions. Five types of disperse systems of MGA have been identified, which provides four types of geochemical reactions: lythoreactions, soling, stone formation reactions. These reactions are the basis of new geoprotective technologies: lithosynthesis, soling and safing. These technologies conserve detoxification products inside the stone functioning as a useful element in construction.

Keywords Geochemical · Geoprotective · Classification · Technology

1 Introduction

The area of the research is geosphere protection from pollutions such as heavy metal ions (HMI)—the most dangerous, super toxicants of the twentieth century. The works [1–6] show that for geosphere protection, mineral geoantidotes (MGA) may be used—the substances similar to natural minerals both by nature and by products,

L. Svatovskaya (✉) · K. Mikhailova · T. Supeliuk · I. Drobyshev
Emperor Alexander I St. Petersburg State Transport University, 9 Moskovsky pr, St. Petersburg
190031, Russia
e-mail: lsvatovskaya@yandex.ru

© Springer Nature Singapore Pte Ltd. 2020

A. Petriaev and A. Konon (eds.), *Transportation Soil Engineering in Cold Regions*,
Volume 2, Lecture Notes in Civil Engineering 50,
https://doi.org/10.1007/978-981-15-0454-9_41

395

in spontaneous reactions ($\Delta G_{298}^{\circ} < 0$) capable of detoxifying pollutions forming the product with useful properties [7–12]. However, the effectiveness of the application of MGA of different nature by detoxification taking into account MPC index was not known, because the main MGA requirement is the formation of low-soluble product with $SP < 10^{-8}$. The aim of the research was to range the effectiveness of MGA use depending on their nature and the pollution level, to classify MGAs by the type of disperse system and to distinguish the features of geochemical reactions for developing new geocoprotective technologies based on them.

2 Methods

In the study, we used chemical, physical–chemical and mathematical methods. The calculations are based on the reference data on solubility product (SP) of substances, ion concentration in saturated solution and MPC values for soil HMI. We also made a geochemical analysis of phosphate systems, carbonates and hydroxides of HMI formed in detoxification.

3 Results and Discussion

Tables 1, 2, 3 present geochemical analysis of phosphates, hydroxides and carbonates as a result of HMI detoxification.

The information presented in Tables 1, 2 and 3 suggests at least two conclusions. First, using the values of ion concentration in the saturated solution of low-soluble substances of different nature it is possible to make the range of their effectiveness (reliability)—the lower the ion concentration in the saturated solution is, the higher the reliability of the detoxification is. Some HMI are given below:

Table 1 Geochemical analysis of phosphates

Free ion of heavy metal, HMI	Phosphates of heavy metals ions, HMI	Solubility product, SP	Concentration of metal Me(II) ion in saturated solution		MPC of soil ions, g/kg
			mol/l	C, g/l(kg)	
Pb(II)	Pb ₃ (PO ₄) ₂	7.94×10^{-43}	1.49×10^{-10}	3.08×10^{-8}	$20(32) \times 10^{-3}$
Cu(II)	Cu ₃ (PO ₄) ₂	1.26×10^{-37}	1.63×10^{-8}	1.03×10^{-6}	3.0×10^{-3}
Ni(II)	Ni ₃ (PO ₄) ₂	5.01×10^{-31}	3.47×10^{-7}	2.01×10^{-5}	4.0×10^{-3}
Zn(II)	Zn ₃ (PO ₄) ₂	9.12×10^{-33}	1.53×10^{-7}	$\sim 1.0 \times 10^{-5}$	23.0×10^{-3}
Cd(II)	Cd ₃ (PO ₄) ₂	2.51×10^{-33}	1.18×10^{-7}	1.32×10^{-5}	0.5×10^{-3}
Fe(II)	Fe ₃ (PO ₄) ₂	1.29×10^{-22}	1.14×10^{-11}	0.63×10^{-9}	0.1×10^{-3}

Table 2 Geochemical analysis of hydroxides

Ion	Hydroxide	SP of hydroxides	HMI concentration in saturated solution of hydroxides		HMI concentration in saturated solution of silicates, C, g/l(kg)	MPC of soil ions, g/kg
			mol/l	C, g/l (kg)		
Cd(II)	Cd(OH) ₂	3.98×10^{-15}	1×10^{-5}	1.12×10^{-3}	$<1.12 \times 10^{-3}$	0.5×10^{-3}
Pb(II)	Pb(OH) ₂	1.0×10^{-20}	1.36×10^{-7}	3.2×10^{-5}	$<3.2 \times 10^{-5}$	32×10^{-3}
Ni(II)	Ni(OH) ₂	6.3×10^{-18}	1.17×10^{-6}	6.9×10^{-5}	$<6.9 \times 10^{-5}$	4×10^{-3}
Cu(II)	Cu(OH) ₂	5.6×10^{-20}	3.8×10^{-7}	2.4×10^{-5}	$<2.4 \times 10^{-5}$	3×10^{-3}
Zn(II)	Zn(OH) ₂	1.2×10^{-17}	3.8×10^{-6}	2.5×10^{-4}	$<2.5 \times 10^{-4}$	23×10^{-3}

Table 3 Geochemical analysis of carbonates

Ion	Carbonate	SP	HMI concentration in saturated solution		MPC of soil ions, g/kg
			mol/l	C, g/l(kg)	
Cd(II)	CdCO ₃	5.25×10^{-9}	2.29×10^{-6}	0.2×10^{-3}	0.5×10^{-3}
Cu(II)	CuCO ₃	2.34×10^{-10}	1.37×10^{-5}	0.87×10^{-3}	3×10^{-3}
Pb(II)	PbCO ₃	7.4×10^{-14}	2.7×10^{-7}	0.5×10^{-4}	32×10^{-3}
Ni(II)	NiCO ₃	1.35×10^{-7}	4.03×10^{-4}	2.37×10^{-2}	4×10^{-3}
Zn(II)	ZnCO ₃	1.45×10^{-11}	3.8×10^{-6}	2.47×10^{-4}	23×10^{-3}

Cu(II); Pb(II); Cd(II); Ni(II); Zn(II)

The range of effectiveness in descending order is presented below:

phosphates → silicates* → hydroxides → carbonates

*the place of silicates is conditional because the SP values are not known, as a rule; however, in the literature there is information that silicates are less soluble than hydroxides.

Second, using the ratio of MPC value and HMI minimum concentration value in saturated solution, it is possible to calculate, to a first approximation, MGA detoxification capability (E_{mga}) as the ratio of MPC to HMI concentration in saturated solution, C g/l (kg):

$$E = \frac{\text{MPC g/kg}}{C \text{ g/kg}} \quad (1)$$

For example, Cu(II) phosphates are capable of detoxification with 10^3 frequency with which MPC is exceeded. Nearly, the same exceedance can be eliminated through soling taking into account row 1 of Table 4.

Table 4 shows ranges of MGA detoxification capability to destroy pollutions which can be eradicated with the help of MGA of certain nature.

Table 5 presents MGA classification by the name of disperse systems. The classification makes it possible to treat geochemical reactions with sediment formation in a new way, taking into consideration the system in which they undergo (Table 6).

Table 6 presents the examples of four types of geochemical reactions in geosystems using MGA.

It should be noted, that in lithoreactions, i.e. reactions in pores and capillaries, from the consequence point of view, the sedimentation is the same as in other chemical reactions—first of all, in lithosystem the substance with the lowest solubility, i.e. minimum SP value, sediments.

The first type of MGA reactions is when lithoreactions undergo in the stone with HMI in polluted solution transported from the geosphere. Then, according to disperse systems classification in colloid chemistry, the stone is called composite material, the first type of disperse system, and consists of solid disperse phase and solid disperse medium. The binded HMI as sediment remain in the stone. The second type of MGA is stone with cellular structure, solid foam, the second type of disperse system [13, 14]. Broken products of composite materials and solid foam are included in this type of MGA. In detoxification using the first and second type of MGA, there is a need for initial act of absorption (capillary suction) of the polluted solution into MGA solid body, where lithoreactions undergo and detoxified products remain in the stone. The third MGA type as disperse system is liquid sol solution, e.g. silica sol. It is assumed to be possible to handle the polluted soil by watering. Detoxified HMI remain in the soil as sediments, which are safe if ion concentration in saturated solution, according to SP, is lower than ion MPC in the soil [15–20]. It should be noted that the mechanism of formation of silicates of HMI of different levels of condensation includes a number of stages [21–24] and needed to be clarified.

Table 4 Approximate evaluation of MGA effectiveness (order of magnitude)

MGA use resulting in formation of	Detoxification capability by heavy metal ions estimated by E value				
	HMI				
	Cu(II)	Pb(II)	Cd(II)	Ni(II)	Zn(II)
Phosphates (\approx silicates)	$\sim 10^3$	$\sim 10^5$	$\sim 10^2$	$\sim 10^2$	$\sim 10^2$
Hydroxides	$\sim 10^2$	$\sim 10^3$	–	$\sim 10^2$	~ 10
Carbonates	–	$\sim 10^2$	–	–	$\sim 10^2$

Table 5 Classification of MGA as disperse systems where pollution detoxification undergoes

Name of MGA as disperse system	Example	Example of HMI detoxification, Me^{n+} as geochemical reaction
Composite material	Silicate concretes and their wastes	$x\text{CaO} \cdot y\text{SiO}_2 \cdot n\text{H}_2\text{O} + \text{Ca}(\text{OH})_2 + (x + 1)\text{Cd}^{2+}$ $= x\text{CdO} \cdot y\text{SiO}_2 \cdot n\text{H}_2\text{O} + \text{Cd}(\text{OH})_2 \downarrow + (x + 1)\text{Ca}^{2+}$
Solid foam (stone sponge)	Foam concretes and their broken products	$x\text{CaO} \cdot y\text{SiO}_2 \cdot n\text{H}_2\text{O} + \text{Ca}(\text{OH})_2 + (x + 1)\text{Cu}^{2+}$ $= x\text{CuO} \cdot y\text{SiO}_2 \cdot n\text{H}_2\text{O} + \text{Cu}(\text{OH})_2 \downarrow + (x + 1)\text{Ca}^{2+}$
Liquid sol	Silica sol, alumina sol	$\text{SiO}_2 \cdot n\text{H}_2\text{O} + 2\text{Pb}^{2+} + 4\text{OH}^-$ $= \text{PbO} \cdot \text{SiO}_2 \cdot n\text{H}_2\text{O} + \text{Pb}(\text{OH})_2 + \text{H}_2\text{O}$
Paste	Phosphate system	$3\text{Zn}^{2+} + 2\text{PO}_4^{3-} + 4\text{H}_2\text{O} = \text{Zn}_3(\text{PO}_4)_2$
Powder	Cement	$\text{C}_3\text{S} + \text{Me}^{2+} + (n + 1)\text{H}_2\text{O} = \text{C}_2\text{S} \cdot n\text{H}_2\text{O}$ $+ \text{Me}(\text{OH})_2 + \text{E}^{2+}, (\text{Me}^{2+} - \text{HMI})$

Table 6 Geochemical reactions of HMI detoxification in geosystem taking into consideration the nature of disperse system where they undergo

Example of HMI in geosystem	Mineral geonitidote (MGA) as disperse system detoxifying pollutions	Special geochemical detoxification reactions depending on disperse system which is MGA
Ba(II)	1. <i>Composite material</i> Calcium-sulphate stone (and its broken products) CaSO_4 , $\text{CaSO}_4 \cdot 2\text{H}_2\text{O}$ pH ≈ 7	1. <i>Lithoreactions</i> —using mineral artificial stone as composite material or solid foam and also their broken products $\text{Ba}_{\text{aq}}^{2+} + \text{CaSO}_4 = \text{BaSO}_4 \downarrow + \text{Ca}^{2+} \text{Ba}^{2+}$ $+ \text{CaSO}_4 \cdot 2\text{H}_2\text{O} = \text{Ca}^{2+}$ $+ \text{BaSO}_4 \downarrow + 2\text{H}_2\text{O}; \Delta G_{298}^{\circ} < 0$
Pb(II)	Calcium-sulphate stone CaSO_4 , $\text{CaSO}_4 \cdot 2\text{H}_2\text{O}$ pH ≈ 7	$\text{Pb}_{\text{aq}}^{2+} + \text{CaSO}_4^{2-} = \text{PbSO}_4 \downarrow + \text{Ca}^{2+} \text{Pb}^{2+}$ $+ \text{CaSO}_4 \cdot 2\text{H}_2\text{O} = \text{Ca}^{2+} + \text{PbSO}_4 \downarrow + 2\text{H}_2\text{O};$ $\Delta G_{298}^{\circ} < 0$
Fe(III)	2. <i>Solid foam</i> “stone sponge”, e.g. D500 foam concrete stone, its broken products, composition— $\text{CaO} \cdot \text{SiO}_2 \cdot n\text{H}_2\text{O} + \text{Ca}(\text{OH})_2$, pH > 7	$2\text{Fe}_{\text{aq}}^{3+} + 3\text{Ca}(\text{OH})_2(\text{s}) = 2\text{Fe}(\text{OH})_3(\text{s}) + 3\text{Ca}_{\text{aq}}^{2+}$ $\text{SP}_{\text{Fe}(\text{OH})_3} < \text{SP}_{\text{Ca}(\text{OH})_2}$ $\Delta G_{298}^{\circ} < 0$
Cu(II) Pb(II) Cd(II)	3. <i>Sol</i> e.g. silica sol, $\text{SiO}_2 \cdot n\text{H}_2\text{O}$, pH > 7	2. <i>Solting</i> $\text{Cu}^{2+} + \text{SiO}_2 \cdot n\text{H}_2\text{O} + 4\text{OH}^- = \text{Cu}(\text{OH})_2$ $+ \text{CuO} \cdot \text{SiO}_2 \cdot n\text{H}_2\text{O} + \text{H}_2\text{O}$ $\Delta G_{298}^{\circ} < 0$
Fe(II)	4. <i>Paste</i> e.g. phosphate system hardening into stone $\text{FeO} + \text{H}_3\text{PO}_4$ <i>slid - liquid</i> pH < 7	3. <i>Stone formation reactions</i> e.g. phosphatization $3\text{Fe}^{2+} + 2\text{H}_3\text{PO}_4 \cdot n\text{H}_2\text{O} = \text{Fe}_3(\text{PO}_4)_2 \cdot n\text{H}_2\text{O} \downarrow + 6\text{H}^+$ $\Delta G_{298}^{\circ} < 0$
Ni(II)	5. Binder powder or clinker mineral	5. Reactions of the hydration activity (can be without stone formation)

Table 7 Geochemical reactions as the basis for new geocoprotective technologies

Geochemical reactions	New geocoprotective technologies	Examples
Lithoreactions	Lithosynthesis ^a	Detoxification with concrete foam of silicate nature
Soling	Soling ^b (silica, alumina, complex)	Soil strengthening
Stone formation (hydrate formation in special conditions according to M.M. Sychov)	Safing ^c	Hardening of phosphate or geopolymer pastes
Reactions of hydratation activity	Hydratation activity ^d	Binder powder or clinker mineral

^aTechnologies are based on the artificial stone absorption. Artificial stone absorbs heavy metal ion contenting solution and detoxicates them

^bTechnologies are based on the use of silica sol in any way

^cTechnologies are based on the safe creation with pollutions. Two ways can be use. First is that the reactions of stone formation and heavy metal ions binding at the same time. The second way is lay creation on the mineral base of any nature

^dTechnologies are based on the use of powder with hydration activity

The fourth type of MGA as disperse system provides chemical reaction of binding HMI when the system is hardening with the formation of artificial stone. Then, according to disperse systems classification in colloid chemistry, MGA is a paste where the reactions of hardening into stone, based on complex formation (hydrate formation), undergo. The paste becomes MGA because, firstly, HMIs sediment inside the paste in stone formation and, secondly, the formed stone functions as a safe and the products of HMI binding remain in the artificial stone, e.g. phosphate stone.

Table 7 presents new geocoprotective technologies based on chemical calculations mentioned above. There are three technologies: lithosynthesis, soling and safing. Their main advantage is that, having served as geocoprotection, the system continues to be a useful product, e.g., through structural properties.

4 Conclusions

1. HMI concentrations in saturated solutions of phosphates, carbonates and hydroxides using SP value have been calculated. It is shown that the concentration is lower, as a rule, than MPC in the soil. The range of MGA effectiveness in HMI detoxification has been made depending on the nature of MGA. The formula of MGA effectiveness evaluation has been presented.
2. The classification of MGA as disperse systems—five types—has been presented. The specificities of geochemical reactions, such as lithoreactions, soling, stone formation and hydratation activity reaction, have been determined.

3. Geochemical reactions are the basis of new geocoprotective technologies: lithosynthesis, soling, safining and hydration activity. Their main advantages are detoxifying properties and the fact that detoxified products remain in the stone functioning as a useful product.

References

1. Svatovskaya LB, Kabanov AA, Sychov MM (2017) The improvement of foam concrete geocoprotective properties in transport construction. IOP Conf Ser Earth Environ Sci 90:012010
2. Svatovskaya LB, Kabanov AA, Sychov MM (2017) Lithosynthesis of the properties in the transport construction on the cement base. IOP Conf Ser Earth Environ Sci 90:012009
3. Svatovskaya LB, Kabanov AA, Sychov MM (2017) Soling, aerating and phosphating for soil strengthening and detoxication. Proc Eng 189:398–403
4. Svatovskaya LB, Urov OV, Kabanov AA (2017) Geocoprotective technology of transport construction using silica sol absorption method. Proc Eng 189:454–458
5. Svatovskaya LB, Shershneva MV, Baidarashvili MM, Yakimova NI, Khitrov AV (2004) Foam concrete construction demolished waste. In: Proceedings of the international conference on sustainable waste management and recycling: construction demolition waste, London, pp 199–203
6. Svatovskaya LB, Sakharova AS, Baidarashvili MM, Petriaev AV (2015) Building wastes and cement clinker using in the geocoprotective technologies in transport construction. In: Proceedings of the 14th international conference of international association for computer methods and recent advances in geomechanics, IACMAG, Taylor and Francis—Balkema, Netherlands, pp 619–622
7. Sychova AM, Svatovskaya LB, Mjakin SV, Vasiljeva IV (2009) Modification of fillers for cements (book chapter). In: Electron beam modification of solids: mechanisms, common features and promising applications, pp 35–37
8. Sychova AM, Svatovskaya LB, Mjakin SV, Vasiljeva IV (2009) Activation of aqueous phase at cement and concrete solidification (book chapter). In: Electron beam modification of solids: mechanisms, common features and promising applications, pp 39–47
9. Maslennikova LL, Svatovskaya LB, Mjakin SV, Vasiljeva IV (2009) Activation of reactions at solid-solid interfaces. Improvement of ceramics materials (book chapter). In: Electron beam modification of solids: mechanisms, common features and promising applications, pp 57–61
10. Svatovskaya LB, Yakimova NI, Trunskaya OY, Rusanova EV, Krylova NB (2004) New complex ecotechnology for oil demolished waste. In: Proceedings of the international conference on sustainable waste management and recycling: construction demolition waste, London
11. Sychova AM, Solomahin A, Kotovich V, Svatovskaya LB, Kamenev Y (2018) Improving of the monolithic foam concrete quality for used in the high-rise construction. In: E3S web of conferences, vol 33, p 02058
12. Gusev N, Svatovskaya LB, Kucherenko A (2018) Effect of changing of the parameters of the cable network of monitoring systems of high-rise buildings on the basis of string converters on their operability. In: E3S web of conferences, vol 33, p 02069
13. Sychova A, Sychov M, Rusanova E (2017) A method of obtaining geonoiseprotective foam concrete for use on railway transport. Proc Eng 189:681–687
14. Sychova A, Solomahin A, Hitrov A (2017) The increase of the durability and geoprotective properties of the railway subgrade. Proc Eng 189:688–694
15. Yamamoto T, Yamoda T, Miyake A (2007) Transparent conductive Ga-doped ZnO films properties on glass, PMMA and COP substrates. In: Proceedings of international display workshop, 2004, Japan

16. Kityk V, Migalska A, Ebothe J, Elchichou A (2002) Anomalously large pockels effect in ZnO-F single crystalline films deposited on bare glass. *Cryst Res Technol* 37:340–352
17. Singha I, Bhatnagara PK, Mathura PC (2008) Optical and electrical characterization of conducting polymer-single walled carbon nanotube composite films. *Carbon* 46(8):1141–1144
18. Kimakis E (2002) Single walled carbon nanotube composites. *Synth Met* 127:59–62
19. Todda MG, Shi FG (2003) Characterizing the interphase dielectric constant of polymer composite materials: effect of chemical coupling agents. *Appl Phys* 94(7):4551–4557
20. Xiaoliang D, Xiaolin L, Yong Z (2009) Improved dielectric strength of barium titanate-polyvinylidene fluoride nanocomposites. *Appl Phys Lett* 95:95
21. Chao F, Liang G, Kong W (2008) Dielectric properties of polymer: ceramic composites based on thermosetting polymers. *Polym Bull* 60:129–136
22. Todd MG, Shi FG (2002) Validation of a novel dielectric constant simulation model and the determination of its physical parameters. *Microelec J* 33:627–632
23. Rao Y, Takahashi A, Wong CP (2003) Di-block copolymer surfactant study to optimize filler dispersion in high dielectric constant polymer-ceramic composite. *Composites: Part A* 34:1113–1116
24. Qi L, Lee BI, Samuels WD (2006) Three-phase percolative silver-BaTiO₃—epoxy nanocomposites with high dielectric constants. *J Appl Polym Sci* 102:967–971

Information Assessment of Natural Geosystem Preservation in Geoconstruction by Improving the Quality of Concrete



Larisa Svatovskaya , Oleg Urov, Kseniia Mikhailova and Tatyana Supeliuk

Abstract The research area is natural geosystem preservation during the geoconstruction operations. The problem is connected with the cold region because of low temperature influence on the quality of the geoconstruction. The aim of the research is: firstly, by improving concrete properties, to improve the quality of concrete articles in geoconstruction, their durability and, therefore, to reduce the consumption of natural substances; secondly, to assess the achieved quality by introducing a new summative assessment called quality index. The methods of the research are physical-mechanical and experimental ones for evaluation of the concrete properties, and rating method of quality assessment which has been developed and presented to testing. The improvement of concrete properties was achieved by using sol adsorption technology. By using quality index, the quality assessment showed 37% increase. The achieved results make it possible to reduce the consumption of natural sand and, consequently, preserve natural geosystems in geoconstruction.

Keywords Assessment · Geosystem · Preservation · Improving · Quality

1 Introduction

Two issues are in the focus of attention of modern construction: material quality improvement and preservation of the natural environment. Every year both in Russia and in the whole world, the need for high-quality reinforced concrete slabs for road and airfield surfaces is increasing. The method of absorbing silica sol by a slab when hardening may become one of the ways of improving the quality of reinforced concrete slabs [1–6]. This work is focused on this method and its application in transport construction for improving the quality and, consequently, reducing the consumption of natural raw materials.

L. Svatovskaya (✉) · O. Urov · K. Mikhailova · T. Supeliuk
Emperor Alexander I St. Petersburg State Transport University, 9 Moskovsky Pr, St. Petersburg
190031, Russia
e-mail: lbsvatovskaya@yandex.ru

© Springer Nature Singapore Pte Ltd. 2020
A. Petriaev and A. Konon (eds.), *Transportation Soil Engineering in Cold Regions*,
Volume 2, Lecture Notes in Civil Engineering 50,
https://doi.org/10.1007/978-981-15-0454-9_42

The aim of the research was to assess the quality of silica sol modified concrete. It was necessary to accomplish the following tasks:

- to study the principal structural properties of the concrete developed by a modified method of silica sol absorption;
- to develop the methodology of integrated assessment of modified articles quality and to analyze the index of concrete quality from the geosystem preservation point of view;
- to introduce the proposed method into experimental-industrial production of road construction.

The object of the research was the articles made of heavy B15 concrete.

The subject of the research was the quality of concrete for road surfacing.

It should be noted that the applied methods of concrete modification often fail to solve the problems related to the operation of concrete articles, e.g., slabs used in road surfacing. The feature of operation of these slabs is that they are subject to repeated loads. On high-density roads, total estimated number of estimated loading may come up to 30 million times. It inevitably leads to concrete spalling at the points of loading application and, therefore, to rutting. The solution of the problem could be the increase in bending tensile strength and hardness of the concrete and the reduction in concrete abrasion, which increases the durability of the concrete.

At the same time, in the structures where it is impossible to provide high-quality drainage there is a problem of pavement capillary pumping. Concrete used for road slab manufacturing has a porous structure which may be represented as the system of capillaries of different diameter. Thus, it is subject to capillary pumping. During operation of the articles, aggressive groundwater passes into the concrete, goes up the capillaries until hydrostatic pressure is balanced by gravity. Groundwater is a natural solution of salts, and when it evaporates from the concrete it leaves salt efflorescence, destroying the concrete from the inside. Thus, preliminary impregnation of the concrete by solutions of particular nature can contribute to reduction in surface porosity and stop moisture from entering the concrete during its operation, i.e., improve the concrete quality.

In the works [7–14], it was assumed that silica sol can be used as a solution capable of improving concrete operational properties and its quality, on the one hand, and solving the problem of capillary pumping, on the other hand. This assumption is based on the fact that solid phase of sol is of silicate nature, and thus, sol impregnation at the hardening stage will lead to additional hydro-silicates. Since hydro-silicates are generated after the pore structure of the concrete is formed, hydro-silicate groups are formed in the pores which block the pores stopping aggressive water from entering the concrete body [15–17]. Lithosynthesis is used here as a method of improving operational properties of concrete and its durability, which is a constituent part of sol absorption technology (SAT).

2 Methods

Absorption method (SAT) is that a concrete article at hardening age of 3 days is wholly put into silica sol solution. The layer of the liquid over the article should be 2–3 cm. The structural properties were in accordance with GOST RF.

The following structural properties have been determined: compressive strength, bending tensile strength, water absorbing capacity, water resistance, frost resistance, and abrasion.

All the samples were weighed during the experiments. We observed weight gain of the samples—0.5 g per each cm^2 of the sample's surface contacting with the sol. This fact made it possible to draw a conclusion that water absorbing capacity depends on the sample's square contacting with the sol, and to introduce a new indicator of concrete modification method—coefficient of surface absorption K , kg/m^2 . This coefficient may be used to determine the quantity (consumption) of sol Q , kg, for modification of different articles. Multiplying the coefficient by the article's square S , we will get the quantity (consumption) of the silica sol in kg for modification of the article:

$$Q = S \cdot K \quad (1)$$

The developed methodology of the assessment of the quality of the modified concrete introduces the indicator—*quality index*.

The value of the quality index is found according to rating method. In accordance with this method, each structural property of a new material holds nondimensional weight factors from 0 to 1 in such a way that the total amount is 1. In compliance with the methods in current normative documents, numerical values of these properties are determined, and the increase/decrease in each property in % compared to the reference material is calculated. The sum of all the changes of all the properties, multiplied by their weight factors, equals the quality index (QI). It is accepted that the higher the level of QI is, the higher the quality of the obtained material is.

Therefore, QI can be calculated by the following formula:

$$\text{QI} = \sum k_i \cdot \Delta_i \quad (2)$$

where k_i —weight factor of i -property, assigned by expert assessment;

Δ_i —percentage change of i -property.

It is proposed to give weight factors to each of the properties after expert assessment taking into consideration the importance of one or another property under operating conditions of the article of a new material. The same material being used for different purposes should go through expert assessment taking into consideration certain purpose, because, for example, structural properties of modified concrete used in wall blocks are different from those of road concrete.

3 Results and Discussion

The experiments showed that silica sol use increases compressive strength by 15%, bending strength by 15%, reduces water absorbing capacity not less than 60%, increases frost resistance by 100%, and reduces abrasion by 25%.

Let us give a calculation of quality index for B15 concrete modified by SAT and used in road slabs. The expert assessment taking into consideration the features of road slab performance made it possible to give the following weight factors:

- Compressive strength—0.1.
- Bending tensile strength—0.3.
- Abrasion—0.3.
- Frost resistance—0.15.
- Water absorbing capacity—0.15.

Let us calculate QI by the formula (2):

$$QI = 1.15 \cdot 0.1 + 1.15 \cdot 0.3 + 1.25 \cdot 0.3 + 2 \cdot 0.15 + 1.6 \cdot 0.15 = 1.37$$

Quality index expressed in percentage is 37%. Thus, as a result of SAT modification the quality of road slab concrete improved by 37%. It is a quality improvement which makes it possible to predict durability and, therefore, inform of geosystem preservation.

The results were implemented according to the technology of building approach motorways which include a number of operations: topsoil removal, planning the top of the formation, filling the sand base 20–30 cm depth, and laying the slabs in design position. After SAT modification technology, reinforced concrete slabs when contacting with water do not need drainage basement. Taking into account increasing problems related to availability and costs of high-quality bulk materials in central regions of our country, it is possible to save considerable resources excluding the operation of filling the sand base.

When building an approach road of prefabricated concrete slabs, we conducted experimental-industrial testing of the slab modified by SAT. The 3-day-old concrete slabs 2 × 6 m were put into wood formwork, filled by 3% silica sol solution. One day later, the slabs were taken back from the formwork and were left for natural hardening. The 28-day-old slabs were laid onto the prepared base.

Together with the slabs to control the quality, we tested standard samples 10 × 10 × 10 cm using the same operations. The 28-day-old modified samples and the unmodified samples were tested by the properties mentioned above, which gave the quality with the coefficient 1.37. The results go in accordance with the works [18–24] on nature and properties of modified surfaces.

Now it is important to discuss the ways' of concrete quality improving development. Thermodynamical calculation, Table 1, shows that the best of all is the reaction 1, because of energy meaning (–740.89 kJ) and the more meaning of reaction's energy, the better strength of the systems and durability. Another way of quality

Table 1 Thermodynamical calculation of the reactions with Ca(II)

Ions	Reactions of silica sol, SiO ₂ .H ₂ O	ΔG_{298}° , kJ of the reactions
Ca(II)	$6\text{Ca}^{2+} + 6(\text{SiO}_2 \cdot \text{H}_2\text{O}) + 12\text{OH}^- = 6\text{CaO} \cdot 6\text{SiO}_2 \cdot \text{H}_2\text{O} + 11\text{H}_2\text{O}$	-740.89
Ca(II)	$\text{Ca}^{2+} + 2(\text{SiO}_2 \cdot \text{H}_2\text{O}) + 2\text{OH}^- = \text{CaO} \cdot 2\text{SiO}_2 \cdot 2\text{H}_2\text{O} + \text{H}_2\text{O}$	-201.65
Ca(II)	$6\text{Ca}^{2+} + 3(2\text{SiO}_2 \cdot 3\text{H}_2\text{O}) + 12\text{OH}^- = 6\text{CaO} \cdot 6\text{SiO}_2 \cdot \text{H}_2\text{O} + 14\text{H}_2\text{O}$	-284.89
Ca(II)	$\text{Ca}^{2+} + 2\text{SiO}_2 \cdot 3\text{H}_2\text{O} + 2\text{OH}^- = \text{CaO} \cdot 2\text{SiO}_2 \cdot 2\text{H}_2\text{O} + 2\text{H}_2\text{O}$	-50.65

Table 2 Interconnection of some structural, geocoprotective, and fundamental properties of artificial mineral hydrate systems

Properties			Fundamental basis	Property formalization to a first approximation
N ^o	Structural	Geocoprotective		
1	Average density D , t/m ³	Absorbing properties of material P_{abs} and raw material costs predicted by the material average density	Physical properties in the form of capillary-pore structure CP, %, and total porosity P, %	$P_{\text{abs}} = k(\text{CP}, \text{P})$ —direct proportionality, k —coefficient of proportionality
2	Water absorption, W, %	Absorption capacity of inorganic and organic pollutions, e.g., oil products O_p , evaluating the amount of the absorbed product		$D_{\text{hmi}} = k(C_{\text{hs}}, \text{CP}, \text{P})$ —direct proportionality, k —coefficient of proportionality
3	Strength, R_{compr} , MPa	D_{hmi} —heavy metal ions (HMI) detoxifying properties of lithosphere	The number of hydro-silicates (hydrates) C_{hs} (theory and practice of chemistry of complex compounds)	
4	Thermal conductivity λ , W/m C	Energy preservation P_{λ} . Predicting it helps to assess fuel costs in the operation of a facility or a building structure	Thermodynamic parameters: $-\Delta H_{298}^{\circ}$, ΔG_{298}° , S_{298}°	$P_{\lambda} = f(-\Delta H_{298}^{\circ})$; $P_{\lambda} = f(S_{298}^{\circ})$ (according to professor A. M. Sychova)

improving is to use data in Table 2. It is possible to use formalization of the first approximation to obtain quality improvement more than 37%.

4 Conclusions

1. The methods of modified concrete quality assessment have been presented, using the improvement of concrete principal structural properties.
2. With the help of these methods, the numerical value of 37% quality improvement in silica sol modification has been found.
3. The improved quality of the modified concrete makes it possible to exclude sand base filling in motorway building, which saves natural products and, consequently, contributes to natural geosystem preservation.

References

1. Svatovskaya LB, Kabanov AA, Sychoy MM (2017) The improvement of foam concrete geocoprotective properties in transport construction. *IOP Conf Ser Earth Environ Sci* 90:012010
2. Svatovskaya LB, Kabanov AA, Sychoy MM (2017) Lithosynthesis of the properties in the transport construction on the cement base. *IOP Conf Ser Earth Environ Sci* 90:012009
3. Svatovskaya LB, Kabanov AA, Sychoy MM (2017) Soling, aerating and phosphating for soil strengthening and detoxication. *Proc Eng* 189:398–403
4. Svatovskaya LB, Urov OV, Kabanov AA (2017) Geocoprotective technology of transport construction using silica sol absorption method. *Proc Eng* 189:454–458
5. Svatovskaya LB, Shershneva MV, Baidarashvili MM, Yakimova NI, Khitrov AV (2004) Foam concrete construction demolished waste. In: *Proceedings of the international conference on sustainable waste management and recycling: construction demolition waste*, London, pp. 199–203
6. Svatovskaya LB, Sakharova AS, Baidarashvilly MM, Petriaev AV (2015) Building wastes and cement clinker using in the geocoprotective technologies in transport construction. In: *Proceedings of the 14th international conference of international association for computer methods and recent advances in geomechanics*, IACMAG, Taylor and Francis—Balkema, Netherlands, pp 619–622
7. Sychova AM, Svatovskaya LB, Mjakin SV, Vasiljeva IV (2009) Modification of fillers for cements (book chapter). In: *Electron beam modification of solids: mechanisms, common features and promising applications*, pp 35–37
8. Sychova AM, Svatovskaya LB, Mjakin SV, Vasiljeva IV (2009) Activation of aqueous phase at cement and concrete solidification (book chapter). In: *Electron beam modification of solids: mechanisms, common features and promising applications*, pp 39–47
9. Maslennikova LL, Svatovskaya LB, Mjakin SV, Vasiljeva IV (2009) Activation of reactions at solid-solid interfaces: improvement of ceramics materials (book chapter). In: *Electron beam modification of solids: mechanisms, common features and promising applications*, pp 57–61
10. Svatovskaya LB, Yakimova NI, Trunskaya OY, Rusanova EV, Krylova NB (2004) New complex ecotechnology for oil demolished waste. In: *Proceedings of the international conference on sustainable waste management and recycling: construction demolition waste*, London

11. Sychova AM, Solomahin A, Kotovich V, Svatovskaya LB, Kamenev Y (2018) Improving of the monolithic foam concrete quality for used in the high-rise construction. In: E3S web of conferences vol 33, p 02058
12. Gusev N, Svatovskaya LB, Kucherenko A (2018) Effect of changing of the parameters of the cable network of monitoring systems of high-rise buildings on the basis of string converters on their operability. In: E3S web of conferences, vol 33, p 02069
13. Sychova A, Sychov M, Rusanova E (2017) A method of obtaining geonoiseprotective foam concrete for use on railway transport. Proc Eng 189:681–687
14. Sychova A, Solomahin A, Hitrov A (2017) The increase of the durability and geoprotective properties of the railway subgrade. Proc Eng 189:688–694
15. Yamamoto T, Yamoda T, Miyake A (2007) Transparent conductive Ga-doped ZnO films properties on glass, PMMA and COP substrates. In: Proceedings of international display workshop, 2044, Japan
16. Kityk V, Migalska A, Ebothe J, Elchichou A (2002) Anomalously large pockels effect in ZnO-F single crystalline films deposited on bare glass. Cryst Res Technol 37:340–352
17. Singha I, Bhatnagara PK, Mathura PC (2008) Optical and electrical characterization of conducting polymer-single walled carbon nanotube composite films. Carbon 46(8):1141–1144
18. Kimakis E (2002) Single walled carbon nanotube composites. Synth Metals 127:59–62
19. Todda MG, Shi FG (2003) Characterizing the interphase dielectric constant of polymer composite materials: effect of chemical coupling agents. Appl Phys 94(7):4551–4557
20. Xiaoliang D, Xiaolin L, Yong Z (2009) Improved dielectric strength of barium titanate-polyvinylidene fluoride nanocomposites. Appl Phys Lett 95:95
21. Chao F, Liang G, Kong W (2008) Dielectric properties of polymer: ceramic composites based on thermosetting polymers. Polym Bull 60:129–136
22. Todd MG, Shi FG (2002) Validation of a novel dielectric constant simulation model and the determination of its physical parameters. Microelectr J 33:627–632
23. Rao Y, Takahashi A, Wong CP (2003) Di-block copolymer surfactant study to optimize filler dispersion in high dielectric constant polymer-ceramic composite. Composites: Part A 34:1113–1116
24. Qi L, Lee BI, Samuels WD (2006) Three-phase percolative silver-BaTiO₃—epoxy nanocomposites with high dielectric constants. J Appl Polym Sci 102:967–971

Safing Technologies for Lithosphere Geocoprotection



Larisa Svatovskaya , Kseniia Mikhailova, Ivan Drobyshev and Elena Bodenko

Abstract The study deals with the methods of environmental protection from pollutions, in particular, safing technologies. Such kind of technologies is important in cold region because of military waste. The aim of the work was to study the specificities of safing technologies as coatings in mineral systems and as dimensional safing. By using a coating has been studied the depth and the composition of the layer on the surface of concretes of self-stressing cement and expanding cement. As dimensional safing, we considered making a phosphate artificial stone which involves binding of heavy metal ions. The methods of the research were electron microscopical image (EMI), electron probe microanalysis (EPM), and chemical and physical-mechanical methods. It is shown that the coating's layer is up to 7 mm. Due to dimensional safing, special heavy metal ions are binding and hardening of system takes place at the same time. The study presents the development of safing technologies of geoprotection.

Keywords Safing · Technology · Lithosphere · Geocoprotection

1 Introduction

The research deals with the issues of geoenvironmental protection from pollutions. One of the possible solutions of these issues could be either involving the pollution in a useful chemical process, e.g., solidification and formation of an artificial stone accompanied by pollution detoxification, conserving the products inside the stone; or blocking the pollutions in a mineral construction building, structure or article by forming a preserving protective layer on the surface. Thus, the main principle of safing technologies is creating a construction system—safe, including throughout the whole volume of either only mineral layers on the surface of articles and construction buildings, or any other mineral system, e.g., on concrete or soil. Mineral layer is a kind of preserving protective screen with useful structural properties—they increase hardness, water resistance and they act as geocoprotection. The mineral surface

L. Svatovskaya (✉) · K. Mikhailova · I. Drobyshev · E. Bodenko
St. Petersburg State Transport University, 9 Moskovsky Pr, St. Petersburg 190031, Russia
e-mail: lbsvatovskaya@yandex.ru

© Springer Nature Singapore Pte Ltd. 2020
A. Petriaev and A. Konon (eds.), *Transportation Soil Engineering in Cold Regions*,
Volume 2, Lecture Notes in Civil Engineering 50,
https://doi.org/10.1007/978-981-15-0454-9_43

can be created by single or numerous impregnations or, in the case of dimensional safing, by solidification with a mineral binder or solution functioning simultaneously as a hardener and a mineral geoadjuvant. The example of forming dimensional geoprotection can be the method of phosphate solidification, when, for example, heavy metal ions bind into low-soluble hydrophosphates, resulting in both hardening due to hydrate formation and geoprotection due to heavy metal ion binding [1–5].

The works [6–9] mentioned that making a surface of one or several layers of silica and (or) hydrosilicate calcium or silica aluminium calcium provides a positive impact to a construction geosystem. These coatings—single or multilayered—may perform the following functions: increase of a structure durability under operation; conserving absorbed pollutants inside an article, structure, construction; protection from dusting, e.g., ash mass. Impregnation layers consist of silica sol which can be applied by several impregnations or mixed with Ca(II) or Mg(II) solutions containing compounds as salt solutions in order to form hydrosilicates. The example of safing coatings for a structure's durability may be road surfaces. The example of dusting protection may be silica sol coatings for dusting ash dumps [10–15].

It should be noted that geoprotective coatings represent a kind of layers of mineral nature with the properties that should be controlled.

The aim of the study was to develop surface and dimensional safing of a certain composition and impregnation layer depth functioning as a surface screen for articles of two types of cements: stressing cement and expanding cement—with 3% silica sol penetration. For dimensional safing, we made the samples of clay-containing material with the additives 15% FeO; ZnO; CuO; NiO; and H₃PO₄. After making surface or dimensional safing, we did industrial experiences on application of safing protection technologies.

2 Methods

For our study, we used a scanning electron microscope (SEM) and an X-ray micro-analyzer (XRM), which allows us to obtain data on the morphology, elemental and phase composition of the sample cross-section in the direction of propagation of the self-fertilizing compound. For this, the section in the central part was opened, and the samples were analyzed using the methods mentioned at a depth of 0.1, 3, 5, 10, 15, and 20 below the impregnation surface to obtain comparative data on the layer-by-layer change of materials.

The accuracy of the data obtained depends on the type of sample hole, which has a destructive effect on the sample. To minimize damage, the dissection was performed using a specialized cutter (Buchler) on a thin diamond disk (0.3 mm) with low rotation and minimal load and power. The cut sample was thoroughly blown, it was given dry polishing (without water) on a 10 micron abrasive, after which it was placed on the board of the microscope.

This type of sample preparation (dry polishing without impregnation with epoxy resin) allows preserving the original structure and composition of samples since

impregnation with epoxy resin (or any other impregnating composition) of samples with a developed surface leads to a significant impoverishment of the overall picture. The use of an aqueous medium during polishing can cause leaching, dissolution and modification of some components of the cement stone, including new formations (hydroxide salts, hydrated silicates, etc.).

To avoid undesirable effects associated with charging non-conductive samples with electron beams, as well as to increase the contrast of X-ray images, a thin Au layer (~200 Å) was sprayed onto the samples using a JFC-1100 cathode sputtering device (JEOL). For the SEM and XRM methods, zones of the bonding matrix (cement stone) were chosen, the porous morphological structure of which determines the level and characteristics of the impregnation of the concrete sample.

As an «indicator» of the depth of impregnation, any element can be selected; the concentration of which varies monotonically in depth and differs from the equilibrium one; or needle-like crystals of new formations formed by the interaction of the impregnating composition and the cement stone. Experiments used concrete B 20–30.

3 Results and Discussion

Tables 1, 2, and 3 present the results of concrete articles impregnated with 3% silica sol.

The XRM and SEM data in RE show that 90% of the impregnation composition (silica sol particles) is concentrated in the near-surface layer, where the highest density of new formations is observed.

With increasing depth, the density and size of new formations represented by sol particles and crystalline hydrates decreases.

In dimensional safing, one can find the correlation between the hardening process of a phosphate system as the basis of manufacturing artificial stone for construction and the show of detoxification properties, which is essential for geoprotection. Table 4

Table 1 Data of the layer-by-layer x-ray image of a self-hardening cement sample impregnated with 3% silica sol (wt%)

<i>h</i> , mm	CaO	SiO ₂	Al ₂ O ₃	Fe ₂ O ₃	MgO	SO ₃
0	52.0	24.0	12.5	0.0	1.0	10.0
1	53.8	22.8	12.4	1.2	0.6	8.9
1.98	55.0	21.3	12.4	2.6	0.6	7.7
3	56.1	19.9	13.0	3.4	0.7	6.5
4.94	57.4	18.1	13.4	4.7	0.6	5.2
>10 ^a	57.5	18.0	13.0	5.0	1.0	5.0

^aThe sample is not exposed to a silica sol, and its chemical composition is the same as that of the reference sample

Table 2 Data of layer-by-layer x-ray image of an expanding cement sample impregnated with 3% silica sol (wt%)

<i>h</i> , mm	CaO	SiO ₂	Al ₂ O ₃	Fe ₂ O ₃	MgO	SO ₃	Na(K)OH
0	52.0	24.1	12.5	0.0	0.9	10.0	0.5
1	49.8	20.6	16.5	0.5	1.3	10.6	0.7
2	48.3	17.7	20.0	1.0	1.0	11.5	0.5
3	47.2	15.8	22.5	1.5	1.1	11.1	0.9
5	46.2	14.5	24.5	1.9	0.8	11.5	0.6
>10^a	46.0	14.0	25.0	2.0	1.0	11.5	0.5

^aThe sample is not exposed to a silica sol, and its chemical composition is the same as that of the reference sample

Table 3 A summary of samples impregnated with 3% silica sol

Sample	<i>h_{re}</i> , mm	<i>h_{xrm}</i> , mm	<i>h_{nf}</i> , mm	<i>S/S₀</i> , %	<i>n/f</i>	Morphological types of <i>n/f</i>
Self-stressing cement	2.0	4.0	7	37	+++	Tobermorite
Expanding cement	2.5	3.8	7	40	++++	Ettringite

h_{re} depth of impregnation, determined by contrast in RE

h_{xrm} the depth of the impregnation is determined by the X-ray microanalyzer

h_{nf} depths of electronic microscope

S/S₀ the square occupied by micropores and microfractures (characterizes the level of the sample)

n/f new formations of crystals and flakes

Table 4 Dimensional safing achieved when phosphate systems are hardening

Heavy metal ion	Oxide powder	The main product providing strength, aquacomplex
Fe(II)	FeO	Fe ₃ (PO ₄) ₂ · 8H ₂ O
Zn(II)	ZnO	Zn ₃ (PO ₄) ₂ · 4H ₂ O
Cu(II)	CuO	Cu ₃ (PO ₄) ₂ · 3H ₂ O
Ni(II)	NiO	Ni ₃ (PO ₄) ₂ · nH ₂ O

shows the composition of a phosphate stone. The table shows that the basis of a hardening process is formation of hydrophosphates of heavy metals and the strength of the system constructed of them.

It should be noted that in dimensional phosphate, safing ions Fe(II), Zn(II), Cu(II), Ni(II) provide quite high strength.

Table 5 presents concentration values of ions in the saturated solution of phosphates unhydrous, which is shown from calculations of solubility product (SP) values compared to maximum permissible concentration (MPC) of soil ions.

The data in Table 5 show that ion concentration in the saturated solution of the sediment is lower compared with MPC of soil ions (columns 5 and 6, Table 5).

Table 5 Estimated values of heavy metal ions concentration in saturated phosphate solution by SP and MPC of soil ions

Free ion of heavy metal	Phosphates of heavy metals ions	Solubility product, SP	Concentration of metal Me(II) ion in saturated solution		MPC of soil ions, g/kg
			mol/l	g/l	
Cu(II)	$\text{Cu}_3(\text{PO}_4)_2$	1.26×10^{-37}	1.63×10^{-8}	1.03×10^{-6}	3.0×10^{-3}
Ni(II)	$\text{Ni}_3(\text{PO}_4)_2$	5.01×10^{-31}	3.47×10^{-7}	2.01×10^{-5}	4.0×10^{-3}
Zn(II)	$\text{Zn}_3(\text{PO}_4)_2$	9.12×10^{-33}	1.53×10^{-7}	$\sim 1.0 \times 10^{-5}$	23.0×10^{-3}
Fe(II)	$\text{Fe}_3(\text{PO}_4)_2$	1.29×10^{-22}	1.14×10^{-11}	0.63×10^{-9}	0.1×10^{-3}

Thus, it supports the hypothesis [16–22] that to increase the geosystem safety, it is necessary for ion concentration of the sediment in the saturated solution to be lower than MPC. The phosphate hardening method of soil geoprotection from heavy metal ions may be presented in the following structure (Fig. 1).

The purpose of the study was to use materials, including those contaminated with oil products and heavy metal ions, to produce artificial stone in which these contaminants will be blocked from interacting with the lithosphere and, thus, to protect it (geo-protective function), as well as to assess the durability of these stones [23, 24]. Durability affects the ability to use geo-protective systems for construction purposes. Geoprotection here is defined as the transformation of contaminated materials into environmentally friendly, as well as the elimination of the need to use them by manufacturing a durable building product. The energy for detoxifying and curing the system with good properties is taken from the energy reserve of the system.

Table 6 shows the energy reserves of some substances. Reactions release energy, and if the amount of mineral powder prevails over the liquid (H_3PO_4), then you can get building products with good properties by reducing the energy supply of the system. Following the purpose of the study, the properties possessed by materials

Fig. 1 Structure of safing technology of phosphate hardening in soil geocprotection

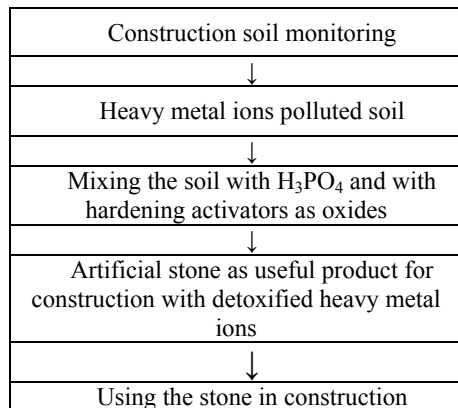


Table 6 Energy reserves of raw materials, ΔH_{298}^2 , kJ/mol

Raw material	$-\Delta H_{298}^2$, kJ/mol
Cambrian clay, $\text{Al}_2\text{O}_3 \cdot 4\text{SiO}_2 \cdot 4\text{H}_2\text{O}$	-5764.6
Kaolin, $\text{Al}_2\text{O}_3 \cdot 2\text{SiO}_2 \cdot 2\text{H}_2\text{O}$	-4116.0
Coal, FeO	-272
H_3PO_4	-289.26
Sand, SiO_2	-901.99
Fuel oil residual, $\text{C}_{20}\text{H}_{42}$; $\text{C}_{20}\text{H}_{40}$	-456.4 -330.8

obtained from artificially contaminated hardened solutions of soil and phosphoric acid have been studied for more than 10 years in order to decide whether they can be used, given their behavior over time. Tables 7 and 8 show the same result for phosphate protection.

Tables 7 and 8 show the natural clay or artificial material in combination with another pollutant, such as iron (II) oxide, which makes it possible to obtain a durable structural system with geo-protective properties, which manifests itself as the mixture hardens. These properties are the process of decontamination, the idea of which is to form sparingly soluble substances, and the process of blocking deactivation in

Table 7 Compressive strength of the protective phosphate cement system of soil contaminated with oil

Composition, weight, %				Density of H_3PO_4 , g/cm^3	Compression strength, MPa, years	
Contaminated soil	Clay material, $\text{Al}_2\text{O}_4 \cdot 4\text{SiO}_2 \cdot 2\text{H}_2\text{O}$	Sand	FeO	1.42 (solids 21%)	5	10
58.0	14.0	–	7.0	1.42	4.5	5.0
12.0	12.0	48.0	7.0	1.42	2.5	3.0
64.0	8.0	–	7.0	1.42	3.5	4.0
53.0	13.0	–	14.0	1.37	7.5	8.0

Table 8 Protective phosphate-containing cement system of Al_2O_4 , 4SiO_2 , $2\text{H}_2\text{O}$, and sand polluted with oil products

Contaminated sand + $\text{Al}_2\text{O}_4 \cdot 4\text{SiO}_2 \cdot 4\text{H}_2\text{O}$ + Fe, %				Compression strength, MPa, timing	
Sand	Clay	FeO	Petroleum product	1 year	10 years
51.5	13.3	16.6	1.5	4.0	5.0
50.4	13.3	16.6	2.7	3.5	4.5
49.4	13.3	16.6	3.7	3.0	4.2

the case when oil mixtures of oil are present in the mixture. Water extracts from the system, which were made at different times (from 1 month to more than 10 years), showed the removal of heavy metal ions.

The industrial testing of safing methods showed that heavy metal ions are not washed away from the phosphate stone, which indicates their total binding. Volatile products (ashes) impregnated with silica sol did not show dusting, which is also important in geocoprotective technologies.

4 Conclusions

1. The coating safing, which is the result of silica sol impregnation of hydrosilicate surface, has been studied. It is shown that the depth of the screen formed is till 7 mm, which depends on the cement used.
2. It has been observed that for ions Fe(II), Zn(II), Cu(II), Ni(II), it is possible to form a stone through phosphate hydrates of these metals which is the result of their binding, in dimensional safing.
3. Study presents the development of safing technologies of geocoprotection for mineral construction system through coatings and dimensional ways.

References

1. Svatovskaya LB, Kabanov AA, Sychov MM (2017) The improvement of foam concrete geocoprotective properties in transport construction. IOP Conf Ser Earth Environ Sci 90:012010
2. Svatovskaya LB, Kabanov AA, Sychov MM (2017) Lithosynthesis of the properties in the transport construction on the cement base. IOP Conf Ser Earth Environ Sci 90:012009
3. Svatovskaya LB, Kabanov AA, Sychov MM (2017) Soling, aerating and phosphating for soil strengthening and detoxication. Procedia Eng 189:398–403
4. Svatovskaya LB, Urov OV, Kabanov AA (2017) Geocoprotective technology of transport construction using silica sol absorption method. Procedia Eng 189:454–458
5. Svatovskaya LB, Shershneva MV, Baidarashvili MM, Yakimova NI, Khitrov AV (2004) Foam concrete construction demolished waste. In: Proceedings of the international conference on sustainable waste management and recycling: construction demolition waste, pp 199–203, London
6. Svatovskaya LB, Sakharova AS, Baidarashvilly MM, Petriaev AV (2015) Building wastes and cement clinker using in the geocoprotective technologies in transport construction. In: Proceedings of the 14th international conference of international association for computer methods and recent advances in geomechanics, IACMAG. Taylor and Francis—Balkema, Netherlands, pp 619–622
7. Sychova AM, Svatovskaya LB, Mjakin SV, Vasiljeva IV (2009) Modification of fillers for cements. In: Electron beam modification of solids: mechanisms, common features and promising applications, pp 35–37
8. Sychova AM, Svatovskaya LB, Mjakin SV, Vasiljeva IV (2009) Activation of aqueous phase at cement and concrete solidification. In: Electron beam modification of solids: mechanisms, common features and promising applications, pp 39–47

9. Maslennikova LL, Svatovskaya LB, Mjakin SV, Vasiljeva IV (2009) Activation of reactions at solid-solid interfaces. Improvement of ceramics materials. In: Electron beam modification of solids: mechanisms, common features and promising applications, pp 57–61
10. Svatovskaya LB, Yakimova NI, Trunskaya OY, Rusanova EV, Krylova NB (2004) New complex ecotechnology for oil demolished waste. In: Proceedings of the international conference on sustainable waste management and recycling: construction demolition waste, London
11. Sychova AM, Solomahin A, Kotovich V, Svatovskaya LB, Kamenev Y (2018) Improving of the monolithic foam concrete quality for used in the high-rise construction. E3S Web of Conf 33:02058
12. Gusev N, Svatovskaya LB, Kucherenko A (2018) Effect of changing of the parametrs of the cable network of monitoring systems of high-rise buildings on the basis of string converters on their operability. E3S Web of Conf 33:02069
13. Sychova A, Sychov M, Rusanova E (2017) A method of obtaining geonoiseprotective foam concrete for use on railway transport. Procedia Eng 189:681–687
14. Sychova A, Solomahin A, Hitrov A (2017) The increase of the durability and geoprotective properties of the railway subgrade. Procedia Eng 189:688–694
15. Yamamoto T, Yamoda T, Miyake A (2007) Tansparent conductive Ga-doped ZnO films properties on glass, PMMA and COP substrates. In: Proceedings of international display workshop, Japan, p 2044
16. Kityk V, Migalska A, Ebothe J, Elchichou A (2002) Anomalously large pockels effect in ZnO-F single crystalline films deposited on bare glass. Cryst Res Technol 37:340–352
17. Singha I, Bhatnagara PK, Mathura PC (2008) Optical and electrical characterization of conducting polymer-single walled carbon nanotube composite films. Carbon 46(8):1141–1144
18. Kimakis E (2002) Single walled carbon nanotube composites. Synth Met 127:59–62
19. Todda MG, Shi FG (2003) Characterizing the interphase dielectric constant of polymer composite materials: effect of chemical coupling agents. Appl Phys 94(7):4551–4557
20. Xiaoliang D, Xiaolin L, Yong Z (2009) Improved dielectric strength of barium titanate-polyvinylidene fluoride nanocomposites. Appl Phys Lett 95:95
21. Chao F, Liang G, Kong W (2008) Dielectric properties of polymer. Ceramic composites based on thermosetting polymers. Polym Bull 60:129–136
22. Todd MG, Shi FG (2002) Validation of a novel dielectric constant simulation model and the determination of its physical parameters. Microelectron J 33:627–632
23. Rao Y, Takahashi A, Wong CP (2003) Di-block copolymer surfactant study to optimize filler dispersion in high dielectric constant polymer-ceramic composite. Compos: Part A 34:1113–1116 (2003)
24. Qi L, Lee BI, Samuels WD (2006) Three-phase percolative silver-BaTiO₃—epoxy nanocomposites with high dielectric constants. J Appl Polym Sci 102:967–971

Specificities of Soling Processes in Technologies of Geoconstruction



Larisa Svatovskaya , Kseniia Mikhailova, Alexander Kabanov
and Nikolay Khamenok

Abstract The study belongs to the field of silica sol technology application in geoconstruction of the cold regions. The aim of the research was to study the specificities of processes of various kinds of soling technologies—detoxification, absorption, blocking and strengthening technologies. The methods of the research were thermodynamic, experimental ones, electronic microscope scanning, x-ray analysis, derivatographic and chemical analysis. The correlation of thermodynamic resolution and formation of calcium-hydrosilicates and heavy metal ions has been found. In the first case, this is the basis for property improvement in absorption and blocking technologies, in the second case—in detoxification technology. In strengthening technology, the nature of the soil should be taken into consideration.

Keywords Soling · Process · Geoconstruction · Specificity

1 Introduction

The research area is geoconstruction with the use of sol solutions, in particular, silica sol. In accordance with the criteria of environmental admissibility of soil mineral substances, one can state that silica sol meets the requirements below [1–6].

1. **Criterion of mineralogical compliance (CMC)** determines the similarity of input binding systems to the principal natural products of the soil—silicates and aluminum silicates (sands, clays). This criterion protects lithosphere from the input of harmful substances such as phenol-formaldehyde resins which are not allowed to be used for soil strengthening within the proposed knowledge system. The criterion is met provided the compliance of chemical and phase compositions. Silica sol is of formula $\text{SiO}_2 \cdot n\text{H}_2\text{O}$.

L. Svatovskaya (✉) · K. Mikhailova · A. Kabanov · N. Khamenok
St. Petersburg State Transport University, 9 Moskovsky pr, St. Petersburg 190031, Russia
e-mail: lsvatovskaya@yandex.ru

Table 1 Silica soling technologies in geoconstruction and the achieved useful properties

Silica sol technology	Achieved useful geocoprotective properties of a geoconstruction system
Silica sol technology of heavy metal ion detoxification Sol Detoxification Technology (SDT)	Heavy metal ion detoxification
Silica sol technology of soil strengthening Sol Strengthening Technology(SST)	Similar to silicization using Na_2SiO_3 , but without alkalization of the system
Blocking pollutions inside a construction system Sol Blocking Technology (SBT)	Blocking absorbed oil products or other organic substances
Increase of quality index of articles by silica soling in geoconstruction system—structures, building facilities Sol Absorption Technology (SAT)	20–80% improvement of structural properties [13, 14]

- Criterion of Gibbs free energy reduction (CEGR)** represents the energy base of detoxification and strengthening by using the full energy of the system, i.e., in this process, this criterion reflects the change of Gibbs free energy ΔG°_{298} , kJ. In accordance with the works [7–12], ΔG°_{298} of silica soling processes comes up negative.
- Criterion of showing geocoprotective properties (CGP)** determines the capability of a binder to detoxify the pollutions in the soil being strengthened. These properties are either already known or predicted by thermodynamic (energy) values, and they are characterized by particular quantitative values, e.g., capacity, g/kg or kg/t. Adsorptive properties of silica sol are well-known.
- Criterion of predicting (CP) useful properties of a strengthened system during or after its life-cycle.** This criterion predicts the possibility of useful life of the substances from a geoconstruction system. For geocoprotective purposes, this criterion can be expressed by various values, for example, a share of a replaced natural product by using the wastes of silica sol modified articles (Table 1).

The aim of the work is to study the specificities of silica sol processes in geoconstruction. The main target is to find out if silica sol forms chemical compounds in reactions and what the depth off the surface of the new formations is.

2 Methods

The methods of the research are instrumental, experimental, thermodynamic and derivatographic ones.

SDT technology was studied by the method of water extract from heavy metal ion soils. The water extract interacted with 3–30% silica sol solution, and the obtained

sediments were analyzed by derivatographic method. SST, SBT and SAT samples were analyzed as samples from consolidated materials.

In order to obtain an electron microscopic image of silica gel deposits with absorbed heavy metal ions and layers on concrete, we used signals from secondary or reflected electrons (SE, RE), which made it possible to obtain a morphological or compositional contrast, respectively.

The determination of the elemental composition of the samples is carried out by electron probe microanalysis, which is based on a comparison of the characteristic x-ray spectra of the analyzed sample and standards of known composition. The sensitivity of the method is ~ 0.1 wt%.

Unanalyzed elements: H, Li.

X-ray phase analysis is based on collecting diffraction reflection spectra from the phase structures included in the sample and their identification according to the catalog. Amorphous component is not collected. Reflections with a large peak width can correspond to different isostructural phases with similar grid parameters. The sensitivity of x-ray phase analysis is ~ 5 wt% (given x-ray microanalyzer).

Equipment for analysis:

1. Scanning electron microscope (SEM) Vega 3SBH (Tescan).
2. Energy dispersive x-ray microanalyzer (XRM) X-act Energy (Oxford Instrumentation).
3. Installation of thermal spraying Q15R (Quortum technology).
4. RIGAKU SmartLab3 diffractometer (Rigaku).
5. Auxiliary equipment for sample preparation.

3 Results and Discussion

Table 2 presents thermodynamic analysis of silica sol systems in the technologies under review.

Tables 3 and 4 present the results of SDT technology analysis. Table 5 presents the results of SAT technology analysis.

Precipitation with heavy metal ions is characterized by a very high degree of condensation. All x-ray amorphous deposits.

Data of the tables show that the sediments (Eqs. 1–8, Table 2) in SDT technology represent chemical compounds, which is confirmed by the data of Tables 3 and 4.

Work on the modification of the surface of a concrete product and the detoxification of the soil with heavy metal ions combine the mechanisms of $\text{SiO}_2 \cdot n\text{H}_2\text{O}$ reactions, studied in the Russian school of academician V. B. Aleskovsky [15–20]. In accordance with these works, it can be assumed that the interaction processes of $\text{SiO}_2 \cdot n\text{H}_2\text{O}$ are controlled by the value of the solubility product SP during the initial interaction event, represented by sorption. Each formed substance has its own

Table 2 Thermodynamic evaluation of silica sol processes in geoconstruction

№	Ions	Chemical reactions	ΔG°_{298} , kJ/mol
1	Cu(II)	$\text{Cu}^{2+} + \text{SiO}_2 \cdot \text{H}_2\text{O} + 2\text{OH}^- = \text{CuO} \cdot \text{SiO}_2 \cdot 2\text{H}_2\text{O}$	-56.7
2	Cu(II)	$2\text{Cu}^{2+} + \text{SiO}_2 \cdot \text{H}_2\text{O} + 4\text{OH}^- = \text{CuO} \cdot \text{SiO}_2 \cdot 2\text{H}_2\text{O} + \text{Cu}(\text{OH})_2$	-56.7
3	Cu(II)	$2\text{Cu}^{2+} + \text{SiO}_2 \cdot 2\text{H}_2\text{O} + 4\text{OH}^- = \text{CuO} \cdot \text{SiO}_2 \cdot 2\text{H}_2\text{O} + \text{Cu}(\text{OH})_2 + \text{H}_2\text{O}$	-6.8
4	Pb(II)	$5\text{Pb}^{2+} + \text{SiO}_2 \cdot \text{H}_2\text{O} + 10\text{OH}^- = \text{Pb}(\text{OH})_2 + 4\text{PbO} \cdot \text{SiO}_2 + 5\text{H}_2\text{O}$	-529.9
5	Pb(II)	$3\text{Pb}^{2+} + \text{SiO}_2 \cdot \text{H}_2\text{O} + 6\text{OH}^- = \text{Pb}(\text{OH})_2 + 2\text{PbO} \cdot \text{SiO}_2 + 3\text{H}_2\text{O}$	-353.9
6	Pb(II)	$5\text{Pb}^{2+} + \text{SiO}_2 \cdot \text{H}_2\text{O} + 10\text{OH}^- = \text{Pb}(\text{OH})_2 + 4\text{PbO} \cdot \text{SiO}_2 + 6\text{H}_2\text{O}$	-480.05
7	Pb(II)	$3\text{Pb}^{2+} + \text{SiO}_2 \cdot 2\text{H}_2\text{O} + 6\text{OH}^- = \text{Pb}(\text{OH})_2 + 2\text{PbO} \cdot \text{SiO}_2 + 4\text{H}_2\text{O}$	-306
8	Pb(II)	$3\text{Pb}^{2+} + 2\text{SiO}_2 \cdot 3\text{H}_2\text{O} + 6\text{OH}^- = \text{Pb}(\text{OH})_2 + 2\text{PbO} \cdot \text{SiO}_2 + 4\text{H}_2\text{O} + \text{SiO}_2 \cdot \text{H}_2\text{O}$	-202.9

Table 3 X-ray microanalyzer data (% wt)

№	N	O	Na	Mg^{2+}	Si	Cl^-	K	Fe	Cu^{2+}	Pb^{2+}	C
1,2	-	53.4	0.7	0.5	46.9	-	-	-	-	-	4
3	-	52.3	0.3	-	45.4	-	-	-	1.9	-	2
4	-	53.9	0.1	-	42.3	-	-	-	0.1	3.7	2
5	-	52.5	-	-	46.0	0.2	-	1.1	0.1	-	2

1, 2—control sample, $\text{SiO}_2 \cdot n\text{H}_2\text{O}$

3—precipitate with Cu^{2+}

4—precipitate with Pb^{2+}

5—precipitate with Fe^{3+}

Table 4 illustrates the difference between control sample $\text{SiO}_2 \cdot n\text{H}_2\text{O}$ -Ca and Cu^{2+} , Pb^{2+} silicasol

Table 4 Calculation of derivatogram

Systems	Mass, mol, ion	Water loss according to derivatogram, %
Silica sol- Ca^{2+}	40.00	25.02
Silica sol- Cu^{2+}	63.50	9.00
Silica sol- Pb^{2+}	207.00	9.89

Table 5 Data layer-by-layer x-ray image of a sample of Portland cement impregnated with 3% silica sol (wt%)

<i>h</i> , mm	CaO	SiO ₂	Al ₂ O ₃	Fe ₂ O ₃	MgO	SO ₃	Na(K)OH
0	57.1	27.0	9.0	2.1	1.6	2.5	0.7
1	59.9	25.3	6.9	3.0	2.0	1.9	1.0
2	61.9	24.2	5.5	3.3	1.8	2.2	1.1
3	63.3	23.8	4.7	3.2	2.0	2.2	0.8
5	64.5	23.5	4.0	3.1	1.8	2.3	0.8
>10 ^a	64.6	23.3	4.0	3.0	1.9	2.2	1.0

^aThe sample is not exposed to a silica sol, and its chemical composition is the same as that of the reference sample

composition and is an individual compound; while the solubility product for polysilicon salts is small in the works of V. B. Aleskovsky it is called the sorbed product (Table 6).

In accordance with Table 6, salts of polysilicic acids tend to have lower values than hydroxides (columns 3 and 5) or in some cases close to Cu(II).

Therefore, SDT technology's feature is that under thermodynamic resolution (reactions 1–8, Table 2) the formation of new silicate phases includes the mechanism of ion sorption SiO₂ · H₂O (sol) (Table 6), and further transition into amorphous silicate phases of new formations (Tables 3, 4). Judging from the data in Table 5, SAT technology provides surface layers of new formations, the depth of which is shown in Table 7, which goes in accordance with the works [21–24].

The data obtained in this article, the thermodynamic calculations we made, and the data in Table 7 illustrates the potential of hydrated silicates and polysilicates responsible for improving the properties of materials in SAT technologies. They increase the durability of materials in geoconstruction; in detoxification technologies, they form poorly soluble compounds of heavy metal ions, which is detoxification. In SBT technology, the penetration rate should be lower, because in this technology, silica gel occurs after curing.

The obtained results make it possible to assume that in SST technology the composition of a generated silicate, or silica gel, depends on the nature of the soil, Table 8.

Table 6 Sorbability product and solubility products of polysilicic acid hydroxides

Metal ions	Polysilicic salts		Hydroxides	
	Sorb. product	<i>C</i> , mol/l	Solub. product	<i>C</i> , mol/l
Ca(II)	10 ⁻⁹	7 × 10 ⁻⁵	5.5 × 10 ⁻⁶	1.1 × 10 ⁻²
Mg(II)	4 × 10 ⁻¹²	2 × 10 ⁻⁶	1.8 × 10 ⁻¹¹	1.65 × 10 ⁻³
Al(III)	10 ⁻⁶⁰	10 ⁻¹²	10 ⁻³²	5 × 10 ⁻⁹
Cd(II)	4 × 10 ⁻¹⁴	10 ⁻⁷	2 × 10 ⁻¹⁴	1.8 × 10 ⁻⁵
Zn(II)	10 ⁻¹⁷	7 × 10 ⁻⁹	7.1 × 10 ⁻¹⁸	1.2 × 10 ⁻⁶

Table 7 Summary of Portland cement samples soaked with 3% silica sol

Sample	h_{re} , mm	h_{xrm} , mm	h_{nf} , mm	S/S_0 , %	n/f	Morphological types of n/f
Portland cement	1.5	3.5	5	33	+	CSH

h_{re} depth of impregnation, determined by contrast in RE

h_{xrm} the depth of impregnation, determined by the change in the chemical composition in the surface layer using an x-ray microanalyzer

h_{nf} maximum depth at which characteristic neoplasms were detected using a scanning electron microscope

S/S_0 the area occupied by micropores and microcracks (characterizes the permeability of the sample)

n/f tumors, represented by needle-like crystals and flakes, and their density

Table 8 Nature of the soil being strengthened

Nature of the soil being strengthened	Possible new formations in silica soling
Sandy soil	$SiO_2 \cdot nH_2O$, gel
Clay-containing soil	$Al_2O_3 \cdot nSiO_2 \cdot mH_2O$
Calcium-containing soil	$nCaO \cdot mSiO_2 \cdot xH_2O$

To develop the result of the paper it is possible to suggest other mineral geoantidotes silicate nature (see Table 9).

In Table 9, there are artificial (C_3S , C_2S , $Al_2O_3 \cdot 2SiO_2$ (metacaolinit) and natural substances ($xMgO \cdot ySiO_2$; $Al_2O_3 \cdot 2SiO_2 \cdot 2H_2O$) of the silicate nature. Such kind of mineral substances is good enough for geosphere protection according to schemes of Table 9.

4 Conclusions

1. The interaction of silica sol in SDT technology is based on thermodynamic resolution and includes the formation of a new phase, most probably, hydrosilicate; the interaction mechanism includes sorption processes.
2. The interaction of silica sol in SAT and SBT technologies includes absorption and generation of new formations as low-basic silicates at the depth till 5 mm.
3. The interaction of silica sol in SST technology includes the formation of an amorphous phase, most probably, silica gel if the sandy soil is strengthened, or more complex hydrosilicates in the other cases.

Table 9 Detoxification with different mineral geoantidotes

Nº	Mineral geoantidotes	Schemes	pH
1	C_3S C_2S	$\left. \begin{array}{l} x'C_3S + nH_2O + C_{i, aq}^* \\ x'C_2S + nH_2O + C_{i, aq}^* \end{array} \right\} \rightarrow x''C_iO \cdot y'SiO_2 \cdot n'H_2O + C_i(OH)_2 + xCaO \cdot ySiO_2 \cdot mH_2O$ $C_2S + Na_2SiO_3(K_2SiO_3) + nH_2O + x'C_i \rightarrow C_i(OH)_2 + xC_iO \cdot ySiO_2 \cdot zH_2O + xCaO \cdot ySiO_2 \cdot n'H_2O$	>7
2	$xMgO \cdot ySiO_2$	$xMgO \cdot ySiO_2 + nH_2O + C_{i, aq} \rightarrow C_iO \cdot xSiO_2 \cdot yH_2O + x'MgO \cdot y'SiO_2 \cdot n'H_2O$	>7
3	$Al_2O_3 \cdot 2SiO_2$	$Al_2O_3 \cdot 2SiO_2 \cdot Na_2SiO_3(K_2SiO_3) + nH_2O + (C_iOH)_{aq}^+ \rightarrow C_i(OH)_2 \downarrow$ + + $xN_{aq}O(K_2O) \cdot yAl_2O_3 \cdot zSiO_2 \cdot mH_2O + \alpha SiO_2 \cdot bH_2O$	>7
4	$Al_2O_3 \cdot 2SiO_2 \cdot H_2O$	$Al_2O_3 \cdot 2SiO_2 \cdot 2H_2O + 3C_i(II)_{aq} + H_3PO_4 \rightarrow (C_i)_3(PO_4)_2 \cdot nH_2O + SiO_2 \cdot mH_2O + Al_2O_3 \cdot xP_2O_5 \cdot n'H_2O$	<7

References

1. Svatovskaya LB, Kabanov AA, Sychov MM (2017) The improvement of foam concrete geoeccoprotective properties in transport construction. *IOP Conf Ser Earth and Environ Sci* 90:012010
2. Svatovskaya LB, Kabanov AA, Sychov MM (2017) Lithosynthesis of the properties in the transport construction on the cement base. *IOP Conf Ser Earth and Environ Sci* 90:012009
3. Svatovskaya LB, Kabanov AA, Sychov MM (2017) Soling, aerating and phosphating for soil strengthening and detoxication. *Procedia Eng* 189:398–403
4. Svatovskaya LB, Urov OV, Kabanov AA (2017) Geoeccoprotective technology of transport construction using silica sol absorption method. *Procedia Eng* 189:454–458
5. Svatovskaya LB, Shershneva MV, Baidarashvili MM, Yakimova NI, Khitrov AV (2004) Foam concrete construction demolished waste. In: *Proceedings of the international conference on sustainable waste management and recycling: construction demolition waste* London, pp 199–203
6. Svatovskaya LB, Sakharova AS, Baidarashvili MM, Petriaev AV (2015) Building wastes and cement clinker using in the geoeccoprotective technologies in transport construction. In: *Proceedings of the 14th international conference of international association for computer methods and recent advances in geomechanics, IACMAG*, Taylor and Francis—Balkema, Netherlands, pp 619–622
7. Sychova AM, Svatovskaya LB, Mjakin SV, Vasiljeva IV (2009) Modification of fillers for cements. In: *Electron beam modification of solids: mechanisms, common features and promising applications*, pp 35–37
8. Sychova AM, Svatovskaya LB, Mjakin SV, Vasiljeva IV (2009) Activation of aqueous phase at cement and concrete solidification. In: *Electron beam modification of solids: mechanisms, common features and promising applications*, pp 39–47
9. Maslennikova LL, Svatovskaya LB, Mjakin SV, Vasiljeva IV (2009) Activation of reactions at solid-solid interfaces. Improvement of ceramics materials. In: *Electron beam modification of solids: mechanisms, common features and promising applications*, pp 57–61
10. Svatovskaya LB, Yakimova NI, Trunskaya OY, Rusanova EV, Krylova NB (2004) New complex ecotechnology for oil demolished waste. In: *Proceedings of the international conference on sustainable waste management and recycling: construction demolition waste*, London
11. Sychova AM, Solomahin A, Kotovich V, Svatovskaya LB, Kamenev Y (2018) Improving of the monolithic foam concrete quality for used in the high-rise construction. *E3S Web Conf* 33:02058
12. Gusev N, Svatovskaya LB, Kucherenko A (2018) Effect of changing of the parametrs of the cable network of monitoring systems of high-rise buildings on the basis of string converters on their operability. *E3S Web Conf* 33:02069
13. Sychova A, Sychov M, Rusanova E (2017) A method of obtaining geonoiseprotective foam concrete for use on railway transport. *Procedia Eng* 189:681–687
14. Sychova A, Solomahin A, Hitrov A (2017) The increase of the durability and geoprotective properties of the railway subgrade. *Procedia Eng* 189:688–694
15. Yamamoto T, Yamoda T, Miyake A (2007) Tansparent conductive Ga-doped ZnO films properties on glass, PMMA and COP substrates. In: *Proceedings of international display workshop, Japan*, p 2044
16. Kityk V, Migalska A, Ebothe J, Elchichou A (2002) Anomalously large pockels effect in ZnO-F single crystalline films deposited on bare glass. *Cryst Res Technol* 37:340–352
17. Singha I, Bhatnagara PK, Mathura PC (2008) Optical and electrical characterization of conducting polymer-single walled carbon nanotube composite films. *Carbon* 46(8):1141–1144
18. Kimakis E (2002) Single walled carbon nanotube composites. *Synth Met* 127:59–62
19. Todda MG, Shi FG (2003) Characterizing the interphase dielectric constant of polymer composite materials: effect of chemical coupling agents. *Appl Phys* 94(7):4551–4557
20. Xiaoliang D, Xiaolin L, Yong Z (2009) Improved dielectric strength of barium titanate-polyvinylidene fluoride nanocomposites. *Appl Phys Lett* 95:95

21. Chao F, Liang G, Kong W (2008) Dielectric properties of polymer. Ceramic composites based on thermosetting polymers. *Polym Bull* 60:129–136
22. Todd MG, Shi FG (2002) Validation of a novel dielectric constant simulation model and the determination of its physical parameters. *Microelectron J* 33:627–632
23. Rao Y, Takahashi A, Wong CP (2003) Di-block copolymer surfactant study to optimize filler dispersion in high dielectric constant polymer-ceramic composite. *Compos: Part A* 34:1113–1116
24. Qi L, Lee BI, Samuels WD (2006) Three-phase percolative silver-BaTiO₃—epoxy nanocomposites with high dielectric constants. *J Appl Polym Sci* 102:967–971

Criteria of Green Geocoprotective Technologies in Transport Construction



Larisa Svatovskaya , Ivan Drobyshev, Kseniia Mikhailova and Nikolay Khamenok

Abstract The paper concerns geocoprotective technologies in transport construction in the cold regions. The aim of the research was to develop criteria for the estimation of geocoprotective properties in the sphere of transport geoconstruction using geoantidotes as an example. Such methods as physical and chemical, physical and mechanical as well as instrumental ones were applied during the study. Five criteria for green geocoprotective technologies with the help of mineral geoantidotes have been developed. They are the following:

- energy of geocoprotective processes must be based only on the internal energy (without the consumption of any kind of natural fuel);
- detoxication products must have a very low solubility product (detoxication technology) or must be kept in a stone-like in a safe (safing technology);
- substances, articles, or structures with useful building properties must be produced as a result of green technology, they being the same as natural ones;
- mineral geoantidotes must have nature-like any natural substance;
- there must be the field of the application of such substances after their life cycle in order to avoid waste.

The examples of the use of precipitations of sparingly soluble compounds of lead and barium, as well as copper, nickel, and zinc, are given.

Keywords Geocoprotective technology · Transport · Cold · Construction · Geoenvironment · Geoantidote · Property

1 Introduction

The study concerns the protection of natural and man-made environment in geoconstruction. In the last decade, special attention has been paid to the neutralization of pollutions that become dangerous when the maximum permissible concentration

L. Svatovskaya (✉) · I. Drobyshev · K. Mikhailova · N. Khamenok
St. Petersburg State Transport University, 9 Moskovsky pr, St. Petersburg 190031, Russia
e-mail: lbsvatovskaya@yandex.ru

© Springer Nature Singapore Pte Ltd. 2020
A. Petriaev and A. Konon (eds.), *Transportation Soil Engineering in Cold Regions*,
Volume 2, Lecture Notes in Civil Engineering 50,
https://doi.org/10.1007/978-981-15-0454-9_45

level increases [1–6]. Substances which are capable of detoxicating pollutions are called mineral geoantidotes. They can be in the form of a dispersion, nanosolutions, solid, or composite materials [7–14]. Thus, in accordance with the works mentioned above, mineral geoantidotes must meet certain requirements:

- they must have a mineral composition which is similar to natural one both in the initial form and in detoxication products;
- they must be able to detoxicate pollutions by using the internal energy of a system;
- they must demonstrate detoxication properties by producing, e.g., sparingly soluble products;
- detoxication system must have useful properties in order not to pollute the environment.

In Tables 1, 2, 3, and 4, there are examples of some mineral geoantidote reactions, namely sulfate, silicate, and phosphate systems. They illustrate that there are substances which are similar to natural ones in the left part of the equality of the reactions of heavy metal ion detoxication. During the reactions, energy is released. The reaction products are also like natural ones in their mineralogical composition, and they are sparingly soluble products.

Tables 1, 2, 3, and 4 demonstrate that any geochemical process has the negative meaning of ΔH°_{298} and ΔG°_{298} , and it is possible to say, that any process is based on the internal energy.

Table 1 Energy evaluation of lithosphere detoxication processes when using calcium hydrosulfate mineral geoantidotes

Chemical processes	ΔH°_{298} , kJ/mol	ΔH°_{298} of detoxication, kJ/mol	ΔG°_{298} , kJ/mol	ΔG°_{298} of detoxication, kJ/mol
$\text{CaSO}_4 \cdot 0.5\text{H}_2\text{O} + 1.5\text{H}_2\text{O}(\text{l}) = \text{CaSO}_4 \cdot 2\text{H}_2\text{O}$ (stone) control	–18.0	–	–5.35	–
$2(\text{CaSO}_4 \cdot 0.5\text{H}_2\text{O}) + \text{H}_2\text{O}(\text{l}) + \text{Pb}^{2+}_{\text{aq}} = \text{PbSO}_4 \downarrow(\text{s}) + \text{CaSO}_4 \cdot 2\text{H}_2\text{O}(\text{s}) + \text{Ca}^{2+}_{\text{aq}}$	–58.12	–40.12	–29.42	–24.07
$2(\text{CaSO}_4 \cdot 0.5\text{H}_2\text{O})(\text{s}) + \text{H}_2\text{O}(\text{l}) + \text{Ba}^{2+}_{\text{aq}} = \text{BaSO}_4 \downarrow + \text{CaSO}_4 \cdot 2\text{H}_2\text{O}(\text{s}) + \text{Ca}^{2+}_{\text{aq}}$	–71.86	–53.86	–42.40	–37.05

Table 2 Energy evaluation of lithosphere detoxication processes when using hydration active minerals as mineral geoantidotes

Chemical processes	ΔH°_{298} , kJ/mol	$\Delta H^{\circ a}_{298}$ of detoxication, kJ/mol	ΔG°_{298} , kJ/mol	$\Delta G^{\circ b}_{298}$ of detoxication, kJ/mol
2(3CaO SiO ₂)(s) + 6.17H ₂ O(l) + Cd _{aq} ²⁺ = 2CaO SiO ₂ · 1.17H ₂ O(s) + CdO SiO ₂ H ₂ O(s) + 4Ca(OH) ₂ (s)	−320.20	−254	−315	−233.13
3(CaO SiO ₂)(s) + 2.17H ₂ O(l) = 2CaO SiO ₂ · 1.17H ₂ O(s) + Ca(OH) ₂ (s)	−66		−81.87	
2(2CaOSO ₂)(s) + 4.17H ₂ O(l) + Cd _{aq} ²⁺ = 2CaO SiO ₂ · 1.17H ₂ O(s) + CdO SiO ₂ H ₂ O(s) + 2Ca(OH) ₂ (s)	−224.25	−165.20	−171.7	−161.70
2(CaO SiO ₂)(s) + 1.17H ₂ O(l) = 2CaOSiO ₂ · 1.17H ₂ O(s)	−59		−10	

Notes (s)—solid substance; (l)—liquid substance

^aEnthalpy of detoxication calculated as the difference of changes of enthalpies of processes 1 and 2; 3 and 4

^bDetoxication useful work calculated as the difference of ΔG°_{298} changes of processes 1 and 2; 3 and 4

In general, the following scheme can be proposed to ensure that the technology is green (see Fig. 1):

The scheme emphasizes five criteria that would allow to name the technology of geocoprotection as a green technology in terms of perfection:

- the internal energy is used, i.e., fuel is not consumed;
- mineral compositions of initial and final products are close to natural ones;
- final products are the same as natural ones;
- reaction products must have a very low solubility product, less than 10^{−8};
- products should have useful properties after detoxication.

It is the last criterion that is of great importance for geocoprotection. In this regard, it should be noted that, if adsorption method is used, when a pollution is absorbed by artificial stone and is neutralized there, or a pollution is involved in the formation of stone, e.g., phosphate system, the artificial stone with neutralized

Table 3 Energy evaluation of lithosphere detoxication processes when using alkali binding systems

Chemical processes	ΔH°_{298} , kJ/mol	ΔH°_{298} of detoxication, kJ/mol	ΔG°_{298} , kJ/mol	ΔG°_{298} of detoxication, kJ/mol
$\text{Al}_2\text{O}_3 \cdot 2\text{SiO}_2 + \text{NaOH(s)} + 2\text{H}_2\text{O(l)} = \text{NaAlSi}_2\text{O}_6 \cdot \text{H}_2\text{O} + 0.5(\text{Al}_2\text{O}_3 \cdot 3\text{H}_2\text{O(s)})$	-274.60	-	-275.45	-
$2(\text{Al}_2\text{O}_3 \cdot 2\text{SiO}_2) + 4\text{NaOH(s)} + 4\text{H}_2\text{O} + \text{Cd}^{2+}_{\text{aq}} = 2(\text{NaAlSi}_2\text{O}_6 \cdot \text{H}_2\text{O(s)}) + \text{Cd(OH)}_2\text{(s)} + \text{Al}_2\text{O}_3 \cdot 3\text{H}_2\text{O(s)} + 2\text{Na}^{+}_{\text{aq}}$	-419.51	-144.9	-709.5	-434.05
$2(\text{Al}_2\text{O}_3 \cdot 2\text{SiO}_2\text{(s)}) + 4\text{NaOH(s)} + 4\text{H}_2\text{O(l)} + \text{Pb}^{2+}_{\text{aq}} = 2(\text{NaAlSi}_2\text{O}_6 \cdot \text{H}_2\text{O(s)}) + \text{Pb(OH)}_2\text{(s)} + \text{Al}_2\text{O}_3 \cdot 3\text{H}_2\text{O(s)} + 2\text{Na}^{+}_{\text{aq}}$	-682.68	-408.5	-732.48	-457.03

Notes (s)—solid substance; (l)—liquid substance

Table 4 Energy release reactions in phosphate systems

№	Chemical processes	ΔH°_{298} , kJ/mol
1	$\text{Al(OH)}_3 + \text{H}_3\text{PO}_4 = \text{AlPO}_4 + 3\text{H}_2\text{O}$	-17.53
2	$\text{Al(OH)}_3 + 3\text{H}_3\text{PO}_4 = \text{Al(H}_2\text{PO}_4)_3 + 3\text{H}_2\text{O}$	-147.60
3	$\text{Al(OH)}_3 + \text{H}_3\text{PO}_4 = \text{Al(OH)}_2\text{H}_2\text{PO}_4 + \text{H}_2\text{O}$	-152.44
4	$\text{Al}_2\text{O}_3 \cdot 2\text{SiO}_2 \cdot 2\text{H}_2\text{O} + 2\text{H}_3\text{PO}_4 = 2(\text{SiO}_2 \cdot \text{H}_2\text{O}) + 2\text{AlPO}_4 + 3\text{H}_2\text{O}$	-22.61
5	$\text{Al}_2\text{O}_3 \cdot 2\text{SiO}_2 \cdot 2\text{H}_2\text{O} + 6\text{H}_3\text{PO}_4 = 2(\text{SiO}_2 \cdot \text{H}_2\text{O}) + 2\text{Al(H}_2\text{PO}_4)_3 + 3\text{H}_2\text{O}$	-282.77
6	$\text{Al}_2\text{O}_3 \cdot 4\text{SiO}_2 \cdot 2\text{H}_2\text{O} + 2\text{H}_3\text{PO}_4 = 4(\text{SiO}_2 \cdot \text{H}_2\text{O}) + 2\text{AlPO}_4 + 3\text{H}_2\text{O}$	-55.72
7	$\text{Al}_2\text{O}_3 \cdot 4\text{SiO}_2 \cdot 2\text{H}_2\text{O} + 6\text{H}_3\text{PO}_4 = 4(\text{SiO}_2 \cdot \text{H}_2\text{O}) + 2\text{Al(H}_2\text{PO}_4)_3 + \text{H}_2\text{O}$	-315.82
8	$\text{Al}_2\text{O}_3 \cdot 4\text{SiO}_2 \cdot 2\text{H}_2\text{O} + 2\text{H}_3\text{PO}_4 + 3\text{H}_2\text{O} = 4(\text{SiO}_2 \cdot \text{H}_2\text{O}) + 2\text{Al(OH)}_2\text{H}_2\text{PO}_4$	-325.54

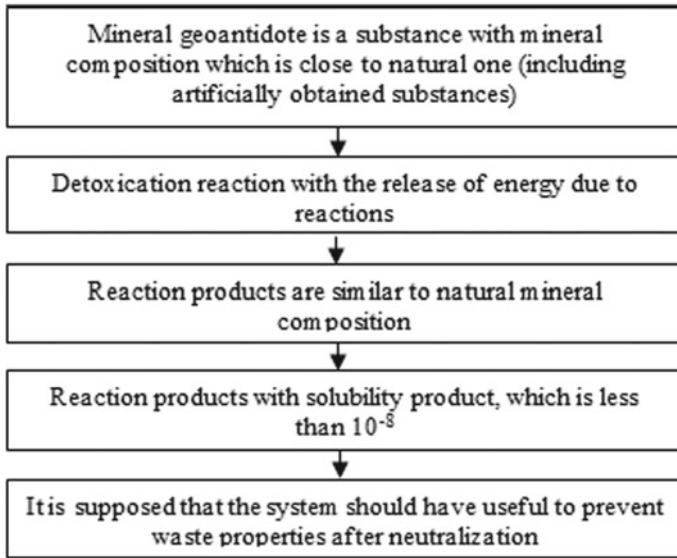


Fig. 1 Method of the absorption of a complex with silica solution by concrete

precipitations or with detoxication products is a product with useful properties, e.g., for construction. But if precipitations, e.g., sparingly soluble sulfates, are not formed in the body of stone, the technology will be green in the case of the application of lead or barium sparingly soluble compounds in an amount of 20–100 maximum permissible concentration, e.g., as additives in the hardening of binding systems.

The aim of the work was to determine the possibility of using lead or barium sparingly soluble salts as additives when hardening cements having silicate, sulfate, or phosphate nature.

2 Methods

Physical and mechanical as well as physical and chemical methods were used during the research, physical and chemical methods including derivatographic, infrared spectroscopic, and X-ray phase analyses.

In order to study the effect of sparingly soluble substances on the strength of stone, samples in the form of cubes with an edge size of 10 mm were made from the neat cement paste having plastic consistency. They were tested for strength at the age of 1, 3, 7, 14, and 28 days. Sparingly soluble compositions were compounded with cement before mixing it with water, and the samples were solidified at 100% moisture: At certain times, hydration was stopped by means of acetone. The samples were investigated by X-ray phase, derivatographic, infrared spectroscopic, and chemical analysis methods.

3 Results and Discussion

Table 5 illustrates the most typical results of nature and concentration effect of the added substances on the strength of stone made from different cements. It follows from the table that the sparingly soluble salts of lead (II) decrease the strength of the stone at all times of hardening, reducing it to zero at the age of 1 day.

Physical and chemical studies of cement stone samples, solidified in the presence of sparingly soluble compounds having different nature, showed that the object of influence in the stone was alite. This fact was confirmed by derivatographic, infrared spectroscopic, and X-ray phase analyses. In the case of negative influence, alite hydration fell. This was the reason of property decrease.

Tables 6 and 7 present a derivatographic analysis of the systems which shows the effects on cement hydration.

The results showed that sparingly soluble lead compounds in silicate cements cannot be used as additives because they prevent hardening, while sparingly soluble barium compositions can be applied as additives.

This conclusion was confirmed by infrared spectroscopic studies. The research of sulfate and phosphate systems has shown that precipitations of sparingly soluble of lead and barium in these systems can be “hidden” without the strength decline.

In a similar way, precipitations of sparingly soluble substances of copper, nickel, and zinc were investigated.

Table 8 demonstrates the overall results, which is consistent with the proceedings [15–20].

The given material about the final property of a neutralized system to be a useful product shows that it is possible to achieve the full implementation of the criteria of green geocoprotective technology of neutralization, taking into account the peculiarities of the chemical behavior of systems in the formation of artificial stone. The mechanisms of these processes can be traced by means of papers [21–24].

Table 5 Cement system strength

Added compound— detoxication product	Solubility product	Amount, %, of cement mass
–	–	0
PbSO ₄	1.6×10^{-8}	2
PbCO ₃	1.0×10^{-13}	2
PbI ₂	1.1×10^{-9}	1
Ba ₃ (PO ₄) ₂	6.03×10^{-39}	2
Ba ₃ CrO ₄	1.2×10^{-10}	0.5
Ba ₃ SO ₄	1.1×10^{-10}	2

Table 6 Derivatographic analysis of binding systems having silicate nature with sparingly soluble precipitations of lead

Added compound	Amount, %, of cement mass	Age, days	Effects on derivatograms, °C, of stone made of paste				Water loss during effects, %					Ultimate compressive strength, %, relative to the check sample
			I	II	III	IV	I	II	III	IV	Σ	
500 grade of cement produced by the plant named after Vorovsky	–	1	120	145	500	775	6.52	3.48	1.30	2.17	13.9	100
	1	1	140	180	490	790	2.04	1.22	0.01	1.22	6.52	38
	2	1	130	190	–	790	1.52	1.74	–	1.74	5.6	9
500 grade of cement produced by the plant named after Vorovsky	3	1	115	160	–	750	2.83	3.04	–	2.83	8.70	9
	–	28	–	150	500	805	–	6.52	1.30	1.95	11.08	100
PbI ₂	1	28	–	150	490	620	–	6.30	1.74	2.17	12.17	76
						795				1.95		
						870				0.65		
PbSO ₄	2	28	120	160	–	690	1.52	1.02	–	4.8	7.2	30
						830				0.215		
						880				0.215		
PbCO ₃	3	28	–	150	510	800	–	6.1	0.87	1.74	10.9	17
						860				0.43		

Table 7 Derivatographic analysis of binding systems having silicate nature with sparingly soluble precipitations of barium

Added compound	Amount, %, of cement mass	Age, days	Effects on derivatograms, °C, of stone made of paste				Water loss during effects, %					Ultimate compressive strength, %, relative to the check sample
			I	II	III	IV	I	II	III	IV	Σ	
400 grade of Slantsy cement	–	1	140	–	500	790	4.34	–	0.43	3.91	10.86	100
BaSO ₄	3	1	150	–	500	795	5.65	–	0.65	4.34	11.74	105
Ba ₃ (PO ₄) ₂	3	1	165	315	510	800 815	4.0	1.25	0.75	1.50 0.75	11.0	118
BaCrO ₄	0.5	1	170	–	545	840	6.54	–	2.17	4.78	17.7	135
Barium waste of lithopone production	1	1	150	–	500	800	7.39	–	0.86	3.91	12.50	–
400 grade of Slantsy cement	–	28	170	–	510	810	7.82	–	0.43	4.78	15.21	100
BaSO ₄	3	28	140	–	490	785	5.65	–	0.43	4.78	13.94	104
BaF ₂	0.5	28	145	–	490	770 810	7.32	–	1.30	2.17 2.18	14.34	115

Table 8 Effect of precipitations containing heavy metal ions on the properties of binding systems^a

Precipitation, its nature	Effect on the properties of binding systems		
	Silicate	Phosphate	Sulfate
PbSO ₄ PbCO ₃ Pb ₃ (PO ₄) ₂	Negative	Neutral or positive	Positive
BaSO ₄	Positive	Neutral or positive	Positive
NiSiO ₃ NiCO ₃	Positive	Neutral or positive	Positive
CuCO ₃ Cu ₃ (PO ₄) ₂	Negative	Positive	Positive
ZnCO ₃ Zn ₃ (PO ₄) ₂	Negative	Positive	Positive

^aAddition in amount of up to 5% mass of cement

4 Conclusions

1. Five criteria of green technologies of neutralizing systems with the use of mineral geoantidotes are assigned. This allows geocoprotection technology to be a green technology.
2. It is shown that the products of detoxication of lead ions in the form of sparingly soluble salts can be used as additives when hardening only sulfate and phosphate systems; they cannot be applied as additives in silicate systems during their hardening.
3. A summary of the efficiency of the use of lead, barium, copper, nickel, and zinc sparingly soluble compounds in the hardening of binders having different nature are given. This allows to make the choice of a system for the implementation of green technology.

References

1. Svatovskaya LB, Kabanov AA, Sychoy MM (2017) The improvement of foam concrete geocoprotective properties in transport construction. IOP Conf Ser: Earth and Environ Sci 90:012010
2. Svatovskaya LB, Kabanov AA, Sychoy MM (2017) Lithosynthesis of the properties in the transport construction on the cement base. IOP Conf Ser: Earth Environ Sci 90:012009
3. Svatovskaya LB, Kabanov AA, Sychoy MM (2017) Soling, aerating and phosphating for soil strengthening and detoxication. Procedia Eng 189:398–403
4. Svatovskaya LB, Urov OV, Kabanov AA (2017) Geocoprotective technology of transport construction using silica sol absorption method. Procedia Eng 189:454–458
5. Svatovskaya LB, Shershneva MV, Baidarashvili MM, Yakimova NI, Khitrov AV (2004) Foam concrete construction demolished waste. In: Proceedings of the international conference on sustainable waste management and recycling: construction demolition waste, London, pp 199–203

6. Svatovskaya LB, Sakharova AS, Baidarashvilly MM, Petriaev AV (2015) Building wastes and cement clinker using in the geocoprotective technologies in transport construction. In: Proceedings of the 14th international conference of international association for computer methods and recent advances in geomechanics, IACMAG, Taylor and Francis—Balkema, Netherlands, pp 619–622
7. Sychova AM, Svatovskaya LB, Mjakin SV, Vasiljeva IV (2009) Modification of fillers for cements. In: Electron beam modification of solids: mechanisms, common features and promising applications, pp 35–37
8. Sychova AM, Svatovskaya LB, Mjakin SV, Vasiljeva IV (2009) Activation of aqueous phase at cement and concrete solidification. In: Electron beam modification of solids: mechanisms, common features and promising applications, pp 39–47
9. Maslennikova LL, Svatovskaya LB, Mjakin SV, Vasiljeva IV (2009) Activation of reactions at solid-solid interfaces. improvement of ceramics materials. In: Electron beam modification of solids: mechanisms, common features and promising applications, pp 57–61
10. Svatovskaya LB, Yakimova NI, Trunskaya OY, Rusanova EV, Krylova NB (2004) New complex ecotechnology for oil demolished waste. In: Proceedings of the international conference on sustainable waste management and recycling: construction demolition waste, London
11. Sychova AM, Solomahin A, Kotovich V, Svatovskaya LB, Kamenev Y (2018) Improving of the monolithic foam concrete quality for used in the high-rise construction. E3S Web Conf 33:02058
12. Gusev N, Svatovskaya LB, Kucherenko A (2018) Effect of changing of the parameters of the cable network of monitoring systems of high-rise buildings on the basis of string converters on their operability. E3S Web Conf 33:02069
13. Sychova A, Sychov M, Rusanova E (2017) A method of obtaining geonoiseprotective foam concrete for use on railway transport. *Procedia Eng* 189:681–687
14. Sychova A, Solomahin A, Hitrov A (2017) The increase of the durability and geoprotective properties of the railway subgrade. *Procedia Eng* 189:688–694
15. Yamamoto T, Yamoda T, Miyake A (2007) Tansparent conductive Ga-doped ZnO films properties on glass, PMMA and COP substrates. In: Proceedings of International Display Workshop, Japan, p 2044
16. Kityk V, Migalska A, Ebothe J, Elchichou A (2002) Anomalously large pockels effect in ZnO-F single crystalline films deposited on bare glass. *Cryst Res Technol* 37:340–352
17. Singha I, Bhatnagara PK, Mathura PC (2008) Optical and electrical characterization of conducting polymer-single walled carbon nanotube composite films. *Carbon* 46(8):1141–1144
18. Kimakis E (2002) Single walled carbon nanotube composites. *Synth Met* 127:59–62
19. Todda MG, Shi FG (2003) Characterizing the Interphase Dielectric Constant of Polymer Composite Materials: effect of chemical coupling agents. *Appl Phys* 94(7):4551–4557
20. Xiaoliang D, Xiaolin L, Yong Z (2009) Improved dielectric strength of barium titanate-polyvinylidene fluoride nanocomposites. *Appl Phys Lett* 95:95
21. Chao F, Liang G, Kong W (2008) Dielectric properties of polymer. Ceramic composites based on thermosetting polymers. *Polym Bull* 60:129–136
22. Todd MG, Shi FG (2002) Validation of a novel dielectric constant simulation model and the determination of its physical parameters. *Microelectron J* 33:627–632
23. Rao Y, Takahashi A, Wong CP (2003) Di-block copolymer surfactant study to optimize filler dispersion in high dielectric constant polymer-ceramic composite. *Compos A* 34:1113–1116
24. Qi L, Lee BI, Samuels WD (2006) Three-phase percolative silver-BaTiO₃—epoxy nanocomposites with high dielectric constants. *J Appl Polym Sci* 102:967–971

Modification of Mineral Substance Surfaces for Geosphere Protection



Larisa Svatovskaya , Maxim Sychov, Kseniia Mikhailova, Alexander Kabanov and Elena Bodenko

Abstract The paper concerns geosphere protection in a cold region which can be increased by means of raw material economy, pollution detoxication and antidusting lay creation on a mineral surface and soil strengthening. Silica sol was chosen as the main agent for modification. Concrete, sand, slag, limestone, ash, perlite and other mineral articles were used as mineral surfaces. Such methods as physical, chemical and instrumental ones were applied during the study. The chosen substances were penetrated with silica sol agent as well as the second agent and after certain operations modified surfaces having improved technical and geocoprotective properties were produced. Besides, obtained compositions had higher mechanical and absorbtion properties. A composition with modified mineral surface can be applied in transport geocostruction for waste detoxication, e.g. heavy metal ion detoxication, for antidusting lay and geocoprotective screen creation. The prospects of modification use are considered in this paper.

Keywords Geotechnology · Geosphere protection · Detoxication · Mineral surface

1 Introduction

The paper concerns problems of geosphere protection from pollutions. One of the possible solutions of this problem may be the involvement of pollutions in a useful chemical process, such as hardening in artificial stone [1–5]. During this process, a neutralization of pollutions with the preservation of products in the body of a stone takes place. Another solution of the problem is either to block pollutions in a mineral building structure, construction or article by creating a preserving, protective layer on a surface or to absorb a pollutant. Thus, the main idea of modifying technologies is to create a geocoprotective building system, including its entire volume, or only to form mineral layers on a surface of articles and structures or any other mineral system, e.g. on concrete surface, on soil one. The mineral layer is a kind of preserving,

L. Svatovskaya (✉) · M. Sychov · K. Mikhailova · A. Kabanov · E. Bodenko
St. Petersburg State Transport University, 9 Moskovsky pr, St. Petersburg 190031, Russia
e-mail: lbsvatovskaya@yandex.ru

© Springer Nature Singapore Pte Ltd. 2020
A. Petriaev and A. Konon (eds.), *Transportation Soil Engineering in Cold Regions*,
Volume 2, Lecture Notes in Civil Engineering 50,
https://doi.org/10.1007/978-981-15-0454-9_46

protective screen that ensures useful properties for construction, namely: the increase of hardness, water resistance and geocoprotective functions [6–11]. The creation of such a mineral surface is achieved by single or repeated impregnation or, if it is a volumetric preservation, by hardening with a mineral binder or a solution having the functions of both a hardener and a mineral geantidot. An example of volume geocoprotection creation can be a method of phosphate and alkaline hardening, e.g. when heavy metal ions bind to sparingly soluble hydrophosphate or hydroalumosilicates. As a result, hardening takes place due to the formation of hydrates while geocoprotection occurs due to binding of heavy metal ions.

We introduce modifying technologies for geocoprotection by creating coatings (see Table 1).

It was previously mentioned that the main positive impact on a building geosystem is the creation of a surface with single- or multilayer coatings: silica, and (or) calcium hydrosilicate, or calcium silicoaluminate ones. These kinds of coatings—single- or multilayer—can perform the following functions: the increase of structure durability during operation; the conservation of absorbed pollutants in an article, construction

Table 1 Mineral building geosystems for the creation of modified surface layers

Mineral building geosystem with modified surface multilayers (<i>n</i> -layers)	Type of building geosystem	Aim of surface multilayer coating	Method of layer creation	Examples
Sulphate (gypsum) geosystem with silica or hydrosilicate layers from complex solutions	Article, construction, structure	Protection against pollutions absorbed from a geosystem Prevention from aggressive environment Strengthening	Impregnation, e.g. with silica sol solution ($\text{SiO}_2 \cdot n\text{H}_2\text{O}$)	Sulphate articles Concrete articles for roads impregnated with silica Screens for site foam concrete in order to protect the lithosphere from pollutions absorbed by foam concrete, e.g. oil products
Hydrosilicate, hydroaluminate, hydrosulphoaluminate geosystem			Immersion in silica solution	
Soils, embankments and other artificial structures made of silica, calcium silicate waste, calcium hydrosilicate, blast-furnace and other slags	Subgrade	Geosystem strengthening and pollution preservation in it	Soils, embankments and other artificial structures made of silica, calcium silicate waste, calcium hydrosilicate, blast-furnace and other slags	Subgrade

or structure; the protection, e.g. of ash mass from dusting. Impregnating layers in the examples of Table 1 consist of silica sol, which can be applied in several impregnations or mixed with solutions of Ca(II) or Mg(II) containing compounds in the form of salt solutions in order to form hydrosilicates. An example of retaining coatings for the durability of structures can be pavements. An example of protection against dust is sol-silicate coatings for dusting ash dumps.

It should be noted that geocoprotective coatings are kinds of layers having mineral nature. Their physical and mechanical properties should be controlled. Table 2 shows an example of changes in two properties of concrete when absorbing 3% silica sol solution.

Table 3 summarizes data obtained by using research of electron microscopical image (EMI) and a method of electron probe microanalysis (EPM).

The authors propose technological solutions of geocoprotection in the form of coatings for mineral geosystems which are single- or multilayer impregnation of articles, constructions or structures using solutions, such as silica sol.

So, modified surface layers are new way for geocoprotection from pollution, but such layers can be used to save natural resources. In addition to the papers [12–15], let us consider the synthesis of hydration active phases in a geosystem as carriers of strength and at the same time as mineral geoantidots at the level of sparingly soluble silicates, aluminates and phosphates. The idea is based on the reaction of binder formation in the form of calcium and magnesium hydroaluminates. But, since there are industrial sols—silica sols and alumina sols—they can be industrially applied as thermodynamically permitted process:

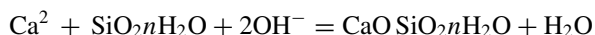


Table 2 Changes of concrete properties when impregnating

Concrete (strength grade)	Changes of properties (when impregnating) concerning test specimens (without impregnation), $\pm\Delta$ %	
	Water absorption	Hardness
B20–B30	–45 to –50	+30 to +40

Table 3 Layer characteristics

Binding article	Impregnation depth by the method of EPM, mm	Maximum depth, on which there was a new phase, mm	Morphological type of new growths	Share of the area occupied by micro pores and micro cracks prior to the formation of a layer, %
Portland cement, concrete B20	3.5	5	CSH (low-basic hydrosilicates)	Not more than 30

Table 4 Gibbs free energy change during the synthesis of hydrosilicates from solutions

Reactions	Gibbs free energy, ΔG°_{298} , kg/mol
$2\text{CaO}(\text{OH}_2) + \text{SiO}_2\text{H}_2\text{O} = 2\text{CaO} \cdot \text{SiO}_2 \cdot 1.17\text{H}_2\text{O} + 1.83\text{H}_2\text{O}$	-95.32
$\text{Ca}(\text{OH}_2) + 2(\text{SiO}_2\text{H}_2\text{O}) = \text{CaO} \cdot 2\text{SiO}_2 \cdot 2\text{H}_2\text{O} + \text{H}_2\text{O}$	-169.19
$2\text{CaO} \text{ SiO}_2 \cdot 1.17\text{H}_2\text{O} + 2(\text{SiO}_2 \cdot \text{H}_2\text{O}) = 2\text{CaO} \cdot 3\text{SiO}_2 \cdot 2.5\text{H}_2\text{O} + 0.67\text{H}_2\text{O}$	-180.56
$\text{Ca}^2 + 3(2\text{SiO}_2 \cdot 3\text{H}_2\text{O}) + 12\text{OH}^- = 6\text{CaO} \cdot 5\text{SiO}_2 \cdot \text{H}_2\text{O} + 14\text{H}_2\text{O}$	287.89

Table 4 shows the variants of ΔG°_{298} reactions depending on the degree of sol and calcium reagent condensation when obtaining hydrosilicates without the use of cement in order to save natural raw materials.

The fact of the matter is that in some construction technologies, the synthesis of hydrosilicates which are carriers of binding properties and strength can be used. That is why one should pay attention to the circumstances related to the protection of geoecosystems: first, it is the methods of technological operations; secondly, the control of geosystem properties. Geosystems require compliance with admissibility conditions: the use of substances of mineral compositions close to natural, spontaneity, the formation of sparingly soluble substances and the usefulness of a product. These conditions are met if hydrosilicates or hydroaluminates are used. Analyzing Table 4, one can assume that the admissibility conditions of substance use are fulfilled for the lithosphere. Another property is the technology of operations which requires the knowledge of soil filtration characteristics, the methods and the sequence of solutions' introduction and their concentration as well as additives, their mixing and the complex of their property control. To obtain binders from solutions is harmless to the environment. Two properties can be considered for control—technical and geocoprotective ones. For technical properties, one can use known techniques from the field of building material science; for geocoprotective purposes, the choice of additives may be oriented to obtain sparingly soluble substances.

The third direction of modification is to use the impregnation of concrete two or more times in order to “work” with the surface of its pore and capillary volume. In so doing, the first impregnating solutions can be contaminated with heavy metal ions which are neutralized in the body of a stone. The second impregnation is carried out with a solution of silica.

The aim of the work was to try to create of surface layers on mineral bases having different nature as well as to meet the requirement of double-layer impregnation during the hardening of concrete.

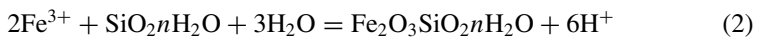
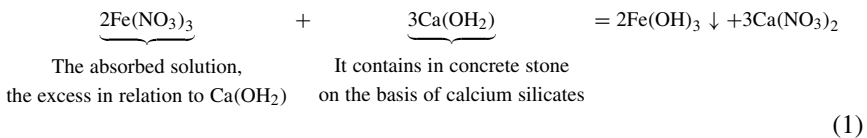
2 Methods

In the experiments specimens of B15-30 class concrete, dispersion of calcium carbonate, ash, perlite, expanded clay and basic blast-furnace slag were used. The specimens were tested by physico-chemical and physico-mechanical methods. Concrete specimens were saturated with Fe(NO₃)₃ solution and then with 3% silica. In 28 days, strength was investigated. The surface of different nature dispersions was saturated with a solution of calcium or magnesium salt, and then with a concentrated silica solution. After that the results were analysed. Finally impregnated systems were tested as aggregates to answer the question: how to use these systems after the end of their life cycle.

3 Results and Discussion

Studies have shown that for B15 class concrete articles, the thickness of the forming layer corresponds to an approximate value which is up to 5 mm when impregnated, first, with Fe(NO₃)₃ solution, and then with 3% silica sol concentrate. The strength of the articles increases by more than 20% compared with the strength of the articles impregnated only with silica. Water absorption is reduced by more than 50% and, thus, frost resistance and water resistance increase. Improving the quality of concrete due to the modified layer and extending its life cycle helps to reduce the level of waste by increasing durability which is important from the standpoint of environmental protection.

The mechanism of action is based on reactions 1, 2 and 3.

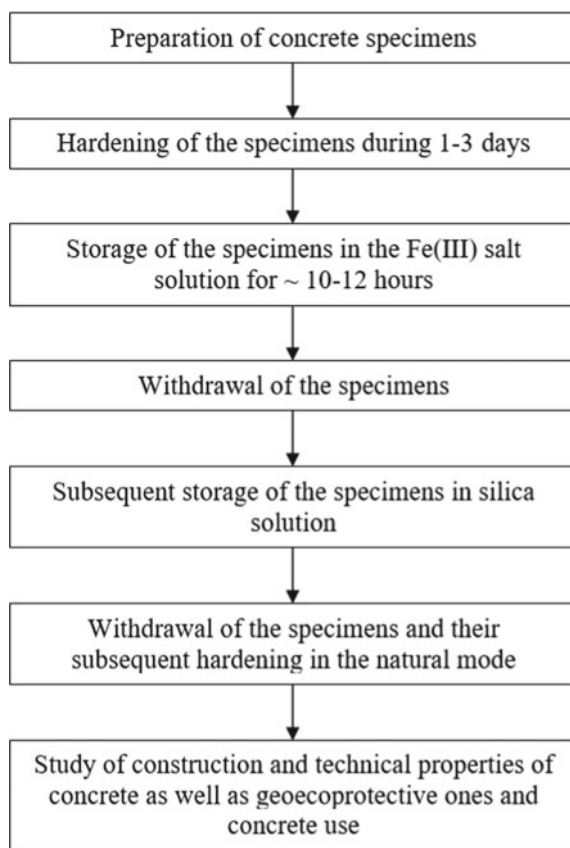


Subsequently, the neutralization of H⁺ ions in pores of concrete, takes place, where pH > 7 (3):



Processes 1, 2 and 3 can enable to heal concrete pores with the formation of a sort of its own waterproofing coating. Thus, this contributes to the increase of construction and technical properties, such as reducing water absorption, increasing frost resistance and water resistance. In accordance with the theoretical assumptions and taking into account the proceedings [16–24], a method was developed (see Fig. 1).

Fig. 1 Method of the absorption of a complex with silica solution by concrete



The method corresponds to the positions of technosphere safety because it helps to prevent the penetration of ions into the environment, on the one hand, and to increase the durability of articles, on the other hand.

Table 5 shows a qualitative result concerning the impregnation of different nature dispersions with concentrated solutions of sols or complexes. It illustrates that there is an effect of creating a screen that is strengthened when using complexes.

Prospects for the development of surface modification in geocoprotection:

1. The production of modified dispersions of mineral geoantidots by method of soling. In this case, it is proposed to use mineral raw materials of natural or technical origin as a basis for soling. The idea is that the surface modified by silica or alumina sol or their solutions can serve as an absorber for pollution. In so doing, the modification can take place by cation or anion. The anion can be double one, $\text{SiO}_2 \cdot \text{H}_2\text{O} + \text{Al}_2\text{O}_3 \cdot n\text{H}_2\text{O}$, $\text{SiO}_2 \cdot n\text{H}_2\text{O} + \text{P}_2\text{O}_5 \cdot n\text{H}_2\text{O}$, or triple one $\text{SiO}_2 \cdot \text{H}_2\text{O} + \text{Al}_2\text{O}_3 \cdot n\text{H}_2\text{O} + \text{P}_2\text{O}_5 \cdot n\text{H}_2\text{O}$. It is possible to carry out modification by cation, for example, using Ca(II) or Mg(II) ions. The technological operation in such cases includes either sequential surface treatment with different solutions

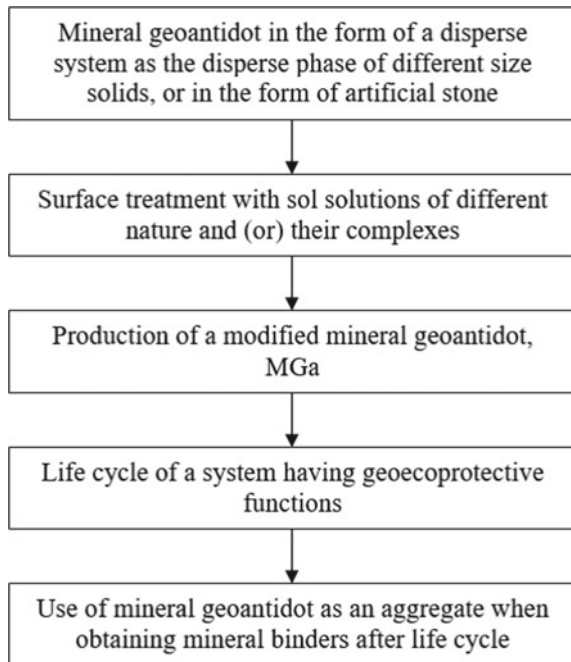
Table 5 Qualitative testing of concentrated sol or complexes to strengthen surface by modification

Mineral substances, dispersions	Strengthening effect—the creation of surface screen—after single- or multilayer impregnation		Article, structure and construction use after their life cycle
	By sol	By complexes	
Slag	+	++	As aggregates in the design of building systems
Limestone	+	++	
Perlite	+	++	
Bloating clay aggregate	+	++	
Ash	+	++	

or obtaining modified sols in advance, and then mineral dispersions are processed by them.

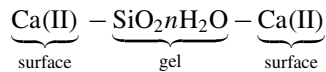
In this case, absorption capacity of the modified layer is important because it cleans the lithosphere: it absorbs a pollutant and neutralizes it. Absorption time and capacity of such modified mineral disperse systems depend on the level of environmental aggression, and after the life cycle of geocoprotective action, the products can be used as aggregates when produced mineral systems. This technique is called “mineral geoantidot modification” (see Fig. 2).

Fig. 2 Mineral geoantidot scheme



Obtained mineral geantidot meets admissibility conditions for applying a mineral geantidot in a geosystem as it has the composition which is like natural one. It means that the processes of mineral geantidot action are spontaneous and Gibbs energy of a system decreases, $\Delta G^{\circ}_{298} < 0$. This forms products similar to natural ones and, as a result, a useful product is obtained.

2. Mineral material obtaining for construction through the modification of building articles, constructions and structures by the method of soling. The idea is to increase durability and, ultimately, to reduce the consumption of natural raw materials due to surface modification of articles and imparting them improved physical and mechanical properties, and, thus, to preserve a productive natural environment. It is important for the life of the present and future people generations. Modification can be carried out with the help of both silica and its complex compositions.
3. The method of soling can be applied to produce articles on the base of Ca(II) or Mg(II) compounds in the form of dispersions of mineral man-made raw materials. In this case, it is possible to synthesize hydrosilicates along phase interfaces and the appearance of strength, i.e. cross-linking of dispersions occurs according to the scheme:



with the formation of calcium hydrosilicates. This strengthens the contact. Such a direction is also related with the economy of natural resources on the basis of geochemical reactions.

4. One more direction is the use of sol dispersions of solid mineral bodies as aggregates and fillers in order to improve physical and mechanical properties and, accordingly, operational ones resulting in the increase of durability and, thus, the reduction of the cost of natural raw materials. In this case, we are talking about increasing and improving the deformation properties of materials.
5. The study of mineral geantidots in the form of pastes having slag-lime nature. The advantages of such substances can be considered the fact that there is unlimited raw material base of clay-containing raw materials having different nature.
6. The study of the processes of lithosynthesis when neutralizing pollutants in artificial solid materials based on aluminates, sulphaluminates and other special binders.
7. A special area of engineering knowledge is geocoprotection calculation of structures that ensures geochemical reactions. This may be structures of transport, civil and special construction.
8. The development of modification creates a base of green geocoprotective technologies that can be evaluated, e.g. by the rating method taking into account weighting coefficient. In this case, the level of internal energy change in the geocoprotective process, absorption ability of mineral geantidots, the accessibility and scale of man-made raw material base, the use of mineral geantidots

in the process of geocoprotection as a useful product in the process and after the life cycle can be used as the main geocological properties.

9. The development of modification can contribute to the creation of special new building structures and constructions having geocoprotective properties: shields, barriers, coatings, fills and other “safety facilities” performing preventive and restoration role.

4 Conclusions

1. The process step of modifying mineral surface of a material, article and structure is suggested with the aim of improving their construction and geocoprotective properties. An example is shown with the use of sol solution or sol complex for a single impregnation, and a combination of impregnation with electrolyte and sol solution during two-time impregnation.
2. Complex modifiers based on sols are proposed to increase the level of construction and geocoprotective properties.
3. Prospects for the use of surface modification in geocoprotection are traced.

References

1. Svatovskaya LB, Kabanov AA, Sychov MM (2017) The improvement of foam concrete geocoprotective properties in transport construction. IOP Conf Ser: Earth Environ Sci 90:012010
2. Svatovskaya LB, Kabanov AA, Sychov MM (2017) Lithosynthesis of the properties in the transport construction on the cement base. IOP Conf Ser: Earth Environ Sci 90:012009
3. Svatovskaya LB, Kabanov AA, Sychov MM (2017) Soling, aerating and phosphating for soil strengthening and detoxication. Procedia Eng 189:398–403
4. Svatovskaya LB, Urov OV, Kabanov AA (2017) Geocoprotective technology of transport construction using silica sol absorption method. Procedia Eng 189:454–458
5. Svatovskaya LB, Shershneva MV, Baidarashvili MM, Yakimova NI, Khitrov AV (2004) Foam concrete construction demolished waste. In: Proceedings of the international conference on sustainable waste management and recycling: construction demolition waste, London, pp 199–203
6. Svatovskaya LB, Sakharova AS, Baidarashvili MM, Petriaev AV (2015) Building wastes and cement clinker using in the geocoprotective technologies in transport construction. In: Proceedings of the 14th international conference of international association for computer methods and recent advances in geomechanics, IACMAG, Taylor and Francis—Balkema, Netherlands, pp 619–622
7. Sychova AM, Svatovskaya LB, Mjakin SV, Vasiljeva IV (2009) Modification of fillers for cements. In: Electron beam modification of solids: mechanisms, common features and promising applications, pp 35–37
8. Sychova AM, Svatovskaya LB, Mjakin SV, Vasiljeva IV (2009) Activation of aqueous phase at cement and concrete solidification. In: Electron beam modification of solids: mechanisms, common features and promising applications, pp 39–47

9. Maslennikova, L.L., Svatovskaya, L.B., Mjakin, S.V., Vasiljeva, I.V.: Activation of reactions at solid-solid interfaces. improvement of ceramics materials. In: Electron beam modification of solids: mechanisms, common features and promising applications, pp 57–61
10. Svatovskaya LB, Yakimova NI, Trunskaya OY, Rusanova EV, Krylova NB (2004) New complex ecotechnology for oil demolished waste. In: Proceedings of the international conference on sustainable waste management and recycling: construction demolition waste, London
11. Sychova AM, Solomahin A, Kotovich V, Svatovskaya LB, Kamenev Y (2018) Improving of the monolithic foam concrete quality for used in the high-rise construction. E3S Web Conf 33:02058
12. Gusev N, Svatovskaya LB, Kucherenko A (2018) Effect of changing of the parametrs of the cable network of monitoring systems of high-rise buildings on the basis of string converters on their operability. E3S Web Conf 33:02069
13. Sychova A, Sychov M, Rusanova E (2017) A method of obtaining geonoiseprotective foam concrete for use on railway transport. Procedia Eng 189:681–687
14. Sychova A, Solomahin A, Hitrov A (2017) The increase of the durability and geoprotective properties of the railway subgrade. Procedia Eng 189:688–694
15. Yamamoto T, Yamoda T, Miyake A (2007) Tansparent conductive Ga-doped ZnO films properties on glass, PMMA and COP Substrates. In: Proceedings of international display workshop, Japan, p 2044
16. Kityk V, Migalska A, Ebothe J, Elchichou A (2002) Anomalously large pockels effect in ZnO-F single crystalline films deposited on bare glass. Cryst Res Technol 37:340–352
17. Singha I, Bhatnagara PK, Mathura PC (2008) Optical and electrical characterization of conducting polymer-single walled carbon nanotube composite films. Carbon 46(8):1141–1144
18. Kimakis E (2002) Single walled carbon nanotube composites. Synth Met 127:59–62
19. Todda MG, Shi FG (2003) Characterizing the interphase dielectric constant of polymer composite materials: effect of chemical coupling agents. Appl Phys 94(7):4551–4557
20. Xiaoliang D, Xiaolin L, Yong Z (2009) Improved dielectric strength of barium titanate-polyvinylidene fluoride nanocomposites. Appl Phys Lett 95:95
21. Chao F, Liang G, Kong W (2008) Dielectric properties of polymer. Ceramic composites based on thermosetting polymers. Polym Bull 60:129–136
22. Todd MG, Shi FG (2002) Validation of a novel dielectric constant simulation model and the determination of its physical parameters. Microelectron J 33:627–632
23. Rao Y, Takahashi A, Wong CP (2003) Di-block copolymer surfactant study to optimize filler dispersion in high dielectric constant polymer-ceramic composite. Compos A 34:1113–1116
24. Qi L, Lee BI, Samuels WD (2006) Three-phase percolative silver-BaTiO₃—epoxy nanocomposites with high dielectric constants. J Appl Polym Sci 102:967–971

A Structure of Atoms of the Main Phase of Industrial Wastes Predict Properties of Building Materials in Transport Construction in Cold Regions



Natalia Babak

Abstract The main object of our research is the transport construction in cold regions. It based on many natural resources for making building materials, which must be adapted to low temperature. We pay the main attention to usage of industrial mineral wastes. Comprehensive analysis of waste including the structure of atoms of the main phase allows predicts properties of building materials. Using industrial mineral wastes instead of mineral raw, one can affect various structural properties of materials. 3d-metals in technogenic raw materials increase the strength characteristics. And s-elements increase the heat efficiency which is crucial in cold regions. We carried out a comparison of various wall materials with waste. S-elements improve heat technical characteristics of bricks.

Keywords Industrial mineral wastes · Geoecological reserve · Reduce thermal losses

1 Introduction

An impact of construction activities on the environment occurs at all its stages. Any civil or industrial engineering begins with structural materials. Production of structural materials is a chain of transformations performed under rock and structural materials as elements of the inorganic world. Transport construction has high capital costs because of structural materials (make more than 55%). Considering this fact apparently, it is possible to claim that application of the industrial mineral wastes is one of the paths of increase production potency of building materials [1–15]. See also [1–8] for usage of industrial wastes in the production of ceramics and [9–15] for the production of concrete.

N. Babak (✉)

Emperor Alexander I St. Petersburg State Transport University (PGUPS), Moskovsky Pr. 9, St. Petersburg 190031, Russia
e-mail: babak.ru@inbox.ru

© Springer Nature Singapore Pte Ltd. 2020

A. Petriaev and A. Konon (eds.), *Transportation Soil Engineering in Cold Regions*, Volume 2, Lecture Notes in Civil Engineering 50, https://doi.org/10.1007/978-981-15-0454-9_47

The amount of energy required to heat transport facilities throughout a cold winter can be staggering. Thermal conductivity is considered to be the main component of thermal losses through walls. Improvement of thermal insulation of walls in the majority of structural technologies happens due to a decrease in their thermal conductivity [16]. Thermal conductivity for a solid phase is entirely defined by porosity and the structure of a solid body. According to the phonon theory, thermal conductivity of solid solutions is much less when its crystal lattice is strongly chaotic. It can be used in the synthesis of new heat effective building materials on the basis of the industrial mineral wastes.

2 Methods and Objects of Research

We introduce a notion of a geoecological reserve of the raw materials used for production of construction materials. The geoecological reserve contains many aspects including efficient use of waste instead of mineral resources.

It is known that the combination of chemical elements and their spatial distribution in earth's crust is in the causal dependence on the properties caused by atomic and ion structures. The analysis of the geochemical table of Zavaritsky and Vernadsky with Fersman says that many chemical compositions of industrial wastes are similar to the natural minerals applied in the production of building materials [17].

Sedimentary rock is the main raw material of the industry; it contains about 70% of clays, about 20% of sands and sandstones, and 5% of carbonates. The main oxides of the building materials industry are SiO_2 , Al_2O_3 , Fe_2O_3 , CaO , MgO , and R_2O . Analyzing the natural minerals composition used for producing building materials and the industrial wastes composition, it can be seen that they are similar.

Building ceramics are composite materials, in which the contact phase is formed during firing to 1000 °C. The phase of industrial waste and the phase of clay containing matrix are involved in the process. The contact formed with the donor–acceptor mechanism. The feature of this interaction depends on the electronic structure of an element of the main phase of waste [18–23]. Substances with donor–acceptor bonds are widespread. The majority of bonds fall into complex compounds.

It is known that the strength of the donor–acceptor bond grow from s- to d-valence electrons, and we see this depends for the cation of the main phase of waste. There is the geoecological reserve of the industrial waste (Table 1).

Possible electron power conditions in the atom are defined by the size of the principal quantum number n . The principal quantum number n defines some energy band where the exact electron energy value is defined by the size l , an azimuthally quantum number. It is known that a radial distribution of electronic density for each atomic orbital consists of several maxima and is described by the difference of the principal and azimuthally quantum numbers ($n - l$) [24]. The exception is made by atomic orbitals 1s, 2p, 3d, and 4f; for each of them, the radial distribution of electronic density consists only the single maximum. This circumstance can have a

Table 1 Fundamental power parameters of the cation electronic structure

Cation power parameters				Orbital energy	
The valence atomic orbital	The principal quantum number n	The azimuthally quantum number l	The number of electronic density maxima on radial distribution curve ($n - l$)		
1s	1	0	1	↓	
2s	2	0	2		
2p	2	1	1		
3s	3	0	3		
3p	3	1	2		
3d	3	2	1		
4s	4	0	4		
Power reserve					↓
$n - l = 1$	$n - l = 2$	$n - l = 3$	$n - l = 4$		
1s (H)	2s (Li)	3s (Na, Mg)	4s (Ca)		
2p (B, C, N, O)	3p (Al, Si)	4p (Se)			
3d (Cr, Mn, Fe, Co, Ni, Cu, Zn)	4d (Mo)				
Communication hardening, neutralization of ions of heavy metals				← →	
Economy of energy during the preparation of ceramics, decrease of pollutions					
Fuel economy, decrease of pollutions					

great influence on ability to form donor–acceptor bonds in atoms which have 2p- or 3d-valence electrons.

The analysis of literature data shows that energy of bonds in complexes changes depending on an electronic configuration of atom. A metal–water bond in the studied model complexes changes from purely electrostatic (To, Sa₂) to donor–acceptor with significant transfer of electronic density on a metal ion orbital (Cu₂, Zn₂). Values of energy of the covalent binding for various complexes are given in Table 2.

We offer the relative reserve energy coefficient of elements based on power characteristics of an electronic level of the substance.

The relative reserve energy coefficient KRE (relate to sodium) for cation elements of the most wastes in the crust can become the power characteristic allowing to predict properties of building materials made with the use of these wastes. For example, low KRE (the Ca s-element has KRE = 1.19) says about weak contact of this cation with a clay matrix. In other words, it gives a decrease of a thermal conductivity of this material. On the contrary, high KRE says about higher strength characteristics of building ceramics (Table 2).

We can describe a formation of a contact zone «waste – matrix» in terms of zone theory. This theory gives us an estimation of the donor–acceptor activity of surfaces of solid waste [23].

Table 2 Power characteristics of various complexes fragments

Metal ion	Configuration	Ionic radius (nm)	The number of electronic density highs on radial distribution curve ($n - l$)	Molar ionization energy (kJ/mol)	The relative reserve energy coefficient KRE
Na ⁺	3s ⁰	0.098	3	495.8	0
Al ³⁺	3p ⁰	0.057	2	577.6	1.16
Ca ²⁺	4s ⁰ d ⁰	0.104	4	589.8	1.19
Cr ²⁺	3d ⁴	0.083	1	652.7	1.32
Mn ²⁺	3d ⁵	0.091	1	717.4	1.45
Fe ²⁺	3d ⁶	0.080	1	761.6	1.54
Co ²⁺	3d ⁷	0.078	1	759	1.53
Ni ²⁺	3d ⁸	0.074	1	736.7	1.48
Cu ²⁺	3d ⁹	0.080	1	745.4	1.50
Zn ²⁺	3d ¹⁰	0.083	1	906.4	1.83

Therefore, it is possible to assume that if technogenic raw materials contain phases with the value of width of the inhibited zone ΔE less than 3.5 eV, then the donor–acceptor activity of a surface on phase boundaries increases when roasting. That leads to the formation of ecologically steady connections which are not washing away from a matrix.

The more phases with ΔE less than 3.5 eV are contained in the waste, the higher probability of formation a contact zone by donor–acceptor interactions of boundary phases. The highest number of such phases (up to 60%) is in d-wastes; therefore, the probability of formation of a contact zone of a matrix with such wastes is highest.

3 Results and Discussion

We carried out a comparison of various wall materials. Results of calculation are presented in Table 3.

The ceramic brick with waste from foam concrete has restrictions on water absorption and can be used only with a good waterproofing. But the usage of the brick with metallurgical slag, and, in particular, in combination with a waste of copper-smelting production, allows to create a highly effective brick.

Table 3 Thickness of the protecting wall from various wall materials

Wall materials	Density (kg/m ³)	Thermal conductivity λ (W/m °C)		Thickness δ (m)
		In a dry state	Under operating conditions	
Corpulent ceramic brick	1800	0.56	0.81	2.44
Ceramic brick with hollows	1250	0.28	0.47	1.43
Blocks from cellular concrete	600–800	0.14–0.21	0.26–0.37	0.8–1.13
Wood	500	0.09	0.18	0.55
Ceramic stone with hollows (a waste—foam concrete, KRE = 1.19)	900	0.15	0.2	0.61
Corpulent ceramic brick (a waste—foam concrete and granulose domain slag, KRE = 1.19)	1500	0.24	0.4	1.22
Corpulent ceramic brick (waste of granulose domain slag and copper slag KRE = 1.19–1.54)	1800	0.29	0.42	1.28

3.1 Calculation of Heat Losses for a Wall from Various Materials

A good warming of houses is important not only from the financial point of view for the consumer. A decrease of consumption of the incinerated fuel sharply reduces quantity of pollutions that significantly improves an ecological situation.

Let us consider a formula of calculation of heat losses $Q(W)$, through enclosing structures (e.g., walls, a floor, a ceiling, and a window):

$$Q = kS\Delta t \tag{1}$$

where S is the area of an enclosing structure (for example walls) in m²; Δt is a temperature difference of internal and outdoor air, °C; k is a heat transfer coefficient of an enclosing structure (W/m² °C).

Analyzing a formula (1), we see that it is possible to reduce thermal losses through a certain wall in two ways: reducing temperature difference (having lower air temperature indoors) or decreasing a heat transfer coefficient of a wall.

Increasing the wall thickness or choosing material for a layer with smaller value of a thermal conductivity λ , we reduce k , and, therefore, heat losses.

Example 1 The external wall 4 m long 3 m high consists of bricklaying 50 cm thick, two red corpuent bricks with cement and sand solution. The layer of internal cement plaster is 1 cm thick can be neglected. Thermal conductivity of such laying $\lambda = 0.8 \text{ W/(m } ^\circ\text{C)}$, heat transfer coefficient of such wall $k = 1/(1/8.7 \cdot 0.5/0.8 \cdot 1/23) = 1.3 \text{ W/(m}^2 \text{ } ^\circ\text{C)}$.

Heat losses through a wall at temperature difference $40 \text{ } ^\circ\text{C}$ (-20 on the street 20 in room): $Q = 1.3 \cdot (3 \cdot 4) \cdot 40 = 624 \text{ W}$.

If one constructs such a wall from the brick made with a waste of foam concrete and granulose domain slag (KRE = 1.19) instead of a sand 75 cm thick, heat conductivity in a laying $\lambda = 0.4 \text{ W/(m } ^\circ\text{C)}$, and then a heat transfer coefficient of such wall: $k = 1/(1/8.7 \cdot 0.75/0.4 \cdot 1/23) = 0.5 \text{ W/(m}^2 \text{ } ^\circ\text{C)}$.

So that heat losses through such wall $Q = 0.5 \cdot (3 \cdot 4) \cdot 40 = 240 \text{ W}$.

Difference in heat losses of walls from a traditional brick and a brick made with the use of wastes $\Delta Q = 624 - 240 = 384 \text{ W}$.

As we see, using bricks with wastes (KRE = 1.19) instead of sand, it is possible to reduce heat losses by 2–2.5 times. And, it will reduce emissions of a carbon dioxide and, as a result, will reduce the greenhouse effect.

Example 2 If one constructs such a wall from the brick made with the copper slag (KRE = 1.54) instead of a sand, heat conductivity in a laying $\lambda = 0.47 \text{ W/(m } ^\circ\text{C)}$, and then a heat transfer coefficient of such wall $k = 1/(1/8.7 \cdot 0.5/0.47 \cdot 1/23) = 0.82 \text{ W/(m}^2 \text{ } ^\circ\text{C)}$.

Therefore, heat losses through such wall $Q = 0.82 \cdot (3 \cdot 4) \cdot 40 = 393.6 \text{ W}$.

Difference in heat losses of walls from the traditional brick and brick made with wastes $\Delta Q = 624 - 394 = 240 \text{ W}$.

As we see, it reduces heat losses by 3.5 times.

These examples show the advantage of using industrial wastes for building materials in cold regions.

4 Conclusions

The ceramic industry uses some waste materials because it is similar to the natural raw materials in structure and chemical properties. The choice of industrial wastes instead of natural ones can provide some possibilities to extend the using building ceramics. 3d-metals in waste increase the strength characteristics of building materials; s-elements improve heat technical characteristics of bricks, which is important in cold regions. This forecast can be made proceeding from the fundamental knowledge about the structure of substance.

References

1. Dvorkin LI (2007) Structural materials from an industry. Phoenix, Rostov-on-Don
2. Arbuzova TB et al (1993) Building materials from industrial wastes. Samara
3. Rodrigue J-P (2017) The environmental impacts of transportation. Routledge, New York
4. Chen Z, Li H, Wong C (2005) Environmental Planning: analytic network process model for environmentally conscious construction planning. *J Constr Eng Manag* 131(1):92–101
5. Cole RJ (2000) Assessing construction practices. *Constr Manag Econ* 18(8):949–957
6. Ametepey SO, Kwame S (2015) The Case of Ghana. *J Environ Sci* 5(3):18–26
7. Babak NA, Maslennikova LL, Slavina AM (2010) Geo-environmental solutions to create effective construction ceramics on the base of technogenic silicate materials. *News PSTU* 2:220–230
8. Maslennikova LL, Babak NA, Abu-Khasan MS (2017) The use of oil-contaminated crushed stone screenings in construction ceramics. *Procedia Eng* 189:867–873
9. Svatovskaya LB, Kabanov AA, Sychoy MM (2017) The improvement of foam concrete geocoprotective properties in transport construction. *IOP Conf. Ser.: Earth Environ. Sci.* 90 012010
10. Svatovskaya LB, Kabanov AA, Sychoy MM (2017) Lithosynthesis of the properties in the transport construction on the cement base. *IOP Conf Ser Earth Environ Sci* 90:012009
11. Svatovskaya LB, Urov OV, Kabanov AA (2017) Geocoprotective technology of transport construction using silica sol absorption method. *Procedia Eng* 189:454–458
12. Svatovskaya LB, Shershneva MV, Baidarashvili MM, Yakimova NI, Khitrov AV (2004) Foam concrete construction demolished waste. In: *Proceedings of the international conference on sustainable waste management and recycling: construction demolition waste*, London, pp 199–203
13. Svatovskaya LB, Sakharova AS, Baidarashvili MM, Petriaev AV (2014) Building wastes and cement clinker using in the geocoprotective technologies in transport construction. In: *Proceedings of the 14th international conference of international association for computer methods and recent advances in geomechanics, IACMAG, Kyoto*, pp 619–622
14. Sychova AM, Svatovskaya LB, Mjakin SV, Vasiljeva IV (2009) Modification of fillers for cements. In: *Electron beam modification of solids: mechanisms, common features and promising applications*, pp 35–37
15. Sychova AM, Svatovskaya LB, Mjakin SV, Vasiljeva IV (2009) Activation of aqueous phase at cement and concrete solidification. In: *Electron beam modification of solids: mechanisms, common features and promising applications*, pp 39–47
16. Babak NA, Maslennikova LL, Slavina AM (2011) Geocological reserve of technologies, materials and structures in construction using industrial mineral waste. SPB: PSTU
17. Saukov AA (1950) *Geochemistry M*
18. Babak NA (2008) The use of natural science classification features of solid technogenic waste to predict their utilization. *Nat Tech Sci* 3:241–246
19. Svatovskaya LB, Maslennikova LL, Babak NA (2011) Engineering-chemical and naturally-scientific bases for new eco- and geoprotective technologies creation. SPb: PGUPS
20. Babak NA (2011) The solution of problems of energy saving when using natural and technogenic building materials. *Ecol Urban Territ* 2:77–79
21. Babak NA (2017) Transport construction negative impact on the environment. *Procedia Eng* 867–873
22. Babak NA, Maslennikova LL (2018) Geocological reserve of industrial mineral waste. *Health Saf* 10(214):57–64
23. Maslennikova LL, Svatovskaya LB, Mjakin SV, Vasiljeva IV (2009) Activation of reactions at solid-solid interfaces. Improvement of ceramics materials. In: *Electron beam modification of solids: mechanisms, common features and promising applications*, pp 57–61
24. Korolkov DV (1982) *Fundamentals of inorganic chemistry M*

Silica Sol in Transport Construction



Ivan Kozlov 

Abstract Research area is transport construction in cold regions in compliance with geoecology. The goal of the article is to develop a new binder for the simultaneous performance of two functions—construction and technical, associated with soil reinforcement, and detoxification of heavy metal ions (HMI). Silica sol was chosen as such binder. The research methods are chemical (assessment of the silica sol detoxifying ability), physical (determination of the required concentration of silica dioxide), and physicommechanical (strength tests of samples). It is traced that sandy soil reinforcement is provided by 30% silica sol with detoxification functions. The author proposes transport construction technology in which the use of the new binder allows to achieve higher strength indicators of reinforced structures, as well as to ensure the implementation of the geoecological function.

Keywords Research of silica sol · Geoecology · Transport construction · Soil reinforcement

1 Introduction

The growth of industry, increase in the number of vehicles, and development of civil and transport construction lead to increase of atmosphere, hydrosphere, and lithosphere pollution [1–5].

A serious danger to the environment is soil contamination with heavy metal ions (HMI). Unlike organic pollutants, heavy metals are stored in it for a long time even after the source of pollution has been eliminated. As a result of a pollutant intake into a human body, the activity of the cardiovascular system is disrupted, and severe forms of allergy occur. Therefore, in order to preserve the health of present and future generations, soils need to be cleaned.

In order to detoxify pollution, the study aimed at detoxifying these pollutants was performed [6–10].

I. Kozlov (✉)

Emperor Alexander I State Transport University, St. Petersburg, Russia
e-mail: kis-84@list.ru

© Springer Nature Singapore Pte Ltd. 2020

A. Petriaev and A. Konon (eds.), *Transportation Soil Engineering in Cold Regions*, Volume 2, Lecture Notes in Civil Engineering 50, https://doi.org/10.1007/978-981-15-0454-9_48

459

Table 1 Functions soling•

Process	Reaction	
	Detoxification	Reinforcing
Soling	$n\text{SiO}_2 \cdot \text{H}_2\text{O} + \text{Cd}_2 \rightleftharpoons \text{CdO} \cdot \text{SiO}_2 \cdot \text{H}_2\text{O} + \text{Cd}(\text{OH})_2$	$\text{SiO}_2 \cdot \text{H}_2\text{O} \rightleftharpoons \text{SiO}_2 \cdot \text{H}_2\text{O}$ <p style="text-align: center;">sol gel</p>
Soil silication (taken for comparison)	$\text{Na}_2\text{SiO}_3 + \text{H}_2\text{O} + \text{Cd}_2 \rightleftharpoons \text{CdO} \cdot \text{SiO}_2 \cdot \text{H}_2\text{O} + \text{Cd}(\text{OH})_2 + 2\text{NaOH}$	$\text{Na}_2\text{SiO}_3 + 2\text{H}_2\text{O} \rightleftharpoons \text{SiO}_2 \cdot \text{H}_2\text{O} + 2\text{NaOH}$ <p style="text-align: center;">gel</p>

However, the physicochemical basis of the processes occurring in soils during soling suggests that in addition to the detoxifying function, there appears the reinforcing one. From the point of view of increasing soils reinforcement, an identical function appears during soil silication. Comparison of the processes is given in Table 1.

The known technological process of soil silication, as shown in the reactions, has a serious minus—soil alkalization. Therefore, soling with the use of a pure substance—silica sol, was chosen for further research.

2 Research Methods

The research methods are chemical (assessment of the silica sol detoxifying ability), physical (determination of the required concentration of silica dioxide), and physicommechanical (strength tests of samples).

2.1 Assessment of the Detoxifying Ability of Silica Sol

The sand fraction of 0.63–1.25 mm was used as contaminated soil. For artificial sand contamination, three solutions were prepared containing a concentration of cadmium ions (II) 20 times or more exceeding approximate permissible concentration in soil (0.5 mg/kg). Qualitative analysis confirmed the presence of cadmium ions in these solutions, since the addition of sodium sulfide (Na_2S) to each sample led to the formation of a yellow settled sludge of cadmium sulfide CdS . This fact proves the presence of cadmium (II) ions.

The experiment showed that a sufficient volume of solution for wetting (artificial pollution) of soil is 20 ml per 100 g of sand. In the course of the qualitative analysis of aqueous extract, it was found out that silica sol is capable of detoxifying contaminated sand containing a concentration of cadmium (II) ions 20 or more times exceeding the approximate permissible concentration.

Table 2 Characteristics of “Silica Sol 30”

№	Indicator	Value
1	pH, unit pH	9.0–10.5
2	Mass concentration of silica dioxide, % mass	29–31
3	Kinematic viscosity, not more	10
4	Density, g/cm ³	1.196–1.210

In order to preserve and purify the natural and man-made environment of the supertoxicants of the twenty-first century, which are heavy metal ions (HMI), such objects as railways and highways were chosen.

It is meant that with the help of silica sol, the following possibilities occur:

- detoxifying and reinforcing of road surface during recycling;
- reinforcing the surface of unpaved roads or the main road surface of the railways;
- reinforcing the slopes of the roadbed of railways and highways in deserts and in the Far North area, where strong winds inflate the roadbed, creating the threat to traffic safety, and there is no possibility of mass reinforcing of slopes by the cheapest way—sowing of grass.

In the experiments, there was used “Silica Sol 30” with the characteristics given in Table 2.

2.2 Determination of the Required Concentration of Silica Dioxide

When carrying out the experiments, “Silica Sol 30” was used, and it was diluted with water to a concentration of 15 and 10%. The filler is quarry sand with particles of a diameter from 0.063 to 2.5 mm. As a form (container) for tests, food transparent plastic cups with a volume of 100 ml were used. The standard soil load is 100 g. The density of the resulting sand (bulk, without additional compaction) is 1.63 g/cm³.

In the course of the experiment, sand was filled with silica sol with a volume of 100 ml (weight—121.43 g) at a certain speed. The quantity of silica sol which managed to be absorbed during the infusion was taken as consumption (soil absorbency). The overflow (unabsorbed) silica sol was drained through the perforated openings from the first cup into the second and was removed.

As the result of testing the samples, it was possible to determine the consumption of silica sol (soil absorbing capacity) per 100 g of sand. The data obtained are summarized in Table 3.

The data obtained in the experiment make it possible to formulate the following conclusions, useful for experiments on manufacturing beams for determining the reinforced soil strength:

Table 3 Silica sol consumption (soil absorbing capacity) per 100 g of sand

Sample number	Silica sol concentration, %		
	10	15	30
	Consumption, g		
1	12.9	22.1	29.6
2	13.4	22.2	29.0
3	13.2	22.0	30.4
Average consumption	13	22	30

- for manufacturing of beams, you should use a larger amount of silica sol (not just soak, but pour the sample to the brim), because silica sol absorbed during the infusion is not enough for hardening the sample throughout the volume;
- silica sol should be poured in two or three stages depending on the state of the sample as the silica sol shrinks.

2.3 *Fabrication and Testing of Beams from Soil, Reinforced with Silica Sol*

Samples were made in standard forms for the manufacture of concrete beams. In order not to waste silica sol and soil for testing, the remaining sieved sand from the first experiment (first form), as well as from ordinary medium-sized quarry sand, which builders usually use when building a roadbed, was used to make the first standard beams $4 \times 4 \times 16$ cm (second form). To prevent silica sol leakage, the form was laid with food wrap. The sand was poured at room temperature and humidity, not compacted.

The first form with sieved sand, which remained after the first experiment, was filled with 15% silica sol in the hope that a greater amount of binder and periodicity of watering will allow obtaining a reinforced soil sample capable of holding the form. Unfortunately, beams have not been formed for 28 days. They crumble. It is even impossible to take beams in hand. Only a small lower part of them has been hardened.

With 15% silica sol, the strength was not reached. With the Silica sol 30, the experiment revealed the following (see Fig. 1).

The test results of the three beams for bending and compression are shown in Table 4.

The results of the first tests suggest that the sandy soil can be reinforced with silica sol. The concentration should not be below 30%, and higher strength is achieved with a higher sample mass.



Fig. 1 Beams 4 × 4 × 16 of ordinary middle-sized sand in 28 days

Table 4 Strength of reinforced material for bending and compression, kgf/cm²

Beam №	Mass (g)	Bending strength	Compressive strength	
1	512.86	1.40	Max	9
2	471.33	1.95	Min	3
3	449.26	0.99	Average	5

3 Results and Discussion

In the development of the studies described above, this article discusses the use of silica sol in modern and progressive construction technology—recycling roads so that the process of road recycling can simultaneously be detoxifying. It is also known that man-made soils can be used in the construction of dirt roads using stabilization technology. However, such products are often polluted by HMI, which prevents their use and the release of land occupied by waste and preservation of natural products. But contaminated man-made products during the construction of dirt roads can be restored (detoxified) by using silica sol solution. Next we consider both of these technologies.

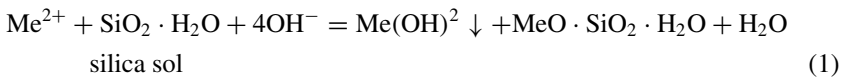
3.1 Cold Recycling Technology

When reconstructing roads with asphalt concrete pavement, it is possible for a recycler, at the same time with its well-known function of removing the old pavement, grinding and mixing it to a certain degree of uniformity, perform a new function—adding a new solution of silica sol during mixing.

From the point of view of geoecoprotection, cold recycling with the use of silica sol will have a significant advantage over other methods of reconstruction, not only due to the full use of old pavement material, but also due to its detoxification. In addition, there is no need for the supply of materials for construction, as the reconstruction is carried out directly at the site, which reduces the pollution of the area that is inevitable when new quarries and chamber nominations are opened.

The silica sol, $\text{SiO}_2 \cdot n\text{H}_2\text{O}$, is safe in its composition for the environment [11–15].

The detoxification function of silica sol is based on spontaneous reactions of interaction of heavy metal ions (HMI) with the formation of low-solubility substances:



So, as tires are worn out in asphalt concrete, HMI accumulates, including zinc, nickel, cadmium, and also lead. The reaction of type (1) in the recycled layer due to the formation of low-solubility products (the right side of Eq. (1)) can reduce the danger of HMI to the value of the maximum permissible concentration (MPC) in the soil, i.e., minimizes danger. The latter is especially important, as it forms a new coating during recycling, which should be safe for the lithosphere.

The principle of repairing (reconstruction) of roads by the method of cold recycling consists in uniform grinding of asphalt concrete pavement, as a rule, with the capture of part of the road base and adding reinforcing additives, such as cement or other inorganic binders, into the resulting granulate, with further mixing, planning and compacting obtained mixes.

The meaning of silica soling is in adding into the resulting granulate the reinforcing additive simultaneously with silica sol for detoxification purpose (Fig. 2).

The destruction of the old coating allows you to eliminate the source of occurrence of new reflected cracks; moreover, the utilization of the old coating is not required.

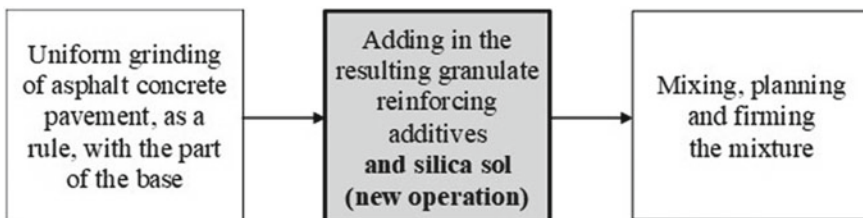


Fig. 2 Geoecoprotective road recycling

The silica sol is introduced in the recovering contaminated raw materials using a pump, equipped with recyclers. The dosage and delivery of the fluid are controlled by the microprocessor in relation to the amount of material in the mixing chamber. Silica sol is pumped through nozzles (channels) that are located on the distribution pipeline and injected with even layer across the entire width of the mixing chamber.

The recycler works together with large tankers (including those containing silica sol), which are combined with the recycler, after which it pushes them or hauls them. The tankers carry a supply of liquid impurities, and separate tankers are used for each type of binders, including for silica sol. The complex is considered usual when the recycler has one tanker.

To obtain a homogeneous mixture, silica sol is mixed with recycled material. The water supply is adjusted so that the moisture percentage is satisfactory for the desired firming. Through the strip, milled with a cutter drum, the solution enters the mixing chamber, where the process of alignment takes place on the back part before filling this strip. After the work of the recycler, the roller performs compaction of asphalt for the grader, which in turn smoothes the road surface to a certain height level.

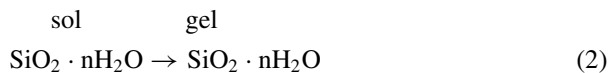
A rather detailed examination of the cold recycling technology has shown that there are no restrictions for giving it a geocoprotective function. The water used in this technology can be replaced by silica sol, which, in addition to the main detoxification function, reinforces the soil.

3.2 Stabilization Technology (Soil Reinforcement)

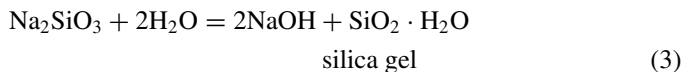
The aim of the work was to propose the possibility of preserving natural and man-made systems during the construction of dirt roads and other road infrastructure objects by using silica sol. It is proposed to use it in the technology of reinforcing dirt roads, including man-made ones, while in cases of contamination by HMI, the above-described process takes place (see Formula 1).

Under the preservation of the natural environment, in this case, the saving of natural resources and the restoration of polluted mineral products are meant.

Furthermore, the silica sol solution (according to [16–20]), due to the possibility of transition to silica gel, in addition to detoxification, HMI holds the soil particles together, reinforcing it, i.e., acts as an inorganic binder:



The mode of silica-firming action for soils is similar to the known use of liquid glass:



However, unlike reaction (3), silica gel obtained by silica soling is pure due to the sol–gel transition and does not alkalize the building system with strong alkali, NaOH, and thus does not pollute the lithosphere, as in reaction (3). This is its principal geocological advantage, i.e., silica gel obtained from silica sol is a pure mineral product with detoxifying and binding properties.

Moreover, in the case of reinforcing of dirt roads and other objects of the road infrastructure, polluted under service, as well as when using for reinforcing polluted mineral waste production, by adding silica sol, spontaneously reacting with dangerous pollutants—heavy metal ions—and forming silica gel as a pollution absorber, the stabilization technology acquires a geocoprotective function. This function works not only when the substance is added into the soil, but also when being under service, since the known absorption properties of $\text{SiO}_2 \cdot n\text{H}_2\text{O}$ in the form of silica gel allows to provide these properties during the road operation—as the dirt absorber will be present in the dirt road.

The analysis of recovery of contaminated products, used as part of soil reinforcement during the dirt roads construction, shows the possibility of adding silica sol into the soil when the HMI soil is contaminated in quantities comparable to the 1000-fold MPC excess (for reference, MPC in soil: Cu (II)—1 mg/kg; Pb (II)—20 (30) mg/kg; Cd (II)—0.5 mg/kg).

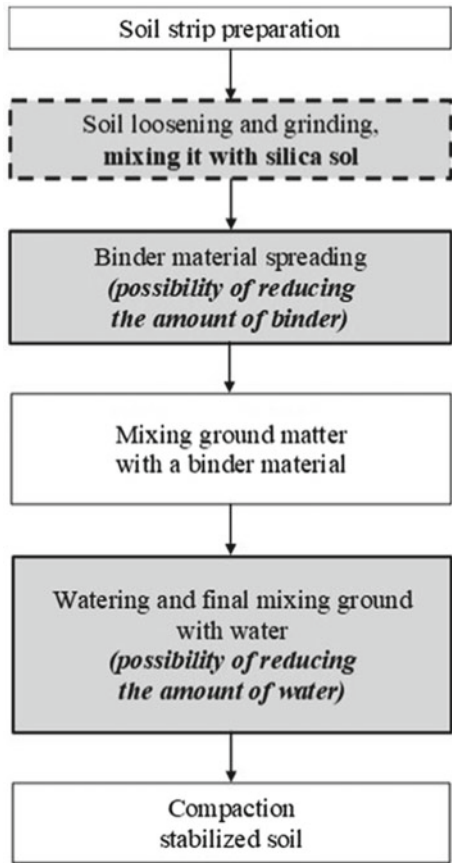
From a practical point of view, the stabilization of soils with modern single-pass means of mechanization (such as WR 2500 from Wirtgen, Germany) includes the grinding of soil and/or man-made product and the supply of cement and water with simultaneous mixing of soil with layer.

In case of soil reinforcement with cement, the amount of water added must also be determined taking into account laboratory tests. In this case, in the technological chain of machines, after the binder dispenser, a water tanker truck is added.

Taking into account the above mentioned, silica sol, being an aqueous solution of silica dioxide, in certain proportions of the laboratory mixes with water, replacing a part of it, or is poured into a tank truck instead of water (Fig. 3).

This technology of dirt roads construction minimizes the negative impact on the lithosphere and is economically beneficial as it not only reinforces the local soil directly on the road, which is a known advantage, but also significantly reduces the amount of imported soil by using man-made materials without detoxification of unsuitable ones—i.e., there is a detoxification of the entire mineral building system, which is the geocoprotective function of silica sol.

Fig. 3 Scheme for adding of silica sol when reinforcing the soil to detoxify pollution and protect the lithosphere



4 Conclusions

The concentration dependence of the strength when using silica sol has been traced, and the values of the strength indicators of soil samples reinforced with silica sol have been obtained.

The possibility of providing a geocoprotective function of soil stabilization technologies and road recycling using silica sol has been proposed. Furthermore, the equipment used in the technological chain of machines in these technologies is provided.

References

1. Sychova A, Solomahin A, Hitrov A (2017) The increase of the durability and geoprotective properties of the railway subgrade. *Procedia Eng* 189:688–694
2. Svatovskaya LB, Sakharova AS, Baidarashvili MM, Petryaev AV, Shershneva MV, Ganchits VV (2012) New geocoprotective technologies in the construction and reconstruction of railways. PGUPS, St. Petersburg
3. Svatovskaya LB, Shershneva MV, Baydarashvili MM, Sycheva AM, Savelieva MYu (2012) Engineering-chemical approaches to the detoxification of the lithosphere using mineral geoantidotes of sulphate-calcium nature. *Nat Tech Sci* 5(61):253–254
4. Svatovskaya LB, Shershneva MV, Sycheva AM, Makarova EI, Baydarashvili MM (2012) Natural science aspect of the nature of mineral geoantidotes (MGA). *Nat Tech Sci* 5(61):255–258
5. Svatovskaya LB et al (2014) New methods of geo-protection of natural and technogenic systems of construction activities in the interests of sustainable development. PGUPS, St. Petersburg
6. Svatovskaya LB (2014) Geocological properties and methods of geo-protection in transport construction. *Transp Constr* 10:28–30
7. Svatovskaya LB, Shershneva MV, Sakharova AS, Baydarashvili MM, Efimova NN, Stepanova IV (2014) Quality assessment of geocoprotective technology solutions at railway transport facilities. *Technosphere Saf Technol* 2(54):34
8. Svatovskaya LB, Baidarashvili MM, Makarova EI, Shershneva MV, Sycheva AM, Kabanov AA (2014) New geocoprotective property of building materials and products. *Technosphere Saf Technol* 1(53):36
9. Svatovskaya LB, Kabanov AA, Sychov MM (2017) Soling, aerating and phosphating for soil reinforcing and detoxication. *Procedia Eng* 189:398–403
10. Svatovskaya LB, Urov OV, Kabanov AA (2017) Geocoprotective technology of transport construction using silica sol absorption method. *Procedia Eng* 189:454–458
11. Svatovskaya LB, Sychova AM, Soloviova VY, Maslennikova LL, Sychov MM (2016) Absorptive properties of hydrate silicate building materials and products for quality and geocoprotection improvement. *Indian J Sci Technol* 9(42):104231
12. Baydarashvili M (2017) Criteria of geocoprotection in construction. *Procedia Eng* 616–621
13. Bayandinova S, Mamutov Z, Issanova G (2018) Geocological bases of nature protection measures and actions. *Environ Sci Eng (Subser: Environ Sci)* 9789811063459:125–134
14. Oliva M, Ruiz-Fernández J, Zarankin A, Casanova-Katny A, Nofre J (2017) Geoecology and historical heritage in the ice-free area of elephant point (antarctica). Proposal for future environmental protection. *Geoheritage* 9(1):97–109
15. Sun D, Li K, Liu F, Sui X, Zhou C (2018) Research of silica aerogels prepared by acidic silica sol under the condition of atmospheric pressure drying. *J Porous Mater* 25(2):341–349
16. Destino JF, Dudukovic NA, Johnson MA, Nguyen DT, Yee TD, Egan GC, Sawvel AM, Steele WA, Baumann TF, Duoss EB, Suratwala T, Dylla-Spears R (2018) 3d printed optical quality silica and silica–titania glasses from sol–gel feedstocks. *Adv Mater Technol* 3(6):1700323
17. Park M-G, Lim HM, Kim DS, Kim H, Choi J (2016) Correlation research of dispersion factors on the silica sol prepared from fumed silica. *Korean J Mater Res* 26(3):136–142
18. Thakur S, Pandey S, Arotiba OA (2017) Sol-gel derived xanthan gum/silica nanocomposite-a highly efficient cationic dyes adsorbent in aqueous system. *Int J Biol Macromol* 103:596–604
19. Pham Q-T, Wang Y-T, Wu Y-T, Chern C-S, Yao Z-H (2017) Preparation and characterization of monodisperse silica nanoparticles via miniemulsion sol–gel reaction of tetraethyl orthosilicate. *J Mater Sci* 52(21):12706–12716
20. Ma J, Ye F, Yang C, Ding J, Lin S, Zhang B, Liu Q (2017) Heat-resistant, strong alumina-modified silica aerogel fabricated by impregnating silicon oxycarbide aerogel with boehmite sol. *Mater Des* 131:226–231

The Method of Producing Non-autoclaved Foam Concrete Based on Polymers for the Construction of Various Road Structures in Cold Regions



Anastasiya Sychova , Yuriy Kamenev, Larisa Svatovskaya and Alexandr Avseenko

Abstract The purpose of the investigation is to obtain the non-autoclaved foam concrete with increased thermal protection properties for various road structures. It is shown that to achieve this goal, polymers and dolomitized limestone are to be introduced into the foam concrete composition, which results in the decrease of the thermal conductivity coefficient of more than a class of average density. The interrelation of thermal conductivity coefficient of foam concrete with physical–chemical characteristic of its stone interlayer (crystal–amorphous ratio characterizing the amorphism degree of its stone structure) is scientifically proved. New technological solutions for road structures construction are proposed. It is shown that the use of foam concrete based on polymers in road structures allows to provide high frost resistance, which is especially important for construction in cold regions. In such regions, in order to arrange road structures on permafrost and heaving soils, they need increased thermal protection characteristics. The use of materials with a reduced thermal conductivity coefficient in their composition will prevent their destruction. When using foam concrete in railway embankments, the load on weak foundations is reduced. It is established that the solutions with simultaneous application of foam concrete of different classes of average density are the most effective. Fourier transform infrared spectroscopy and derivatographic methods of analysis were used in the study of the material obtained. The calculation of road structures was carried out in accordance with the regulatory documentation and showed a significant margin of frost resistance and the load reduction in a weak base.

Keywords Non-autoclaved foam concrete · Thermal protection properties · Polymers · Frost resistance · Road and rail structures

A. Sychova (✉) · Y. Kamenev · A. Avseenko
Military Space Academy Named After A.F. Mozhaysky, St. Petersburg 197198, Russia
e-mail: amsychova@yandex.ru

L. Svatovskaya
Emperor Alexander I St. Petersburg State Transport University, St. Petersburg 190031, Russia

© Springer Nature Singapore Pte Ltd. 2020
A. Petriaev and A. Konon (eds.), *Transportation Soil Engineering in Cold Regions*,
Volume 2, Lecture Notes in Civil Engineering 50,
https://doi.org/10.1007/978-981-15-0454-9_49

1 Introduction

The relevance of the work is due to the fact that 60% of the territory of Russia is in the first road-climatic zone. This zone is characterized by low average daily temperatures of the cold period of the year, as well as the presence of heaving and subsidence of soils. So, in order to ensure the durability of pavement structures operating in difficult climatic and hydrogeological conditions, the use of the following materials is required: with a reduced density for decreasing the load on a weak base, with high thermal protection properties for increasing the frost resistance of the entire road structure [1, 2].

The use of polystyrene foam in road embankments on weak soils is known from the literature [3–5]. Road structures with light materials require little time for their construction [6, 7]. It is known to use geofam EPS as an embankment for the foundations of bridges [8]. In recent years, expanded polystyrene (EPS) geofam has successfully been used to reduce the acting vertical and horizontal stresses in several geotechnical applications due to its lightweight, compressibility, and durability [9–11]. Material such as foam polystyrene (EPS) can be used as an energy-absorbing material [12]. But foam polystyrene (EPS) has the following disadvantages: high cost, the ability to destruction, and the possibility of using only blocks (the use of monolithic material is not possible).

To create a non-autoclaved foam concrete with increased thermal characteristics, it is proposed to increase the degree of amorphism of its stone structure. The amorphous structure will be known to reduce [13] the rate of thermal wave's propagation and the coefficient of the material's thermal conductivity.

It is proposed to increase the degree of the phase structure amorphism of foam concrete by introducing polymers with amorphous structure and dolomitized limestone into its composition. High fineness of limestone grinding increases the amorphous phase in its composition. With the introduction of the polymer together with the limestone into the of the foam concrete composition, it is possible to increase the amorphism degree of its stone structures significantly [14].

The degree of amorphism is supposed to be estimated by a new characteristic—the crystal–amorphous ratio (Ω), formula is (1):

$$\Omega = \frac{\text{crystalline phase, mg}}{\text{amorphous phase, mg}} \quad (1)$$

The calculation is based on the results of derivatographic analysis of the foam concrete samples and gives the possibility to determine the amount of crystalline and amorphous phase in the material.

The greater the amorphous phase in the material, the lower is the value Ω and the coefficient of thermal conductivity of foam concrete and higher its thermal properties. It should be taken into account that the crystalline phase largely provides the strength of foam concrete to a considerable degree. That is why the ratio of these phases in the material is especially important.

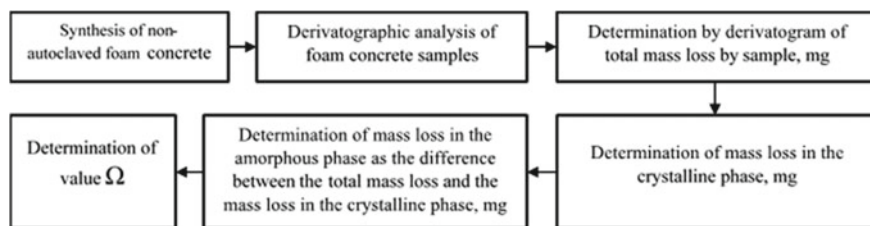


Fig. 1 Method of determining the value of the crystal–amorphous foam concrete ratio, Ω

For Fig. 1, the method of determining the value of the crystal–amorphous ratio of foam concrete is based on polymers.

2 Experiment

Then, the synthesis of non-autoclaved foam concrete with the increased heat-shielding properties was carried out. In developing the composition of the material, the following factors were taken into account:

1. To exclude the slowing effect of polymers on the processes of cement hydration, they are supposed to be introduced into the foam concrete in the form of a complex additive together with a hardening accelerator. NaCl was chosen as a hardening accelerator, as it can exert a significant activating influence on the cement hydration processes [2].
2. It is necessary to choose the stabilizers of a construction foam on a protein basis because the hardening accelerators can cause its destruction. As a stabilizer, a polymer (latex SCS-65 GP) was also proposed [15] because it was supposed to be able to form chemical bonds with the molecules of the protein foaming agent, which would strengthen the protein film and ensure the stability of the building foam in the presence of the introduced hardening accelerator [15, 16].

The experiment showed that the foam resistance time will increase by more than 2.5 times. Fourier transform infrared spectroscopy confirmed that the effect of the foam stability increase is connected with the formation of hydrogen bonds between the molecules of the foaming agent and latex SCS 65-GP [17].

Further, the composition of the complex additive was selected for the introduction into the foam concrete mixture, as well as the composition of non-autoclaved foam concrete classes in the average density D500 and D1000. On the basis of experimental studies, the following composition of the complex polymer additive (mass%) was selected: 77 (polyvinyl acetate): 23 (NaCl).

The complex additive was introduced into the mixture together with mixing water in an amount of 13% by weight of cement. The fast-hardening Portland cement CEM I 42.5 B was used as a binder. A part of the aggregate (sand with a grain size of not

more than 0.63 mm) was replaced by the dolomitized limestone with a specific surface area of 3000 cm²/g in the amount of 30%. Hardening of samples was carried out in the mode of heat and humidity treatment.

3 Results and Discussion

Physical and mechanical tests of the developed foam concrete show that the compressive strength increases up to 65%; tensile strength in bending—up to 25%; frost resistance increases up to 27%; the coefficient of thermal conductivity decreases by more than a class of average density (Table 1) [18–20].

The derivatographical analysis of samples carried out (Table 2) shows the presence of the low-basic hydrosilicates—CSH (II) and C₆S₆H in the material which are

Table 1 Physical and mechanical properties of the foam concrete developed

Physical and mechanical characteristics	Samples			
	Class on average density			
	D500		D1000	
	Control sample	A sample of the complex polymer additives	Control sample	A sample of the complex polymer additives
Bending tensile strength (MIIa)	2.7	3.1	6.9	9.3
Compressive strength (MIIa)	3.7	5.6	14.8	18.2
Thermal conductivity (W/m °C)	0.12	0.10	0.29	0.19
Frost resistance (cycles)	15	19	41	52

Table 2 Derivatographic analysis of the foam concrete samples

Sample type	Effects (°C)				Mass loss in the crystalline phase, mg	Mass loss in gel (amorphous) phase, mg
	I-(64-120)CSH(II)	II-(463-513)Ca(OH) ₂	III-(613-725)C ₆ S ₆ H	IV-(725-888)C ₆ S ₆ H		
	Weight loss on effects, mg					
Control sample	16.4	6.4	16.0	–	38.4	25.3
A sample of the complex polymer additives	22.5	9.0	13.5	29.25	74.25	64.75

Table 3 Relationship between the crystal–amorphous ratio and the thermal conductivity coefficient of the developed foam concrete

Sample type	Crystal–amorphous ratio	Thermal conductivity, λ (W/m °C)
Control sample	1.5	0.19
A sample with the complex polymer additives	0.9	0.155

characterized by high strength [21]. Also, the results of the analysis show an increase in the amount of $\text{Ca}(\text{OH})_2$, which indicates an increase in the degree of cement hydration in the presence of the introduced complex additive. These results explain the increase in physical and mechanical characteristics [16] of the foam concrete obtained.

The results of the calculation data of the derivatographical analysis (Table 3) show that the proposed value of the crystal–amorphous ratio is reduced by 1.6 times, and the coefficient of thermal conductivity—by more than one class of the average density in comparison with the control sample. These results confirm the previously stated assumptions about the influence of the degree of amorphous stone structure of foam concrete on its thermal properties.

Further, new technological solutions of the received foam concrete application in various road designs were developed.

The first technological solution for the pavement construction (Fig. 2) proposes to use the developed foam concrete as a carrier base performing simultaneously a heat-shielding function (D1000), as well as an additional heat-insulating layer (D500). This solution allows to reduce the thickness of other layers of the road structure, to improve the water-heat regime of the roadbed and frost resistance of the entire structure. This is necessary for their arrangement in the Northern regions where the permafrost and heaving soils are present [22–24].

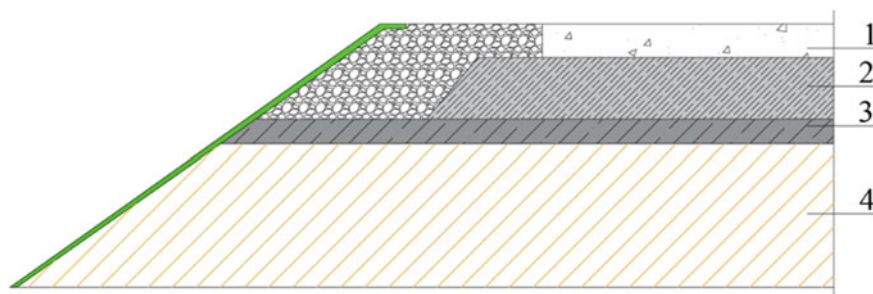
**Fig. 2** Road construction with the use of the developed foam concrete of different average densities: 1 coating; 2 foam concrete D1000; 3 foam concrete D500; 4 soil subgrade

Table 4 Design strength characteristics of the road pavement when the developed foam concrete is used

Calculation conditions	Margin according to the terms of the calculation when using a new technological solution $N = 7.68 \cdot 106$
According to the permissible elastic deflection of the entire structure	1.9
According to the resistance to stresses arising under the influence of the repeated short-term loads	1.86
According to the unacceptable residual deformation in the underlying soil and low connective layers of road pavement	2.14
According to the resistance	2.83

Table 4 shows the characteristics of the road constructions with the use of the foam concrete developed. The developed pavement calculation was carried out for the group of the design load A3 which corresponds to the standard static load on the axis 130 kN [25].

Table 4 shows that the reserves according to the frost resistance exceed the required ones superior to 2.83 times [26]. From this result, it follows that the developed foam concrete is an effective building material which is advisable to use in road structures in the Northern regions.

The second technological solution offers to use the developed foam concrete as a material of railway embankment (Fig. 3).

Instead of a part of the railway embankment material, the developed foam concrete of the average density of D500 with a layer height of 4 m is placed.

The construction of a railway embankment with foam concrete is carried out under the condition of its quick fill whole the, which is impossible when using sand or local soil are used [25, 27, 28].

Table 5 shows the design characteristics of the railway embankment while using the foam concrete developed [29].

The table shows that the load from the embankment with the foam concrete use is lower compared to the sand embankment by 32%; the weak base is able to withstand

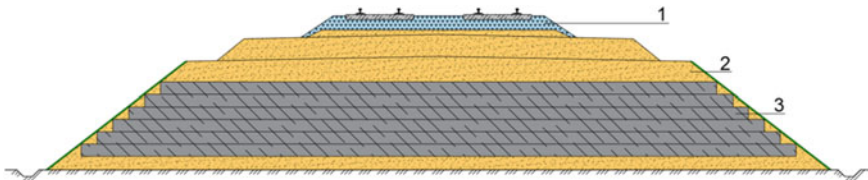


Fig. 3 Railway embankment with the use of the foam concrete developed: 1 ballast layer; 2 embankment soil; 3 non-autoclaved foam concrete of medium density D500

Table 5 Calculation results of the railway embankment while using the developed foam concrete of the average density D500

Calculation type	Design characteristics	Value
The calculation of load on a weak basis	The estimated load from the embankments with the use of foamed concrete (kN/m ²)	104
	The estimated load from the sand, embankment (kN/m ²)	320
	Safe loading (kN/m ²)	112
The calculation of the precipitation of the weak base	A finite amount of precipitation of the foundation within the active zone of compression (cm)	19.7
	Permissible value of the base precipitation (cm)	20

the embankment with foam concrete, while in using the sand embankment additional measures are required to strengthen it.

The developed technological solutions can be recommended for areas of the permafrost soils (the Far North and the Arctic), since the frost resistance of such structures ensures the preservation of soils in the frozen state throughout the service life, and their reduced weight decreases the load on the weak bases.

For both technological solutions, it is assumed to lay monolithic foam concrete at the average daily air temperature of up to minus 15 °C, and to lay foam concrete mats at the average daily temperature below minus 15 °C.

4 Conclusions

1. To assess the degree of the foam concrete stone structure amorphism, it is proposed to use the value of the crystal–amorphous ratio Ω , determined by the results of derivatographic analysis.
2. It is proposed to introduce a polymer in the form of a complex polymer additive (polyvinyl acetate + NaCl), as well as dolomitized limestone in order to increase the heat-shielding properties of cellular concrete.
3. It is shown that the developed foam concrete with a complex polymer additive reduces the value of the crystal–amorphous ratio by 1.6 times, increases strength characteristics up to 65%, and decreases the thermal conductivity coefficient by more than a class of average density.
4. The use of foam concrete with different densities in the pavement layers which perform the carrier and thermal insulation function as well as a railway embankment is presented.

5. The calculation of road structures with the use of the foam concrete developed showed a significant margin of frost resistance as well as the load decrease on a weak base.

References

1. Sychova A, Solomahin A, Gera V, Kotovich V (2018) The use of monolithic polymer-cement foam concrete in the construction of the roadway. *Way Track Facil* 6:32–34
2. Sycheva A, Kamenev Yu, Avseenko A, Abu-Hassan M, Aleshichev S (2018) The method of calculating the value of the crystal-amorphous ratio of the stone layer of cellular concrete in order to assess its heat-shielding properties and the use of road structures. *Transp Constr* 12:24–27
3. Wang F, Miao L (2009) A proposed lightweight fill for embankments using cement-treated Yangzi River sand and expanded polystyrene (EPS) beads. *Bull Eng Geol Environ* 68:517
4. Duškov M, Erkelens W (2018) Dutch N201 road embankment with EPS geofoam. In: 5th international conference on geofoam blocks in construction applications, pp 89–97
5. Aabøe R, Bartlett SF, Duškov M, Frydenlund TE, Mandal JN, Negussey D, Özer AT, Tsukamoto H (2018) Geofoam blocks in civil engineering applications. In: 5th international conference on geofoam blocks in construction applications, pp 3–38
6. Duškov M, den Uil M, Fütterer M (2018) Dutch A76 highway widening using EPS embankment with a vertical side. In: 5th international conference on geofoam blocks in construction applications, pp 81–87
7. Taneichi K, Konami T, Tsukamoto H, Kubota T, Yasuhara K (2018) Opening traffic for a temporarily remediated EPS road after the 2016 kumamoto earthquake: a world first. In: 5th international conference on geofoam blocks in construction applications, pp 351–359
8. Vaslestad J, Bartlett SF, Aabøe R, Burkart H, Ahmed T, Arellano D (2018) Bridge foundations supported by EPS geofoam embankments on soft soil. In: 5th international conference on geofoam blocks in construction applications, pp 281–294
9. AbdelSalam SS, Anwar MB, Eskander SS (2018) Long term behavior of EPS geofoam for road embankments. In: *GeoMEast. Advances in Geosynthetics Engineering*, pp 97–107
10. El-kady MS, Alzara MA, Farouk MA (2018) Reduction of lateral earth pressure using Geofoam blocks. *Innov Infrastruct Solut* 3:40
11. Gendy ME, Araby IE, Kamash WE, Sallam E, Labban AE (2018) Effect of using EPS geofoam on deformation behavior of square footings on clay subjected to static and dynamic loads: experimental study. In: 5th international conference on geofoam blocks in construction applications, pp 251–266
12. Ouyang Chaojun, Liu Yang, Wang Dongpo, He Siming (2019) Dynamic analysis of rockfall impacts on geogrid reinforced soil and EPS absorption cushions. *KSCE J Civ Eng* 23:37–45
13. Komokhov P, Gryzlov V (1992) *Structural mechanics and thermophysics of light concrete*. Publishing House of the Vologda Scientific Center, Vologda
14. Sycheva AM, Stepanova IV, Eliseeva NN et al (2010) Nanoadditives in compositions of inorganic binders. Monograph
15. Gel'fman M (2005) *Workshop on colloidal chemistry*
16. Sychova A, Solomahin A, Kotovich V, Svatovskaya L, Kamenev Y (2018) Improving of the monolithic foamconcrete quality for used in the high-rise constructions. In: *E3S web of conferences*, vol 33, p 02058
17. Sychova A, Eliseeva N, Samborsky S (2010) Improvement of quality non-avtoclavic foam concrete by foam stabilisation. *Concr Zhelezobeton* 5:13–15
18. Svatovskaya L, Shershneva M, Baidarashvili M, Yakimova N, Khitrov A (2004) Foam concrete construction demolished waste. In: *Proceedings of the international conference on sustainable waste management and recycling: construction demolition waste*, pp 199–203

19. Svatovskaya L, Sychova A, Mjakin S, Vasiljeva I (2009) Modification of fillers for cements In: Electron beam modification of solids: mechanisms, common features and promising applications, pp 35–37
20. GOST 25485-89 (1989) Concrete cellular. Specifications. The state building committee of the USSR. M
21. Mikulski V, Kupriyanov V et al (2000) Building materials 536
22. Sychova A, Solomahin A, Hitrov A (2017) The increase of the durability and geoprotective properties of the railway. Subgrade transportation geotechnics and geoecology. In: TGG 2017, Procedia Engineering, vol 189, pp 688–694
23. Sychova A, Sychov M (2017) A method of obtaining geoniseprotective foam concrete for use on railway transport. Subgrade transportation geotechnics and geoecology. In: TGG 2017, Procedia Engineering, vol 189, pp 681–687
24. Svatovskaya L, Sychov M, Sychova A, Gravit M (2016) New geocoprotective properties of the construction materials for underground infrastructure development. Procedia Eng
25. Sakharova A, Svatovskaya L, Baidarashvili M, Petriaev A (2016) Sustainable development in transport construction through the use of the geocoprotective technologies. Procedia Eng
26. ODN 218.046-01, Engineering of non-tough pavement
27. Sakharova AS, Svatovskaya LB, Baidarashvilly MM, Petriaev AV (2015) Building wastes and cement clinker using in the geocoprotective technologies in transport construction. In: 14th international conference of international association for computer methods and recent advances in geomechanics, IACMAG
28. Sakharova AS, Svatovskaya LB, Baidarashvili MM, Petriaev AV (2016) Sustainable development in transport construction through the use of the geocoprotective technologies. In: The 3rd international conference on transportation geotechnics, Procedia Engineering, pp 1401–1408
29. The joint venture 32-104-98 (1998) Designing of an railway subgrade with a track of 1520 mm

Conservation of Mineral Resources in Transport and Civil Construction



Marina Baydarashvili , Antonina Sakharova  and Natalia Shrednik

Abstract Mineral resources conservation has been gaining importance in transport and civil construction, including in cold climates. Numerous experiments have established that conservation of mineral resources is possible when using silicic acid nano-solution at the stage of production of cement-base building systems. Some resource-saving technological decisions are present. The article presents the calculated data on the economy of natural resources using these decisions. Resource consumption coefficient is offered. This coefficient determines natural raw materials efficiency. There is another way to preserve natural resources—geocoprotective decoration of white cement construction products. This decision involves the use of colored solutions of metals instead of the natural mineral pigment. The calculation of the mineral coloring component consumption per 1 m³ of the concrete product was carried out. The valuation showed that the use of colored solutions when painting the surface of the product significantly reduces the cost of natural mineral raw materials.

Keywords Mineral resources conservation · Resource consumption coefficient · Silicic acid nano-solution · Geocoprotective decoration

1 Introduction

There are various ways to preserve mineral resources in construction. On the one hand, it can be the development of buildings, structures projects that provide minimal costs for construction and operation. On the other hand, it is possible to create resource-saving types of building materials, products, and related technologies of their production [1–8]. In the article [9] were conducted studies that showed the possibility of using waste foundry in the hot sand-asphalt production. Studies have shown that replacing 25% of sand with burnt earth improves performance. In foreign practice, great attention is paid to the possibility of using various wastes as aggregates in the concrete production [10–19]. Such concretes are referred to as «green»

M. Baydarashvili · A. Sakharova (✉) · N. Shrednik
Emperor Alexander I St. Petersburg State Transport University, St. Petersburg 190031, Russia
e-mail: assakharova@list.ru

© Springer Nature Singapore Pte Ltd. 2020
A. Petriaev and A. Konon (eds.), *Transportation Soil Engineering in Cold Regions*,
Volume 2, Lecture Notes in Civil Engineering 50,
https://doi.org/10.1007/978-981-15-0454-9_50

or «ecological» concretes, because they have less impact on the environment, help in solving the problem of construction and industrial wastes utilization, and contribute to the natural resources preservation.

It should be noted that the problems of building long-term buildings and structures and their operation are particularly acute in cold climates. A significant part of these problems is related to the stability of buildings and structures on frozen soils, the impact of snow loads on buildings and structures, environmental protection, and recycling of man-made waste. As a result of high requirements to the quality of buildings and structures construction, environmental safety, builders use the most efficient, energy- and resource-saving building materials, structures and technologies.

2 Scientific Basis of Resource Conservation in Construction

It is possible to distinguish two fundamental characteristics of construction systems that will lead to resource-saving in construction activities and in construction technologies. The first is the size of the particles, including nanoscale (1–100 nm). Nanoparticles provide additional energy. The second is the ability of a capillary-porous mineral body (for example, a building product of a cement base) to absorb nanoparticles and their further participation in processes that provide resource economy [20–23].

As nano-solution was taken from the solution of silicic acid sol, which has excess surface energy and surface area, which ensures high reactivity.

As a result of capillary rise, silicic acid sol interacts with the components of the building hydrosilicate system. This process is energetically beneficial and is accompanied by the formation of an useful product. The results of research have shown that the use of silica solution increases the strength of building materials, which increases the structural quality coefficient (SQC) of the material. This coefficient is calculated as the ratio of the strength to the relative average density. It characterizes the technical and economic quality of the material (Table 1).

To assess the consumption of natural resources in the various construction materials and products production have been proposed geoeological indicator—the ratio of the mineral resources cost k_{rc} . This coefficient is associated with the coefficient of

Table 1 Results of the calculation of SQC samples of control and saturated with silica solution

Average density of hydrosilicate systems (kg/m ³)	SQC, MPa, determined at the age of 28 days	
	Test	With absorbed silicic acid sol
400	1.12	2.00
500	1.86	4.18
600	2.28	4.45
2000	7.04	12.3

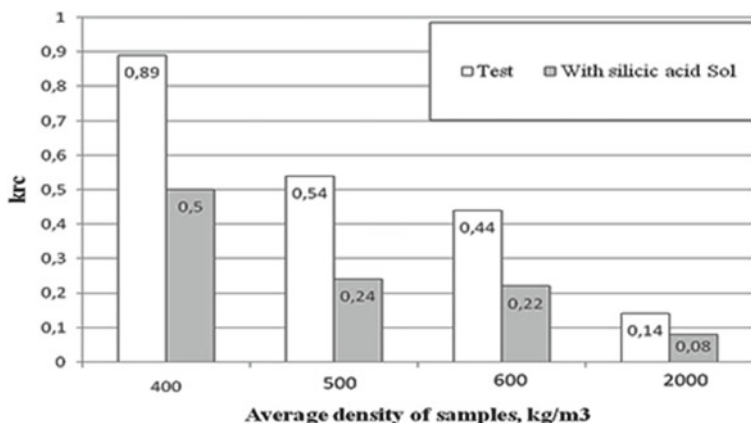


Fig. 1 Resources cost indicators of control concretes and concretes with absorbed silica

constructive quality inverse relationship. It shows the following. The lower its value, the less natural raw materials are consumed. Therefore, decreasing this coefficient shows that such technical and technological solutions in the construction activities become geoenvironmental protective.

Figure 1 shows the values of k_{rc} for control samples of building systems and systems modified with silica solution.

Figure 1 illustrates the idea that the absorption of nano-solution construction hydrosilicate system leads to saving of resource consumption by increasing the properties level of the building system. In other words, the absorption of the silica solution and its further interaction with the components of the construction hydrosilicate system leads to the synthesis of the properties of such a system, which were previously provided by the use of natural raw materials [24–28].

3 Technological Solutions for the Mineral Resources Conservation in Construction

The first solution was applied to underground construction structures operated in high humidity conditions—strip foundations, piles, pasture columns, etc., when it is important to increase geosecurity to provide reduced water absorption of the underground part. Studies have shown (Fig. 2) that the processing of such structures of average density of 2000 kg/m^3 silica solution leads to a decrease in water absorption and to an increase in the life of such products and structures of them.

Figure 3 shows the calculated data on the amount of natural raw materials that will be saved when using resource-saving technologies that provide for an increase in the service life of the construction system.

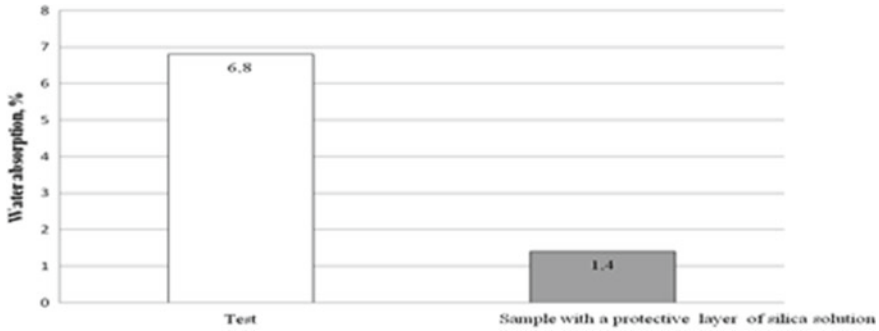
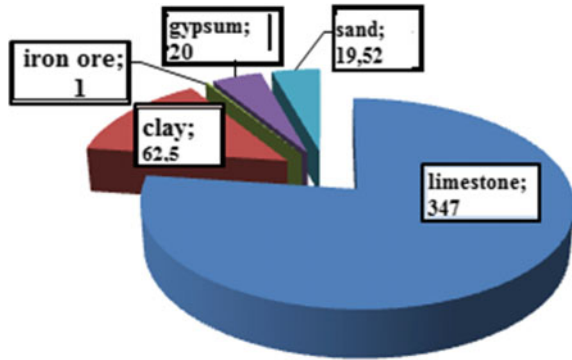


Fig. 2 Geoenvironmental protective (for waterproofing) properties that determine the material durability

Fig. 3 Saving of natural raw materials



The second solution is applied to the resource-protection technology of painting the surface of finished building products of white color for decorating products. Such products do not carry a surface load and are operated in favorable (non-aggressive) conditions for this material (for example, small-piece products made of silicate brick, foam, aerated concrete remaining after construction, repair, reconstruction, etc.). This solution is based on the absorption and interaction of colored solutions with the components of the building system, which leads to the coloring of the product. This reduces the resource costs for the production of pigments used for decoration. There are two ways of painting concrete products in construction. The first is to add dyes at the stage of mixing the solution; the second method involves applying paint to the surface of the finished product.

To paint the building products in yellow, red, black, and brown colors are often used iron oxide pigments containing in their composition of iron oxides and hydroxides [29]. In this case, the amount of pigment administered varies from 0.2 to 5% of the weight of the prepared cement. The pigment content depends on the intensity of staining (Table 2).

Table 2 Consumption of natural mineral iron oxide pigment depending on the color intensity

Pigment consumption per 100 kg of cement (kg)	Color intensity
1–2	Weak color, pastel colors
3–4	Average intensity
5–6	Intense color

Iron oxide (III) is the basis of iron oxide pigments. Analysis of reference data [19] showed that its content is 90%. Then, for the production of 1 m³ of colored concrete product of the initial average density of 2000 kg/m³, painted in pastel colors, with a cement consumption of 500 kg, it is necessary $2 \times 500/100 = 10$ kg of pigment, that is $10 \times 0.9 = 9$ kg of iron oxide (III). Iron (III) oxide is about 70% of enriched iron ores. Then for producing 1 m³ of colored concrete products will be required to 12.9 kg of natural raw materials, for 1000 m³ of 12.9 tonnes, which speaks of resource-intensive technologies of this type of construction.

Thus, the development of technological solutions aimed at reducing resource consumption in this type of construction activity will be the geoenvironmental protective.

The first studies were aimed at determining the lowest concentration of the initial solution at which the color of the product appears. These studies are dictated by the need for safe disposal of such solutions. Samples of foam concrete and silicate brick were chosen as construction materials to be painted.

Staining products occurred at the following minimum concentrations: when using a solution of copper (II)—0.025%; when using a solution of Nickel (II)—0.025%; when using a solution of iron (III)—0.005% (Fig. 4).

The following studies were aimed at determining the “washout” of metal cations from painted products. To do this, the stained samples were immersed in distilled water. After 1, 7, and 30 days, water samples were taken to detect heavy metal cations.

These studies showed the absence of metal cations in all samples. This fact indicates the safety of the color of the product, on the one hand, and the environmental safety of such technology for the environment, on the other.

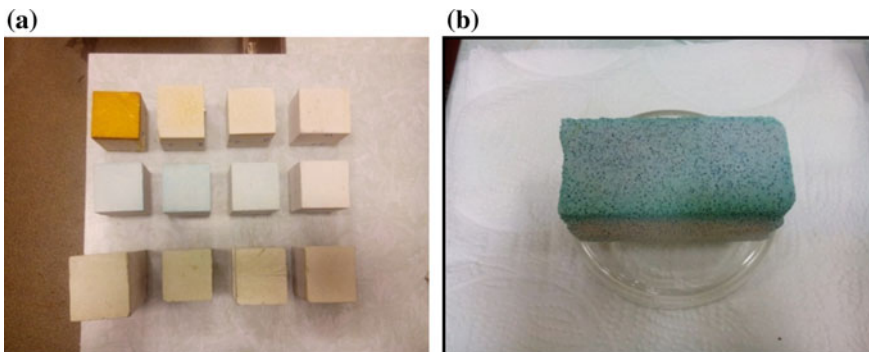


Fig. 4 Result of the process of decorating samples of silicate bricks (a) and foam concrete (b)

Table 3 Consumption of mineral coloring component per 1 m³ of concrete product, which determines the consumption of natural mineral resources

Nº	Pigment (contains iron (III) compound)	Pigment consumption per 1 m ³ to create a weak color	In what form is used	The content of the coloring component (%)	Consumption of the coloring component, kg/m ³ , to create a weak color (pastel colors)
1	Red iron oxide	10 kg	Solid	97	9.7
2	Brown iron oxide	10 kg	Solid	84	8.4
3	Orange iron oxide	10 kg	Solid	83	8.3
4	Yellow iron oxide	10 kg	Solid	87	8.7
5	Iron (III) nitrate	1 L	Solution	0.025	0.00025

Thus, the processes of absorption and interaction of metal cations with the components of the construction system can be used in the decoration technologies of building cement products using colored solutions with copper (II), Nickel (II), and iron (III) ions. It can significantly reduce the consumption of natural ores, which are also mined for the pigments and dyes production. Table 3 shows the quantities of coloring components (containing iron (III) compounds) per 1 m³ of finished cement products with an initial average density of 2000 kg/m³ and a cement consumption of 500 kg/m³. It should be noted that the first four pigments are added at the stage of mixing solutions that stain the product throughout. The fifth, which is proposed in this article, involves painting the surface of the finished product. In this regard, a condition is introduced that the goal of decoration is to paint the product surface.

According to Table 3, the use of solutions of non-ferrous metal ions on the example of iron nitrate (III) can significantly save natural resources related to non-renewable.

4 Conclusions

1. To assess the consumption of natural resources in the various construction materials and products production have been proposed geoecological indicator—the ratio of the mineral resources cost k_{rc} . The lower its value, the less the natural raw materials are consumed.
2. Conservation of mineral resources is possible with the use of solution silicic acid sol at the stage of cement products production. The absorption of the silica solution and its interaction with the components of the hydrosilicate system

leads to the synthesis of the properties of such a system, which were previously provided by the use of natural raw materials.

3. Conservation of mineral resources is possible in the technology of coloring concrete products in white. The technology allows to refuse the pigments received from natural ores.
4. Painting the surface of the product with a colored metal solution reduces the consumption of mineral resources by four orders of magnitude.
5. These decisions on the conservation of mineral resources allow us to solve some of the problems of building long-term buildings and structures in cold climates, which were described in the article.

References

1. Svatovskaya L, Sychova A, Sychov M, Okrepilov V (2016) New parameter of geoeological protective ability of construction articles. *MATEC Web Conf* 53:01024
2. Svatovskaya L, Sychov A, Sychov M, Okrep V (2016) Quality improvement of concrete articles. *MATEC Web Conf* 53:01023
3. Sakharova A, Svatovskaya L, Baidarashvili M, Petriaev A (2016) Sustainable development in transport construction through the use of the geoeoprotective technologies. *Procedia Eng* 143:1401–1408
4. Svatovskaya LB, Kabanov AA, Sychov MM (2017) The improvement of foam concrete geoeoprotective properties in transport construction. In: *IOP conference series: earth and environmental science*, p 90
5. Sychova A, Sychov M, Rusanova EA (2017) Method of obtaining geonoiseprotective foam concrete for use on railway transport. *Procedia Eng* 189:681–687
6. Sychova A, Solomahin A, Hitrov A (2017) The increase of the durability and geoprotective properties of the railway subgrade. *Procedia Eng* 189:688–694
7. Svatovskaya LB, Shershneva MV, Baidarashvili MM, Yakimova NI, Khitrov AV (2004) Foam concrete construction demolished waste. In: *Proceedings of the international conference on sustainable waste management and recycling: construction demolition waste London*, pp 199–203
8. Svatovskaya LB, Sakharova AS, Baidarashvili MM, Petriaev AV (2015) Building wastes and cement clinker using in the geoeoprotective technologies in transport construction. In: *Proceedings of the 14th international conference, computer methods and recent advances in geomechanics*, pp 619–622. Taylor and Francis—Balkema, Netherlands
9. Maisuradze N (2006) Use of burnt earth in asphalt mixtures. *Izvestiya KGASU* 5:39–41
10. Hossain MU, Xuan D, Poon CS (2017) Sustainable management and utilization of concrete slurry waste: a case study in Hong Kong. *Waste Manag* 61:397–404
11. Gajendran KA, Anuradha R, Venkatasubraman GS (2016) Strength study on eco friendly high performance concrete by replacing the cement by flyash, silica fume and metakaolin. *Asian J Microbiol Biotechnol Environ Exp Sci* 18(2):495–497
12. Radonjanin V, Malešev M, Marinković S (2013) Green recycled aggregate concrete. *Constr Build Mater* 47:1503–1511
13. Lin K-L, Chen B-Y, Chiou C-S (2010) An Cheng waste brick's potential for use as a pozzolan in blended Portland cement. *Waste Manag Res* 28(7):647–652
14. De'Gennaro R, Graziano SF, Cappelletti P, Langella A, De'Gennaro M (2009) Structural concretes with waste-based lightweight aggregates: from landfill to engineered materials. *Environ Sci Technol* 43(18):7123–7129

15. Demir I (2009) Reuse of waste glass in building brick production. *Waste Manag Res* 27(6):572–577
16. Baldwin DA, Gericke WA, Potgieter N, Van Niekerk WC (2007) A criteria for utilization of by-products from the ferro-alloy industry innovations in the Ferro alloy industry. In: *Proceedings of the XI international conference on innovations in the Ferro alloy industry, Infacon XI*, pp 489–498
17. Emery JJ (1978) Utilization of wastes and by products as construction materials in Canada. *Conserv Recycl* 2(1):31–41
18. Zhu JQ, Wu SP, Zhong JJ, Wang DM (2011) A review of the recycling of construction and demolition wastes in asphalt pavement. *Adv Mater Res* 211–212
19. Marinković S, Radonjanin V, Malešev M, Ignjatović I (2010) Comparative environmental assessment of natural and recycled aggregate concrete. *Waste Manag* 30(11):2255–2264
20. Svatovskaya LB, Urov OV, Kabanov AA (2017) Geocoprotective technology of transport construction using silica sol absorption method. *Procedia Eng* 189:454–458
21. Svatovskaya L, Shershneva M, Baydarashvily M, Sychova A, Sychov M, Gravit M (2015) Geocoprotective properties of cement and concrete against heavy metal ions. *Procedia Eng* 117:350–354
22. Svatovskaya L, Sychova A, Sychov M, Gravit M (2016) New geocoprotective properties of the construction materials for underground infrastructure development. *Procedia Eng* 165:1771–1775
23. Svatovskaya LB et al (2016) Improvement of the level of the concrete properties by means of surface modification. *Transp Constr* 7:30–32
24. Svatovskaya LB, Baidarashvili MM, Shershneva MV (2014) New methods of geocodefense of natural and technogenic systems of structural activity for the benefit of sustainable development. *Monograph, PGUPS*
25. Sychova AM, Svatovskaya LB, Mjakin SV, Vasiljeva IV (2009) Modification of fillers for cements. In: *Electron beam modification of solids: mechanisms, common features and promising applications*, pp 35–37
26. Sychova AM, Svatovskaya LB, Mjakin SV, Vasiljeva IV (2009) Activation of aqueous phase at cement and concrete solidification. In: *Electron beam modification of solids: mechanisms, common features and promising applications*, pp 39–47
27. Svatovskaya L, Sychova A, Soloviova V, Maslennikova L, Sychov M (2016) Obtaining foam concrete applying stabilized foam. *Indian J Sci Technol* 9(42):104304
28. Sakharova A, Svatovskaya L, Baidarashvili M, Malchevskaya K, Petriaev A (2018) Buildings and construction infrastructure with geocoprotective properties. *Way Track Facil* 9:28–31
29. Information on iron oxide pigments, http://www.yarpigment.ru/folders/pigments_info. Last accessed 2019/01/20

The Acceleration of Hardening of Non-autoclaved Foam Concrete with the Mechano-Activated Binder When Constructing in the Arctic and Cold Regions



Andrey Solomahin, Larisa Svatovskaya and Yuriy Kamenev 

Abstract The purpose of the investigation is to obtain high strength characteristics of foam concrete during its hardening at sub-zero temperatures and using in road embankment structures. It is scientifically proved that the introduction of the granulated slag and waste molding mixture jointly ground with cement into the binder composition reduces the time of cement hydration in winter without using the modern methods of concrete hardening acceleration. The optimal combination of the complex binder components and the amount of injected polymer for foam stabilization are determined. The kinetics of the calcium release in the process of hydration at the initial phases is shown, and the rate of decrease of the alite component in the samples with the mechano-activated binder and polymer foam stabilizer is estimated. It was found that the introduction of the polymer into the active foam does not slow down the hydration process of silicates when introducing a mechano-activated binder. It is shown that the joint grinding of silicate components violates the crystal lattice of minerals and leads to the change in their surface properties. The method of X-ray phase analysis was used in the study of cement stone hardening processes. The paper proposes constructive solutions of road embankments with the use of non-autoclaved foam concrete on the basis of a mechano-activated binder. The use of non-autoclaved foam concrete based on mechano-activated binder is relevant to the construction in the Northern regions. Receive when you activate the secondary of active sites of hydration helps to reduce the binding time binding.

Keywords Non-autoclaved foam concrete · Mechano-activated binder · Polymer stabilizer · Hydration of silicates · Roads

A. Solomahin (✉) · Y. Kamenev
Military Space Academy named after A. F. Mozhaysky, St. Petersburg 197198, Russia
e-mail: solomahina@mail.ru

L. Svatovskaya
Emperor Alexander I St. Petersburg State Transport University, St. Petersburg 190031, Russia

© Springer Nature Singapore Pte Ltd. 2020
A. Petriaev and A. Konon (eds.), *Transportation Soil Engineering in Cold Regions*,
Volume 2, Lecture Notes in Civil Engineering 50,
https://doi.org/10.1007/978-981-15-0454-9_51

1 Introduction

The use of polystyrene foam in road embankments on weak soils is known from the literature [1–3]. Road structures with light materials require little time for their construction [4, 5]. It is known to use geofoam EPS as an embankment for the foundations of bridges [6]. In recent years, expanded polystyrene (EPS) geofoam has successfully been used to reduce the acting vertical and horizontal stresses in several geotechnical applications due to its lightweight, compressibility, and durability [7–9]. Material such as foam polystyrene (EPS) can be used as an energy-absorbing material [10]. But foam polystyrene (EPS) has the following disadvantages: high cost, the ability to destruction, and the possibility of using only blocks (the use of monolithic material is not possible). Non-autoclaved foam concrete can serve as an alternative to polymer products. It is free from the disadvantages of polymeric materials.

To obtain high strength characteristics of foam concrete of non-autoclaved hardening used in the construction of buildings and structures as well as in the process of construction of road and railway embankments in the Arctic and cold regions is quite a difficult task. The problem of reducing the time of cement hydration becomes even more important with the introduction of the concrete mix composition for obtaining higher physical–mechanical characteristics of polymeric components. Moreover, polymer components (polyvinyl acetate, divinyl-styrene latex) can be introduced as a foam stabilizer both into the mixing water and into the foam concentrate.

The introduction of a dispersion of polyvinyl acetate (PVA) into the foam concrete promotes an increase in compressive strength and flexural tensile strength [11–13]. This effect is due to the fact that polyvinyl acetate molecules (1 mk. long) are attracted by adhesion to the crystalline particles of the cement stone. When testing the foam concrete for stretching in the process of bending, a polymer film which works in stretching increases the strength and special properties of foam concrete several times.

The main disadvantage of polymer-cement foam concrete with latexes of various modifications and dispersions of PVA is the high shrinkage during hardening. According to A. V. Satalkina, it is necessary to use polymer additives that interact with cement and give concrete the positive properties of cement and polymers in polymer-cement concretes. These properties can correct the disadvantages of the cement binder due to the individual properties of polymers [14].

2 Results and Discussion

The problem of obtaining high-quality foam concrete with a stable rheological composition and the required physical and mechanical characteristics can be solved by polymer foam stabilization and joint mechanical activation of the hydraulic binder (cement) and foundry waste based on the molding mixture and quick cooling slag.

Portland cement (CEM 1 of the classes 32.5 (GOST 31108-2003)) of Pikalevsky plant was used as a hydraulic binder. As the initial components of the mineral additive, wasted molding mixtures (WMM) and granulated slags of several metallurgical enterprises of St. Petersburg were selected. The main components of the WMM are SiO_2 , Al_2O_3 , Fe_2O_3 , the amount of Al_2O_3 , Fe_2O_3 being increased in comparison with the initial molding sands. The increase of Al_2O_3 , Fe_2O_3 , CaO , Na_2O_3 , K_2O , MgO content increases the pH value in comparison with the initial sands. In order to assess correctly, the effectiveness of the WMM and the metallurgical slag use as an additive in cement, and special studies were conducted concerning the correspondence of WMM and slag requirements to the mineral additives in cement. It was concluded that all the additives investigated met the requirements of TU to the active mineral additives in cement. This conclusion appeared to be decisive in the choice of the main directions for the next stage of our research.

Further fine grinding of raw materials is the most important technological operation in the production of the binders which determines the quality of the binder to a great extent [15, 16]. In accordance with the principle of Gibbs-Curie, the higher the substance dispersion the higher is its solubility and chemical activity. In general, the mechanism of mechano-chemical processes can be defined as the initiation of chemical reactions under the influence of elastic energy. The degree of the processes proceeding during the mechanical activation can be estimated only by the products of chemical reactions after testing. A common feature of the activation processes is the increase in the excess energy of solids which occurs due to the increase of the free surface and because of the defects of the spatial atomic or molecular structure of the treated bodies.

During the study of hydration processes, it was assumed that the introduction of the granulated slag and WMM with joint activation with cement and subsequent mixing with the polymer would significantly increase the rate of the alite phase decrease as a result of the significant increase in the concentration of the active centers, which leads to the intensification of the complex binder hydration (Figs. 1 and 2).

Thus, it will give the opportunity to hydrate more binder (Figs. 1 and 2). This assumption is based on the fact that the activated slag with added water will have a pronounced alkaline medium which, in its turn, also makes it possible to carry out the hydration reaction in the most complete form.

This assumption was confirmed by the results of X-ray phase analysis which allowed us to come to the following conclusions:

1. The polymer introduction slows down the process of silicates hydration.

The reason is the form of the polymer particles of the introduced polymer (latex globules, polyvinyl acetate film). The films provide a greater overlap of the hydrated minerals surface than the balls. Hydration in the presence of latex stabilized by liquid glass can be increased at the initial stage (up to 3 days) of the process compared with the PVA dispersion:

- (a) due to the presence of soluble silicate ions;
- (b) due to the alkaline environment.

Fig. 1 Rate of alite decrease: (1) samples based on CEM 1 of the classes 32.5 with polymer-free mixing; (2) samples based on CEM 1 of the classes 32.5, MD with polymer-free mixing

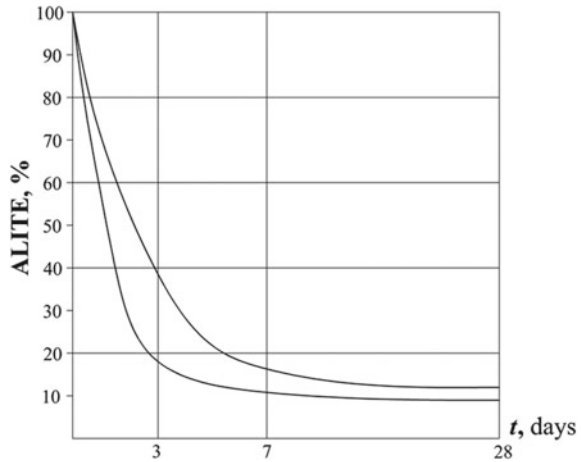
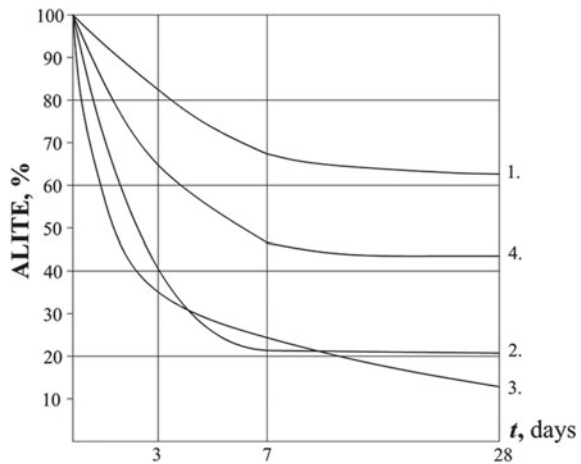


Fig. 2 Rate of alite decrease: (1) samples based on CEM 1 of the classes 32.5 and PVA; (2) samples with the mechano-activated binder with mineral additives (MAV M) and PVA; (3) samples on the basis of MAV MD and latex; (4) samples based on CEM 1 of the classes 32.5 and latex



2. The introduction of the additives leads to the acceleration (as compared with the number 1) of the hydration reaction due to a faster set of alkalinity by the system (Fig. 1), despite the fact that the reaction completeness is different (Fig. 3). The set of alkalinity is due to the fact that according to the X-ray phase analysis, the CFS is almost a pure crystalline quartz while slags are amorphous silica with pH = 10.
3. When introducing the additives, there is a sharp increase in the rate of alite hydration at the initial stage-up to 3 days. During the period from 3 to 7 days, there is a redistribution of the speeds. The slowest speed takes place in the cement samples with mineral additive based on polyvinyl acetate dispersion (Fig. 4). Further, there are samples on the basis of cement without additives and PVA. An even higher speed of samples hydration on the basis of latex takes place.

Fig. 3 Release of CA during the hydration process of the initial phases in the samples based on cement and binder MD at the unparallelled mixing: (1) samples based on CEM 1 of the classes 32.5 with polymer-free mixing; (2) samples based on CEM 1 of the classes 32.5, MD at polymer-free mixing

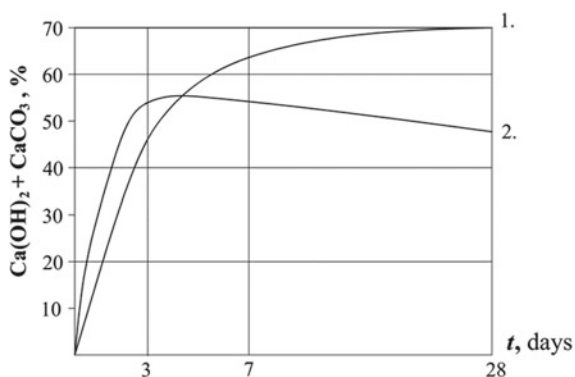
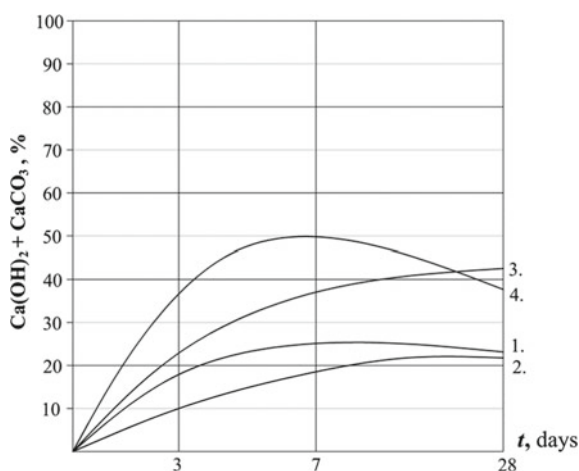


Fig. 4 Release of CA during the hydration process of the initial phases in samples based on MV MD at polymeric mixing: (1) samples based on CEM 1 of the classes 32.5 and PVA; (2) samples based on MAV MD and PVA; (3) samples based on MAV MD and latex; (4) samples based on CEM 1 of the classes 32.5 and latex



The most complete process of hydration occurs in polymer-free samples on pure cement, although the rate of alite decrease they have is the slowest (Fig. 2).

As mentioned above, the introduction of a polymer binder usually slows down the process of cement hydration. However, its introduction in the range of 15–25% of the weight of the hydraulic binder and the implementation of mechano-chemical activation of the binder by means of a mineral additive allows to activate the hydration process. The tables shows the indicators of increase in bending strength (Table 1) and compression (Table 2) of foam concrete samples of beams of different composition for grades D900, D500.

It should be noted that it is not always possible to use standard approaches to the embankment device. This is due to the construction area, the terrain relief, and the ground characteristics at the base.

Table 1 Strength characteristics of samples—beams of foam concrete D900, D500 (R_{bt})

Name of samples	R_{bt} , MPa 3 days D900/D500	R_{bt} , MPa 7 days D900/D500	R_{bt} , MPa 28 days D900/D500
Model No. 1 cement + water	1.39/1.03	2.48/1.83	4.2/3.1
Model No. 2 cement + PVA	1.74/1.28	3.1/2.28	5.25/3.86
Model No. 3 cement + WMM + slag + PVA	1.65/1.22	2.95/2.18	5.0/3.68
Model No. 4 cement + WMM + slag + water	1.26/0.93	2.25/1.66	3.8/2.8
Model No. 5 cement + WMM + slag + latex	1.13/0.83	2.01/1.48	3.4/2.5
Model No. 6 cement + latex	1.32/0.98	2.36/1.74	4.0/2.95

Table 2 Strength characteristics of samples—beams of foam concrete D900, D500 (R_{bt})

Name of samples	R_b MPa. 3 days D900/D500	R_b MPa. 7 days D900/D500	R_b MPa. 28 days D900/D500
Model No. 1 cement + water	3.57/1.85	6.38/3.31	11.0/5.8
Model No. 2 cement + slag + latex	2.55/1.34	4.55/2.4	7.7/4.06
Model No. 3 cement + slag + PVA	2.00/1.06	3.57/1.89	6.05/3.19
Model No. 4 cement + WMM + latex	1.31/0.69	2.34/2.09	3.96/2.09
Model No. 6 cement + WMM + slag + latex	1.42/0.75	2.54/1.34	4.29/2.27
Model No. 5 cement + WMM + PVA	2.25/1.19	4.03/2.13	6.82/3.60
Model No. 7 cement + WMM + slag + PVA	4.57/2.44	6.38/3.31	10.8/5.6

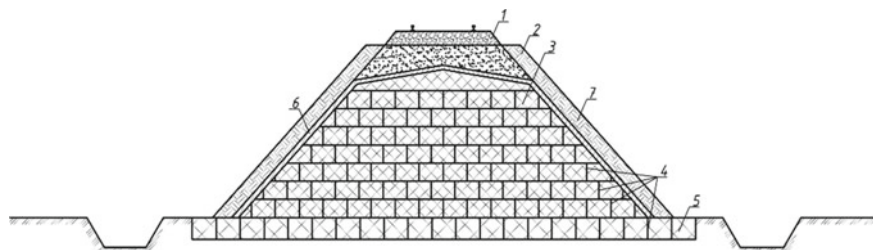


Fig. 5 Example of an embankment structure on a weak base for a railway track: (1) ballast layer of crushed stone; (2) sand drainage layer; (3) monolithic polymer-cement foam concrete D900; (4) spatial polymer lattice; (5) foam concrete D500; (6) waterproofing polymer layer; (7) ground dusting

In this paper, we propose to use non-autoclaved polymer-cement foam concrete based on the mechanically activated binder in typical and individual embankments structures (Fig. 5) for the railways and highways when building on weak soil foundations [17–19].

3 Conclusions

1. The use of man-made products of the metallurgical processes with a high content of R2O allows to increase the concentration of alkaline ions, resulting in the increase in the calcium ions concentration in the solution. This leads to the intensification of the hydration processes and increased exothermia.
2. As a result of the mechano-chemical activation of the binder with mineral additives, the chemical bonds of the raw material particles break. Having no time to recombine with each other, they form acidic and basic centers which also activate the hydration processes.
3. The use of mineral additives with a high content of R2O in polymer-cement concretes activates the processes of formation of portlandite and calcium carbonate, which results, respectively, in a higher degree of the alite phase decrease. The crystal structure of alite is formed already at the early stages of the foam concrete curing.

References

1. Wang F (2009) A proposed lightweight fill for embankments using cement-treated Yangzi River sand and expanded polystyrene (EPS) beads. *Bull Eng Geol Env* 68:517–524
2. Duškov M, Erkelens W (2019) Dutch N201 road embankment with EPS geof foam. In: Arellano D, Özer A, Bartlett S, Vaslestad J (eds) 5th international conference on geof foam blocks in construction applications. Springer, Cham, pp 89–97

3. Aabøe R (2019) Geofam blocks in civil engineering applications. In: Arellano D, Özer A, Bartlett S, Vaslestad J (eds) 5th international conference on geofam blocks in construction applications. Springer, Cham, pp 3–38
4. Duškov M, den Uil M, Fütterer M (2019) Dutch A76 highway widening using EPS embankment with a vertical side. In: Arellano D, Özer A, Bartlett S, Vaslestad J (eds) 5th international conference on geofam blocks in construction applications. Springer, Cham, pp 81–87
5. Taneichi K, Konami T, Tsukamoto H, Kubota T, Yasuhara K (2019) Opening traffic for a temporarily remediated EPS road after the 2016 kumamoto earthquake: a world first. In: Arellano D, Özer A, Bartlett S, Vaslestad J (eds) 5th international conference on geofam blocks in construction applications. Springer, Cham, pp 351–359
6. Vaslestad J, Bartlett SF, Aabøe R, Burkart H, Ahmed T, Arellano D (2019) Bridge foundations supported by EPS geofam embankments on soft soil. In: Arellano D, Özer A, Bartlett S, Vaslestad J (eds) 5th international conference on geofam blocks in construction applications. Springer, Cham, pp 281–294
7. Abdelsalam S, Badr El-Din A (2019) Long term behavior of EPS geofam for road embankments. In: Proceedings of the 2nd GeoMEast international congress and exhibition on sustainable civil infrastructures, SSIGE, Egypt, pp 97–107
8. Samir El-kady M, Alzara MA, Anwar Farouk M (2018) Innovative infrastructure solutions, reduction of lateral earth pressure using Geo-fam blocks. *Innov Infrastruct Solut* 3:40
9. Gendy ME, Araby IE, Kamash WE, Sallam E, Labban AE (2018) Effect of using EPS geofam on deformation behavior of square footings on clay subjected to static and dynamic loads: experimental study. In: 5th international conference on geofam blocks in construction applications. Springer, pp 251–266
10. Ouyang C (2019) Dynamic analysis of rockfall impacts on geogrid reinforced soil and EPS absorption cushions. *KSCE J Civ Eng* 37–45
11. Sychova A (2018) Improving of the monolithic foamconcrete quality for used in the high-rise constructions. In: Solomahin A, Kotovich V, Svatovskaya L, Kamenev Y (eds) E3S web of conferences, vol 33, HRC 2017, pp 02058. <https://doi.org/10.1051/e3sconf/20183302058>
12. Shahova L (2010) The technology of foam concrete. Theory and practice. Publishing House Association Building Universities, Moscow
13. Tikhomirov V (1983) Foam. Theory and practice of generation and destruction. Publishing House “Chemistry”, Moscow
14. Satalkin A, Solntseva V, Popov O (1971) Cement-polymer concrete. Stroiizdat, Leningrad
15. Svatovskaya A, Sychev M (1983) Activated hardening cements. Stroyizdat, Leningrad
16. Sychova A, Svatovskaya L, Mjakin S, Vasiljeva I (2009) Modification of fillers for cements. In: Electron beam modification of solids: mechanisms, common features and promising applications, Saint-Petersburg
17. Solomakhin A (2017) The use of polymer-cement concrete to increase the service life of the railway. *Transp Constr* 6:21–23
18. Sychev M (2016) The use of non-autoclaved polymer-cement foam concrete in the device of pavement. *Bull Constr Mach* 11:62–64
19. Sychova A (2017) The increase of the durability and geoprotective properties of the railway. *Procedia Engineering. Subgrade transportation geotechnics and geoecology, TGG*, vol 189, pp 688–694

Effective Building Ceramics for Transport Infrastructure



Ludmila Maslennikova , Natalia Babak, Anna Slavina and Igor Naginskii

Abstract In this article the possibility of using porous silicate-containing waste when receiving an effective ceramic brick (which is used for erection of a transport infrastructure buildings and constructions at low temperature) is considered. The purpose of study was development of ceramic brick compositions made with using of granulated blast-furnace slag and with using of a ground foam concrete crush, which has a lower thermal conductivity coefficient of a brick, and meets the requirements of state standards for other indicators. Optimum compositions of materials and physical-mechanical characteristics of received materials are given. To study the composition of technogenic raw materials and the structure of synthesized ceramic materials the following methods were used: X-ray phase and differential-thermal methods, IR- Fourier-transform spectroscopy, electron microscopy, mercury porosimetry method. The estimation of ecological and economic efficiency of use of porous silicate-containing waste is given. This estimation shows a significant reduction of anthropogenic load on the environment, a reduction of the cost of production of ceramic bricks with improved heat technical characteristics, what is needed for erection of buildings and constructions in cold regions.

Keywords Effective brick · Granulated slag · Foam concrete waste · Conductivity coefficient

1 Introduction

Currently, more and more attention is being paid to improving energy saving and energy efficiency worldwide. This makes it urgent to improve the heat-shielding properties of building materials, including ceramic bricks, especially in cold regions. At the same time, the emergence of new requirements for thermal protection of buildings

L. Maslennikova (✉) · N. Babak · A. Slavina · I. Naginskii
Emperor Alexander I St. Petersburg State Transport University (PGUPS), St. Petersburg 190031,
Russia
e-mail: llmaslennikova@yandex.ru

© Springer Nature Singapore Pte Ltd. 2020

A. Petriaev and A. Konon (eds.), *Transportation Soil Engineering in Cold Regions*,
Volume 2, Lecture Notes in Civil Engineering 50,
https://doi.org/10.1007/978-981-15-0454-9_52

495

and structures dictates the need to create new building materials with improved thermal protection properties. In this regard, research, aimed at reducing heat conduction of ceramic crock by attracting porous silicate-containing technogenic components, is relevant. Research on the decline of heat conductivity of ceramic brick with the use of porous silicate-containing technogenic components are actual, as allow complex to decide the questions of resource and energy-savings, guard of environment and deficit of separate raw material.

1.1 Purpose and Objectives of the Study

The aim of the work was to develop and study the compositions of effective ceramic bricks using porous silicate-containing technogenic raw materials.

To solve this problem, the following research objectives were formulated:

- to determine the criteria for assessing the choice of technogenic raw materials for improving the performance characteristics of ceramic bricks;
- to develop optimal compositions of effective ceramic bricks with the use of porous silicate-containing technogenic raw materials;
- to establish the regularities of the effect of the injected silicate-containing technogenic raw materials on the pore structure, thermal conductivity coefficient and other physical-mechanical characteristics of a ceramic brick.

1.2 Short Literary Review

The influence of technogenic components on the improvement of the physical and mechanical properties of ceramic bricks has been considered in many works [1–25], however, the existing technological methods (such as burnout additives, increase of emptiness) for receiving an effective ceramic brick are largely exhausted. Moreover, issues of reducing the thermal conductivity of wall ceramic materials by adding of technogenic raw materials with its own porosity and chemical nature insufficiently studied.

In this regard, to reduce a density of a ceramic it is advisable to consider the use of porous silicate-containing technogenic raw materials.

2 Methods and Experiments

In order to improve the thermal properties without significantly reducing the strength, it is necessary to take into account two contradictory points: on one hand, the higher the porosity of the ceramic material, the lower the density and thermal conductivity,

on the other hand, the increase in porosity leads to a decrease in strength and frost resistance. This is consistent with research of [26], who additionally allocated an interval of intermediate pores with size from 0.5 to 10 μm in the existing classification of A. S. Berkman and I. G. Melnikova.

Along with the porosity, it is necessary to take into account the chemical nature of the solid, because the prevailing mechanism of heat transfer in ceramics is a phonon conductivity, which is realized by lattice vibrations. In research of U. D. Kingery [27] is shown that the complication of the crystal lattice (which is characterized by a large violation of the systematicity and by a scattering of phonons in a ceramic matrix) leads to a decrease in the thermal conductivity of the entire composition.

The complexity of the structure of a material can be assessed using energy indexes. Lower values of a standard enthalpy (energy content) formation of $-\Delta H_{298}^0$, kJ/mol, and more high molar masses M , g/mol of the basic phases of the material inform about its lower values of heat conductivity. It was found by research of scientists of the department «Engineering chemistry and natural sciences» PSTU under the guidance of the professor L. B. Svatovskaya in a cement materials science.

In accordance with the above ideas, it is possible to formulate criteria for the selection of technogenic raw materials in order to obtain an effective ceramic brick. These criteria are: own porosity with a preferential pore size of less than 10 μm , complex mineral composition in the form of silicates, alumo-silicates and hydrosilicates of calcium and magnesium, which have lower values of an enthalpy and higher values of molar masses in comparison with quartz.

A granulated blast-furnace slag (GBFS), which is formed as a waste at metallurgical plants satisfies such conditions. It has a size modulus 2.4–2.9, its phase composition is represented by helenite, akermanite and other silicates of calcium and magnesium. The conducted studies of porosity by the mercury porosimetry method showed that pores with size less than 10 μm occupy 80–85% of the total volume of a GBFS. It was also taken into account that during the heat treatment of GBFS stable crystalline phases of slag glass can be formed (they affect the increase in bending strength of the material). The second technogenic component which meets the selected criteria is a foam concrete crush autoclave and non-autoclave hardening, whose phase composition is represented by quartz, tobermorite, xonotlite and by other hydrosilicates. By using the mercury porometriya method, it was found that pores with a size of less than 10 μm occupy 80–85% of the non-autoclave foam concretes volume and 90–94% of the autoclave foam concretes volume (of the total volume). During the firing the final dehydration product of hydrosilicates is wollastonite, this will facilitate the simplification of the entire structure of the material with the additional effect of lightening the brick.

Cambrian clay (Krasny Bor deposit) was used as a clay component. This clay is widely distributed in the North-West region of Russia and the Baltic countries. Sand for construction works with the size modulus 1.9–2.4 was used as an emaciating material for control samples.

Table 1 Physical-mechanical characteristics of laboratory samples

Composition wt%	Water absorption by weight, W, %	Average density, g/sm ³	Coefficient of thermal conductivity, λ , W/(m K)	Strength limit, MPa		Brick color
				At bending, R_b	At compression, R_c	
Control composition: Clay—70 Sand—30	7.1	1.91	0.31	Av. 3.9 Min. 2.9	Av. 15.9 Min. 13.6	Brick-red
Composition 1 Clay—65 foam Concrete—35	26	1.41	0.15	Av. 3.1 Min. 2.9	Av. 12.2 Min. 11.5	Light beige

Physico-mechanical studies were carried out on laboratory samples—beams the size $160 \times 40 \times 40$ mm samples—cubes $50 \times 50 \times 50$ mm. The firing temperature, traditionally adopted in the North-West region for firing ceramic bricks on the Cambrian clay, is 980°C .

The foam concrete crush was coarsely ground to a particle size of less than 1 mm and was injected into a burden as an emaciating material.

Using the method of mathematical modeling, the optimal composition was found, it contains 65 wt% of clay and 35 wt% of foam concrete crush. The results of physical-mechanical studies of the obtained samples are presented in Table 1.

As can be seen from Table 1, injecting 35 wt% of ground foam concrete allowed to reduce the density of the brick by 26% and to reduce the coefficient of thermal conductivity by 2 times in comparison with the control sample.

The color of the front surface of the material is light beige. Strengths of a sample of composition 1 are decreased, however, despite the decrease in bending and compressive strength, the ratio R_b/R_c of the composition with a foam concrete remained at the level of the control. By the X-Ray phase method and IR- spectroscopy it was established that in the “clay—foam concrete” system during the firing, the phases of wollastonite crystallize $\beta\text{-CaO-SiO}_2$ ($-\Delta H_{298}^0 = 1634.2$ kJ/mol, $M = 116.1$ g/mol) and melilite phases $\text{Ca}_2(\text{Al,Mg,Si})\text{Si}_2\text{O}_7$ ($-\Delta H_{298}^0 = 3898.1$ kJ/mol, $M = 326.7$ g/mol). Melilite is a continuous series of solid solutions of a helenite with an akermanite.

In order to increase the strength of the products while maintaining the light beige tone of the ceramic matrix, the foam concrete was used in the finely ground state (the remainder on a sieve with a cell size of 0.14 mm is not more than 2%). For comparison building sand and GBFS were injected into the burden as an emaciating material.

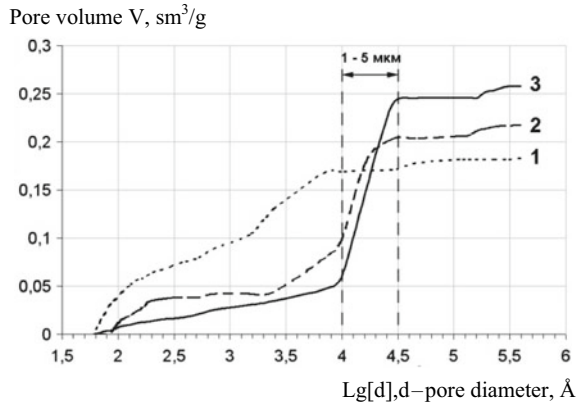
For further research a composition with a 20% content of foam concrete and GBFS was taken. The results of physical-mechanical studies of the samples obtained are presented in Table 2.

The porosity characteristic determined by the mercury porosimetry method is shown on Fig. 1 and in Table 3. An analysis of the results obtained showed that

Table 2 Physical-mechanical characteristics of brick samples

Composition, wt%	Water absorption by weight, W, %	Average density, g/sm ³	Strength limit, MPa		λ, Wt/(m K)	Brick colour
			At bending R _b	At compression, R _c		
Composition 2 Clay—60 Fine-grained foam concrete Crush—20 Sand—20	20.9	1.54	Av. 1.8 Min. 1.7	Av. 11.1 Min. 0.2	0.29	Light beige
Composition 3 Clay—60 Fine-grained foam concrete Crush—20 GBFS—20	22.0	1.52	Av. 4.2 Min. 3.9	Av. 15.3 Min. 3.2	0.24	Light beige

Fig. 1 Integral curves of pore size distribution:
1—control sample;
2—sample with sand and foam concrete;
3—sample with slag and foam concrete



in samples with fine ground foam concrete (compositions 2 and 3) a predominant increase in the pore volume of 1–5 μm. In the same time in a control sample the pore volume of this size does not practically increase.

Curves 2 and 3, which reflect the increase in pore volume in samples with fine ground foam concrete, have a jump in the pore size range from 1 to 5 μm. It means that pores of this size predominate in the total pore volume.

Pore volume size 1–5 μm increases (Table 3) in the row from the control sample to the sample 2 and further to the sample 3. In the same sequence the structure of the material becomes more complicated, this should lead to a corresponding decrease in

Table 3 Characterization of porosity of ceramic samples

Composition ceramic brick	Average density, g/sm ³	Specific surface of pores m ² /g	Total pore volume, sm ³ /g	Pore volume size 1–5 μm from the total volume	
				sm ³ /g	%
Control Composition	1.86	32.44	0183	0009	4.9
Composition 2 (sample 2)	1.54	13.22	0217	0106	48.8
Composition 3 (sample 3)	1.52	7.53	0258	0188	72.8

the thermal conductivity of the brick. The measured coefficients of thermal conductivity of the samples under stationary thermal conditions (National State Standard of Russia 7076-99) confirm the revealed dependence.

Comparing the available data on the reduction of thermal conductivity in the samples compositions 2, 3 and in the control one, also the obtained data on the distribution of pores we can conclude that the maximum contribution to the improvement of the heat-shielding properties of the ceramic material is introduced by pores with a diameter from 1 to 5 μm.

In a Fig. 2a, b the slag grain (III) with spheroidal pores and the inclusion of foam concrete (II) are shown. They form channel porosity in the clay matrix and have their own capillary porosity (Fig. 2c).

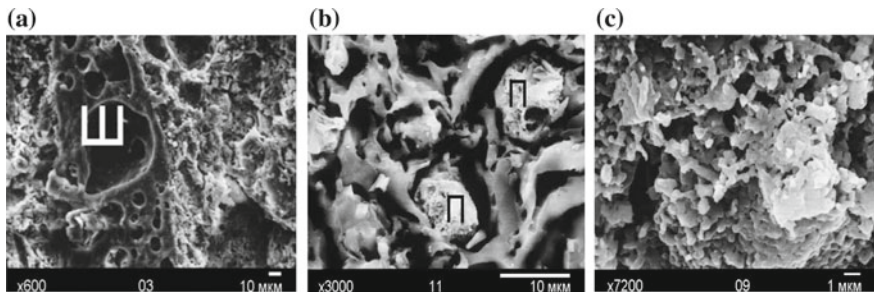


Fig. 2 Microstructure of sample 3 after firing: **a** slag grain (III); **b** foam concrete parts (II) in ceramic matrix; **c** foam concrete grain with its own capillary porosity

Table 4 Physical-mechanical characteristics of laboratory samples of effective brick with the selected technogenic raw material

Compositions	The main identified phases of neoplasms after firing	Physical-mechanical characteristics of the material obtained			
		Average density, g/sm ³	λ , Wt/(m K)	Ratio R_B/R_C	Coefficient of constructive quality, CCQ
Control with sand	CaO·Al ₂ O ₃ ·2SiO ₂ , SiO ₂	1.91	0.31	0.25	8.3
Composition 2	CaO·Al ₂ O ₃ ·2SiO ₂ , β -CaO·SiO ₂ , 2CaO·Al ₂ O ₃ ·SiO ₂ , 2CaO·MgO·2SiO ₂ , 3CaO·MgO·2SiO ₂	1.52	0.24	0.28	10.1
Composition 3	CaO·Al ₂ O ₃ ·2SiO ₂ , β -CaO·SiO ₂ , Ca ₂ (Al,Mg,Si)Si ₂ O ₇	1.41	0.15	0.26	8.7

3 Results and Discussion

The achieved results on improving the operational properties of effective ceramic bricks with the selected technogenic raw materials are presented in the summary Table 4.

As expected, the combined injection of GBFS and fine-grained foam concrete makes it possible to obtain a light beige color of a brick, to reduce the thermal conductivity coefficient by 23% and to increase the coefficient of constructive quality by 22% in comparison with the control sample.

Thus, possibility of decline of coefficient of heat conductivity of ceramic brick is reasonable due to using silicate-containing of technogenic raw material. This technogenic raw material should have its own porosity with a predominant pore size of less than 10 μ m. The use of such bricks in the construction of transport infrastructure buildings will reduce the load on the foundation and reduce the thermal conductivity of the walls, which is an important factor for cold regions.

References

1. Zong Y-B, Chen W-H, Liu Y-X, Liu Z-B, Cang D-Q (2019) Influence of slag particle size on performance of ceramic bricks containing red clay and steel-making slag. *J Ceram Soc Jpn* 127(2):105–110
2. Mao L, Wu Y, Zhang W, Huang Q (2019) The reuse of waste glass for enhancement of heavy metals immobilization during the introduction of galvanized sludge in brick manufacturing. *J Environ Manage* 231:780–787
3. Gayarre FL, González JS, López MAS, Pérez CL-C, Arias PJF (2019) Mechanical properties of prestressed joists made using recycled ceramic aggregates. *Constr Build Mater* 194:132–142
4. Fíla J, Eliášová M, Sokol Z (2019) Experimental investigation of mortar mechanical properties for glass brick masonry. *Glass Struct Eng* 4(1):127–141

5. Gayarre FL, González JS, López MAS, Pérez CL-C, Arias PJF (2019) Mechanical properties of prestressed joists made using recycled ceramic aggregates. *Constr Build Mater* 194:132–142
6. Hassan AM, Moselhy H, Abadir MF (2019) The use of bagasse in the preparation of fireclay insulating bricks. *Int J Appl Ceram Technol* 16(1):418–425
7. Horckmans L, Nielsen P, Dierckx P, Ducastel A (2019) Recycling of refractory bricks used in basic steelmaking. *Resour Conserv Recycl* 140:297–304
8. Wilkerson RP, Gludovatz B, Ell J, Hilmas GE, Ritchie RO (2019) High-temperature damage-tolerance of coextruded, bioinspired (“nacre-like”), alumina/nickel compliant-phase ceramics. *Scr Mater* 158:110–115
9. Čáchová M, Scheinherrová L, Doleželová M, Keppert M (2019) The effect of ceramic application in design of ceramic-based plasters. *Adv Struct Mater* 98:97–106
10. Baptista A, Carneiro A, Parsekian G, Fonseca F (2019) A proposed test to evaluate efflorescence potential of ceramic blocks RILEM bookseries 18:532–539
11. Colombia Monroy R, Romero YA, Gelves JF (2018) Consumption of energy in the manufacturing of ceramic bricks in the metropolitan area of Cúcuta. *J Phys: Conf Ser* 1126(1):012014
12. Shershneva MV, Makarova EI, Savelyeva MY (2017) Oil products absorbing properties of foam concretes. *Procedia Eng* 189:320–324
13. Svatovskaya LB, Shershneva MV, Bobrovnik AB (2017) Geocoprotective properties of binders for transport systems. *Procedia Eng* 189:440–445
14. Łapka P, Wasik M, Furmański P, Wiśniewski TS, Jaworski M (2018) Preliminary mathematical and numerical transient models of convective heating and drying of a brick. In: *M. MATEC Web of Conferences* 240, 01022
15. Arbuzova TB, Shabanov VA, Korenkova SF, Chumachenko NG (1993) Building materials from industrial wastes. Samara
16. Bozhenov PI (1994) Complex use of mineral raw materials and ecology. Association of Construction Universities. Stroyizdat, Moscow
17. Babak NA, Maslennikova LL, Slavina AM (2010) Geocological solutions for creating efficient building ceramics on the basis of technogenic silicate raw materials. *News of PSTU* 2:220–230
18. Babak NA, Maslennikova LL, Slavina AM (2011) Geocological reserve of technologies, materials and structures in construction using industrial mineral waste. PSTU, St.-Petersburg
19. Komokhov PG, Maslennikova LL, Abu-Khasan MS (2003) Controlling the strength of ceramic materials by forming a contact zone between the clay matrix and the emaciating material. *Constr Mater* 12:44–45
20. Maslennikova LL (2000) Development and introduction of ceramic materials with predictable properties and taking into account the nature of the introduced technogenic raw materials. Dissertation for the degree of Doctor of Technical Sciences. Saint-Petersburg
21. Maslennikova LL, Slavina AM (2009) The use of waste cellular concrete in the production of ceramic materials with improved thermal protection properties. *Pop Concr Sci* 6(32):30–35
22. Maslennikova LL, Abu-Khasan MS, Babak NA (2017) The use of oil-contaminated crushed stone screenings in construction ceramics. *Procedia Eng* 189:59–64
23. Maslennikova LL, Naginskii IA, Troshev AN (2017) Use of waste from aluminothermic welding of railroad tracks in structural materials science. *Procedia Eng* 189:94–98
24. Maslennikova LL, Svatovskaya LB, Mjakin SV, Vasiljeva IV (2009) Activation of reactions at solid-solid interfaces. In: *Improvement of ceramics materials (book chapter)*. Electron beam modification of solids: mechanisms, common features and promising applications, pp 57–61
25. Svatovskaya LB, Shershneva MV, Savelyeva MY (2017) Geocoprotective technologies of storage of used wooden sleepers. *Procedia Eng* 189:605–609
26. Lkhova NA, Makarova IA, Patramanskaya SV (2002) Firing materials based on microsilica. BrSU, Bratsk
27. Kingery UD (1977) Introduction to ceramics. Stroyizdat, Moscow